The tectonic evolution of the Eastern Limassol Forest Complex, Cyprus

Thesis

THE TECTONIC EVOLUTION OF THE EASTERN LIMASSOL FOREST COMPLEX, CYPRUS

A thesis presented for the degree of

Doctor of Philosophy

by

Christopher John MacLeod

B.Sc. (Hons.) Dunelm

(1984)

Department of Earth Sciences

The Open University

September 1988

Any maps, pages, tables, figures graphs,or photographs, missing from this digital copy, have been excluded at the request of the university.

"They've just heard that ophiolites are bits of ancient oceanic lithosphere and they're so excited that they've come to see if anyone can confirm the news."

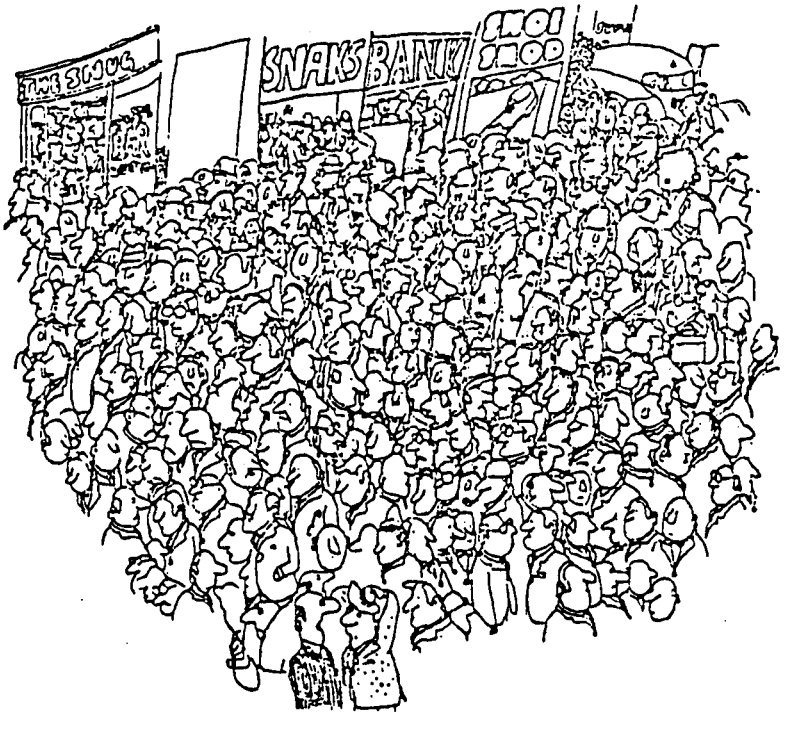

ABSTRACT:

The Eastern Limassol Forest Complex (ELFC) lies at the southern margin of the Troodos ophiolite, Cyprus, and preserves a Penrose-type stratigraphy with a 4km-thick crustal sequence. The ELFC is separated from the main part of the Troodos Massif by an east-west trending fault zone, the Arakapas Fault Belt, which earlier studies suggest formed the northern wall of an oceanic transform fault. Transform-related structures are identifiable in the northern part of the ELFC, and volcaniclastic turbiditic sediments intercalated with lava flows attest to the existence of a bathymetric depression coincident with the fault zone. A southern boundary to the transform fault zone is recognised within the ELFC, with the abrupt disappearance of interlava sediments and E-W trending structures. Crust to the south of the boundary was generated at an 'Anti-Troodos' ridge axis. A width of *c.*5km is implied for the transform.

The accretionary geometry of the ELFC has been extensively modified by post-volcanic tectonism. Sustained extension oblique to the trend of the transform has resulted in the reactivation of transform-related structures as normal faults, which have been rotated 'falling domino' style, together with the greater part of the axis sequence crust, above a décollement horizon located near to the petrological Moho. Extensional strain was preferentially accommodated in the transform-tectonised north of the ELFC. In the south, NW-striking normal faults are more steeply dipping, and block tilting is less extreme. Mesostructural data suggest that these normal faults have been reactivated as oblique dextral strike-slip faults and, with subsidiary NE-trending structures, are responsible for clockwise block rotations about steeply plunging axes.

The timing of the deformation is constrained with respect to the overlying pelagic sediments, which suggest that the extension continued from the Turonian (*i.e.* almost immediately after ophiolite formation) to the late Campanian, and that the strike-slip reactivation occurred in late Campanian to early Maastrictian times. Palaeomagnetic studies have shown that Cyprus experienced a 90° anticlockwise rotation, which commenced in the Campanian–Maastrichtian interval, and it is argued that the late dextral strike-slip movements in the southern ELFC reflect deformation close to the margin of the rotating Cyprus microplate. The extensional reactivation of the transform in the Turonian–Campanian may correspond to an anticlockwise torque applied to the Troodos ocean floor prior to actual rotation. The rotation of Cyprus is thought to have been a consequence of the collision of the Arabian continental promontory to the east with an intra-oceanic subduction zone (above which Troodos was created) in the Upper Cretaceous.

ACKNOWLEDGEMENTS:

The completion of this project would have been considerably more difficult and taken even longer without the assistance of a number of people. I wish to thank the following in particular for their help:

—Ian Gass, my supervisor, for his sage wisdom and advice throughout, and for his prompt and (very) critical reviews of earlier versions of the tome.

—Costas Xenophontos, for his generosity and invaluable help with logistics in the field, and useful discussions over cups of coffee on Saturday mornings in Nicosia.

—Simon Allerton, for bouncing ideas around, for fine company and showing by example how fieldwork in Cyprus needn't be too taxing, and not least for undertaking all the palaeomagnetic sampling, demagnetising, and fiddling of data *etc.*

—Bramley 'Pink Adonis' Murton, the Grandfather of Cyprus Geology, for help and hindrance over the years, and for Indiana Jones lessons in Limassol.

—Sabine Schregle, for 'diplomatic initiatives'.

—The 'grown-ups': Fred Vine, Eldridge Moores, John Malpas and Alastair Robertson, for interesting chats.

In Cyprus:

—Andreas Panayiotou and Eleni Georgiou of the Cyprus Geological Survey Department.

—Stuart Swiny of the Cyprus American Archaeological Research Institute, Nicosia, for his generous permission to allow me to use CAARI as a home from home.

—David Pearlman, Kalavasos, for getting me out of nasty scrapes when my Greek just wasn't up to it, and introducing me to many of the finer points of Cypriot life.

—all the people of Kalavasos for their extraordinary hospitality over the ten months of my stay in the village, particularly Nikolas Stratouras and Stavros Elia.

—all the archaeologists

—The Nirvana, Nicosia

At the Open University:

—Nick Rogers for INAA analyses, commenting on chapter 4 and teaching me some geochemistry (quite a lot, really); Pam Owen for typing bits and pieces and warning me of the Gassman's whereabouts; Ian Chaplin for prompt thin sectioning (apart from the May '85 lava samples); Johnny Watson for XRFing; Andy Tindle and Ben van Wyk de Vries for probing; Dave Ormerod and Andy Tindle (again) for computing (Thank God for the Macintosh); John Taylor and Andy Lloyd for trying repeatedly to teach me how to draw; the micropal. boys, Simon Houghton and Paul Gamson for helping me in my attempts to extract microbeasts, and Tony King for helping me try to find them on the SEM; Jim Miller and Dave Ormerod for putting up with me in T19 for the duration; Fiona McGibbon for just being there; Cherry Lewis for almost coping with the mental abuse; and Graham Hill for being enough of a gentleman not to lap me at the last.

to my parents

CONTENTS:

CHAPTER 1: Introduction 1

1.1 Regional Setting 1
1.1.1 Cyprus: geography and present tectonic setting 1
1.1.2 The Eastern Limassol Forest Complex 2

1.2 The Troodos Ophiolite 3
1.2.1 General description 3
1.2.2 Ophiolites: definition and history of the term 3
1.2.3 The Troodos ophiolite as oceanic lithosphere 5

1.3 Cyprus in the Context of the Evolution of Tethys 6
1.3.1 The Tethys Ocean 6
1.3.2 Brief geological history of Cyprus in the context of Tethys 8

1.4 Previous Research: the Arakapas Fault Belt and Limassol Forest 9
1.4.1 The Arakapas Fault Belt 9
1.4.2 The Western Limassol Forest Complex 10
1.4.3 The Eastern Limassol Forest Complex 11

1.5 Aims and Presentation of this Thesis 13
1.5.1 Aims, preconceptions, approach and progress 13
1.5.2 Presentation of this thesis 15

CHAPTER 2: Ophiolite Stratigraphy 17

2.1 Introduction 17

2.2 Mantle Sequence 18
2.2.1 Introduction 18
2.2.2 The mantle sequence in the Limassol Forest Complex 18
2.2.3 Tectonised harzburgite 19
2.2.4 Dunite pods in harzburgite 21
2.2.5 Massive dunite 22
2.2.6 Intrusives in the mantle sequence 23
2.2.7 Alteration of mantle sequence lithologies 24

2.3 Layered Sequence 27
2.3.1 Introduction 27
2.3.2 The layered sequence in the ELFC 28
2.3.3 Cumulate peridotite 29
2.3.4 Cumulate peridotite and gabbro: the 'transition zone' 30
2.3.5 Cumulate gabbro 31
2.3.6 Intrusives in the layered sequence 31
2.3.7 Attitude of layering 32
2.3.8 High-temperature deformation of the layered sequence 33

2.4 High-Level Plutonic Suite 34
2.4.1 Introduction 34
2.4.2 Field relations 35
2.4.3 Petrography 36

2.5 Sheeted Dyke Complex 38
2.5.1 Introduction 38
2.5.2 The base of the Sheeted Dyke Complex 39
2.5.3 Field relations and mineralisation 40
2.5.4 Basal Group 42
2.5.5 Petrography 43
2.5.6 Attitude of the Sheeted Dyke Complex across the ELFC 44

2.6 Post-Axis Sequence Intrusives 47
2.6.1 Field relationships 47
2.6.2 Petrography 48
2.6.3 Geochemistry 50
2.6.4 Significance of the post-axis sequence intrusives 50

2.7 Discussion 52
2.7.1 Lateral variations in crustal structure across the ELFC 52
2.7.2 A reconstruction of the thickness of the axis sequence crust 53

CHAPTER 3: Lava Stratigraphy 55

3.1 Introduction 55

3.2 Sub-Division of the Extrusive Sequence 56

3.3 The Kalavasos Mines 57
3.3.1 Lower Pillow Lavas 58
3.3.2 Mineralisation 59
3.3.3 Upper Pillow Lavas (limburgites) 60
3.3.4 Upper Pillow Lavas (olivine basalts), and associated intrusives 61
3.3.5 Interlava sediments 62

3.4 The Northern ELFC: Dhrapia–Vavla 64
3.4.1 Dhrapia–Palaeodhrapia 64
3.4.2 Palaeodhrapia–Parsata 65
3.4.3 Vathyrkakas, Vavla 66

3.5 The Southern ELFC: Asgata–Parekklisha 68

3.6 Discussion 71
3.6.1 A reconstruction of the ELFC palaeobathymetry 71
3.6.2 The 'Anti-Troodos' plate fragment 71

CHAPTER 4: Lava Petrography and Petrogenesis 73

4.1 Introduction 73
4.1.1 Background 73
4.1.2 Evidence for the supra-subduction zone origin of Troodos lavas 75
4.1.3 On boninites, and reasons for studying them 76

4.2 Petrography 77
4.2.1 Plagioclase–clinopyroxene suite 78
4.2.2 Olivine–clinopyroxene suite 78
4.2.3 Olivine–orthopyroxene–clinopyroxene suite 80
4.2.4 Other lavas 82

4.3 Alteration: Petrological and Geochemical Effects 83

4.4 The Kalavasos Mines Geochemical Traverse 85
4.4.1 Introduction 85
4.4.2 Major element variation 86
4.4.3 Picrites 87

4.5 Petrogenesis 90
4.5.1 Introduction 90
4.5.2 The nature of the mantle source region 92
4.5.3 Evidence for enrichment of the incompatible elements in the ELFC lavas 95
4.5.4 Origin and significance of the enriched component 98
4.5.5 Summary of petrogenesis and discussion of nomenclature 101
4.5.6 Tectonic controls on boninite genesis 103

CHAPTER 5: Structural History 106

5.1 Preconceptions 106

5.2 Palaeomagnetism 107

5.3 Transform-Related Structures 111
5.3.1 Serpentinite shear zones 111
5.3.2 Deformation of the axis crustal sequence 112
5.3.3 Palaeomagnetic sites from the northern ELFC 114
5.3.4 Mazoukambos, Vasilikos River 116

5.4 Post-Volcanic Deformation I: the Northern ELFC 118
5.4.1 Introduction 118
5.4.2 The Mavridhia and Vasilikos Reservoir Faults 119
5.4.3 Faulting style in the Parsata–Kalavasos Mines area 120
5.4.4 The Akapnou Forest Décollement 122
5.4.5 Discussion of deformation style in the northern ELFC 124
5.4.6 Reverse faulting, Layia–Akapnou 127

5.5 Post-Volcanic Deformation II: the Southern ELFC 129
5.5.1 Dyke intrusion and block rotation in the Asgata River 129
5.5.2 Antithetic faulting and block rotation, Monagroulli 130
5.5.3 The Pevkos Fault 131
5.5.4 Discussion: faulting mechanisms 133

5.6 Neogene Deformation 137
5.6.1 Uplift of the central Limassol Forest block 137
5.6.2 North–south normal faulting 138

CHAPTER 6: Lava–Sediment Relationships 140

6.1 Introduction 140

6.2 Sedimentary Stratigraphy 141
6.2.1 The Perapedhi Formation 141
6.2.2 The Moni mélange 142
6.2.3 Age of the Perapedhi and Kannaviou Formations 143

6.3 Angular Relationships, Asgata 144
6.3.1 Pillow collapse breccias 145
6.3.2 Relationship of the Perapedhi sediments to faulting 146

6.4 Angular Relationships, Dhrapia–Vavla 148
6.4.1 The Kalavasos Mines and Dhrapia 148
6.4.2 Parsata 149
6.4.3 Vathyrkakas 150

6.5 Synthesis: Sequence and Timing of Faulting 150

CHAPTER 7: The Tectonic Evolution of the ELFC 153

7.1 Introduction 153

7.2 Reconstruction of the Oceanic Geometry of Southern Troodos 154
7.2.1 Summary of the accretionary geometry of the ELFC 154
7.2.2 Implications for the geometry of the Southern Troodos Transform Fault 156
7.2.3 Discussion: alternative models 157

7.3 Rotation of the Cyprus Microplate 159
7.3.1 Timing of the rotation: palaeomagnetic evidence 159
7.3.2 Size of the rotated microplate 160

7.4 Regional Setting: A Synopsis of the Geology of SW Cyprus 162
7.4.1 The Kannaviou Formation 162
7.4.2 The Mamonia Complex 162
7.4.3 Juxtaposition of Troodos against the Mamonia Complex 164

7.5 The ELFC in the Context of the Rotation of the Cyprus Microplate 167
7.5.1 Summary of post-volcanic deformation in the ELFC 167
7.5.2 Relevance of the ELFC deformation to microplate rotation 169
7.5.3 Significance of the extensional reactivation of the STTF 170
7.5.4 Implications for rotation mechanisms 172

7.6 Summary of Conclusions 174

REFERENCES 176

APPENDIX 1: Analytical Techniques 199

A1.1 Whole-Rock Major and Trace Element Analysis 199
A1.1.1 XRF Sample Preparation 199
A1.1.2 X-ray fluorescence analysis 199

A1.2 Instrumental Neutron Activation Analysis 201

A1.3 Mineral Analysis 201

APPENDIX 2: Sample Localities 203

APPENDIX 3: XRF Analyses 205

APPENDIX 4: INAA Analyses 212

APPENDIX 5: Microprobe Analyses 213

APPENDIX 6: Palaeomagnetic Data 225

LIST OF FIGURES:

CHAPTER 1:

following page:

Figure 1.1: Outline map of the Eastern Mediterranean 1
Figure 1.2: Geological sketch map of Troodos 2
Figure 1.3: Consensus oceanic spreading model as deduced from ophiolites 5
Figure 1.4: Reconstruction of Pangaea in the early Jurassic 7
Figure 1.5: Location of the Tethyan ophiolites 7
Figure 1.6: Model for the emplacement of Troodos from gravity data 8
Figure 1.7: N-S cross-section across the Arakapas Fault Belt 9
Figure 1.8: N-S cross-section across the Western Limassol Forest Complex 9
Figure 1.9: Geological map of Troodos from the early 1960s 12
Figure 1.10: Simplified geological map of the Limassol Forest Complex 14

CHAPTER 2:

following page:

Figure 2.1: Simplified geological map of the Eastern Limassol Forest Complex 18
Figure 2.2: Sketch map of cumulate–metacumulate contact, Lestóvounos 33
Figure 2.3: Dyke rooting at the base of the Sheeted Dyke Complex 39
Figure 2.4: Hypothetical relationship between dyke intrusion and faulting 44
Figure 2.5: Original dyke strikes for ELFC sheeted dykes, from palaeomagnetics 46
Figure 2.6: TiO_2 v Zr for cross-cutting dykes in the ELFC 50
Figure 2.7: Simplified geological map of the Western Limassol Forest Complex 51
Figure 2.8: Reconstructed cross-section through ELFC axis sequence crust 53

CHAPTER 3:

following page:

Figure 3.1: Comparative maps of the Kalavasos Mines area 57
Figure 3.2: Sketch of the Mavridhia Fault, to accompany plate 3.3 59
Figure 3.3: Sedimentary logs of interlava sediment, Kalavasos Mines 62
Figure 3.4: Geological map of the northeastern ELFC 64
Figure 3.5: Sketch map of the Asgata River area 70
Figure 3.6: Restacked logs of lava stratigraphy across the northern ELFC 71

CHAPTER 4:

following page:

Figure 4.1:	MORB-normalised patterns for a range of ELFC glassy lavas	75
Figure 4.2:	Summary diagrams showing geochemical effects of alteration	84
Figure 4.3:	TiO_2 v stratigraphic height, Kalavasos Mines	85
Figure 4.4:	Zr v stratigraphic height, Kalavasos Mines	85
Figure 4.5:	Major element variation diagrams, Kalavasos Mines lavas	86
Figure 4.6:	TiO_2 v Zr, Kalavasos Mines lavas	86
Figure 4.7:	Calculation of picrite intercumulus liquid composition	88
Figure 4.8:	Model to explain differences between ELFC and N. Troodos picrites	89
Figure 4.9:	REE patterns for ELFC and other primitive Troodos lavas	91
Figure 4.10:	Cr v Y modelling for ELFC lavas	92
Figure 4.11:	CaO/TiO_2 v Al_2O_3/TiO_2 for ELFC lavas	94
Figure 4.12:	TiO_2 v Zr from McCulloch and Cameron (1983)	96
Figure 4.13:	Chondrite-normalised trace element abundances, ELFC lavas	97
Figure 4.14:	Ce/Yb v Ta/Yb, LFC lavas	97

CHAPTER 5:

following page:

Figure 5.1:	The Allerton palaeomagnetic technique	108
Figure 5.2:	Location of palaeomagnetic sites in the ELFC	109
Figure 5.3:	Cumulative length v orientation, serpentinite shear zones	111
Figure 5.4:	Strike-slip slickenside lineations from serpentinite shear zone	112
Figure 5.5:	Summary of palaeomagnetic results, Dhrapia	115
Figure 5.6:	Summary of palaeomagnetic results, Klonari	115
Figure 5.7:	Geological map of the Mazoukambos area, Vasilikos River	116
Figure 5.8:	Geological cross-section, Parsata–Kalavasos Mines	119
Figure 5.9:	Geological map of the northeastern ELFC	119
Figure 5.10:	Summary of palaeomagnetic results, Kalavasos Mines	119
Figure 5.11:	Sketch of the Vasilikos Reservoir Fault, to accompany plate 5.3	120
Figure 5.12:	Stereograms illustrating relationships of faulting, Kalavasos Mines	120
Figure 5.13:	Geological map of the Karyakia area, Vasilikos River	121
Figure 5.14:	Summary of serpentinite deformation experiments	124
Figure 5.15:	Cartoons illustrating extension by listric and planar faulting	126
Figure 5.16:	Simplistic estimates of extension across the Vasilikos Reservoir Fault	126
Figure 5.17:	Geological cross-section, Layia and Mavrovouni	127
Figure 5.18:	Sketches illustrating footwall uplift in extensional systems	128
Figure 5.19:	Summary of palaeomagnetic results, Asgata River	129
Figure 5.20:	Cartoon cross-section illustrating anithetic faulting, Stenoman	130
Figure 5.21:	Contoured stereonets of lava dips, northern and southern ELFC	130

following page:

Figure 5.22: Summary of palaeomagnetic results, Monagroulli 131
Figure 5.23: Summary of palaeomagnetic results, Pevkos 132
Figure 5.24: Multiple slickenside lineations, Lestóvounos 133
Figure 5.25: Summary of palaeomagnetic results, Asgata–Vasa road 133
Figure 5.26: Model illustrating how large rotations require multiple fault sets 134
Figure 5.27: Contoured stereonets, poles to fault planes, Pevkos Quarry 135
Figure 5.28: Fault plane and slickenside data from Pevkos Quarry 135
Figure 5.29: Mechanism of block rotation as deduced from Pevkos 136
Figure 5.30: Geological cross-section, Pevkos area 138
Figure 5.31: Cartoon cross-section across the central Limassol Forest 138

CHAPTER 6: following page:

Figure 6.1: Composite stratigraphic column of Upper Cretaceous sediments 140
Figure 6.2: Sketch map and cross-section, Asprolaona 145
Figure 6.3: Geological map of the Asgata area 146
Figure 6.4: Fault plane and slickenside data from Konnin, Asgata 147
Figure 6.5: Summary of lava–sediment relations, Asgata–Dhrapia–Parsata 150
Figure 6.6: Cartoon illustrating the order of fault block activity 151

CHAPTER 7: following page:

Figure 7.1: (a) Tectonic features associated with a medium slip-rate transform 156
(b) Reconstruction of the geometry of the STTF 156
Figure 7.2: Cartoon showing reinforcement of dyke swing by fault reactivation 158
Figure 7.3: Simplified geological map of SW Cyprus 165
Figure 7.4: Sketch map of serpentinite fault lineaments in Mamonia Complex 165
Figure 7.5: Inferred configuration of basement types in southern Cyprus 169
Figure 7.6: Schematic illustration of deformation at margin of rotating microplate 170
Figure 7.7: Summary block diagram of basement relationships, southern Cyprus 170
Figure 7.8: (a)–(e) Possible models for microplate rotation mechanisms 172

LIST OF TABLES:

CHAPTER 2: following page:

Table 2.1: Summary of harzburgite mineral compositions 20

CHAPTER 3: following page:

Table 3.1: Summary of LPL-UPL characteristics 56

CHAPTER 4: following page:

Table 4.1: Summary of petrographic alteration indices 83
Table 4.2: Petrography and stratigraphic position of Kalavasos Mines samples 85

APPENDIX 1: following page:

Table A1.1: Repeated XRF analyses of standard AGV-1 200

ENCLOSURE:

1: 20,000 scale geological map of the Eastern Limassol Forest Complex

LIST OF PLATES:

CHAPTER 2:

		following page:
Plate 2.1:	Incomplete serpentinisation of harzburgite	26
Plate 2.2:	Low angle dolerite dyke cutting steeply dipping layered plutonics	26
Plate 2.3:	Ductile shear zone truncating layering in plutonics	33
Plate 2.4:	Plagiogranite stoping dolerite xenoliths at base of Sheeted Complex	35
Plate 2.5:	Sheeted Dyke Complex	40
Plate 2.6:	Gossan along mineralised NE fault (ridge parallel)	40
Plate 2.7:	Cross-cutting sheeted dykes	41

CHAPTER 3:

		following page:
Plate 3.1:	Vertical Lower Pillow Lavas	58
Plate 3.2:	Umber at Lower Pillow Lava–Upper Pillow Lava contact	59
Plate 3.3:	The Mavridhia Fault	59
Plate 3.4:	Glassy 'limburgite' Upper Pillow Lavas	60
Plate 3.5:	Close-up of the base of a picrite flow	60
Plate 3.6:	Fine-grained sedimentary intercalation in limburgites	62
Plate 3.7:	19m thick intervolcanic sediment horizon, Mandra tou Alykou	62
Plate 3.8:	3m thick intervolcanic sediment horizon, Polemikon	63
Plate 3.9:	Massive lava and dyke-rock scree breccia	64

CHAPTER 4:

		following page:
Plate 4.1:	Photomicrograph of clinopyroxene–plagioclase glomerocrysts	78
Plate 4.2:	Photomicrograph of 'hopper' olivine phenocryst in fresh glass	78
Plate 4.3:	Photomicrograph of twinned radial olivine crystal	79
Plate 4.4:	Photomicrograph of quenched 'cockscomb' clinopyroxene	79
Plate 4.5:	Photomicrograph of plagioclase spherule	80
Plate 4.6:	Photomicrograph of orthopyroxene jacketed by clinopyroxene	80
Plate 4.7:	Photomicrograph of strained olivine phenocryst in picrite	82
Plate 4.8:	Photomicrograph of cumulus orthopyroxene-phyric flow	82

CHAPTER 5:

following page:

Plate 5.1:	Serpentinite shear zone	111
Plate 5.2:	Large gabbro block incorporated into serpentinite shear zone	111
Plate 5.3:	Vasilikos Reservoir Fault, Mavrolaona	120
Plate 5.4:	Low angle fault contact between sheeted dykes and mantle sequence	122
Plate 5.5:	The Akapnou Forest Décollement	122
Plate 5.6:	Sheared serpentinised ultramafics and boudinaged gabbros	123
Plate 5.7:	Photomicrograph of the Akapnou Forest Décollement	123
Plate 5.8:	View SE along the Pevkos Fault	131
Plate 5.9:	Oblique-slip fault, Pevkos	135

CHAPTER 6:

following page:

Plate 6.1:	Pillow collapse breccias and deformed umbers, Asgata	145
Plate 6.2:	Pillow collapse breccias, umberiferous matrix, Asgata	145
Plate 6.3:	Slump-folded radiolarites, Asgata	147
Plate 6.4:	Angular unconformity in umber deposit, Dhrapia	148
Plate 6.5:	Tilted umbers and lava breccia horizons, Parsata	148
Plate 6.6:	Radiolarites banked against hill of brecciated sheeted dykes, Vavla	150
Plate 6.7:	Slump-folding in radiolarites, Vavla	150

CHAPTER 1:
Introduction

1.1 Regional setting

1.1.1 Cyprus: geography and present tectonic setting

The island of Cyprus is situated in the northeastern corner of the Mediterranean Sea, 75km south of Turkey and 105km west of Syria (figure 1.1). It lies within a broad zone of seismic activity which marks the plate boundary between the Afro-Arabian plate to the south and Eurasian plate to the north (McKenzie 1970, 1972). An arcuate belt of earthquake epicentres to the south of and beneath Cyprus suggest that an active subduction zone, the 'Cyprean Arc', dips northwards beneath the island at the present time; recent studies (*e.g.* Ben-Avraham *et al.* 1988) have identified a belt of active deformation corresponding to its surface expression lying approximately 50km offshore, parallel to the south and west coastline of the island. Subduction processes are being interrupted to the south by the impending collision of a microcontinental block, the Eratosthenes Seamount, with the trench, and to the east of this the plate boundary is poorly defined (Kempler and Ben-Avraham 1987).

The island of Cyprus itself is dominated physiographically by two major mountainous regions, the Troodos and Kyrenia Ranges, separated by the flat Mesaoria plain. The Kyrenia Range, on the north coast of the island, is an arcuate E-W belt of Mesozoic sediments folded and thrust southwards in Eocene to Miocene times, and forms the southernmost expression of the Tauric Alps of Turkey (figure 1.1).

The Troodos mountains, in the central part of the island, have the shape of a lozenge, or flattened oval, with long axis oriented west-northwest. The mountains are *c.*3000km^2 in area, and the highest point, Mount Olympus, rises to an elevation of

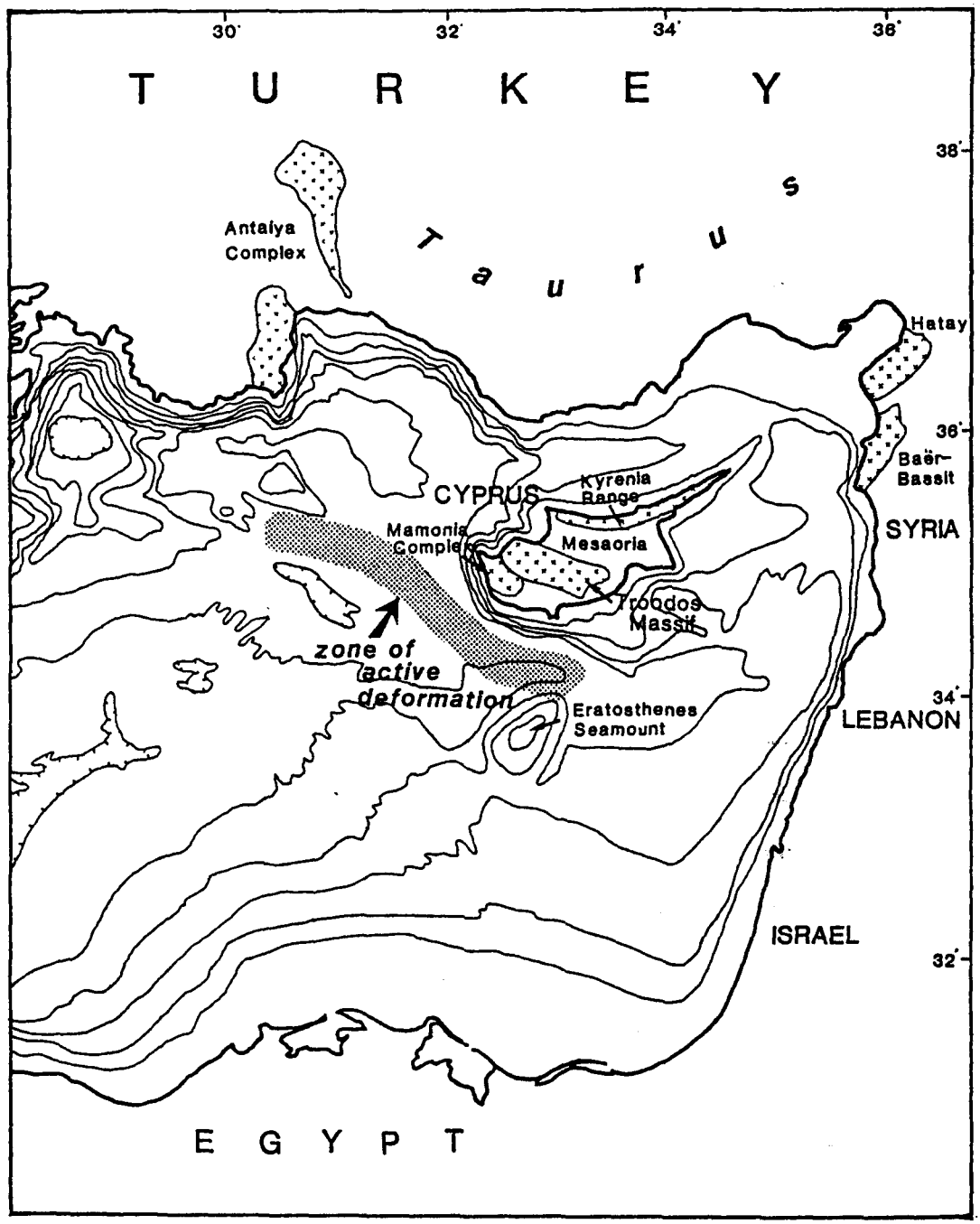

Figure 1.1: Outline map of the Eastern Mediterranean, showing the location of Cyprus and various tectonic and bathymetric features discussed in text. Bathymetric contours are at 500m intervals. Redrawn and modified after Robertson and Woodcock (1980) and Kempler and Ben-Avraham (1987).

1951m. They are composed of ultrabasic–basic igneous rocks of Middle Cretaceous age (see below), blanketed by Upper Cretaceous–Recent sediments. Beneath these same sediments in the southwest of Cyprus is a suite of highly disrupted igneous, sedimentary and metamorphic rocks of Triassic–Cretaceous age referred to as the Mamonia Complex.

1.1.2 The Eastern Limassol Forest Complex

The subject of the present study is the Eastern Limassol Forest Complex (ELFC), an area of almost 200km^2 lying at the southern margin of the Troodos Massif (figure 1.2). The Limassol Forest, which is situated approximately 20km northeast of the city of Limassol, is a rugged, generally sparsely populated mountainous area, rising to a height of 1010m in its western part, and 790m (Mt. Sinoas) in the east. It is capped by erosion surfaces probably of Miocene age (de Vaumas 1959, 1961). The term 'Forest' is somewhat of a misnomer in the eastern part of the Limassol Forest, as extensive (pine) afforestation is rare; instead, the greater part of the area, particularly the more elevated central portion, is covered by a variety of (usually prickly) bushes, including spiny burnet, prickly broom, rockrose and lavender.

The Limassol Forest is separated from the main part of the Troodos mountains by a prominent 0.5-1.5km wide E-W trending valley running through the village of Arakapas, which can be traced for almost 40km from Kato Dhrys in the east to Perapedhi in the west. The Arakapas valley and the Limassol Forest areas have suffered a distinct and more protracted tectonic and magmatic history than the remaining portions of the igneous massif to the north; previous geological research on these areas is documented and discussed in section 1.4.

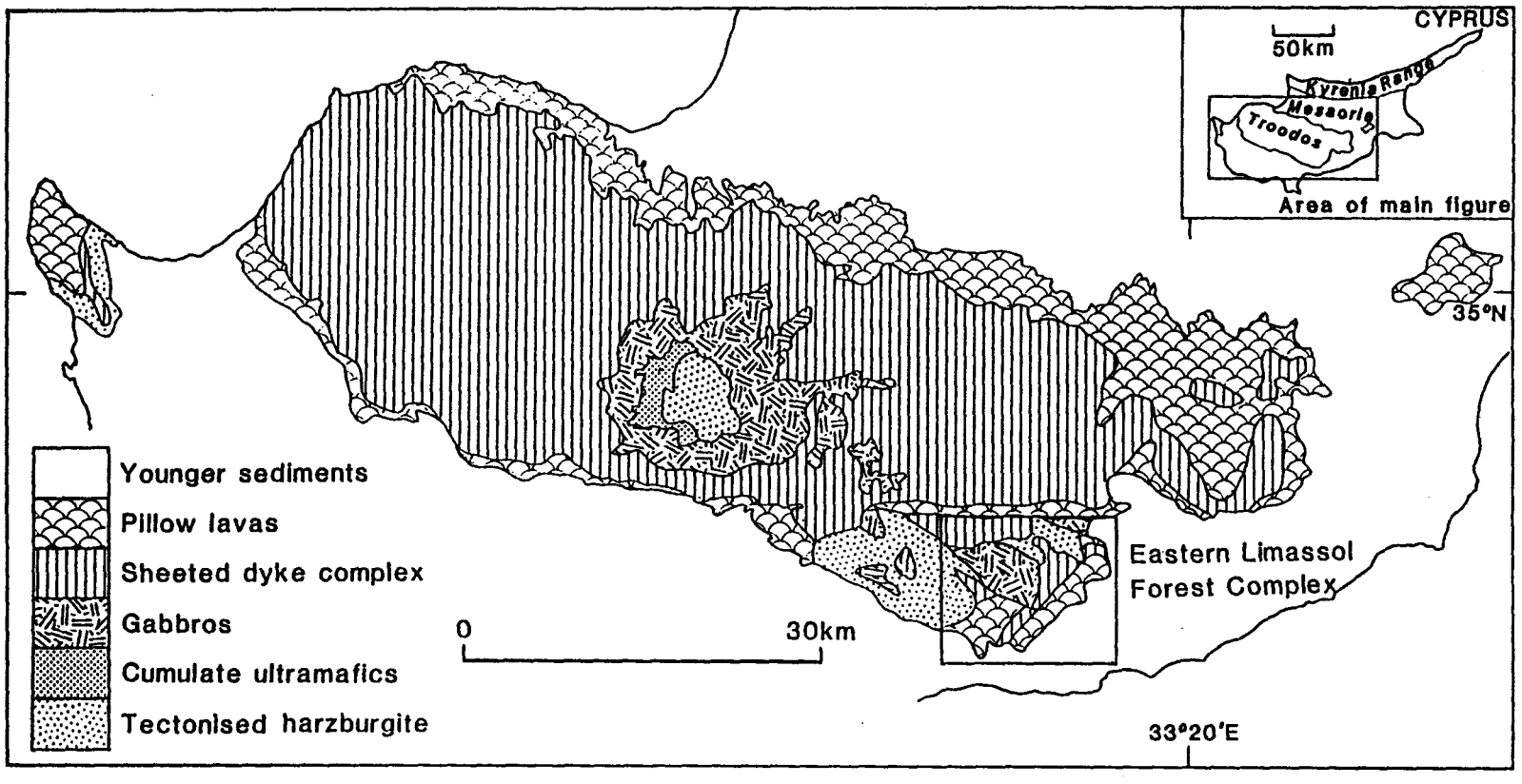

Figure 1.2: Geological sketch map of the Troodos Massif, showing the location of the Eastern Limassol Forest Complex area.

1.2 The Troodos Ophiolite

1.2.1 General description

The Troodos Massif is an crudely stratiform igneous body which has been deformed into an overall dome shape by differential uplift centred on Mt. Olympus. As a result, the deepest stratigraphic levels crop out in the central, highest part of the massif, and successively shallower levels exposed in annular outcrop toward the periphery (figure 1.2; Wilson 1959).

The igneous sequence is composed (from bottom to top) of the following: ultramafic rocks (usually serpentinised) predominantly of harzburgite but also dunite and pyroxenite, upon which have been superimposed a high temperature deformation fabric; cumulus textured plutonic rocks, initially ultramafic and thence mafic, with well developed igneous phase layering; massive mafic 'high-level' plutonics, which are locally differentiated to an acidic composition; a remarkable dolerite dyke swarm which, in the most part, is composed of 100% sheeted dykes with no intervening host rock, generally striking N-S and extending for more than 100km across strike; and an extrusive suite, dominated by pillowed flows, which was subdivided by early workers into Upper and Lower Pillow Lava units. The succession is surmounted by patchy metalliferous sediments (brown umbers) and radiolarian cherts, and thence widespread pelagic chalks.

1.2.2 Ophiolites: definition and history of the term

The succession given above fits almost exactly the ideal definition of an 'ophiolite', as defined by participants of the Geological Society of America's Penrose Field Conference (Anon. 1972):

> "a distinctive assemblage of mafic to ultramafic rocks occurring in the following sequence, from bottom to top:
>
> –ultramafic complex consisting of varying proportions of harzburgite, lherzolite and

dunite, usually with a metamorphic tectonite fabric (more or less serpentinised)
–gabbroic complex ordinarily with cumulus textures commonly containing cumulus peridotites and pyroxenites, and usually less deformed than the ultramafic complex
–mafic sheeted dyke complex
–mafic volcanic complex commonly pillowed

Associated rock types include (i) an overlying sedimentary section typically containing ribbon cherts, thin shale interbeds, and minor limestones; (ii) podiform bodies of chromite generally associated with dunite; (iii) sodic felsic intrusive and extrusive rocks. Faulted contacts between mappable units are common. Whole sections may be missing. An ophiolite may be incomplete, dismembered or metamorphosed. . . . Use of the term should be independent of its supposed origin."

This definition of an ophiolite (*lit.* 'snake rock') was given after *c.*150 years of *ad-hoc* usage of the term, following its introduction by Brongniart (1827) to describe the rock-type serpentinite, on account of its green and mottled, supposedly reptilian, appearance. A notable modification of its usage was made by Steinmann (1906, 1927), who used it to describe the *assemblage* of serpentinite, pillow lava and radiolarian chert (the 'Steinmann Trinity'), which he had frequently observed in close association within thrust slices in the Apennines of Italy; he also suggested that the igneous rocks in such associations might be consanguineous.

The deep-sea marine affinities of ophiolites were recognised by most authors (including Steinmann himself) at an early stage. From this arose the concept of ophiolites as colossal 'magma balloons' erupted along the submarine flanks of geosynclines (Dubertret 1955, Brunn 1961, Auboin 1965). These supposedly became differentiated after emplacement to form a regular stratigraphic sequence with peridotites and gabbros in the centre, surrounded by a chilled carapace through which dolerite dykes were injected to feed pillow lavas on top.

1.2.3 The Troodos ophiolite as oceanic lithosphere

Troodos is one of the best preserved ophiolite complexes in the world, and was the first to be studied in detail. Systematic mapping of the greater part of the Troodos Massif was undertaken by the Cyprus Geological Survey Department at a scale of 1: 5,000 in the late 1950s and published as a series of memoirs (Wilson 1959, Carr and Bear 1960, Bear 1960, Gass 1960, Bagnall 1960 and Bear and Morel 1960); consequently Troodos became central to the development of ideas on the origin and significance of ophiolites in general from the 1960s through to the present day, and still remains by far the most well-studied example.

Although Bishopp (1952) and Gass and Masson-Smith (1963) suggested that the Troodos Massif represented a volcanic pile with no underlying *sialic* crust developed in an oceanic region that once lay between Eurasia and Africa, and Wilson (1959) concluded that "the *sialic* crust appears to have moved apart under great tensional stress while the numerous dykes of the diabase (Sheeted Dyke Complex) and pillow lava series were intruded", it was not until the advent of the seafloor spreading hypothesis (Dietz 1961, Hess 1962, Vine and Matthews 1963) that the suggestion was made (Gass 1968) that the Troodos ophiolite might represent an actual fragment of oceanic lithosphere. The Vine–Matthews model stated that oceanic crust is continually being created at mid-oceanic ridges and spreads laterally, supplied and driven by convection currents in the upper mantle beneath, and it was Gass (*op. cit.*) who first appreciated that "the structure of the Sheeted Intrusive Complex is the type that would be formed on the crest of a mid-ocean ridge where diverging cells in the mantle would produce crustal tension". This was emphasised by Moores and Vine (1971), also working on Troodos, who stated explicitly that "100% dykes imply . . . 100km of extension in 100km of exposure. The only possible mechanism which has been proposed to account for such extension is seafloor spreading".

Moores and Vine (*op. cit.*) also arrived at an integrated model for the Troodos

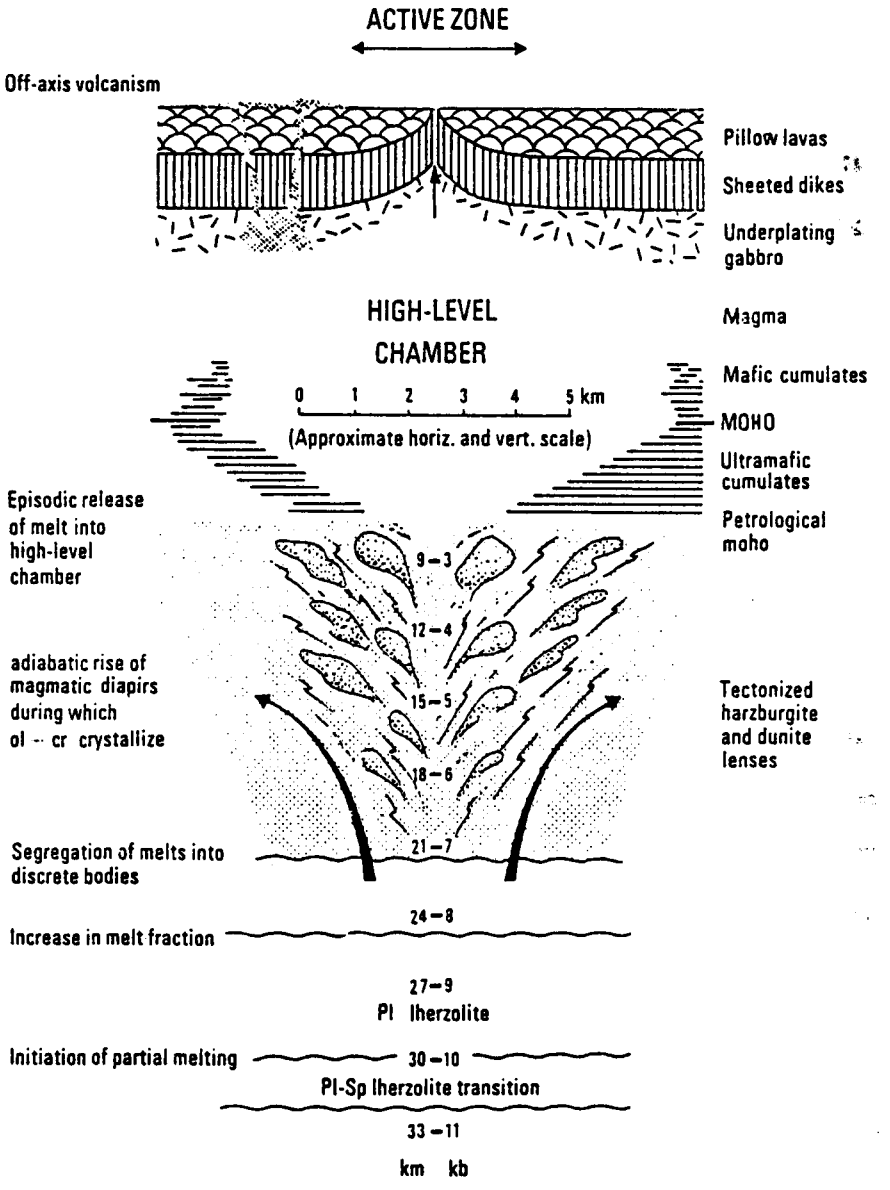

Figure 1.3: Consensus oceanic spreading model, as deduced from ophiolites. From Gass (1980).

ophiolite as a whole which, although modified by subsequent, more detailed study (*e.g.* Greenbaum 1972, Gass and Smewing 1973, Allen 1975), is essentially the same as the 'consensus' ophiolite model accepted almost universally at the present time (Gass and Smewing 1981; figure 1.3). In this, the harzburgite and dunite of the ultramafic rocks represent depleted upper mantle, from which a basaltic melt has been extracted to produce the overlying oceanic crust, and the layered plutonic rocks represent the cumulate portions of a ridge axial magma chamber or chambers. The high-level plutonics and sheeted dykes form a carapace to the magma chamber, and correspond to seismic layer 3 of ocean crust, the extrusive sequence to layer 2, and overlying sediments to layer 1.

These concepts are dwelt upon in slightly greater detail in chapter 2, in which the major lithological units of the ophiolite are described as observed in the Eastern Limassol Forest Complex. For a more thorough review of the history of research and the concepts introduced above the reader is referred to Coleman (1977), Gass (1980) and Gass and Smewing (1981).

1.3 Cyprus in the Context of the Evolution of Tethys

1.3.1 The Tethys Ocean

Wegener's (1924) first palispastic reconstruction of the fit of the continents in the Permo-Triassic, showing a wedge-shaped, westward-narrowing gulf between the super-continents of Gondwanaland and Laurasia, has been essentially confirmed by subsequent palaeomagnetic palaeopole data (*e.g.* Bullard *et al.* 1965, Smith and Briden 1977). The tectonic evolution of this gulf, named the 'Tethys Ocean', can be divided into two, *viz.* an essentially Palaeozoic 'Palaeotethys', and a Mesozoic 'Neotethys'. Most models suggest that Palaeotethys in the late Permian to Triassic was undergoing consumption beneath Eurasia; at the same time on its southern margin continental fragments were rifted

from Gondwanaland and Neotethyan oceanic crust formed behind them. According to Sengör *et al.* (1985) the largest of these continental fragments was the 'Cimmerian' continent (now incorporated into the Balkans, Turkey and the Caucasus), which migrated northwards across the ocean as Palaeotethys closed before it and Neotethys opened behind (figure 1.4).

It is within the Neotethyan Ocean that Troodos and other similar ophiolites were created. In Greece and Yugoslavia two belts of ophiolites, the Pindos and the Vardar, are Jurassic (Spray *et al.* 1985); to the east, a string of ophiolites (including Cyprus) form the "croissantes ophiolitique peri-arabe" of Ricou (1971), stretching from Cyprus in the west to Oman and thence the Himalayas in the east (figure 1.5). All of the latter so far dated appear to be of Cretaceous age (Thuizat *et al.* 1981).

Geochemical evidence (discussed in chapter 4) from Troodos and several of the other 'croissante ophiolitique' (Hatay, Baër-Bassit, Oman) suggests that these fragments of oceanic lithosphere were created above a subduction zone, rather than at a mid-ocean ridge *sensu stricto* (Miyashiro 1973, Pearce 1975, Smewing *et al.* 1975, Pearce *et al.* 1984). Although the exact mechanism is not completely clear, it appears that subduction was initiated within Neotethys, away from a continental margin (*cf.* Lippard *et al.* 1986)–possibly even at the ridge crest itself (Smith and Spray 1985, Robertson and Dixon 1985)–and then the ophiolite crust generated by spreading, probably short-lived, at E-W striking ridge axes (Whitechurch *et al.* 1985; see next section) directly above the subduction zone. This almost occurred in response to the shift in relative motion of Africa relative to Eurasia at this time (the early–mid Cretaceous), from one of lateral (sinistral) movement to one dominated much more by convergence (Livermore and Smith 1984).

With continued convergence of Africa with respect to Eurasia intraoceanic slicing took place and ophiolitic nappes were emplaced in Upper Cretaceous times, both onto the Arabian promontory and onto continental fragments further to the north, where subduction continued until Eocene times (Sengör and Yilmaz 1981, Robertson and Dixon 1985, Aktas and Robertson 1985).

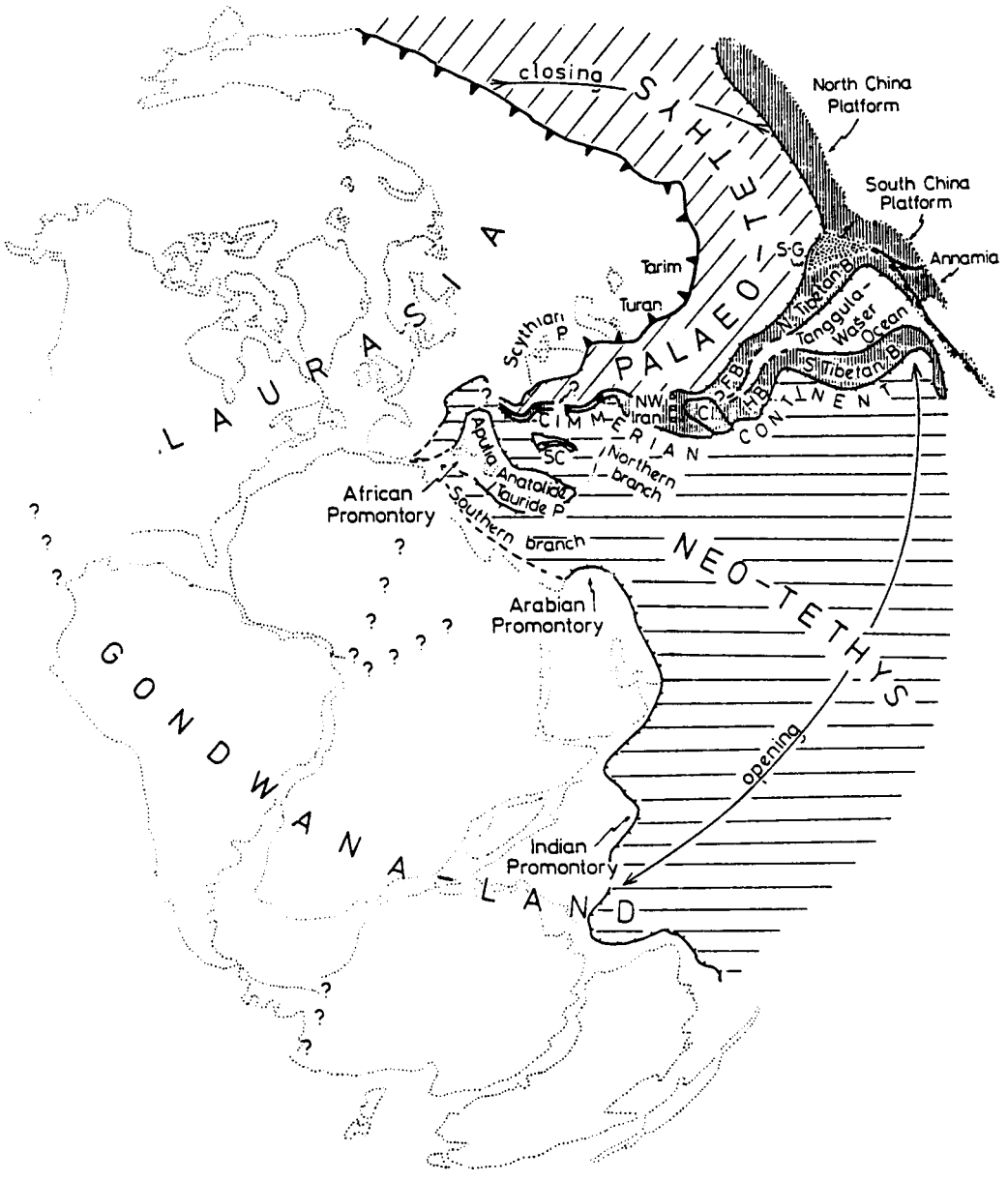

Figure 1.4: Reconstruction of Pangaea in the Liassic, showing the relationship between Palaeotethys and Neotethys. The Cimmerian continent drifts northwards as Palaeotethys is subducted beneath Laurasia, and Neotethys opens behind it. Subduction (probably northward-dipping) is initiated within the Southern branch of Neotethys, sometime in the early–mid Cretaceous, and Troodos created by spreading above the subduction zone. Simplified after Sengör *et al.* (1985).

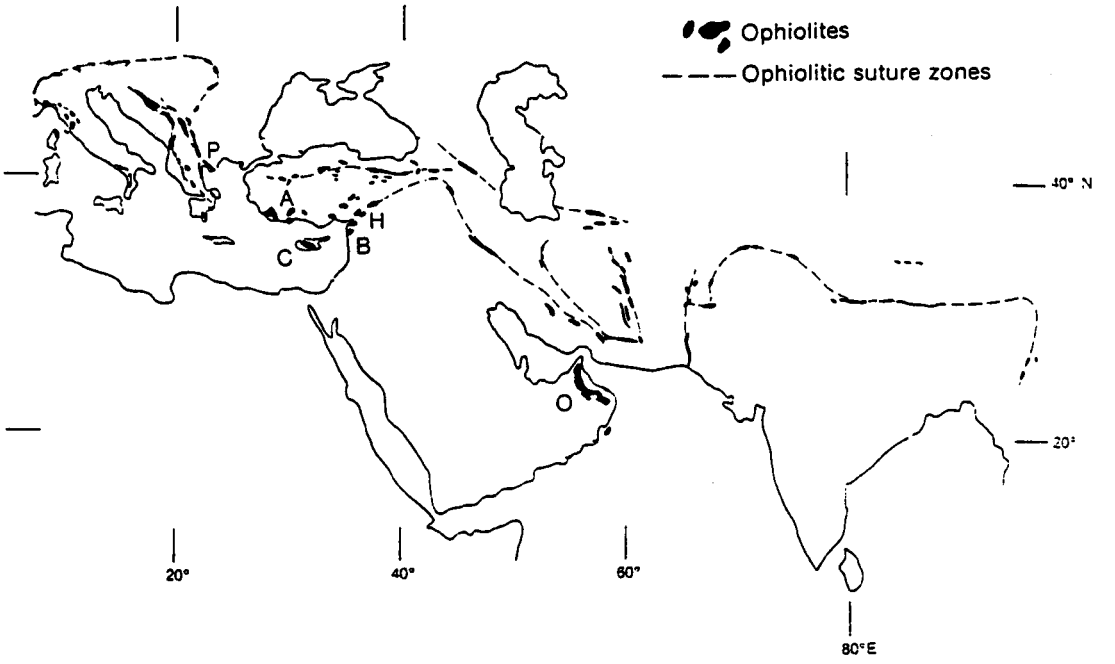

Figure 1.5: Map showing the location of the Tethyan ophiolites, simplified after Lippard *et al.* (1986). P -Pindos; A -Antalya; C -Troodos; B -Baër-Bassit; H -Hatay, and O Oman.

1.3.2 Brief geological history of Cyprus in the context of Tethys

Troodos was formed in the Upper Cretaceous (Cenomanian–Turonian, 91.6 ± 1.4 Ma: Mukasa and Ludden 1987) by seafloor spreading directly above a subduction zone, which probably dipped northwards, as at the present day (Sengör and Yilmaz 1981, Robertson and Dixon 1985). Unlike the remainder of the Tethyan ophiolites, however, Troodos appears to be essentially autochthonous. No basal metamorphic aureole has been identified, and the massif itself is not internally sliced into imbricate thrust sheets as suggested by Lapierre and Rocci (1967) and Biju-Duval *et al.* (1976) (see section 1.4.3).

Palaeomagnetic studies indicate a westerly-directed remanence vector for Troodos lavas (Moores and Vine 1971), suggesting that Cyprus suffered a 90° anticlockwise rotation subsequent to its genesis. This restores the original spreading direction, as indicated by the strike of the Sheeted Dyke Complex, back to an E-W orientation, *i.e.* the same as that indicated for the Turkish and Syrian Tethyan ophiolites (Gass 1968, Moores and Vine *op. cit.*, Whitechurch *et al.* 1985). Clube *et al.* (1985) have shown that this rotation took place between the Upper Cretaceous and Lower Eocene, and that *c.*60° of this occurred in the Campanian–Maastrichtian interval. At this time the Mamonia Complex of southwest Cyprus, which is a disrupted remnant of one of the continental passive margin successions rifted in the Triassic (Clube and Robertson 1986), was juxtaposed against Troodos. Magnetic inclination data (Abrahamsen and Schönharting 1986) suggest that Cyprus became effectively attached to the African plate (with respect to its polar wandering curves) at this time. The mechanism and cause of the rotation of Cyprus is one of the major themes of this thesis, and is discussed in detail in chapter 7.

Gravity data from Cyprus (Gass and Masson-Smith 1963) suggest that the high density ophiolite slab dips northwards beneath the Mesaoria plain, and that the island is underlain by thinned continental crust (figure 1.6(a)). The uplift and emergence of Cyprus commenced in the Miocene, and it is thought that this was the result of the

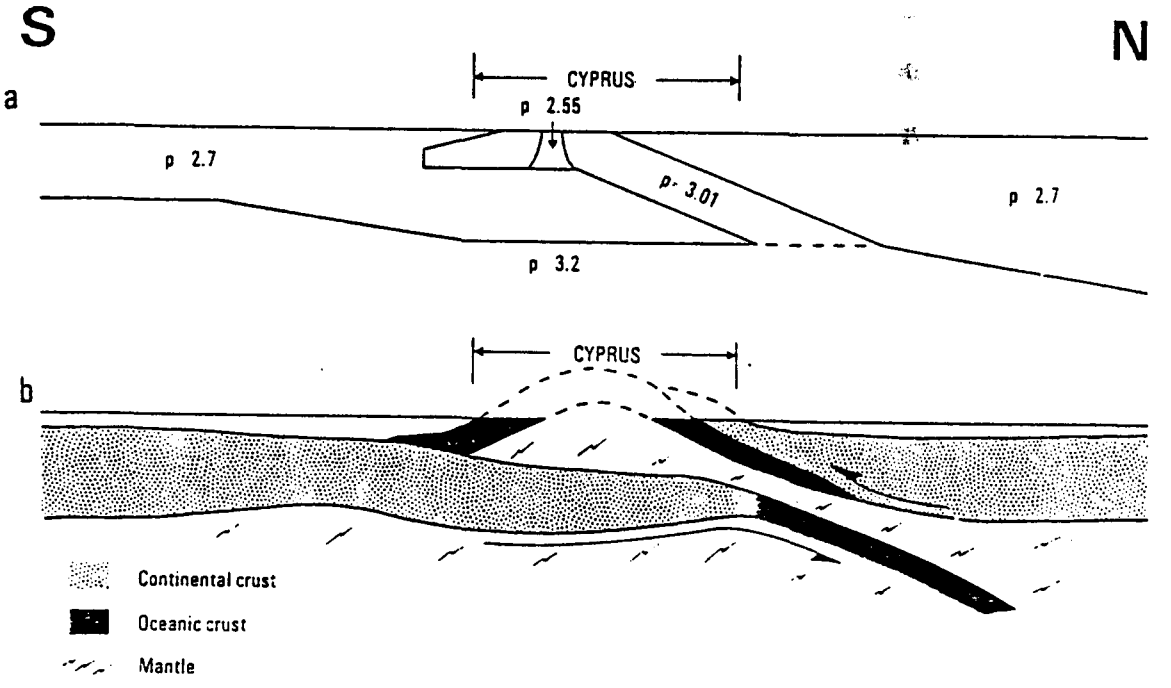

Figure 1.6: Model for the emplacement of the Troodos Massif. (a) Space form of high density (ophiolite) slab beneath Cyprus, as deduced from gravity data (Gass and Masson-Smith 1963). (b) Interpretation: uplift of Troodos occurs in response to the attempted subduction of thinned continental crust belonging to the African plate (Gass 1980, after Gass and Masson-Smith *op. cit.*).

attempted northward subduction and underthrusting of a microcontinental fragment at this time (figure 1.6(b)), in similar manner to the present-day incipient collision of the Eratosthenes Seamount (section 1.1.1; Robertson 1977c).

Rapid uplift of Mt. Olympus commenced in the Plio-Pleistocene, and was almost certainly caused by the serpentinisation of ultramafics at depth, possibly by fluids liberated from the subducting slab beneath Cyprus. In this time it has risen approximately 2000m, and a negative gravity anomaly of 120 mgal beneath it at the present day (Gass and Masson-Smith 1963) suggests that it is still rising.

1.4 Previous Research: The Arakapas Fault Belt and Limassol Forest Complex

1.4.1 The Arakapas Fault Belt

The E-W trending valley which separates the Limassol Forest Complex (LFC) from the main Troodos Massif was named the 'Arakapas Fault Belt' (AFB) by Simonian (1975). It had long been recognised as an important fault zone by early workers (Wilson 1959, Bear 1960, Bagnall 1960, 1964, Lapierre and Rocci 1967, and Pantazis 1967), but it was Moores and Vine (1971) who first suggested that the fault zone might represent an oceanic transform fault, following the definition of Wilson (1965). The area was investigated in detail for the first time by Simonian (1975, — and Gass 1978), and the transform hypothesis substantiated in detail.

Simonian and Gass (1978) showed that the AFB is an elongate zone of intense E-W transcurrent faulting, in which wholesale fault brecciation of the Sheeted Dyke Complex is common. Erupted unconformably onto this brecciated dyke complex 'basement', and infilling small basins between upstanding fault blocks, are irregular sequences of lava flows intercalated with volcaniclastic sediments (figure 1.7). These sediments are derived by the submarine erosion of fault scarps within and on the flanks of the fault belt, and are

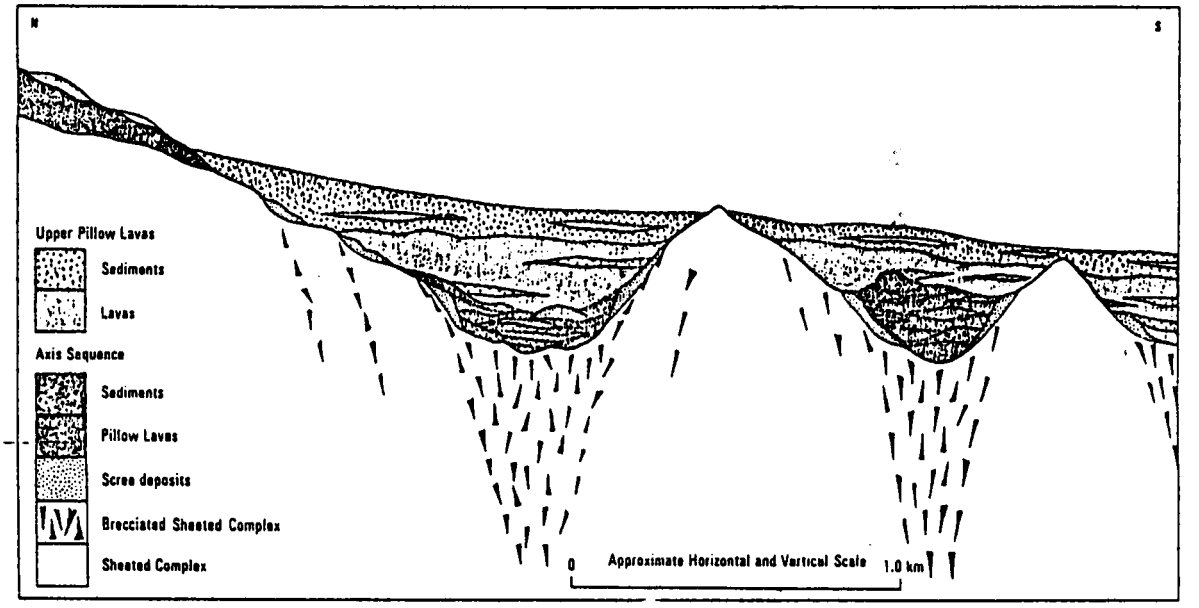

Figure 1.7: Composite schematic N-S cross section across the Arakapas Fault Belt in the Layia area, showing rugged brecciated basement, and infill of fault-controlled basins by lava flows and volcaniclastic sediments. From Simonian and Gass (1978).

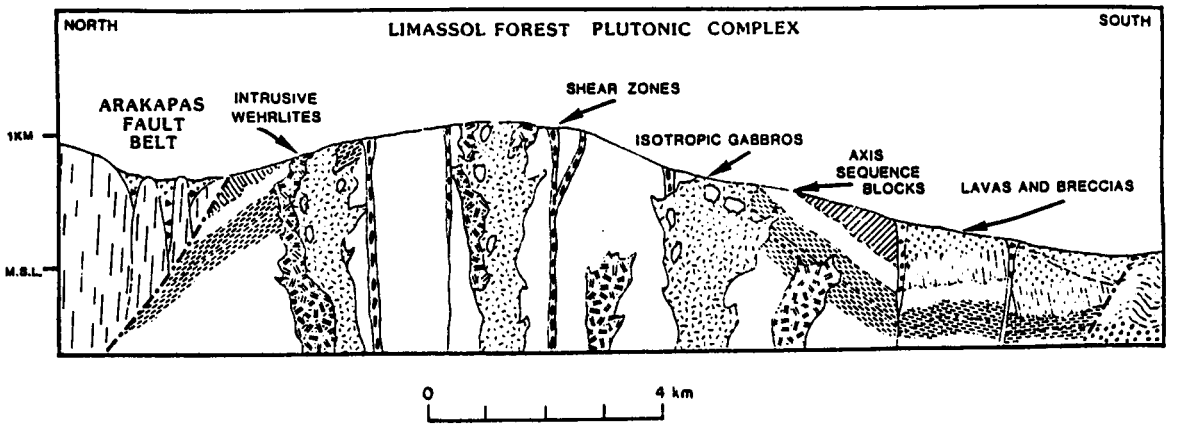

Figure 1.8: Schematic N-S cross section across the Western Limassol Forest Complex. Troodos-type 'axis sequence' blocks have been tilted and disaggregated prior to the intrusion of wehrlites and isotropic gabbros. Transcurrent serpentinite shear zones cut and are cut by the intrusives. Southwestward thrusting at the south of the complex is of Miocene age. from Murton (1986a).

evidence for considerable bathymetric relief across the area at the time. The nature of the lava sequence in the AFB contrasts markedly to the regular, orderly lava successions from the north flank of Troodos, which contain no volcaniclastic sediments; the present Arakapas valley, therefore, appears to reflect, albeit in a subdued manner, the bathymetry of the original seafloor. In this, a clear analogy can be drawn with modern-day oceanic fracture zones, in which a broad fault zone several kilometres in width is associated with a marked bathymetric depression (*e.g.* Menard and Atwater 1969, Bonatti and Honnorez 1976).

Many of the lavas erupted in the AFB are more primitive than those of the remainder of the massif, and have been interpreted (Simonian and Gass *op. cit.*) as reflecting the ease of eruption of melts in an environment where open fractures are plentiful. This is discussed further in chapter 4.

To the north of the AFB the average N-S attitude of the Sheeted Dyke Complex over the greater part of Troodos swings clockwise progressively to a NE-SW and thence E-W alignment over a distance of *c.*10km. This was interpreted by Simonian and Gass (1978) as a result of either: (i) fault drag imposed upon originally N-S striking dykes, or (ii) dyke intrusion in a sigmoidal stress field, both at a dextrally-slipping transform (in the latter case, however, they incorrectly identified the orientation of the stress field; such an intrusion mechanism should instead imply that the transform was sinistrally-slipping). The relative merits of these models in the light of more recent evidence are discussed in chapters 5 and 7.

1.4.2 The Western Limassol Forest Complex

Simonian and Gass (1978) envisaged the AFB as only the northern wall of a transform fault, and suggested that the entire Limassol Forest Complex (LFC) was also part of the structure. In the Western Limassol Forest Complex (WLFC) large areas of serpentinite are exposed, with isolated blocks of peridotites and gabbros (Bear and Morel 1960). The serpentinites were considered to have been intruded diapirically into the

transform (as observed in modern oceanic fracture zones: Bonatti 1976), and the plutonic rocks ridge axis-generated material which had been entrained within the rising serpentinite diapir (Bear and Morel 1960, Panayiotou 1977, Simonian and Gass *op. cit.*).

That the WLFC indeed represented part of the transform was verifed by Murton (1986a, b, — and Gass 1986), who observed E-W serpentinite shear or 'mélange' zones and occasional mylonites, both indicating transcurrent slip, occurring across the entire width of the WLFC. He also showed that the serpentinite outcrops, supposedly diapiric, were in fact passively serpentinised 'mantle sequence' tectonised harzburgites and dunites, and that the peridotites and gabbros blocks were multiple plutons intruded into the mantle lithologies whilst strike-slip deformation was continuing (figure 1.8). Abundant dyke swarms associated with, and emanating from, the intrusives, fed the primitive pillow lavas that now crop out in the AFB and around the periphery of the LFC. As much as 22% extension may have been accommodated by the magmatism in the WLFC, leading Murton (1986a, b) to conclude that the AFB and LFC represented part of a 'leaky' transform fault. He also presented structural arguments to suggest that the transform was a sinistrally-slipping structure. These are discussed in more detail in chapter 7.

1.4.3 The Eastern Limassol Forest Complex

The ELFC has received relatively little study before now. Apart from reconnaissance surveys by Gaudry (1862) and Bellamy and Jukes Brown (1905), the only early geological investigations were carried out on the Kalavasos Mines ore deposits. The work of Cullis and Edge (1927) on Cyprus sulphides led to the reopening of mines in the district, and was followed up by further (mostly unpublished) reports by Mousoulos (1957), Gordon-Smith (1963), Searle (1967) and Searle and Constantinou (1967a, b).

The ELFC, with the Makhaeras Forest region directly to the north, formed the

subject of the last of the memoirs of the Cyprus Geological Survey Department (Memoir No.8: Pantazis 1967; figure 1.9). In this, Pantazis produced a 2 inch to the mile map of the whole of the ELFC. However, although he worked in some detail on the sediments that overlie the ophiolite, and made deductions as to the sedimentary history, he made little attempt to interpret the igneous rocks (which, in the most part, he identified correctly), and none whatsoever concerning the structural evolution of the area.

At the same time Lapierre and Rocci (1967) published the results of a reconnaissance study of the petrology and structure of the Limassol Forest Complex (or 'le massif pluto-volcanique basique de Kellaki'). They reported "intense thrusting", southward directed, throughout the entire area, based presumably upon the observation of local reverse faulting at the southwestern margin of the WLFC (of Miocene age: see section 5.6), and consequently interpreted all other structures in the area in the same fashion. In particular, they described a "NW-striking, NE-dipping low angle thrust" in the central part of the ELFC which, in this study, is named the 'Pevkos Fault' (see section 5.5.3), and is shown instead to be a *normal* fault, dipping 55-60° *southwestwards*.

Arising from these erroneous observations came the interpretation that the Limassol Forest Complex represented an imbricate southward-directed thrust pile immediately above an 'obduction plane', and hence 'evidence' that the Troodos Massif was allochthonous (Biju-Duval *et al.* 1976, Searle and Panayiotou 1980). Panayiotou (1977), working on mineralisation in the Limassol Forest, suggested that ductile deformation in the plutonics represented an early manifestation of obduction-related thrusting. Searle and Panayiotou (*op. cit.*) did, however, recognise (following Robertson 1975) that lavas in the Kalavasos Mines had been tilted steeply northeastwards and the succession repeated by gravity slides (southwesterly-directed) prior to the deposition of the overlying metalliferous umbers (see chapter 6). Searle and Panayiotou suggested that the tilting represented the collapse of fault blocks into a 'Mamonia Complex trough' in response to the obduction of Troodos.

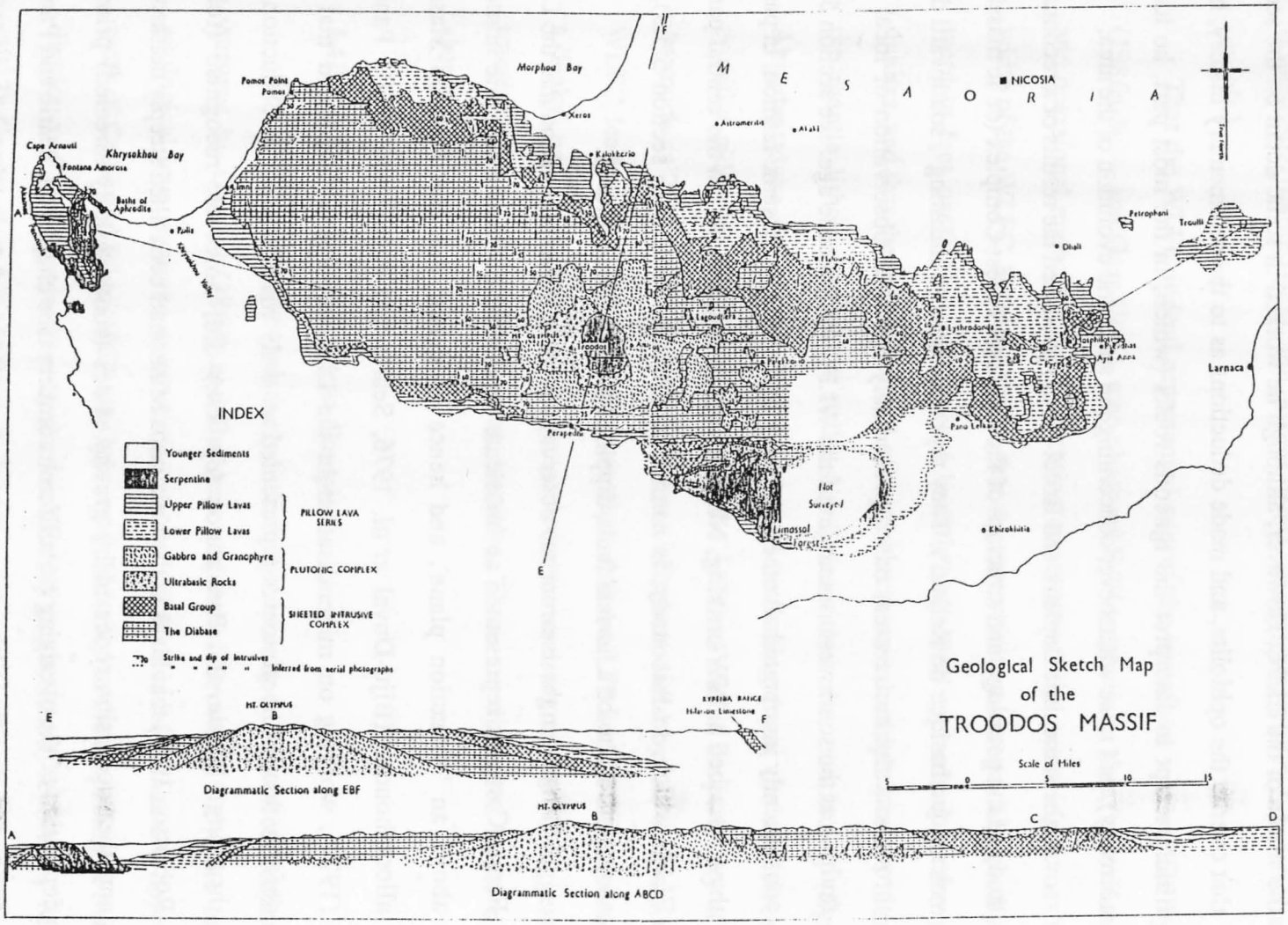

Figure 1.9: Geological map of the Troodos Massif by Gass and Masson-Smith (1963). The Eastern Limassol Forest Complex was the last area of Troodos to be surveyed.

By far the most important and best piece of work to previously have been undertaken on the ELFC was the detailed investigation of the geology of the Kalavasos Mines region carried out by Adamides (1980, 1984). He confirmed Searle and Panayiotou's observations of extensive pre-umber tilting of the lava sequences and gravity sliding, and also discovered the highly significant 'Mavridhia Fault', which is a very early, now low angle, fault controlling mineralisation and lava extrusion in the mines. This he considered a subsidiary of the Arakapas Fault Belt 5km to the north. In addition, he identified interlava volcaniclastic sediments in the northern part of the Kalavasos Mines and suggested that they, too, were related to transform fault activity.

Adamides' (1984) 1: 5000 scale geological map of the Kalavasos Mines, which utilised large quantities of borehole data, was found to be excellent. Modifications of parts of this were incorporated into the 1: 20,000 scale map of ELFC accompanying this thesis (enclosure 1), as the greater part of the Kalavasos Mines region is now inaccessible. Adamides (1984) also carried out a less detailed study of the geology of the area surrounding the Mangaleni sulphide deposit, 3km northwest of Parekklisha, and produced a 1: 10,000 scale map of the vicinity.

The most recent pieces of research to be carried out on the ELFC are by Georgiou (1987) on the chromite deposits of the Akapnou Forest (in the northern part of the ELFC), and by Remond (1986) on the plutonic rocks of the Kellaki area. Remond's studies were primarily mineralogical and petrological, and essentially confirmed the work of Allen (1975) from Mt. Olympus.

1.5 Aims and Presentation of this Thesis

1.5.1 Aims, preconceptions, approach and progress

The aim of this thesis in the first instance was very simple, and that was to undertake a multidisciplinary structural, petrological and geochemical investigation of the hitherto

unstudied eastern portion of the Limassol Forest Complex, in the light of work by Murton on the west and Simonian on the AFB to the north.

Murton (1986b) demonstrated in the WLFC that the lithospheric mantle within the transform had been invaded by ultramafic and mafic plutons whilst strike-slip deformation was continuing. These plutons gave rise to dykes, locally sheeted, and chemically distinct primitive lavas, thus forming anomalous 'transform sequence' oceanic crust (Murton 1986a). In the ELFC, where erosion levels are not so deep, and blocks of an apparently more conventional axis-generated 'Penrose-style' crust are exposed, one might presuppose that a study of the area might ultimately become concerned with mechanisms of crustal disaggregation within a transform fault, perhaps modified by 'transform sequence' magmatic activity.

Fieldwork was carried out over two major field seasons, the first of three months' duration from January to April 1985, and the second of six months, from February to August 1986. A brief visit was also made in September–October 1987. In the light of Murton's observations above, the initial approach to the project was to look for intrusive relationships within the crustal sequence blocks and for evidence of syn-magmatic deformation, unconformities within the lava sequences *etc.*, whilst mapping the *c.*200km^2 of the ELFC at 1: 5000 scale. Sampling of dykes and lavas was undertaken to try to distinguish between the relatively evolved 'axis sequence' products, thought to be geochemically similar to the remainder of Troodos, and the distinctive, highly primitive, 'transform sequence'.

It became apparent in the first season that there was little evidence in the ELFC for large-scale intrusion by Murton's 'transform sequence' plutons; indeed, there was little obvious sign even of the vertical E-W transform trend so prominent in the WLFC and AFB (*cf.* figure 1.10). No angular unconformities were identified in the lava sequences, even in areas such as the Kalavasos Mines, where volcaniclastic sediments indicative of fault activity are interbedded between lava flows. Instead, the importance of Robertson's

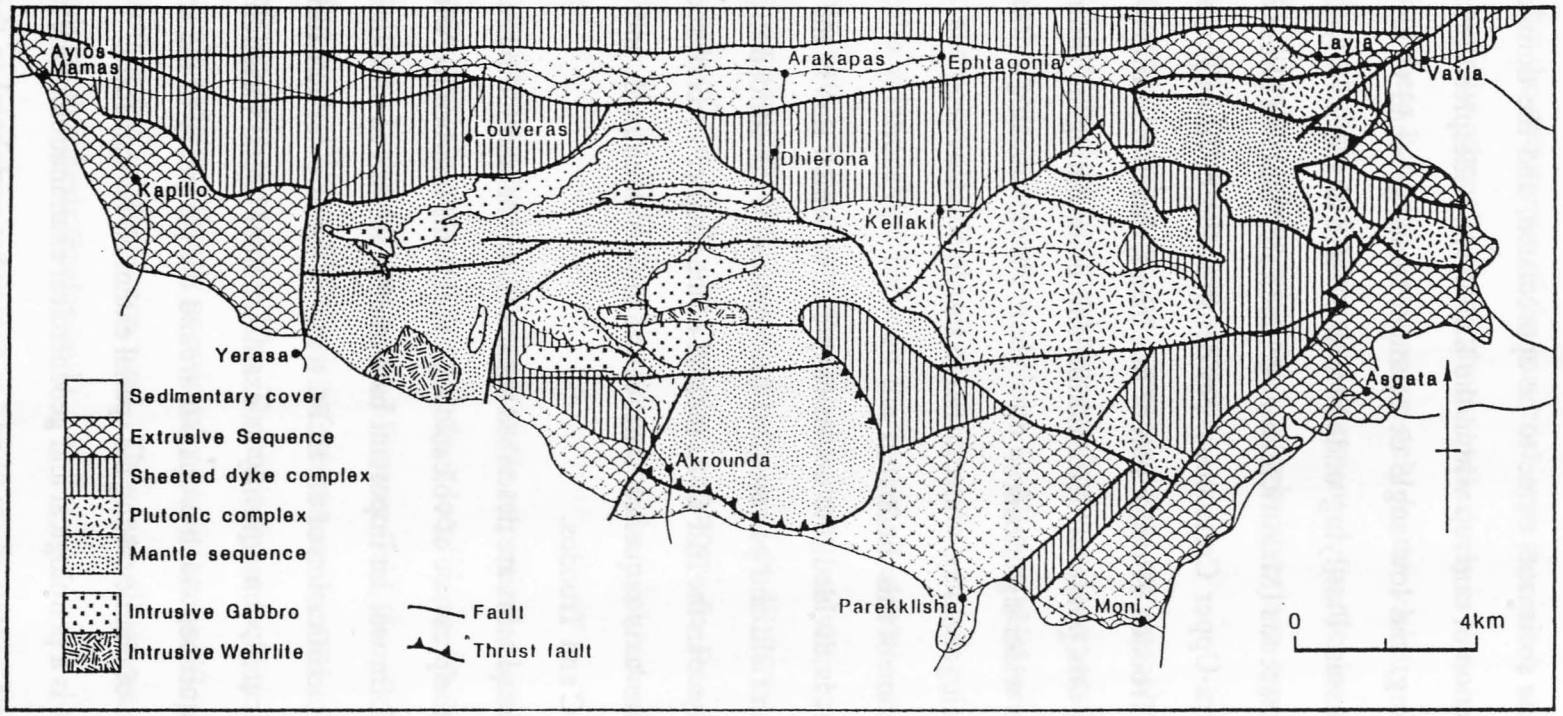

Figure 1.10: Highly simplified geological sketch map of the Arakapas Fault Belt and Limassol Forest Complex. A strong E-W fabric is evident in both the western Limassol Forest and in the Arakapas Fault Belt, but is significantly less obvious in the eastern Limassol Forest.

(1975) and Adamides' (1980) observations of the tilting of lavas prior to the deposition of metalliferous sediments came to be appreciated, and the dominant control on the present disposition of outcrop within the ELFC–*viz.* widespread brittle normal faulting and block tilting, and low angle detachment faulting–found to be the result of post-volcanic processes. Flat-lying undeformed pelagic chalks overlying the ophiolite, of uppermost Cretaceous (Maastrichtian) age, indicated that this phase of deformation was essentially intra-Upper Cretaceous. No deformation of this age had previously been recognised in Troodos. A major part of this thesis, therefore, came to be concerned with characterising this phase of deformation and determining its timing, with a view to appreciating its wider significance.

1.5.2 Presentation of this thesis

The thesis is divided into seven chapters, of which this is the first. Chapter 2 is concerned with field and petrological descriptions of the lithostratigraphic units of the 'Penrose' sequence in the ELFC. At the end of the chapter a reconstruction of the original thickness of the 'axis sequence' crust in the area is attempted, and comparisons made with the WLFC and Troodos.

The lava sequences are described separately in chapter 3. Simonian and Gass (1978) showed, with the presence of volcaniclastic sediments interbedded with lavas in the AFB, that the transform was an important bathymetric as well as structural feature. With the post-volcanic modification of the ELFC many of the original transform-related structures have been obscured; consequently an examination of lateral variations in the stratigraphy of the lava sequence, which crops out around the periphery of the area, provides one of the best means of characterising the spatial extent of the transform.

Chapter 4 is a petrological and geochemical examination of the lavas in the ELFC. It is a largely self-contained study and is somewhat peripheral to the central aim of the thesis. For this reason conclusions from it are discussed at the end of the chapter, rather

than the end of the thesis. The Limassol Forest Complex and Arakapas Fault Belt are notable for the occurrence of the rare rock type 'boninite', which is a highly primitive basaltic andesite otherwise found almost exclusively in Western Pacific marginal basins. In Cyprus these boninitic lavas occur only in the vicinity of the transform. A brief discussion of their petrogenesis is presented, particular attention being paid to stratigraphic relationships with the less primitive lava types, and possible tectonic controls on their generation and extrusion.

The remaining chapters are concerned with the tectonic evolution of the ELFC. Chapter 5 examines the structural history of the area, incorporating the results of a limited collaborative palaeomagnetic study with S. Allerton (University of East Anglia). Syn-volcanic and post-volcanic phases of deformation are distinguished. Chapter 6 deals with the angular relationships between the igneous basement and the overlying pelagic sediments, with a view to constraining the timing and sequence of deformation. In the final chapter a model for the tectonic evolution of the ELFC is erected. A brief review of the geology of the Mamonia Complex and Kyrenia Range is presented, and the significance of the ELFC in the context of the evolution of Cyprus as a whole is discussed.

Throughout the thesis reference is made to particular localities, given with a six or eight figure grid reference and, frequently, a local name. The grid references are based upon the 1000m Universal Transverse Mercator Grid, Zone 36S, International Spheroid (100,000m square: WD). Six figure references are located to the nearest 100m, eight figure references to the nearest 10m. The majority of locality names are taken from the 1: 5000 scale cadastral sheets; occasionally names or modifications of names conveyed to the author by villagers are used. They are all given on the 1: 20,000 map accompanying this thesis (enclosure 1).

CHAPTER 2:
Ophiolite Stratigraphy

2.1 Introduction

In this chapter descriptions are given of the major lithostratigraphic units of the ophiolite as observed in the ELFC, with the exception of the extrusive suite, which is considered separately in chapter 3. Section 2.2 deals with stratigraphic units below the petrological Moho, termed the 'mantle sequence', and sections 2.3-2.5 with the crustal rocks above this datum. These crustal rocks are taken to be the products of a constructive margin magma chamber and are henceforth referred to as belonging to the 'axis sequence'. In the WLFC, in addition to the axis sequence, Murton (1986b) described an association of plutonic, hypabyssal and volcanic rocks to which he ascribes an origin within the transform fault and termed 'transform sequence'. The representatives of these rocks within the ELFC are described in section 2.6.

In the past a great deal of energy has been expended in the development of the concept of ophiolites as oceanic crust, and in discussion of their tectonic setting, whether created at a mid-ocean ridge or marginal basin constructive plate margin. Much of this has centred on the Troodos Massif (see chapter 1), which is undoubtedly the best-studied ophiolite complex in the world. It is not the intention of this chapter to reiterate in detail the reasons for the identification of the Troodos and Limassol Forest Complex sequences as oceanic lithosphere. Rather, the lithostratigraphic units are described with reference made to their position and significance within the ophiolite consensus model (figure 1.3). Complexities within this model and features relevant to the tectonic evolution of the ELFC are discussed.

2.2 Mantle Sequence

2.2.1 Introduction

The term 'mantle sequence' was first used by Allen (1975) to describe the tectonised peridotites that crop out around Mt. Olympus, at the centre of the Troodos Massif. In common with the majority of ophiolite complexes, the peridotites occur at the deepest structural levels and have a pervasive tectonite fabric resulting from syntectonic re-crystallisation at elevated temperatures and pressures (Nicolas and Poirier 1976, George 1978). The sequence around Mt. Olympus is composed of about 80% harzburgite, which is widely held to represent the residue left behind after partial fusion and the extraction of a basaltic melt from a previously lherzolitic upper mantle peridotite (Moores and Vine 1971, Greenbaum 1972), and 20% dunite, commonly in the form of irregular lenticular masses enclosed within the harzburgite. The dunite pods are thought to represent cumulates precipitated from small magma chambers within the partially melting upwelling asthenospheric mantle (Greenbaum *op. cit.*, Menzies and Allen 1974).

2.2.2 The mantle sequence in the Limassol Forest Complex

Similar stratigraphic levels are exposed in the LFC. Previous workers described the lithologies as 'bastite serpentinite', and interpreted the 45km^2 outcrop in the western LFC as a serpentinite diapir (Bear and Morel 1960, Panayiotou 1977). However, Murton (1986b) has shown that these rocks are in fact tectonised harzburgites and dunites which have subsequently been passively serpentinised.

In the ELFC the mantle sequence is exposed in the Akapnou Forest, forming an area of *c.*10km^2 (figure 2.1). North of northing 53 harzburgite predominates, whereas to the south dunite is the major rock type. Minor pyroxenitic bodies cut all parts of the sequence (see section 2.2.6) and rare poikilitic wehrlite and gabbro intrusives are locally developed (section 2.6).

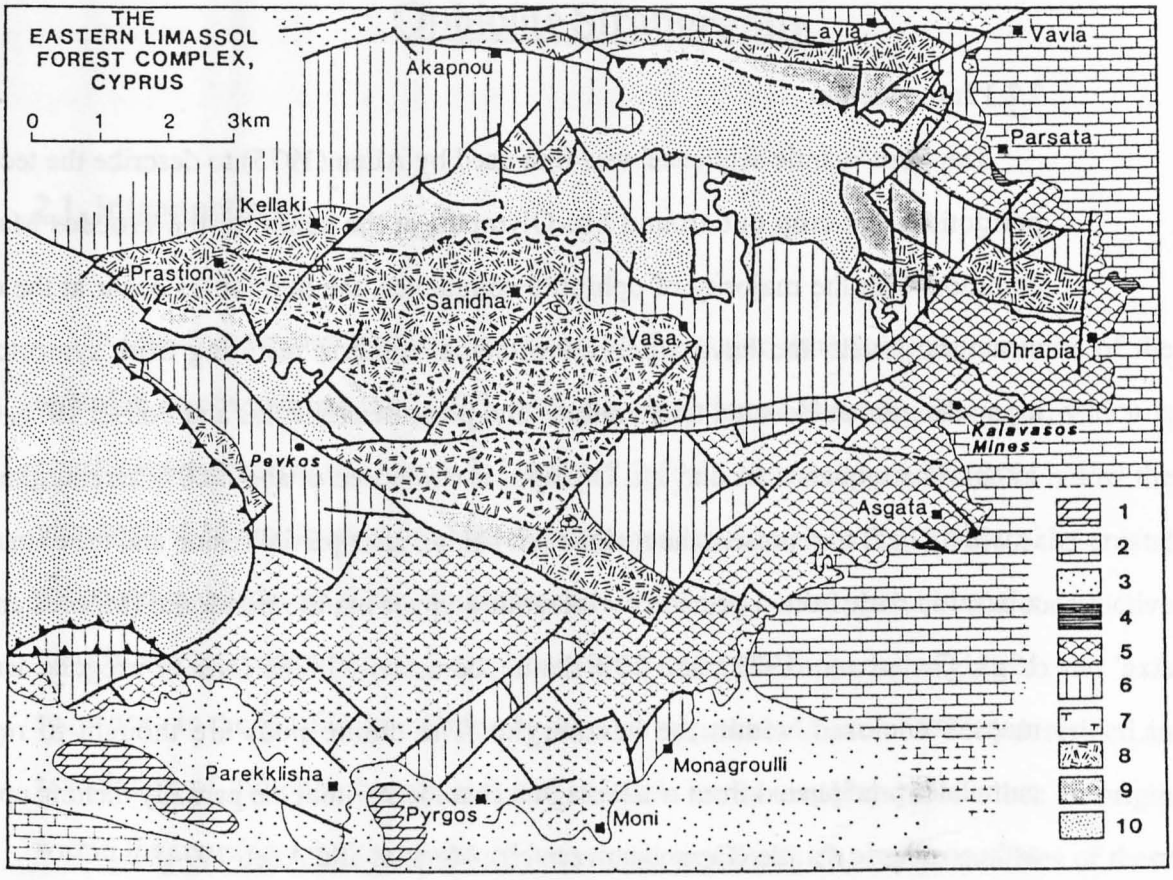

Sediments:

(1): Miocene–Recent
(2): Maastrichtian–Miocene
(3): Campanian–Maastrichtian Moni mélange
(4): Turonian–Campanian Perapedhi Formation

Igneous Rocks:

(5): Pillow lavas
(6): Sheeted Dyke Complex
(7): Plagiogranites
(8): Gabbros
(9): Peridotites
(10): Tectonised harzburgites and dunites

Figure 2.1: Simplified geological map of the Eastern Limassol Forest Complex.

2.2.3 Tectonised harzburgite

The harzburgite gives rise to a rugged and deeply incised terrain which weathers to a rich orange-brown colour; sheared sections have a distinctive blue-silver hue. In hand specimen fresh harzburgite is dark green, and contains prominent elongate 1cm-long orthopyroxene plates with a lustrous bronze colour. However, fresh harzburgite is rare, even in freshly-cut sections, and is most commonly altered to an orange-brown colour upon the oxidation of magnetite liberated from olivine upon serpentinisation (see section 2.2.7). Orthopyroxene may be pseudomorphed to bastite but grains retain their morphology, and commonly their elongation defines a foliation. In the ELFC chrome spinel is rare, and it proved impossible to identify any lineation from the orientation of such grains as were visible in hand specimen.

As a result of the high degree of serpentinisation and subsequent extensive brittle deformation, the (metamorphic) compositional ratio layering visible in the Mt. Olympus mantle sequence (Allen 1975, George 1978) is rarely apparent on a mesoscopic scale, particularly in the Akapnou Forest, although differences in pyroxene concentration between outcrops are apparent. Where visible, the foliation was usually sub-vertical, and when the effects of local rotation-inducing faulting were removed, between N-S and NW-SE in orientation.

In thin section the harzburgite has a mosaic porphyroclastic texture (Harte 1976), with strained orthopyroxene porphyroclasts set in a matrix of tabular olivine and accessory spinel. The orthopyroxenes have a prominent cleavage with clinopyroxene exsolution lamellae parallel to (100), which is frequently deformed; extinction is undulose and kink bands are occasionally developed. The grains are allotriomorphic, with serrated cuspate margins, and may be elongate with a length to width ratio of up to 5:1, emphasised by dislocation glide planes parallel to (100). In extreme cases the grains are broken down into clusters of more equant tabular grains with differing orientations.

The olivines may reach 8mm in size, the larger grains having kink bands and

undulose extinction, and the smaller with straight extinction. Serpentinisation in even the freshest samples obscures most olivine-olivine grain boundaries, but rare gently curving lobate boundaries are occasionally visible.

Chrome spinels are deep red in colour and either form equant anhedra up to 1mm long with ragged edges, or highly irregular amoeboid forms at olivine and orthopyroxene grain margins that partially enclose silicate fragments.

Clinopyroxene is a rare accessory in the harzburgite, but several grains occur in specimen 86/169, forming <1% of the mode. The largest is 1.5mm in length and, like the chrome spinel, is developed at the interstices of the olivine and orthopyroxene grains. The olivine and orthopyroxene have lobate margins where in contact with the clinopyroxene, giving rise to a 'holly-leaf' shape to the clinopyroxene grains. Unlike the orthopyroxene, the clinopyroxene has regular extinction and no exsolution lamellae.

The mineral chemistry of the harzburgite is summarised in table 2.1. The primary minerals (*i.e.* olivine, orthopyroxene, spinel) have a relatively restricted range of compositions that fall within the range defined by harzburgite from Mt. Olympus (Allen 1975) and Oman (Brown 1982, Browning 1982). The clinopyroxene, however, is an endiopside, with higher En and Fs components and lower Wo than primary lherzolite clinopyroxene (*e.g.* Lippard *et al.* 1986).

The flexed cleavage, undulose extinction, kink bands and physical modification of the orthopyroxene porphyroclasts are unequivocal evidence for high strain at elevated (asthenospheric) temperatures and pressures (Nicolas and Poirier 1976, Lippard *et al. op. cit.*). The larger olivines are also strained, but the smaller grains with straight extinction may be analogous to the recrystallised olivine neoblasts observed by George (1978) in less-serpentinised harzburgites from Mt. Olympus, which are interpreted as a static post-strain annealing phenomenon (Dick 1977).

Deformational textures in chrome spinel are limited to the larger grains, which have irregular dilatant cracks suggesting low temperature fracturing; no elongation of the

	Olivine 86/169WAC (core)		Chrome spinel 86/169WCA (core)		
SiO_2	41.88		SiO_2	0.57	
FeO^{tot}	8.26		TiO_2	0.18	
MnO	0.12		Al_2O_3	20.81	
MgO	49.58		FeO*	13.89	
Cr_2O_3	0.02		Fe_2O_3*	3.22	
NiO	0.41		MnO	0.12	
TOTAL	100.27		MgO	14.48	
		range:	CaO	0.01	
$100^{Mg}/_{Mg+Fe}$	91.5	91.2-91.5	Cr_2O_3	46.82	
			NiO	0.10	
			TOTAL	100.20	
					range:
			$100^{Mg}/_{Mg+Fe"}$	65.0	58.3-65.0
			$100^{Cr}/_{Cr+Al}$	60.1	56.4-60.1
			$100^{Fe'''}/_{R'''}$	3.8	2.2-11.1

* calculated assuming stoichiometry

	Orthopyroxene 86/169WBF (core)		Clinopyroxene 86/169WBB (core)	
SiO_2	57.48		53.42	
TiO_2	0.04		0.13	
Al_2O_3	1.86		3.08	
FeO^{TOT}	5.26		2.80	
MnO	0.13		0.09	
MgO	32.58		17.77	
CaO	1.69		20.21	
Na_2O	0.01		0.17	
Cr_2O_3	0.72		1.14	
NiO	0.09		0.05	
TOTAL	99.86		98.86	
		range:		range:
$100^{Mg}/_{Mg+Fe+Ca}$	88.7	87.4-89.7	52.5	52.5-52.8
$100^{Fe}/_{Mg+Fe+Ca}$	8.0	8.0-8.4	4.6	4.6-4.8
$100^{Ca}/_{Mg+Fe+Ca}$	3.3	1.9-4.4	42.9	42.4-42.9

Table 2.1 Summary of harzburgite mineral compositions from the ELFC

spinels parallel to the orthopyroxene foliation was apparent.

Relict (primary) clinopyroxene from Oman harzburgites forms ragged anhedral grains with orthopyroxene exsolution lamellae and a strain fabric (Lippard *et al.* 1986). The clinopyroxene in specimen 86/169, however, is strain-free and its interstitial texture suggests a secondary origin. Dick (1977) interprets lobate orthopyroxene and olivine boundaries (as above) as partial melting textures involving dissolution-reprecipitation creep. As such, the clinopyroxene may therefore represent either trapped melt generated *in situ*, or melt generated elsewhere and impregnated into the residual harzburgite.

2.2.4 Dunite pods in harzburgite

In places pods of dunite occur within the harzburgite. They range from a centimetre-metre scale up to perhaps 100m in length, forming bodies apparently sub-parallel to the harzburgite tectonite foliation. The contact between the dunite and harzburgite is sharp but may be intricate: in the field the rough harzburgite surface changes to a characteristic smooth-weathering one characteristic of dunite with the disappearance of orthopyroxene (Allen 1975). Within the dunite, in accessory concentrations, are lustrous black chrome spinel grains which may locally become abundant enough to form chromitite bodies at the margins of the dunite pods. These are rare in the Akapnou Forest (E. Georgiou *pers. comm.* 1986), but a deposit at Mandra tou Veli–Mazoukambos (21355360) was sufficiently large for limited mining to be undertaken in the 1920s (Pantazis 1967). The remaining chromitite ore there forms veins or lenses of disseminated to massive chromite, rarely greater than 5cm in width and of limited lateral extent, in sheared and pervasively serpentinised dunite which is in turn surrounded by harzburgite. Within the massive chromite layers of occluded silicate (*i.e.* serpentinised olivines) and fine chromite define a primary magmatic layering, which is crossed by perpendicular 'pull-apart' cracks related to the later brittle fracture of the chromite body. The preservation of such magmatic textures leads most workers to conclude that the chromitites are of cumulate

origin, and that the dunite pods crystallised from magmatic bodies within the harzburgite and deformed by continued mantle tectonism (*e.g.* Brown 1980, 1982; Bartholemew 1983).

2.2.5 Massive dunite

In the southern part of the Akapnou Forest, north of the village of Vasa, several square kilometres of massive dunite crop out. They are usually faulted against other rock types, although E. Georgiou (*pers. comm.* 1987) reports an unfaulted contact between harzburgite and massive dunite transitional over a few metres in the Kaloussi area, *c.*0.5km from the chromite locality described above. Weathered outcrops of the dunite may be smooth and buff-coloured, but more frequently assume a purplish mottled colour where serpentinisation is extreme (see section 2.2.7). The freshest material is dark green, with individual grains or stringers of lustrous black chrome spinel, though even here serpentinisation approaches 100% and no relict olivine has been found. At some localities cumulus textures are visible in hand specimen. These are more obvious in thin section: rounded pseudomorphs after olivine up to 5mm in diameter are enclosed by clinopyroxene pseudomorphs, which form 0-10% of the mode, mimicking an adcumulate–orthocumulate texture. Euhedral black chrome spinel up to 1mm in diameter is present in accessory quantity and may be rimmed by ferritchromit.

The cumulate textures and appearance of intercumulus clinopyroxene indicates that the massive dunite is transitional into massive wehrlite and should be regarded as the lowest portion of the layered plutonic sequence (see section 2.3). The 'petrological Moho', *i.e.* the boundary between residual mantle peridotites and magma chamber precipitates, should therefore strictly be sited at the harzburgite–massive dunite contact. It is convenient, however, to include the massive dunites in this section as their appearance, particularly in the most highly serpentinised areas, and their behaviour in response to later tectonism (see chapter 5), is very similar to that of the harzburgites.

2.2.6 Intrusives in the mantle sequence

The mantle sequence is host to two distinct suites of intrusives. The later set consists of dykes and bosses of ultramafic and mafic material, which intrude all levels of the crust. They will be discussed in more detail in section 2.6.

The earlier set comprises irregular masses of clinopyroxenite, commonly of pegmatitic aspect, which mostly intrude the massive dunite. Sinuous bifurcating veins and dykelets up to 0.5m wide are locally abundant: *e.g.* at 200520 Koufkia, 0.5km north of Vasa, where elongate bodies on occasion up to 40m x 10m may develop. The orientation of the intrusives is variable, but most are steeply dipping and strike close to east-west, and are therefore transform parallel. The margins are generally diffuse and unchilled. Well-formed pyroxene crystals are up to 20cm long, and occasionally are aligned sub-parallel to (100), locally defining a foliation parallel to the margins of the body. In the centre of the larger pyroxenite bodies olivine may be present as millimetre-sized grains, poikilitically enclosed by the pegmatitic clinopyroxene; such areas locally approach wehrlite in composition.

In thin section the pyroxenites are seen to comprise almost 100% clinopyroxene, with accessory chrome spinel forming aggregates of tiny black euhedra. Orthopyroxene forms a minor constituent of one specimen only. The pyroxenes are usually ragged and anhedral; grain boundaries are interlocking and sutured, and fine-grained recrystallisation is developed. This recrystallisation may be developed enough to give rise to a porphyroclastic texture. Strain features are abundant: undulose extinction, pull-apart fractures, flexure of cleavage, kink bands and formation of sub-grains. Many of the latter are brittle features which could be related to the mechanical fracture of the intrusive bodies acting incompetently with respect to the serpentinised dunite, perhaps following earlier deformation at elevated temperatures and pressures.

Similar veins and dykelets are described from Troodos (Menzies and Allen 1974, Allen 1975), and other ophiolite complexes. In Oman, pyroxenites are found throughout

the mantle sequence, changing from orthopyroxenite at deep levels to clinopyroxenite near to the Moho (Browning 1982). This is consistent with observations from the Limassol Forest Complex: Murton (1986b) describes orthopyroxenite dykes from the harzburgite core of the WLFC, nearly 1km below the petrological Moho, with the clinopyroxenites (as described above) occurring much closer to the Moho.

The development of a poikilitic texture and local transition to wehrlite suggests that the pyroxenite was intruded as a melt phase, rather than forming by the metasomatic alteration of wallrock adjacent to a fracture, as proposed by Murton (1986b). An origin similar to that proposed by Montigny *et al.* (1973) and Menzies and Allen (1974), is perhaps the most applicable, with the pyroxenites representing the final partial melt fraction extracted from the harzburgite.

2.2.7 Alteration of mantle sequence lithologies

Mantle sequence lithologies have been much affected by alteration processes. By far the most important of these is serpentinisation, which involves the hydration of olivine, and to a lesser extent orthopyroxene, according to the reactions (taken from Coleman 1977):

$$2Mg_2SiO_4 + 3H_2O \rightarrow Mg_3Si_2O_5(OH)_4 + Mg(OH)_2$$

olivine — serpentine — brucite

$$2Mg_2SiO_4 + 2H_2O \rightarrow Mg_3Si_2O_5(OH)_4 + MgO$$

olivine — serpentine — removed

$$3Mg_2SiO_4 + SiO_2 + 4H_2O \rightarrow Mg_3Si_2O_5(OH)_4 + Mg(OH)_2$$

olivine — silica — serpentine — brucite

or in harzburgite:

$$Mg_2SiO_4 + MgSiO_2 + H_2O \rightarrow Mg_3Si_2O_5(OH)_4 + Mg(OH)_2$$

olivine orthopyroxene serpentinite brucite

In general, the serpentinisation reaction is considered essentially isochemical, involving only the uptake of 12-13.5 wt% water (Coleman *op. cit.*). It can only proceed at temperatures below about 430°C, at which point forsterite becomes unstable in the presence of water (Bowen and Tuttle 1949). Natural serpentinites normally consist of mixtures of three principal serpentine minerals, *viz.* antigorite, lizardite and chrysotile, which have similar chemical compositions but distinct atomic structures and crystal habits (Deer *et al.* 1966, Prichard 1979). They have similar appearance in thin section, forming low relief, low birefringence microcrystalline aggregates, and can normally only be distinguished by X-ray diffraction.

The mechanism of serpentinisation can be deduced from thin section. Almost all terrestrial olivines are crossed by irregular fractures, and it is a ubiquitous feature of Limassol Forest mantle olivines that these fractures are infilled by veinlets or 'cords' (Maltman 1978) of fibrous serpentine and small black grains of magnetite (the latter liberated during the serpentisation reaction). In the very freshest specimens of harzburgite the cords enclose polyhedral remnants or 'cores' (Maltman *op. cit.*) of primary olivine, forming a characteristic mesh-like texture. More frequently, however, the cores are also replaced by serpentine. This is presumably by means of a passive diffusive process, as the mesh texture and often even the primary igneous or metamorphic texture is preserved, even though the primary mineralogy has been completely replaced. This is true particularly of the poikilitic wehrlite horizons within the massive dunite and of the harzburgite, in which orthopyroxene, although commonly partly replaced by its pseudomorph bastite, retains its grain morphology and cleavage trace, and hence tectonite

fabric, even when no fresh olivine is preserved.

The mesh texture visible in thin section is identifiable in hand specimen. The more heavily altered rocks are purplish in colour and are criss-crossed by innumerable black veinlets with green clots, probably of antigorite. This type of alteration is especially apparent adjacent to fractures, as shown in plate 2.1. Here, a block of harzburgite delineated by joint planes has a rind of purple pervasively serpentinised material 2-3cm thick enclosing the more familiar orange-weathering, haematite-stained, partially-serpentinised peridotite. The iron-staining has itself percolated only 5-10cm into the block, preserving a core of relatively fresh harzburgite which has suffered only 10-20% serpentinisation. Sample 86/169 was taken from the core of this block.

This clearly shows that minor fractures, as are prevalent over the entire mantle sequence outcrop, are capable of acting as fluid channelways and thus as serpentinisation loci. Macdonald and Fyfe (1985) have shown that serpentinisation by diffusion at a water-filled crack in a seafloor environment is a geologically rapid process at temperatures >100°C. In a transform fault environment, therefore, with its plethora of open fractures, serpentinisation of significant thicknesses of mantle peridotite is possible in «1Ma.

At what stage, therefore, was the Akapnou Forest mantle sequence serpentinised? Veins of antigorite in the massive dunite cross pyroxenite dykes undeflected, and must therefore post-date intrusion. This is in accord with the interpretation of the pyroxenites being produced from magmatic bodies associated with melt extraction beneath a ridge axis, and therefore generated at temperatures well above the stability field of serpentine.

The later post-axial intrusives, however, (section 2.6) appear to be little affected by serpentinisation. At 200520 Koufkia, north of Vasa, pervasively serpentinised dunites and cumulate poikilitic wehrlites of the massive dunite unit are intruded by bosses and dykes of fresh poikilitic wehrlite. The marked difference in alteration states between identical lithologies leaves little doubt that much of the serpentinisation preceded the later plutonism and was therefore largely a seafloor phenomenon.

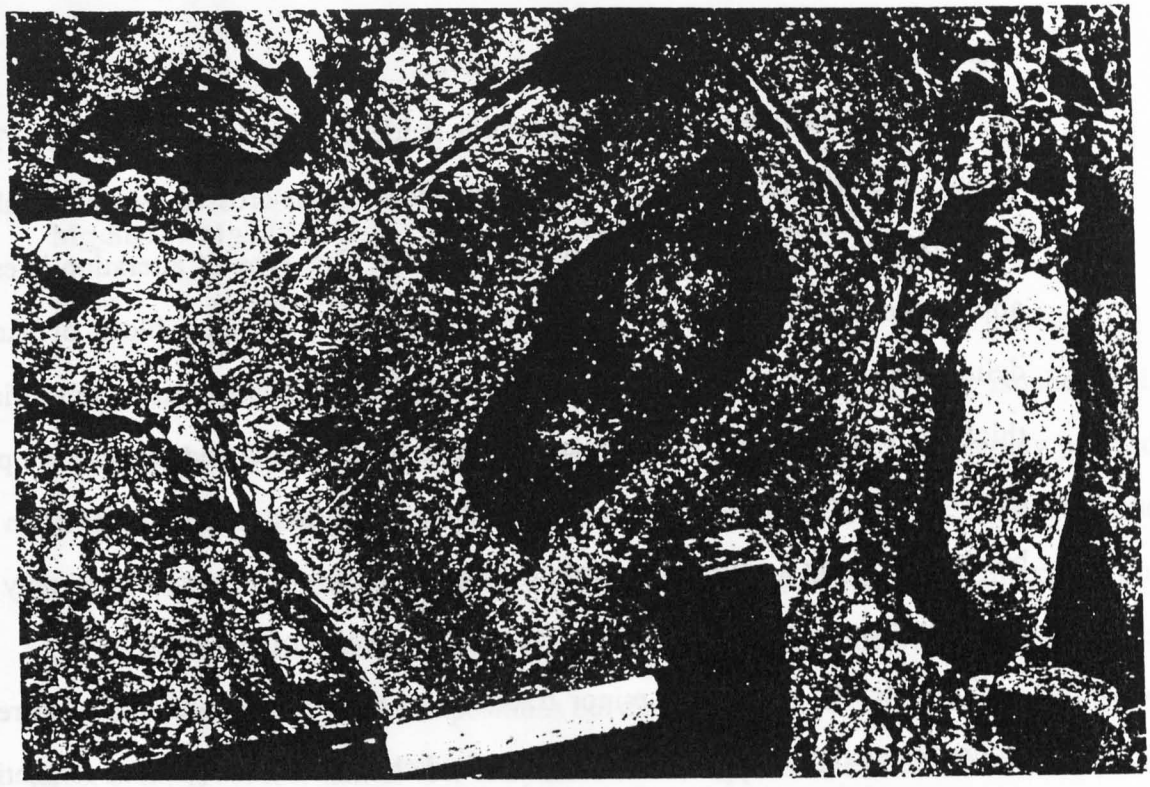

Plate 2.1: Alteration of harzburgite. The degree of serpentinisation increases from ~20-30% in the centre of the block to 100% at the edge. 19455450 Akapnou Forest, 2.5km E of Akapnou village.

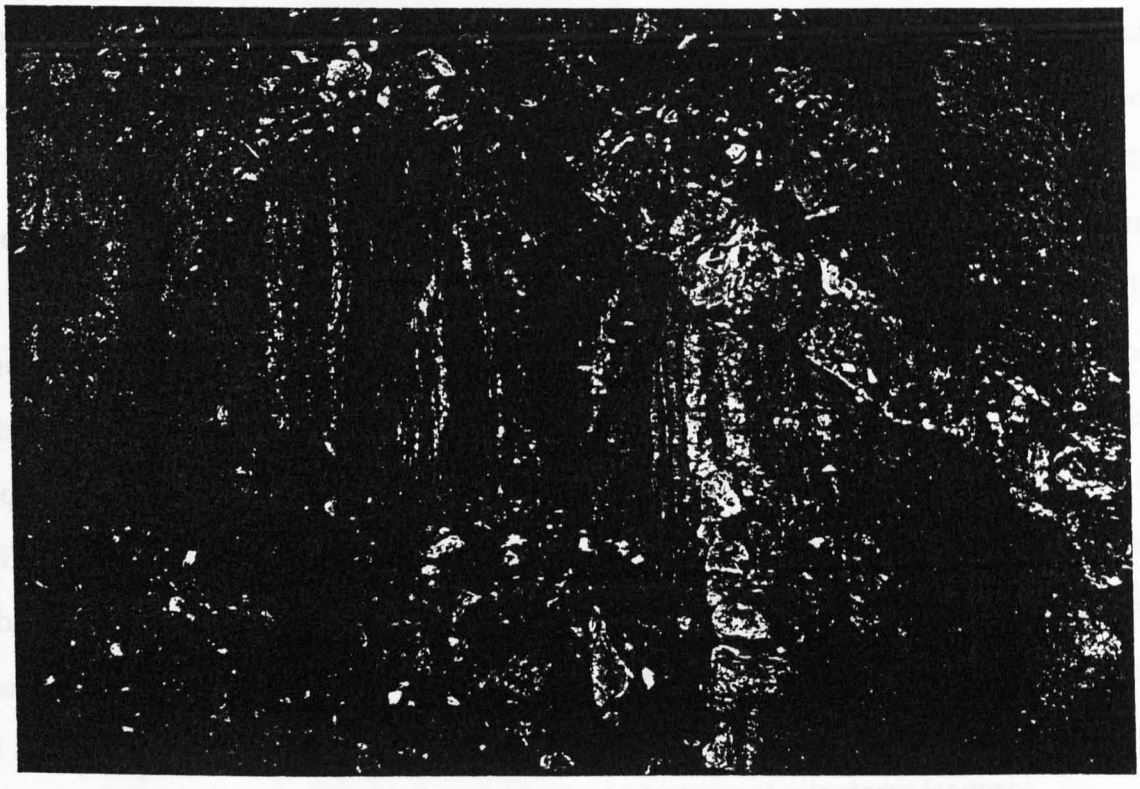

Plate 2.2: Low angle chilled dolerite dyke through steeply dipping layered sequence. 14835112 Lestóvounos.

2.3 Layered Sequence

2.3.1 Introduction

The mantle sequence is overlain stratigraphically by a plutonic complex, which is here subdivided into the 'layered sequence' and the 'high level plutonic suite' (described in section 2.4). The plutonic section of the ophiolite association has long been recognised as the frozen relict of a major magma chamber or chambers beneath a spreading ridge axis (see chapter 1); it is therefore considered to be the lowest part of the axis sequence crust (*e.g.* Moores and Vine 1971, Greenbaum 1972).

The massive dunite at the transition zone of the petrological Moho grades upwards into a suite of layered plutonic rocks dominated by peridotites in the lower part and gabbros in the upper. The layering is most commonly defined by variation in the modal proportions of the mineral phases present, often forming repetitive cyclic ultramafic-mafic units. The presence of these repeated units, coupled with their cumulus textures (see below), as observed in petrographic section, gave rise to the classical interpretation of such rocks as the products of the mechanical settling of crystals out of batches of magma introduced into the chamber (Wager and Deer 1939, Wager and Brown 1968), although modern studies have shown that more complex and partly *in situ* physico-chemical processes must be invoked to explain some features of the layering (*e.g.* McBirney and Noyes 1979). The term 'cumulate', however, is retained, but with a non-genetic implication.

George (1978) showed that the cumulate textures of some of the layered plutonics had been modified by a penetrative deformation fabric analogous to that observed in the underlying mantle sequence. He claimed that the intensity of the deformation diminished rapidly and progressively with stratigraphic height and died out within the cumulate ultramafics, and emphasised the lack of correspondence between the levels of the residual-magmatic and tectonite-cumulate transitions at the base of the crust. Early

authors (*e.g.* Greenbaum 1972), however, had reported intrusive contacts between the metacumulates and undeformed cumulates; recent studies (Malpas *et al.* 1987, Malpas and Robinson 1987, Benn and Laurent 1987) have shown that these correspond to an intrusive boundary between an earlier magmatic suite, now pervasively deformed, and a later, largely undeformed, suite.

2.3.2 The layered sequence in the ELFC

The layered sequence crops out extensively in the ELFC, forming the rugged, elevated terrain of the Lestóvounos region to the south of Kellaki village, in the heart of the Limassol Forest. The ground rises abruptly to a height of 790m from the low-lying Parekklisha plain to the south across a prominent NW-striking fault at Pevkos (see plate 5.8 and section 5.5.3), and the layered plutonics are well-exposed on the higher ground along the Parekklisha–Kellaki road. As in all other parts of the ELFC, the plutonics at Lestóvounos are highly tilted and heavily block faulted, but provide the most continuous and extensive sections for more detailed observation.

The layered sequence also crops out along the northern flanks of the Akapnou Forest, between Akapnou and Vavla, at the southern margin of the Arakapas Fault Belt. The peridotites and gabbros grade up into high-level gabbros near Layia, although the section has been modified by transform processes and the post-transform uplift of the Akapnou Forest (see chapter 5). Similar layered plutonics are found at the base of the gabbro section exposed west of Dhrapia, immediately to the north of the Kalavasos Mines. Although drill-hole data obtained by this author from 25645181, 500m north of Dhrapia village, show that melagabbros underlie the lavas beneath at least part of the Kalavasos Mines, only a *c.*200m sequence of layered rocks is exposed at the surface. Further to the west, the layered sequence is again visible in the Vasilikos River, 2km above the dam. This particular area has suffered exceptional tectonic disruption, and is discussed further in section 5.3.

The intensity of tectonism is such that no unbroken sections through the layered sequence exist in the ELFC. Uninterrupted progressions from harzburgite through massive dunite to cumulate peridotite have not been identified: layered plutonics are most frequently separated from the underlying harzburgites by a thick sub-horizontal serpentinite shear zone, *e.g.* at 141508 (Lestóvounos) and 162533 (1km southwest of Klonari). Tha nature and significance of this shear zone is discussed in section 5.5.4.

For mapping purposes it was found convenient to subdivide the ELFC layered plutonics into four lithological, pseudostratigraphical units (in ascending order): the 'cumulate peridotite' (cP), 'cumulate peridotite and gabbro' (cPG), 'cumulate gabbro and peridotite' (cGP) and 'cumulate gabbro' (cG), and they are described in that sequence hereafter. The first and last correspond to Remond's (1986) 'wehrlite zone' and 'layered gabbro zone' respectively, and the cPG and cGP units to her 'transition zone'.

2.3.3 Cumulate peridotite

The massive dunite grades up into the layered sequence with increasing proportion of modal clinopyroxene, so that wehrlite is the dominant rock type in the lower part of the layered series. Although serpentinisation is still strong at the base of the sequence, the wehrlites can be distinguished by the 1-2mm diameter brown spots of clinopyroxene on the otherwise smooth-weathering surface of the dunite. Closer examination reveals flat cleavage surfaces dotted with numerous millimetre-sized oval pits, where tiny poikilitically enclosed olivine grains have been preferentially weathered. Serpentinsation decreases with stratigraphic height, revealing (*e.g.* around 155528, to the north of the Panayia tou Glossa monastery) monotonous sections of massive and layered poikilitic wehrlite (Remond 1986).

In higher parts of the cumulate ultramafic pile the intercumulus clinopyroxene is joined by plagioclase, giving rise to horizons of plagiowehrlite, and occasionally of gabbro. Cyclic units become apparent, as displayed at a small outcrop at Lestóvounos (149509). Here, a 9m section reveals three cycles, each grading from dunite at the base,

to poikilitic wehrlite and plagiowehrlite, and thence to gabbro before being superseded by another dunite unit. The dunite layer is typically only a *c.*5-10cm thick and is always highly serpentinised. It has a relict adcumulus texture, with outlines of subhedral olivines up to 5mm in length still visible, and differs from the massive dunite (section 2.2.5) in its apparent absence of chrome spinel. It grades over a centimetre or so into wehrlite with the appearance of intercumulus clinopyroxene, which rapidly attains a size of 1cm or more. Olivines in contact with the clinopyroxene have convex lobate margins, such that completely enclosed grains assume a circular outline in thin section, with a typical diameter of 1mm. This is interpreted as a resorption texture (Jackson 1961, 1971). The plagiowehrlites contain intercumulus plagioclase in addition to clinopyroxene, textural relations indicating that the plagioclase crystallised last. Plagiowehrlite grades into gabbro with the appearance of cumulate clinopyroxene and typically rapid disappearance of olivine. The cumulus pyroxenes in the gabbros also assume a rounded form, typically 0.5mm in diameter, and are poikilitically enclosed by large clinopyroxene and plagioclase oikocrysts, giving rise to a heteradcumulus texture.

2.3.4 Cumulate peridotite and gabbro: the 'transition zone'

Plagioclase becomes an increasingly important phase with increasing stratigraphic height in the layered sequence. Intermediate levels in the cumulate pile are characterised by the rapid alternation of ultramafic and mafic lithologies in phase layered cyclic units (plate 2.2), and by the first appearance of plagioclase as a cumulus phase. Cycles similar to those described in the previous section are common, but the clinopyroxene cumulus gabbros are succeeded by and alternate with plagioclase cumulus horizons. In these, the feldspar crystals form abundant tabular euhedral lozenges up to 3mm in length, enclosed by adcumulus plagioclase and orthocumulus clinopyroxene. Orthopyroxene, which is rare in the ultramafic part of the sequence, occurs in some of these gabbros (strictly gabbronorites), possibly in part as a cumulate phase, although both pyroxenes are heavily

replaced by uralitic amphibole and their primary relation is thus obscured.

Alteration in the ultramafic cumulates is moderate. Serpentinisation is heavy in the most olivine-rich rocks, and in the wehrlitic horizons the first-formed intercumulus plagioclase, and to a lesser extent pyroxene, has been replaced. The gabbro has suffered a partial replacement by an intergrowth of colourless hornblende of ragged appearance; the crystals, which grow to 2-3mm in length, contain numerous irregular exsolution blebs and have sutured grain boundaries. Where it occurs, this completely destroys the primary texture of the rock, but here it only affects small patches less than a centimetre in diameter.

2.3.5 Cumulate gabbro

Ultramafic lithologies diminish and gabbroic ones increase towards the top of the layered sequence. The regular phase layering characteristic of the intermediate stratigraphic levels becomes poorly defined, and massive gabbros lacking any kind of lamination in outcrop but retaining a cumulate texture in petrographic section become commonplace. In some instances, however, as at 148516 Vrysi tou Koutalari, 1.5km south of Kellaki, a weak and highly impersistent wispy layering is visible, apparently defined by an irregular variation in the proportion of the mafic minerals present.

2.3.6 Intrusives in the layered sequence

The layered sequence in the central part of the ELFC appears to have been intruded by one or more ultramafic and mafic bodies. At 169520, west of Sanidha, for example, a 25m wide stock or dyke of unchilled poikilitic wehrlite intrudes laminated and massive gabbro from the very topmost part of the layered sequence. Elsewhere, however, where the host and intrusive lithologies are similar, the bodies are more difficult to identify. Remond (1986) describes ultramafic and mafic bodies in the southern part of Lestóvounos, which intrude intermediate stratigraphic levels in the layered sequence.

These are in the order of 100-200m in size, are highly irregular in shape and have diffuse unchilled margins. They are lithologically similar to their cumulate counterparts and may only become visible when their margins are discordant with respect to the igneous layering in the host rock. Remond (*op. cit.*) notes that the mafic intrusives are gabbronorites (*sensu stricto*) and interprets them as late stage melts, possibly remobilised cumulates, which were injected into higher levels of the magma chamber.

In addition to the intrusive bosses described above, the layered sequence in the Lestóvounos (Vrysi) area is intruded by numerous dykes (figure 2.2 and plate 2.2). These are discussed in section 2.6.

2.3.7 Attitude of layering

Early models of magmatic processes at spreading ridges involved large steady-state magma chambers crystallising sub-horizontal layers of cumulates by gravity settling mechanisms (Greenbaum 1972). With the appreciation of the importance of *in situ* crystallisation, however, (McBirney and Noyes 1979) it was realised that crystal nucleation was not only possible but likely parallel to the walls of the magma chamber, and that layering could therefore form at very steep angles. Casey and Karson (1981) were able to demonstrate the non-parallelism of the igneous layering in the Bay of Islands ophiolite, and Browning (1982) and Rothery (1982) concluded from studies of the plutonic section of the Oman ophiolite that the attitude of the layering steepened and became more irregular in orientation with stratigraphic height.

In the ELFC, given the high degree of disruption and differential rotation suffered by blocks of the axis sequence crust (chapter 5) and lack of any reliable palaeohorizontal indicators, the spatial organisation and original attitude of the cumulates is difficult to discern. In the Lestóvounos area the layering is close to vertical, and may dip either towards the north or the south, although way-up indicators consistently 'young' northwards. Although brittle tectonism has locally modified the attitude of the layering, over a scale of tens to hundreds of metres it is relatively consistent, generally swinging

only gently in strike from ENE in the eastern Lestóvounos area to E-W and thence WNW to the west of the Kellaki-Parekklisha road (although see below; figure 2.2). Remond (1986) attributes this swing to primary magmatic processes, and suggests that a primary difference of some 20–30° in dip originally existed between the cyclically layered ultramafics low in the plutonic sequence and the laminated gabbros at the top.

In the area around 149512 doleritic dykes, occasionally multiple, are locally abundant and have shallow southerly dips, which are at a uniformly high angle to the layering (74°± 10°, according to Remond 1986; plate 2.2). Although the assumption is not likely to be strictly true, under normal circumstances dykes are thought to be intruded close to the vertical (see section 2.5), suggesting that tectonic rotation of the Lestóvounos block was significant and that the original dip of the layering was moderate.

2.3.8 High-temperature deformation of the layered sequence

To the south of Kellaki high-level plutonics grade down into cumulate gabbros and thence, without significant tectonic interruption, into 'transition zone' layered gabbros and ultramafics at Vrysi (148512 Lestóvounos; see sections 2.3.4 and 2.4). These rocks have regular, uniform phase layering, and in thin section display primary cumulus textures modified only by minor hydrothermal alteration.

However, a marked change in the character and attitude of the layering is apparent at 14835101, a roadside exposure on the main Kellaki–Parekklisha road. To the south of this point (figure 2.2) the layering becomes disturbed: boudinaging of ultramafic horizons is common, and in places is accompanied by the open flexure and occasional wholesale truncation of the layering (plate 2.3). The deformed cumulates generally have NW strike, but within a hundred metres of the contact boudinage of the ultramafics becomes extreme, and the layering deflected clockwise to a N and thence NNE strike, before being truncated abruptly by the undeformed cumulates, which dip steeply and strike E-W. Deformation in the cumulates can be identified for at least 0.5km to the south of the

Plate 2.3: Ductile shear zone truncating layering in plutonic complex. 14815053 Lestóvounos.

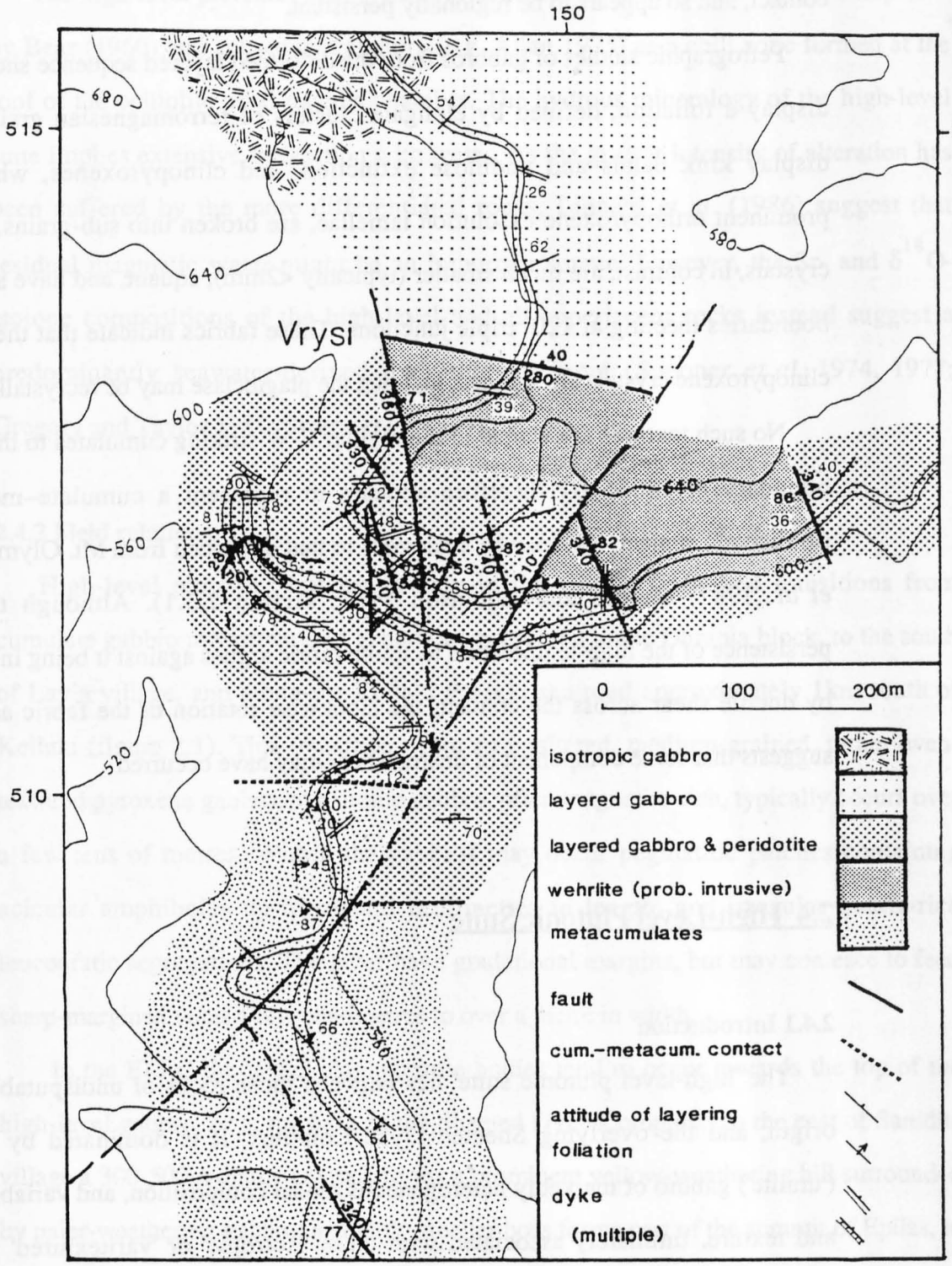

Figure 2.2: Geological sketch map of the Vrysi (Lestóvounos) area, Kellaki–Parekklisha road. Isotropic gabbros to the north grade down into layered gabbros and thence gabbros and peridotites. At 14875101, however, the regular layering is replaced by highly irregular, disturbed layering with heavy boudinage of ultramafic layers and a foliation in mafic layers. Note presence of thick massive wehrlites, probably intrusive, and numerous mafic dykes now tilted to a low angle.

contact, and so appears to be regionally persistent.

Petrographic studies of gabbros from the deformed layered sequence shows that they display a foliation, defined by elongate clusters of ferromagnesian grains. Olivines display kink bands and undulose extinction, and clinopyroxenes, which contain prominent orthopyroxene exsolution lamellae, are broken into sub-grains. Plagioclase crystals, in contrast, are much smaller (typically <2mm), equant, and have straight grain boundaries meeting at 120° triple junctions. These fabrics indicate that the olivine and clinopyroxene crystals are strained, and that the plagioclase may be recrystallised.

No such textures are visible in the regular E-W striking cumulates to the north. The boundary at 14835101 therefore appears to represent a cumulate–metacumulate (intrusive?) contact, and may be analogous to that described from Mt. Olympus (Malpas *et al.* 1987, Malpas and Robinson 1987; section 2.3.1). Although the regional persistence of the high-temperature tectonite fabric argues against it being induced solely by ductile shear across the contact, the clockwise rotation of the fabric adjacent to it suggests that some component of dextral shear may have occurred.

2.4 High-Level Plutonic Suite

2.4.1 Introduction

The 'high-level plutonic suite' lies between those rocks of undisputably cumulate origin, and the overlying Sheeted Dyke Complex. It is dominated by hornblende ('uralite') gabbro of markedly heterogeneous modal composition, and variable grain size and texture. Intimately associated with these 'isotropic' or 'varitextured' gabbros are veins and minor plutons of low-potassium diorite, tonalite, trondhjemite and granophyre, collectively referred to as 'plagiogranites' by Coleman and Peterman (1975) and Aldiss 1978).

The high-level plutonic rocks were first described by Wilson (1959), and interpreted by Bear (1960) and subsequent authors (*e.g.* Allen 1975) as a chill zone formed at the roof of the ophiolite axial magma chamber. The hydrous mineralogy of the high-level suite implies extensive interaction with water. As the greater intensity of alteration has been suffered by the more differentiated rocks, Lippard *et al.* (1986) suggest that residual magmatic water might be an important source; however, the Sr- and $\delta^{18}O$-isotope compositions of the high-level and all superjacent rocks instead suggest a predominantly seawater-derived hydrothermal input (Spooner *et al.* 1974, 1977; Gregory and Taylor 1981; Stakes *et al.* 1984).

2.4.2 Field relations

High-level plutonics outcrop widely in the ELFC. Unfaulted transitions from cumulate gabbro to varitextured gabbro are preserved in the Dhrapia block, to the south of Layia village, and along the Kellaki-Parekklisha road approximately 1km south of Kellaki (figure 2.1). This transition, from an unaltered, medium-grained, rather even-textured pyroxene gabbro, to a uralite gabbro, often magnetite-rich, typically occurs over a few tens of metres. Within the gabbros may occur pegmatitic patches containing acicular amphiboles up to several centimetres in length, and irregular quartz-rich leucocratic segregations. The latter have gradational margins, but may coalesce to feed sharp-margined veins a few centimetres to over a metre in width.

In the ELFC the larger plagiogranite bodies tend to occur towards the top of the high-level gabbro, or at the base of the Sheeted Dyke Complex. To the east of Sanidha village a 300-500m diameter stock forms a prominent yellow-weathering hill surrounded by paler-weathering gabbro; a slightly smaller boss forms part of the summit of Epilas, to the north of Monagroulli. Columnar jointing has been reported in such bodies (Aldiss 1978), implying that they existed as true melts and cooled statically. Net-like feeder veins of plagiogranite may be visible in the high-level gabbros surrounding them, but the margins of these plutons with gabbro are rarely sharp. They may rather be regarded as

Plate 2.4: Pale plagiogranite (tronhjemite) stoping up into and incorporating xenoliths from a (dark grey) dolerite dyke at the base of the Sheeted Dyke Complex. 19765116 Vasa village.

segregations on a much larger scale than described above, derived by the upward migration and coalescence of acidic material through a gabbroic host presumably still partly plastic. The upper margins of the plagiogranites, however, when in contact with the base of the Sheeted Dyke Complex, may display more obvious intrusive relationships: the incorporation of dyke xenoliths of diabase into trondhjemite by stoping is observed at 19765116 Vasa (plate 2.4), and has been identified as an important means of introducing water into the plagiogranite melt (*e.g.* Gass and Smewing 1973, Aldiss 1978).

2.4.3 Petrography

The varitextured gabbros are characterised by the replacement of primary igneous pyroxene by uralite, which is defined by Deer *et al.* (1966) as a 'secondary fibrous light blue-green amphibole of undetermined composition'. In the stratigraphically lower parts of the high-level plutonic sequence the pyroxene may be only partially pseudomorphed, and rare (usually clino-) pyroxene may be preserved in the cores of the subhedral-euhedral crystal outlines. Plagioclase, in contrast, remains relatively fresh, although the larger equant phenocrysts in particular may become markedly zoned. Smaller interlocking laths of plagioclase give rise to a hypidiomorphic granular texture; these are commonly rimmed by tiny green amphibole fibres. Quartz is rare in the pyroxene-bearing gabbros, but may occur in accessory quantity as an interstitial phase. The co-existence of fresh calcic plagioclase with fibrous green amphibole is taken to be indicative of upper actinolite facies metamorphism (Smewing 1975).

Certain gabbro and diorite–trondhjemite samples contain significant proportions (occasionally up to 10%) of opaque minerals, apparently dominated by magnetite. In the more evolved rocks these opaques form tiny (~0.1mm) equant subhedra, but in the gabbros large crystals up to 4mm in diameter showing skeletal textures, indicative of rapid growth, occur. The sudden precipitation of magnetite from the melt is thought to

result from a critical increase in oxygen fugacity following saturation of the magma by seawater (Aldiss 1978). This leaves a high-silica residuum which, with the consequent lowering of the plagioclase liquidus temperature, is able to segregate efficiently from the varitextured gabbro host.

Rare millimetre-sized patches of quartz with allotriomorphic granular textures form the microscopic equivalents of the leucocratic segregations. However, quartz is more frequently observed as a minor interstitial phase in diorites and quartz diorites, in which green acicular hornblende, probably primary, forms the dominant mafic phase. No pyroxene has been identified. In these intermediate rocks plagioclase may show signs of partial saussuritisation: grains have a dusty appearance with the growth of minute hornblende, epidote, clinozoisite and probably also prehnite, albite, sericite and quartz crystals. Sphene may also be present as tiny equant subhedra with the alteration of opaques and plagioclase, and epidote may form aggregates up to 2mm in length. This secondary mineral assemblage suggests deuteric alteration or metamorphism at upper greenschist or lower actinolite facies, confirmed by the trapping temperatures of 370–450°C obtained from saline fluid inclusions in secondary quartz grains in plagiogranite (J.G. Cowan *pers. comm.* 1987). The presence in some examples, however, of chlorite replacing hornblende suggests that some retrogression has occurred.

The most evolved compositions within the plagiogranite spectrum are tonalites (20–40% mafics) and trondhjemites (<20% mafics), which are found in the larger bodies. The texture in these rocks varies from allotriomorphic or hypidiomorphic granular to granophyric. Secondary quartz-albite granophyre may form spectacular plumose intergrowths forming up to 50% of the mode, surrounding partially saussuritised, strongly zoned plagioclase. Intergrowths of secondary epidote and clinozoisite are common, and in some examples the granophyric texture is overprinted by secondary allotriomorphic granular quartz.

2.5 Sheeted Dyke Complex

2.5.1 Introduction

Dykes of the Sheeted Complex ('the diabase' of earlier workers, *e.g.* Bishopp 1952, Wilson 1959) are hypabyssal rocks which represent feeders from the plutonics of the axial magma chamber below (section 2.5.2) to a volcanic, largely pillowed, suite above (section 2.5.4). The gradational lower and upper margins of the complex with the high-level gabbros and the pillow lavas respectively is good evidence for their consanguinuity. As its name suggests, the Sheeted Dyke Complex consists essentially of 100% near-parallel, originally vertical, basic dykes (Wilson 1959) which, on Troodos, are predominantly north-south trending and extend across strike for more than 90km, from Pomos near Polis in the west to Stavrovouni Monastery in the east.

The presence of 100% dykes, representing 100% extension, is still the strongest evidence for the formation of the Troodos ophiolite at a constructive plate margin (Gass 1968, Moores and Vine 1971). Theoretical models of dyke intrusion at a spreading centre, based on average dyke thicknesses and preferential chilling directions (Kidd and Cann 1974, Kidd 1977) suggest that the injection zone at the Troodos ridge was narrow, possibly less than 50m wide. Recent studies of the spreading structure of the Troodos ridge (*e.g.* Varga and Moores 1985, Allerton and Vine 1987) have demonstrated the complexity of the spreading geometry, and the temporal and spatial instability of individual ridge systems. The spreading structure of the Troodos ridge–transform system is discussed in more detail in chapter 7.

2.5.2 The base of the Sheeted Dyke Complex

In places varitextured gabbros and plagiogranites form screens up to 2m in width between dykes for at least 200m above the base of the sheeted complex. The proportion of such screens increases with depth until high-level plutonics predominate; however, the most rapid increase in dyke density (from perhaps >70% to <30%) takes place over a vertical distance of a few tens of metres, and this is arbitrarily taken as the base of the sheeted dyke complex. In Oman (Rothery 1983) and on Troodos (Allen 1975) it has been possible to observe individual dykes rooting in isotropic gabbro (figure 2.3). Pairs of vague doleritic chill zones up to 10m apart effectively delineate gabbro dykes within a gabbroic host. Over a vertical distance of *c.*25m the distance between chills narrows to *c.*1m and the grain size of the internal portion diminishes to that of a typical dolerite (Rothery *op. cit.*).

Lack of exposure and tectonic complexity preclude such a complete description of dyke rooting in the ELFC. Here, in outcrops of high-level varitextured gabbro close to the sheeted dyke transition (e.g. 124524, 1km west of Prastion, figure 2.1), vaguely defined areas up to 10-20m in width of finer-grained microgabbro and dolerite are observed, with which chilled dolerite veinlets are occasionally associated. Immediately below the base of the dyke swarm these doleritic–microgabbroic bodies may themselves display chilled margins against the gabbro, forming 'megadykes' 4-5m in width with similar strike to the overlying sheeted dykes, which have an average width of less than 1m.

Intrusions of trondhjemitic material into the dolerite 'megadykes' (plate 2.4) suggest that the latter, as feeder zones or dyke 'precursors', are an integral part of the axial spreading process. The mutually contradictory intrusive relationships between the dykes and the plagiogranites attest to the continuation of magmatic activity in the magma chamber roof zone away from the immediate environs of the sheeted dyke injection zone (*cf.* Bear 1960, Rosencrantz 1983, Pedersen 1986).

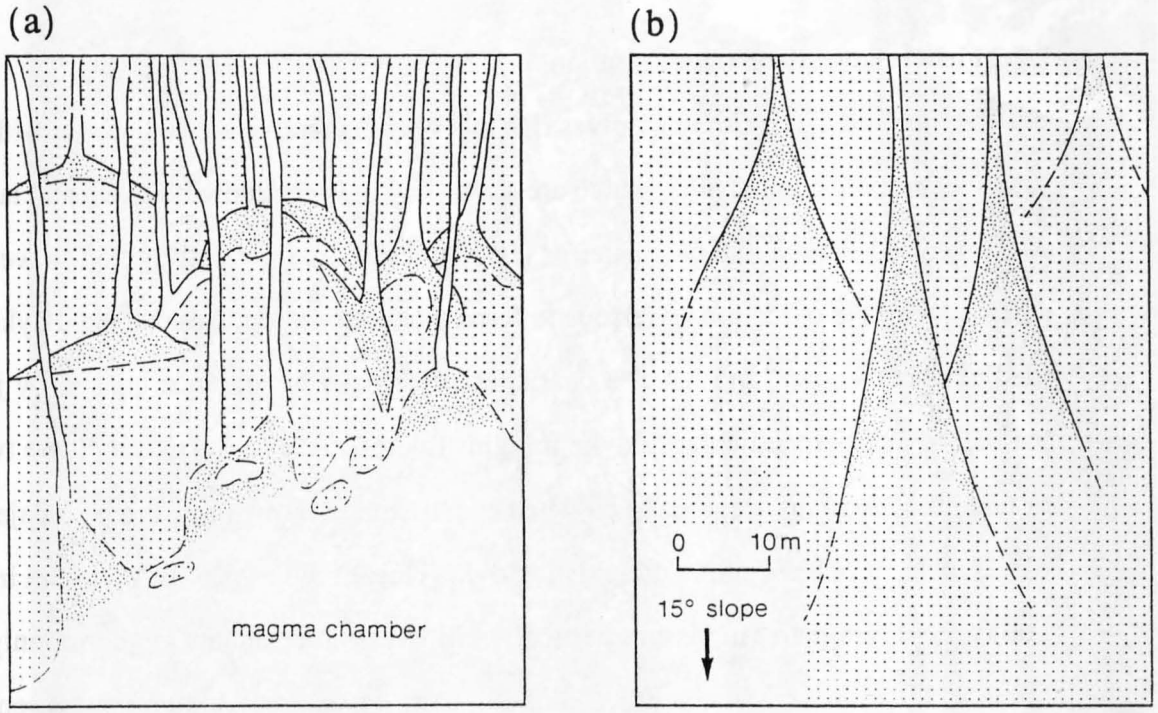

Figure 2.3: Rooting of dykes at the base of the Sheeted Dyke Complex. (a) as proposed by Allen (1975) for Troodos; (b) as proposed by Rothery (1982) for Oman. Blank = dolerite dyke; close stipple = fine-grained gabbro and diorite; coarse stipple = coarse gabbro and diorite. From Lippard *et al.* (1986).

2.5.3 Field relations and mineralisation

The Sheeted Dyke Complex gives rise to a very distinctive incised terrain with steep-sided but smooth conical hills, which are often thickly vegetated with thorn and lavender. A marked red-orange hue of greater or lesser intensity is frequently given to weathered surfaces with the oxidation of ferrous to ferric iron. In outcrop, fresh sheeted dykes are a medium-grey colour, and have a characteristic blocky appearance caused by jointing parallel to and perpendicular to dyke margins (plate 2.5). The dykes may have two, one or no chilled margins, depending on whether subsequent intrusions have been injected up a dyke margin or have split a pre-existing dyke. Unsplit dykes may be up to 2m in width, but average less than 1m; assymmetrically-chilled dyke remnants are commonly in the range 0.3-0.75m thick. The chilled margins themselves are usually about a centimetre wide and have a dark, flinty appearance and glassy basaltic texture. They may be highly sinuous and follow minute irregularities in the surface of their host exactly, suggesting that they were intruded passively.

Brittle shearing sub-parallel to the dyke margins is very common, giving rise to a ribbon-like appearance in sections oblique to the strike, and frequently obliterates the chilled margins. For this reason analyses of preferential chilling directions in order to determine the possible position of the palaeo-spreading axis with respect to the ELFC (as attempted by Kidd and Cann 1974 and Kidd 1977) were not possible.

Indurated interdyke fault breccias, whose formation distinctly predates the brittle deformation noted above, are common in some areas. They are usually a few centimetres in width, contain angular dolerite fragments cemented by epidote and quartz, and may be weakly mineralised. A blue coloration in fresh outcrops weathers to a vivid rusty red. Uniquely, a 200m wide zone of such breccia is developed between Kokkinokhomata (215502) and Kokkines (220510), 1km west of the Kalavasos Mines, giving rise to a prominent NE-trending oxidised zone (*N.B. kokkina* [Gk.] = red). In view of its

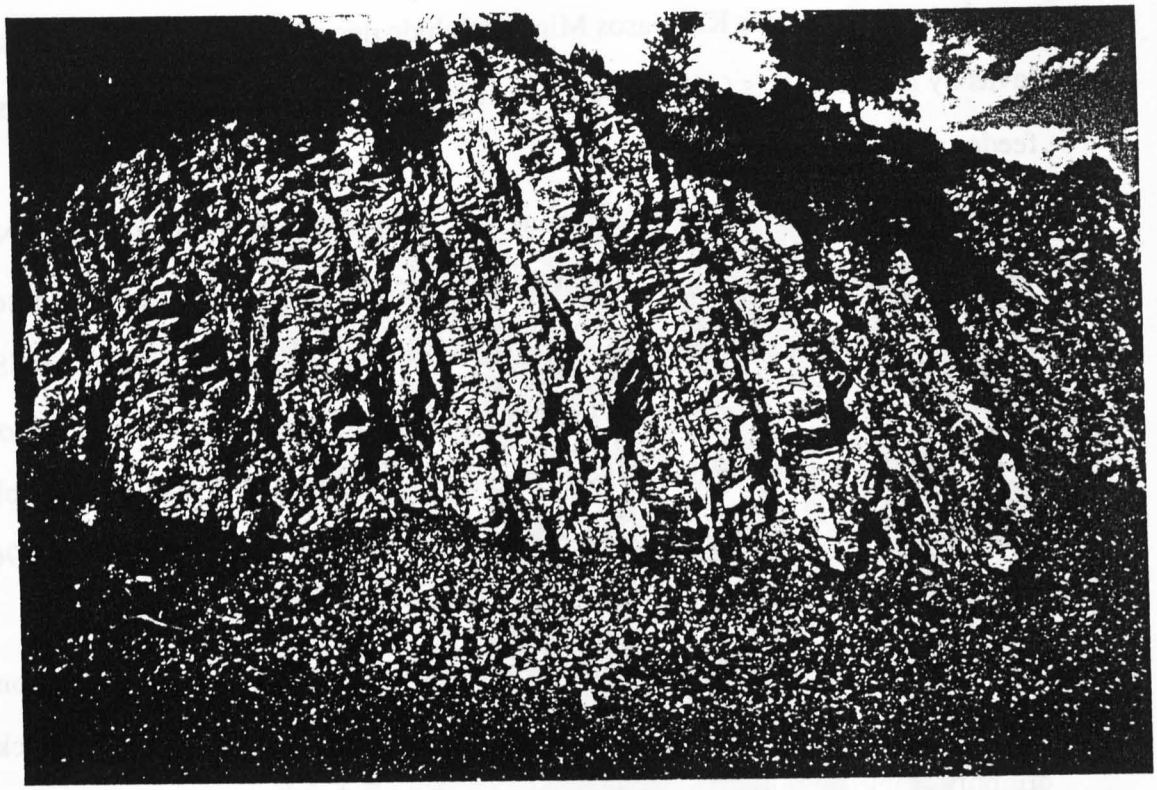

Plate 2.5: Typical appearance of relatively pristine Sheeted Dyke Complex. 18944880 Epilas.

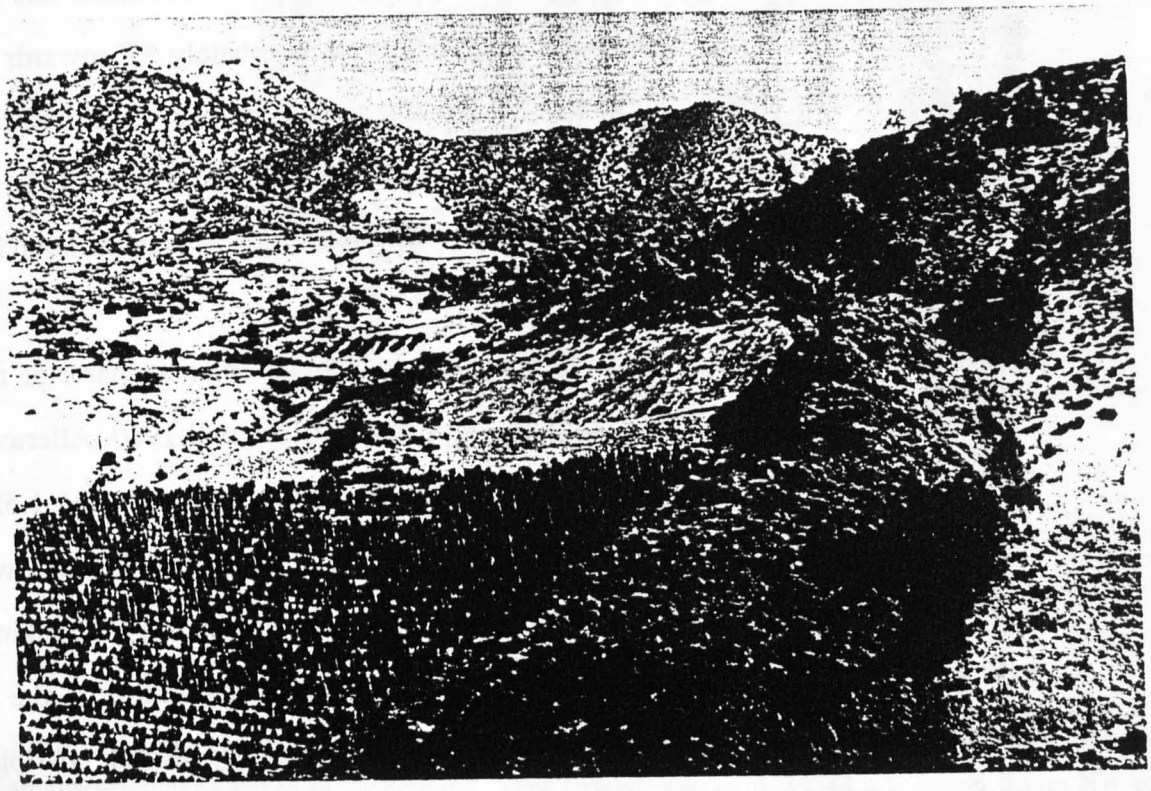

Plate 2.6: View looking northeastwards along the line of the prominent NE fault at Ornitha/Ornithouri. The fault separates lavas to the left from oxidised Basal Group (with NE-striking dykes) to the right, is mineralised, and is now marked by an elongate zone of red-brown gossan. 173465, 2km N of Pyrgos.

proximity to the major Kalavasos Mines sulphide deposits, known to be localised in the lavas by NE structures (Adamides 1980, 1984), it is possible that this represents a major feeder zone to the ore bodies.

Elsewhere in the ELFC gossan zones often lie along major dyke-parallel NE faults within or bounding the Sheeted Dyke Complex. The most prominent of these can be traced for nearly two kilometres along a NE fault from the Pyrgos River (163458, 1.5km NNW of Pyrgos) to Ornithouri 175467), and downthrows aphyric 'lower' pillow lavas on its NW flank down against 'Basal Group' sheeted dykes with lava screens (plate 2.6; see below). This zone was the subject of several prospects in the 1950s and 1960s, but was not found to be economically viable (Pantazis 1967).

In the Kythreotis roadstone quarry at Pevkos (138497), sheeted dykes containing disseminated pyrite are cut by a broad shallow angle fault zone with a 2-3m thickness of crumbly black sulphide-rich gouge and veins of fresh massive pyrite. Palaeomagnetic studies of the area (site B1: see chapter 5) suggest that prior to rotation this fault was originally parallel to the dyke strike but dipped at approximately 55° towards the east-southeast; it thus appears identical in character to the ore-bearing structures in the Kalavasos Mines, which have been interpreted by Adamides (1980, 1984) as ridge-parallel normal faults, and compared to the mineralised fracture systems bounding mid-ocean ridge axial valleys (*e.g.* Macdonald 1982).

Cross-cutting sheeted dyke relationships, locally common in parts of the main Troodos Sheeted Complex (*e.g.* Lefkara–Stravrovouni: Bagnall 1960, Allerton 1988), have in the ELFC been identified only in the Monagroulli area. In the 1.5km long Monagroulli block sheeted dykes have an ENE strike and dip at *c.*50-75° northwards. At 19084529 these dykes are cut by individual brownstone-weathering NE-striking dykes with a moderate southeasterly dip. At 19344561 (palaeomagnetic drill site B8: see sections 2.5.6 and 5.5.2) the N-dipping sheeted dykes are cut by several, possibly many, sheeted multiple dykes with a SE dip. These are hard, grey-weathering dolerites and are themselves cut by sinuous, highly chilled basaltic-textured veinlets (plate 2.7). The two

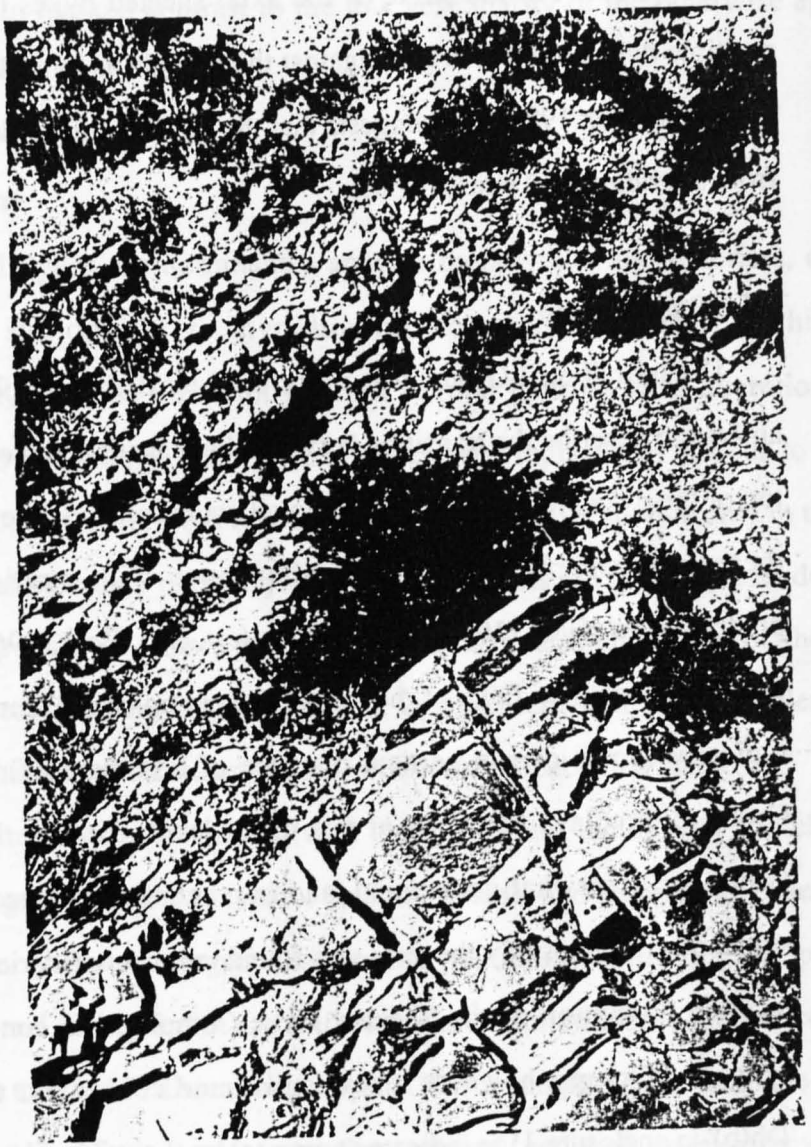

Plate 2.7: Cross-cutting sheeted dykes. Northward-dipping dykes in the foreground are cut by thinner southward-dipping dykes in background. View looking westward. 19344561, stream 0.5km NW of Monagroulli village.

dyke sets have the same magnetisation vectors (chapter 5), which suggests that no significant rotation of the first set took place before the intrusion of the second. The 80° difference between the strike of the axial sheeted dykes (ENE) and the cross-cutting multiple dykes (NNW) argues against their origin as hybrid extensional shear/conjugate pairs (Hancock 1985) and suggests that the cross-cutting dykes were intruded later, away from the ridge axial stress regime.

2.5.4 Basal Group

The term 'Basal Group' was introduced by Bishopp (1952) and subsequent Survey authors to describe the transition between the diabase and the lava sequence. Towards the top of the dyke swarm screens of pillow lava become visible between dykes; thenceforth these increase progressively in abundance with stratigraphic height until lava predominates. Gass (1980; after Wilson (*op. cit.*), Bear (1960), and Gass (1960)) notes that on the northern flank of the massif a rapid transition from <5% to >50% pillow lava typically occurs over a vertical distance of less than 100m, and he places his Basal Group–pillow lava boundary at this upper level. Clearly, the boundaries to the Basal Group are somewhat gradational, and in practice their placement in the field is highly subjective. In this study the term was found to be unwieldy in the field on account of the tectonic disruption of the Sheeted Dyke Complex and consequent lack of continuity between outcrops; however it was still found convenient to retain 'Basal Group' (as 'Db(p)' in enclosure 1) to indicate at map scales the approximate stratigraphic positions of outcrops within the sheeted dykes (*sensu lato*).

Basal Group terrain is relatively less elevated and prominent than sheeted dyke country, because it is commonly metamorphosed to the zeolite, rather than lower actinolite, facies. Consequently, dykes and lavas in Basal Group outcrops have a greenish to khaki-buff colour and are softer than the uniformly mid-grey fresh sheeted dykes. The pillows are globular, interlocking, range from 0.5-1.0m in diameter and are

clearly cut (and occasionally brecciated) by the intruding dykes. The lava itself is aphyric, completely devitrified and frequently highly vesicular (estimated at >20% at the top of the pillow). This is in marked contrast to the low vesicularity of the otherwise apparently identical dyke rock.

2.5.5 Petrography

The sheeted dykes are dominantly aphyric metabasalts and dolerites, originally possessing a sub-ophitic to hypidiomorphic granular texture, which have characteristically suffered ubiquitous partial or total hydrothermal alteration of their primary igneous mineralogy. Clinopyroxene has been replaced by fibrous to prismatic green or brown hornblende; fresh relicts are rare and normally survive only in the centres of the occasional pyroxene phenocrysts. Plagioclase laths are typically pseudomorphed by a dusty aggregate of albite, possibly with quartz, although hints of the original twinning (and occasional zoning) may remain. Opaques remain in the metadolerite, but as minute disseminations of secondary origin, which are probably haematite.

Granular intergrowths of quartz (with abundant fluid inclusions) and chlorite are common in the groundmass, as is minor epidote, sphene, and prehnite. In examples from the Pevkos quarry these intergrowths become important, destroying the plagioclase pseudomorphs and giving rise *in extremis* to a quartz-albite-chlorite-epidote rock, which may contain up to 10-15% disseminated pyrite. These samples come from the vicinity of the major mineralised fault zone (see previous section), and their more extreme degree of alteration is presumably a reflection of the more vigorous hydrothermal activity along the fault zone.

The end product of this extreme deuteric alteration in sheeted dykes and high-level plutonics alike is the formation of an epidosite, which is a quartz-epidote rock (± sphene). These are highly leached rocks which delineate upflow zones below the major sulphide ore bodies on Troodos (*e.g.* Schiffman *et al.* 1987). No epidosites

proper have been observed in the ELFC.

The presence of actinolite (hornblende) in many of the metadolerites is taken to be indicative of lower actinolite facies metamorphism (Elthon and Stern 1978, Lippard *et al.* 1986). However, this hornblende, which replaces clinopyroxene, is itself partially replaced by chlorite. Such disequilibrium textures are common and are always retrogressive; this is characteristic of ocean-floor type hydrothermal metamorphism and appears to reflect the waning of individual convective cells (*e.g.* Cann 1979). Rare vesicles in the metadolerites are infilled with quartz, albite, epidote, calcite, chlorite and prehnite, indicative of lower greenschist facies metamorphism.

Basal Group dykes share a similar doleritic (sub-ophitic to intergranular) texture to that of the sheeted dykes (*sensu stricto*). Plagioclase, occasionally forming phenocrysts, is albitised, but clinopyroxene is frequently fresh or has suffered only partial replacement by chlorite. Secondary alteration in the groundmass is characterised by intergrown granular quartz and calcite. The absence of hornblende after clinopyroxene suggests that the Basal Group never reached more than zeolite–lower greenschist facies,.

Basal Group lavas have an intersertal texture, with radiating plumes of plagioclase laths and acicular clinopyroxene set in a matrix of brown devitrified palagonite glass. Quartz and calcite infill vesicles. The palagonitised glass may indicate further retrogression to zeolite facies. It is significant to note that some late dykes, characterised by greenschist facies metamorphic assemblages, cross-cut lower actinolite facies sheeted dykes, thus emphasising the 'off-axis' origin of the late intrusives (see section 2.6).

2.5.6 Attitude of the Sheeted Dyke Complex across the ELFC

Theoretical considerations of the mechanisms of magma intrusion into brittle and semi-brittle rock (Anderson 1951, Roberts 1970) have shown that dykes are intruded along a plane approximately perpendicular to σ_3, the minimum principal compressive stress direction. In both normal and strike slip systems σ_3 is horizontal (figure 2.4; Anderson *op. cit.*), and so dykes injected in either stress regime (or a combination of

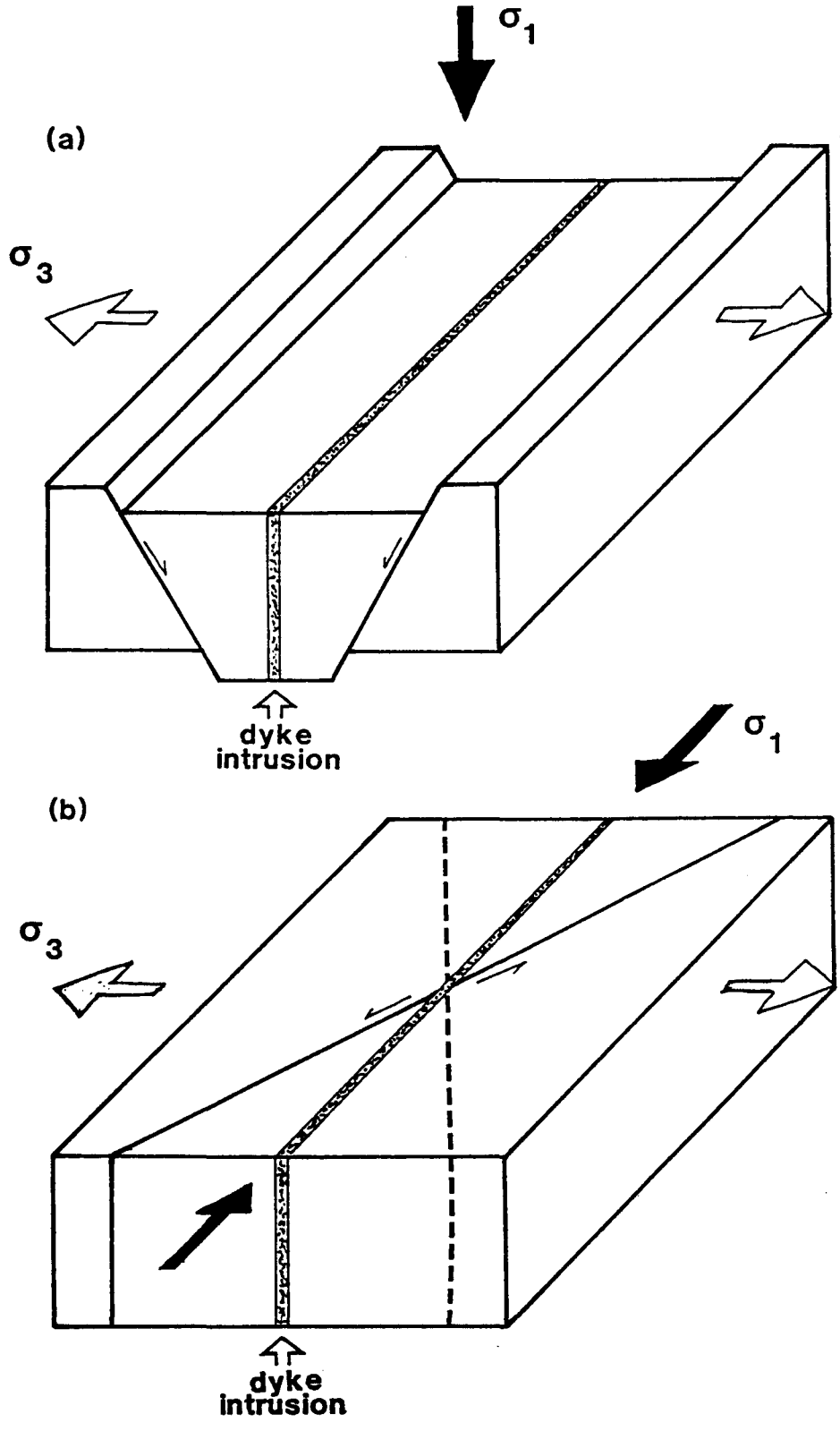

Figure 2.4: Block diagram illustrating the hypothetical relationship between the orientations of the maximum (σ_1) and minimum (σ_3) principal stress axes, faults and dykes in (a) normal faulting, and (b) strike-slip faulting regimes. Dyke injection is approximately perpendicular to σ_3 and is thus vertical in both normal and strike-slip regimes.

both) will be intruded close to the vertical.

Sheeted dykes intruded at a constructive margin must be a product of a relatively long-lived and stable stress regime, unless rotations and cross-cutting relationships can be demonstrated. It therefore appears justifiable to assume that the dykes do indeed represent a palaeovertical, and implicit that the strike of the dyke on intrusion was the same as that of the constructive margin at which they were generated.

In the ELFC Sheeted Dyke Complex crops out across much of the area (figure 2.1). In the more southerly part, the blocks of Pevkos, Ornithouri (Pyrgos), Monagroulli, Epilas and Vasa-Kalavasos Mines, are all characterised by dykes with a regional NE trend and a moderate, usually SE, dip. On a smaller scale, however, this orientation is frequently modified by proximity to what often appear to be quite insignificant-looking faults, but which nevertheless must be responsible for sizeable local rotations.

In the remaining sheeted dyke outcrops in the northern ELFC (*viz.* Dhrapia–Klonari, Akapnou–Klonari, and the Akapnou Forest area to the north of Vasa), tectonic disruption is exceptionally widespread. The term 'Sheeted' Dyke Complex is somewhat of a misnomer here, as dyke margins are frequently obliterated, or can be traced for a few centimetres only. Such dykes as can be measured tend to have been tilted to a low angle and have a variable strike, indicating that tectonic rotation has been significant.

A detailed palaeomagnetic study of the SE part of the Troodos massif by Allerton (1988), has recently suggested that large areas of apparently quite coherent sheeted dykes in the Ayii Vavatsinias–Stavrovouni area have in fact suffered hitherto unsuspected rotations of up to 100° away from their original strike directions, about high angle axes of rotation (see section 7.2.3). In light of this, it must be questioned whether the NE regional orientation of sheeted dykes in the southern ELFC has any relevance to the orientation of the original spreading axis at which they were generated.

A limited palaeomagnetic study of the ELFC was carried out with S. Allerton with the initial intention of attempting to quantify some of the tectonic rotations geometrically

necessary to explain the structure of much of the area. The methodology and detail of the results is presented and discussed in chapter 5. However, one consequence of Allerton's method is that it gives two possible solutions for the original strike of a dyke upon intrusion, assuming that it was emplaced vertically. The sites are described individually in chapter 5 and the merits of the two alternative solutions at each site are debated; however, it is pertinent to discuss the solutions for the original dyke strikes here. The solutions obtained are shown schematically in figure 2.5. Of the five sites drilled in the sheeted dykes, preference can be indicated for one or other of the solutions at three of them (*viz.* B1 Pevkos, B6 Klonari and B8 Monagroulli) from external geological considerations discussed in chapter 5. At Klonari and Pevkos the paleomagnetics indicate an original N to NNE strike for the Sheeted Dyke Complex upon intrusion, and this is consistent with the inferred probable northerly strike of mineralised faults in the Kalavasos Mines (section 5.3).

The remaining data, however, are far from consistent. The Monagroulli site, with the cross-cutting sheeted dykes, yields an ENE strike (identical to the present-day strike) for the earlier set of dykes and a NNW strike for the later set, and the two remaining sites (B2 Asgata–Vasa road and B5 Dhrapia) give widely disparate solutions, with either NW or NE strikes. It is not thought that the wide scatter of original dyke strikes, particularly at the latter two sites, has any tectonic significance. It is beyond the scope of this study to discuss the statistical significance of the data, but in simplistic terms the orientations of the dyke magnetisation vectors with respect to the regional vector, and the orientations of the dykes relative to the poles of rotation, in the latter cases maximise and compound potential errors in the original dyke strike such that small inaccuracies in the measurement of dyke strikes in the field are magnified greatly (S. Allerton *pers. comm.* 1987). The statistics of the method are discussed in detail in Allerton (1988).

In conclusion, it is tentatively suggested that the original strike of the Sheeted Dyke Complex, and hence of the constructive margin at which they were generated, was

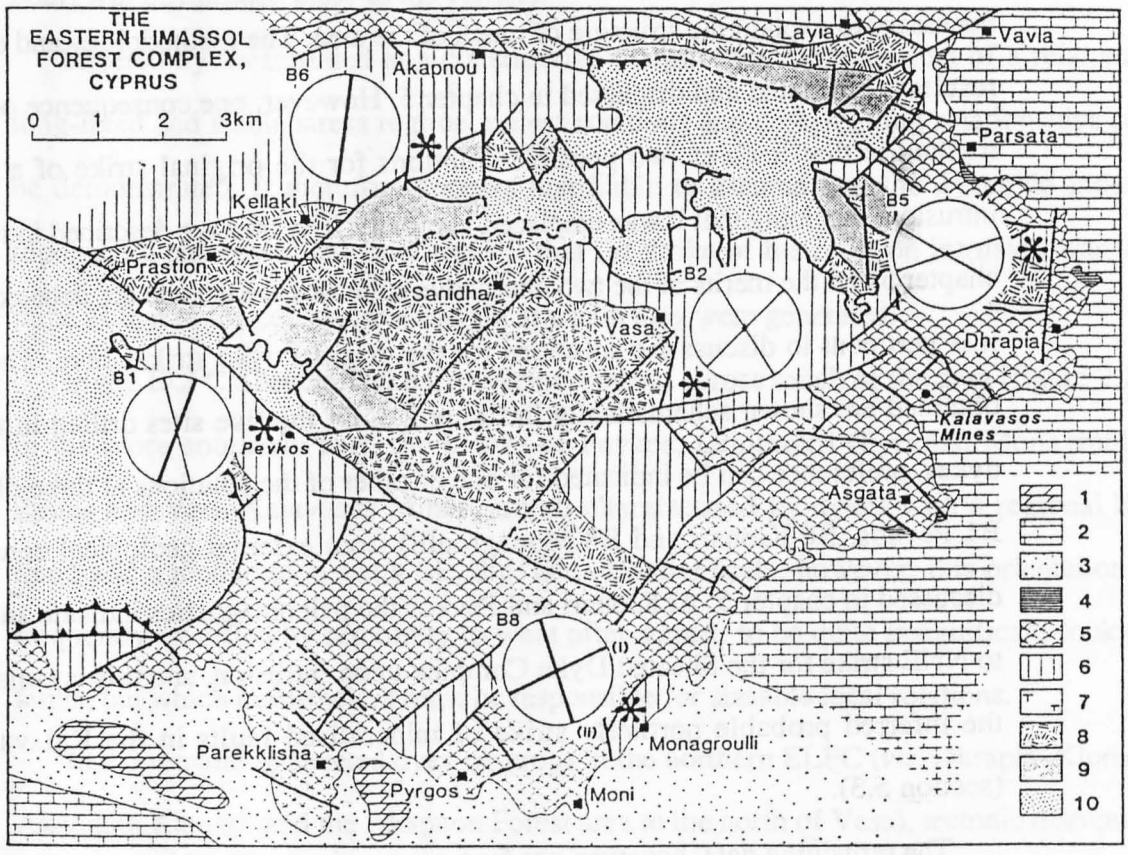

Figure 2.5: Simplified geological map of the Eastern Limassol Forest Complex., showing the original dyke strikes for sheeted dykes at (B1) Pevkos, (B2) Asgata–Vasa road, (B5) Dhrapia, (B6) Klonari and (B8) Monagroulli, deduced from palaeomagnetic data (sites denoted by asterisk *). Bold line at site B1 indicates preferred solution; at B8 (i) indicates early and (ii) late sets of dykes. At B2 and B5 no preference is indicated.

Sediments: (1): Miocene–Recent; (2): Maastrichtian–Miocene; (3): Campanian–Maastrichtian Moni mélange; (4): Turonian–Campanian Perapedhi Formation.

Igneous Rocks: (5): Pillow lavas; (6): Sheeted Dyke Complex; (7): Plagiogranites; (8): Gabbros; (9): Peridotites; (10): Tectonised harzburgites and dunites.

oriented between N-S and NE-SW (possibly NNE?). It is argued in sections 5.4 and 5.5 that the present day NE strike of the dykes across much of the area is a consequence of later rotations taking place about axes approximately perpendicular to the planes of the dykes. Wholesale rotations of *c.*100° of the sheeted dykes about high angle axes, as proposed by Allerton (1988) for Troodos do not appear to have occurred.

2.6 Post-Axis Sequence Intrusives

2.6.1 Field relationships

In preceding sections reference has been made to the presence at all stratigraphic levels, from the mantle sequence to the sheeted complex, of intrusive rocks that appear to postdate the crustal-generating ridge axial processes.

Fresh to partly serpentinised poikilitic wehrlites, petrologically similar to their layered counterparts, form rare dykes and bosses up to 50m in diameter in mantle sequence harzburgites and dunites, and the lowermost cumulate ultramafics of the Akapnou Forest. The dunites and cumulates are pervasively serpentinised, implying that the intrusion of the wehrlite postdated much of the serpentinisation, and that the host must therefore have been relatively cool (*i.e.* below the upper stability limit of serpentine of approximately 430°C (Bowen and Tuttle 1949)) at this time. Vague chilled (*i.e.* olivine-deficient) margins are occasionally visible (plate 2.14).

At 20095202 Koufkia (0.5km north of Vasa) a small wehrlite stock intruding serpentinised dunite is itself intruded by irregular gabbroic dykelets. In the Mazoukambos area, near the Vasilikos River, mafic dykes are locally very common. An east-west belt of strongly chilled sheeted multiple dolerite dykes up to 50m wide can be traced for almost a kilometre from 215530 to 222528, whence they are rotated into and deformed within a major N-S shear zone (see section 5.3.4). Undeformed dykes cutting this shear zone are evidence of the syntectonic nature of the magmatism, and recrystallisation of serpentine at

dyke margins again suggests that the serpentinisation at least partly predated intrusion.

Remond (1986) reports the presence of unlayered ultramafic and mafic bodies intruding the layered sequence at Lestóvounos, which she interprets as cumulates remobilised from the lower levels of the axial magma chamber (see section 2.3.6). Locally abundant in the same area (around 149512 Vrysi, see fig 2.2) are chilled dolerite and microgabbro dykes, occasionally multiple, which may be derived from these plutons.

At higher crustal levels (*i.e.* the high-level plutonics and sheeted complex) late-stage intrusives become more difficult to identify. However, cross-cutting dykes, which cannot have been intruded under the same stress regime as the axial dykes, are occasionally observed in the dyke complex (*e.g.* Monagroulli River: plate 2.7). Late, sinuous, bifurcating brownstone dykes up to 2m wide also intrude the sheeted complex, typically sub-parallel to the axial dyke sheeting. These have a crumbly-weathering appearance, which is thought to be the result of seafloor alteration at temperatures below ~50-100°C (Cann 1979).

2.6.2 Petrography

In the mantle sequence, dykes, when fresh, are typically orthopyroxene-, clinopyroxene- and occasionally plagioclase-phyric dolerites. They may also contain the distinctive and highly unusual composite phenocrysts of orthopyroxene mantled by clinopyroxene, which are characteristic of some of the more primitive Limassol Forest lavas (section 4.2.3). Possible genetic relationships between these dykes and the primitive lavas are discussed in the following section.

The primary texture of the dykes is reminiscent of the intersertal basaltic textures of the lavas, but with the interstices between plagioclase laths and elongate pyroxene prisms now occupied by fibrous chlorite and quartz, giving rise to an intergranular to ophitic texture. The texture is also commonly modified by fabrics indicative of brittle deformation, particularly of the pyroxene phenocrysts. This is a ubiquitous feature of

pyroxenite dykes in the mantle sequence (section 2.2.7), and has also been reported in similar doleritic intrusives in the WLFC (Murton 1986a).

The igneous texture of the intrusive dolerites may be partially or totally obliterated by the growth of a felted mat of fibrous tremolite and chlorite. Accessory sphene, prehnite and calcite may occur, and irregular isotropic patches may be hydrogrossular. This secondary mineral assemblage is characteristic of a rodingite, which is a metasomatic alteration product formed in a variety of mafic-silicic and sedimentary protoliths upon contact with serpentinite (Coleman 1977). The process of 'rodingitisation' covers a series of chemical reactions, all of which involve the addition of calcium and water and subtraction of silica. The calcium required for this is thought to be derived from the small amounts contained within peridotite, which is liberated upon its serpentinisation (Coleman *op. cit.*). In hand specimen, rodingites are distinctive white, flinty, sugary-textured rocks which are typically observed forming at the margins of dolerite bodies, or completely replacing the smaller dykes. They are invariably restricted in their occurrence to intrusives in the serpentinised mantle sequence and basal cumulates.

In the layered sequence intrusives are hydrothermally altered metadolerites and metagabbros characterised by actinolite facies metamorphic assemblages. Rare relict orthopyroxene and clinopyroxene phenocrysts survive, but are usually pseudomorphed by uralite, which in some specimens is accompanied by chlorite. Plagioclase may either be fresh or saussuritised.

In the sheeted complex, petrological and metamorphic differences exist between the axial dykes and the late cross-cutting intrusives. At 19574828 (Hellenic Mining Company old quarry, Epilas), aphyric lower actinolite facies sheeted dykes are cut by a porphyritic dyke containing phenocrysts of olivine (pseudomorphed by serpentine and carbonate), and fresh orthopyroxene, clinopyroxene and orthopyroxene/clinopyroxene composites. Originally glassy interstices between groundmass plagioclase laths are infilled by fibrous chlorite and accessory sphene, and there is little evidence to suggest that the rock was

ever metamorphosed beyond lowermost greenschist facies. Together with the ultra low-grade brownstone facies dykes (which also intrude actinolite facies sheeted dykes), there is clear evidence that a metamorphic discontinuity exists between the axis sequence and the late-stage intrusives.

2.6.3 Geochemistry

The similarity in petrology between the primitive lavas from the LFC and AFB and the late dykes suggests that they might be related. The lavas are also geochemically distinct, being characterised by extremely low abundances of the incompatible elements, particularly Ti and Zr, when compared with lavas from all other parts of Troodos (see chapter 4). If the dykes are cogenetic with the primitive lavas then they should share this unusual geochemistry. To investigate this, a number of dykes cutting the mantle sequence and layered sequence, and obviously discordant dykes from the Sheeted Dyke Complex, were analysed by X-ray fluorescence for the trace elements (see appendix 3).

The fields occupied on a Ti v Zr variation diagram by lavas and dykes from the main Troodos Massif (the 'axis sequence') and the LFC/AFB are indicated in figure 2.6(a). The cross-cutting dykes clearly share the depletion in Ti and Zr displayed by lavas erupted in the transform. More specifically, figure 2.6(b) shows that the dykes span the range of compositions displayed by lavas from the Kalavasos Mines analysed in this study (chapter 4). Flow units 'b' to 'e' represent 'off-axis' upper pillow lavas (see chapter 3) not genetically related to the underlying Sheeted Dyke Complex; instead it is possible that they were fed from the late cross-cutting dykes.

2.6.4 Significance of the post-axis sequence intrusives

Sub-Moho intrusives are generally rare in ophiolites. On Troodos Malpas *et al.* (1987) describe a 400m diameter layered body cutting harzburgites near the Hadjipavlou chromite mine, 1.5km south of Mt. Olympus, but this is similar to plutonics from the second, post-kinematic suite described by Malpas and Robinson (1987), and considered

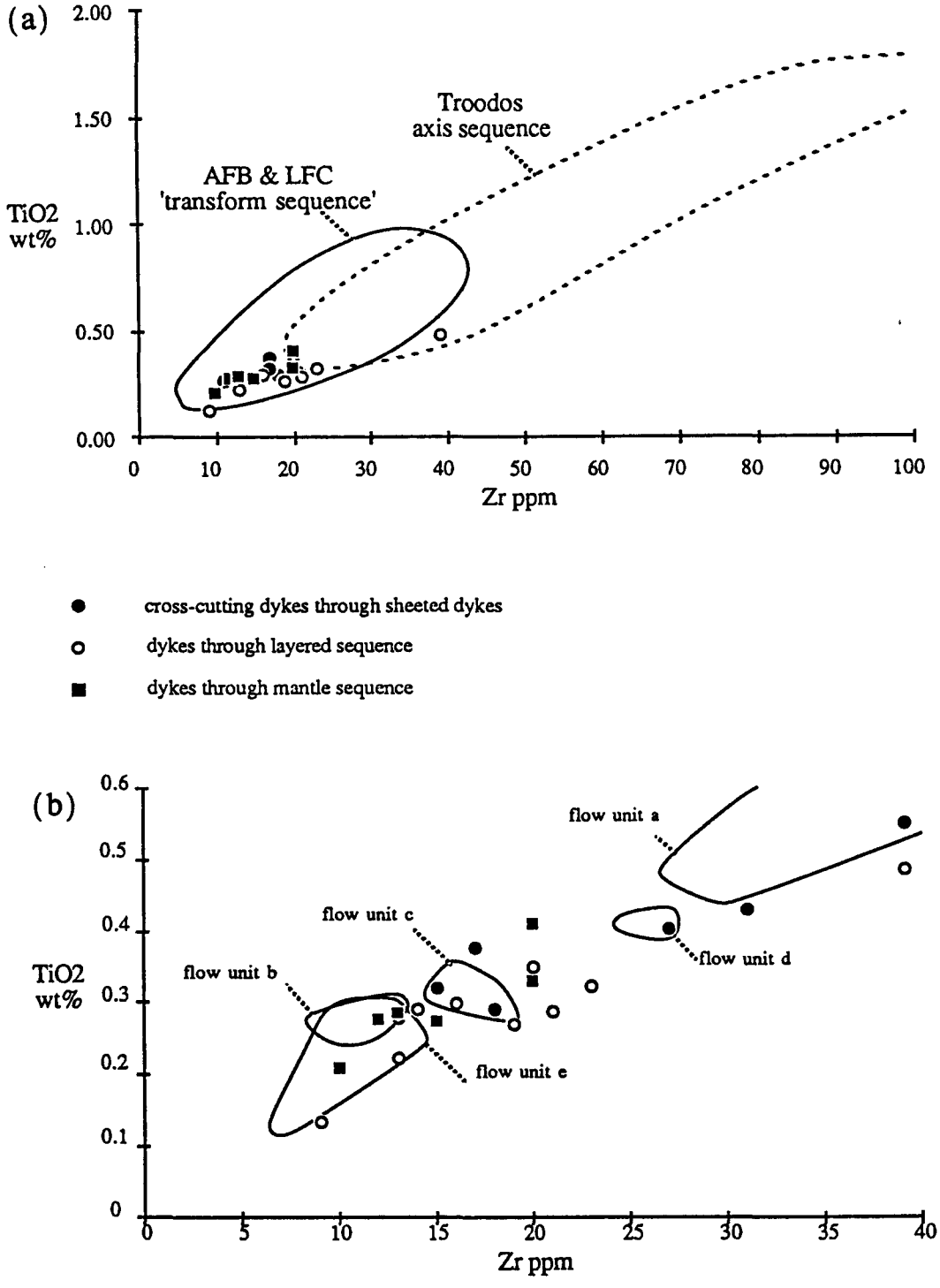

Figure 2.6: TiO_2 v Zr for late cross-cutting dykes in the ELFC: (a) showing their low Ti and Zr abundances and clear affinity with transform sequence, rather than axis sequence, lavas (fields after Simonian and Gass 1978); and (b) demonstrating the similarity of dyke and ELFC lava compositions. Lava flow units from the Kalavasos Mines, defined in chapter 4.

an integral part of the Troodos spreading structure.

In the western part of the LFC, however, Murton (1986a,b; — and Gass 1986; — and MacLeod 1987) describes abundant multiple plutons and associated dykes of massive wehrlite and of gabbro intruding the mantle sequence and a rotated and disaggregated axis crustal sequence (figure 2.7). These cut and are themselves cut by E-W strike slip shear zones associated with transform tectonism, suggesting that the intrusives are genetically related to transform processes. This led Murton (1986a,b) to define the ultramafic and mafic plutonics, dykes and associated extrusives collectively as 'transform sequence' oceanic lithosphere, distinct from that formed at a constructive plate boundary.

The cross-cutting post-axis sequence dykes in the ELFC are identical in their field characteristics, petrology and geochemistry to the 'transform sequence' dykes of the WLFC, and there is little doubt that they are consanguineous. However, important differences do exist between the two areas. In the WLFC, wehrlite plutons range from 0.6–1.2km in diameter, and the gabbros 1–5km. They are locally abundant; for instance, in the central core of the WLFC the transform sequence plutons, together with the dykes, account for up to 24% extension (Murton 1986b). The ELFC equivalent of the transform sequence, in contrast, is represented by a handful of wehrlite 'pips', a few tens of metres in diameter, and only a couple of dozen dolerite dykes.

The absence of major plutons in the Akapnou Forest could conceivably be explained by the difference in erosion levels between it and the central WLFC. The latter is much more deeply eroded, possibly as much as 1km below the petrological Moho, yet even at this level the plutons are frequently only partially unroofed. However, if major plutons were to exist beneath the Akapnou Forest or other parts of the ELFC, high density dyke swarms would be expected in the superjacent host rock, and this is rarely obseved. Although the distribution of transform sequence intrusives in the WLFC is patchy–the plutonics are mainly concentrated in two broad ENE-trending belts (figure 2.7), and significant areas (*e.g.* to the east of Akrounda) are apparently devoid of intrusives–it is

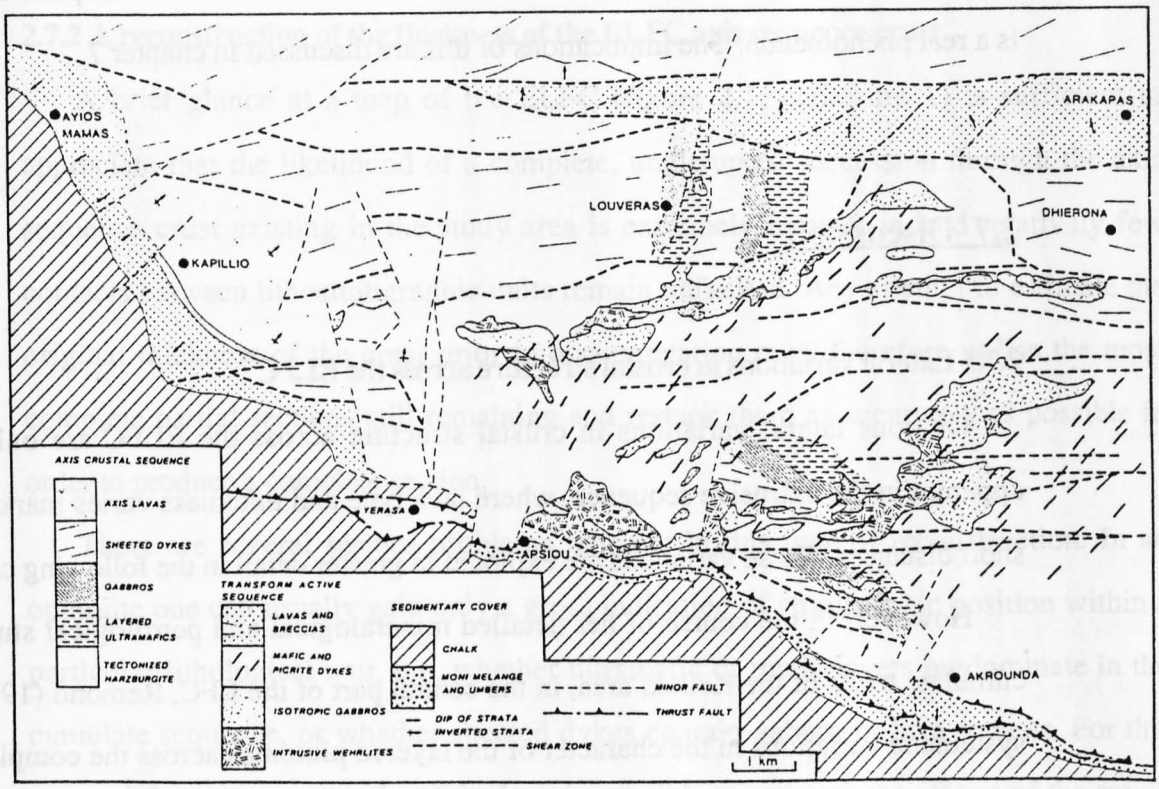

Figure 2.7: Simplified geological map of the Western Limassol Forest Complex, from Murton (1986a). Note large (≤5km) plutons of wehrlite and gabbro, and abundant dykes intruding the mantle sequence, in marked contrast to the ELFC, where dykes are rare and plutons absent.

concluded that the apparent difference between the eastern and western parts of the LFC is a real phenomenon. The implications of this are discussed in chapter 7.

2.7 Discussion

2.7.1 Lateral variations in crustal structure across the ELFC

Obvious lateral variations in crustal structure across the ELFC are only readily apparent in the extrusive sequence, where lava type and thickness varies markedly over short distances. These variations are explored in greater detail in the following chapter.

However, in the course of her detailed mineralogical and petrological study of the cumulate rocks of the Kellaki area, in the central part of the LFC, Remond (1986) noted systematic variations in the character of the layered plutonics across the complex. In the north, around Kellaki and Panayia tou Glossa, chrome spinel is abundant, and clinopyroxene relatively subordinate, so that dunites and troctolites predominate amongst the ultramafic lithologies. These rocks are fine-grained and the layering is regular. However, to the south, in the Lestóvounos area, the igneous layering is much less regular, clinopyroxene is abundant, and chrome spinel rare. The pyroxenes are much coarser grained than in the north, and have exsolution textures indicative of sub-solidus re-equilibration, suggesting that cooling was much less rapid than in the north. This led Remond (*op. cit.*) to suggest that the more southerly plutonics formed in the heart of the ophiolite magma chamber, whereas those to the north crystallised at its termination (presumably against the Arakapas Fault Belt).

Although this hypothesis is attractive, and probably preferable, it is also possible, if the disturbed contact zone at 14835101 does indeed represent an intrusive boundary (section 2.3.8), that the distinction she recognises could be the result of differences in composition and thermal history between two distinct magma chambers.

2.7.2 A reconstruction of the thickness of the ELFC axis sequence crust

A brief glance at a map of the ELFC (figure 2.1; enclosure 1) is sufficient to appreciate that the likelihood of a complete, undisrupted succession through the axis sequence crust existing in the study area is extremely remote; indeed relatively few contacts between lithostratigraphic units remain unfaulted. Any attempt to estimate the original thickness of the crust prior to disaggregation must therefore utilise the most complete partial sections still remaining and restack them as accurately as possible in order to produce a complete section.

There are several serious problems inherent in this type of reconstruction. In an ophiolite one can usually gain only a gross indication of stratigraphic position within a particular lithological unit, *e.g.* whether ultramafic or mafic layers predominate in the cumulate sequence, or whether sheeted dykes contain gabbro or lava screens. For this reason it becomes extremely difficult or impossible to estimate the effects of the small, apparently insignificant faults that are present in every section and which may cause parts of the sequence to be repeated or omitted. To complicate matters still further, dependable palaeohorizontal indicators are rarely present away from the lava sequence, so accurate estimations of the attitude of a particular block of crust are difficult to make. It should also be noted that boundaries between lithostratigraphic units are unlikely to be planar surfaces–data from the ICRDG borehole CY-4, for instance, suggests a relief of up to 300m on the base of the Troodos Sheeted Dyke Complex–so that estimates of thickness made in a particular area may not be representative of the complex as a whole.

Taking these imponderables into account, and where possible quoting a range of values from different parts of the complex, a reconstructed composite section through the ELFC axis sequence crust is presented in figure 2.8. The estimates are based mainly upon the present mapping, but incorporate the data of Adamides (1980, 1984) from the lava sequence and Remond (1986) from the layered plutonics. The total thickness thus obtained is between 3.5km and 4.4km, though it is probably wisest to conclude, bearing

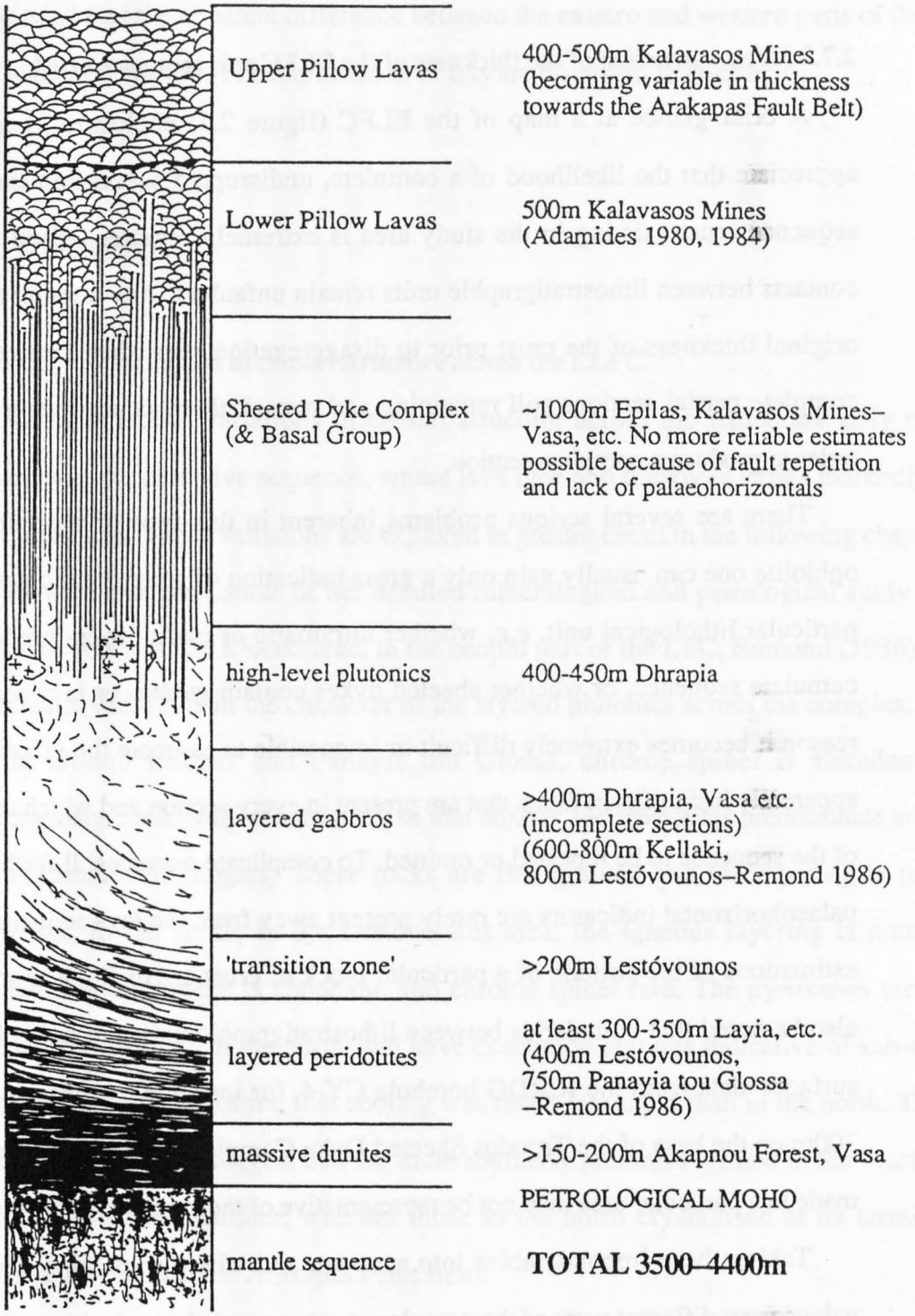

Figure 2.8: Reconstructed cross-section through the axis sequence crust in the ELFC. Approximately true scale. For discussion see text.

in mind the uncertainties involved, that the ELFC crustal thickness was approximately 4km ± ½km.

This is remarkably similar to Murton's (1986b) quoted estimate of 3690-4410m for the WLFC axis sequence, derived by similar means to the above. This led him to compare his preferred estimate of 3.6km (*sic*) with Allen's (1975) calculated crustal thickness of 6-8km for Troodos (*i.e.* upper lavas 0.5km, lower lavas 1.0km, sheeted complex 1-1.5km, plutonics 4-5km), and to conclude that the Limassol Forest ridge axis-generated crust was anomalously thin, probably from its proximity to the transform fault (Murton 1986a, Murton and Gass 1986).

Although superficially attractive, this hypothesis is not borne out by data from the ICRDG drillholes CY-1, CY-1a and CY-4, which suggest that Allen's calculations are overestimates. These indicate that the lava sequence, Sheeted Dyke Complex, and total mafic plutonics (layered and isotropic gabbros) each total approximately 1000m in thickness (Vine and Smith 1987). These figures are identical to the equivalent thicknesses estimated for each lithostratigraphic unit in the ELFC; therefore, although CY-4 did not penetrate mantle sequence, for which reason an accurate estimate of the total thickness of the Troodos crust is not possible, on available data it is not valid to claim that the LFC axis sequence crust is thinner than Troodos.

CHAPTER 3:
Lava Stratigraphy

3.1 Introduction

In the previous chapter it was shown that the syn-tectonic plutonism that gives rise to the anomalous 'transform sequence' oceanic lithosphere in the western half of the Limassol Forest is poorly represented in the east. Furthermore, it will be shown in chapters 5 and 6 that widespread post-volcanic tectonism has extensively modified the original seafloor spreading geometry of the ELFC, therefore making identification of any transform-related structures in the area extremely difficult. With this paucity of unequivocal structural and magmatic evidence, can the claim that the ELFC originated in a transform fault setting be justified?

Deep erosion levels, mostly in the mantle sequence, are preserved in the WLFC. In the Arakapas Fault Belt, however, sheeted dykes and lavas are preserved. Simonian (1975, — and Gass 1978) showed that the lavas in the AFB are interbedded with thick volcaniclastic turbiditic sediments, which were produced by the submarine erosion of fault scarps. This suggests that the AFB existed as a linear trough with rugged bathymetry during volcanic activity there. The resulting chaotic lava stratigraphy, preserved in small, irregular, fault-bounded basins, contrasts with the regular, ordered lava successions of the north flank of the Troodos Massif (*e.g.* Schmincke *et al.* 1983, Taylor 1988).

The transform is therefore apparently identifiable on bathymetric, as well as purely structural, grounds. In light of this, it should be possible to document the bathymetric extent of the transform (and hence to see if a potential southern boundary to it can be recognised) by a detailed examination of the lava stratigraphy across the ELFC, paying particular attention to structural controls on lava accumulation, and documenting the

spatial occurrence of interlava volcaniclastic sediments. As lavas crop out around the periphery of the ELFC, from Vavla in the AFB south to Asgata, and in the southern part of the complex from Monagroulli to Parekklisha (figure 2.1), it is possible to reconstruct a two-dimensional north-south palaeobathymetric cross-section perpendicular to the strike of the transcurrent faulting in the AFB. To do this, the lava stratigraphy of the Kalavasos Mines, as the best preserved and the most well-known area in the ELFC, is described first (section 3.3), and then compared with lavas to the north of the mines in section 3.4, and those to the south in section 3.5.

3.2 Sub-Division of the Extrusive Sequence

The early Survey workers (*e.g.* Wilson 1959, Carr and Bear 1960, Bear 1960, Gass 1960, Bagnall 1960) recognised that systematic differences existed in the character of the lavas within the Troodos extrusive sequence. In addition to the Basal Group (described in section 2.5.4) they sub-divided the extrusives into 'Lower Pillow Lavas' (LPL) and 'Upper Pillow Lavas' (UPL), based on field and petrological criteria. Although some workers initially believed that the boundary between the lavas and the Sheeted Dyke Complex was partly erosional (Gass *op. cit.*, Gass and Masson-Smith 1963), it became generally accepted that the transition from sheeted dykes to Basal Group and thence LPL was gradational, with the rapid decrease in abundance of dykes with stratigraphic height, and change from zeolite to greenschist grade of metamorphism, and that the units were cogenetic (Bear *op. cit.*).

Several criteria were used by the Survey authors to distinguish between the Lower and Upper Pillow Lavas, and these are summarised in table 3.1. In places they were able to demonstrate that the two groups were separated by an unconformity, but elsewhere there appeared to be a transitional relationship between them. Gass and Smewing (1973) later suggested that the LPL-UPL boundary along the northern flank of Troodos, whether

Lower Pillow Lavas:	Upper Pillow Lavas:
abundant contemporaneous dykes and sills. massive flows (often with columnar jointing) common. pillows average ~50% of outcrop.	minor intrusives rare. pillowed flows predominate.
pillows spherical to elongate, usually ellipsoidal. typically 0.5-1m in length.	pillows ellipsoidal to elongate or irregular. size variable.
pillowed lava mid-grey, with thin, dark, glassy chilled margins (when fresh).	fresh lava black and glassy, sometimes with thick vitreous interpillow spall, but devitrified lava altered to pale grey colour and argillised.
lava predominantly aphyric	frequently olivine phyric, occasionally enough to give rise to picrites with up to 60% modal olivine. in altered lavas olivine is pseudomorphed by bright orange-brown Fe-stained calcite.
vesicularity generally high in pillows and minor intrusives alike. vesicles large (up to 10%),elongate, and of irregular shape.	vesicularity often very low. where present, vesicles are small and usually spherical.
vesicles infilled by milky-white chalcedony, calcite, various zeolites, and distinctive bluish-green celadonite.	vesicles may be infilled by zeolites, typically analcite, natrolite and gmelinite, and by calcite.
celadonite frequently coats joint surfaces and occurs in lava groundmass, imparting distinct green colour to rock.	some parts of UPL may be pink-stained from alteration of volcanic glass to ferruginous chlorophaeite by submarine weathering.
primary and secondary quartz common in thin section.	chalcedonic silica absent, calcite common secondary mineral.
LPL typically andesitic in composition, with occasional basalts, quartz andesites and dacites	UPL usually basaltic, sometimes ultrabasic

Table 3.1: Summary of characteristics used by Survey authors to distinguish between Lower and Upper Pillow Lavas (after Bear 1960, Gass 1960 *etc.*).

conformable or not, corresponded to a metamorphic discontinuity separating the gabbros, sheeted dykes and LPL, all metamorphosed adjacent to a ridge crest, from the 'off-axis' UPL.

In his mapping of the Pharmakas-Kalavasos area (including the ELFC), Pantazis (1967) used the criteria in table 3.1 to sub-divide the lavas. He appears to have had certain difficulties in distinguishing between the groups, and his memoir notes exceptions to many of the 'rules' formulated by the earlier Survey authors, particularly in the AFB-ELFC area. In addition to the 'tuffaceous agglomerates' developed in the Layia-Vavla area, he reports that lavas of basaltic, rather than andesitic, composition are locally common in the LPL, and may be olivine-phyric. He also notes that dykes may be extremely abundant in the UPL and are celadonite stained, containing typical LPL secondary mineral assemblages.

The difficulty in distinguishing between the two lava groups, particularly in faulted terrains where no unequivocal stratigraphic control is present, is illustrated in fig 3.1, with a comparison between Pantazis' (1967) map of the Kalavasos Mines area, and that of Adamides (1984). Wide differences exist between the two maps. Clearly, ambiguity will exist between any attempts to sub-divide the lava sequence solely on the criteria set out in table 3.1 above. However, the two-fold distinction does appear to have validity across the entire ophiolite, and is valuable in the field even in highly faulted areas. It is recognised and used under a variety of names by virtually all workers in Cyprus and is therefore retained in this study.

3.3 The Kalavasos Mines

The Kalavasos Mines are amongst the most important of the Cyprus massive sulphide deposits, in recent times producing more than six million tons of ore (Adamides 1980) until their closure in 1977.

The area was surveyed in detail by Adamides (1984) for mineral exploration

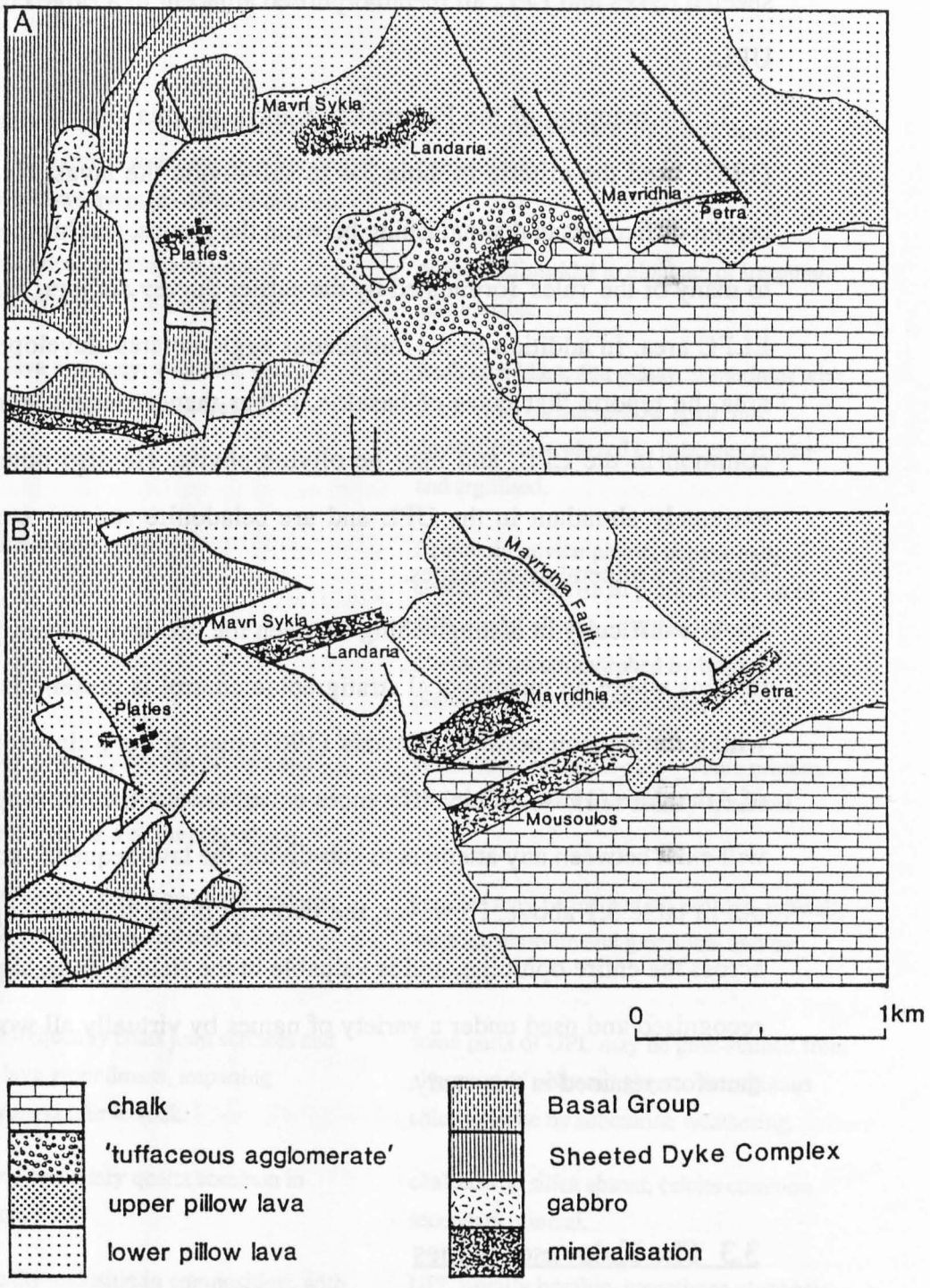

Figure 3.1: Comparative maps of the Kalavasos Mines area by (A) Pantazis (1967), and (B) Adamides (1980). The differences in interpretation, particularly in distinguishing between Upper and Lower Pillow Lavas are noteworthy; the distinctions (table 3.1) often prove highly subjective to implement in practice.

purposes. Unfortunately, the mines and much of their surroundings are now a restricted area and it was not possible to re-visit anywhere to the south of the Kalavasos–Platies road. However, mapping in the present study of the area to the north of the Vasilikos River up to Dhrapia, and around the Kalavasos Dam, was sufficient to establish the accuracy of Adamides' work, and this author is in general agreement with his interpretations.

Adamides (1980, 1984) retained the Survey terminology of 'Lower' and 'Upper' pillow lavas, but preferred to sub-divide the latter into two lithostratigraphic units, *viz.* a lower 'limburgite' unit and an upper 'olivine basalt' unit. These are described separately below.

3.3.1 Lower Pillow Lavas

Lower Pillow Lavas crop out most extensively around the SW abutment of the Kalavasos Dam and along the southern bank of the Vasilikos Reservoir (figure 3.4). They dip moderately to steeply northeastward, as do all the lavas in the area, and are in faulted contact with Basal Group exposed to the west of the mines. Pillows are usually dark grey or green with the presence of celadonite, and weathered outcrops tend to assume a characteristic khaki colour. In such outcrops argillisation of the pillows and minor intrusives may obscure their chilled margins, so that the material tends to have a massive, featureless appearance except in favourable light. Vesicularity is almost always high (*c.*20%), and although celadonite, chalcedony and heulandite may be present, the vesicles are usually empty. Fresh LPL are exposed in the vicinity of the sluice gate of the Kalavasos Dam (238510). Pillows are up to 1.5m in diameter, typically somewhat globular, and are intimately interlocking, with regular dark grey-green glassy margins a few centimetres in width (plate 3.1). The pillows are interbedded with hyaloclastites, and are cut by numerous penecontemporaneous sills and NE-trending dykes (plate 3.3). Fresh material from pillow and dyke centres is usually aphyric, though occasionally contains sparse plagioclase microphenocrysts, and varies in colour from pale grey to a

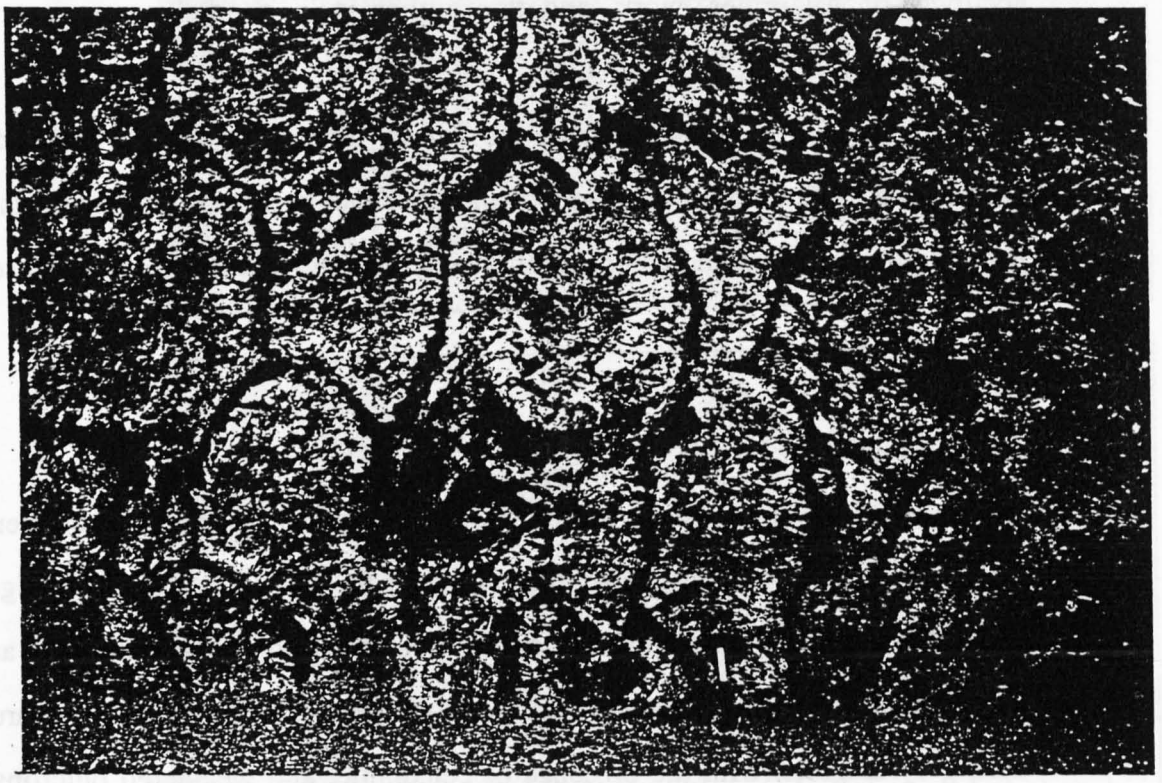

Plate 3.1: Vertical Lower Pillow Lavas. Large, globular, pillows with thin interlocking chilled margins, and traces of green-blue celadonite, are characteristic of LPL pillows. Note small daughter 'bud' in centre-left of picture, fed from larger pillow (now above, half visible). 23895104 Kalavasos Dam, sluice gate.

medium grey with a distinct bluish tinge. This distinguishes it from the dark slate grey–black colour of the much more mafic fresh limburgite lavas (see below).

3.3.2 Mineralisation

The consensus amongst early workers (Cullis and Edge 1927, Mousoulos 1957, Gordon-Smith 1963) was that the Cyprus massive sulphide deposits were post-Perapedhi Formation in age, localised in the pillow lavas by the entrapment of ascending hydrothermal fluids beneath impervious umbers and marls. Pantazis (1967) suggested that the Kalavasos deposits were post-UPL, but it was Adamides (1980, after Bear 1960) who showed unequivocally that mineralisation took place in the interval between the extrusion of the Lower and Upper Pillow Lavas.

The UPL lie conformably on the LPL, and a thin band of red-brown laminated umberous sediment up to 40cm thick frequently occurs at the interface between them (*e.g.* at 24415068 Petra Mine: plate 3.2, and at the Kalavasos Dam NE buttress: Loizides 1971). The LPL are brecciated and veined with this material for up to 2m below the contact, and may be distinctly reddened. Note that this reddening, representing the seafloor alteration or weathering of volcanic glass, has been cited by Survey authors as characteristic of UPL (table 3.1). The sediment horizon, thought by Constantinou (1972) to be oxidised ore, thickens into stratiform massive sulphide at the SE or hangingwall sides of several NE-trending faults. These faults, with their associated stockworks are interpreted as ridge-parallel by Adamides (1980), and appear similar to a mineralised fault at Pevkos (section 2.5.3).

The ore bodies are localised close to the intersection of the NE faults with the Mavridhia Fault (Adamides *op. cit.*), which is a major low angle fault dipping at approximately 25-30° to the south and striking WNW (plate 3.3 and figure 3.2). This important fault has been traced for over 2.5km on the surface, and for more than 1km underground by borehole (N.G. Adamides *pers. comm.* 1986). Its dip is practically perpendicular to that of the lavas, which dip on average 60-70° northeastwards, and so

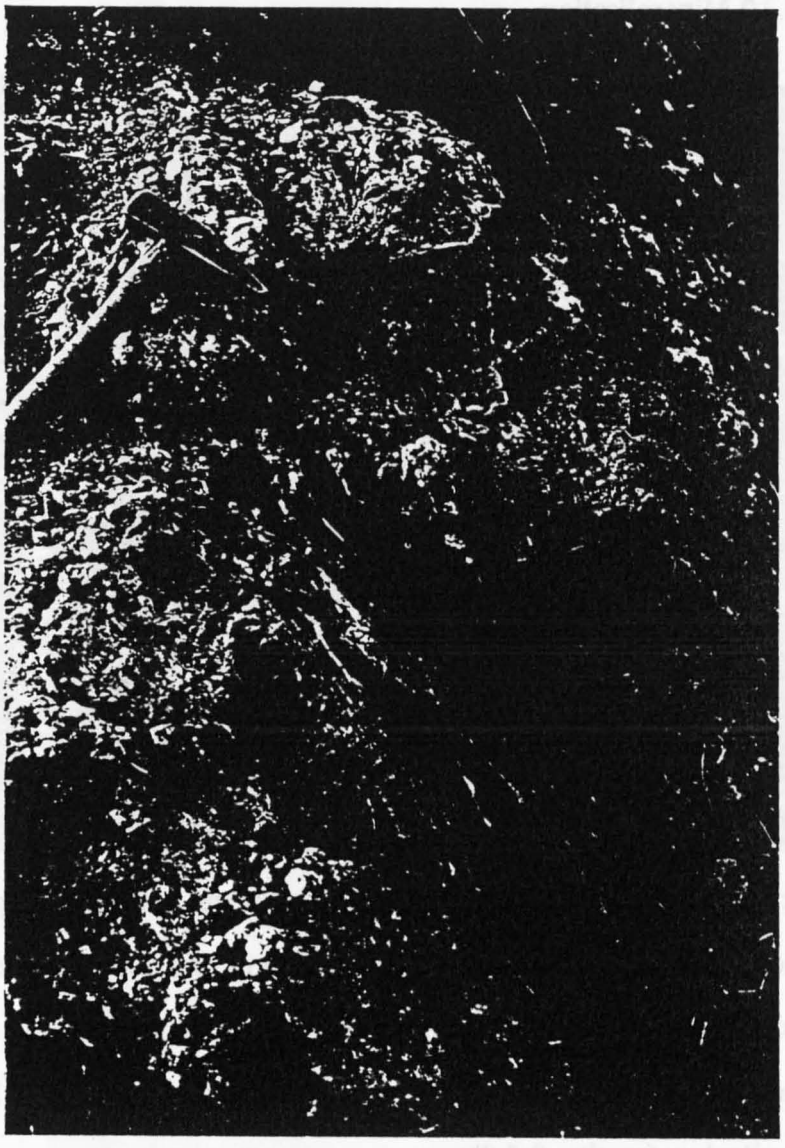

Plate 3.2: Partly silicified umber horizon at Lower Pillow Lava–Upper Pillow Lava contact, 24415068 Petra, Kalavasos Mines. This lies at the same stratigraphic level as the massive sulphide deposits nearby. Note steep dip (towards the northeast).

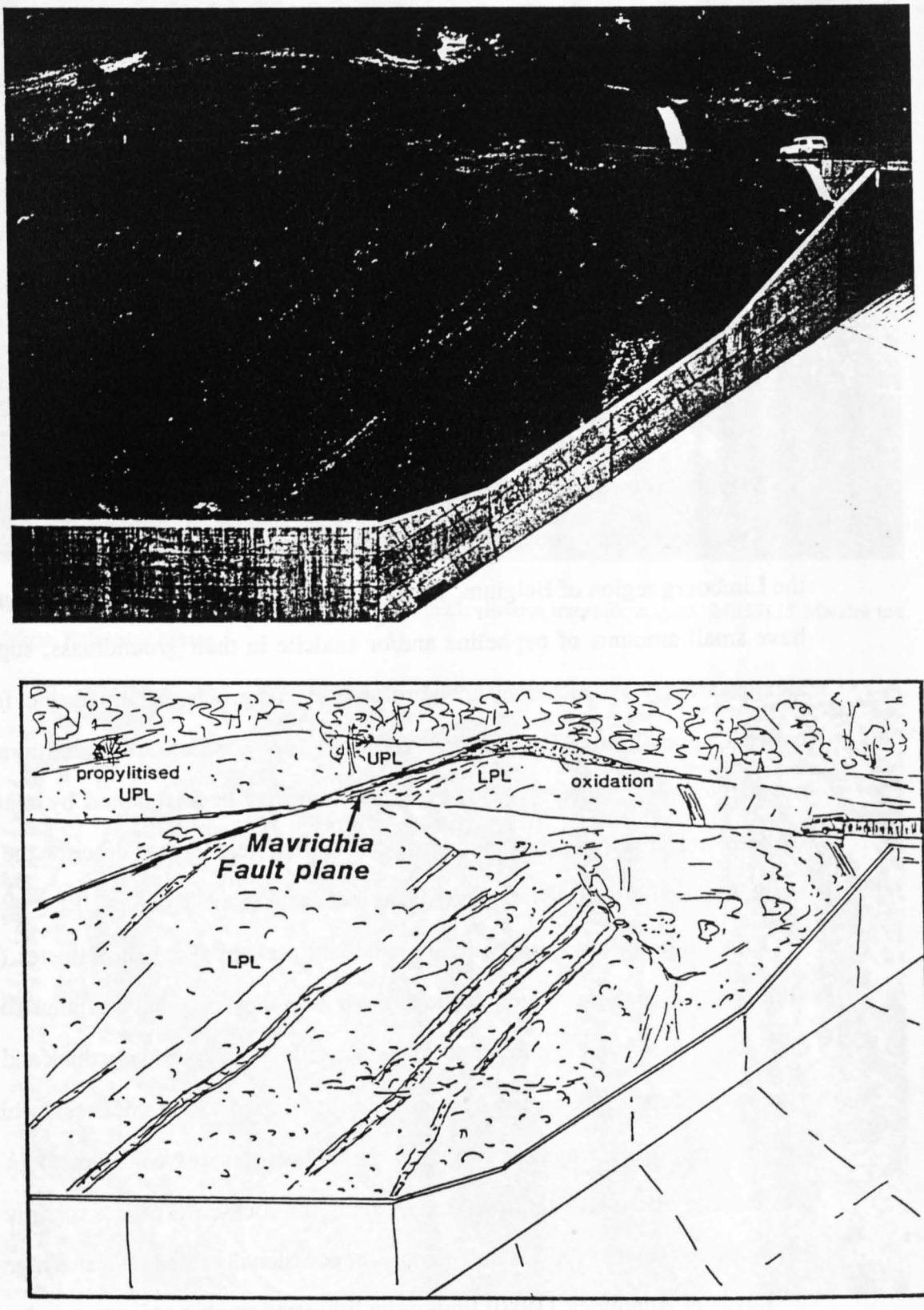

Plate 3.3 and Figure 3.2: The Mavridhia Fault. Note slight oxidation along the fault plane itself. LPL on footwall are cut by abundant dykes; UPL on hanging wall are veined with white propylite. 23785095 Kalavasos Dam.

prior to their rotation must have been oriented close to vertical, probably with an E-W strike (see chapter 5 for discussion).

Adamides (1984) considers the Mavridhia Fault to have been a very early structure. The ore bodies are all located on its southern side and the NE faults all terminate against it, so there is no correspondence of geology between the two sides. The fault plane itself is propylitised and oxidised (plate 3.3), and borehole cores of it are impregnated with pyrite, so, although no ore bodies are found along it, it has probably acted as a channelway for the mineralising hydrothermal fluids. Adamides (*op. cit.*) also suggests that the Mavridhia Fault may have been active after mineralisation, localising UPL in a small basin on its southern side.

3.3.3 Upper Pillow Lavas (limburgites)

Type limburgites are feldspar-free, glassy olivine-clinopyroxene-phyric basalts from the Limbourg region of Belgium. They may contain hornblende or biotite, and typically have small amounts of nepheline and/or analcite in their groundmass, suggesting an alkaline affinity. As such, they are petrologically and geochemically distinct from the so-called Cyprus 'limburgites' (Bear 1960, Gass 1960), which are tholeiitic and quartz-normative (see chapter 4). However, the term has been retained by many authors working in Cyprus, who have found it a convenient field term to describe the distinctive black, usually olivine-phyric, glassy lavas that occur in the Troodos UPL.

Limburgite pillows are typically smallish, perhaps 0.5m in diameter (plate 3.4), although favourably-oriented sections show that they may have tubular form and be distinctly elongate in the third dimension. Interpillow spall is usually thick and frequently vitreous, and may give rise to hyaloclastite flows up to 1m in thickness, which contain rounded eggs-like fragments of very fresh lava several centimetres in diameter. Vesicularity of the lavas is low (at least along the southern Troodos margin: *cf.* Taylor 1988) and the cavities are generally empty, or occasionally filled with analcite.

Lavas of Adamides' (1980) limburgite lithostratigraphic unit are not always glassy. Grey argillised flows and pillows with orange olivine pseudomorphs, and pillows with

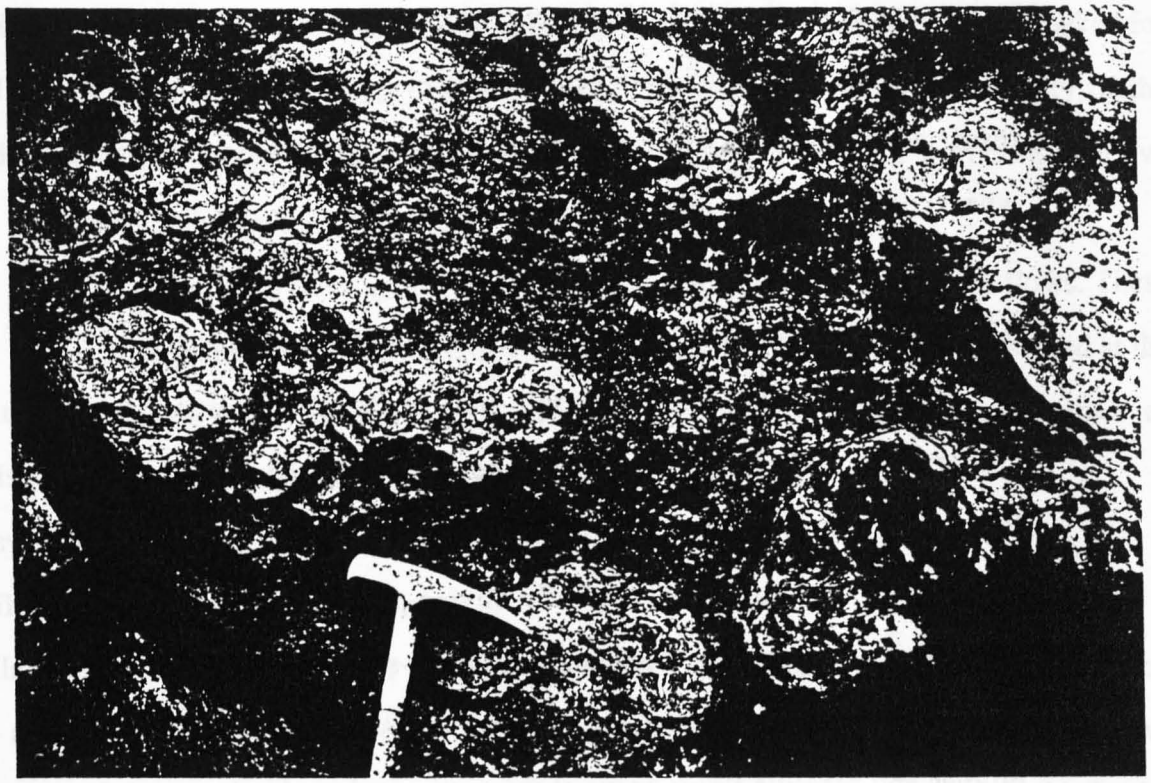

Plate 3.4: Glassy 'limburgite' pillow lavas, with thick vitreous interpillow spall. 24855115 Mandra tou Alykou, Kalavasos Mines.

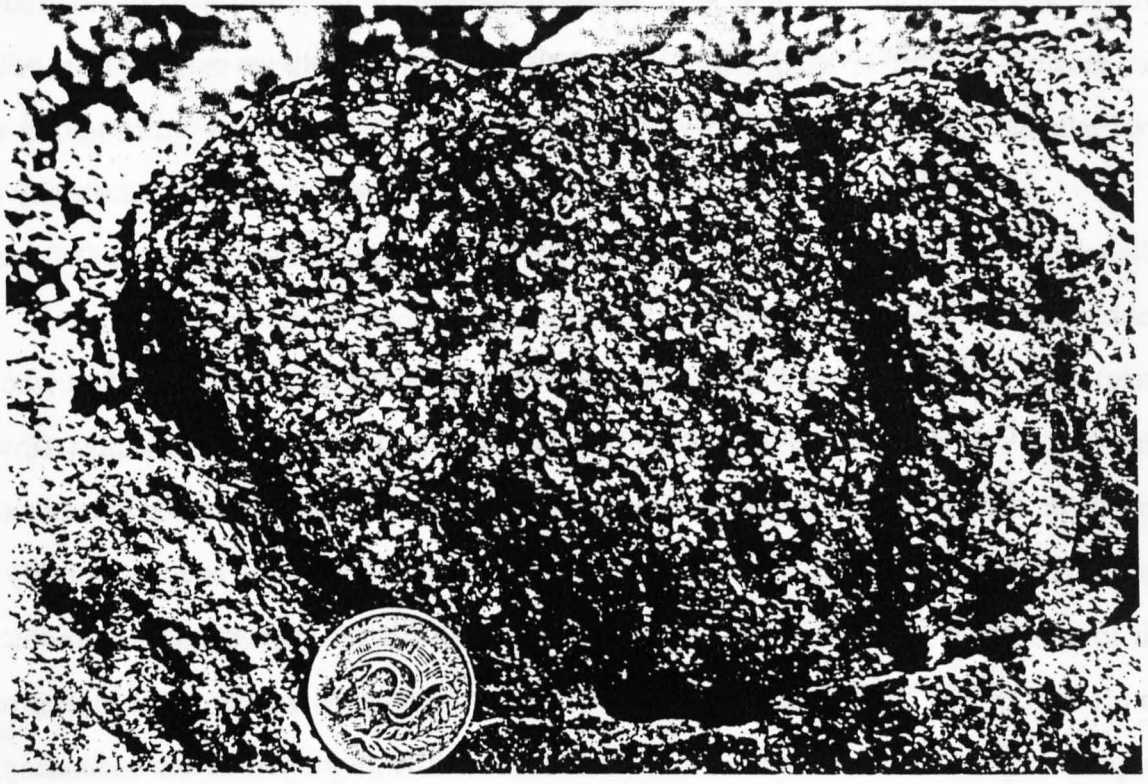

Plate 3.5: Close-up of a portion of the base of a picrite flow, showing the high proportion of accumulated olivine phenocrysts. 24865121 Mandra tou Alykou, Kalavasos Mines.

tachylitic margins but devitrified cores, are common. It is usually the larger pillows that are altered, and it appears from petrographic evidence (chapter 4) that the argillisation is restricted to those rocks in which groundmass plagioclase is present, *i.e.* in those areas where cooling rates are relatively slower.

3.3.4 Upper Pillow Lavas (olivine basalts), and associated intrusives

Adamides' (1980) 'olivine basalt' unit of the UPL overlies the limburgite unit conformably, either directly or with intervening interlava sediment (see below). The lowermost part of the unit at Polemikon (235510, 200m west of the Kalavasos Dam sluice gate) is an argillised, markedly olivine-phyric basaltic–picritic sheet flow 1-4m thick, which appears to be ponded against a NE-striking fault. In the stream gullies to the north of the Vasilikos River, *e.g.* Mandra tou Alykou (249512), up to 20m of picrite pillows and massive flows occur at the same stratigraphic level (*cf.* Searle and Vokes 1969). These are vitrophyric, containing an abundance of bright green euhedral olivines up to 1cm long (plate 3.5) which tend to settle in the lower parts of flows and pillows. The settling is very marked–the modal proportion of olivine may fall from >50% to zero in the space of a few centimetres in the middle part of a flow a metre thick–suggesting either that the magma was of extremely low viscosity, or that the density difference between the olivine and magma was high. The origin and significance of these lavas is discussed further in chapter 4.

Picritic lavas were first recognised in the Margi area by Gass (1958), who described bosses, dykes and sills feeding pillowed and massive picritic lava flows. In the Kalavasos Mines two large picrite sills intrude lower pillow lavas at Polemikon (234511) and Mavrolaona (237521: Vasilikos Reservoir, north bank), and are probably feeders to the picrite basalts and olivine basalts. Both sills are approximately 25m thick, display columnar jointing, and form dark brown lozenge-shaped areas of high ground (*N.B. Mavrolaona* [Gk.] = 'dark crag'; plate 5.3). The picrite is careous weathering, but fresh material is tough, with green millimetre-sized olivines in a dark green crystalline matrix,

and homogeneous across the entire body. Lavas above and below the sills are baked for 1-2m away from the contact. Minor picrite sills are observed in the vicinity of the Mavrolaona body, and are presumably fed by it; they also occur intruding interlava sediment at Polemikon (figure 3.3).

The extrusive picrites grade up into grey, altered pillows and massive flows. These lavas are usually, but not always, olivine-phyric, with phenocrysts usually settled at the bases of the flows or pillows. They may also contain orthopyroxene, either as phenocrysts, microphenocrysts or microlites (see chapter 4).

3.3.5 Interlava sediments

In the sections north of the Vasilikos River, particularly the Mandra tou Alykou (248511) stream gulley (figure 3.4), glassy pillows and (celadonite-stained) massive flows in the upper 20-30m of the UPL limburgite unit become interbedded with increasingly common bands of discontinuous sediment up to 0.5m thick. The sediment is usually a red-brown finely-laminated haematitic clay, with occasional fine sand layers, that drapes over the underlying partly brecciated pillows (plate 3.6). In some places this is capped by a band up to 10cm thick of unsorted grey breccia, containing angular lava fragments up to 1cm in diameter.

The top of the limburgite unit is marked by a much thicker and more regionally extensive sedimentary horizon. At Mandra tou Alykou red mudstones are interbedded with volcaniclastic silts, sands, grits and breccias, forming a sequence 19m thick (plate 3.7). This is the section logged by Adamides (1980), and is shown in figure 3.3. Within this sequence are two major breccia influxes, the larger more than 8m thick and containing poorly-sorted angular clasts of Lower Pillow Lava, mineralised Basal Group, sheeted dyke, indurated fault breccia and very rarely microgabbro. The bases of the breccia units, which show slight reverse grading, are erosive, and incorporate rip-up clasts of the underlying fine interbedded clay and sandstone. The upper parts display slight normal grading and are normally succeeded by cross-bedded gritty and sandy

Plate 3.6: Fine-grained sedimentary intercalation in flow unit d, below 19m sediment horizon (plate 3.7). 24875116 Mandra tou Alykou, Kalavasos Mines.

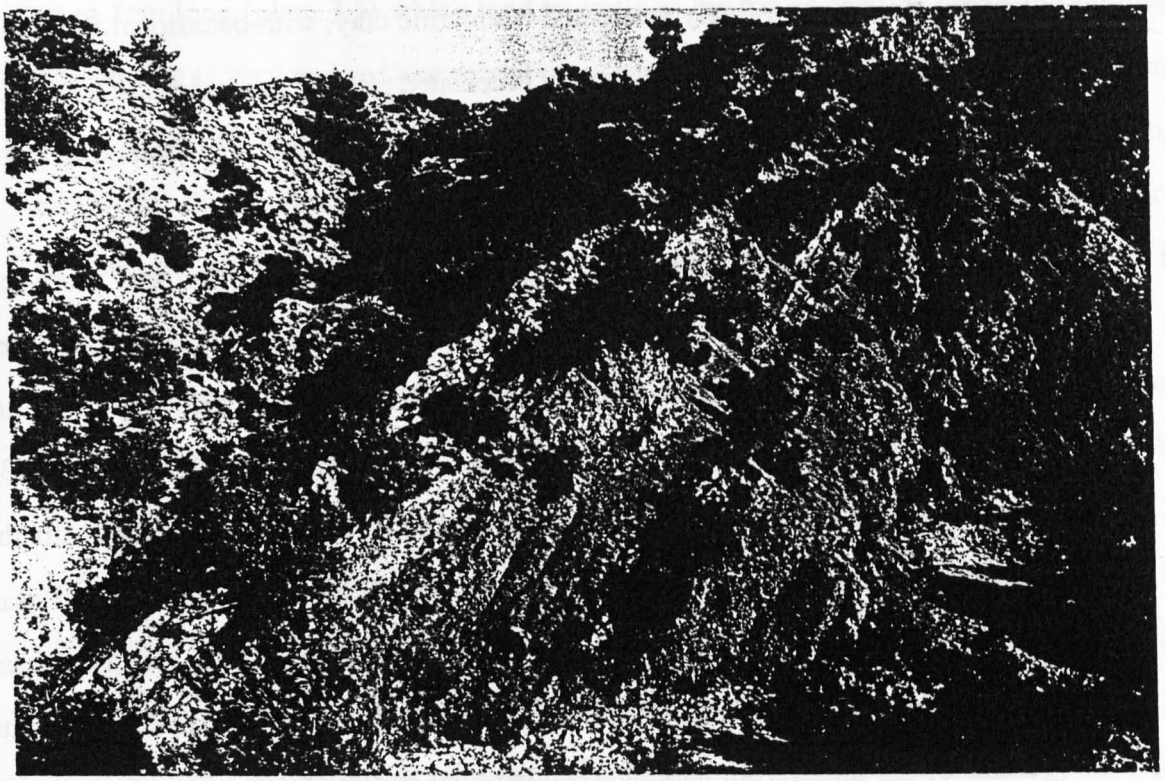

Plate 3.7: 19m thick intervolcanic sedimentary horizon, dipping northeast, 249512 Mandra tou Alykou, Kalavasos Mines (fig. 3.3, log C). Note two sills (more resistant to weathering) intruding fine sediments.

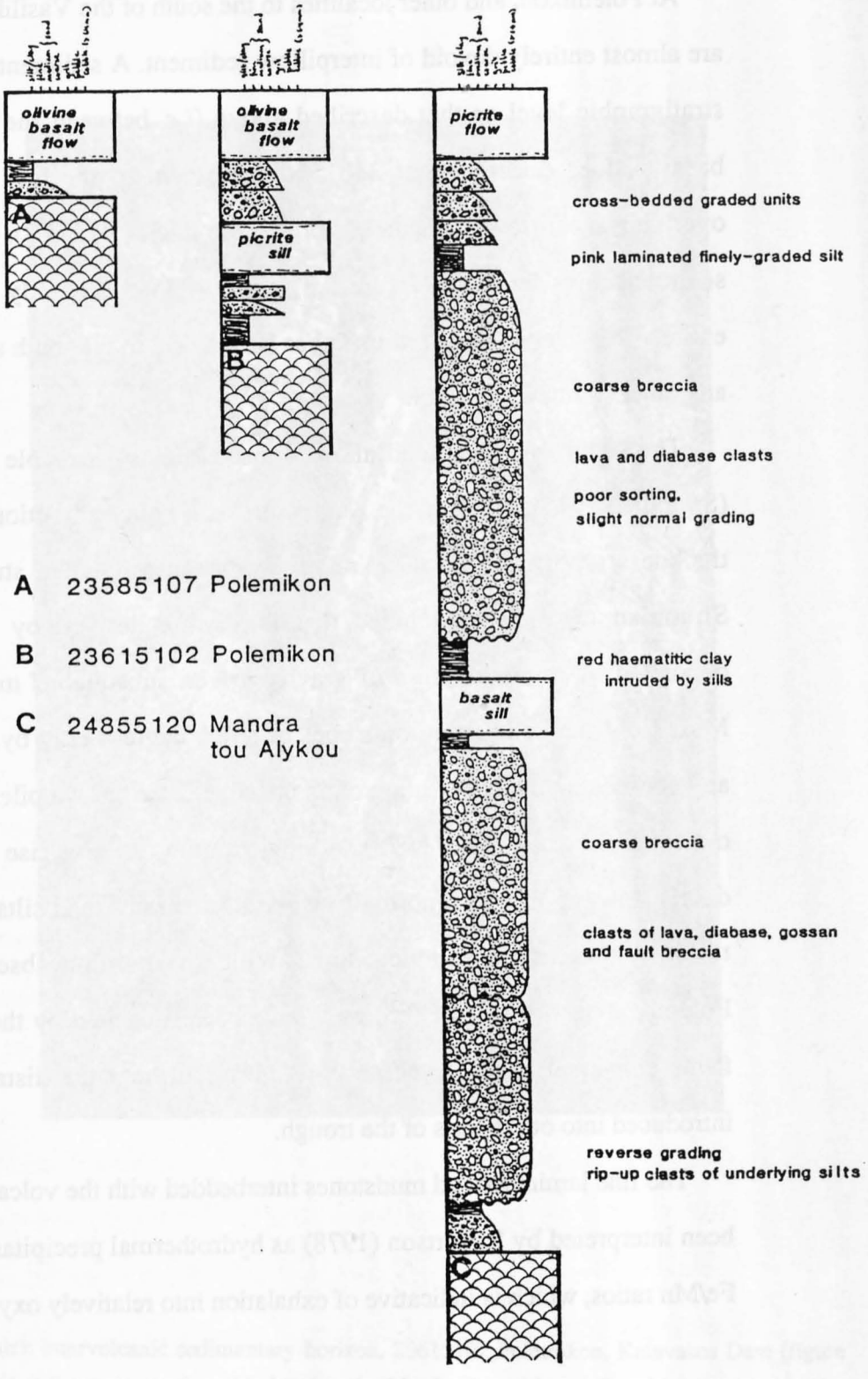

Figure 3.3: Logged sections of interlava sediment from the same stratigraphic level (between the 'limburgite' and 'olivine basalt' units of the UPL) at Polemikon (Kalavasos Dam) and Mandra tou Alykou (Vasilikos River), showing the marked increase in sediment thickness from south (Polemikon) to north (Mandra tou Alykou). These two localities are summarised in figure 3.6(b) as logs 2 and 3 respectively.

layers.

At Polemikon, and other localities to the south of the Vasilikos River, the limburgites are almost entirely devoid of interpillow sediment. A sedimentary sequence at the same stratigraphic level as that described above (*i.e.* between the limburgites and olivine basalts) does occur, but at 23615102, adjacent to the NE fault against which the overlying sheet flow is ponded, is only 2.4m thick (plate 3.8). Away from this fault the sediment thins to 60cm (figure 3.3) and at 23545111, only 130m away, disappears entirely. No intervolcanic sediment has been found to the south and west of here at this or any other stratigraphic level.

The sediments described above appear indistinguishable from those of the AFB (Simonian 1975), albeit in the Kalavasos Mines only a fraction of the 500m maximum thickness reported from the Arakapas area. In a detailed study of these sediments, Simonian (*op. cit.*) concluded that they were derived by submarine erosion and deposited by a combination of gravity-driven subaqueous mass transport processes. Mass flow can be initiated on slopes of a few degrees only by, for example, the tilting and consequent oversteepening of an unstable scree or lava pile, extra sediment loading, or seismic shock (Carter 1975). A single slump can give rise to a breccia dumped by debris flow, upon which normally-graded grits, sands and silts may be deposited from turbidity currents. Incomplete units, with fine fraction absent (e.g. from the 2.4m Polemikon section, figure 3.3) may have been truncated by the influx of a new debris flow; conversely, repeated fine units may represent the distal portions of turbidites introduced into other parts of the trough.

The fine laminated red mudstones interbedded with the volcaniclastic sediments have been interpreted by Robertson (1978) as hydrothermal precipitates because of their high Fe/Mn ratios, which is indicative of exhalation into relatively oxygen-depleted waters.

Plate 3.8: 3m thick intervolcanic sedimentary horizon, 23615102 Polemikon, Kalavasos Dam (figure 3.3, log B). This is at the same stratigraphic level as the 19m horizon (plate 3.7) at Mandra tou Alykou, 1km to the northeast. Fine sediments are again intruded by (picrite) sills.

3.4 The Northern ELFC: Dhrapia–Vavla

3.4.1 Dhrapia–Palaeodhrapia

The Mandra tou Alykou and Klitari lava sections are truncated by a major low angle WNW-trending normal fault that runs from just north of Dhrapia village along the north bank of the Vasilikos Reservoir to Mavrolaona (figure 3.4). This fault, here named the 'Vasilikos Reservoir Fault', dips at 20-30° southward and is almost exactly parallel to the Mavridhia Fault, which lies 1km to the south. On its footwall side, however, are steeply tilted layered plutonics, which pass up into high-level gabbros and thence sheeted dykes (see chapter 5). This block is bounded to the east by a steep N-S fault which cuts the Vasilikos Reservoir Fault and downthrows lavas on its eastern side, now exposed between Dhrapia and Palaeodhrapia (256530).

The representatives of the extrusive sequence here differ markedly from the Kalavasos Mines succession. Pillowed flows are absent; instead massive breccias occur across the entire area. The utter lack of sorting in the breccia is noteworthy: fragments range in size from many metres (*e.g.* a 12m block of oxidised Basal Group, or a 10m block of pillowed lava, internally coherent but with pillows now overturned) down to sub-millimetric granules (plate 3.9). Lava is the most common clast type, but dyke-rock is locally predominant. Some of the larger dolerite blocks preserve internal chilled dyke margins, and confirm their Sheeted Dyke Complex origins. No gabbro fragments were observed.

Vague suggestions of bedding in the breccia (plate 6.6) indicate that the Dhrapia area, like the Kalavasos Mines, been tilted towards the northeast, but a lack of reliable palaeohorizontal indicators makes it difficult to make an accurate estimation of its thickness. Taking the dip of the base of the umber as a minimum estimate for the dip of the deposit, the breccia is at least 275m and possibly as much as 450m thick. The total lack of sorting, grading and clast imbrication, and virtual absence of stratification, suggest that the Dhrapia breccias suffered little transport prior to deposition. They appear

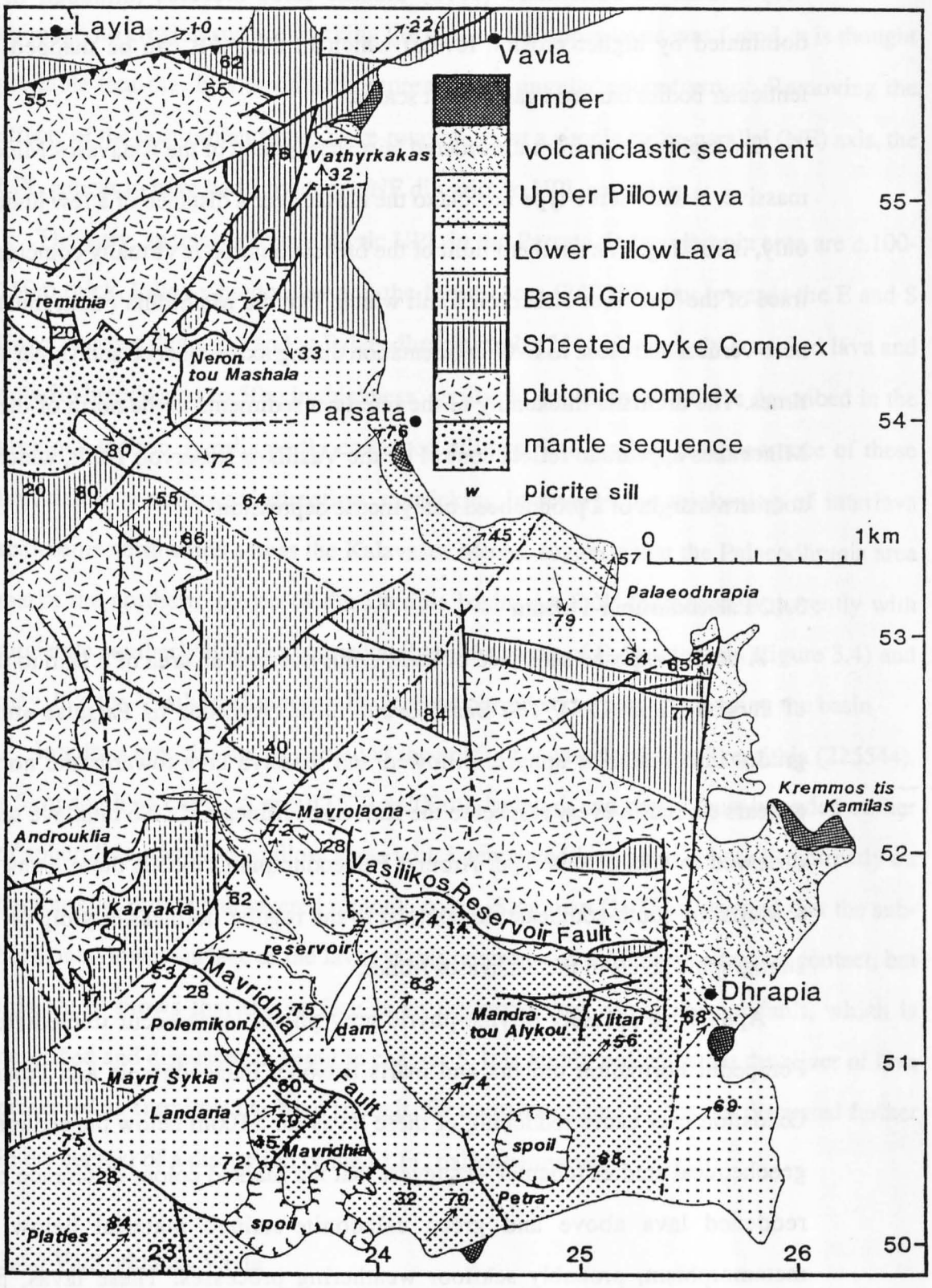

Figure 3.4: Geological map of the northeastern part of the ELFC.

very similar to Simonian's (1975) diabase scree breccias (although in the ELFC dominated by higher erosion levels) which in the AFB can be mapped as discrete lenticular bodies banked against fault scarps.

The rapid change from the ordered lava stratigraphy of the Kalavasos Mines region to massive, chaotic scree-type breccia to the north, over a distance of a few hundred metres only, is striking. The southern limit of the breccia outcrop is virtually coincident with the trace of the Vasilikos Reservoir Fault which, like the Mavridhia Fault, must have been near-vertical and close to E-W in orientation during axis sequence and Upper Pillow Lava times. The dramatic thickening of the interlava sediments to the north of the Kalavasos Mines thus appears to reflect control by the Vasilikos Reservoir Fault, which marks the southern margin of a pronounced bathymetric depression.

3.4.2 Palaeodhrapia–Parsata

A poorly exposed sequence of lavas crops out over an area of *c.*1km to the S and W of Parsata (figure 3.4). The Basal Group in the Ayiasma tis Parsatas area (232534) grades into vesicular aphyric pillowed and massive lava towards the northeast; this appears similar in every respect to the Kalavasos Mines LPL. No interlava sediment was observed in lava of this type. Around Palaeodhrapia (250530) these lavas dip steeply towards the south-southeast, in contrast to the regular northeasterly dip of lavas of all stratigraphic levels in the Kalavasos Mines.

Aphyric to sparsely olivine-phyric grey pillow lavas occur immediately beneath Perapedhi Formation umbers and marls between Palaeodhrapia and Parsata village. Oxidation may cause reddening of these lavas for >100m below the sediment contact; geochemical studies (chapter 4) suggest that the marked colour difference between the reddened lava above and green celadonite-stained material below is due to metamorphism, probably seafloor weathering processes. These lavas, presumably equivalent to the UPL, dip moderately towards the northeast, at the same angle as the overlying umbers (see chapter 6) but with marked angular discordance with respect to the

Palaeodhrapia LPL. No major faults appear to separate the two lava types and so, although no erosion surface marking the base of the upper lavas was found, it is thought probable that the dip discordance represents an angular unconformity. Removing the effects of the post-umber tilting by re-rotation about a simple strike-parallel (NE) axis, the LPL appear to have had a moderate NE dip prior to UPL extrusion.

The grey, sparsely olivine-phyric UPL in the Parsata–Palaeodhrapia area are *c.*100-150m thick. Pillows predominate in the former area (242537), but towards the E and S flows become degraded and at Palaeodhrapia itself (251533) vaguely stratified lava and dolerite breccias up to 50m in thickness, similar in appearance to those described in the previous section, overlie partly collapsed pillows. The gradual disappearance of these breccias in a northward direction, mimicking in reverse the thickening of interlava sediments northwards across the Kalavasos Mines, suggests that the Palaeodhrapia area marks the northern margin of the Dhrapia basin. An E-W fault zone, apparently with moderate southerly dip, lies immediately to the south of Palaeodhrapia (figure 3.4) and may, like the Vasilikos Reservoir Fault, have played some part in bounding the basin.

Interlava breccias are preserved to the north of Palaeodhrapia at Tremithia (225544), 1.5km south of Layia. A small (500 x 200m), isolated, and partly fault-bounded outlier of spherulitic and glassy pillow lavas with intercalated lava breccia here lies directly on harzburgite, dunite and layered plutonic rocks. Simonian (1975) suggested that the sub-horizontal lower surface of the lavas at this outcrop was a primary extrusive contact, but this study shows that the surface is an important low angle normal fault, which is described and discussed in detail in chapter 5. It is highly probable that the sliver of lava preserved at Tremithia has been tectonically transported, and so it is not discussed further in the context of a discussion of the ELFC palaeobathymetry.

3.4.3 Vathyrkakas, Vavla

North of Parsata sheeted dykes are overlain directly by Perapedhi Formation marls and, at 240554 (0.5km west of Vavla, immediately south of the Layia road), by radiolarites. To the south, in a hollow at the 'Vathyrkakas' locality, a small area of lava, a

few hundred metres square, occurs between the dykes and the sediment. In the main part of the outcrop the lavas have a regular 10-30° northward dip, similar to that of those radiolarites not affected by syn-sedimentary deformation (see chapter 6), and 60-100m of lava are preserved.

The upper few tens of metres of this sequence are a chaotic mixture of intact olivine-phyric pillows, partly collapsed flows and volcaniclastic breccias and grits. Breccias decrease in proportion down section, and as a result regular pillowed and massive flows, with minor intrusives, predominate at lower stratigraphic levels. These lavas are aphyric, celadonite-stained and have heulandite amygdales, so appear similar to typical LPL. Seafloor weathering has stained the upper 20m or so of the section pink though, as at Parsata, the colour change does not appear to correspond to any volcanological or geochemical distinction (see chapter 4).

To the south and west of the Vathyrkakas outcrop the lavas are in faulted contact with the Sheeted Dyke Complex, itself partly fault brecciated by regional transform-related deformation. To the northwest however, the uppermost lavas are banked against sedimentary polymict breccias which contain gabbro and, in places, lava clasts in addition to dolerite that appear similar to Simonian's (1975) diabase scree breccias. These breccias give rise to a small hill at 240555 lying on the SE side of a major NE-trending fault, from which they may be derived. The pillows adjacent to the scree breccias have irregular but generally steep dips towards the SE, *i.e.* away from the hill, contrasting markedly with the gentle and regular northerly lava dips elsewhere in the section. These are almost certainly depositional dips, and suggests that the upper lavas at least were erupted into a small, probably fault-controlled hollow adjacent to a hill of brecciated sheeted dyke basement, which was aproned by scree.

3.5 The Southern ELFC: Asgata–Parekklisha

The claim made in section 3.3.5 that no interlava sediment horizons occur to the west and south of the Kalavasos Mines is apparently contrary to the interpretation of Pantazis (1967), who on his map marks extensive areas of 'tuffaceous agglomerate' on his map of the ELFC in the Dhrapia and Layia–Vavla areas, but also around Asgata and Parekklisha. In the latter areas the 'tuffaceous agglomerates' (*sic*) lie immediately below the contact with Perapedhi and Moni Formation sediments.In chapter 6 it is shown that these deposits, better described as 'pillow collapse breccias', are post-volcanic and totally unrelated to the syn-volcanic Dhrapia and Arakapas Fault Belt sediments.

The steep, regular NE dip of the extrusive sequence in the Kalavasos Mines is maintained in the Asgata area and for *c.*3km to the west of the village, as far as an important WNW-trending fault near the 'Stenoman' locality (200477; see chapter 5). To the south and west of this fault, across the remainder of the southern ELFC (figure 3.6(a)), lavas and sheeted dykes have been compartmentalised into small, independently-rotated fault blocks, usually tilted towards the SW. The lack of structural continuity over distances of a few hundred metres only, coupled with the lack of intervolcanic sediments (which form distinctive marker horizons), precludes the reconstruction of stratigraphic sections as detailed as those presented for the Kalavasos Mines and northern ELFC.

With the exception of the Asgata River locality (which is described separately below), the lava sequence across the entire southern ELFC, from Asgata to Parekklisha, is strikingly uniform, and its similarity to a typical section through the extrusive sequence of the northern flank of the Troodos Massif (*e.g.* Gass 1960), rather than to the Arakapas Fault Belt, is noteworthy.

Three kilometres north of Parekklisha, at Mangaleni (125465), lies a small lava-hosted massive sulphide deposit. This was investigated by Adamides (1984), who also mapped the surrounding area. He subdivided the upper part of the stratigraphic column into Basal Group–LPL–UPL (limburgite)–UPL (olivine basalt), as in the Kalavasos

Mines, although it is the view of the present author that the use of lithology alone to determine stratigraphic position within the UPL in the ELFC is not justified (see chapter 4). Mangaleni is in close proximity to the serpentinised harzburgite massif of Kyparissia (in the central Limassol Forest), which was uplifted in the Miocene (chapter 5); consequently tectonism in the lavas is extreme, and the sulphide deposit has been highly dismembered. No stockwork zone is preserved, although extensive alteration of large areas of 'Basal Group' pillows to quartz-epidote rocks has taken place (Adamides *op. cit.*). Adamides reports the presence of limburgite lavas resting directly upon these lavas, suggesting that the LPL-UPL transition is unconformable in this area.

In the Ornithouri block, north of Pyrgos, Basal Group grades northeastwards into pale grey or buff aphyric vesicular lower pillow lavas at ~180470. These are widely exposed in adjacent fault blocks where, like the LPL of the remainder of the ELFC (and Troodos), are frequently cut by minor intrusives, and weather to a dull khaki colour. One notable difference between the LPL of this southern area and the Kalavasos Mines/northern ELFC is the relative scarcity of celadonite in the former. This contrasts with descriptions of the LPL given in sections 3.3 and 3.4, in which the mineral was virtually ubiquitous. Since celadonite is indicative of higher metamorphic grade within the zeolite facies, its scarcity in the southern ELFC might indicate that hydrothermal circulation there was relatively less vigorous, or that geothermal gradients were lower than in the north.

In a small fault-bounded block at 188461, 1km north of Monagroulli village, pillow lavas with the typical appearance of LPL (here with celadonite and heulandite) are succeeded by very fresh limburgite pillow lavas containing olivine and, at 18694585, orthopyroxene (sample 86/147: see chapter 4). The flows are apparently conformable, and no umber, sediment or brecciation of the underlying lava is visible at the contact. Olivine-phyric UPL, frequently glassy, crop out widely between Monagroulli and Pyrgos. These lavas, with secondary analcite and gmelinite infilling vesicles, fit closely the Cyprus Survey's ideal definition of Upper Pillow Lavas (table 3.1). One notable

difference, however, is the common presence of dykes in the UPL of the southern ELFC, contrasting with the Kalavasos Mines–Parsata and AFB areas (Simonian and Gass 1978), where they are very unusual (although they may be very common along the western continuation of the AFB: I.G. Gass *pers. comm.* 1988). The dykes in the southern ELFC may form locally dense swarms, as at 218479 Asprolaona, 2km west of Asgata (figure 6.2), where parallel N-S trending high-angle dykes up to 5m in width cut pillow lavas dipping 70-80° NNE, and are often olivine-phyric, occasionally picritic.

The most spectacular development of intrusives in the UPL is in the Asgata River, 0.5km east of the village (figure 3.5). At least three generations of dykes are present, the most prominent of which being a high-angle NE-trending set. At 23934882 these form a multiple swarm of at least six parallel dykes, some with assymmetrically split chilled margins, totalling 10-15m in width. Individual dykes parallel to this are up to 8m wide, truncate a few thin, scattered, E-W trending dykes and are themselves cut by abundant shallowly northward-dipping sills.

These dykes and sills are spatially associated with a large celadonite-stained dolerite body at 238488, possibly up to 40m in thickness, which displays crude columnar jointing and dips *c.*60° northwards. Its chilled upper margin suggests that it is a sill. The chemistry of the body, the dykes and pillow lavas from this locality are very similar (chapter 4) and it is likely that they are consanguineous. No systematic chemical distinctions can be made between successive dyke generations. Although no instances of minor intrusives feeding lava flows directly were observed, most dykes and sills are strongly chilled and many are highly sinuous, compatible with their intrusion at shallow levels. It is suggested that this locality represents a small high-level magma chamber below a local eruptive centre.

The area was the subject of palaeomagnetic investigation (site B4) in an attempt to document its rotation history. The results of this are presented and discussed in section 5.5.1.

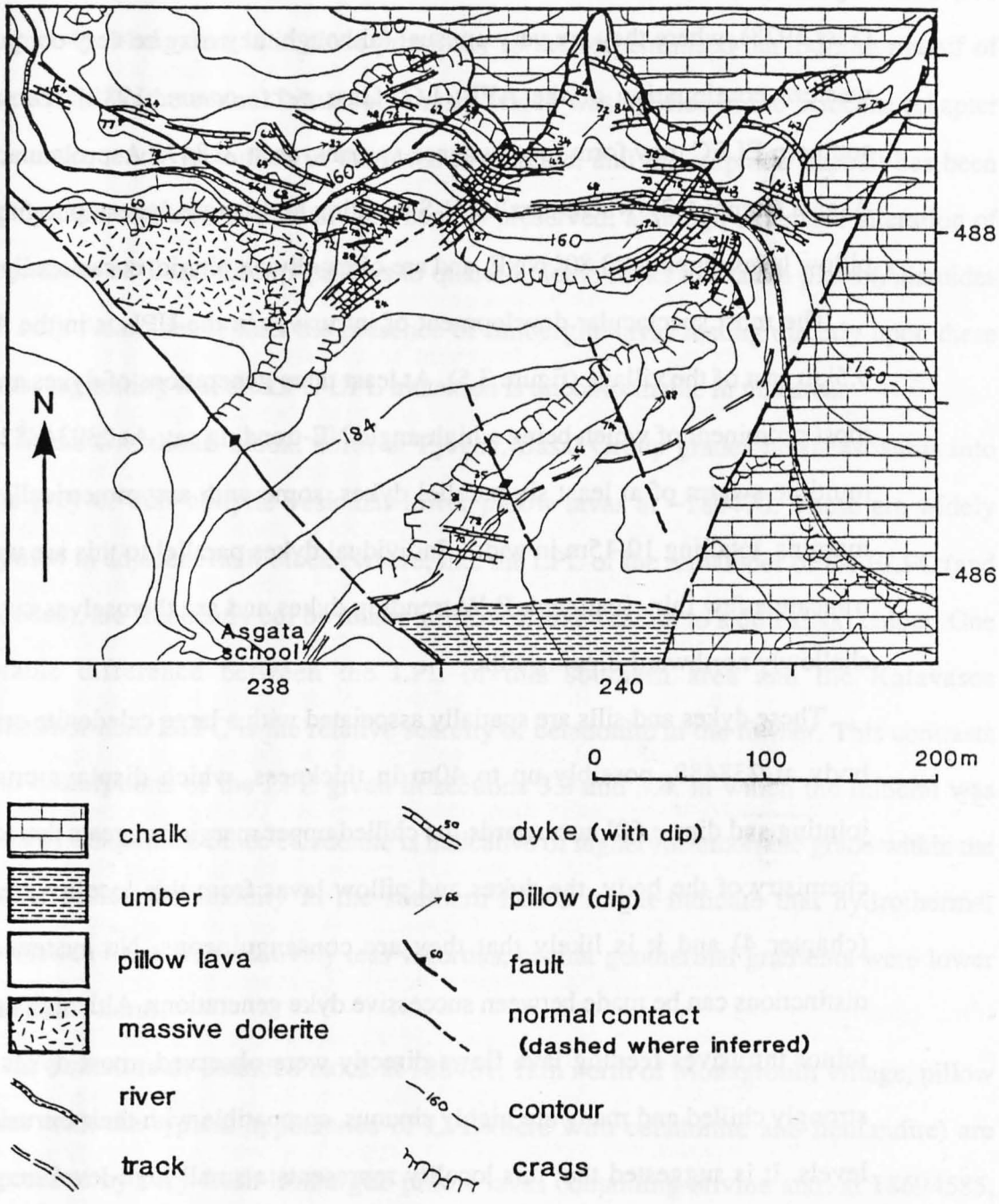

Figure 3.5: Geological sketch map of the Asgata River area, showing the high concentration of minor intrusives around the large dolerite boss or sill. Note NE-trending multiple dykes, which formed the subject of palaeomagnetic site B4 (see chapter 5).

3.6 Discussion

3.6.1 A reconstruction of the ELFC palaeobathymetry

An E-W reverse fault to the south of Layia, which brings gabbros northwards over the lavas and sediments of the Arakapas Fault Belt, was taken by Simonian and Gass (1978) to be a southern boundary to the eastern part of the AFB. As they note, this fault was activated after the main syn-volcanic transcurrent movements, so this boundary has no particular significance in the context of the ocean floor bathymetry (although it may have been a reactivation of an earlier feature: see chapter 5). The similarity of the Vathyrkakas basin (section 3.4.3) to Simonian's (1975) description of localised lava- and sediment-filled basins, occasionally up to 200m thick, lying between steep hills of a brecciated sheeted dyke basement in the Layia–Vavla–Kato Dhrys area, leaves little doubt that Simonian's bathymetric depression extended southwards to include at least part of the ELFC.

In figure 3.6(b) stratigraphic sections through the extrusive sequence from eight areas from Layia (in the AFB) to Asgata, are stacked to form what approximates to a N-S cross-section, perpendicular to the strike of the transform. The irregularity of the lava stratigraphy of the more northerly sections is striking. Two major volcaniclastic sediment-filled troughs at Layia (log 8) and at Dhrapia (log 4) are separated by a horst between Parsata and Vavla. In this area brecciation of the Sheeted Dyke Complex (logs 6 and 7) and tilting of the LPL (log 5) prior to UPL lava/sediment accumulation attest to syn-volcanic tectonism and seafloor uplift.

3.6.2 The 'Anti-Troodos' plate fragment

The lateral equivalent of the 275m+ of volcaniclastic sediment at Dhrapia is, in the Kalavasos Mines (Mandra tou Alykou) area 19m thick and at the Kalavasos Dam (Polemikon) between 0 and 3m (figure 3.6(b), logs 3 and 2 respectively). To the south of the latter locality the sediments disappear completely and none are found across the entire

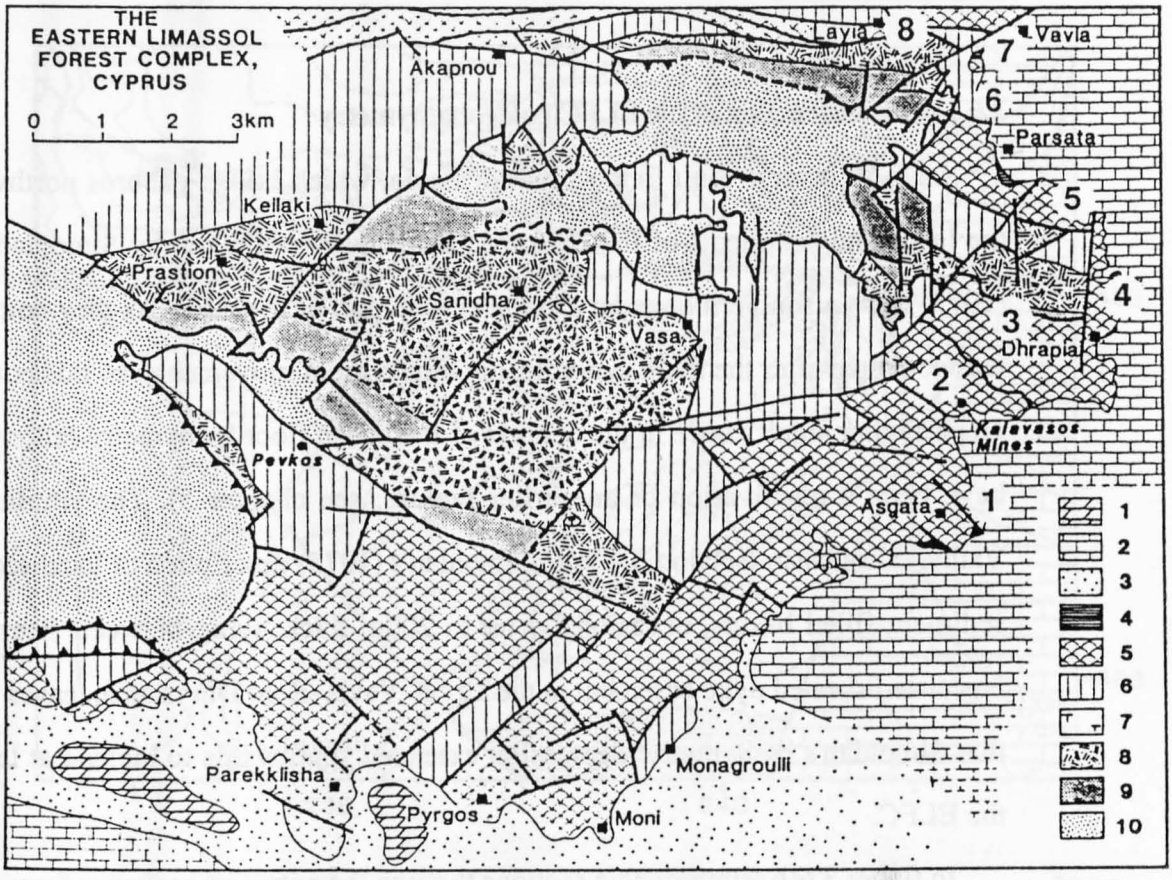

1: Asgata

2: Kalavasos Mines, Polemikon

3: Kalavasos Mines, Mandra tou Alykou

4: Dhrapia

5: Palaeodhrapia

6: SW Vavla

7: SW Vavla: Vathyrkakas

8: Layia (Arakapas Fault Belt)

Figure 3.6 (a): Simplified geological map of the ELFC, showing the location of the eight stratigraphic logs presented in figure 3.6(b). *Sediments:* (1): Miocene–Recent; (2): Maastrichtian–Miocene; (3): Campanian–Maastrichtian Moni mélange; (4): Turonian–Campanian Perapedhi Formation. *Igneous Rocks:* (5): Pillow lavas; (6): Sheeted Dyke Complex; (7): Plagiogranites; (8): Gabbros; (9): Peridotites; (10): Tectonised harzburgites and dunites.

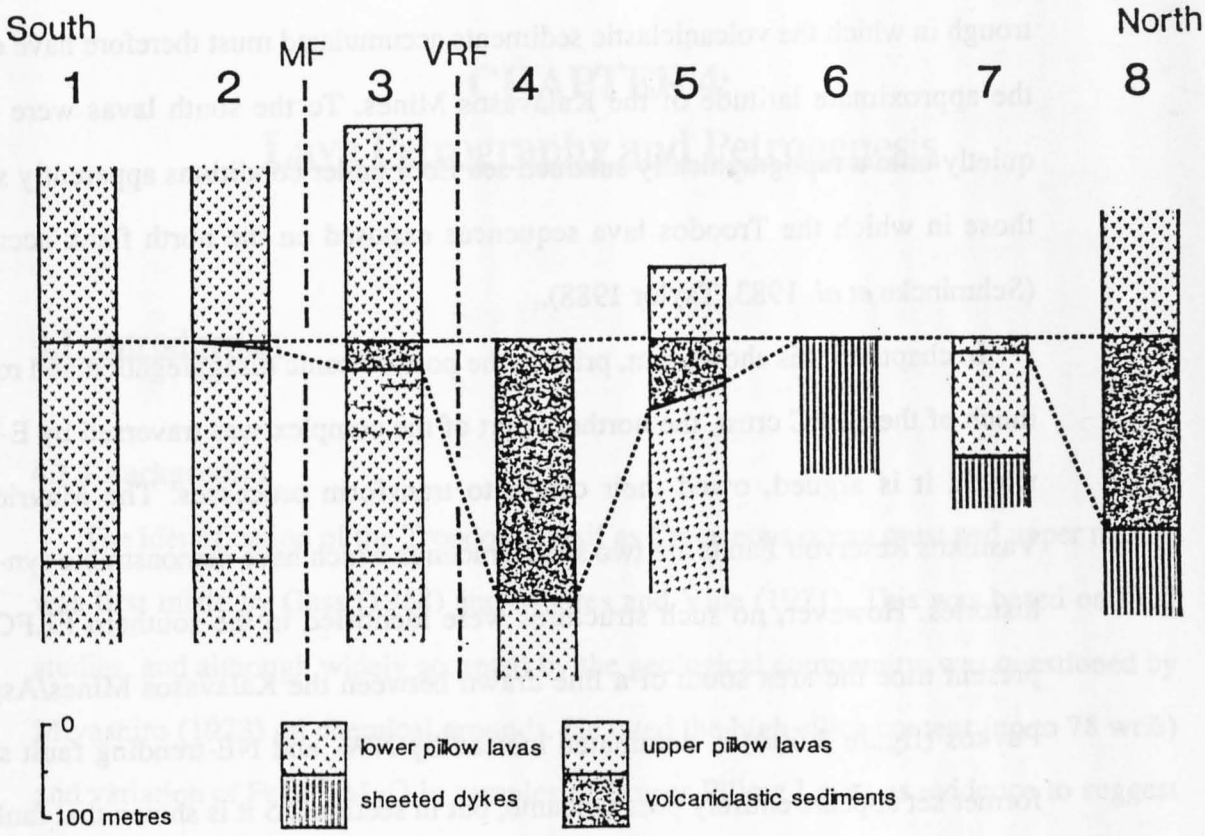

1: Asgata
2: Kalavasos Mines, Polemikon
3: Kalavasos Mines, Mandra tou Alykou
4: Dhrapia
5: Palaeodhrapia
6: SW Vavla
7: SW Vavla: Vathyrkakas
8: Layia (Arakapas Fault Belt)

Figure 3.6 (b): Schematic stratigraphic logs from lava sequences in the ELFC (location of sections shown in figure 3.6(a)), stacked to form a reconstructed N-S bathymetric profile across the transform. Skewed Lower Pillow Lava ornament in log 5 indicates tilting of the LPL there prior to UPL extrusion. Lava sequences at all other sections appear conformable. MF = Mavridhia Fault; VRF = Vasilikos Reservoir Fault. Note thick volcaniclastic sediments at both Dhrapia and at Layia, indicating two troughs, and control of the Dhrapia trough by the Vasilikos Reservoir Fault. An E-W trending fault shown on figure 3.6(a), immediately south of log 5, probably controls the northern margin of the trough.

southern ELFC from Asgata–Parekklisha. A southern boundary to the rugged irregular trough in which the volcaniclastic sediments accumulated must therefore have existed at the approximate latitude of the Kalavasos Mines. To the south lavas were extruded quietly onto a topographically subdued sea floor under conditions apparently similar to those in which the Troodos lava sequences exposed on the north flank accumulated (Schmincke *et al.* 1983, Taylor 1988).

In chapter 5 it is shown that, prior to the post-volcanic disaggregation and rotation of much of the ELFC crust, the northern part of the complex was traversed by E-W faults which, it is argued, owed their origin to transform processes. The Mavridhia and Vasilikos Reservoir Faults are two such structures which have demonstrable syn-volcanic histories. However, no such structures were identified in the southern ELFC. At the present time the area south of a line drawn between the Kalavasos Mines/Asgata and Pevkos (figure 3.6(a)) is dominated instead by NW- and NE-trending fault sets. The former set appears entirely post-volcanic, but in section 2.5 it is shown that faults of the latter set, which are oriented parallel to the trend of the Sheeted Dyke Complex across most of the area, are often mineralised and, it is concluded, were probably active as ridge-parallel normal faults during seafloor spreading.

It would appear, therefore, that the southern margin to the bathymetric depression also coincides with the disappearance of transform-parallel structures (to the south of the Mavridhia Fault), and a transition to wholly ridge-related deformation. A width of approximately 5km is thus calculated for the transform fault zone in the eastern part of the Limassol Forest Complex, after subtracting the effects of post-volcanic extension (see chapter 5).

The crust making up the southern part of the ELFC to the south of this transform boundary is considered to have been generated at a N- to NE-oriented 'Anti-Troodos' spreading axis, on the opposite side of the transform to the remainder of the Troodos Massif. Approximately 50km^2 of Anti-Troodos crust between Asgata and Parekklisha is preserved.

CHAPTER 4:
Lava Petrography and Petrogenesis

4.1 Introduction

4.1.1 Background

The identification of the Troodos Massif as Cretaceous ocean crust and upper mantle was first made by Gass (1968) and Moores and Vine (1971). This was based on field studies, and although widely accepted by the geological community, was questioned by Miyashiro (1973) on chemical grounds. He cited the high silica content (up to 78 wt%) and variation of FeO^{tot}/MgO in samples of Lower Pillow Lavas as evidence to suggest that some of the lavas were of calc-alkaline rather than tholeiitic affinity, and that the Troodos and other ophiolites were therefore formed in island arcs rather than at mid-ocean ridges. This conclusion was challenged on several grounds by subsequent correspondents (Hynes 1975, Moores 1975 and Gass *et al.* 1975), who stressed the unreliability of an interpretation based solely on the geochemistry of samples which display evidence of extensive mineralogical alteration, and therefore the potential for large-scale metasomatism, and they rejected unequivocally Miyashiro's (1975b) claim that the Sheeted Dyke Complex might not be composed of 100% near-vertical dykes but instead represent "swarms of radial dykes around several eruptive centres in an island arc" (Gass *et al. op. cit.*).

To circumvent the alteration problem, Pearce and Cann (1971, 1973) examined the concentrations of elements known to be unaffected by seafloor weathering at up to lower greenschist facies, *viz.* Ti, Zr and Y (Cann 1970), in the Troodos lavas and compared them with the equivalent concentrations in basalts erupted in a variety of known tectonic settings. Ewart and Bryan (1972) noted the similarities between the unusually low TiO_2

abundances of the Troodos lavas and basalts from Eua (Tonga), and suggested that both were erupted in the early stages of island arc development. Pearce (1975) showed that the chemistry of the Troodos LPL had affinities both with mid-ocean ridge and island arc basalts, and that the UPL resembled primitive low-potassium arc tholeiites. This led him to propose that the Troodos ophiolite was formed at a constructive margin but in a marginal basin setting above a subduction zone rather than at a mid-ocean ridge.

In a similar study Smewing *et al.* (1975) concurred with this view; however, they showed that, although *average* Ti and Zr contents decreased systematically with increasing stratigraphic height, considerable overlap existed between the Lower and Upper Pillow Lavas across the ophiolite as a whole, and that metamorphic boundaries within the extrusive sequence did not necessarily coincide with chemical ones, except where obvious unconformities could be demonstrated. It was not therefore possible to invoke different tectonic settings to explain the formation of the LPL and UPL.

Later, more detailed work on individual sections through the lava sequence on the northern flank of Troodos by Robinson *et al.* (1983) and Schmincke *et al.* (1983) showed that the extrusive pile was in fact composed of numerous, often chemically distinct, volcanic units. They identified two major magma groups: a lower highly evolved andesite–dacite–rhyolite suite, and an upper, more depleted, basalt–basaltic andesite assemblage of boninitic affinity (see below), and showed that the transition between the suites occurred at a much lower stratigraphic level than the LPL-UPL boundary (defined on metamorphic grounds) of Gass and Smewing (1973).

On the southern flank of Troodos Simonian (1975) identified several petrographically distinct lava types in the AFB; however, he was unable to erect a coherent lava stratigraphy, suggesting instead that the lavas in the AFB were randomly interbedded. In a comparative study, Simonian (*op. cit.*) found none of the highly evolved dacites and rhyolites typical of Troodos LPL; instead, he showed that the major element composition of the average AFB lava was similar to that of the average Troodos *Upper* Pillow Lava,

although its incompatible trace element abundances were lower at a given index of fractionation, *e.g.* MgO content. Low rare-earth element (REE) abundances in the most depleted group of AFB lavas (with the "type C" chondrite-normalised pattern of Simonian and Gass *op. cit.*), which have no equivalents on the northern flank of Troodos, were indicative of a distinct mantle source apparently not available to the north. Simonian and Gass (*op. cit.*) suggested that the differences in magma-genetic and eruptive mechanisms between the northern and southern flanks of Troodos could be explained by higher degrees of partial melting beneath the transform, coupled with the greater ease of magma egress through the plentiful fracture zones, and thus more limited opportunity to fractionate.

4.1.2 Evidence for the supra-subduction zone origin of Troodos lavas

Much of the early uncertainty as to the significance of the differences between Troodos lavas and mid-ocean ridge basalts (MORBs) was clarified by the work of Pearce (1980). He showed very clearly the nature of the differences by normalising the Troodos lavas to typical MORB and plotting the relative abundances of trace and minor elements in order of decreasing incompatibility. This revealed a systematic enrichment with respect to MORB in all Troodos lavas of the large-ion lithophile elements (LILE), *viz.* Sr, K, Rb and Ba, and a depletion in the high field strength elements (HFSE: Ta, Nb, Zr, Hf, and Ti). A typical plot is shown in figure 4.1 for lavas (from this study) from the ELFC, selected to span the entire range of observed compositions.

The LILEs are mobile in aqueous media, and their enrichment is most easily explained by the input of aqueous fluids derived from the dehydration of subducted ocean lithosphere into their mantle source regions (Pearce 1982). Almost identical patterns are found in island arc tholeiites. The low abundances of the HFSE with respect to MORB in the Troodos lavas can be explained either by the generation of the magmas at higher degrees of partial melting, or their derivation from a mantle source depleted in the incompatible (magmatophile) elements by a previous episode of melting (Pearce op. cit.).

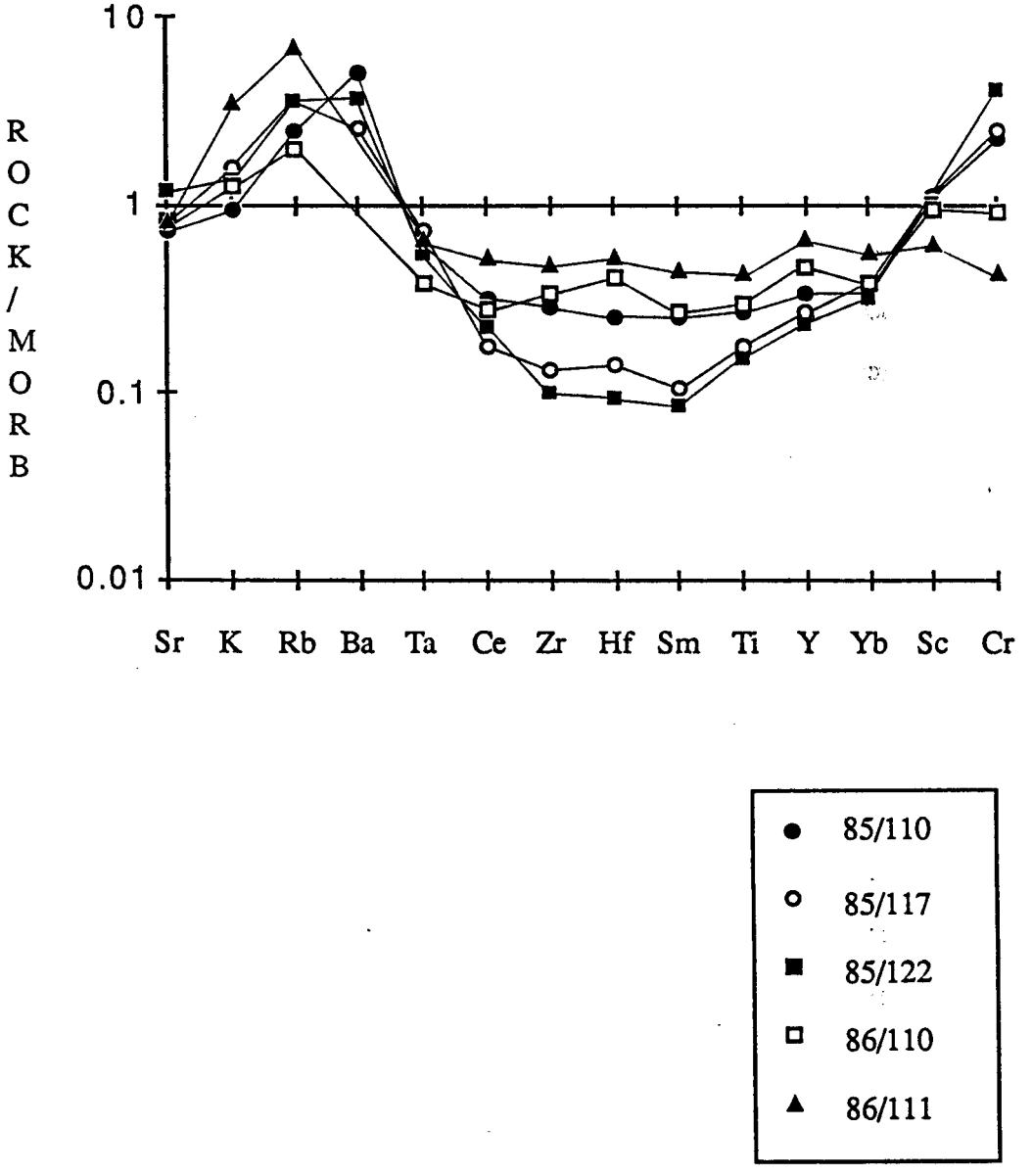

Figure 4.1: MORB-normalised trace element patterns for typical ELFC lavas. The samples are all fresh glasses, chosen to minimise alteration effects, and span the entire range of compositions observed in the ELFC. Enrichment of the large-ion lithophile elements (Sr, K, Rb and Ba) is observed in all Troodos lavas and, as these elements are mobile in aqueous media, is most easily explained by the input to their source of fluids derived from the dehydration of subducted oceanic lithosphere. Depletion of the high field strength elements (Ta, Zr, Hf and Ti) can be explained either by the generation of the Troodos magmas at very high degrees of partial melting or (more likely: see section 4.5.2), by their derivation from a mantle source already depleted in these elements by a previous melting event. Normalising values (from Pearce 1982): Sr = 120ppm; K_2O = 0.15wt%; Rb = 2.0ppm; Ba = 20ppm; Ta = 0.18ppm; Ce = 10.0ppm; Zr = 90ppm; Hf = 2.4ppm; Sm = 3.3ppm; TiO_2 = 1.5wt%; Y = 30ppm; Yb = 3.4ppm; Sc = 40ppm and Cr = 250ppm.

This is discussed further in section 4.5.

4.1.3 On boninites, and reasons for studying them

Simonian and Gass (1978) classified the primitive AFB lavas as 'basaltic komatiites', after Brooks and Hart (1974), on mineralogical, textural and geochemical grounds. The use of this term was, however, criticised by Sun and Nesbitt (1978) on the basis of the low CaO/Al_2O_3 ratios and incompatible trace element abundances of the AFB rocks, and because it implied that they were derived, like Archaean komatiites, from large-degree anhydrous melting of relatively undepleted mantle.

Cameron *et al.* (1979) and many subsequent authors have suggested that the rocks are better described as 'boninites' or 'transitional boninites' (Beccaluva and Serri 1988), after the rare high-magnesium andesites of the Chichijima (Bonin) Islands of Japan (Kikuchi 1890, Petersen 1891). The definition and repeated redefinition of the term, and its relevance to the Troodos lavas, has been the subject of much debate, the pertinent details of which are discussed in the latter parts of this chapter. Most (Anglo-Saxon) authors agree that boninites are petrographically distinct rocks containing rapidly crystallised pyroxene and/or olivine, often mimicking a spinifex texture (Cameron and Nisbet 1982), and that plagioclase, if present at all, crystallises after clinopyroxene (in contrast to normal MORB). Chemically they are characterised by high SiO_2, MgO and volatile contents, and by extremely low incompatible element abundances.

Boninites from the type locality and elsewhere in the Western Pacific are situated in supra-subduction zone (nominally 'fore-arc') settings, although their origin from a tectonic point of view is poorly known. Their interest to the geochemist far outweighs their volumetric abundance, for their primitive, unfractionated character is virtually unique amongst arc-related volcanic rocks, and they can thus offer the most direct opportunity to investigate the nature of processes operating in the sub-arc mantle wedge.

Whilst it is beyond the scope of this study to construct as rigorous a petrogenetic

model as has been formulated by other (specialist) geochemists (*e.g.* Flower and Levine 1987), this author has the advantage of a relatively well-constrained model for the structural and volcanic history of part of the Southern Troodos Transform Fault, and the newly-recognised Anti-Troodos crustal fragment (chapter 3). An opportunity therefore exists to investigate the local tectonic controls on boninite genesis, which are very poorly known, by means of an examination of the spatial extent and temporal occurrence of the primitive lavas in and adjacent to the transform in the ELFC and, in discussion, more generally across the Troodos Massif as a whole. The basis of this study is a geochemical traverse through the Kalavasos Mines lava section, and a comparison of these rocks with others from elsewhere in the transform-tectonised and non-transform parts of the ELFC.

4.2 Petrography

Three distinct petrographic sub-groups can be identified within the ELFC lavas, based upon the mineralogy of the groundmass and, where present, the phenocryst assemblage. The primary igneous assemblage is usually modified, to a greater or lesser extent, by hydrothermal alteration; however, this appears to be a passive process which does not destroy the original fabric of the rock, so it is usually possible to identify the primary mineralogy even in the most highly-altered samples. In sections 4.2.1–4.2.3 examples from each of the three petrological groups least affected by secondary processes are described. In section 4.2.4 more unusual lavas from the ELFC are discussed. The petrological and geochemical consequences of hydrothermal alteration are described in section 4.3.

4.2.1 Plagioclase–clinopyroxene suite

This group of lavas is typically aphyric, and characterised by a plagioclase-dominated assemblage, usually in conjunction with clinopyroxene. In the groundmass plagioclase needles and equant anhedral to subhedral clinopyroxene, both less than *c*.0.5mm in length, give rise to an intersertal texture, with the interstitial glass appearing always to be devitrified. Magnetite is an important accessory in many samples, particularly those in which clinopyroxene is subordinate or absent, forming tiny equant grains *c*.0.01mm across. Orthopyroxene is occasionally present in the more ferromagnesian-rich samples, and, like clinopyroxene, has an equant form.

Sample 86/110 is the sole example found by this author of a non-devitrified lava belonging to this group. It comes from a vitreous chilled pillow margin and is unusual for the presence of glomeroporphyritic aggregates of plagioclase and clinopyroxene up to 2mm long set in fresh, pale green glass with perlitic cracks (plate 4.1). The feldspar and pyroxene are of compositions $An_{86\text{-}90}$ (bytownite–anorthite) and $Ca_{42\text{-}44}Mg_{50\text{-}51}Fe_{6\text{-}8}$ (endiopside) respectively, and appear to have crystallised simultaneously. Another porphyritic sample, 86/111, contains some tabular euhedral bytownite feldspar phenocrysts ($An_{81\text{-}84}$) which display oscillatory zoning. This sample contains accessory magnetite and is devoid of pyroxene in the groundmass.

4.2.2 Olivine–clinopyroxene suite

The second petrographically distinct sub-type amongst the ELFC extrusives is a suite of olivine-phyric lavas, with a hyalopilitic groundmass of essential olivine and clinopyroxene displaying a range of quench morphologies. Glass is common at pillow margins (see plate 4.2), and may be sufficiently fresh for whole-rock defocused-beam microprobe analysis to be possible (see section 4.4). The olivine phenocrysts, which occur in both pillow margin and core alike, are up to 2mm long and frequently display characteristic 'hopper' morphologies (plate 4.2) indicative of rapid cooling (see below).

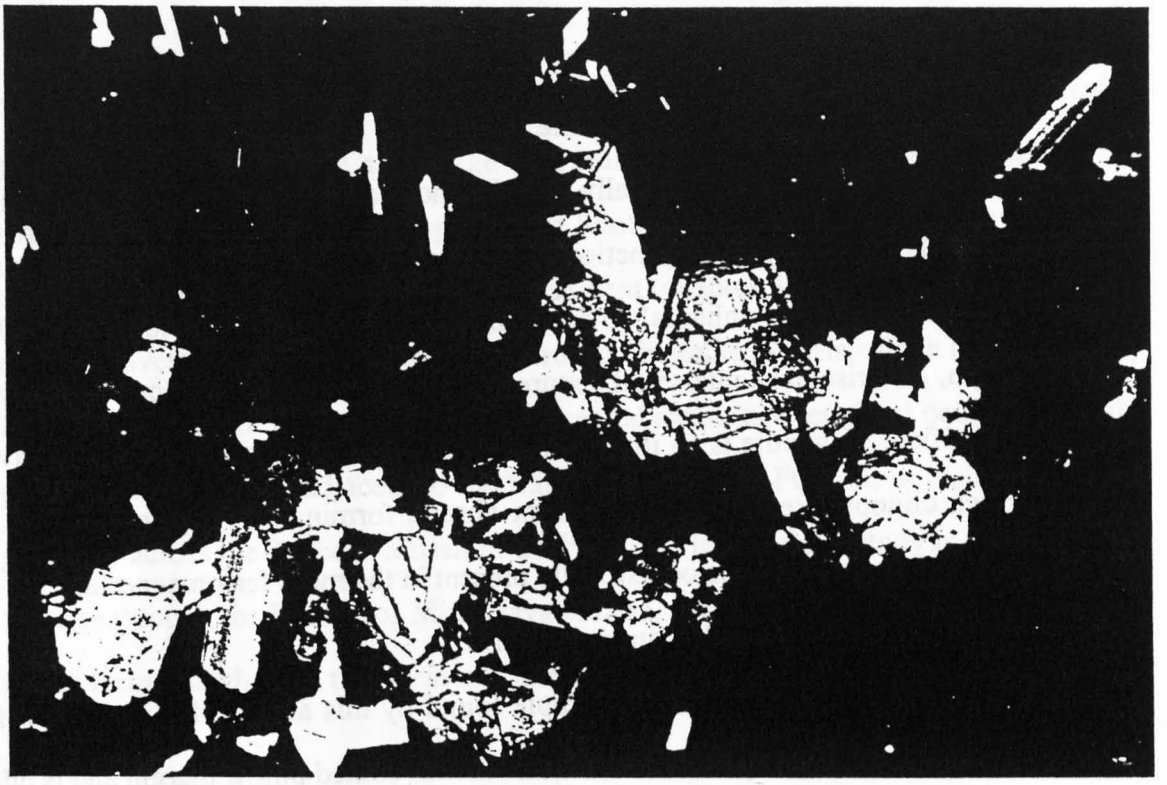

Plate 4.1: Glomeroporphyritic clinopyroxene–plagioclase-phyric hyaloclastite, with fresh vitreous glassy matrix. 86/110 Lower Pillow Lava (flow unit a). 23835105 Kalavasos Dam. FOV 3.5mm, X-polars.

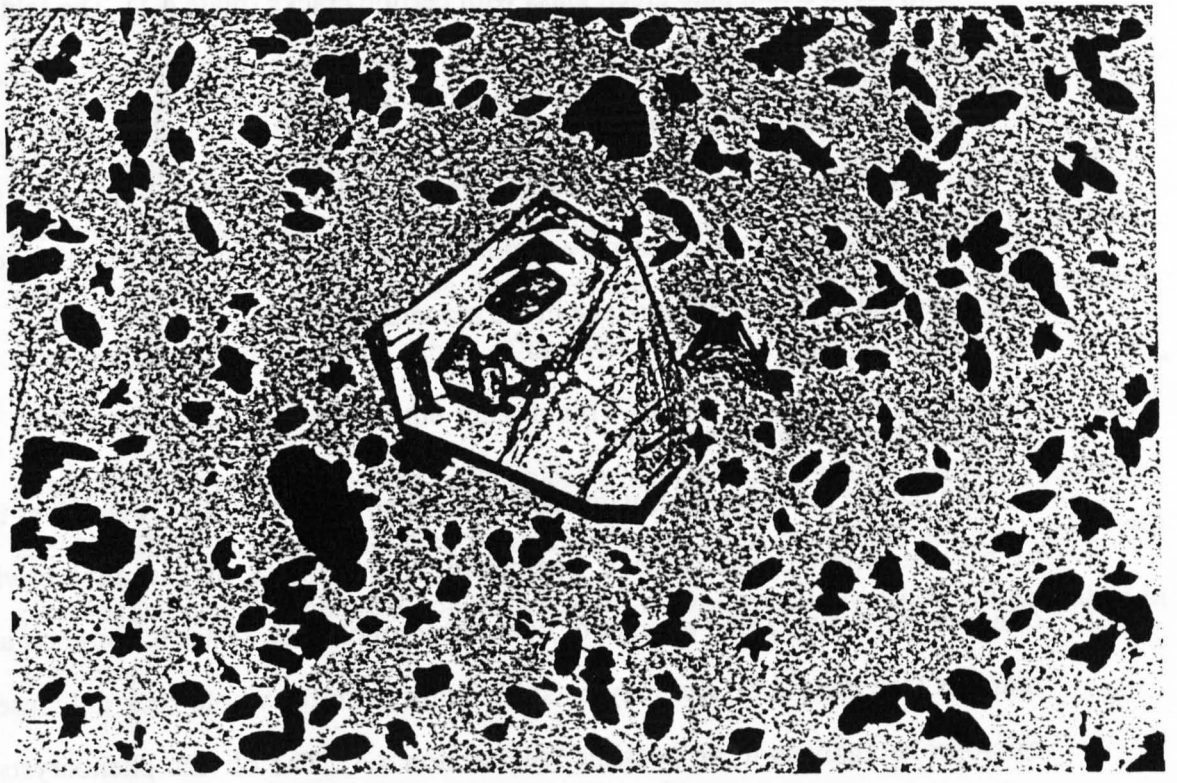

Plate 4.2: 'Hopper' olivine phenocryst set in vitreous isotropic glass, with bundles of olivine/ clinopyroxene microcrystallites. 86/74 'limburgite' pillow margin (flow unit d). 24845115 Mandra tou Alykou, Kalavasos Mines. FOV 2.8mm, PPL.

The texture of the groundmass varies systematically from pillow rim to core. Colourless isotropic glass at the rim develops sheaf-like aggregates of microcrystalline olivine needles *c*.0.2mm long, which increase rapidly in abundance towards the interior of the pillow and coalesce to form a felted mat-like texture. From this, acicular olivine and clinopyroxene crystals with a variety of quench morphologies have developed.

Olivine most commonly occurs as long chains or 'vertebrae' (in optical continuity) up to 0.5mm long but only 0.01-0.02mm wide. In one petrographic section of sample 85/110, taken *c*.1cm from the pillow margin, chain olivines are accompanied by several twinned radial olivines (plate 4.3), which consist of two crystals intergrown with their 'c'-axes at a 60° angle. This morphology is extremely rare in nature, having been decribed only from the Taiwan coast ophiolite (Liou 1974), and one other sample from the ELFC (Jørgensen and Brooks 1981). Experimental studies (Donaldson 1976) suggest that such twinned, radiate morphologies form only under very restricted conditions, *viz.* at *c*.20°C supercooling (*i.e.* crystallisation at a temperature 20°C below the olivine liquidus). The appearance of, in turn, sheaf-like (variolitic), chain and twinned radial olivines with increasing distance from the cooling interface (*i.e.* the pillow margin) suggests that they crystallised *in situ* and is in accord with experimental observations that the respective morphologies form at progressively lower degrees of supercooling (Donaldson *op. cit.*). However, the presence of the hopper olivine phenocrysts throughout the pillow core and glassy margin implies that they crystallised when the magma was still liquid, and that flow was thus taking place at supercooling rates of *c*.5-10°C (Jørgensen and Brooks *op. cit.*). This in turn implies that the phenocrysts are unlikely to be magma chamber crystallisates, but were probably nucleated on magma ascent immediately prior to or upon eruption.

Clinopyroxene crystallises after olivine in these rocks and forms abundant curved, branching dendrites with compositions $Ca_{38-47}Mg_{36-49}Fe_{11-18}$. These may give rise, *in extremis*, to spectacular fans of crystals forming 'cockscomb' textures up to 2.5mm in

Plate 4.3: Twinned radial olivine crystal (colourless; lower centre part of picture) surrounded by acicular branching clinopyroxenes and olivine needles in fresh (colourless) to devitrified (brown) glassy matrix. 85/110 (flow unit d). 24805112 Mandra tou Alykou, Kalavasos Mines. FOV 0.7mm, PPL.

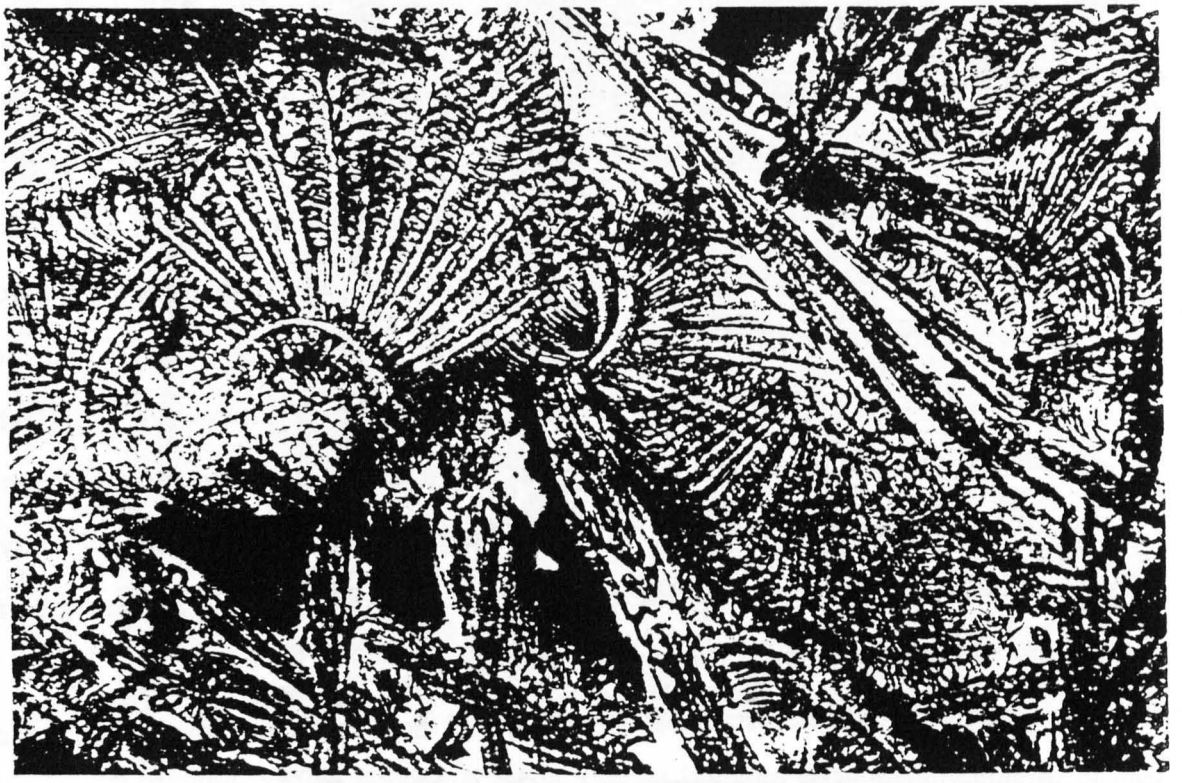

Plate 4.4: Curved branching 'cockscomb' and straight 'vertebral' clinopyroxenes, and olivine needles. 85/110 (flow unit d). 24805112 Mandra tou Alykou, Kalavasos Mines. FOV 0.9mm, PPL.

diameter (plate 4.4). These appear to be nucleated on pre-existing crystallites, either clinopyroxene or, in one observed case, a small chrome spinel crystal. Spinels are generally not common in these lavas, occurring as tiny diamond-shaped euhedra within a few olivine phenocrysts, and very rarely in the groundmass.

With decreasing cooling rate, *i.e.* towards the centre of the larger pillows, the clinopyroxene gradually assumes a more blocky, prismatic appearance, albeit often elongate. This is accompanied by the appearance of discrete circular patches or spherules of very fine-grained devitrified brown or yellowish material up to 2mm in diameter (plate 4.5). These are aggregates of clay minerals, which appear to be pseudomorphing equally fine-grained feldspar microlites (see section 4.3). In the centres of these spherules acicular plagioclase (An_{71-74}) may be preserved. The spherules increase in proportion rapidly towards the centres of the pillows, and thenceforth form the major part of the groundmass. The onset of plagioclase crystallisation is very obvious in the field, as the concomitant devitrification of the glassy interstices changes the dark, hard appearance of the olivine–clinopyroxene–glass lava to a crumbly argillised 'metabasalt', giving rise to some pillows with a dark glassy 'limburgitic' pillow margin but grey devitrified core.

4.2.3 Olivine–orthopyroxene–clinopyroxene suite

This group is characterised by the presence of orthopyroxene, either as a phenocryst or microphenocryst phase, or in the groundmass. A few examples are aphyric, but in the majority of cases the lava is olivine-phyric, with the olivines, as in the previous group, up to 2mm long and displaying 'hopper' morphologies. Orthopyroxene typically ranges in size from 0.1-2mm in a single section and forms equant or slightly elongate euhedral–subhedral prisms, occasionally with skeletal growth textures. Microphenocrysts of clinopyroxene up to 0.5mm long are also present, frequently forming irregular, blocky agglomerations or intergrowths with orthopyroxene (see below).

Similar textures to those reported from the olivine–clinopyroxene suite occur in the groundmass, though olivine microlites are not so abundant and twinned radial

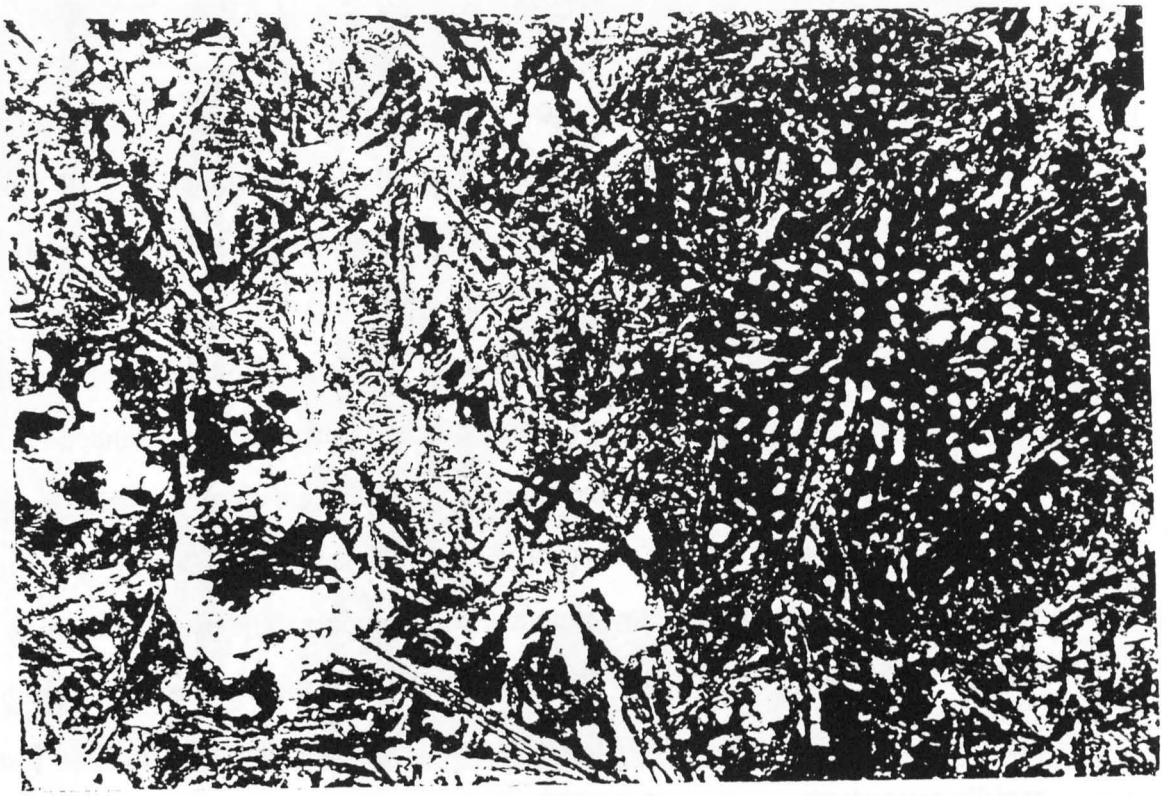

Plate 4.5: 2mm diameter spherulite marking the site of incipient plagioclase crystallisation in an olivine-phyric lava. The yellow colour represents smectite. 85/110 (flow unit d). 24805112 Mandra tou Alykou, Kalavasos Mines. FOV 3.5mm, PPL.

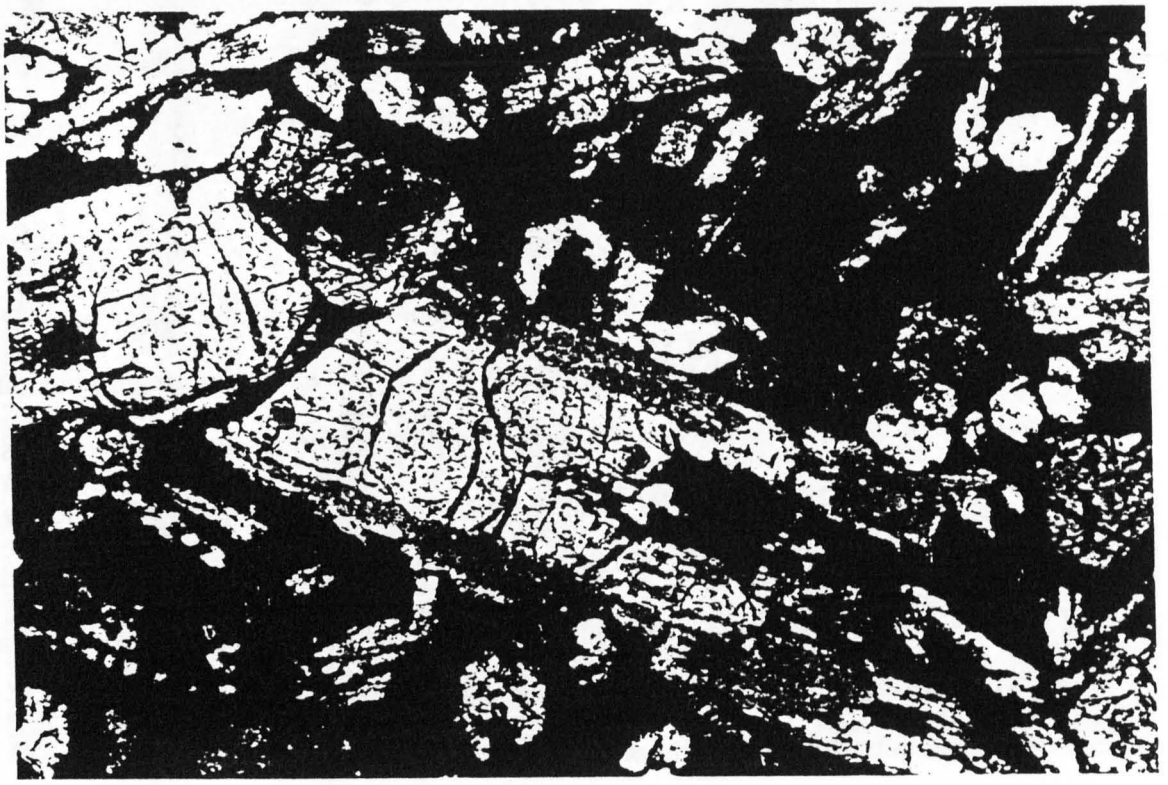

Plate 4.6: Orthopyroxene phenocryst jacketed by clinopyroxene. 85/117 (flow unit e). 24875120 Mandra tou Alykou, Kalavasos Mines. FOV 0.9mm, X-polars.

morphologies were not observed. Sheaf-like variolites appear in the olivine- and orthopyroxene-bearing vitreous glassy pillow margin, and from these aggregates gently curved, branching clinopyroxene dendrites grow rapidly in size and abundance in the interior parts of the pillow. Orthopyroxenes do not appear to assume this dendritic habit, but form equant to slightly elongate prisms with length to width ratios rarely greater than *c*.5:1. Chrome spinel is an early-formed phase within the olivine phenocrysts and also in the groundmass, where occasional equant, euhedral microphenocrysts up to 0.25mm in diameter may occur. Plagioclase appears in exactly the same manner described for the previous petrological group above.

A characteristic feature of the olivine–orthopyroxene–clinopyroxene suite of lavas is the presence, in addition to the blocky two-pyroxene intergrowths mentioned above, of orthopyroxenes ($Ca_5Mg_{84}Fe_{11}$) with marginal overgrowths or 'jackets' of clinopyroxene ($Ca_{37}Mg_{56}Fe_7$) (plate 4.6). These occur on both phenocryst and groundmass orthopyroxenes–more strictly low-Ca pyroxenes or 'magnesian pigeonites'–which have undulose and inclined extinctions indicative of lattice defects, and a monoclinic rather than orthorhombic structure; this is probably a function of extremely rapid growth. It should be noted here that these are *not* the same as the clinoenstatite crystals reported from Cape Vogel, Papua New Guinea (Dallwitz *et al.* 1966) and Bonin Islands (Komatsu 1980) boninites, which are exceptionally low in Ca (<1% Wo) and display ubiquitous closely-spaced multiple twin lamellae. 'Jacketed' clinopyroxene-on-orthopyroxene textures identical to those described here do, however, occur in Bonin Islands boninites, and have been reported from boninites in the Mariana fore-arc by Natland (1981). They have been interpreted by him as a disequilibrium phenomenon, caused by the rapidity of orthopyroxene growth depleting the surrounding medium in (particularly) Mg ions faster than the rate of diffusion towards the site of nucleation, and consequent enrichment of the immediate surroundings in Ca, Al and Ti to form an environment favourable for high-Ca pyroxene crystallisation. In support of this he cites

systematically lower En contents in the Mariana clinopyroxene borders than in coexisting microphenocrysts; however, the single analysis 85/117ZJX (appendix 5) from a clinopyroxene rim in an ELFC lava does not show such a distinction, and it is possible that some of the borders are simply dendritic overgrowths of quenched groundmass clinopyroxene which have nucleated on pre-existing microphenocrysts at high degrees of undercooling. Similar overgrowth textures occur in other boninites and appear to be characteristic of the rock type: Komatsu (1980) describes rims of clinoenstatite on olivine, and bronzite on olivine and clinoenstatite, and Dallwitz *et al.* (1966) report clinopyroxene bordering clinoenstatite and bronzite.

4.2.4 Other lavas

In section 3.3.4 picrite flows and pillows containing olivine crystals up to 1cm long were reported occurring in conjunction with orthopyroxene-bearing lavas in the Kalavasos Mines (see section 4.4). The olivine shows pronounced crystal settling (*cf.* Searle and Vokes 1969), and in the lower parts of the flows can form up to 50% of the modal proportion of the rock. The upper parts, in contrast, may be virtually olivine-free and have textures and mineralogies identical to the overlying non-picritic lavas (described in section 4.2.3 above). In thin section some of the olivines display strain morphologies *viz.* undulose extinction, kink bands and sub-grains (plate 4.7). Resorption features (*i.e.* rounded embayments) have been described in olivine crystals from other picrites in the northern Troodos lavas (Gass 1958, Cameron 1985) but, significantly, in the Kalavasos Mines examples are extremely rare. The picrite olivines are texturally quite distinct when compared to the quenched phenocrysts described in the preceding sections, which suggests that they might instead be xenocrysts. This assertion is explored further in a study of the mineralogy and chemistry of the picrite lavas in section 4.4.3.

In the Monagroulli area olivine–orthopyroxene–clinopyroxene flows (sample 86/147) also carry what appear to be xenocrysts (*sensu lato*), this time of orthopyroxene, either

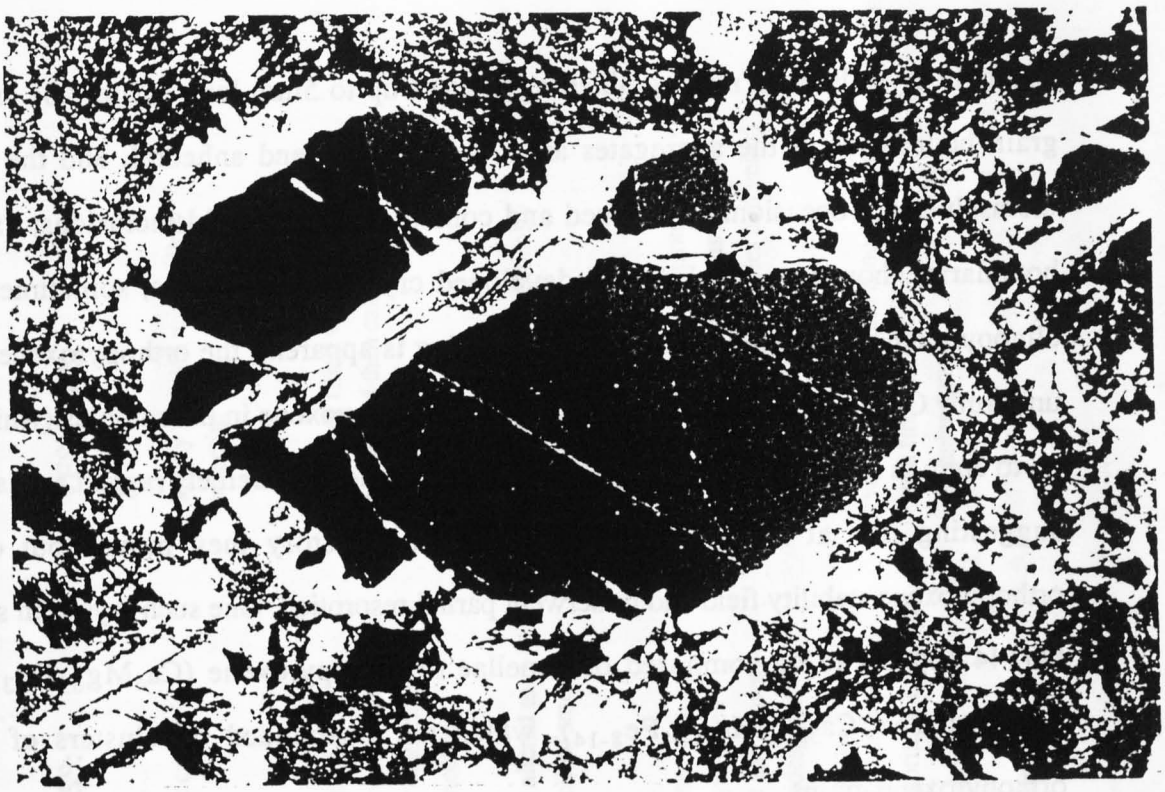

Plate 4.7: Strained olivine phenocryst in picrite. Sub-grain formation is parallel to fractures within the crystal, suggesting brittle deformation? The crystal is partially rimmed by serpentine. The groundmass consists of olivine, clinopyroxene and euhedral chrome-spinel set in devitrified glass. 85/124 (flow unit e), base of flow. 24865120 Mandra tou Alykou, Kalavasos Mines. FOV 5.5mm, X-polars.

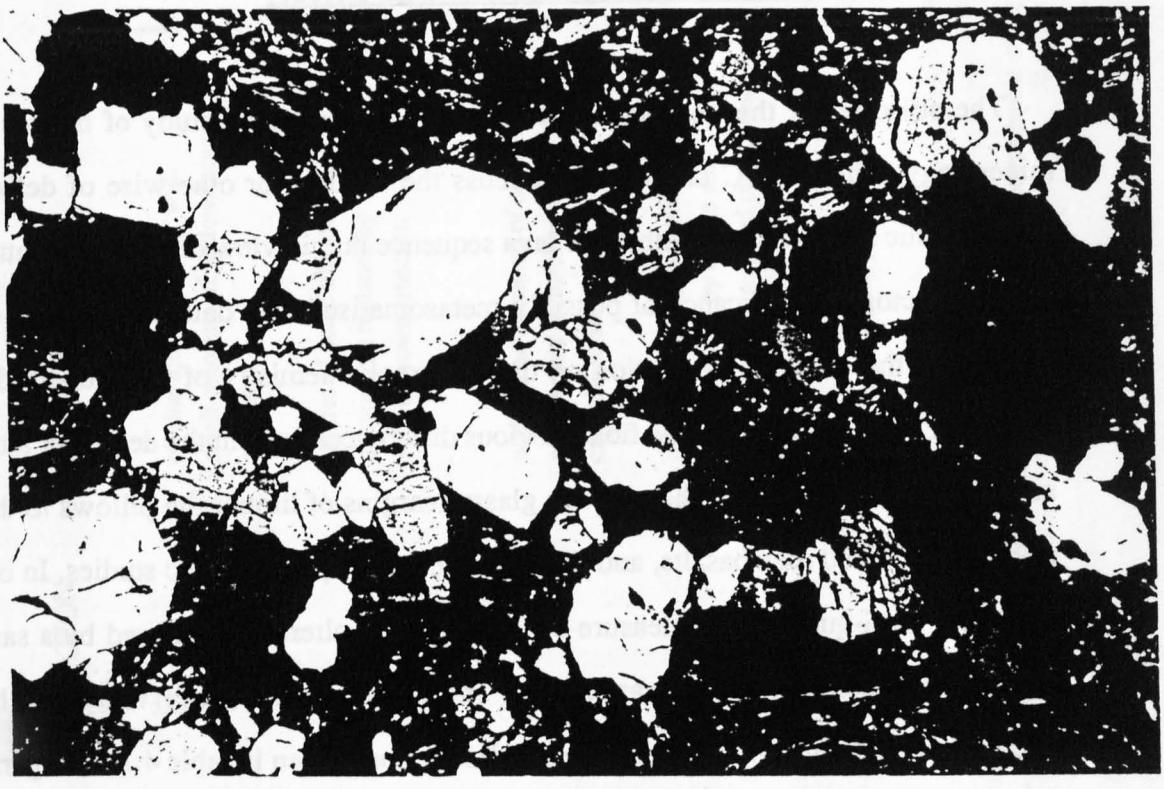

Plate 4.8: Aggregates of orthopyroxene xenocrysts in heavily porphyritic flow. Some crystals have thin clinopyroxene jackets. 86/147. 18694585 Monagroulli. FOV 4.5mm, X-polars.

as single crystals or as multi-grained aggregates up to 5mm long (plate 4.8). Internal grain boundaries in the aggregates are always curved and anhedral, and the grains themselves are occasionally strained and contain abundant fluid inclusions; external boundaries, however, display well-developed crystal terminations, sometimes with clinopyroxene jackets. No compositional zoning is apparent, the orthopyroxene being uniformly $Ca_4Mg_{84}Fe_{12}$. The single crystals of orthopyroxene in the samples (which are up to 3mm in length) are, in contrast, sieve-textured and of extremely ragged appearance, suggesting that at some stage in their eruptive history they moved out of the orthopyroxene stability field and underwent partial resorption. One such crystal in sample 86/144 appears to be composed of lamellae of orthopyroxene ($Ca_4Mg_{83}Fe_{13}$) and clinopyroxene ($Ca_{38-40}Mg_{46-54}Fe_{8-14}$), which are surrounded by clusters of small orthopyroxene grains.

4.3 Alteration: Petrological and Geochemical Effects

The objective of this section is not to undertake a detailed study of the secondary mineralogy of the ELFC lavas, or to discuss the wisdom or otherwise of delineating metamorphic sub-divisions within the lava sequence but, in view of the past controversy over the tectonic significance of possibly-metasomatised lava data (see section 4.1), to investigate the effects of alteration on the bulk-rock chemistry of samples used in the remainder of this chapter. In the field, obvious differences exist in the degree of alteration suffered by the lavas, from the vitreous glassy margins of limburgite pillows to the grey or green argillised metabasalts, and this is borne out by petrographic studies. In order to provide a semi-quantitative measure of the degree of alteration suffered by a sample a petrographic 'alteration index' was devised. This ranges from 1 (fresh) to 5 (most heavily altered) and is defined by the petrographic descriptions given in table 4.1. Categories 1-3 correspond to lavas of glassy appearance in the field (1 to vitreous pillow spall only) and

ALTERATION INDEX:	PHENOCRYSTS:	GROUNDMASS:	VESICLES:
1:	olivine totally fresh or with small amounts of yellow/brown smectite	occasional perlitic cracks in isotropic glass	empty or filled with yellow smectite
2:	centres of some olivine phenocrysts replaced by yellow/brown smectite	fresh olivine and pyroxene microlites; glassy mesostasis partly replaced by colourless to dusty brown smectite	empty or filled with fibrous zeolite and then calcite
3:	widespread alteration of olivine phenocrysts (centres or whole crystals) to smectite	glassy mesostasis altered to dusty brown or yellow smectite, rarely calcite	fibrous zeolite, occasionally calcite also
4:	olivine phenocrysts pseudomorphed by smectite or by calcite and goethite. pyroxenes and plagioclase fresh	acicular plagioclase fresh, but incipient microcrystallites altered to smectite and brown goethite. calcite widespread	occasional celadonite (sometimes widespread), then fibrous zeolite and then calcite (vesicles and veins)
5:	clinopyroxene and plagioclase fresh	widespread alteration to smectite and celadonite (chlorite in Basal Gp)	voids filled by thin rime of smectite then fibrous chalcedony and granular quartz

Table 4.1: 'Alteration indices', and a summary of the petrographic effects of hydrothermal alteration

category 5 restricted to those lavas which show petrographic evidence for silica metasomatism (*i.e.* chalcedony infilling vesicles) These categories correspond approximately to those used by Cameron (1985). The alteration indices of the Kalavasos Mines samples considered in section 4.4 are shown in table 4.2.

The effects of hydrothermal alteration on the major and trace element contents of the lavas are summarised in figure 4.2. TiO_2, along with Zr and Y (and Nb) are considered immobile under conditions of seafloor weathering and alteration (Cann 1970), and the close correlation between TiO_2 and Zr, and coincidence of fresh (filled circles: alteration indices 1-3) and altered (open circles: alteration indices 4 & 5) lava analyses, supports this for these two elements. Y values for the altered lavas, however, are more dispersed, and suggest that this element might be slightly mobilised by hydrothermal processes.

Gillis and Robinson (1988) identified five mineralogically and petrologically distinct hydrothermal alteration zones in the upper parts of ophiolitic and *in situ* oceanic crust, *viz.* (in descending order): (i) a 'seafloor weathering zone', (ii) a 'low-temperature zone', (iii) a 'transition zone', (iv) an 'upper dyke zone', and a separate 'mineralisation zone' (v). Figure 4.2 shows that, in general terms, the altered samples from the ELFC have suffered a loss to the whole-rock of Si and Ca, and gain of Na, K, Rb and Sr (the latter appearing to have been mobile in some of the glassy samples too). This corresponds to the 'low-temperature zone', implying that they have undergone highly variable degrees of low temperature alteration (<50-100°C) at low–moderate water–rock ratios (<5-10). Of the remaining elements displayed in figure 4.2, Al remains stable under these conditions, FeO^{tot} and Mg show a possible minor increase amongst the more TiO_2-rich samples, and Mn displays both gains and losses. A single sample of Basal Group lava (86/163), in contrast, shows a relative enrichment in Mn and Na, but loss of Ca, K, Rb and Sr, which Gillis and Robinson (*op. cit.*) show is characteristic of their 'upper dyke zone', with alteration at low water/rock ratios (<5-10) and higher temperatures (≥200°C).

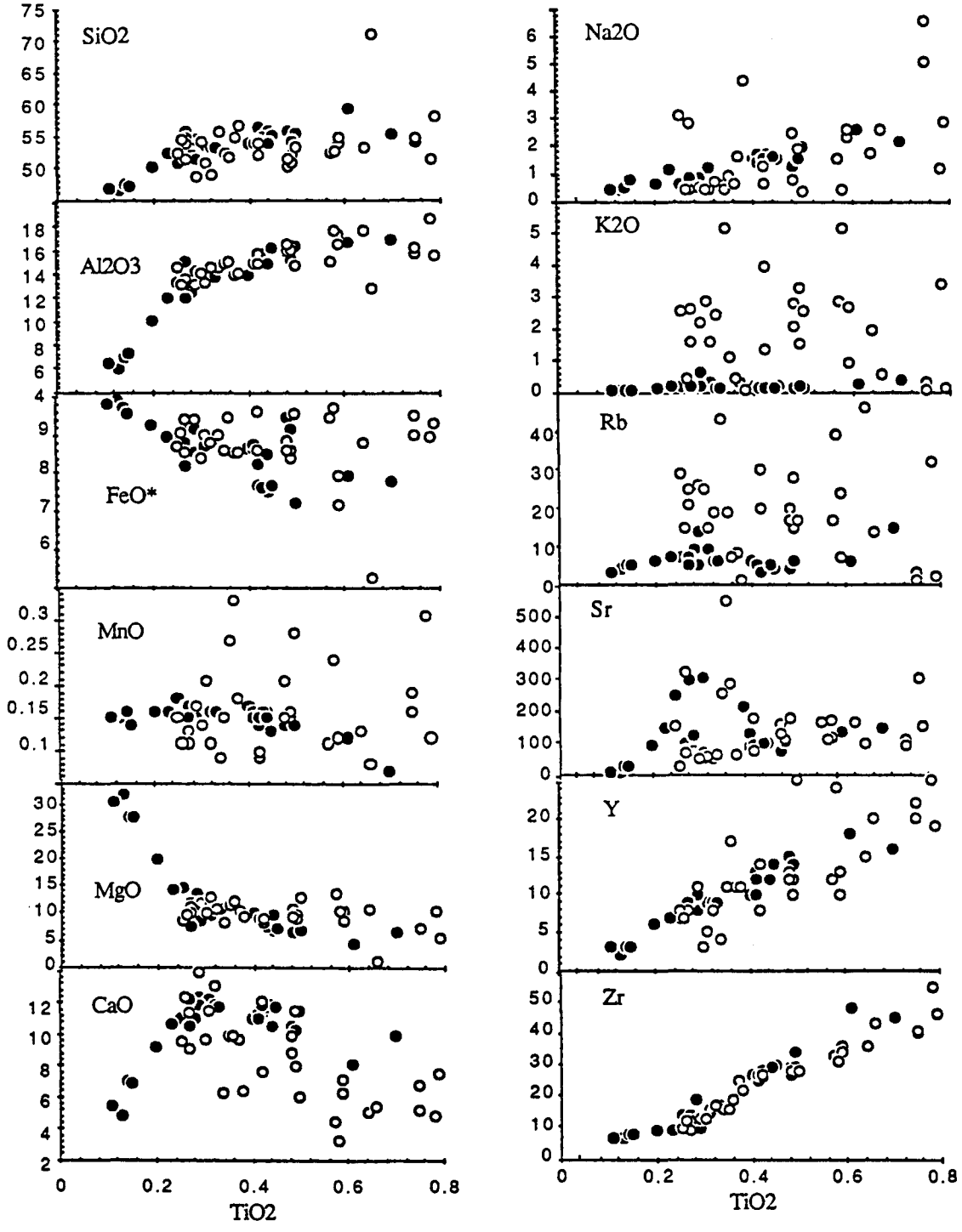

Figure 4.2: Summary diagrams illustrating the effects of hydrothermal alteration on the major and trace element concentrations of lavas from the ELFC. Ti, Zr and Y are considered immobile under conditions of seafloor alteration and metamorphism up to lower greenschist facies (Cann 1970); elements are therefore plotted against TiO_2. Black circles = fresh glassy lavas (alteration indices 1-3 in table 4.1); white circles = altered 'metabasalts' (alteration indices 4&5).

4.4 The Kalavasos Mines Geochemical Traverse

4.4.1 Introduction

Thirty-five samples from the Kalavasos Mines and five from the Asgata River were analysed for the major and trace elements by X-ray fluorescence (see appendices 1 and 3). They were taken from known stratigraphic levels within the extrusive sequence, particularly from the vicinity of known volcanological boundaries, such as Adamides' (1980) LPL-UPL umber horizon and the limburgite-olivine basalt intervolcanic sediment horizon, in an attempt to identify if flow units were chemically distinctive, and if so whether a geochemical stratigraphy could be erected. In figure 4.3 TiO_2 is plotted against stratigraphic height, with Adamides' LPL-UPL boundary as the zero datum. TiO_2 is chosen here as it is the most incompatible of the immobile major elements, and is therefore least likely to be affected by partitioning into the major mineral phases during fractional crystallisation; thus differences in its concentration can give information reflecting primary (*i.e.* mantle source-related) differences. Zr is an equally good discriminant for the same reasons, and is used in figure 4.4, which shows in more detail chemical variation across the LPL-UPL boundary. From these plots the lava sequence is subdivided into five distinct flow units labelled respectively 'a' to 'e' (from bottom to top). The LPL were not sampled extensively in this study, as structural complexity and the lack of distinctive marker horizons made it difficult to assign samples to a definite stratigraphic level with any degree of confidence. Unit a, therefore, may include several geochemically distinct lava flows. A general correspondence exists between flow and petrographic group (section 4.2): the clinopyroxene-plagioclase lavas equate to flow unit a and are not found at any other stratigraphic level; above them the olivine–clinopyroxene suite form flow unit d, and orthopyroxene-bearing types units b, c and e (table 4.2).

The lateral persistence of this sequence of flow types is not thought to be great. Although a transition between flow units of types c and d is well documented in the

SAMPLE: (+ flow units)		POSITION ± DATUM:	PETROLOGY: PHENOCRYSTS	GROUNDMASS	ALTN CHEM: INDEX:	(fresh/alt)
85/119	e	+330m	[ol] opx opx/cpx	opx cpx plag	4	A
85/117	e	+260m	ol opx	sp ol opx opx/cpx cpx	2	F
85/123	e	~+200m	—	sp opx cpx	2	F
85/122	e	~+200m	sp ol(x)	sp ol opx cpx	2	F
85/121	e	~+200m	sp ol(x) opx/cpx	ol cpx	2/3	F
85/124	e	~+200m	sp ol(x) opx cpx	ol opx cpx plag	2/3	F
85/116	e	~+200m	sp ol(x)	ol cpx	2	F
85/115	e	~+200m	sp ol(x)	ol cpx	2	F
85/114	e	~+200m	sp ol(x)	ol cpx	2	F
85/113	e	~+200m	sp ol(x)	plag	2/3	F
		SEDIMENT				
85/127	d	+175m	ol	glass cpx	1	F
86/74	d	+170m	ol	glass	1	F
85/109	d	+130m	ol	glass	1	F
85/110	d	+130m	ol	ol cpx	1/2	F
85/108	d	+80m	[ol]	ol cpx plag	4	A
86/56	d	?	ol	ol cpx	1/2	F
85/29	d	Asgata	ol	ol cpx	3	F
85/172	d	Asgata	[ol]	cpx plag	4	A
85/4	c	Asgata	[ol]	cpx plag	4	A
85/171	c	Asgata	[ol]	cpx	3	F
85/21	c	Asgata	sp ol opx	opx opx/cpx cpx	3	F
85/179	c	+3m	ol	ol opx cpx	2	F
85/178	c	+1.5m	ol	ol opx cpx	2	F
85/161	c	+0.5m			4*	A
85/177	c	+0m			4*	A
		DATUM:				
85/180	b	-0m			4*	A
85/160	b	-1m			4*	A
85/181	b	-1.5m	—	opx opx/cpx cpx plag	4	A
85/182	b	-3m	[ol]	opx opx/cpx cpx plag	4	A
85/184	b	-10m			3*	F
86/96	a	(-1m)			4*	A
85/183	a	-20m	—	cpx plag	4	A
85/185	a	-25m			4*	A
85/186	a	-30m			4*	A
86/110	a	~-200m	cpx plag	glass	1	F
86/106	a	~-275m			2*	F
86/108	a	~-275m			2*	F
86/111	a	~-300m	plag	plag mgt	5	A
86/84	a	?	—	cpx plag	4/5	A
86/85	a	?			4/5	A

datum = Adamides' (1980) LPL-UPL interface.
F/A = chemically unaltered/altered. * = estimated from hand specimen
— = aphyric; sp = chrome-spinel; ol = olivine; opx = orthopyroxene; opx/cpx = pyroxene composite; cpx = clinopyroxene; plag = plagioclase; mgt = magnetite; [ ] = pseudomorph; (x) = xenocryst.

Table 4.2: Petrography and stratigraphic position of samples from the Kalavasos Mines geochemical traverse.

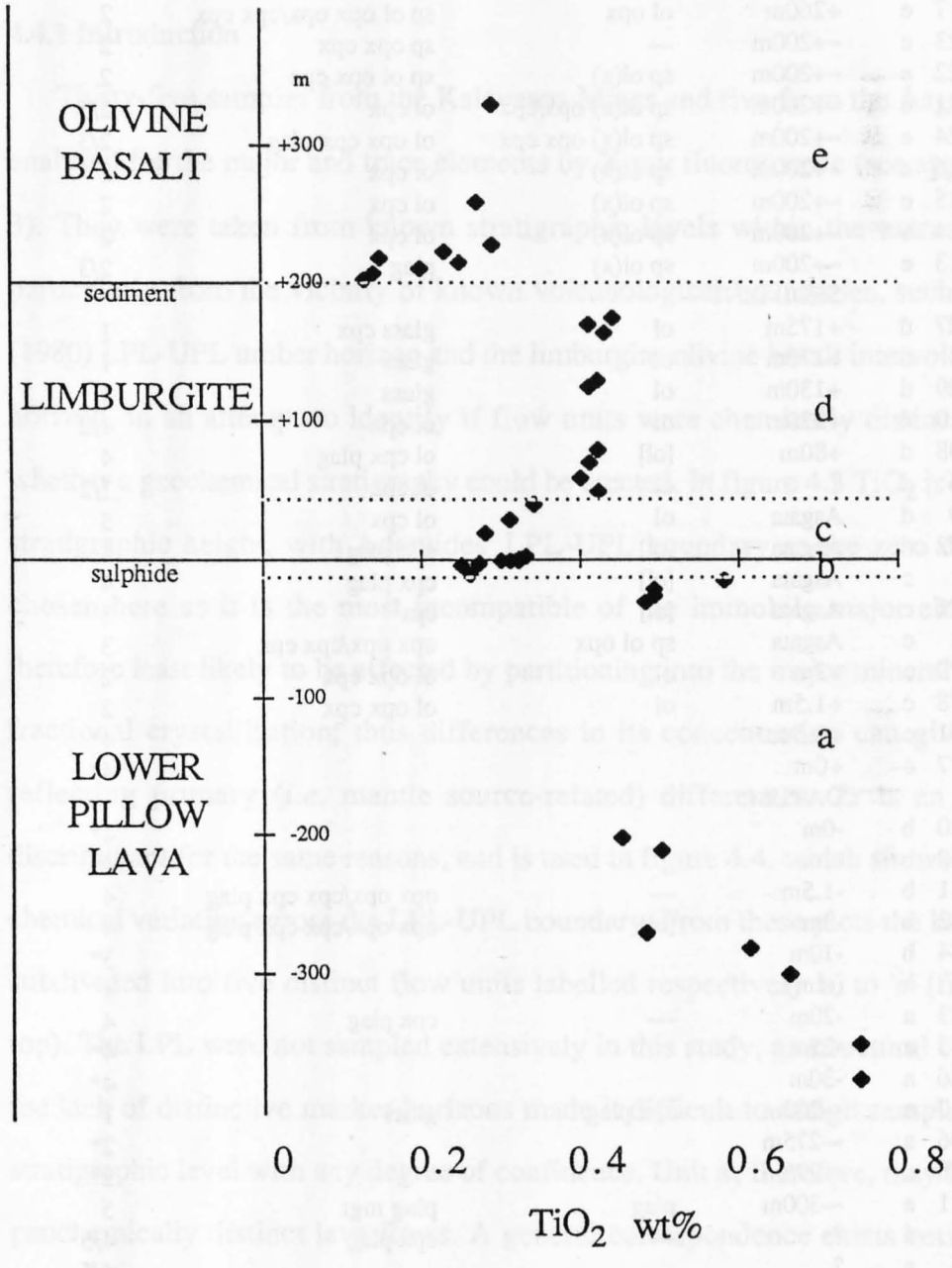

Figure 4.3: Ti content *versus* stratigraphic height, Kalavasos Mines. The 'limburgite' and 'olivine basalt' units (after Adamides 1980) correspond to the Survey's 'Upper Pillow Lavas'. Differences in TiO_2 concentrations enable five geochemically distinct units to be defined (flow units 'a' to 'e', with increasing stratigraphic height). As elsewhere in Troodos, there is a general decrease in TiO_2 with increasing height.

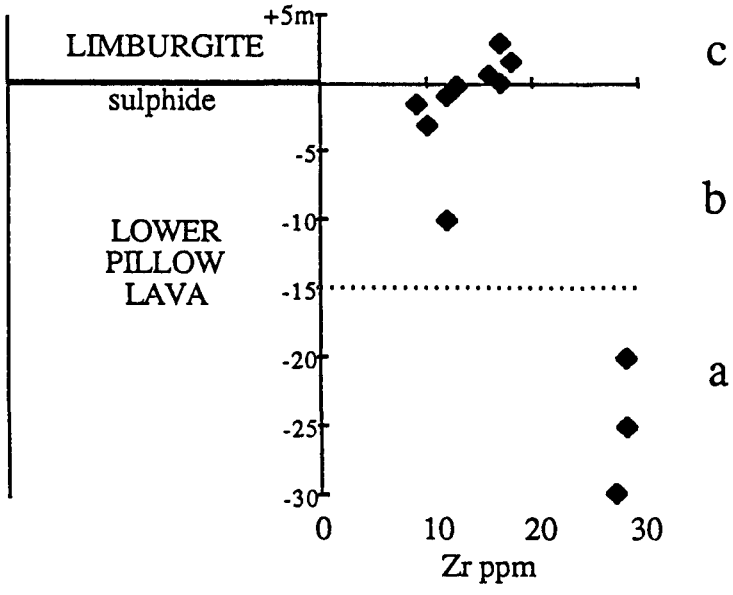

Figure 4.4: Zr content *versus* stratigraphic height in the Kalavasos Mines (Petra) at Adamides' (1980) Lower Pillow Lava–limburgite (Upper Pillow Lava) contact. Note that the change from evolved (high Zr) to depleted (low Zr) compositions occurs between flow units a and b, *i.e. below* the LPL-UPL boundary (defined with respect to the sulphide mineralisation horizon: see chapter 3).

Asgata River (and so is included in this study even though not strictly relevant in a stratigraphic context), along-strike differences exist even within the Kalavasos Mines. The LPL-UPL boundary shown in figure 4.4 was sampled in the vicinity of Petra Mine (~244507); however, at the same stratigraphic level at Polemikon (23485092), sample 86/96, taken from about a metre below the umber horizon, is chemically akin to flow type a, and flow unit b appears to be absent.

4.4.2 Major element variation

In figures 4.3 and 4.4 systematic differences in the incompatible element concentrations of the Kalavasos Mines lavas with stratigraphic height were used to establish discrete flow units. To explore the geochemical characteristics of these units, and particularly to investigate the possible effects of fractionation of the major mineral phases, it is necessary to examine the co-variation of pairs of the major and minor elements. In figure 4.5 six diagrams show the variation between SiO_2, TiO_2, Al_2O_3, CaO and MgO, with the fields occupied by olivine, ortho- and clinopyroxene and plagioclase (averaged from microprobe analyses of phenocrysts in appendix 5) for reference. The large variation in MgO in unit e, which gives rise to a perfect control line towards olivine, is a result of the large proportion of olivine 'xenocrysts' in the picrite lavas, and is discussed in the following section.

In figure 4.5(f) (SiO_2 v Al_2O_3), a slight trend away from orthopyroxene in two samples of unit e suggests that they have suffered a few percent fractionation of this mineral. Units c and d show limited co-variation, again defining good trends towards olivine; simple mass balance calculations (for the above five elements combined) suggest that all major element chemical variation within these flows can be explained by the fractionation of 13% and 8% olivine respectively. Close co-variation of Cr with MgO in these groups suggests that olivine is accompanied by a small amount of chrome spinel fractionation, probably carried in the observed inclusions within the olivine phenocrysts. Variation within flow unit a, in contrast, cannot be explained by simple olivine

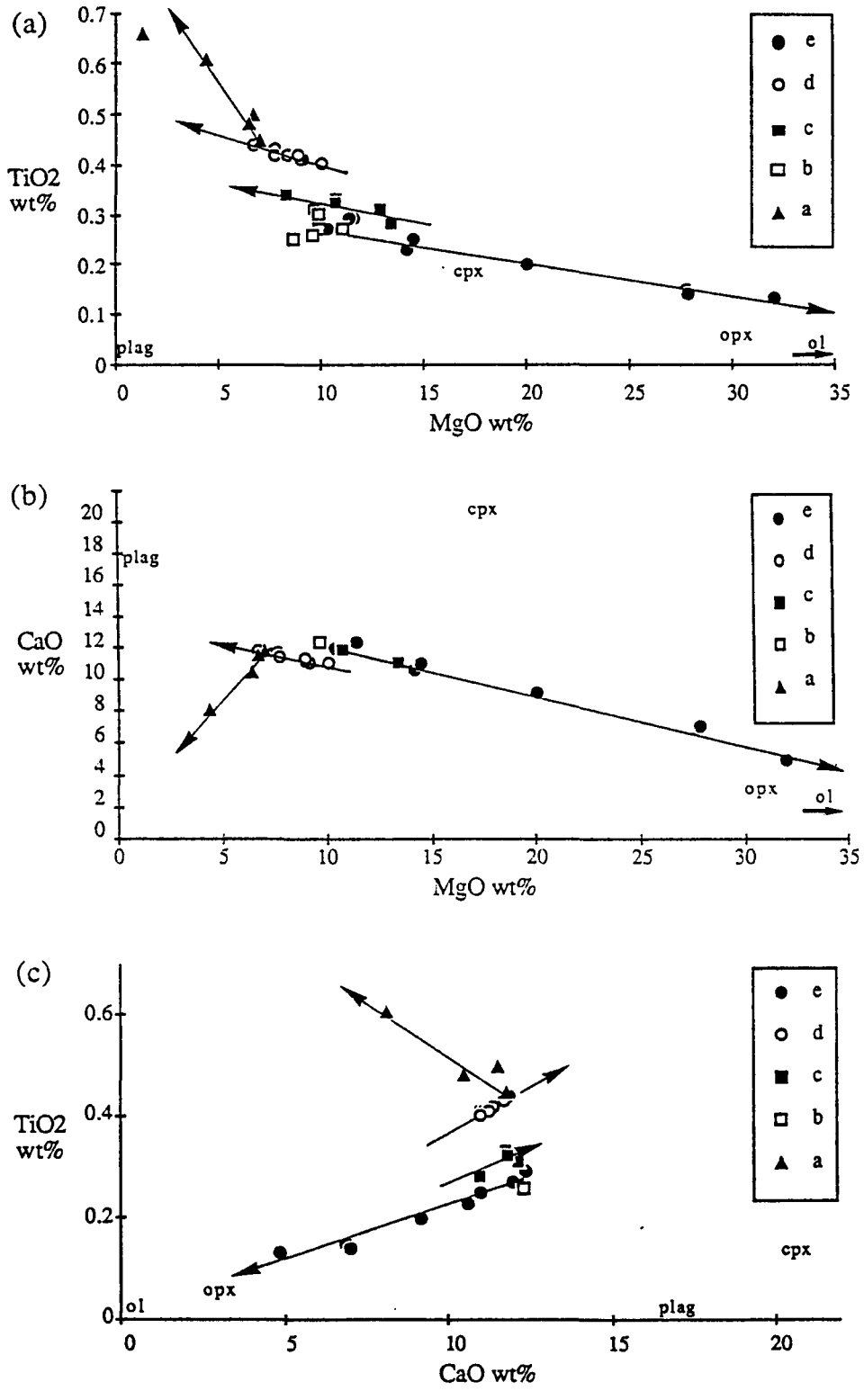

Figure 4.5 (a)–(c): Major element variation diagrams for Kalavasos Mines lavas. The positions on the diagrams of the text 'ol', 'opx', 'cpx' and 'plag' indicate the approximate compositions of these minerals as determined by microprobe analysis (appendix 5). The pronounced straight line trending towards olivine in the picrites of flow unit e reflects olivine accumulation (see text), variation in units c and d olivine fractionation. The trend in flow unit a is indicative of simultaneous clinopyroxene plus plagioclase fractionation.

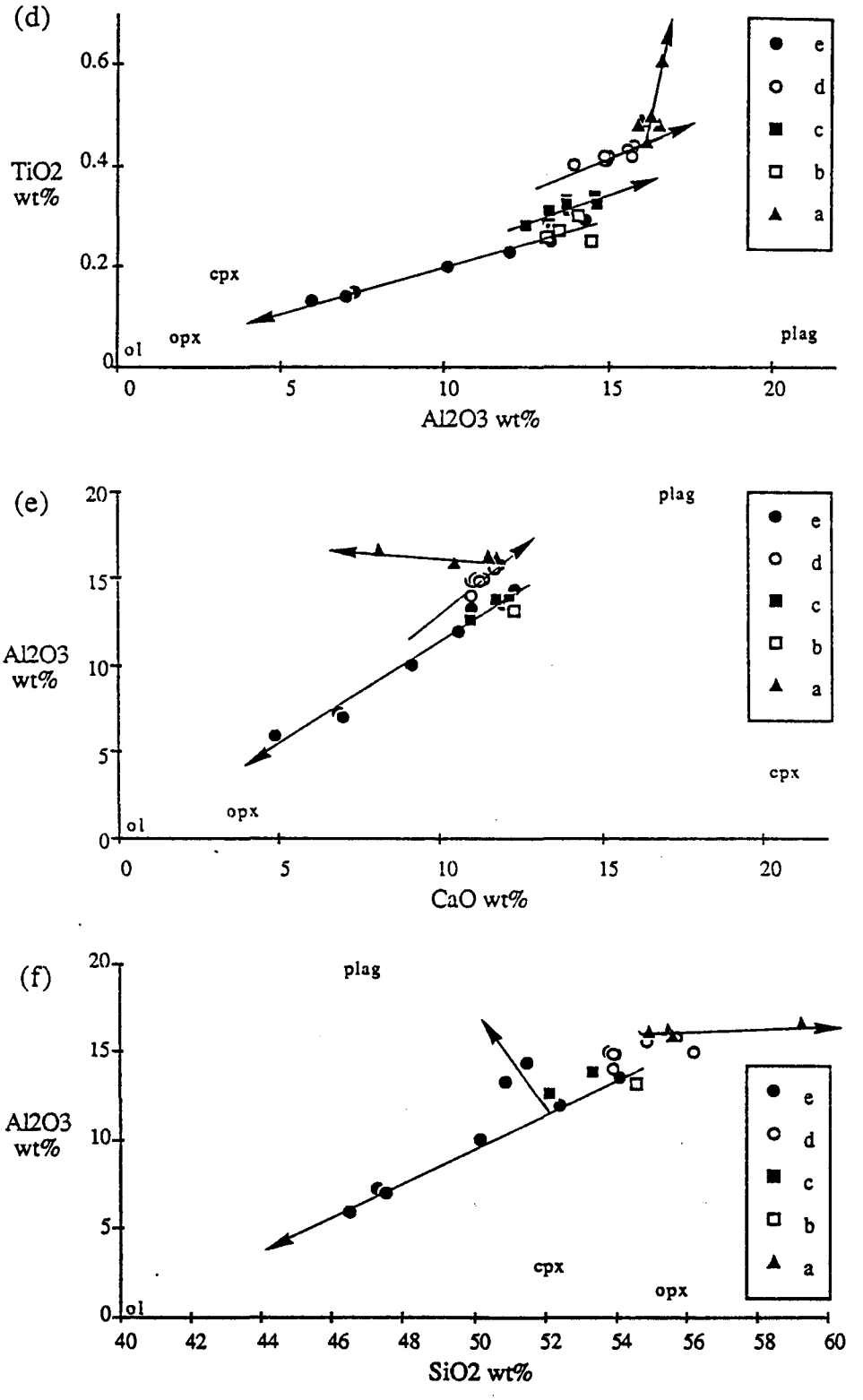

Figure 4.5 (d)–(f): Major element variation diagrams for Kalavasos Mines lavas (continued). In diagram (f) (Al_2O_3 v SiO_2), displacement of two samples from flow unit e away from orthopyroxene suggests that they have suffered limited fractionation of that mineral. Note the similarity in composition between the most primitive of the unit a lavas and most evolved of the unit d, suggesting that unit a is potentially derived from a unit d-like parent. Units a and d cannot, however, be related to units b, c and e by fractional crystallisation. ol = olivine; opx = orthopyroxene; cpx = clinopyroxene; plag = plagioclase.

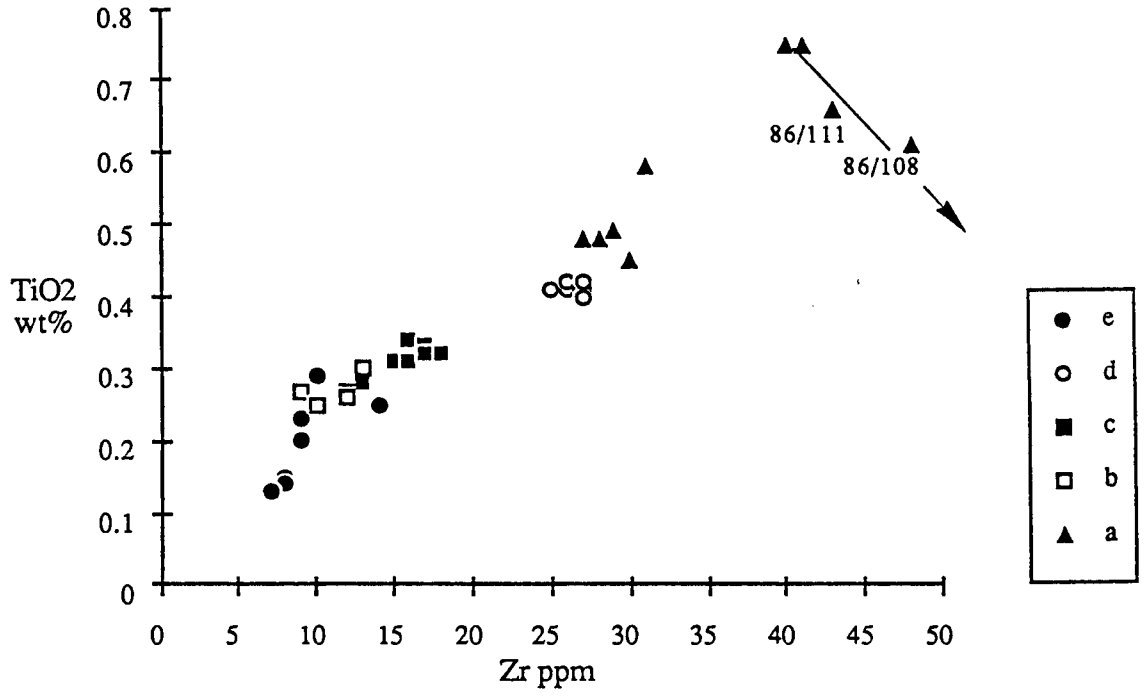

Figure 4.6: TiO_2 v Zr for Kalavasos Mines lavas. Titanium and zirconium are incompatible with respect to the major fractionating phases, hence their variations are more likely to reflect source-related differences. Note how flow units a and d in particular are well distinguished. A trend towards zero TiO_2 and Zr in the picrites of flow unit e reflects simple dilution of the unit e liquid by addition of up to 50 modal % olivine (which contains virtually nothing of either element). The most evolved rocks, 86/111 and 86/108, have the highest Zr contents of all; however, they have lower TiO_2 (and hence lower Ti/Zr ratios) than others of unit a. Titanium is strongly partitioned into magnetite, suggesting that some degree of precipitation and fractionation of this mineral (indicated by arrow) has taken place in these two samples.

fractionation, the more evolved samples from the group having lower MgO, CaO and SiO_2, higher TiO_2 and similar concentrations of Al_2O_3. Using the lever rule, this can be explained by the simultaneous fractionation of (in total) 23% clinopyroxene and 16% plagioclase, from a parent with composition equivalent to the most evolved member of flow unit d. Two rogue samples from flow unit a, however (86/108 and 86/111), lie off this clinopyroxene–plagioclase control line at still more evolved compositions. A plot of TiO_2 v Zr (figure 4.6) shows that, in addition to their unusually low FeO, MgO and CaO contents, the rocks have a significantly lower Ti/Zr ratios than others of flow unit a. Titanium behaves as an incompatible element in basic rock systems, but is strongly partitioned into opaque oxide phases in intermediate and acid systems, suggesting that the two samples have undergone a small amount of magnetite precipitation. This is supported by petrographic evidence (table 4.2).

4.4.3 Picrites

The picrite flows described in section 3.3.4 occur in the lower part of flow unit e. Individual flows and pillows show marked olivine settling, so that the samples used in this study (85/113-116, 85/121-124), which are taken from the bases, middles and tops of individual flows, contain differing proportions of olivine crystals. As expected therefore, the analyses lie on very straight olivine control lines in figure 4.5. Clearly, these trends do not represent olivine fractional crystallisation (*i.e.* crystallisation and removal of the phase prior to eruption)–which would require the initial liquid from which they crystallised to have an MgO content at least as high as that of the most magnesian sample (here 32wt% MgO)–but must instead represent *in situ* post-eruption differentiation by simple gravity settling.

In section 4.2.4 the observation was made that the olivine crystals in the picrites were frequently very large (up to 1cm long) and sometimes displayed strain features, in marked contrast to the small (*c.*2mm) skeletal phenocrysts in the other lavas, thus

leading previous authors (*e.g.* Cameron 1985) to interpret the crystals as xenocrysts. In order to investigate the validity of this claim for the Kalavasos Mines picrites, the relationship of the crystals to their groundmasses, and to other lavas of flow unit e, is examined below by means of Fe-Mg partition coefficients.

Roeder and Emslie (1970) established that the partitioning of Fe and Mg between olivine and its co-existing liquid was independent of pressure and temperature, and could therefore be quantified in terms of a single partition coefficient:

$$K_D = \frac{X^{d}_{FeO}}{X^{liq}_{FeO}} \frac{X^{liq}_{MgO}}{X^{d}_{MgO}} = 0.30$$

(where X = molar proportion)

This can also be expressed in terms of the whole-rock Mg# and Fo% (*i.e.* $100Mg/(Mg + Fe^{2+})$ for liquid and olivine respectively), to allow calculation of the Mg# of a melt from which olivine of known Fo% crystallised, and *vice versa*:

$$Mg\# = \frac{K_D}{1 - Fo + K_D Fo} \text{ and } Fo = \frac{Mg\#}{Mg\# + K_D - K_D Mg\#}$$

Mg#s calculated for the individual picrite samples by this method are, however, meaningless, as they contain added crystals and do not therefore represent true liquid compositions. In order to work out a composition for the interstitial liquid in the picrites, the modal percentage of olivine in each sample was determined by point counting (average *c.*1000 counts per sample) and compared with a picrite olivine composition from microprobe analysis (see appendix 5). The concentration of each element for each sample was plotted against the modal percentage of olivine and the intercept, as 0% olivine, taken as the concentration of that element in the interstitial liquid. In figure 4.7 MgO is shown as an example and the results for all elements tabulated to give to give a calculated liquid composition. This has 12.5 wt% MgO and is chemically similar to, if slightly more primitive than, the other (non-picritic) samples from flow unit e, and also from unit b. This calculation confirms the suggestion made on petrographic grounds that

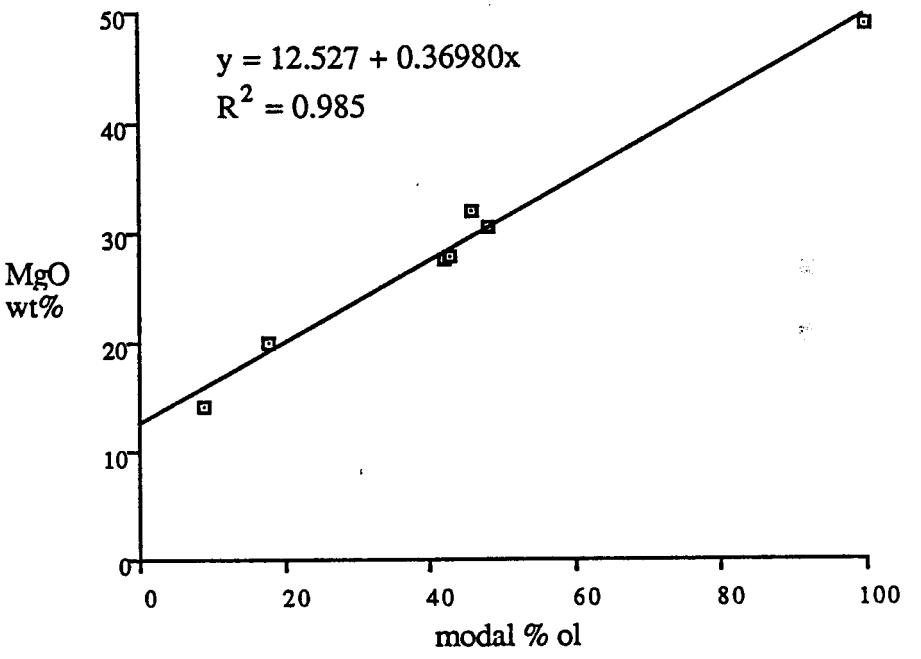

	wt%	sum of residuals:
SiO_2	52.74	$R^2 = 0.983$
TiO_2	0.24	$R^2 = 0.976$
Al_2O_3	12.59	$R^2 = 0.989$
Fe_2O_3*	8.79	$R^2 = 0.943$
MnO	0.17	$R^2 = 0.801$
MgO	12.53	$R^2 = 0.985$
CaO	11.28	$R^2 = 0.965$
Na_2O	0.84	$R^2 = 0.999$
K_2O	0.23	$R^2 = 0.953$
TOTAL:	99.41	
Cr	951	$R^2 = 0.880$
Ni	176	$R^2 = 0.970$
Y	8	$R^2 = 0.961$
Zr	11	$R^2 = 0.906$

modal % olivine:

85/113:	46%
85/114:	43%
85/115:	18%
85/121:	42%
85/122:	9%
85/123:	6%
85/124:	48%

*total Fe-oxide as Fe_2O_3

Figure 4.7: Calculation of a bulk intercumulus liquid composition for the picrite flows (unit e) by the subtraction of the measured modal olivine content of individual samples.

the picrites differ from the olivine–orthopyroxene–clinopyroxene lavas only in the presence of olivine 'xenocrysts' in the former.

The use of the term 'xenocryst', however, (*i.e.* derived from a foreign, usually more magnesian, liquid) is not strictly relevant in this context. The interstitial liquid has an Mg# = 75.8 ($Fe^{3+}/Fe^{2+} + Fe^{3+} = 0.10$), which would theoretically crystallise olivine $Fo_{91.3}$, and the most magnesian olivine analysed in the picrites is 85/121ZHG ($Fo_{91.5}$), which is of identical composition to olivines from a harzburgite in the Akapnou Forest (table 2.1). This implies that the picrite liquid (~13 wt% MgO) was in approximate equilibrium with depleted harzburgite mantle. Duncan and Green (1980) calculate a parental melt to the northern Troodos UPL (in equilibrium with $Fo_{91.7}$) by comparable means, but arrive at an MgO content of 15.8 wt%. The discrepancy in MgO values arises from the unlikely assumption by Duncan and Green that all iron in the source is present as Fe^{2+} (Cameron 1980).

Picrite flows also occur on the northern flank of the Troodos Massif, particularly in the Margi area (Gass 1958, 1960). They contain similarly magnesian olivines ($Fo_{91.7}$: Duncan and Green 1980) but, significantly, calculations of their groundmass composition (Gass 1958) suggest an MgO content of only ~7.5 wt% (equating to an Mg# of *c.*66) for the interstitial liquid, and at considerably higher levels of TiO_2 (0.57 wt%). Lavas with MgO > 8 wt% are relatively rare on northern Troodos, suggesting that fractional crystallisation (both of olivine and clinopyroxene: Robinson *et al.* 1983) was a far more important and effective process than on the southern flank, where lavas of 10-14 wt% MgO are common (this study; Simonian and Gass 1978; Cameron 1985; Murton 1986b). Picrite horizons form the lowermost parts to many flow units in the Margi UPL (Taylor 1988); chemical variations between these flow units can be modelled in terms of open-system fractionation in a periodically replenished magma chamber (Taylor *op. cit.*). The contrast in interstitial liquid compositions suggests that significant differences may have existed in the magma-genetic and eruptive mechanisms that gave rise to the Margi and Kalavasos Mines picrites. It is suggested here (in the explanation to figure 4.8) that the

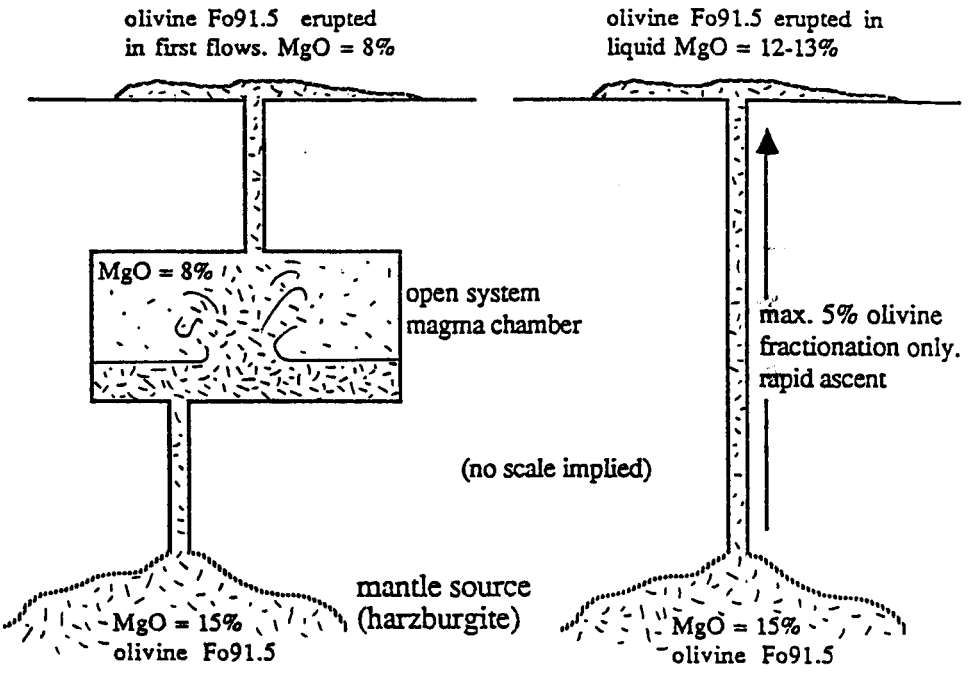

In figure 4.8(a) a hot, dense ultrabasic magma (here in equilibrium with olivine $Fo_{91.5}$) is introduced into the base of a basaltic magma chamber. Its density is such that it does not mix with the cooler, lighter and more evolved basaltic magma, but forms a discrete layer at the base of the chamber. The layers convect vigorously but remain separate, transferring heat by diffusion across a stable interface. As the ultrabasic magma cools it fractionates olivine (which is retained in suspension in the convecting system by turbulence) and becomes less dense until the two layers are of similar temperatures. Convection diminishes as the temperatures equalise, olivine begins to sediment and the interstitial (now basaltic) liquid is liberated, mixing rapidly with the magma in the main part of the chamber. If this rapid mixing coincides with (or causes) eruption, then the first erupted melts are likely to contain suspended olivines, the most magnesian of which will be approximately $Fo_{91.5}$ (from Huppert and Sparks 1980a, b).

In figure 4.8(b) such retention and fractionation of the mantle-derived melt in a magma chamber is not required. Melt forms and segregates in the harzburgite mantle source and begins to precipitate olivine $Fo_{91.5}$. At some stage it is liberated, ascends rapidly, carrying the first-formed crystals, and fractionates no more than 5% olivine before eruption onto the seafloor.

Figure 4.8: Model to explain the differences between picrites erupted on the northern flank of Troodos and in the Kalavasos Mines to the south (*i.e.* adjacent to the transform fault).

eruption of the Margi picrites, and the markedly more fractionated composition of their interstitial liquids, can be explained by a double diffusive convection model analogous to that described by Huppert and Sparks (1980a, b). For the Kalavasos Mines such a model is not necessary, as the interstitial liquid composition is close to equilibrium with the primary melt, and requires little modification between extraction from the mantle and extrusion on the seafloor (figure 4.8(b)). Indeed, to erupt such a primitive magma implies extremely rapid ascent rates and probably turbulent flow (perhaps explaining the occurrence of strain features in some of the olivine crystals (plate 4.7)?), and is most easily accomplished in areas of high geothermal gradient (Huppert and Sparks 1985).

4.5 Petrogenesis

4.5.1 Introduction

In the preceding sections it has been shown that variations in major element chemistry within the five flow units can be explained by fractionation of the observed phenocryst phases, whether by accumulative or fractional crystallisation processes. It is clear from figure 4.5 that the lavas from flow unit a can be derived from a liquid equivalent in composition to the most evolved sample of unit d, and that flow unit b is chemically very similar to the more evolved members of unit e. It is *not* possible, however, to explain the variations *between* flow units a/d, b/e and c by the fractional crystallisation of any observed phase, and in view of the highly primitive, near-primary nature of the majority of the rocks, it is necessary to invoke source-related processes–*i.e.* differing mantle sources and/or melt production/extraction processes–to explain the variations.

Previous studies of primitive lavas from the Troodos ophiolite by McCulloch and Cameron (1983) and Cameron (1985) have shown that they fall naturally into three geochemically distinct groups (named by them 'I', 'II' and 'III'), characterised

respectively by progressively lower TiO_2, Zr and middle rare-earth element (REE) (*i.e.* Nd, Sm and Eu) abundances. Inter-laboratory calibration problems, particularly acute at such low Zr abundances, preclude direct comparisons with other authors: Flower and Levine (1987) also report a three-fold division of lavas from the WLFC, but at slightly differing TiO_2 and Zr abundances; similarly, the Kalavasos Mines data fall into several distinct groups (figure 4.6), but these do not correspond directly to those of McCulloch and Cameron (*op. cit.*; see figure 4.12). Chondrite-normalised REE profiles are, however, more profitably compared (see figure 4.9). Although Ce and Nd are unfortunately below the detection limits of INAA for the samples from flow units b, c, and e (analysis 85/117 is by isotope dilution, anal N.W. Rogers), it is clear that units b, c, and e correspond to Cameron's (1985) group III, and units a and d to group II. A distinction between group II and group I is not considered justifiable, at least in the Kalavasos Mines, as sample 86/111, which corresponds most closely to the group I REE profile, can be related to unit d (*i.e.* group II) by fractional crystallisation of clino-pyroxene and plagioclase (see section 4.4.2). The relatively minor degree of fractional crystallisation required will not markedly fractionate the REE (*cf.* Schilling 1971), but simply raise the profile of the fractionated sample sub-parallel to that of its parent.

In the remainder of this chapter, for the purposes of their petrogenesis, the stratigraphically-defined *volcanological* flow units b, c, and e are henceforth referred to as 'group III' (defined *geochemically*, and prefixed 'ELFC' where necessary to distinguish them from the work of other authors), and flow units a and d as (geochemical) 'group II'. Possible mechanisms to explain the differences between the two groups are explored and, in a slightly wider context, they are compared with the suite of lavas studied by Rautenschlein *et al.* (1985) from the Akaki Canyon on the northern flank of Troodos, and briefly with type boninites from the Western Pacific.

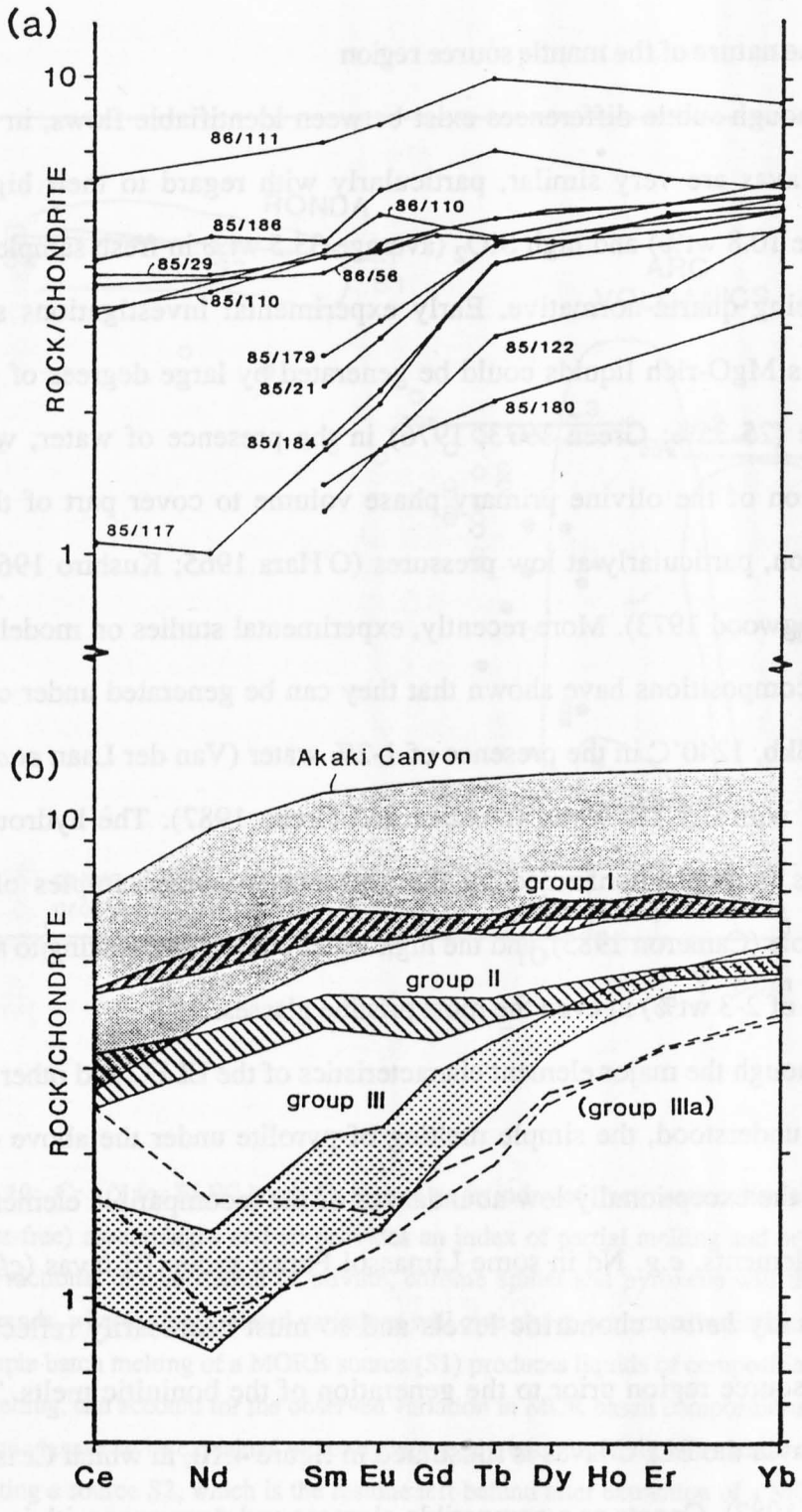

Figure 4.9(a): Chondrite-normalised rare-earth element plots of ELFC lavas (this study). (b): REE characteristics of Cameron's (1985) groups I, II and III/IIIa lavas, with the field occupied by Rautenschlein *et al.*'s Akaki Canyon suite for reference. Note the 'U-shaped' REE patterns of the group III and IIIa lavas, shared by sample 85/117, requiring the addition of a Ce-enriched component; also the *higher* Ce contents of the group II lavas (and higher Ce/Yb ratios) compared with the Akaki rocks, suggesting that the group II (and group I) lavas are also enriched.

4.5.2 The nature of the mantle source region

Although subtle differences exist between identifiable flows, in general terms the ELFC lavas are very similar, particularly with regard to their high MgO contents (average 10.8 wt%) and high SiO_2 (average 53.5 wt% in fresh samples), which leads to their being quartz-normative. Early experimental investigations showed that such siliceous MgO-rich liquids could be generated by large degrees of partial melting of pyrolite (25-35%: Green 1973, 1976) in the presence of water, which allowed the expansion of the olivine primary phase volume to cover part of the plane of silica saturation, particularly at low pressures (O'Hara 1965; Kushiro 1969, 1972; Nicholls and Ringwood 1973). More recently, experimental studies on model Troodos boninite parent compositions have shown that they can be generated under conditions ranging from >3kb, 1240°C in the presence of 1-2% water (Van der Laan *et al.* 1988) to 7-8kb, 1360°C with 0.5-1% water (Duncan and Green 1987). The hydrous nature of these magmas is amply confirmed by the presence in some samples of primary quench amphibole (Cameron 1985), and the high water content (translating to a minimum loss on ignition of 2-3 wt%) in even the most pristine glasses.

Although the major element characteristics of the ELFC and other boninites are thus readily understood, the simple melting of pyrolite under the above conditions cannot explain the exceptionally low abundances of the incompatible elements in these rocks. Some elements, *e.g.* Nd in some Limassol Forest group III lavas (*cf.* Cameron 1985), are actually *below* chondritic levels and so must necessarily reflect depletion of the mantle source region prior to the generation of the boninitic melts. The extent of this depletion in the ELFC lavas is illustrated in figure 4.10, in which Cr is plotted against Y (Pearce 1982). Cr acts as a compatible element and decreases with increasing fractional crystallisation; in contrast, Y is incompatible in garnet-free assemblages and varies only with degree of partial melting and initial concentration in the source. There is no evidence for garnet having existed in the source: the heavy REE are compatible in garnet and hence

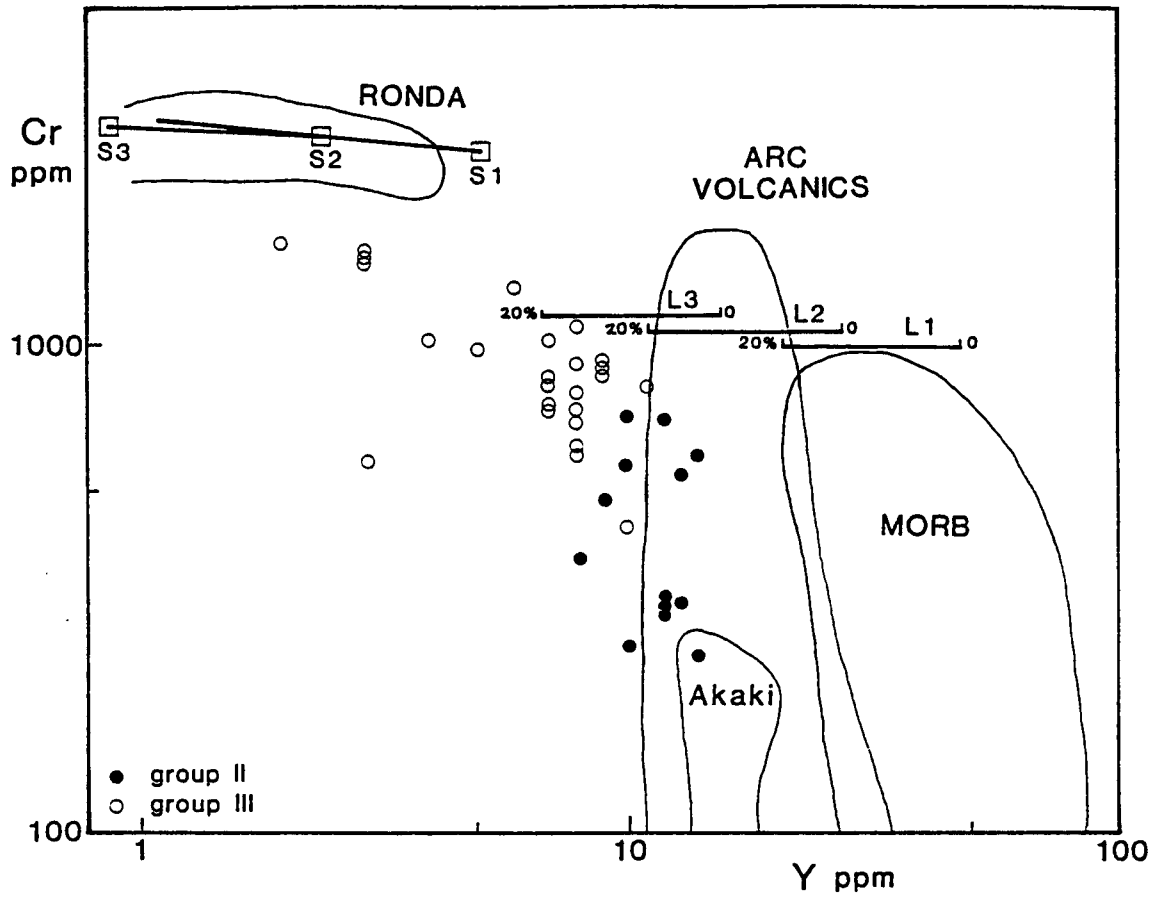

Figure 4.10: Cr v Y for ELFC lavas. Cr is used as an index of fractionation; however, Y is incompatible in (garnet-free) assemblages and so provides an index of partial melting and or melt depletion in the source. Fractional crystallisation of olivine, chrome spinel and pyroxene will therefore produce sub-vertical trends, whereas melt-related variations will give rise to horizontal variations.

Simple batch melting of a MORB source (S1) produces liquids of composition L1 which, at 0-20% partial melting, can account for the observed variation in MOR basalt compositions. Lower Y contents in arc volcanic lavas can be explained either by larger degrees of melting of a similar source, or alternatively by remelting a source S2, which is the residue left behind after extraction of a MORB-like melt. 0-20% melting of S2 (to generate liquids L2) can reproduce the range occupied by arc volcanic rocks. The Akaki Canyon suite can be explained in this fashion; however, the ELFC lavas lie at even lower Y levels, implying either very large degrees of melting of S2, or *further* remelting of a source S3 residual after Akaki melt removal. Note that the range of compositions of the residues S1-S3 left behind after such melting episodes correspond closely with actual peridotite compositions from the Ronda peridotite of southern Spain, which is thought to be a fragment of upper mantle residual after basaltic melt extraction (Frey *et al.* 1985).

fractionate the right-hand side of the REE profile, but this is not evident in figure 4.9, and at the pressures estimated by Van der Laan *et al.* (1988) and Duncan and Green (1987) garnet is not expected to be stable. In figure 4.10, therefore, fractional crystallisation of olivine, chrome spinel and pyroxene will produce sub-vertical trends, whereas melting differences will give rise to horizontal variations. The low Y abundances in the arc lavas and still lower levels in the ELFC samples imply derivation either by higher degrees of melting of a MORB-like source, or by similar degrees of melting of a source already depleted in the magmatophile elements by a previous episode or episodes of melt extraction; the Cr v Y diagram alone cannot distinguish between these two possibilities. However, to produce the levels of Y in the ELFC samples by simple batch melting of a MORB source with 5ppm Y (S1 on figure 4.10) would require unrealistically large degrees of partial melting well in excess of 20%. Instead, the Y levels can be more successfully reproduced by means of multiple melt extraction from such a source, as shown in figure 4.10 (modified after Rogers, MacLeod and Murton 1988). 0–20% melting of S1 gives rise to liquids L1, which cover the spectrum of MORB, and leaves a depleted residue S2. Remelting of S2 by 0–20% partial melting produces liquids L2, which are consistent with arc lava (and Akaki) compositions. The ELFC lavas can be derived from S2 by a minimum of *c.*25% melting, but even this amount is questionable in light of the work of McKenzie (1984, 1985), which predicts the extraction of small degree melts before such extensive melting can develop. This is supported by thermal considerations: high degrees of partial melting of a source imply that large volumes of magma are produced, whereas individual flows in the Kalavasos Mines lava sequence may only be a few tens of metres thick, and are laterally impersistent (*cf.* Bechon 1982). It is preferable, therefore, to derive the ELFC lavas from 0–10% melting of a source such as S3, which is the residue left after the extraction of both L1 and L2 (*i.e.* MORB *and* arc lavas, such as the Akaki suite).

The depleted nature of the source or sources to the ELFC lavas is also illustrated with

respect to their CaO/TiO_2 and Al_2O_3/TiO_2 ratios (figure 4.11). These ratios are significantly higher than chondritic values (*i.e.* ~MORB source) for both group II and group III lavas. Sun and Nesbitt (1978) showed that these ratios both increase with increasing degrees of partial melting, until they have the same ratio as that of their source, after which they remain approximately constant. Clearly, therefore, the ELFC lavas must have been derived from a source with significantly higher CaO/TiO_2 and Al_2O_3/TiO_2 ratios than chondrites. figure 4.11 separates groups II and III effectively, but the CaO/TiO_2 and Al_2O_3/TiO_2 ratios alone, like Cr v Y, do not distinguish between the two most likely scenarios to explain the differences between the groups, *viz.*: (i) similar degrees of partial melting, but group III derived from a still more refractory source than group II; and (ii) a similar source, but group III derived by a higher degree of partial melting. A distinction can be made between these two models, however, with reference to CaO/Al_2O_3 ratios. Most Ca in a mantle peridotite resides in clinopyroxene, which is consumed more rapidly than the other major phases during partial melting. CaO/Al_2O_3 will therefore increase in the melt with increasing degree of partial melting until clinopyroxene is exhausted (whence the ratio will remain constant or even decrease slightly with continued melting). The residue after a melting episode will necessarily have relatively less clinopyroxene remaining, so subsequent liquids (produced at an equivalent degree of partial melting) will have *lower* CaO/Al_2O_3 ratios. CaO/Al_2O_3 represents the gradient of figure 4.11, and it is apparent that the group III lavas indeed have steeper gradients (average 0.88, $\sigma_N = 0.03$) than the group II (average 0.74, $\sigma_N = 0.03$). Model (ii) above therefore appears more applicable, *i.e.* the differences between the group II and group III lavas can be explained in terms of the slightly larger degrees of partial melting required to derive the latter from a single, depleted (but still clinopyroxene-bearing) source.

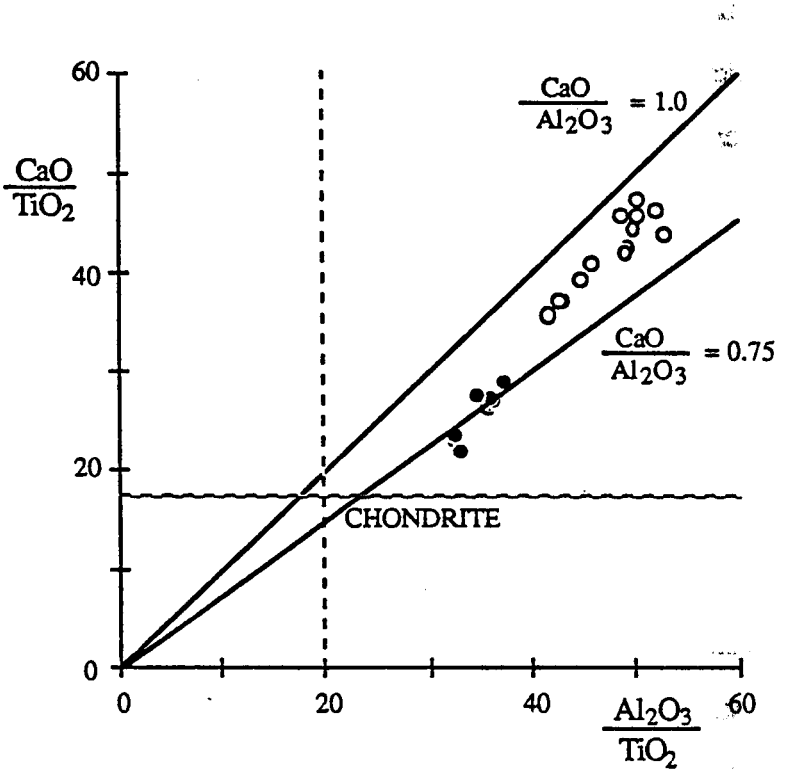

Figure 4.11: CaO/TiO_2 v Al_2O_3/TiO_2 for ELFC lavas: group II = black circles; group III = white circles. CaO/TiO_2 and Al_2O_3/TiO_2 ratios increase with partial melting until they have the same ratio as that of their source; clearly, therefore, both groups of lavas were derived from a source with significantly higher ratios than chondrites. CaO/Al_2O_3 increases with partial melting in a clinopyroxene-bearing source, but decreases with successive episodes of source depletion. Higher CaO/Al_2O_3 ratios in the group III lavas, therefore, imply that they were derived from a similar source to the group II lavas, but at a higher degree of partial melting, rather than being derived from a more depleted source. See text for discussion.

4.5.3 Evidence for enrichment of the incompatible elements in the ELFC lavas

Heavy REE (HREE) abundances in the group II and group III lavas are very similar and are sub-parallel (figure 4.9). The small differences between the two are not statistically significant (average group II Yb = 1.24 ppm, σ_N = 0.05 ppm; average group III Yb = 1.05 ppm, σ_N = 0.17 ppm), but if real are consistent with the model proposed in the previous section, as Yb will decrease in the liquid with increasing degree of partial melting of a given (single) source. Gross differences, however, exist between the groups with respect to their light REE (LREE) and middle REE (MREE) contents, the former disappearing below INAA detection limits in the group III lavas (figure 4.9).

Although the LREE are more incompatible than the HREE, so that smaller degree melts will have a relatively greater $(Ce/Yb)_N$ ratio than large degree melts, differences in the bulk distribution coefficients (after Irving 1978, Hanson 1980 and Nicholls and Harris 1980) for any realistic lherzolitic–harzburgitic source are not sufficiently great to explain the great disparity in LREE concentrations between the group II and group III lavas, given the similarity of their HREE abundances, under any permutation of partial melting conditions (Rogers *et al.* 1988). In other words, it does *not* appear to be possible to account for the differences in light and middle REE abundances between the group II and group III lavas simply by varying the degree of melting of a single source; instead, a further mechanism is necessary.

Repeated equilibrium partial melting of a (MORB-depleted) peridotite source will result in progressively lower $(Ce/Yb)_N$ ratios and a REE profile decreasing monotonically towards the LREE end (*i.e.* Sm/Nd < Nd/Ce < Ce/La). The kick in the REE pattern ($Ce_N > Nd_N$) displayed by the sole group III sample for which reliable Nd data are available (85/117, figure 4.9) must therefore imply that the Ce has been added to the melt by some other mechanism. Although the incomplete REE analyses in this study unfortunately preclude the detection of such patterns in the remaining group III lavas, all those analysed by Cameron (1985) possess similar 'U'-shaped profiles (figure 4.9(b)).

The style of LREE addition in his samples is variable, from profiles with minima at Nd (as 85/117) through to broad, more symmetrical, concave-upward REE patterns with minima at Eu.

Addition of an analogous LREE-enriched component to the group II lavas potentially provides a mechanism to account for their relatively high light and middle REE abundances, given that simple equilibrium partial melting variations are unable to account for their flat REE pattern. Detection of such a component is less easy in the group II lavas, as the postulated lower degrees of partial melt will also contribute to the higher $(Ce/Yb)_N$ ratios and possibly mask its effect. A comparison of the group II profiles with the Akaki Canyon suite (Rautenschlein *et al.* 1985) shows lower HREE contents in the former, consistent with extraction from a more depleted source, as predicted from Cr v Y arguments (figure 4.10); however, La (where quoted), Ce and sometimes Nd in the group II lavas are *higher* than in the Akaki rocks (figure 4.9), apparently implying instead that the Akaki source was *more* depleted in the LREE. This suggests that the ELFC group II suite was also subject to some measure of LREE addition.

Cameron *et al.* (1983) invoked a two-component mixing model to explain the U-shaped group III REE profiles, with the addition of variable amounts of a LREE-enriched hydrous fluid phase to a depleted peridotite source. Accurate reproduction of the patterns, however, required adding fluids of differing $(Ce/Yb)_N$ ratios for different samples, implying that the component could not be of fixed composition. Although the group II lavas were not included in the modelling, McCulloch and Cameron (1983) and Cameron (1985) noted that their Nd isotopes also required addition of some component, and that this had to be isotopically distinct from that added to the group IIIs.

Cameron *et al.* (1983) and Cameron (1985) noticed that those samples with the most symmetrical U-shaped REE patterns (and hence, by inference, the greatest proportion of added component) contain higher abundances of Zr, implying that this element was also carried in the LREE-enriched phase. These samples (named 'group IIIa' by Cameron

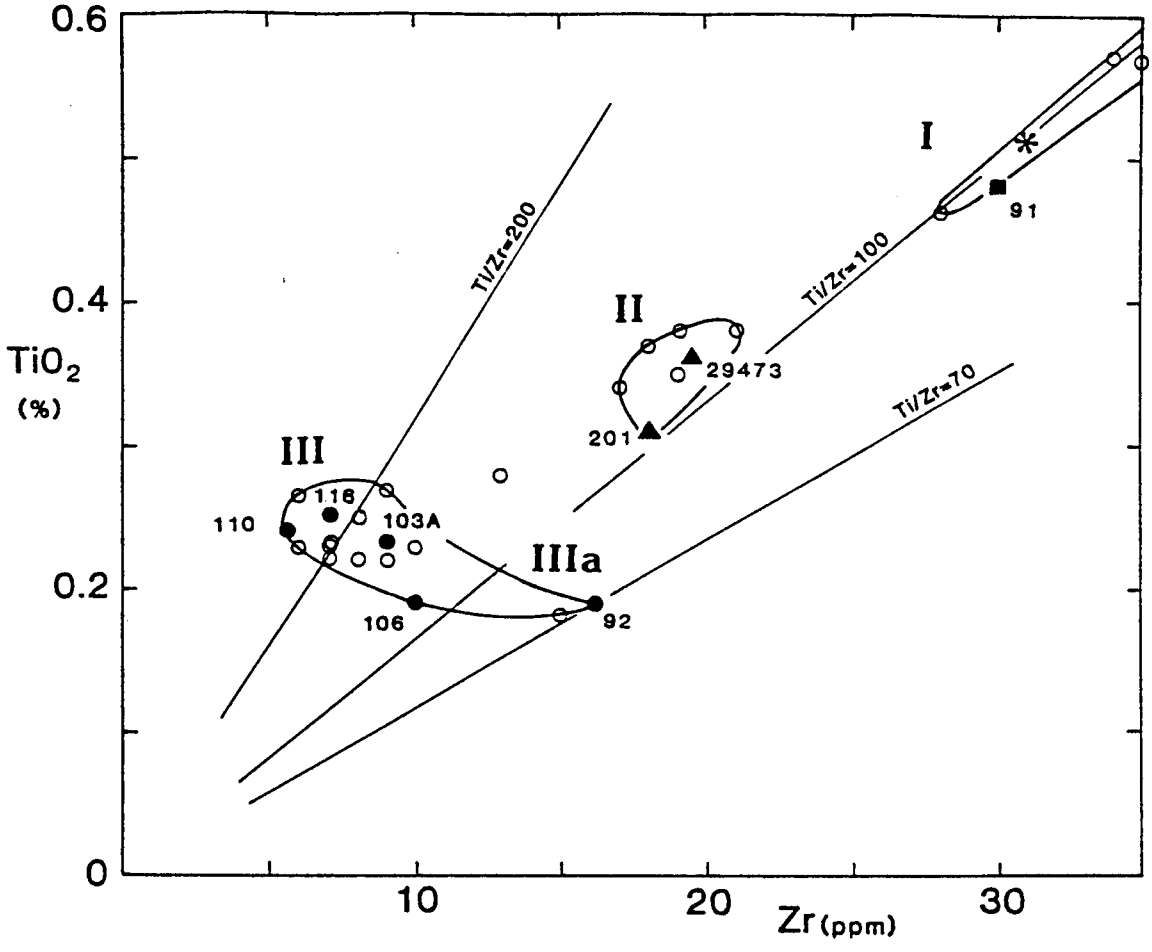

Figure 4.12: TiO_2 v Zr diagram for primitive Troodos lavas from McCulloch and Cameron (1983) (*cf.* figure 4.6). Group III lavas are subdivided by them into groups III and IIIa; Zr is added to the latter in addition to the LREE, leading to significantly lower Ti/Zr ratios. The group IIIa samples also have the most symmetrical, dished REE patterns (figure 4.9), consistent with enrichment of the MREE as well as the LREE.

op. cit.; figure 4.9(b)) have correspondingly lower Ti/Zr ratios of between 70 and 115, as opposed to 150-260 in the remaining group III lavas (figure 4.12). Although Ti/Zr ratios in the ELFC group IIIs vary from 100-175, theoretically overlapping the group IIIa range, this is an artifact of the uncertainty of the Zr analyses in this study, which are at XRF detection limits and may be up to 5ppm too high (see appendix 1). It is therefore not wise to attempt to invoke analogous Zr enrichment in the ELFC data set.

To investigate the possible addition of other elements together with the LREE, chondrite-normalised abundances of the immobile incompatible elements of the group II, III and Akaki lavas are plotted in figure 4.13. Of the HFSE other than Ti and Zr, Nb is unfortunately below XRF detection limits and is therefore omitted; Ta and Hf, however, are analysed by INAA and are therefore reliable. Hf abundances are lowest in the group III suite, and are lower in the group IIs than Akaki. The element varies regularly with Sm, Ti and Yb but does not correlate with the LREE, and does not therefore appear to have participated in the enrichment process. The ultra-incompatible Ta, in marked contrast, shows a large increase in the Limassol Forest lavas with respect to Akaki and, moreover, has higher abundances in the group III samples than the group II. Ta has a very high Z/r ratio (*i.e.* ionic charge/ionic radius) at normal oxidation states, for which reason it is totally immobile in aqeous fluids (Pearce 1983). This applies also to Zr and suggests that the added component must be a *melt* phase, not an aqueous fluid as suggested by Cameron *et al.* (1983) and Cameron (1985) (*cf.* Murton 1986a, Rogers *et al.* 1988). This is emphasised in figure 4.14, in which Ce is plotted against Ta, both normalised to Yb to minimise partial melting and fractionation effects, for lavas from both the eastern and western parts of the Limassol Forest (from Rogers *et al.* 1988). On this diagram volcanic arc basalts display vertical trends ('SZ') due to the relative immobility of Ta with respect to Ce in fluids in subduction-related environments, but MORB, within-plate basalts and ocean island basalts *etc.* occupy the dashed field in the diagram and show diagonal trends ('WP') with the concomitant increase of Ta with Ce in silicate melts. Neither the Limassol Forest nor the Akaki lavas show any evidence for preferential

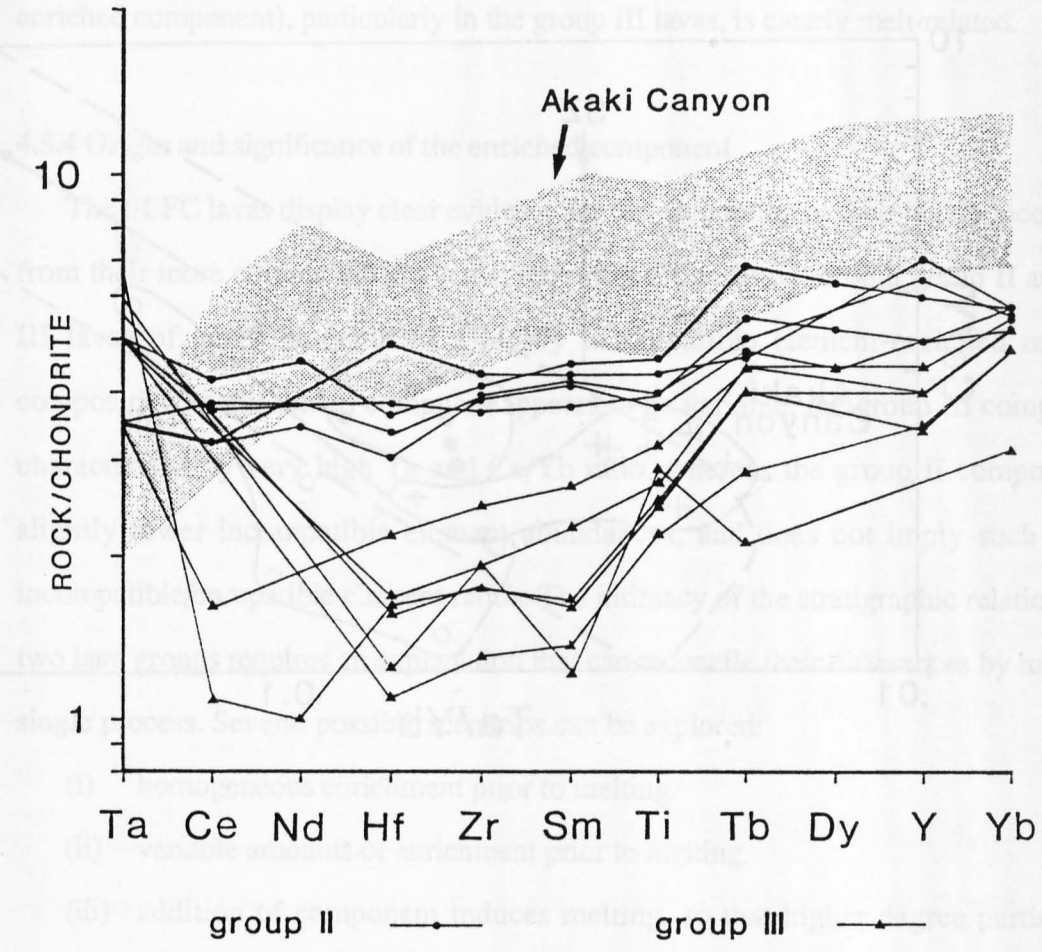

Figure 4.13: Chondrite-normalised trace element abundances of the ELFC lavas. Diagram arranged with increasing incompatibility towards the left. Both group II and group III lavas show marked enrichment of the most incompatible element, tantalum, with respect to the Akaki suite, and moreover, group III lavas have generally higher abundances than the group II. Ta has a very high ionic charge/radius ratio, and so is totally immobile in aqueous fluids, implying that the added component is a melt, rather than aqueous, phase.

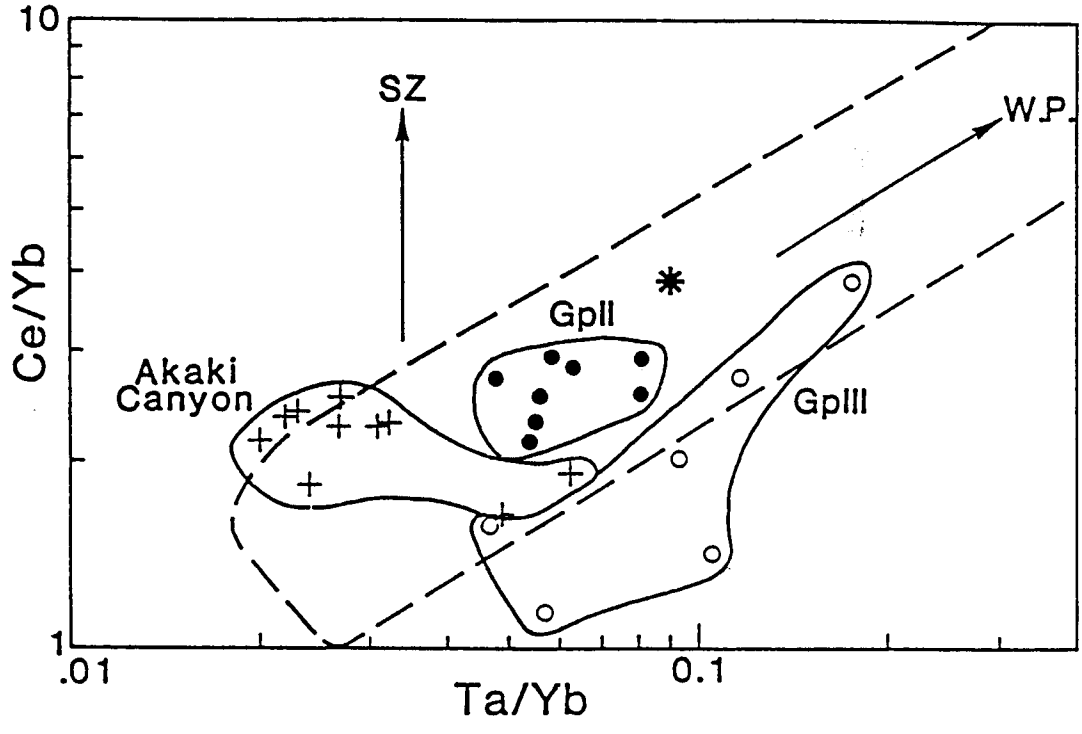

Figure 4.14: Ce/Yb v Ta/Yb diagram for LFC lavas, with Akaki suite for reference (from Rogers *et al.* 1988). Normalisation of Ce and Ta with respect to Yb minimises partial melting and fractionation effects. In subduction zone environments Ce is far more mobile than Ta, giving rise to vertical trends on the diagram in subduction-related lavas ('SZ' trend). Mid-ocean ridge, within-plate and ocean island basalts, in contrast, occupy the dashed field, reflecting the concomitant increase of Ta with Ce in silicate melts, thus giving rise to diagonal trends ('WP', or 'within-plate'). Neither the LFC nor the Akaki lavas show any evidence for subduction-related enrichment with respect to Ce; instead, the group III lavas display a clear increase of Ta with Ce, demonstrating that enrichment was melt-related. * = bulk earth. From Rogers *et al.* (1988).

subduction-related enrichment of Ce; instead the Ce (and hence remainder of the LREE-enriched component), particularly in the group III lavas, is clearly melt-related.

4.5.4 Origin and significance of the enriched component

The ELFC lavas display clear evidence for the decoupling of their highly incompatible from their more compatible elements, requiring the addition to both group II and group III lavas of small amounts of a highly incompatible element-enriched melt. The composition of this added compnent appears to be variable: the group III component is characterised by very high Ta and Ce/Yb ratio, whereas the group II component has slightly lower incompatible element abundances, and does not imply such extreme incompatible/compatible element ratios. The intimacy of the stratigraphic relations of the two lava groups requires an explanation that can reconcile their differences by means of a single process. Several possible scenarios can be explored:

(i) homogeneous enrichment prior to melting.

(ii) variable amounts of enrichment prior to melting.

(iii) addition of component induces melting, so that higher degree partial melts have more enrichment.

(iv) interaction between added melt and LREE-depleted peridotite source, but incomplete equilibration.

Suggestion (i) implies that the source has been 'doped' by a (potentially ancient) enrichment event and that it, too, must have U-shaped REE profiles. Such profiles are indeed common in ophiolitic peridotites (*e.g.* Montigny *et al.* 1973) and their origin is the subject of some debate (Prinzhofer and Allègre 1985). However, the melting of such peridotite cannot smooth the REE patterns sufficiently to reproduce the group II profiles (section 4.5.3). Varying the amount of this enrichment (suggestion (ii)) and thus 'sampling' different degrees of mixing between it and the source with successive melt batches could explain the random interbedding of the group IIs and group IIIs, but would

imply that the liquids should be quite heterogeneous, whereas the group IIs are striking in their homogeneity. Critically, this process would still appear to the trace elements as simple two-component mixing, which does not agree with observation.

The third suggestion implies that enrichment coincided with, and therefore triggered or aided melting, so that the group IIIs (which appear to be larger degree partial melts) should preserve evidence of a greater proportion of enriched component than the group IIs. The differing Ta abundances can be explained this way, but it is extremely difficult to reproduce the smooth group II REE profiles, which appear to require the addition of the MREE as well as the LREE. Accepting that the differences between the group II and group III profiles cannot be generated by the simple admixing of a component of fixed composition (*i.e.* Ce/Yb ratio), as quietly conceded by Cameron *et al.* (1983) and Cameron (1985), a slight modification of suggestion (ii) might be to invoke addition of heterogeneous melt increments from different areas of a partial melting zone (O'Hara 1985). The degree of partial melting F in a zone where melt is being generated varies from zero at the edge to a maximum in the centre, and although the geochemical consequences of these variations are usually averaged out as the melt segregates, it is conceivable that they could be preserved for a time, say, in the case of melting at the base of the lithosphere. However, for this process to work in the context of the ELFC lava petrogenesis the higher 'apparent F' melt fractions (*i.e.* the group II added component), which would be hotter, should induce the larger degrees of partial melting of the depleted lithospheric source, and this is the opposite to what is observed.

The final suggestion is based upon the work of Navon and Stolper (1987), who modelled the geochemical effects and consequences of melt migration through a permeable matrix when the melt and matrix are out of equilibrium, by analogy to ion-exchange processes in a chromatographic column. This has obvious parallels with the percolation of a relatively enriched asthenospheric melt upward through a 'column' of depleted mantle lithosphere. Navon and Stolper (*op. cit.*) showed that the first melts that

migrate through the depleted matrix will undergo ion exchange, be 'stripped' of their enriched fractions, and emerge from the top of the column with the character of a small volume partial melt of the matrix. The rate of exchange of each element with the matrix is strictly dependent upon its partition coefficient, so that the most incompatible element re-equilibrates most rapidly. This results in 'fronts' for each element in the succeeding melts, before which the element is in equilibrium with the matrix, and behind which it has the characteristics of the original melt put in at the base of the column. Successive liquids emerging from the top of the column therefore show abrupt increases in incompatible element abundances and highly incompatible/moderately incompatible element ratios, as each 'front' reaches the surface and the concentration changes rapidly from that of the matrix to that of the original liquid. Compatible elements equilibrate much more slowly, so that although eventually the melt output will be the same as the original melt input if the process is allowed to continue to completion, intervening melts will contain compatible element abundances reflecting the (depleted) matrix composition, yet incompatible elements reflecting the (enriched asthenospheric) melt put in to the base of the column.

Navon and Stolper (*op. cit.*) specifically applied this model to show how U-shaped REE profiles could be generated. With small quantities of melt only passing through a depleted peridotite column, enrichment is apparent only in the most incompatible of the REE (*i.e.* La and then Ce), and a profile exactly similar to that of the group III lavas is generated (figure 4.9). If more melt arrives, with equilibration 'fronts' of the heavier REE, then the point of minimum concentration moves towards the more compatible elements, (*cf.* group IIIa, figure 4.9(b)), and eventually a flat REE pattern (*cf.* group II) mimicking the shape of that of the initial asthenospheric source will result. In the case of the ELFC lavas this implies that the group II suite has undergone relatively more equilibration than the group III (explaining its more homogeneous character), although it does not necessarily imply that the melt introduced into the column from the asthenosphere was of the composition of the group II liquid. For complete equilibration

to take place melt-matrix ratios would need to be extremely large; indeed, it is likely if the proportion of added melt is relatively small (as was probably the case) then no melt may reach the surface, and the peridotite source is simply 'doped' ready for a later, potentially unrelated, melting event. Alternatively, the melt may segregate into veins and then dykes, so that further chemical interaction with the matrix is minimised and the effects of partial equilibration are preserved.

4.5.5 Summary of petrogenesis and discussion of nomenclature

The lava stratigraphy of the Kalavasos Mines reveals a transition, as elsewhere on Troodos (Robinson *et al.* 1983), from a relatively fractionated LPL suite which is apparently cogenetic with the axis sequence sheeted dykes and plutonics, to a markedly more primitive (occasionally primary) and chemically variable UPL sequence. The transition is abrupt, and lies at or slightly below the LPL-UPL boundary defined by Adamides (1980) in the Kalavasos Mines on field criteria. Above this boundary the primitive lavas are to all intents and purposes randomly interbedded, and the stratigraphy defined in the Kalavasos Mines does not appear to persist on a regional scale.

The Kalavasos Mines lavas range in composition from basaltic andesite to dacite. They all have relatively low HFSE abundances, which suggests that they were derived from a melt-depleted source, and the high silica (average 53.5 wt%) high magnesia (average 10.8 wt%) character of the majority of the rocks suggests melting in the presence of water at shallow depths. Ubiquitous enrichment of the LIL elements (figure 4.1), which are easily mobilised in aqueous fluids, can only be interpreted in terms of the introduction of a volatile-rich phase to the source region of the lavas, and this is most easily accomplished above an active subduction zone (section 4.1.2). Field relationships require the creation of the Troodos oceanic crust by seafloor spreading, but the geochemistry suggests that this must have occurred directly above a subduction zone. The absence of any well-defined volcanic arc, either preserved in Cyprus or in its

environs in the present-day Eastern Mediterranean, makes discussion of the tectonic setting of Troodos in terms of 'fore-arc' or 'back-arc' *etc.* irrelevant.

In the ELFC, and elsewhere along the southern flank of the ophiolite, the lavas also reveal evidence for incompatible element enrichment by another component, this time a melt phase which, although most obvious in the most depleted (*i.e.* group III) lavas, has a subtle effect on all the lavas. This addition cannot be explained (as has previously been claimed) by simple two-component mixing between a refractory source and an enriched (and by implication asthenospheric) melt, and it is suggested that the differences between lava groups may reflect differing degrees of equilibration between the depleted peridotite and this melt.

The above chemical characteristics, including the LREE and HFSE enrichment, are shared by all Western Pacific boninites (*e.g.* Hickey and Frey 1982). There are petrographic similarities also, particularly with respect to the crystallisation sequence of clinopyroxene after plagioclase (the opposite to normal MORB), and in the presence of vitrophyric textures and quench groundmass crystals, and sometimes rimmed ('jacketed') phenocrysts. Subtle chemical differences do, however, exist. Western Pacific boninites tend to have slightly lower CaO contents (from *c.* 5-11 wt%), suggesting a more depleted (possibly clinopyroxene-free) source, and higher silica (up to 58 wt%), reflecting an increased presence of water during melting. The latter allows peritectic melting (*i.e.* the incongruent melting of orthopyroxene), and consequent dominance of low-Ca pyroxene fractionation in the type boninites, whereas the Troodos lavas were generated by eutectic melting (Van der Laan *et al.* 1988).

Debate still continues concerning the nomenclature of the primitive lavas, even now that their boninitic affinity has been recognised, and there is little consensus as to how wide to cast the term 'boninite'. It is clear that the Cyprus and Western Pacific lavas result from similar combinations of processes, even if the effects of each of these are slightly more extreme in the latter. There is naturally a great potential for heterogeneity in

a magma type that results from a combination of three probably unrelated 'components', so it is difficult, and not particularly helpful, to to put rigid chemical or petrological constraints on a definition for the term. Of the more recent proposals for a suitable qualifying term for the primitive Troodos lavas 'high-Ca boninite' (as opposed to 'low-Ca boninite' for Bonin Island and Cape Vogel: Van der Laan *et al.* 1988) recognises this dilemma and accommodates it more constructively than does Beccaluva and Serri's (1988) term 'transitional boninite', and so the former is preferred.

4.5.6 Tectonic controls on boninite genesis

The boninitic lavas in Cyprus (*i.e.* the group IIIs and LREE-enriched group IIs) are restricted to the southern flank of Troodos, occurring in the LFC, the AFB and in disaggregated blocks entrained in the Mamonia Complex (see chapter 7). This implies that there is some connection between the transform fault and the conditions required for boninite genesis.

In the WLFC ultramafic and mafic plutons were intruded into uplifted and partially serpentinised mantle sequence, whilst transform-related structures were still active (Murton 1986a). These plutons and their hypabyssal equivalents account for up to 22% extension across parts of the WLFC (Murton 1986b), implying that the transform had a significant component of extension across it. The lack of such intrusives in the ELFC, apart from a limited number of scattered dykes (which mostly have group III chemistry: see chapter 2), coupled with the lack of evidence for synmagmatic extension across the ELFC (see chapter 3), suggests that the transtension and plutonism was limited to an extensional 'relay zone' centred on the WLFC (Murton 1986b; see chapter 7), and hence that the localised extension within the transform was the necessary tectonic control on the boninite genesis. Murton (1986b) suggested that this might indicate partial melting of the depleted lithospheric mantle in the relay zone as a result of its thinning, rapid uplift, and consequent adiabatic decompression.

The predominance of primitive lavas in the LFC and AFB compared with northern

Troodos suggests that the transform allowed easy egress for magmas, with little retention and fractionation in magma chambers, as was first suggested by Simonian and Gass (1978). With respect to fractionation, therefore, there indeed appears to be a 'geochemical' signature to the transform. However, it remains to be proved that the *melt enrichment component* of the boninitic magmas is related to the transform. Group III lavas (samples 86/144 and 86/147: appendices 2 and 3) occur at Monagroulli, which is 4-5km to the south of the transform margin, and Cameron (1985) has also published two analyses of group III lavas from Parekklisha. Now that the melt component has also been identified in the group II lavas, it seems that it forms an integral part of all of the ELFC lavas and, by implication, all of the axis sequence crust. From this it is possible to argue that the melt enrichment is temporally, rather than simply spatially, controlled, and that its absence from the Akaki area on the northern flank of Troodos is because the Akaki crust was formed only when the melt enrichment had died away, or *vice versa* that the Akaki crust had already been formed before the melt component was introduced.

It is tempting to speculate further on the significance of this melt introduction. In those situations where the stratigraphic setting of boninites is known, boninite volcanism occurs at the cessation of arc tholeiite volcanism and *immediately prior to MORB eruption* (Betts Cove, Newfoundland: Coish and Church 1979, Coish *et al.* 1982; Heathcote, Australia: Crawford and Keays 1978, Crawford and Cameron 1985; West Pacific–Mariana region: Crawford *et al.* 1981). Crawford *et al.* (*op. cit.*) show that this marks the sundering and splitting of an island arc and switch to back-arc basin opening, and can be documented on two separate occasions in the Mariana region. This led Flower and Levine (1987) to propose that the transition from arc tholeiite (*i.e.* axis sequence) to boninite volcanism in the AFB/LFC represented the "lengthwise splitting of a submarine arc". Although clearly these authors have not read the comments on Miyashiro's (1973) contribution (Hynes 1975, Moores 1975, Gass *et al.* 1975), nor Simonian and Gass (1978), Murton (1986a) and Murton and Gass (1986), the intriguing possibility remains

that the enriched melt component might be heralding the first signs of a transition to incipient asthenospheric 'back-arc' volcanism, which was arrested before any such melts could be extruded. This could also provide a suitable heat source of sufficient magnitude to enable melting of the refractory peridotite to take place.

CHAPTER 5:
Structural History

5.1 Preconceptions

Simonian and Gass (1978) showed that the zone of tectonised sheeted dykes and lavas that constitute the Arakapas Fault Belt formed the northern wall of an E-W trending transform fault, which they suggested included the entire Limassol Forest Complex to the south. This claim was corroborated by Murton (1986a, b), who demonstrated widespread E-W transcurrent deformation in the predominantly mantle sequence erosion levels of the western half, and showed that this was accompanied by the simultaneous intrusion of 'transform sequence' mafic and ultramafic plutons. From this it might be predicted that the disruption of the Penrose-type crustal sequence lithologies that form the major part of the ELFC might also be a product of transform tectonism, possibly modified by 'transform sequence' magmatism. However, the E-W fabric so prominent in the AFB and WLFC (figure 1.10) is not obvious in the ELFC where, if anything, NW- (or WNW-) and NE-trending lineaments predominate. Instead, the detailed remapping of the ELFC in this study (enclosure 1) reveals a distinct structural style, with the large scale disaggregation and differential rotation of blocks of the axis sequence crust about low angle normal faults. An examination of the pelagic sedimentary cover overlying the ophiolite at the periphery of the ELFC reveals that the deformation is of Upper Cretaceous age, apparently immediately post-dating the cessation of volcanism in the area. The lava–sediment relations give much detailed information as to the mechanisms and timing of the deformation, and particularly its regional tectonic significance, and so is treated separately in the following chapter. A description of the style and effect of this deformation episode, hitherto unrecognised, is given in section 5.4 and 5.5, and forms a

major part of the remainder of this thesis. This post-volcanic brittle tectonism is very widespread in the ELFC, and overprints or re-uses existing ocean-floor structures relating to the transform and the Anti-Troodos ridge. Such evidence as remains for the earlier transform-related deformation is discussed in section 5.3; structures pertaining to crustal *formation* have been described already in chapters 2 and 3.

5.2 Palaeomagnetism

A significant problem encountered when attempting a study of brittle deformation processes in ophiolites is the lack of reliable palaeohorizontal and palaeovertical indicators. Plutonic layering can form at high angles of repose and is therefore of little use (see chapter 3); even pillow lavas can be erupted on moderately steep slopes, and thus may have potentially significant components of 'eruptive dip'. Interlava sediment bands probably form the most reliable horizontals, although the generally close agreement between pillow and sediment attitudes where measured together suggests that the former can be taken as reasonable approximations to a palaeohorizontal in most cases. Although dykes of the Sheeted Complex probably were intruded close to the vertical (section 2.5.6) their use as an orientation tool is limited, especially in areas where strike-slip or oblique-slip faulting is suspected, unless their original strikes upon intrusion are known. This is also true for the palaeohorizontal indicators, which give no clue as to possible rotations or components of rotation about vertical axes.

An attempt to address the problem of the orientation of fault blocks, and particularly to obtain quantitative information on block rotations, by the use of palaeomagnetism has recently been described by Allerton (1988). His method is summarised in Allerton and Vine (1987), and repeated briefly here. A limited collaborative palaeomagnetic study was undertaken in the ELFC with Allerton, who undertook both drilling and analysis, and so

whose input to the following section is therefore considerable; interpretation of the results, however, was made by the present author. The results of the study are also presented and discussed in Allerton (1988).

Cyprus is possibly uniquely suitable for the use of palaeomagnetism as a structural tool. Pioneering palaeomagnetic investigations by Moores and Vine (1971) showed that gabbros and lavas from the ophiolite preserved stable primary thermo-remanent magnetisation vectors, which could be distinguished from the present-day field. The inclinations of these vectors (all normally polarised) suggest a northward movement of Cyprus of some 15° since they were formed, consistent with data from Africa (Abrahamsen and Schönharting 1986); however, magnetic declinations are *westerly*-directed, implying that Troodos has been rotated anticlockwise about a vertical axis by approximately 90°. Such vectors are obtained across the entire width of the ophiolite, from the Akamas peninsula in the west to the Troulli inlier 120km to the east, suggesting that the main part of the massif at least has suffered bulk rotation as a coherent body. The mechanism and implications of this rotation are discussed in chapter 7; for the purposes of the present discourse, however, the significant result of this observation is that a single, very tightly constrained, primary magnetisation vector is known for the Troodos ophiolite and its immediately overlying sediments (azimuth 276°, inclination 32°: Moores and Vine 1971).

Allerton's technique is based upon the assumption that deviations of an individual dyke or lava sample magnetisation vector (SMV) from this average Troodos magnetisation vector (TMV) result from structural rotations alone. It further assumes that: (i) the observed stable remanent magnetisation predates the structural rotation and has not suffered subsequent remagnetisation; (ii) dykes were intruded vertically, and (iii) all deformation is brittle, and internal deformation of a sample is minimal, such that the angle between the magnetisation vector and the normal to the plane of the dyke does not change upon rotation (Allerton and Vine 1987). The principle of the method is illustrated in figure 5.1, and involves finding a rotation vector that will rotate the SMV back to the

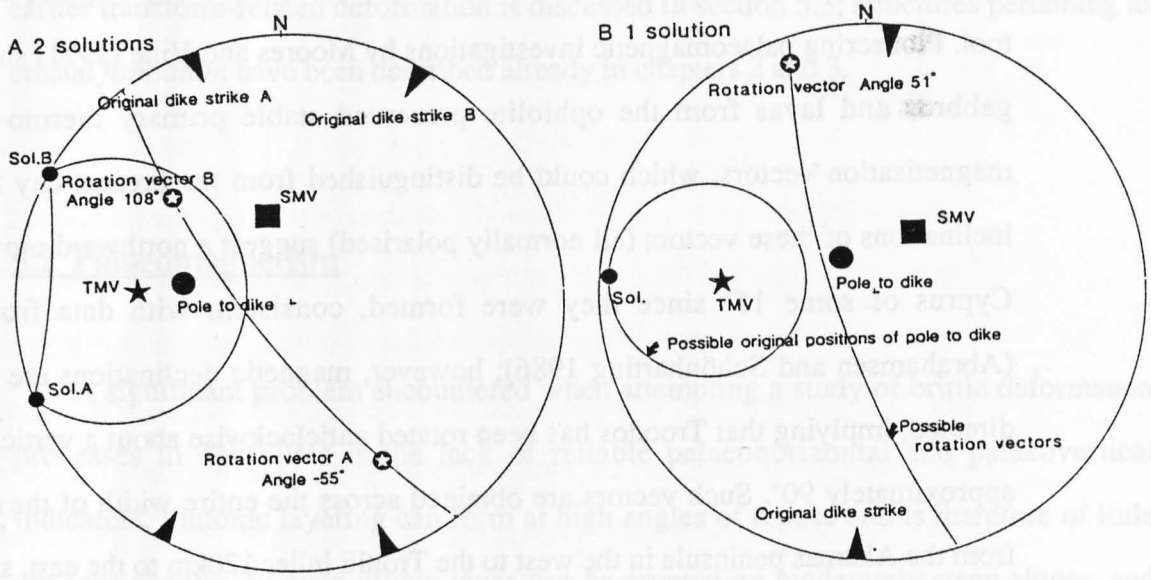

Figure 5.1: The Allerton palaeomagnetic technique attempts to find the vector or vectors that will, by a single rotation, restore the sample magnetisation vector (SMV) back to the Troodos magnetisation vector (TMV), and simultaneously restore the pole to the sample dyke to the horizontal. The locus of all possible rotation vectors lies on the great circle bisectrix of the SMV and TMV and, as the angle β between the SMV and pole to dyke does not change upon rotation, the locus of all possible original positions of the pole describes a small circle of radius β centred upon the TMV. In case A, the small circle intersects the primitive in two places, hence the condition that the dyke was vertical is met by two possible solutions, A and B; in case B the angle β is less than the inclination of the TMV (*i.e.* less than 32°), so the dyke could not have been intruded vertically, and a solution is chosen that assumes that intrusion was as close to the vertical as possible. From Allerton and Vine (1987).

TMV, and simultaneously restore the sample dyke plane to the vertical. Once the SMV has been made coincident with the TMV, the locus of possible original positions of the pole to the dyke plane is given by the small circles in figure 5.1(a) and (b), as the angle between the SMV and the pole to the dyke plane is fixed (assumption iii). The condition that the dykes were originally vertical is met where the small circle cuts the primitive, *i.e.* where the pole to the dyke plane is horizontal. Normally two possible solutions will result (case (a) in figure 5.1), but occasionally the small circle does not cut the primitive, in which case the dyke could never have been vertical and a single solution is chosen that assumes the dyke was intruded at as steep an angle as possible (case (b)). A useful by-product of the method is that two solutions for the original strike of the dyke upon intrusion are also found. Although most frequently applied by Allerton (1988) with dykes, as above, the technique can be easily adapted for use with pillows, massive flows and sills, in which case the pole to the measured palaeohorizontal plane is rotated as close to the vertical as possible with the SMV and TMV coincident, and a single solution is obtained. This has the great advantage over conventional palaeomagnetic approaches that it calculates a single pole to account for all of the rotation–*i.e.* it is capable of yielding solutions with inclined axes–and thus avoids the problems of 'apparent' tectonic rotations generated by the application of conventional bedding corrections (MacDonald 1980). Standard practice is to assume that bedding tilt took place about a simple strike-parallel axis, so that when the effects of the tilting are removed, the resulting deviation of measured declination from the expected value is due to a component of tectonic rotation about a vertical axis. This assumption is highly questionable in regions where oblique-slip tectonism is suspected, as in southern Cyprus (see sections 5.4, 5.5 and chapter 7): both horizontal and vertical components of rotation are implicit in such areas as the result of a single tectonic event and cannot therefore be separated.

For this study seven sites were drilled in the Sheeted Dyke Complex and Extrusive Sequence. Their locations are shown in figure 5.2. An average of eight cores was drilled

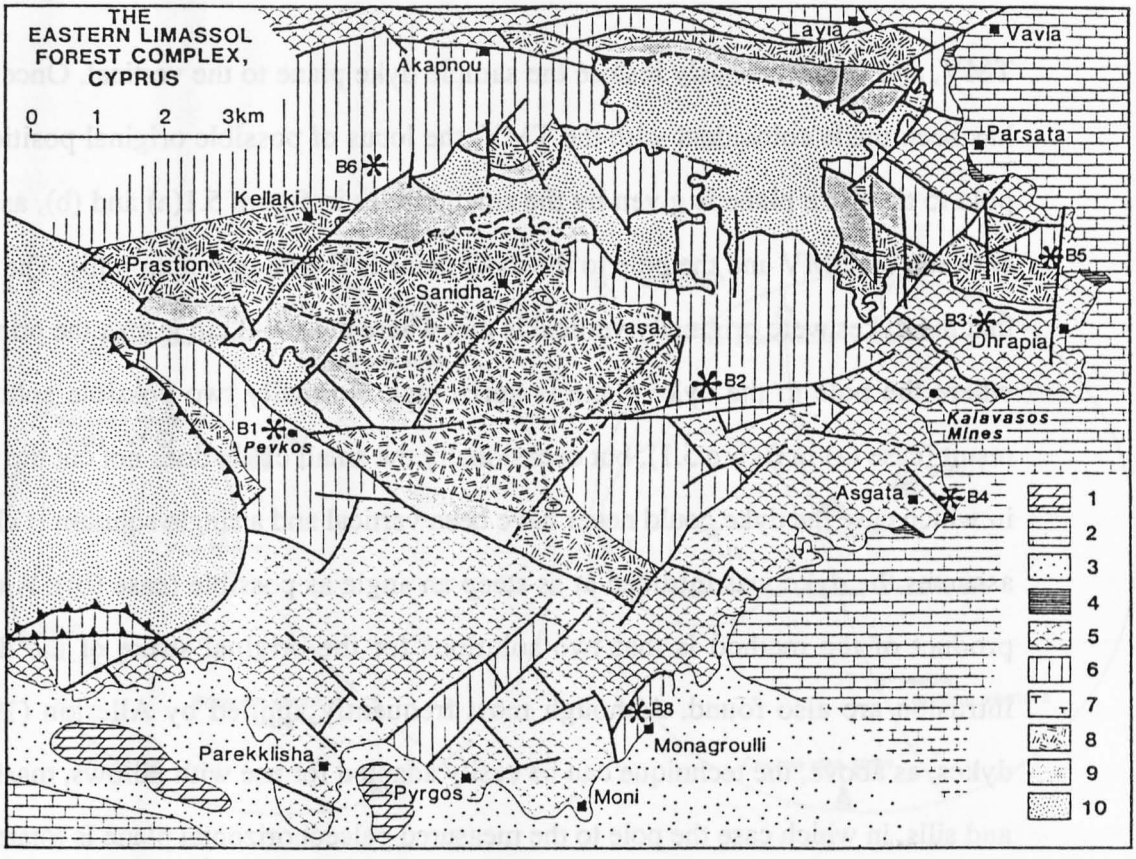

B1: Pevkos quarry 13904983 (sheeted dykes)

B2: Asgata–Vasa road 202503 (sheeted dykes)

B3: Kalavasos Mines 248512 (flows, sills and megapillows)

B4: Asgata River 239488 (dykes through lavas)

B5: Dhrapia River 25485258 (sheeted dykes)

B6: Klonari 15475379 (sheeted dykes)

B8: Monagroulli River 19344561 (sheeted dykes)

Figure 5.2: Simplified geological map of the ELFC showing location of the seven palaeomagnetic sites B1–B8, marked with an asterisk *. Legend: *Sediments:* (1) Miocene–Recent; (2) Maastrchtian-Miocene; (3) Campanian–Maastrichtian Moni Mélange; (4) Turonian–Maastrichtian Perapedhi Formation. *Igneous rocks:* (5) pillow lavas; (6) sheeted dykes; (7) plagiogranites; (8) gabbros; (9) ultramafic rocks, and (10) tectonised harzburgites.

in total at each site into dykes with well-developed chilled margins, in order to establish the most accurate constraint of dyke orientations as possible. Several different dykes were sampled at each site, and usually two holes drilled in each, to minimise possible core orientation errors. Core orientation was measured by sun compass. At one site (B3: Mandra tou Alykou, Kalavasos Mines) cores were taken from massive flows, a sill and an elongate megapillow adjacent to interlava sediments, to which the palaeohorizontal adaptation of the analysis was used. Sample demagnetisation was carried out by S. Allerton at the University of East Anglia on as many individual one-inch sub-samples as could be cut from each core. These were demagnetised in an alternating field at 20mT and a stable, assumed primary, remanent magnetisation was measured. Doubt has been expressed as to the oceanic origin of the magnetisation measured in greenschist facies sheeted dykes (Hall *et al.* 1987), but an examination of the magnetic carriers by various techniques, and the consistency of results from greenschist and zeolite facies sites elsewhere on Troodos suggest that application of the method is justified (Allerton 1988, Bonhommet *et al.* 1988). A full explanation of analytical procedures, pilot demagnetisations and statistical treatment of the results is given in Allerton (*op. cit.*). Doubt may be expressed also as to the validity of the assumption of a TMV for the Limassol Forest, as it lies in part on the opposite side of the transform to the main body of Troodos and may therefore be of considerably different age and geographical position. However, palaeomagnetic results from the Kalavasos Mines and Parekklisha by Clube and Robertson (1986) are close to the average TMV (declination 274°, inclination 36°), and suggest that the assumption is indeed valid.

The seven sites were chosen to address a variety of specific problems brought up by the field studies, and so are discussed individually in the relevant sections of the remainder of this chapter. They give an overall impression of the range of rotational mechanisms operative in the ELFC, rather than forming a basis or framework for the structural field studies, for which many dozens of sites would be necessary, and which is

obviously far beyond the scope of the collaboration. With regard even to these more limited objectives the project was only partially successful, as in three of the seven sites the resultant solutions could not be explained simply in terms of the local structural relationships, and appear to be the product of compound rotations, which cannot be resolved by this analysis. What did become apparent from a consideration of all the sites, however, was the complexity and localised nature of the rotation, which could apparently be accommodated by the small fractures evident at virtually every outcrop. Internal deformation of what are treated as relatively coherent 'blocks' for the purposes of structural interpretation is therefore likely to be considerable.

5.3 Transform-Related Structures

5.3.1 Serpentinite shear zones

Brittle fracture is widespread in the mantle sequence and lowermost plutonics of the Akapnou Forest; however, zones of more intense deformation are identifiable. These take the form of serpentinite 'mélanges', with phacoids of harzburgite, dunite, pyroxenite and occasionally wehrlite and gabbro set in a silvery-blue schistose serpentine matrix. Clast size varies widely, from a few centimetres (plate 5.1) to 20m, the larger blocks tending to be the mechanically more resistant (non-serpentinised) pyroxenites and, where present, gabbros (plate 5.2).

The largest of the shear zones is visible at 197519, a few hundred metres north of Vasa village, where it has been brought into contact with sheeted dykes by a late normal fault. The serpentinite mélange is at least 100m wide and, although disrupted by several later faults, can be traced laterally for more than a kilometre. Excepting one large north-striking shear zone of dubious origin at Mazoukambos in the Vasilikos River (described in section 5.3.4), the serpentinite shear zones have an extremely strong preferred E-W orientation (figure 5.3), and dip steeply either to the north or the south. The schistose

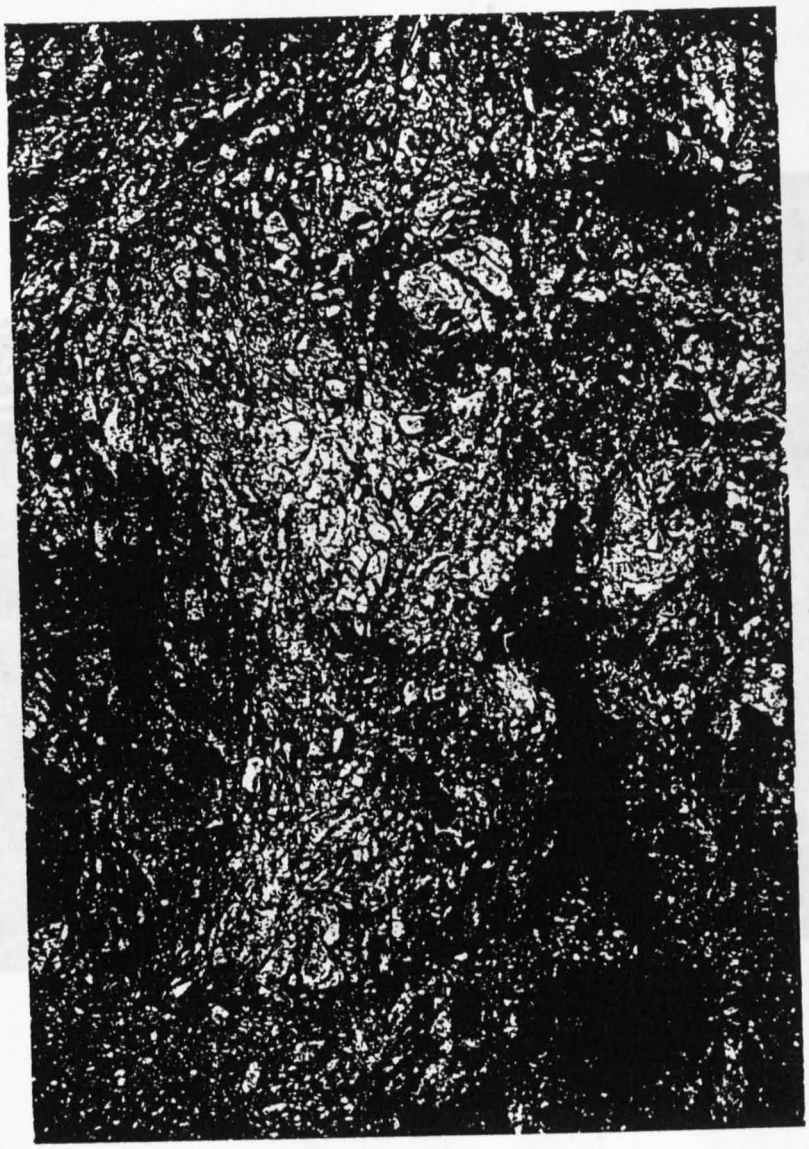

Plate 5.1: Serpentinite shear zone, southwest of Prastion. Note characteristic blue-silver sheen of sheared serpentinite, and slightly more coherent (lower strain) areas at extreme top right and lower left of picture.

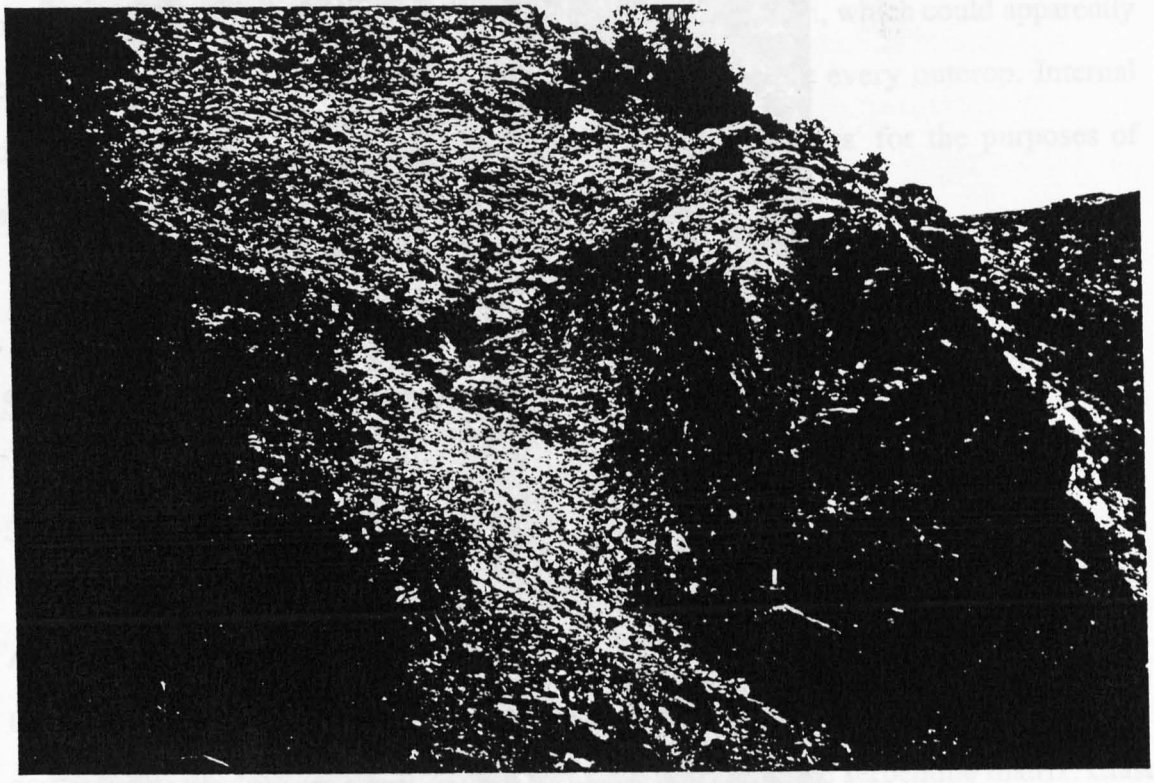

Plate 5.2: 3-4m gabbro block incorporated into E-W serpentinite mélange zone. Note sub-horizontal lineations, indicative of strike-slip displacement, near top of block. 22475259 Vasilikos River.

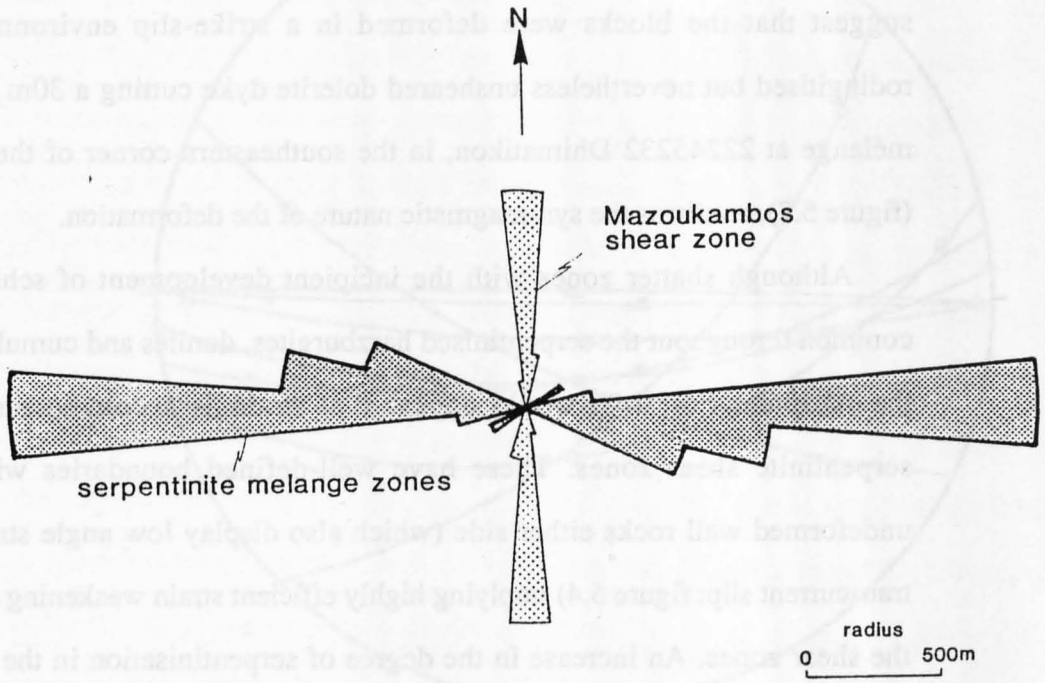

Figure 5.3: Cumulative length *versus* orientation rose diagram for serpentinite shear zones cutting the mantle sequence and lower plutonics, Akapnou Forest.

fabric of the shear zones has a variable orientation on a small scale, the crude foliation being deflected around blocks, and modified with apparent ease by later cross-cutting fault lines. Fractures traverse the larger blocks in the mélanges and are generally oriented E-W or ENE-WSW. Consistent sub-horizontal slickensides on these fracture planes suggest that the blocks were deformed in a strike-slip environment. A partially rodingitised but nevertheless unsheared dolerite dyke cutting a 30m wide serpentinite mélange at 22245232 Dhimatikon, in the southeastern corner of the Akapnou Forest (figure 5.7), confirms the syn-magmatic nature of the deformation.

Although shatter zones with the incipient development of schistose fabrics are common throughout the serpentinised harzburgites, dunites and cumulate ultramafics of the Akapnou Forest, it would appear that strain is accommodated mostly in the serpentinite shear zones. These have well-defined boundaries with the relatively undeformed wall rocks either side (which also display low angle striations indicating transcurrent slip: figure 5.4) implying highly efficient strain weakening and localisation in the shear zones. An increase in the degree of serpentinisation in the wall rocks as the shear zones are approached suggests an increased role for water, and deformation perhaps being aided by locally elevated pore fluid pressures. This is discussed further in the context of post-volcanic deformation later in this chapter.

5.3.2 Deformation of the axis crustal sequence

In the Akapnou Forest the harzburgites, dunites and, in places, layered plutonics are broken up into semi-coherent blocks by the E-W trending serpentinite shear zones. Analogous structures are less obvious in the upper parts of the crustal sequence, which have been tectonically separated from this 'basement' and modified by post-volcanic processes, described in section 5.4. Evidence does, however, remain for early oceanic deformation in the Sheeted Dyke Complex. Across virtually all of the northern half of the ELFC the dykes display greater or lesser degrees of brecciation. Although much is

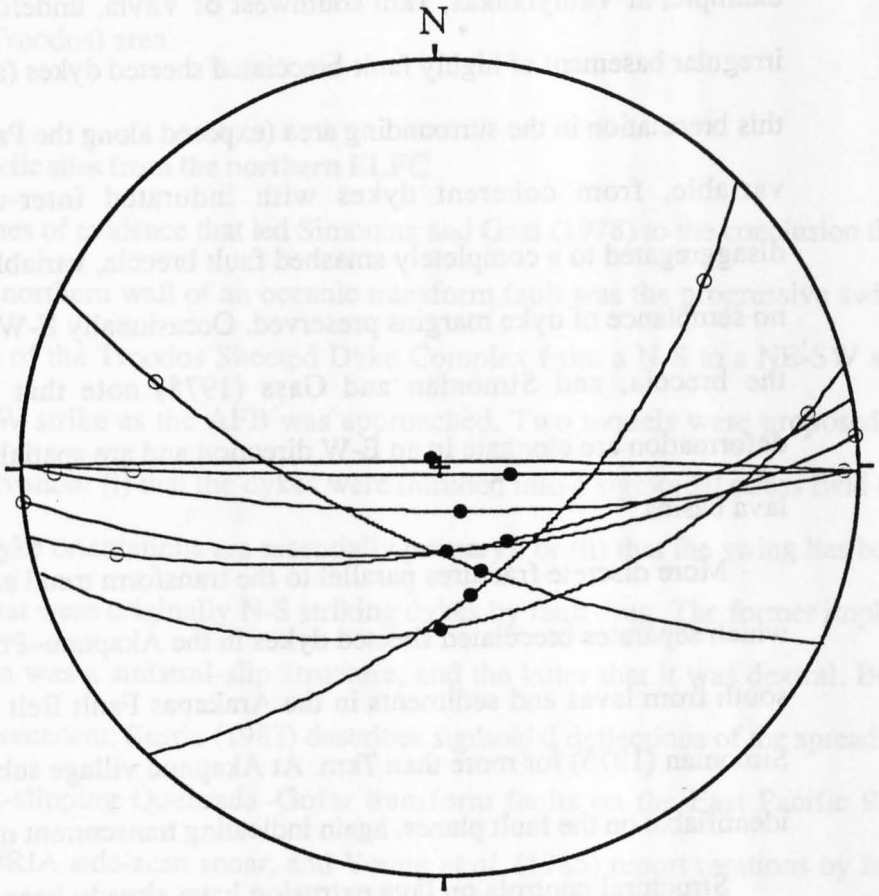

Figure 5.4: Slickenside lineations from the walls of a serpentinite shear zone, Vasa, indicating strike slip movement. Wulff equal angle projection.

undoubtedly due to the post-volcanic tectonism, some has to be syn-volcanic. For example, at Vathyrkakas, 1km southwest of Vavla, undeformed pillow lavas infill an irregular basement of highly fault-brecciated sheeted dykes (see chapter 3). The degree of this brecciation in the surrounding area (exposed along the Parsata–Vavla road section) is variable, from coherent dykes with indurated inter-dyke crush progressively disaggregated to a completely smashed fault breccia, variably oxidised or reduced, with no semblance of dyke margins preserved. Occasionally E-W fractures are visible within the breccia, and Simonian and Gass (1978) note that these zones of maximum deformation are elongate in an E-W direction and are spatially associated with the small lava basins.

More discrete fractures parallel to the transform trend are also visible. A fault zone which separates brecciated sheeted dykes in the Akapnou–Prastion–Dhierona area to the south from lavas and sediments in the Arakapas Fault Belt graben itself was traced by Simonian (1975) for more than 7km. At Akapnou village sub-horizontal slickensides are identifiable on the fault planes, again indicating transcurrent motion.

Structural controls on lava extrusion have already been described and discussed in chapter 3. Most noteworthy are the Mavridhia and Vasilikos Reservoir Faults in the neighbourhood of the Kalavasos Mines. Both now dip at a low angle towards the south and the VRF has been reactivated as a normal fault (see section 5.4), but their consistent orthogonal relationship with the lavas suggests that they were originally vertical. Their original strike depends upon the axis of rotation chosen, but was probably close to E-W. No kinematic indicators survive on these fault planes, and so no direct inferences can be made as to their original slip sense.

As stressed in chapter 3, no such structural controls on lava extrusion are evident in the lava sequence to the south of the Kalavasos Mines. The only 'early' faults which can be identified (from their role in localising mineralisation) are NE- or NNE-trending normal faults which lie parallel to the sheeted dyke trend and are thought to mirror the

attitude of the Anti-Troodos ridge (see sections 2.5.6 and 3.6.2). It is significant also to note that no areas of regionally brecciated sheeted dykes are to be found in the southern ELFC (*i.e.* Anti-Troodos) area.

5.3.3 Palaeomagnetic sites from the northern ELFC

One of the lines of evidence that led Simonian and Gass (1978) to the conclusion that the AFB was the northern wall of an oceanic transform fault was the progressive swing in the orientation of the Troodos Sheeted Dyke Complex from a N-S to a NE-SW and thence ENE-WSW strike as the AFB was approached. Two models were proposed to explain this observation: (i) that the dykes were intruded into a sigmoidal stress field (so that the present dyke orientations are essentially primary), or (ii) that the swing has been imposed upon what were originally N-S striking dykes by fault drag. The former implies that the transform was a sinistral-slip structure, and the latter that it was dextral. Both have geological precedent: Searle (1983) describes sigmoidal deflections of the spreading fabric at the fast-slipping Quebrada–Gofar transform faults on the East Pacific Rise revealed by GLORIA side-scan sonar, and Young *et al.* (1985) report rotations by fault drag at the southern margin of the Tjörnes fracture zone in Iceland.

Murton (1986a, b) argued that the predominantly NE-trending 'transform sequence' dykes cutting the WLFC mantle sequence were intruded along Riedel shears, and therefore that the transform had left-lateral slip; this assumes that the NE dyke direction is original and has not been modified by bulk rotation. In contrast, recent work by Allerton (1988) and Bonhommet *et al.* (1988), following earlier studies by Clube and Robertson (1986), has demonstrated significant clockwise rotations of dyke magnetisation vectors in the Sheeted Complex to the north of the AFB, leading them to suggest an originally N-S orientation for the dykes, and deformation by fault drag along a dextrally-slipping transform. However, a model arising from the present study, discussed in chapter 7, suggests that the clockwise rotations need not relate to the syn-magmatic transform history at all, but instead to a post-volcanic reactivation of the transform in a dextral

transcurrent sense. This debate can only be resolved beyond dispute by palaeomagnetic investigations of Murton's transform sequence dykes to see if their NE intrusion direction is original, or whether they have also suffered clockwise bulk rotation.

Two palaeomagnetic sites were drilled in sheeted dykes in the northern part of the ELFC, *i.e.* that known to have been influenced by transform tectonism, to see if analogous block rotations similar to those reported by Bonhommet *et al.* and Allerton could be detected. The results, presented in figures 5.5 and 5.6, are unfortunately equivocal: both sites lack reliable geological control, and even though the site at Klonari (B6) yields a single solution only (a huge 150° clockwise rotation about a moderately-dipping, westerly-directed axis), the rotation vector cannot be ascribed to any of the nearby structures. It is more likely that the vector is the resultant of two or more separate, unrelated rotations which are now superimposed; note that it is not possible to separate these components by palaeomagnetic means alone.

At the Dhrapia River site (B5) the Sheeted Dyke Complex forms part of a fault block tilted northward by post-volcanic processes (see section 5.4), and so it is again probable that the palaeomagnetic solutions represent compound rotations. If one assumes that the late rotation was, say, 80° clockwise (*i.e.* northward) about a horizontal axis directed toward 280°, which restores the dyke/gabbro contact back to an approximate horizontal and is therefore likely to be a reasonable estimation, an 'early' component of rotation can be calculated. Qualitatively, it is possible to see that the model A solution, which is about a high angle axis, will not modify the now sub-horizontal attitude of the rerotated block significantly, whereas the model B solution (about a sub-horizontal axis) will rotate the block *back* to the vertical again. This suggests that the model A solution, despite its relatively extreme angles of rotation, may be more realistic. This is in agreement with the single solution from Klonari and, significantly, implies high degrees of *clockwise* block rotation about a vertical axis, *i.e. dextral* strike slip, in agreement with Bonhommet *et al.* (1988) and Allerton (1988). Although it is conceivable that the 150° of clockwise

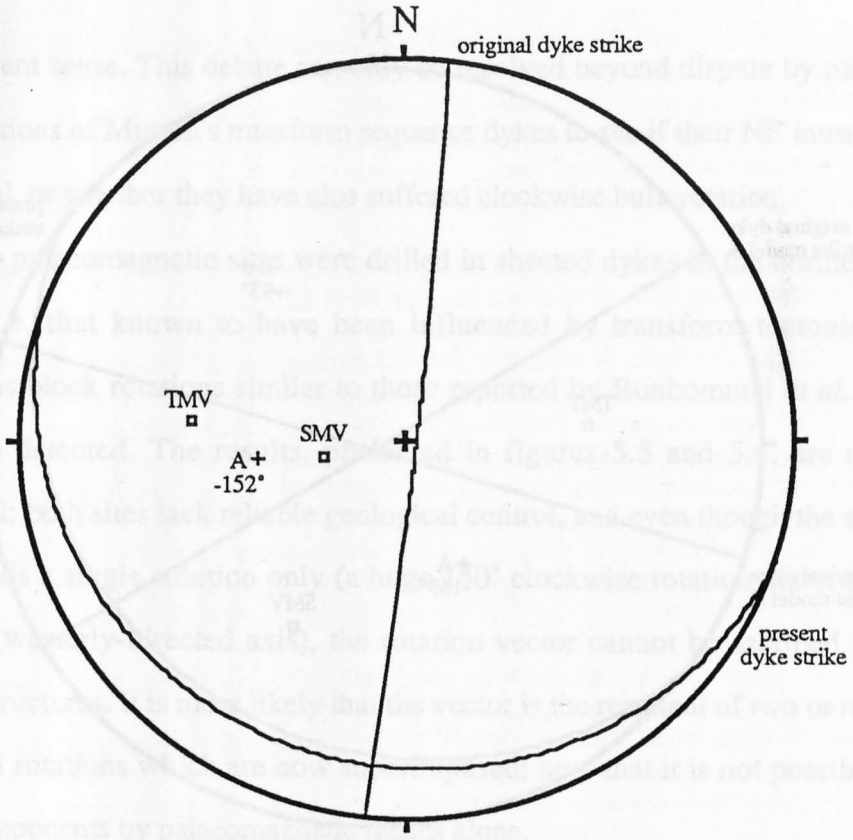

SITE B6: Klonari (15475379)

N = 6

mean present-day dyke orientation: 9°(S)/290°

mean sample magnetisation vector (SMV): 259°; 66°

Troodos magnetisation vector (TMV): 276°; 32°

dyke strike:	decl:	incl:	angle:
A: 87°(E)/185°	264°;	48°	-152°
(single solution)			

+ve angle = anticlockwise rotation by faulting

Figure 5.6: Summary of palaeomagnetic site B6 Klonari. Raw data presented in appendix 6. Wulff equal angle projection.

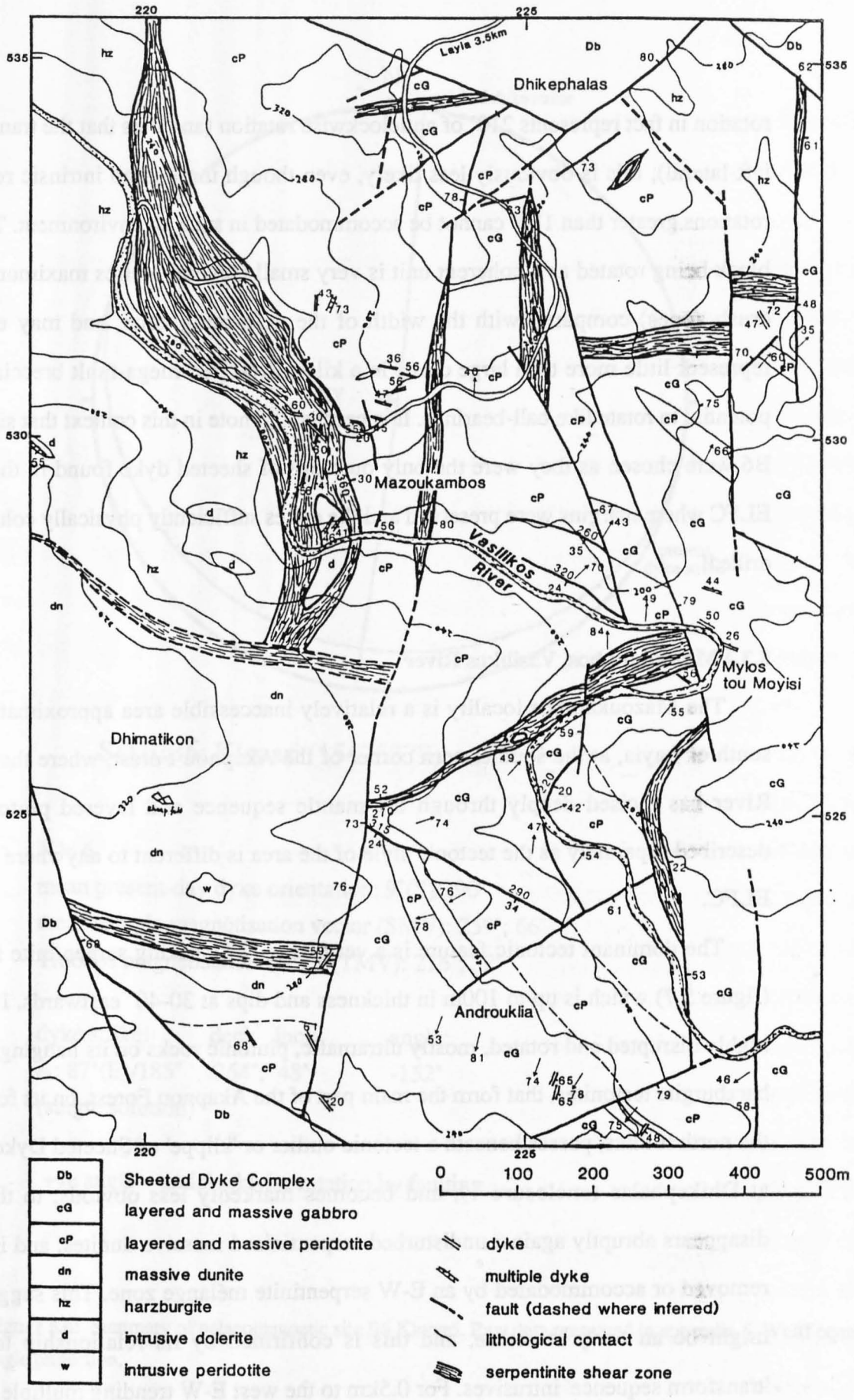

Figure 5.7: Geological map of the Mazoukambos area, Vasilikos River

dolerite pods (with group III boninitic chemistry) cut mantle sequence harzburgite. As the shear zone is approached these are abruptly rotated clockwise into a N or NNE direction, parallel to the fabric of the shear zone. A similar situation is observed on the eastern side, where dolerite dykes cut massive wehrlites. Within the shear zone itself a large dolerite body 150m x 50m, with internal chilled dyke margins, has been rotated into parallelism with the shear, and a smaller body has suffered extreme boudinaging. Significantly, however, the shear zone is cut by dolerite dykes of identical chemistry, but which are totally undeformed, implying that the tectonism and transform sequence magmatism were synchronous.

Several E-W serpentinite mélange zones, some with evidence for strike slip motion, are disrupted on the hanging wall of the major shear zone by later N-S faults. Some of these utilise serpentinised ultramafic layers in the plutonics, along which strain is preferentially concentrated and a schistose fabric developed, and incorporate the boudinaged gabbroic layers into the fault zones; others do not involve serpentinite and instead cut the schistose fabrics. The latter may be related to the N-S normal faulting of Upper Miocene age which, elsewhere in the LFC, is the last phase of deformation observed (see section 5.6.2), and may have reactivated the earlier fault sets.

The significance of the N-S synmagmatic structures in the Vasilikos River is not immediately obvious in the context of transform tectonics. However, in real strike slip fault systems, fracture patterns usually bear little relationship to the predicted 'ideal' orientations of synthetic and antithetic Riedel shears *etc.* (*e.g.* Wilcox *et al.* 1973), which are formed at infinitesimal degrees of strain, and must then be modified immediately by continued strain. In observed natural systems (*e.g.* the Builth inlier, central Wales: Woodcock 1987) several fault sets must be active concurrently, and low angle 'flats' or 'ramps' are kinematically necessary to accommodate differential displacement and block rotation between adjacent strike slip fault strands (Woodcock and Fischer 1987), and it is possible that the Vasilikos River shear zone represents such a structure.

5.4 Post-Volcanic Deformation I: the Northern ELFC

5.4.1 Introduction

Across much of the northern ELFC, from Parsata to Asgata (and several kilometres further west), the lavas at the periphery of the complex are tilted steeply (occasionally as much as 90°) towards the northeast (plates 3.1, 3.7 and 3.8). Sheeted dykes are often very shallowly dipping–note the attitudes of the dykes from the palaeomagnetic sites at Klonari and Dhrapia (figures 5.5 and 5.6)–and layering in the plutonics (for example in the Lestóvounos area) is usually high angle or inverted and cut by gently-dipping cross-cutting dykes (plate 2.2). It is obvious from these general observations that much of the crustal sequence has suffered substantial rotation, the style and mechanism of which is explored in the following sections.

In the northern part of the ELFC, around the Akapnou Forest in particular, lithologies from widely differing stratigraphic levels are juxtaposed, mostly separated by low angle contacts, which mirror the deeply incised topography and hence give rise to a rather confusing appearance in map view (*e.g.* figure 5.2). Sheeted dykes, for example, lie on massive dunites to the north of Vasa, and lavas directly overlie harzburgites and layered plutonics at Tremithia, 1.5km south of Layia. The latter outcrop was interpreted by Simonian (1975) as an extrusive (igneous) contact, but it is shown below that the lavas are in fact separated from the plutonics and tectonites by a low angle fault plane. Low angle faulting in the ELFC is common, and has previously been interpreted in terms of thrusting (Lapierre and Rocci 1967, Remond 1986); however, this does not take into account the consistent juxtaposition of *higher* stratigraphic levels on the hanging wall onto *lower* stratigraphic levels on the footwall. Thrusting implies repetition of stratigraphic units rather than omission, as is observed, which instead implies *normal* faulting. The widespread occurrence of these faults in the northern ELFC suggests that the area has been subject to a considerable degree of extension.

Nowhere are dykes observed cutting or otherwise utilising the low angle faults (unlike the Mazoukambos shear zone, section 5.3.4), and neither are any angular unconformities visible in the uppermost parts of the extrusive sequence; for this reason the faulting and block rotation are interpreted as post-dating the cessation of volcanism in the area. The exact timing of the faulting is discussed in chapter 6.

5.4.2 The Mavridhia and Vasilikos Reservoir Faults

A geological cross-section from Palaeodhrapia (Parsata) south-southwest to the Kalavasos Mines is presented in figure 5.8, and its location shown in figure 5.9. A northeasterly dip is apparent in all the lavas except for an area of SSE-dipping LPL at Palaeodhrapia and Parsata, which must have suffered some local tilting prior to UPL extrusion (chapter 3). Palaeomagnetic site B3 was drilled in pillows, flows and sills at Mandra tou Alykou, and gives a single solution of a simple northeasterly tilt of 60° for the site about a sub-horizontal NW axis (figure 5.10).

The dominant structures in the area are the Mavridhia and Vasilikos Reservoir Faults. They crop out on either side of the Kalavasos Dam, approximately 1km apart, both dip at *c.*25-28°(S)/280°, and can each be traced on the ground for more than 2km. The significant difference between the two is that, whereas the Mavridhia Fault at the surface separates UPL and LPL only, the Vasilikos Reservoir Fault (VRF) has layered gabbros and ultramafics on its (northern) footwall and UPL on its hanging wall, implying a normal displacement of *c.*3km down to the south or southwest (plate 5.3 and fig. 5.11).

Both faults were demonstrably active during the eruption of the lava sequence (chapter 3); what role did they play during the post-volcanic deformation episode? It is not geometrically possible to accommodate the rotation of the lavas with the faults maintained in their present orientations: the faults have a consistent orthogonal relationship with the lavas and must themselves have been rotated together with the

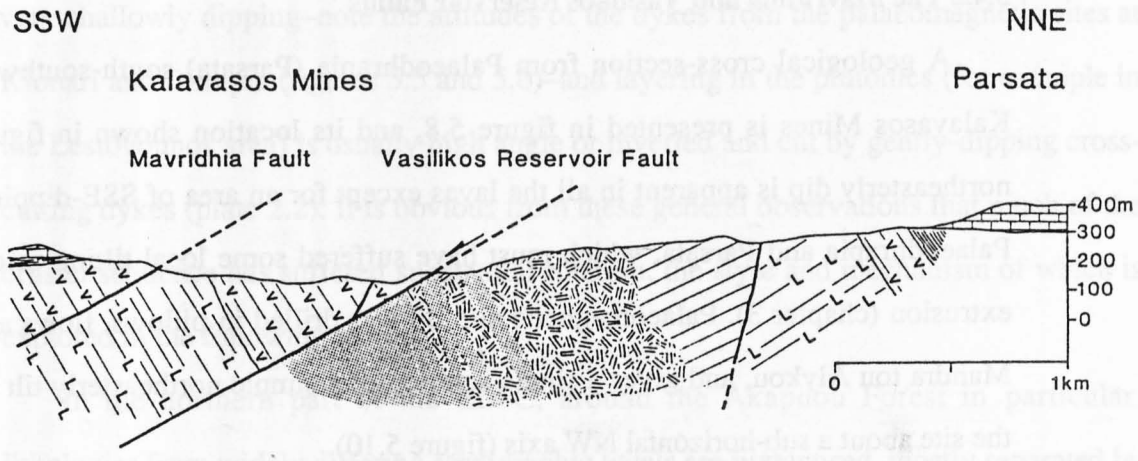

Figure 5.8: Geological cross section from Parsata to the Kalavasos Mines, showing the orthogonal relationship between the low angle Vasilikos Reservoir and Mavridhia Faults and steeply-tilted crustal sequence. L = LPL and V = UPL, with bars indicating dip; random dashed ornament = gabbro, close stipple = ultramafics. Note the angular unconformity between the LPL and UPL near Parsata. Location of cross section is shown on figure 5.9.

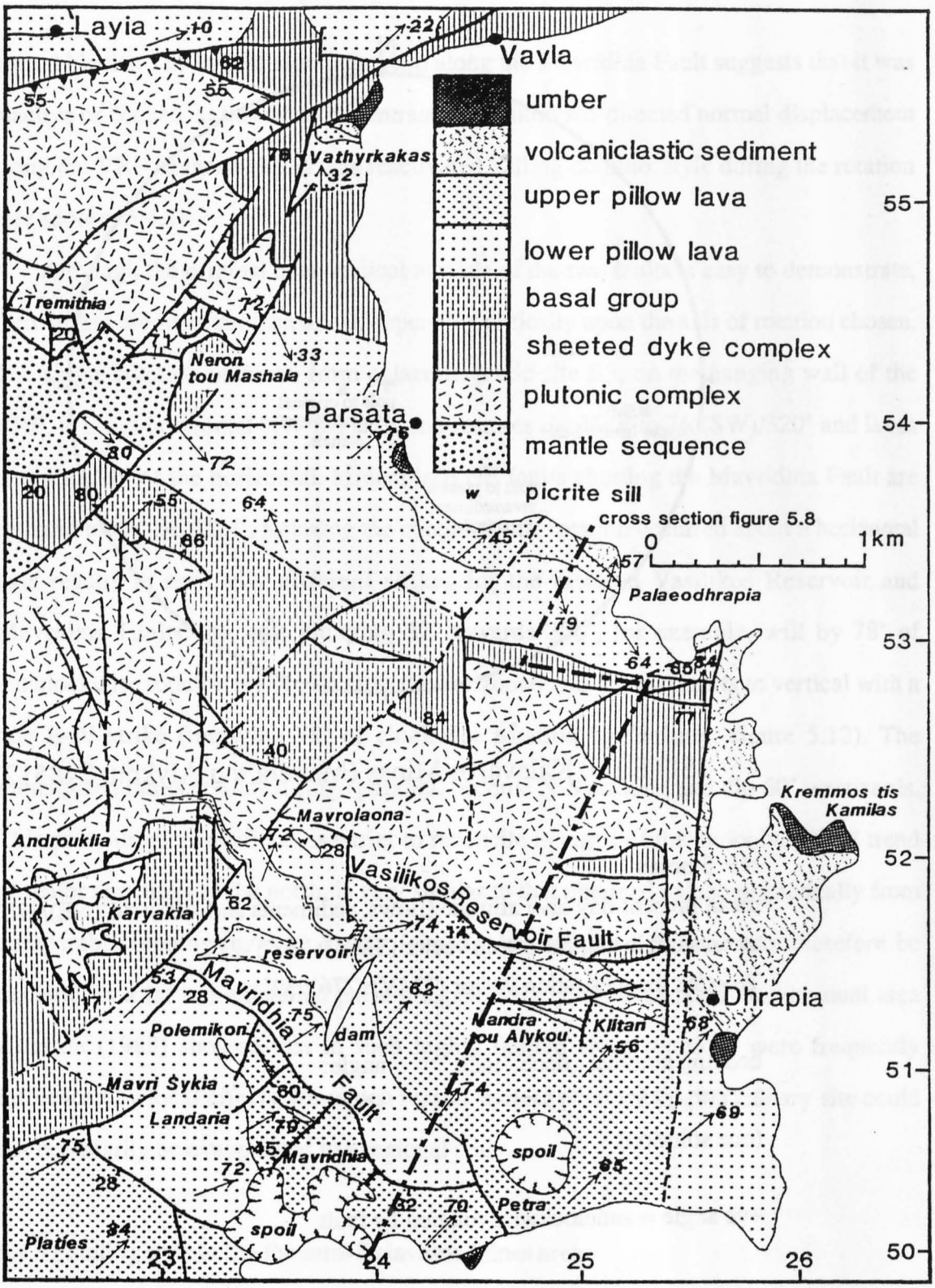

Figure 5.9: Geological map of the northeastern ELFC, showing the Mavridhia and Vasilikos Reservoir Faults and the location of the cross section in figure 5.8 (dot-dashed line).

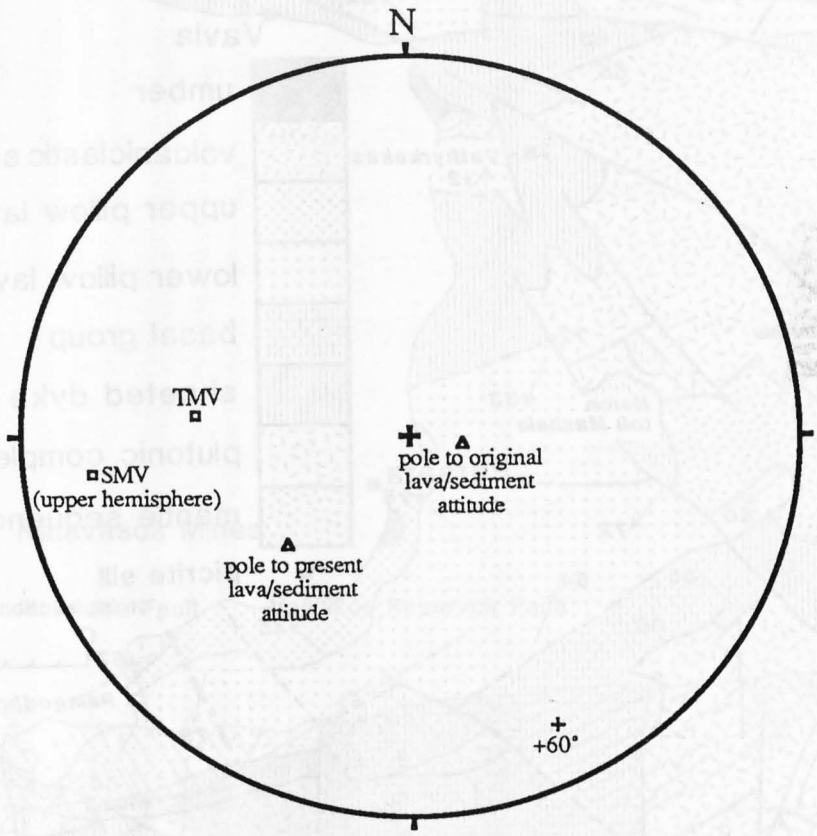

SITE B3: Kalavasos Mines (Mandra tou Alykou; 248512)

N = 3 holes
mean present-day lava attitude (flows, sediments and sills): 46°(NE)/320°
mean sample magnetisation vector (SMV): 263°; -22°
Troodos magnetisation vector (TMV): 276°; 32°

bedding attitude:	decl:	incl:	angle:
15°(W)/185°	154°;	9°	+60°
(one solution)			

+ve angle = anticlockwise rotation by fault

Figure 5.10: Summary of palaeomagnetic site B3 Kalavasos Mines. Raw data presented in appendix 6. Wulff equal angle projection.

crustal blocks. The lack of significant slip along the Mavridhia Fault suggests that it was inactive or 'locked' at this time; in contrast, the southward-directed normal displacement along the VRF suggests that it was reactivated 'falling domino' style during the rotation (see section 5.4.5).

Although the original near-vertical attitude of the two faults is easy to demonstrate, their strikes are more problematical, depending critically upon the axis of rotation chosen. The single solution obtained from palaeomagnetic site B3, on the hanging wall of the VRF, is a sub-horizontal NW-SE axis, and restores the VRF to 76°(SW)/320° and lavas to within 20° of the horizontal. Mineralised NE faults abutting the Mavridhia Fault are restored to 88°(SE)/224°. Relaxing the condition that rotation occurred about a horizontal axis results in markedly different strikes for the restored Vasilikos Reservoir and Mavridhia Faults. An axis plunging 22° towards 300°, for example, will by 78° of anticlockwise rotation restore lavas to the horizontal and the two faults to vertical with a due E-W strike (implying 78° of clockwise rotation by faulting; figure 5.12). The mineralised faults, assumed ridge parallel, become N-S striking and dip 60° westwards. This pole, although artificial, is easier to reconcile in terms of the undoubted E-W trend of major structures to the north, is very similar to that obtained palaeomagnetically from comparably dipping lavas at Asgata (site B4: see section 5.5), and may therefore be realistic. In a far more detailed palaeomagnetic study in the Lefkara–Stavrovouni area Allerton (1988) showed that in such highly faulted areas rotations were frequently influenced by local effects, for which reason vectors obtained from a solitary site could not necessarily be extrapolated to a regional scale.

5.4.3 Faulting style in the Parsata–Kalavasos Mines area

The low angle southward dip of the Mavridhia and Vasilikos Reservoir Faults is mirrored by numerous gravity faults in the Kalavasos Mines–Dhrapia area. A sliver of brecciated sheeted dykes, for example, lies on top of varitextured gabbros 0.75km north of Dhrapia (figure 5.9), and appears to have slid southward from the main outcrop of the

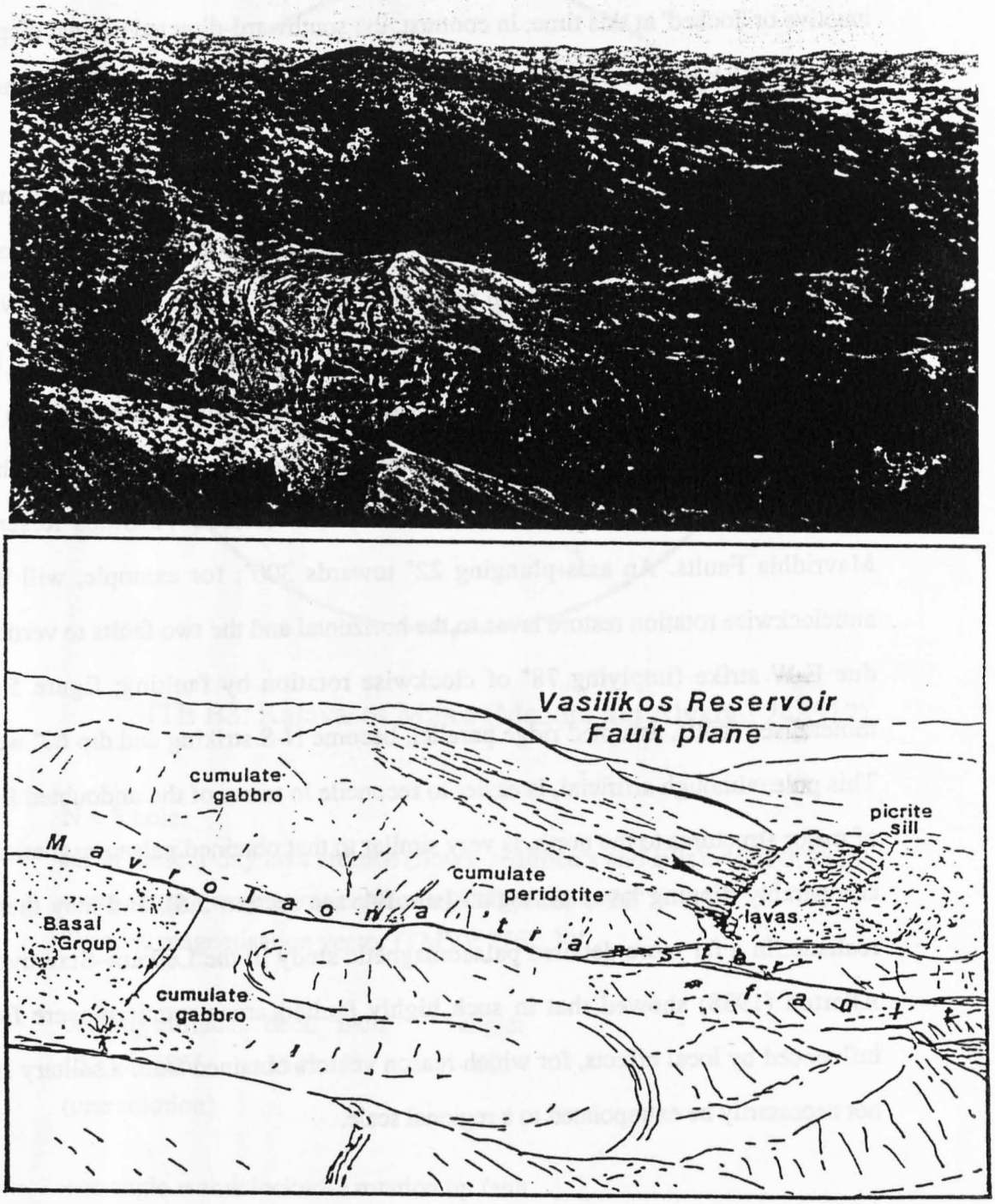

Plate 5.3 and figure 5.11: View eastwards along the north bank of the Vasilikos Reservoir towards Mavrolaona. In the middle distance lavas and a columnar jointed picrite sill dip steeply towards the left of the picture (NE), and are separated from (also NE-dipping) layered peridotites and gabbros by the low angle S-dipping Vasilikos Reservoir Fault. The gently sloping hillside in the centre of the picture (marked with an arrow on the figure) forms the fault plane itself, patches of propylitised fault breccia adhering to much of the hill surface. A NE-striking fault, the 'Mavrolaona transfer fault', runs across the picture down a stream gulley just beyond the white car. The Vasilikos Reservoir Fault does not persist to the NW of this fault (*i.e.* in the foreground); instead oxidised (orange) Basal Group is faulted down against (white) cumulate gabbros along a NW-striking, NE-dipping fault (foreground, left).

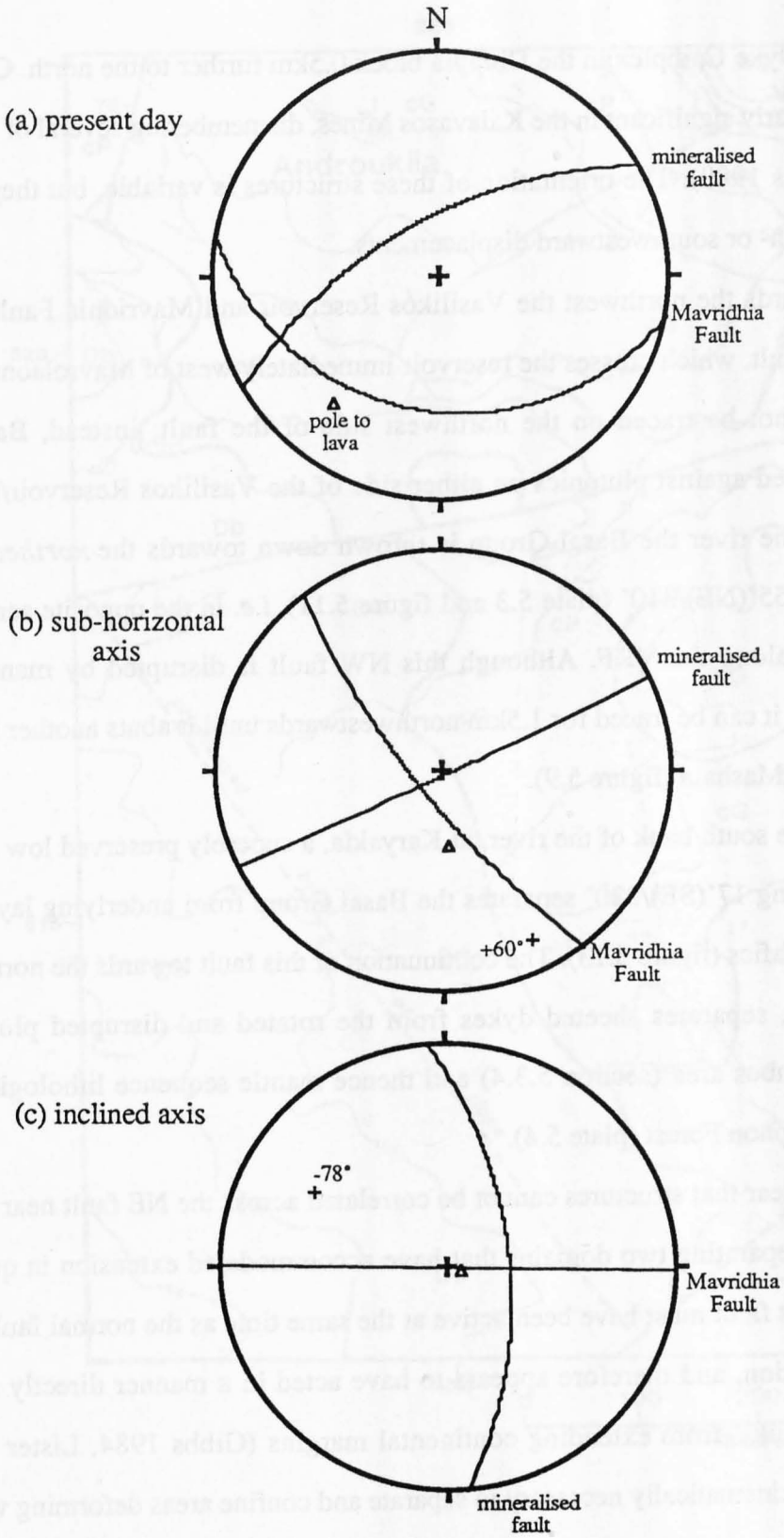

Figure 5.12: Equal area stereograms showing the relationship between the Mavridhia Fault, mineralised fault planes and pillow lavas in the Kalavasos Mines area, and the effects of rotating them about sub-horizontal and inclined axes. For discussion see text.

Sheeted Dyke Complex in the Dhrapia block 0.5km further to the north. Gravity sliding is particularly significant in the Kalavasos Mines, dismembering several of the ore bodies (Adamides 1980). The orientation of these structures is variable, but they consistently show south- or southwestward displacements.

Towards the northwest the Vasilikos Reservoir and Mavridhia Faults abut a NE-striking fault, which crosses the reservoir immediately west of Mavrolaona (figure 5.9). They cannot be traced on the northwest side of the fault; instead, Basal Group is downfaulted against plutonics on either side of the Vasilikos Reservoir/River. To the north of the river the Basal Group is thrown down towards the *northeast* by a fault dipping *c.*55°(NE)/310° (plate 5.3 and figure 5.11), *i.e.* in the opposite sense to the slip direction along the VRF. Although this NW fault is disrupted by many small later structures, it can be traced for 1.5km northwestwards until it abuts another NE fault near Neron tou Mashala (figure 5.9).

On the south bank of the river, at Karyakia, a superbly preserved low angle normal fault dipping 17°(SE)/220° separates the Basal Group from underlying layered gabbros and ultramafics (figure 5.13). The continuation of this fault towards the northwest is sub-horizontal, separates sheeted dykes from the rotated and disrupted plutonics in the Mazoukambos area (section 5.3.4) and thence mantle sequence lithologies across the entire Akapnou Forest (plate 5.4).

It is clear that structures cannot be correlated across the NE fault near Mavrolaona, which is separating two domains that have accommodated extension in quite different styles. This fault must have been active at the same time as the normal faults during the block rotation, and therefore appears to have acted in a manner directly analogous to 'transfer faults' from extending continental margins (Gibbs 1984, Lister *et al.* 1986), which are kinematically necessary to separate and confine areas deforming with differing extension rates and styles.

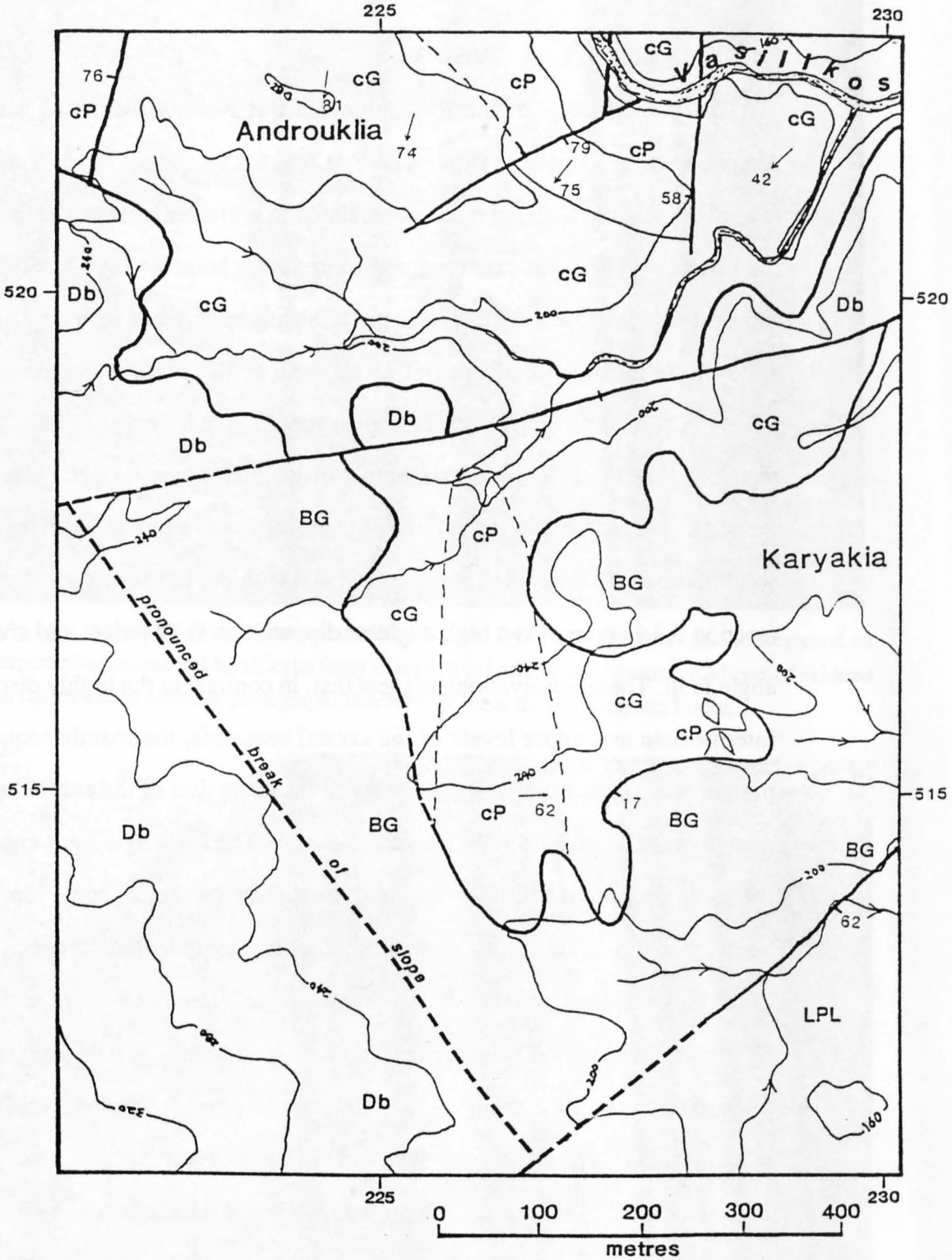

Figure 5.13: Geological map of the Karyakia area (north of the Kalavasos Mines), showing the low angle normal faulting of sheeted dykes (Db) and Basal Group (BG) down over disrupted layered plutonics (cP and cG).

5.4.4 The Akapnou Forest Décollement

The continuation of the low angle fault at Karyakia extends across the entire Akapnou Forest for at least 6km (plate 5.4), and has a regional dip of a couple of degrees towards the south. Sheeted dykes, brecciated to a greater or lesser extent, usually form the hanging wall to the structure, and more rarely lavas or high-level gabbros. On the footwall mantle sequence lithologies predominate, but layered plutonics underlie the fault zone in the north (to the south of Layia) and at Karyakia–Mazoukambos (Vasilikos River). The mantle sequence outcrop in the Akapnou Forest is laterally continuous, tectonised harzburgites in the northern part gradually passing into massive dunites and thence, in places, up into (serpentinised) axis sequence cumulate ultramafics towards the south. Serpentinite mélange zones associated with the transform in the mantle sequence (section 5.3.1) remain at a high angle of dip, with an E-W strike, and are cut by the low angle fault. These observations suggest that, in contrast to the highly disrupted and tilted intermediate and upper levels of the crustal sequence, the mantle sequence and lower plutonics are substantially unrotated (with the exception of the anomalous syn-volcanic disruption described from the Vasilikos River). The low angle fault appears to separate the rotated and unrotated domains and must therefore act as some kind of detachment horizon, kinematically necessary to accommodate the upper crustal extension documented in the previous section. It is henceforth termed the 'Akapnou Forest Décollement' (AFD).

In the field the AFD is often an impressive structure. In many places it is up to 5m thick, rarely even 10m, though ~2m between recognisable lithologies on the footwall and hanging wall is typical. Sheeted dykes on the hanging wall become brecciated from about 10m above the décollement zone proper, and this is accompanied by moderate to heavy oxidation. From 3-4m above the shear zone the oxidation vanishes and the now highly comminuted dyke rock is leached to a distinctive pale grey colour, with irregular white veins of chalcedonic silica. This passes down into a foliated but poorly lithified floury cataclasite, which in turn becomes serpentinous, with a schistose fabric (plate 5.5).

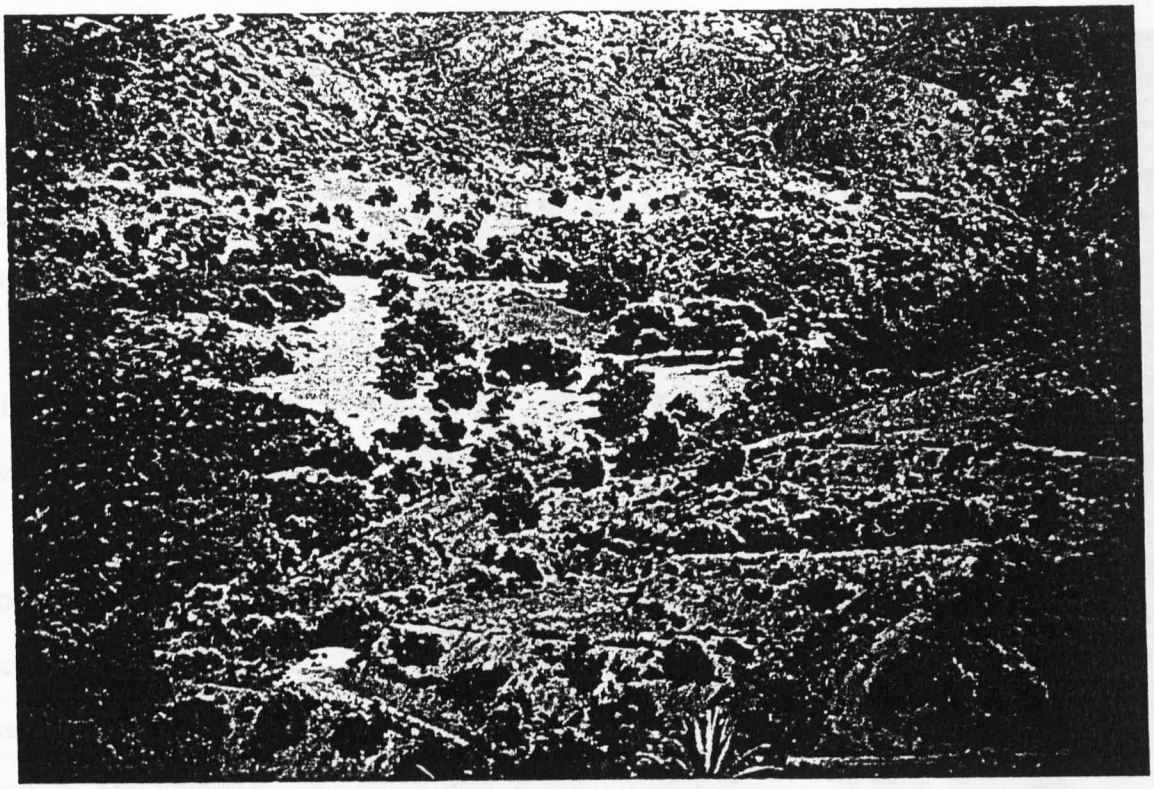

Plate 5.4: Low angle fault contact between oxidised Sheeted Dyke Complex (orange) in foreground on top of serpentinised dunite and harzburgite (grey to brown) in background. Note small 'klippe' of oxidised dykes on flat ground in centre of photograph. 2km NNE of Vasa, darkest Akapnou Forest.

Plate 5.5: The Akapnou Forest Décollement. Pale grey leached and crushed Basal Group lavas lie upon serpentinised layered ultramafics, separated by 1.5m thick crush zone of comminuted lava (white) grading down into schistose serpentinite with low angle fabric. 232543 Neron tou Mashala, 1km NW of Parsata.

Incorporated within the schistose serpentinite and the foliated rock flour may be rounded blocks of any of the major lithologies, frequently so altered as to be virtually unrecognisable. These may also be veined by chalcedony. The intensity of the low angle fabric in the serpentinised footwall diminishes over 1-2m or so below the contact, and passes down into unsheared but still serpentinised harzburgites and dunites *etc.* Gravity sliding frequently removes part or all of this fault zone, such that sheeted dykes lie directly upon dunite and harzburgite without any intervening crush, and it is also cut by numerous small-throw high angle faults.

The AFD is also exposed between the village of Prastion and the Pevkos roadstone quarries (*e.g.* figure 5.2), where steeply tilted layered ultramafics and gabbros of the Lestóvounos area form the hanging wall to a thick low-angle serpentinous shear zone. Harzburgites lie on the footwall. Although disrupted by many later faults in the intervening 3.5km, the difference in elevation between the outcrops of the AFD to the north of Sanidha and near Pevkos suggests a regional dip of some 2-3° southwards, similar to its dip across the Akapnou Forest itself. A major WNW-trending fault near Pevkos, which extends towards Monagroulli and is described in some detail in section 5.5.4, truncates the AFD (figure 5.30) and it is not exposed again in the ELFC further to the south.

An examination of the layered plutonics in the tens of metres above the AFD in the area north of Pevkos gives some insight as to the mechanism of detachment. The degree of serpentinisation of the ultramafic portions of the layered sequence increases in intensity down section, and this is accompanied by a concomitant increase in the amount of deformation, such that scaley serpentinite dislocations develop in the ultramafic rocks parallel to the layering. As the serpentinous shears proliferate, the competent gabbroic layers become progressively more boudinaged (plate 5.6) and thence eventually disaggregated into phacoids enclosed within low angle schistose serpentinite. Below the shear zone are shattered serpentinised harzburgites.

It is very clear from these observations that strain is taken up by the deformation of

Plate 5.6: Sheared serpentinised ultramafics (brown) and boudinaged gabbro horizons in layered plutonic complex, a few tens of metres above the Akapnou Forest Décollement. 14105080, 1km N of Pevkos.

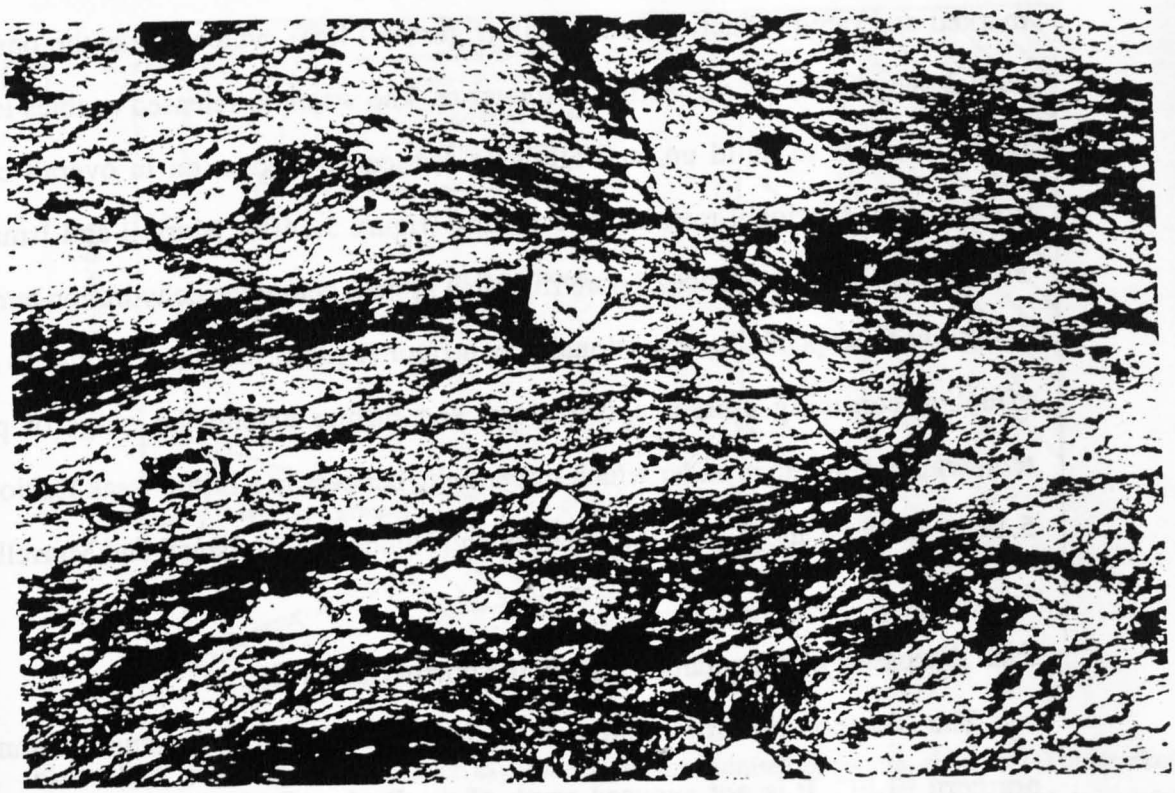

Plate 5.7: Photomicrograph of material from Akapnou Forest Décollement surface. Schistose fabric is defined by elongate serpentines (light) traversed by multiple small-scale dislocations, and tiny grains of iron oxide (dark). More resistant fragments are chrome-spinel and serpentinised but *unsheared* olivine *etc.*, suggesting that serpentinisation preceded deformation. Field of view 5.5mm, plane polarised light.

serpentinite, and this is confirmed by an examination of thin sections of material from the AFD surface itself (plate 5.7). A strong fabric is defined by layers of dark very fine-grained iron oxide (probably after magnetite) and elongate slivers of serpentine with discrete multiple dislocations. Within this fabric are larger fragments of mechanically resistant chrome spinel, and tectonically rounded pips of wehrlite or dunite up to 1.5cm long, in which mesh-textured passively-serpentinised olivine (which is quickly destroyed at low degrees of strain: Raleigh and Paterson 1965, Maltman 1978) are visible. The texture is very obviously one of a mechanically deformed serpentinite, and not a fault rock subsequently serpentinised.

Experimental studies of the deformation of serpentinite (Bowen and Tuttle 1949; Raleigh and Paterson 1965) reveal that, at low temperatures and low-moderate pressures, serpentinised peridotite has an ultimate strength comparable to that of granite; however, at some temperature in the range 300-600°C it suddenly becomes very brittle and shows a marked and rapid reduction in strength (figure 5.14(a)), which marks the onset of the partial dehydration of serpentine to forsterite. The water so released enables local pore fluid pressures to build up, and allows a consequent reduction in overall confining pressure and frictional resistance to sliding (figure 5.14(b); Murrell and Ismail 1976, Sibson 1977). The presence of pore fluid in a system below the dehydration temperature (as might be expected in a tensional ocean-floor regime) has the potential to decrease effective confining pressures still more, and further extend the range of pressure-temperature conditions under which serpentinite behaves in a brittle weak fashion (figure 5.14(c); Hubbert and Rubey 1959, Rubey and Hubbert 1959, Ismail and Murrell 1976).

5.4.5 Discussion of deformation style in the northern ELFC

The Akapnou Forest Décollement is clearly the dominant structural feature of the northern ELFC. It is not exposed south of the Pevkos Fault, but it is possible that it underlies much, if not all, of the southern ELFC. Two exploration boreholes sunk at

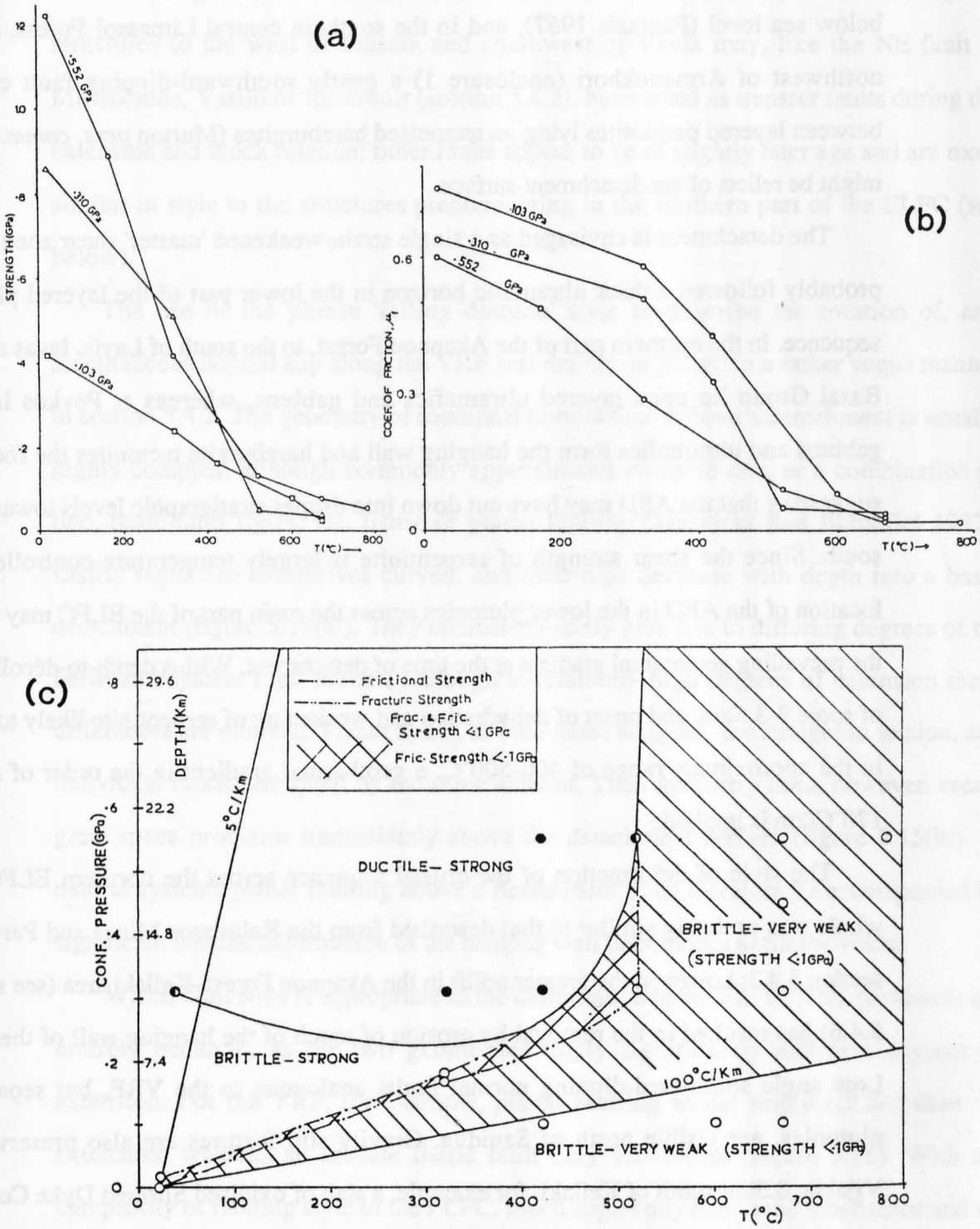

Figure 5.14: Summary of deformation experiments on serpentinised peridotite, showing (a) the marked loss of ultimate strength and (b) reduction of the coefficient of friction as a result of the partial dehydration of serpentine; and (c) the range of P-T conditions under which such weakening might occur (from Murrell and Ismail 1976).

Ornithouri in the late 1950s, which encountered serpentinite at depths of 100-200m below sea level (Pantazis 1967), and in the southern central Limassol Forest, *c.*3km northwest of Armenokhori (enclosure 1) a gently southward-dipping fault contact between layered peridotites lying on tectonised harzburgites (Murton *pers. comm.* 1987) might be relicts of the detachment surface.

The detachment is envisaged as a single strain-weakened 'master' shear zone which probably followed a thick ultramafic horizon in the lower part of the layered plutonic sequence. In the northern part of the Akapnou Forest, to the south of Layia, lavas and the Basal Group lie upon layered ultramafics and gabbros, whereas at Pevkos layered gabbros and ultramafics form the hanging wall and harzburgite tectonites the footwall, suggesting that the AFD may have cut down into deeper stratigraphic levels towards the south. Since the shear strength of serpentinite is largely temperature-controlled, the location of the AFD in the lower plutonics across the main part of the ELFC may reflect the prevailing geothermal gradient at the time of detachment. With a depth-to-décollement of some 3-3.5km, and onset of dehydration and weakening of serpentinite likely to occur in the approximate range of 400-500°C, a geothermal gradient in the order of *c.*110-170°C/km is implied.

The style of deformation of the crustal sequence across the northern ELFC as a whole was probably similar to that described from the Kalavasos Mines and Parsata in section 5.4.2; however, the greater uplift in the Akapnou Forest–Kellaki area (see section 5.4.6) has resulted in the removal by erosion of much of the hanging wall of the AFD. Low angle southward-dipping normal faults analogous to the VRF, but separating plutonics, are visible north of Sanidha. Gravity slip features are also preserved: at Vijakia, 0.5km south of Kellaki, for example, a slab of oxidised Sheeted Dyke Complex with a flat basal contact forms a prominent hill rising 70m above the surrounding layered plutonics, and appears to have slid southward from the main outcrop of sheeted dykes to the north of Kellaki village (enclosure 1). This may be a remnant of a much larger fault

slab.

Many high angle faults also traverse the northern ELFC. Some of the NE-trending structures to the west of Parsata and southwest of Vavla may, like the NE fault at Mavrolaona, Vasilikos Reservoir (section 5.4.3), have acted as transfer faults during the extension and block rotation; other faults appear to be of slightly later age and are more similar in style to the structures predominating in the southern part of the ELFC (see below).

The use of the phrase 'falling domino' style to describe the rotation of, and simultaneous normal slip along the VRF was deliberately used in a rather vague manner in section 5.4.2. The geometry of rotational normal faults above a detachment is usually highly complex, although commonly approximates either to one, or a combination of two, basic fault styles, *viz.* listric or planar faulting (Wernicke and Burchfiel 1982). Listric faults are themselves curved, and their dips decrease with depth into a basal detachment (figure 5.15(a)). They characteristically give rise to differing degrees of tilt between adjacent fault blocks, although at relatively high degrees of extension these differences are minimal. Planar faults, as their name suggests, are straight in section, and individual blocks are tilted by the same amount. Their geometry does, however, create great space problems immediately above the detachment surface (figure 5.15(b)). In natural systems planar faulting above a detachment must therefore be accompanied by significant internal deformation of the hanging wall fault blocks to fill the voids.

Which fault style is appropriate to the deformation in the ELFC? The question is not entirely pedantic, as the two geometries imply significantly different degrees of extension. For the VRF, for example, planar faulting would imply *c.*2.2–2.6km of extension, whereas an arcuate listric fault only 1.2–1.4km (figure 5.16). With the complexity of faulting style in the ELFC, much apparently due to the inheritance and re-use of pre-existing lineaments, and significant erosion of the tilted fault blocks, it is not feasible to attempt a calculation of the total extension across the northern ELFC, nor is it possible to distinguish unequivocally between the two possible fault geometries. The lack

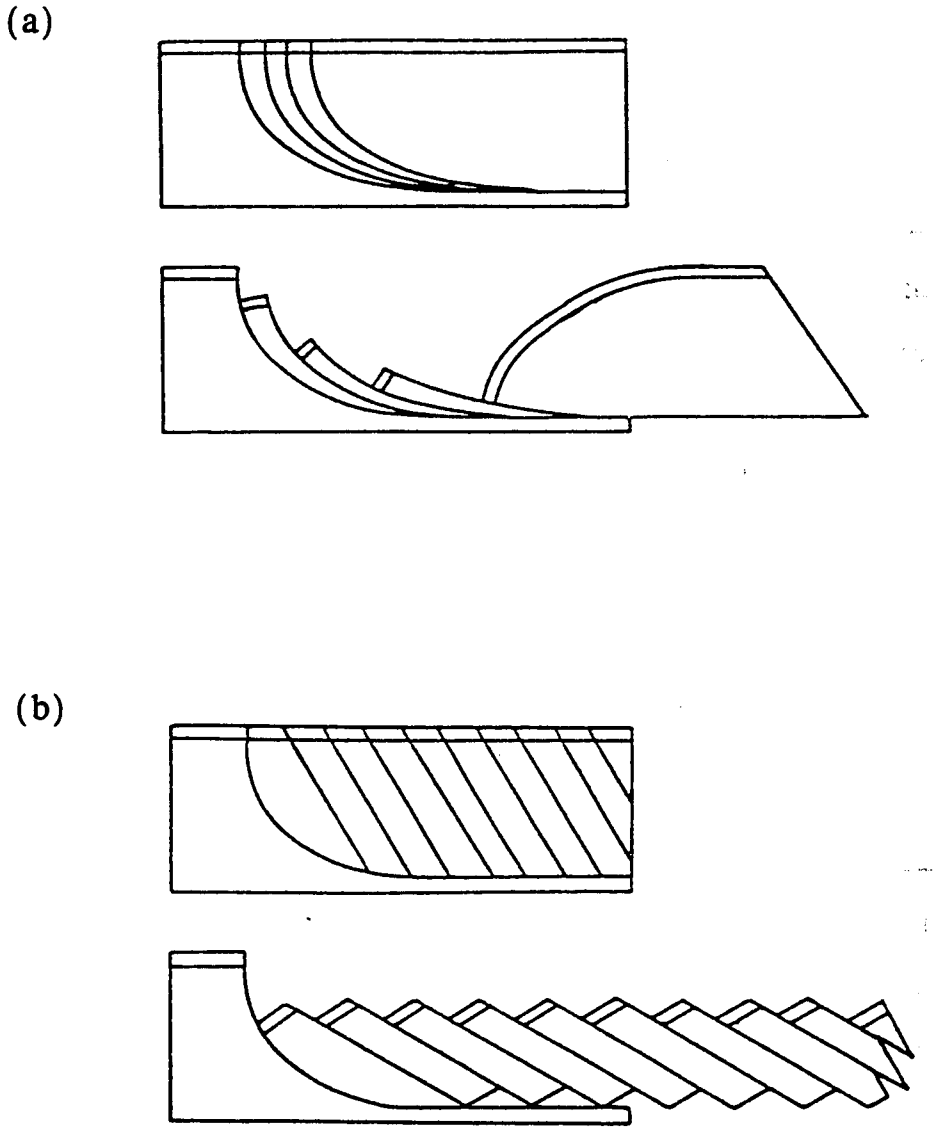

Figure 5.15: Cartoon block diagrams illustrating how extension is accommodated by: (a) listric, and (b) planar rotational normal faults above a basal décollement. The latter are shown bounded by a listric fault; note the space problem created above the detachment horizon, which in natural systems might be filled by small-scale faulting. From Wernicke and Burchfiel (1982).

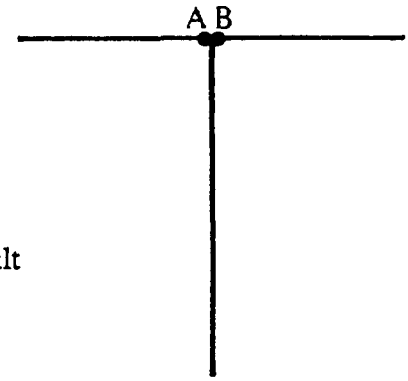

θ = angle of dip of hanging wall
ϕ = angle of dip of fault (here $\theta + \phi = 90°$)
d = displacement along Vasilikos Reservoir Fault
r = radius of curvature of listric fault
x = extension

(a) planar faulting:

$x = d.\sin\theta$

$\theta = 60°$; $\phi = 30°$
for d = 2.5km
x = 2.2km
for d = 3km
x = 2.6km

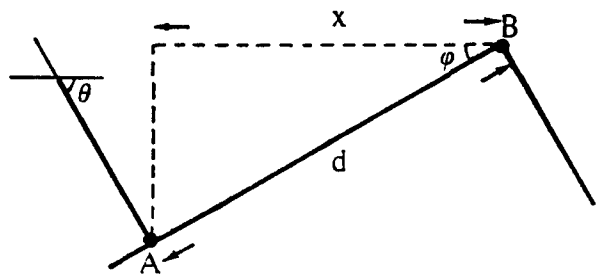

(b) listric faulting:

$d = r.\theta$
$\cos\theta = (r - x) / r$

$\theta = 60°$; $\phi = 30°$
for d = 2.5km
x = 1.2km
for d = 3km
x = 1.4km

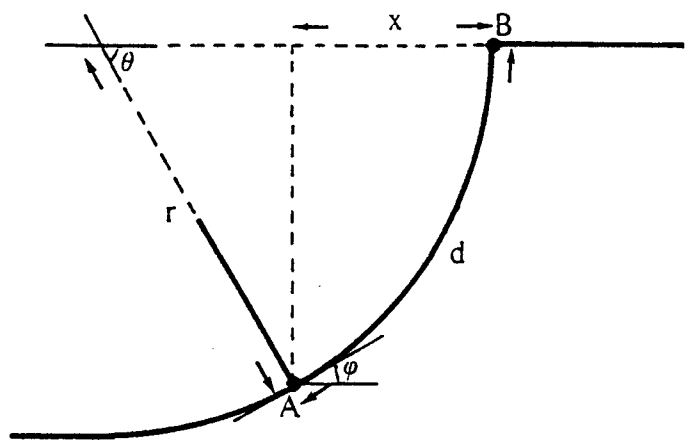

Figure 5.16: Simplistic estimates of the amount of extension accommodated along the Vasilikos Reservoir Fault, assuming (a) planar and (b) listric geometries for the fault.

of reliable palaeo-orientation indicators in the Dhrapia block precludes the identification of any differential tilt between it and the Kalavasos Mines block, and no systematic difference in the orientation of the VRF itself is detectable. However, the originally vertical orientations of the VRF and other now low angle rotated faults, and still vertical transform-related structures in the AFD footwall, suggest that these faults must themselves have been initially planar, and would therefore have retained their planar geometries during reactivation. The widespread small-scale brittle faulting that is so common in the northern ELFC may thus represent the kinematically necessary internal deformation of the planar fault-bounded blocks.

5.4.6 Reverse faulting, Layia–Akapnou

Along the northern margin of the Akapnou Forest, from Layia westwards towards Akapnou village, tectonised harzburgites are reverse-faulted northwards over layered plutonics which are, in turn, reverse-faulted northwards over lavas and brecciated sheeted dykes of the Arakapas Fault Belt (figure 5.17). The faults dip steeply southwards (up to 70°) and are E-W striking. A kilometre to the east of Akapnou the southerly fault truncates the northerly one, so that the former must have been active later. This implies that the reverse faults were propagating southward into the hanging wall, opposite to their sense of translation. This 'overstep propagation' (Butler 1982) is the reverse of the more commonly reported 'piggy-back' or foreland propagation in large-scale thrust belts.

Activity on the reverse faults apparently post-dated the AFD, yet Maastrichtian-Miocene Lefkara chalks along strike to the east are undeformed (note that the E-W trending fold axes marked by Pantazis on his (1967) map to the southeast of Vavla do not in fact exist). The reverse faulting must therefore be of late Cretaceous age, which is similar to that of the extensional structures across the ELFC (see chapter 6). If this is the case, how can the apparent evidence for compression implied by these structures be reconciled with the evidence for extension everywhere else in the ELFC?

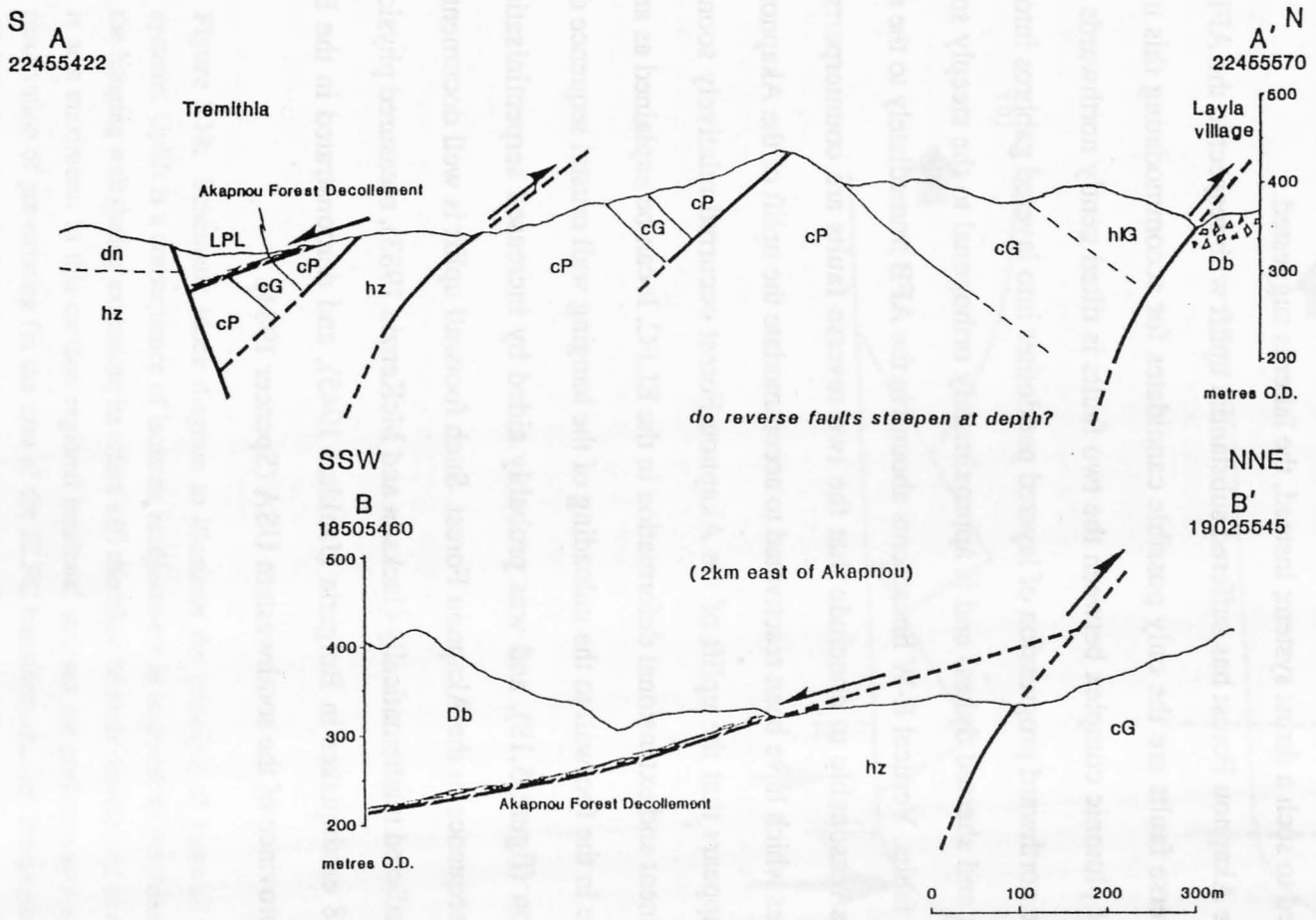

Figure 5.17: Cross sections at Layia village (A-A') and Mavrovouni (B-B': 2km east of Akapnou village), showing reverse faulting at the northern margin of the Akapnou Forest, and the low angle Akapnou Forest Décollement.

It is not possible to determine directly the attitude of the reverse faults at depth, *i.e.* whether they are frontal ramps to a deep, shallowly-dipping thrust plane to the south, or whether they instead steepen and become vertical. However, there is no evidence anywhere in the Limassol Forest for the former, nor are there any structures which could be related to such a thrust system; instead, the latter is suggested.

The Akapnou Forest has suffered substantial uplift with respect to the AFB, and the two reverse faults are the only possible candidates for accommodating this uplift. The block of plutonic complex between the two faults is tilted gently northwards (deduced from the northward progression of layered peridotites into layered gabbros into isotropic gabbros and sheeted dykes) and is approximately orthogonal to the steeply southward-dipping faults. Vertical E-W lineaments abound in the AFB immediately to the north, and it seems reasonable to conclude that the two reverse faults are counterparts of these structures which have been reactivated to accommodate the uplift of the Akapnou Forest.

It appears that the uplift of the Akapnou Forest occurred relatively soon after the décollement and extensional deformation in the ELFC. It can be explained as an isostatic response in the footwall to the unloading of the hanging wall crustal sequence during the extension (figure 5.18), and was probably aided by increased serpentinisation of the mantle sequence in the Akapnou Forest. Such footwall uplift is well documented: it has been predicted mathematically (Jackson and McKenzie 1983), measured physically after the 1928 earthquakes in Bulgaria (Jankhof 1945), and demonstrated in the Basin and Range province of the southwestern USA (Spencer 1984).

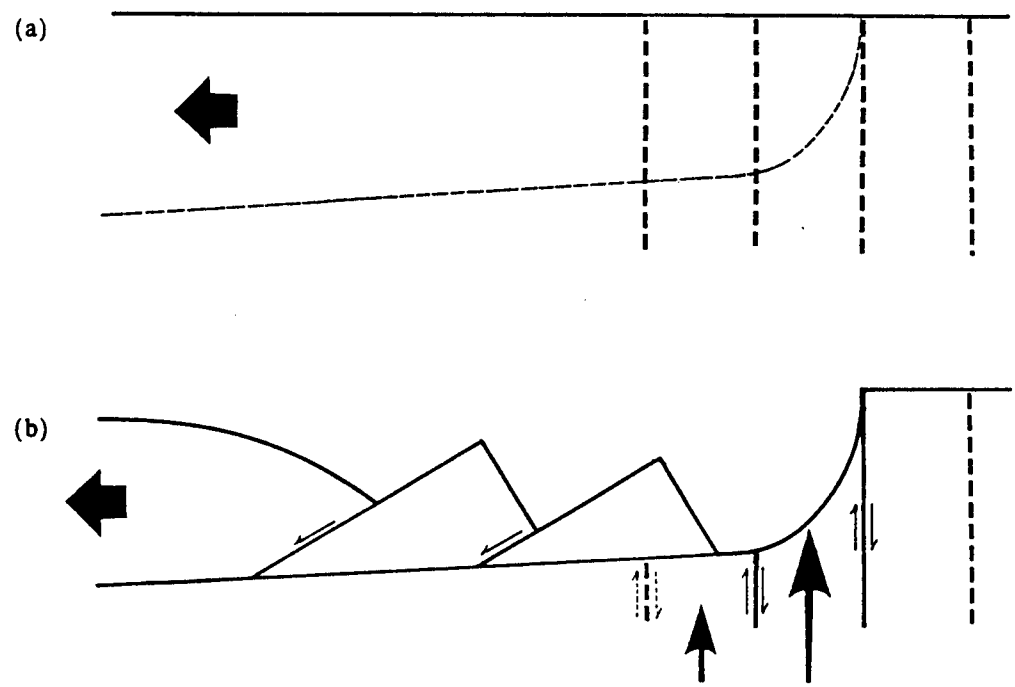

Figure 5.18: Schematic block diagram to illustrate the principle of footwall uplift in extensional systems. Uplift is a consequence of isostatic readjustment in response to the thinning and unloading of the hanging wall during extension; its effect will therefore be most pronounced in areas where extension is at a maximum. In this cartoon regional tensional stresses are preferentially accommodated by the reactivation of pre-existing (in the case of the ELFC transform-related) lineaments, represented by the thick broken lines in (a), above a detachment or delamination surface at some level within the crust. Extension is thus concentrated close to the original (transform) tectonised zone, and isostatic uplift (represented by the vertical arrows in (b)) can be accomplished utilising pre-existing (transform) features in the footwall. No scale is implied.

5.5 Post-Volcanic Deformation II: the Southern ELFC

In the southern half of the ELFC low angle faults with the extreme normal displacements so characteristic of the northern part are not obvious. Instead, more steeply-dipping faults predominate, many having either NE or NW/WNW orientations, and this gives rise to a very different appearance to the area in map view. Some of these faults cut the Akapnou Forest Décollement where it crops out at Pevkos, as indeed do many in the Akapnou Forest itself, and so they must be of younger age. A more detailed examination of the structures (see below) reveals cross-cutting relationships and multiple striations on some surfaces, suggesting a protracted period of fault activity post-dating the décollement.

To the northeast of Parekklisha lavas and dykes are in faulted contact with serpentinised tectonised harzburgite, which then crops out continuously across the western half of the LFC. The contacts between the mantle rocks and the lavas and dykes, which are partly thrust, are thought to be considerably younger than the rest of the deformation in the ELFC and so are discussed separately in section 5.6.

5.5.1 Dyke intrusion and block rotation in the Asgata River

Around Asgata village, and for 3km to the west, pillow lavas are tilted steeply towards the northeast, as in the Kalavasos Mines. Palaeomagnetic site B4 was drilled at the volcanic centre in the Asgata River (section 3.5 and figure 3.5), which is intruded into the steeply-dipping lavas. Field relations indicate a complex intrusive history there, with at least three sets of cross-cutting dykes or sills displaying a wide variety of orientations.

The most prominent of the intrusives are large (up to 8m wide), high-angle, NE-trending dykes, some of which form multiple swarms. The majority of the remainder dip towards the northwest, north or northeast, with no consistent angular relationship either to pillows at the site or to the NE dykes. Many of these individual dykes/sills are highly

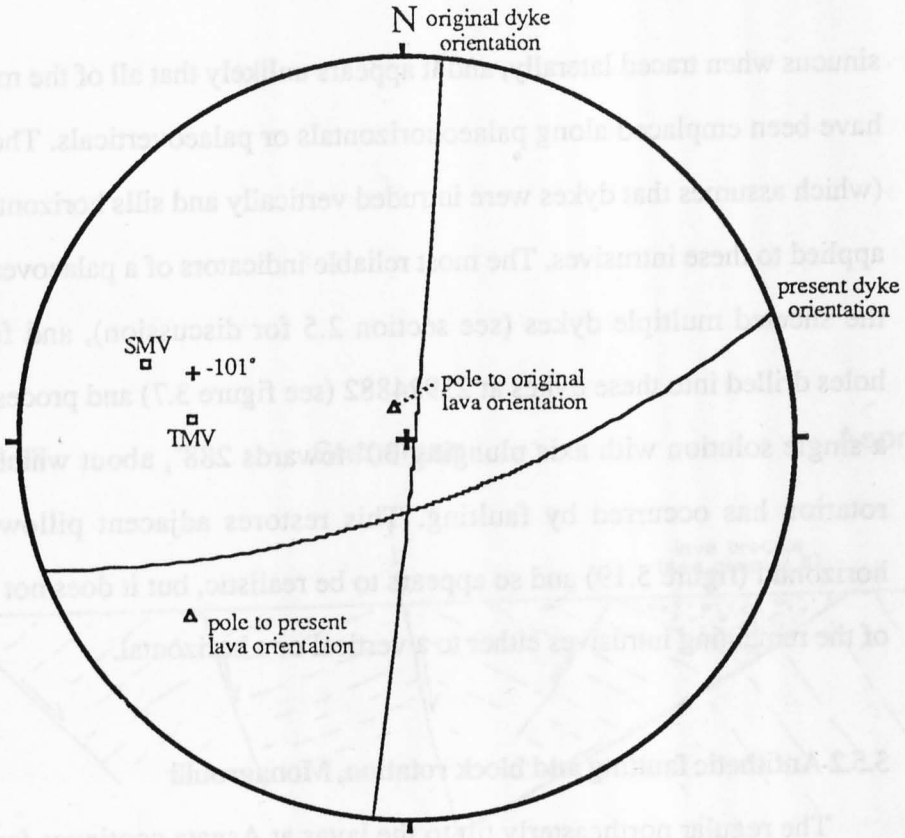

B4: Asgata River (239488)

N = 4 holes

mean present-day dyke orientation: 70°(SE)/230°
(multiple dykes)

mean sample magnetisation vector (SMV): 287°; 20°

Troodos magnetisation vector (TMV): 276°; 32°

original dyke attitude:	decl:	incl:	angle:
88°(E)/185°	288°;	30°	-101°

(one solution)

+ve angle = anticlockwise rotation by fault

Figure 5.19: Summary of possible rotation vectors at palaeomagnetic site B4 Asgata River, for multiple dykes only. Raw data for all dykes presented in appendix 6. Wulff equal angle projection.

sinuous when traced laterally, and it appears unlikely that all of the minor intrusives could have been emplaced along palaeohorizontals or palaeoverticals. The Allerton technique (which assumes that dykes were intruded vertically and sills horizontally) can thus not be applied to these intrusives. The most reliable indicators of a palaeovertical are likely to be the sheeted multiple dykes (see section 2.5 for discussion), and four palaeomagnetic holes drilled into these dykes at 23924882 (see figure 3.7) and processed separately yield a single solution with axis plunging 30° towards 288°, about which 101° of clockwise rotation has occurred by faulting. This restores adjacent pillow lavas back to the horizontal (figure 5.19) and so appears to be realistic, but it does not restore the majority of the remaining intrusives either to a vertical or a horizontal.

5.5.2 Antithetic faulting and block rotation, Monagroulli

The regular northeasterly tilt to the lavas at Asgata continues for 3km to the west of the village, the succession being repeated by several late NW-striking faults in the neighbourhood of the Konnin locality (see section 5.5.4 and chapter 6). Near Asprolaona (215478) a shallowly southward-dipping E-W trending fault can be traced for nearly a kilometre within UPL; to the south of this structure the lavas become rather heavily faulted, and there are indications of their having a much shallower northeasterly dip. At Stenoman (200477) a prominent WNW-striking fault dips steeply northwards, and on its footwall lavas are tilted consistently towards the *southwest* (figure 5.20). The Stenoman fault appears, therefore, to play the role of a major antithetic structure: nowhere to its south or west do lavas again have a steep, regular northeasterly dip. Instead, across the remainder of the southern ELFC, from Monagroulli to Parekklisha, moderate southwesterly or westerly dips predominate. Figure 5.21 shows contoured plots of dips/dip directions of pillow lavas from the northern ELFC (*i.e.* north of Stenoman to the Kalavasos Mines) and southern ELFC (south and west of Stenoman), and emphasises the differing styles of block rotation either side of the Stenoman fault. In the

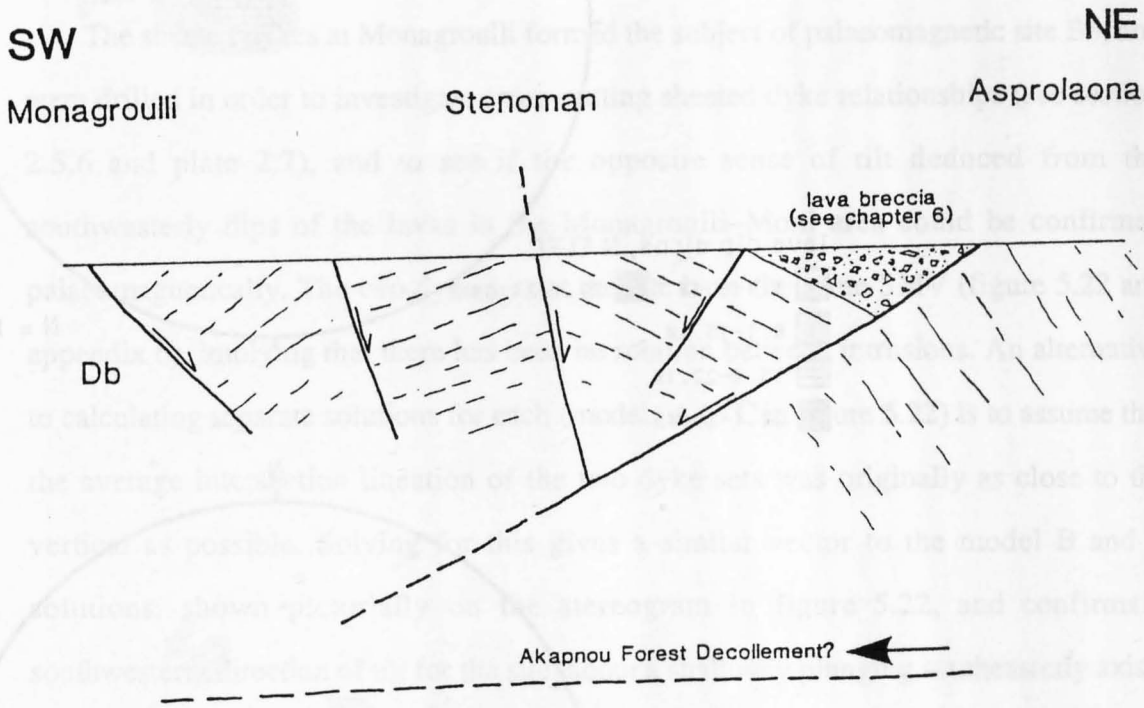

Figure 5.20: Cartoon cross section to illustrate antithetic faulting and change from northeasterly to southwesterly dip of lavas (represented by fine broken lines) at Stenoman (200477). No vertical or horizontal scale implied, but angular relationships approximately correct. True cross section of Asprolaona area is shown in figure 6.2.

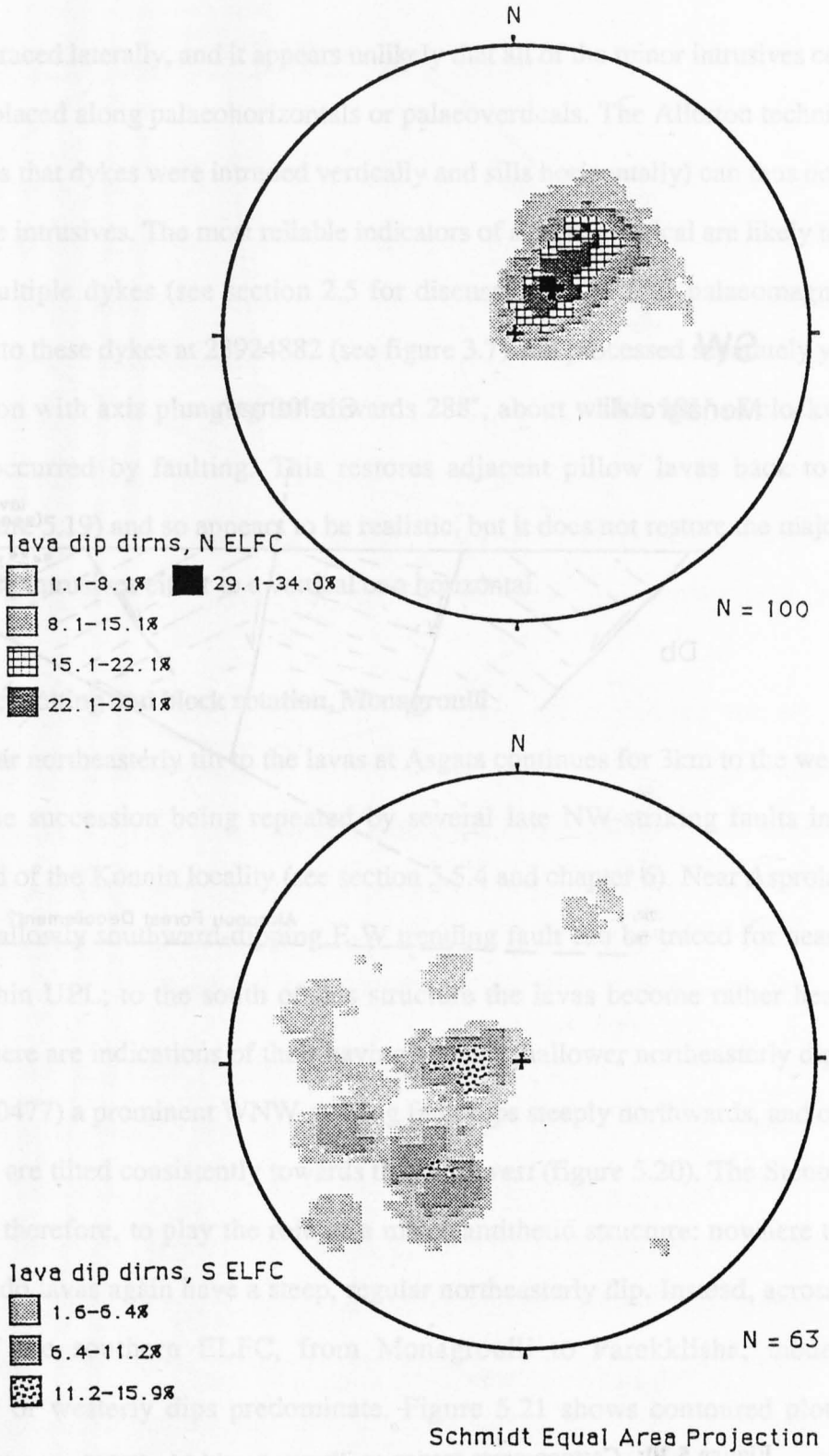

Figure 5.21: Contoured stereonets of lava dip/dip directions from (a) the Kalavasos Mines to Asgata and thence the antithetic fault at Stenoman, and (b) south of Stenoman to Parekklisha.

southern ELFC tilting in the lavas is on a much more local scale and can often be related to specific faults. Pillow lavas northwest of Monagroulli, for instance, are tilted towards the northwest, away from the NE fault bounding the outcrop of Sheeted Dyke Complex at the village itself. Their dips increase as the fault is approached, and close to the contact the lavas have been rotated to the vertical by normal fault drag.

The sheeted dykes at Monagroulli formed the subject of palaeomagnetic site B8, and were drilled in order to investigate cross-cutting sheeted dyke relationships (see section 2.5.6 and plate 2.7), and to see if the opposite sense of tilt deduced from the southwesterly dips of the lavas in the Monagroulli–Moni area could be confirmed palaeomagnetically. The two dyke sets at the site have the same SMV (figure 5.22 and appendix 6), implying that there has been no rotation between intrusions. An alternative to calculating separate solutions for each (models A to C in figure 5.22) is to assume that the average intersection lineation of the two dyke sets was originally as close to the vertical as possible. Solving for this gives a similar vector to the model B and C solutions, shown pictorially on the stereogram in figure 5.22, and confirms a southwesterly direction of tilt for the site, about a shallowly plunging southeasterly axis.

5.5.3 The Pevkos Fault

To the east of the Pevkos roadstone quarries the Akapnou Forest Décollement is cut by an E-W fault, which appears to continue eastwards as far as Gyrisman tou Kanniou (213502) on the Asgata–Vasa road. This in turn is cut at Pevkos by a major WNW-striking fault dipping 55-60° towards the southwest which extends for 9km, from 2km south of Prastion to 2km north of Monagroulli. This impressive structure, henceforth referred to as the 'Pevkos Fault', gives rise to a change in elevation of up to 300m over a distance of less than a kilometre (plate 5.8), from the lavas and dykes of the topographically subdued Parekklisha plain to the rugged Lestóvounos hills and layered plutonics to the north (figure 5.30). The juxtaposition of these lithologies suggests that the structure is a normal fault with a substantial downward displacement to the

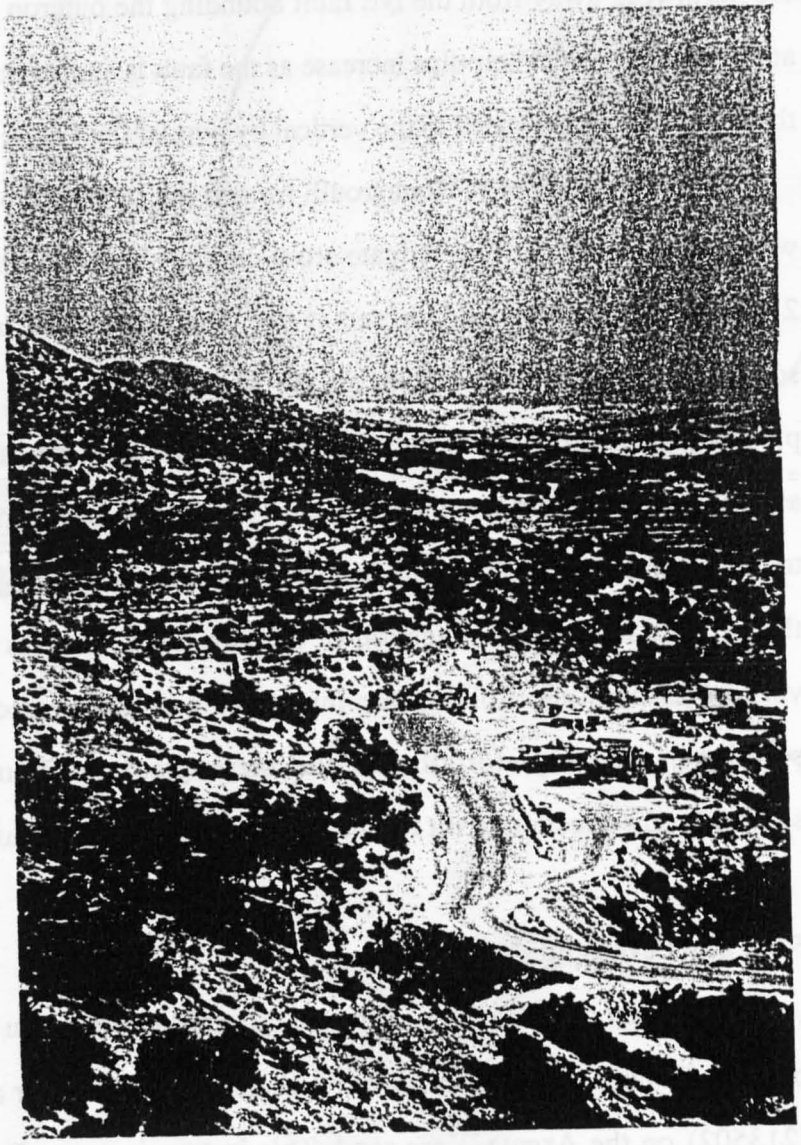

Plate 5.8: View looking southeastwards along the line of the Pevkos Fault, showing the prominent change in relief across the fault, from the subdued lava topography of the Parekklisha plain on the hanging wall (to the right) at *c.*150m O.D., to the rugged terrain of the layered plutonic complex on the footwall at *c.*500m O.D. (to the left). Taken from Kythreotis Quarry, Pevkos, ~138503.

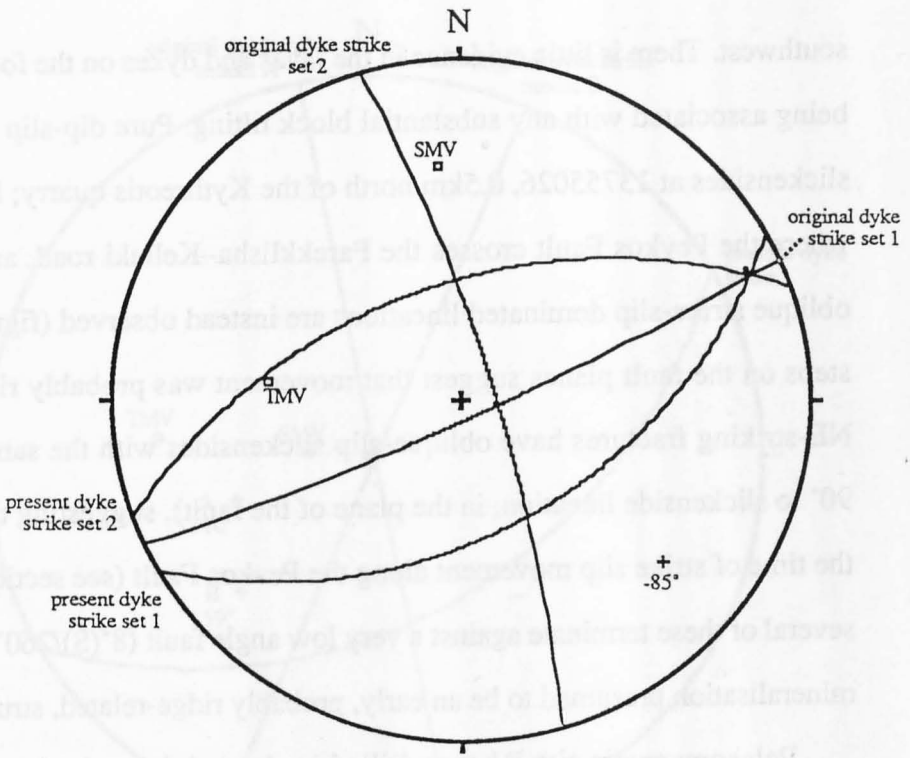

SITE B8: Monagroulli village (19344561)

N = 10 holes

mean present-day dyke orientation set 1: 52°(N)/250°
set 2: 48°(SE)/240°

single mean sample magnetisation vector (SMV): 355°; 21°

Troodos magnetisation vector (TMV): 276°; 32°

set 1:

dyke strike:	decl:	incl:	angle:
A: 312°	327°;	59°	-114°
B: 060°	128°;	23°	-80°

set 2:

C: 87(E)/185° (one solution)	313°;	8°	+117°

alternatively assume that both were intruded approximately vertical and restore the dyke intersection lineation 065°; 6° as close to the vertical as possible:

init. intersection:	decl:	incl:	angle:
096°; 78°	129°;	17°	-85°

original dyke strike set 1: 84°(SE)/245°; set 2: 79°(E)/345°

Figure 5.22: Summary of possible rotation vectors at palaeomagnetic site B8 Monagroulli village. Raw data presented in appendix 6. Wulff equal angle projection.

southwest. There is little evidence in the lavas and dykes on the footwall of the fault for it being associated with any substantial block tilting. Pure dip-slip motion is indicated by slickensides at 13755026, 0.5km north of the Kythreotis quarry; however, at 15104937, where the Pevkos Fault crosses the Parekklisha–Kellaki road, and in the quarry itself, oblique strike-slip dominated lineations are instead observed (figure 5.28). Grooves and steps on the fault planes suggest that movement was probably right-lateral. Subsidiary NE-striking fractures have oblique-slip slickensides with the same no-slip vectors (*i.e.* 90° to slickenside lineation, in the plane of the fault), suggesting that they were active at the time of strike slip movement along the Pevkos Fault (see section 5.5.4). In the quarry several of these terminate against a very low angle fault (8°(S)/260°) with extensive pyrite mineralisation presumed to be an early, probably ridge-related, structure.

Palaeomagnetic site B1 was drilled in sheeted dykes in the quarry (approximately 200m away from the Pevkos Fault) and yields two solutions, each recording clockwise rotations about moderately inclined westerly- to southwesterly-directed axes (figure 5.23). The model B solution restores the mineralised fault to 54°(E)/209°, parallel to the original dyke strike (205°), whereas the model A solution rotates it to an angle oblique to the dyke strike. Model B also requires a smaller angle of rotation, and so is tentatively preferred. Both rotation axes lie approximately in the plane of the Pevkos Fault and, significantly, the preferred model B axis parallels the no-slip lineations on fault planes at the quarry and the roadside locality. Rotation on a fault must take place about an axis perpendicular to the slip direction (*i.e.* about its no-slip vector); thus the strike slip-dominated lineations on the Pevkos Fault and its subsidiaries were potentially produced by the block rotation, or rather that slip along the fault induced the rotation by drag. This is discussed in the following section.

The E-W fault at Gyrisman tou Kanniou, which is cut by the Pevkos Fault, has a similar compound slip history. It cuts northeasterly-tilted plutonics and sheeted dykes, dips steeply southwards and has a normal displacement; however, it also has two sets of

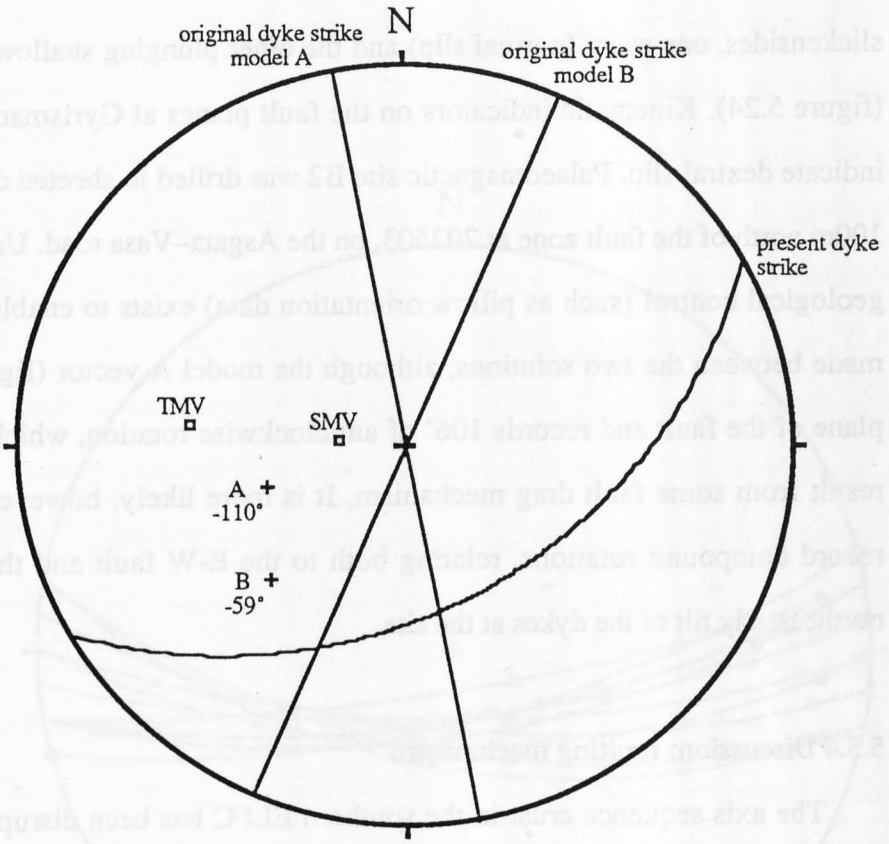

SITE B1: Pevkos Quarry (13904983)

N = 6 holes

mean present-day dyke orientation: 44°(SE)/240°

mean sample magnetisation vector (SMV): 274°; 71°

Troodos magnetisation vector (TMV): 276°; 32°

dyke strike:		decl:	incl:	angle:
A:	349°	254°;	49°	-110°
B:	023°	225°;	37°	-59°

+ve angle = anticlockwise rotation by faulting

MODEL B PREFERRED (see text)

Figure 5.23: Summary of possible rotation vectors at palaeomagnetic site B1 Pevkos Quarry. Raw data presented in appendix 6. Wulff equal angle projection.

slickensides, one steep (normal slip) and the other plunging shallowly towards the west (figure 5.24). Kinematic indicators on the fault planes at Gyrisman tou Kanniou again indicate dextral slip. Palaeomagnetic site B2 was drilled in sheeted dykes approximately 100m north of the fault zone at 202503, on the Asgata–Vasa road. Unfortunately no local geological control (such as pillow orientation data) exists to enable a distinction to be made between the two solutions, although the model A vector (figure 5.25) lies in the plane of the fault and records 106° of anticlockwise rotation, which could conceivably result from some fault drag mechanism. It is more likely, however, that the solutions record compound rotations, relating both to the E-W fault and the postulated earlier northeasterly tilt of the dykes at the site.

5.5.4 Discussion: faulting mechanisms

The axis sequence crust in the southern ELFC has been disrupted and tilted about rotation axes inclined gently to both the northwest and southeast. As in the northern ELFC, this was probably accommodated above the AFD, although in the south blocks were preferentially tilted towards the southwest, and the magnitude of the extensional strain was less. At Pevkos at least two generations of faults cut the décollement horizon and the rotated crust, and these display evidence for both dip-slip and strike-slip dominated phases of movement. Substantial normal displacement is required on the Pevkos Fault, with southwesterly downthrow and postulated extension direction (*i.e.* axis of minimum compressive stress) probably northeast–southwest. This is similar to the extension direction implied for the block rotation above the AFD, and it is therefore possible that the Pevkos normal fault and the supra-décollement rotational deformation might simply represent different manifestations of strain in the same regional stress regime.

It has long been recognised in fault systems, where strain is accommodated by fault slip and concomitant block rotation, that slip along a fault surface will increase with

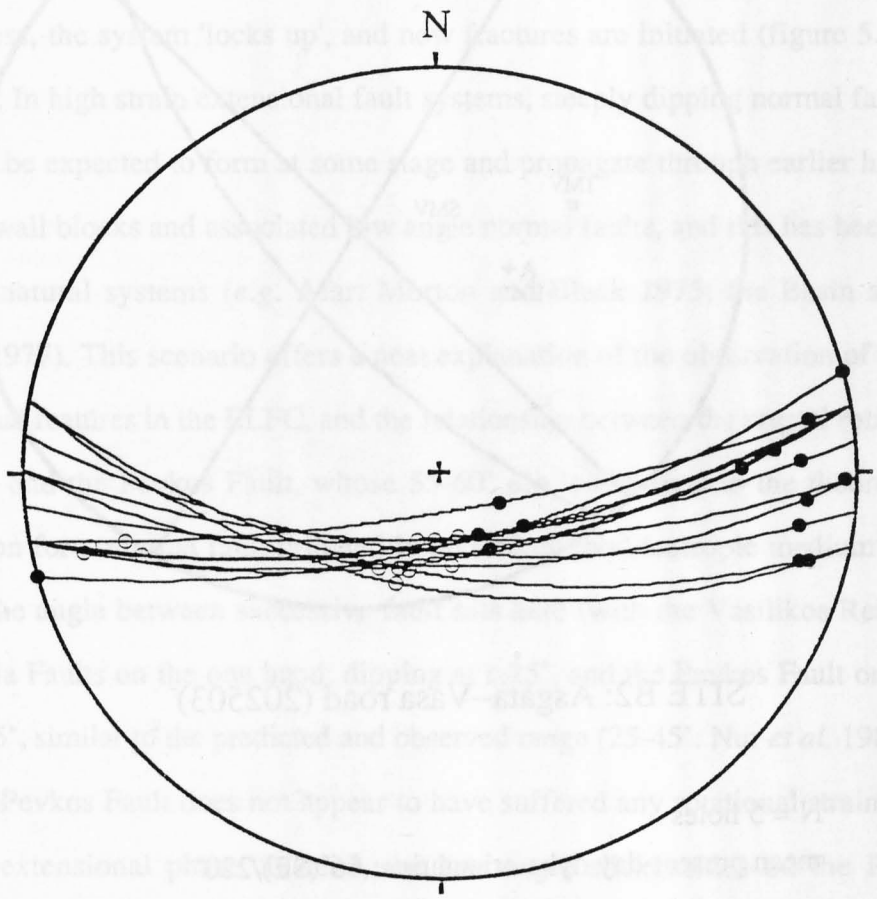

Figure 5.24: Fault planes and slickenside lineations from the Gyrisman tou Kanniou fault at Lestóvounos, showing both dip slip and strike slip phases of motion.

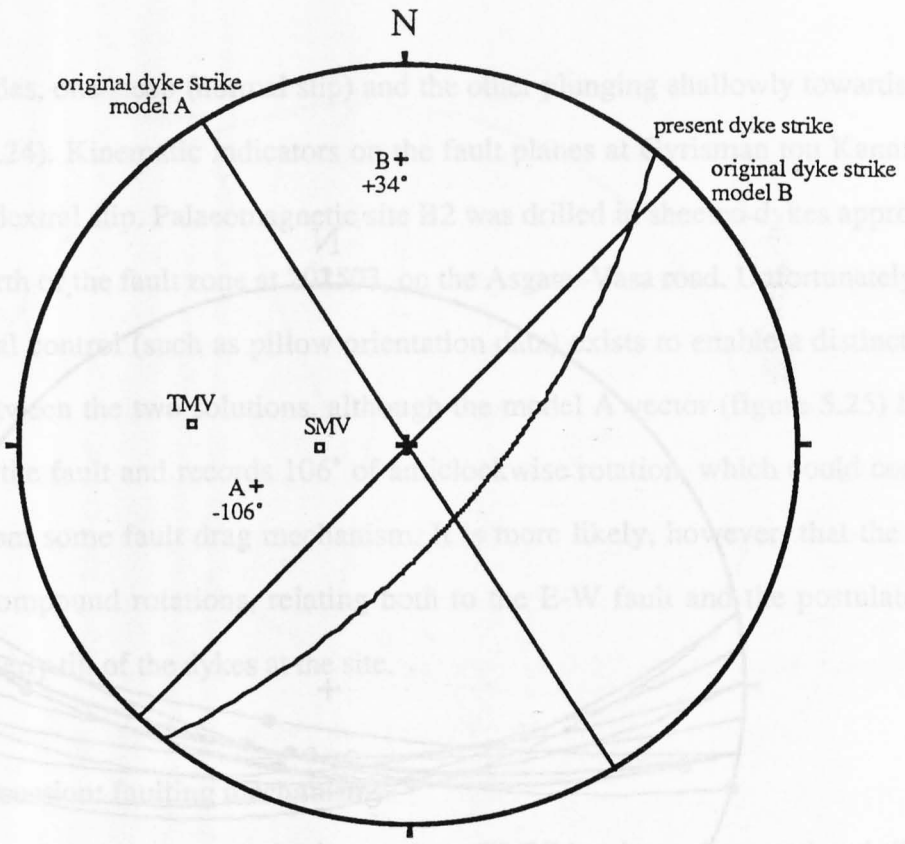

SITE B2: Asgata–Vasa road (202503)

N = 5 holes
mean present-day dyke orientation: 66°(SE)/220°
mean sample magnetisation vector (SMV): 269°; 65°
Troodos magnetisation vector (TMV): 276°; 32°

dyke strike:		decl: incl:	angle:
A:	328°	255°; 46°	-106°
B:	044°	359°; 16°	+34°

+ve angle = anticlockwise rotation by faulting

Figure 5.25: Summary of possible rotation vectors at palaeomagnetic site B2 Gyrisman tou Kanniou, Asgata–Vasa road. Raw data presented in appendix 6. Wulff equal angle projection.

constant stress up to a certain maximum value–when it is at an optimum orientation to the stress field–and then decrease as it is rotated further (DeSitter 1958). At some point slip will decrease to zero as the frictional resistance to sliding becomes equal to the applied shear stress, the system 'locks up', and new fractures are initiated (figure 5.26; Nur *et al.* 1986). In high strain extensional fault systems, steeply dipping normal faults should therefore be expected to form at some stage and propagate through earlier highly tilted hanging wall blocks and associated low angle normal faults, and this has been observed in some natural systems (*e.g.* Afar: Morton and Black 1975; the Basin and Range: Proffett 1977). This scenario offers a neat explanation of the observation of two sets of extensional features in the ELFC, and the relationship between the crustal rotation above the AFD and the Pevkos Fault, whose 55-60° dip is identical to the theoretical ideal orientation for a normal fault initiated in an (effectively) isotropic medium (Anderson 1951). The angle between successive fault sets here (with the Vasilikos Reservoir and Mavridhia Faults on the one hand, dipping at *c.*25°, and the Pevkos Fault on the other) is *c.*30-35°, similar to the predicted and observed range (25-45°: Nur *et al.* 1986).

The Pevkos Fault does not appear to have suffered any rotational strain associated with its extensional phase. Instead, the low angle slickensides on the Pevkos and Gyrisman tou Kanniou fault planes indicate an important change in the regional stress field, and reactivation of these structures in an oblique (dextral) strike-slip shear sense. Although it is difficult to ascertain unequivocally the order of activity on a multiply-striated fault surface, it is thought that the strike-slip phase must post-date the extension, or else two or even three fundamental changes in regional stress regime are required.

Palaeomagnetic site B1 indicates that sheeted dykes up to 250m away from the Pevkos Fault have suffered at least 60° of clockwise bulk rotation about an axis parallel to the no-slip vector on the fault plane. With the relatively large fault-slip data set obtained from both the Pevkos Fault plane itself (at the contact between sheeted dykes and layered plutonics) and from fractures within sheeted dykes on the footwall, an opportunity exists here to examine in slightly greater detail possible mechanisms for the accommodation of

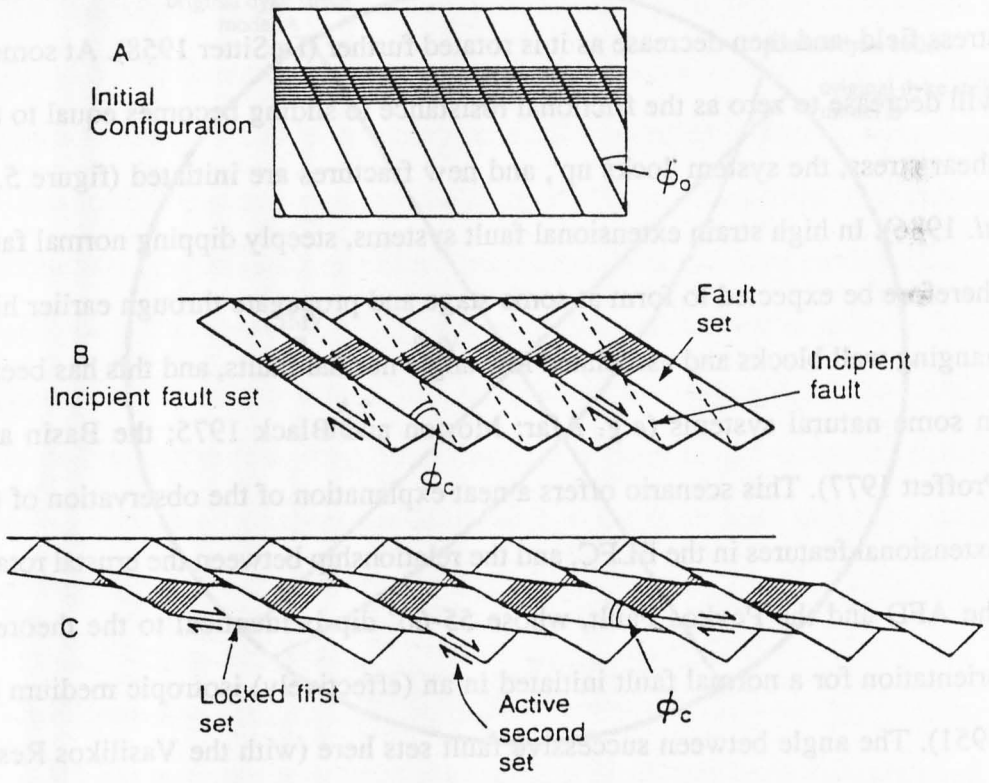

Figure 5.26: Model to show how large magnitude block rotations require multiple sets of fractures. First faults allow block rotation by themselves rotating, but in doing so move away from their optimum slip orientations, eventually becoming geometrically incapable of accommodating further strain. A second set of faults is thus initiated, cutting across the first, and rotates both blocks and the (now inactive) early faults by a similar mechanism. This model is theoretically applicable both to normal-slip and strike-slip faulting. From Nur *et al.* (1986).

distributed rotational strain on a mesoscopic scale (loosely 'fault drag').

There is a wide variation in the orientation of fault planes (figure 5.27) and their associated slickenlines both from the roadside locality and within the quarry. In contrast, there is a relatively tight grouping of their no-slip vectors about the palaeomagnetic rotation poles (figure 5.28). Many of the larger planes, particularly at the dyke/gabbro contact, are parallel to or displaced slightly clockwise from the regional trend of the fault; however, the most numerous fractures, especially in the quarry, are NE-striking and dip moderately southeastward. These have slickensides which are consistently oblique, and indicate normal–*sinistral* slip (plate 5.9) towards the northeast and east, *i.e.* opposite to the *dextral* sense of motion along the zone as a whole, and perpendicular to the direction of overall displacement.

The obliquity of slip on both fault sets shows that the displacement direction cannot be exactly parallel to the trend of the Pevkos Fault. McKenzie and Jackson (1983) have shown that a single strike slip fault in such cases is geometrically unstable, and that strain must instead be distributed on many faults, across a zone of finite width. A second set of faults in such a system might preferentially be initiated in an antithetic Riedel shear direction (Wilcox *et al.* 1973); however, such a configuration is stable only at infinitesimal degrees of strain, and deformation can proceed further *only* if the angle between the two sets of faults changes continuously with time. This requires the concomitant rotation of the intervening fault blocks (McKenzie and Jackson 1983, 1986; figure 5.29).

Clockwise block rotation in the hanging wall of the Pevkos Fault is thus accommodated by oblique sinistral slip on the NE fault planes, which are themselves rotated in a clockwise sense. Small dextrally-slipping subsidiary fractures originally parallel to the main fault trend also potentially suffer minor rotations in the same sense (*cf.* figure 5.28). The angle between the NW and NE fault sets is variable, but may be as much as 100° or so; this spread of fault orientations possibly implies heterogeneous

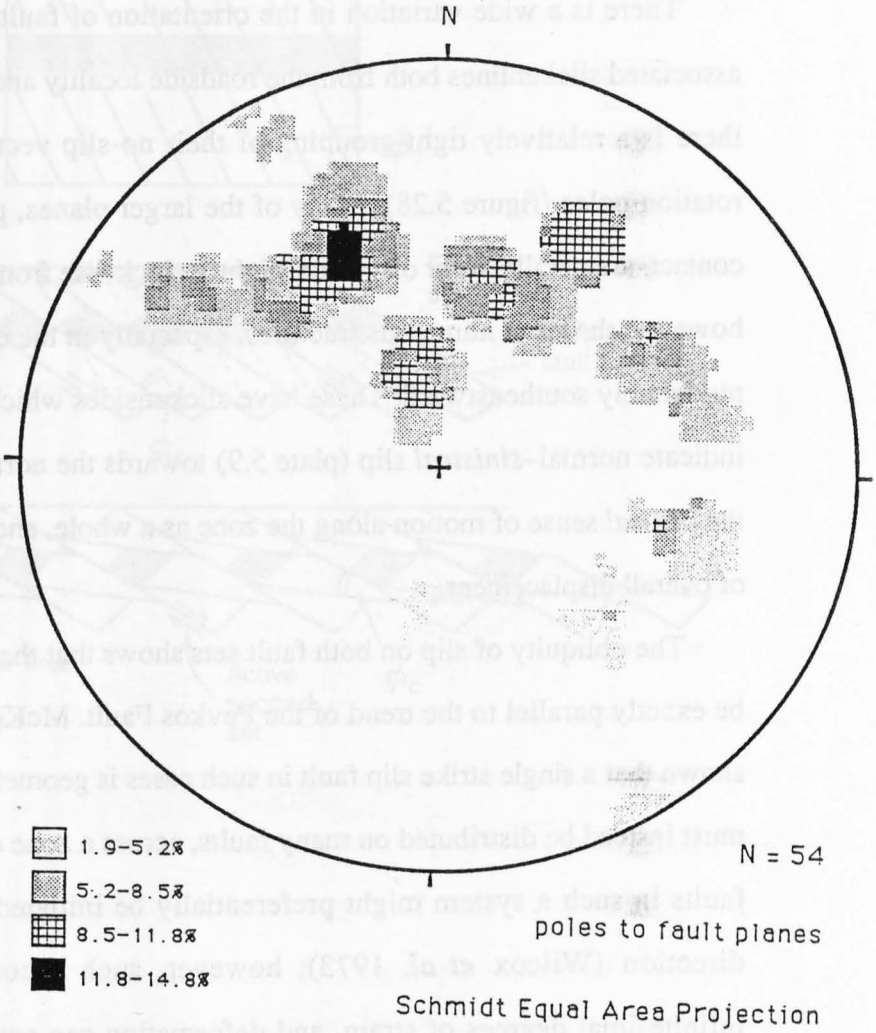

Figure 5.27: Contoured equal area plot of poles to all fault planes, Pevkos quarry and roadside. Note the preponderance of NE-striking, southeasterly-dipping fractures, even though the regional trend of the Pevkos Fault is NW-SE.

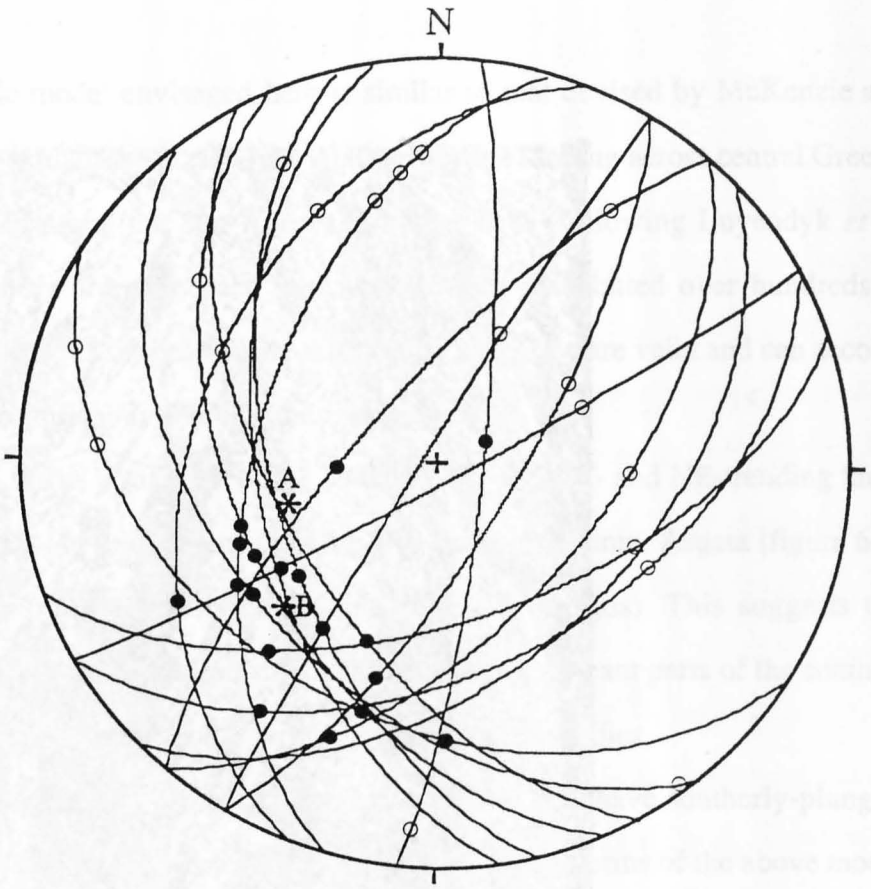

Figure 5.28: Fault planes and slickenside lineations from the Pevkos quarry and roadside locality, showing the close correspondence between the no-slip vectors from the sites and the palaeomagnetic rotation vectors (site B1).

Plate 5.9: Oblique-slip slickensides on NE-striking fault in layered gabbros on the footwall of the Pevkos Fault. Slip indicators suggest a normal–sinistral sense of motion. Parekklisha–Kellaki road.

strain.

The kinematic model envisaged here is similar to that devised by McKenzie and Jackson (1983) to explain the present-day oblique normal faulting across central Greece, and block rotations along the San Andreas Fault system (following Luyendyk *et al.* 1980). These authors are concerned with deformation distributed over hundreds of kilometres; however, it is suggested here that similar processes are valid and can account for rotations on a significantly smaller (mesoscopic) scale.

Across much of the remainder of the southern ELFC, NW- and NE-trending faults have similar slickenside orientations (*e.g.* the NW faults at Konnin, Asgata (figure 6.4), and also the large mineralised NE fault at Ornithouri, Pyrgos). This suggests that analogous clockwise block rotations might characterise significant parts of the southern ELFC, and should be detectable with further palaeomagnetic studies.

In Lestóvounos some NW faults (dipping southwesterly) have southerly-plunging (oblique) slickensides. These are not instantly interpretable in terms of the above model, although their slip sense (whether normal–sinistral or reverse–dextral) is not known, and so they could represent internal deformation of the fault slabs rotating about the NE faults, which all have the same slip sense as those described from Pevkos. A single exception is the NE-striking, southeasterly dipping fault at Kellaki, which has a well-constrained dextral reverse slip vector. A trondhjemite body near the village has been bisected by the fault and offset by 700m of dextral and possibly up to 200m of reverse movement. Analysis of its slip vectors and those of the Pevkos faults (*à la* Angelier and Mechler 1977) indicate that the Kellaki fault could not have been active in the same regional stress field as that which induced the dextral block rotations at Pevkos. No information as to the timing of activity along this fault is available, and so its significance must for now remain obscure.

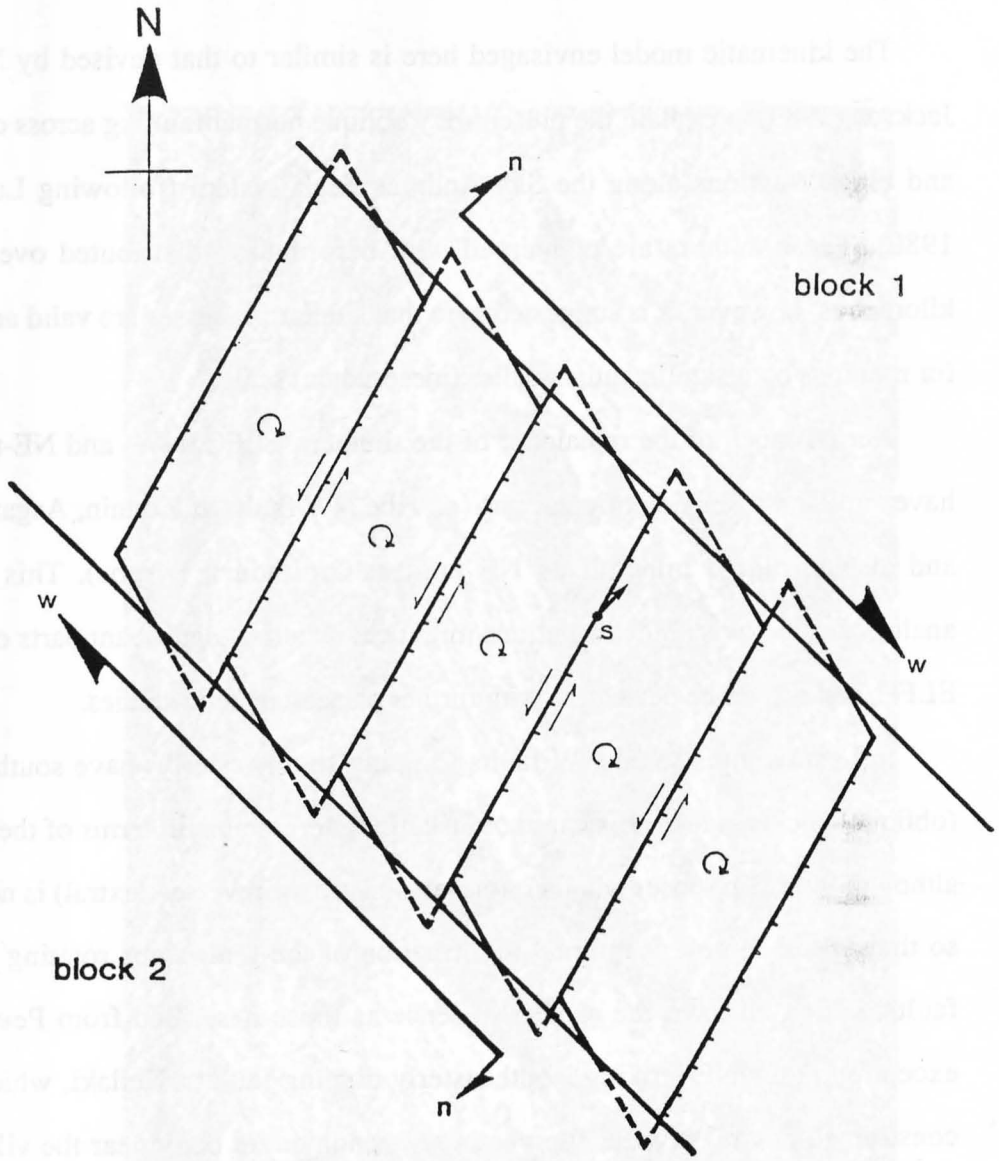

Figure 5.29: Schematic diagram looking down the plane of the Pevkos Fault to illustrate the mechanism of block rotation by means of distributed oblique deformation. Subsidiary NE-trending fractures separating slats within the fault zone have both normal and left-lateral components of motion (downthrow on the former indicated by ticks), and are rotated clockwise together with the slats as deformation proceeds. The slip vector 's' between adjacent slats is perpendicular to the boundary of the deforming zone, and the overall motion of block 1 relative to block 2 can be resolved into components 'w' and 'n' parallel and perpendicular to the boundaries of the zone respectively. The boundaries between the slats and the rigid blocks is shown schematically: differential rotation between them is assumed to be accommodated by internal deformation (*i.e.* smaller scale faulting). Modified after McKenzie and Jackson (1986).

5.6 Neogene Deformation

5.6.1 Uplift of the central Limassol Forest block

The central and western portions of the Limassol Forest Complex have suffered marked differential uplift with respect to the eastern part, such that serpentinised harzburgites are now at elevations of up to 1000m above sea level. Along the southwestern margin of the WLFC the serpentinised mantle sequence and slivers of the crustal sequence have been thrust southwestwards over Maastrichtian to Middle Miocene Lefkara Formation chalks, which have been deformed into upright or southwest-facing folds, and developed a prominent axial planar cleavage adjacent to the thrusts (Bear and Morel 1960, Robertson 1977c, Murton 1986b). Undeformed Koronia reef limestones overlie the deformed sediments and onlap onto the igneous basement between Parekklisha and Pyrgos; these are probably of late Tortonian (pre-Messinian) age–*i.e.* Upper Miocene-and confirm a largely intra-Middle Miocene age for the deformation and uplift of the Limassol Forest block (Robertson *op. cit.*; Eaton 1986). The so-called 'Yerasa fold and thrust belt' is up to 5km in width, and has a pronounced WNW trend along the southwestern margin of the Limassol Forest. Murton (1986b) showed that the reverse and thrust faults were founded upon pre-existing normal faults which, significantly, are parallel to the strike of the Pevkos Fault. This suggests that the effects of the deformation that gave rise to the Pevkos Fault, described in the preceding sections, might be widespread along the southern Troodos margin.

In the ELFC itself the continuation of the thrust belt takes the form of two reverse faults to the west of Mangaleni opencast pit (north of Armenokhori), which carry serpentinised harzburgites over sheeted dykes and sheeted dykes over Basal Group. These are associated with a great deal of brittle deformation and greatly disrupt the Mangaleni sulphide body (Adamides 1984). To the northeast of Mangaleni the contact between the mantle sequence and lavas swings round to a northeasterly and then northerly strike, and its dip becomes easterly, so that the boundary becomes a normal

fault. It once again becomes reversed southwest of Pevkos, but this time displacement is directed towards the *northeast*, opposite to that of the main fold and thrust belt bordering the WLFC. Several complementary thrusts, also northeasterly directed, have been identified in the mantle sequence on the hanging wall of this structure by Murton (*unpubl. data*; see enclosure 1). The reverse fault to the southwest of Pevkos is almost exactly parallel to the Pevkos Fault, so isolating a 1km-wide southwesterly-inclined slab of Sheeted Dyke Complex and high-level gabbro surrounded by serpentinised harzburgite (figure 5.30). The similarity in the orientations of the two structures again suggests that the reverse fault might represent the reactivation of a counterpart of the Pevkos Fault.

Uplift of the central Limassol Forest block appears to have taken place very rapidly in the Middle Miocene by means of thrusting and reverse faulting both towards the southwest and northeast, utilising NW lineaments initiated in the Upper Cretaceous (see figure 5.31 and chapters 6 and 7). Preservation of tectonite fabrics *etc.* in the mantle sequence of the central Limassol Forest suggests that uplift was of coherent blocks, rather than of a diapir (Murton 1986a, b). The causes of the uplift are not known but may reflect either some regional compression or, as with the drastic uplift of Mt. Olympus in the Pleistocene, be related to isostatic instabilities resulting from the large-scale serpentinisation of the mantle sequence (possibly, as speculated by Robertson 1977c, by fluids liberated from a subducting slab dipping northwards beneath Cyprus). The reason for the restriction of the uplifted area to the central and western LFC may relate to the seafloor spreading geometry of the complex (see chapter 7).

5.6.2 North–south normal faulting

The youngest tectonic features visible in the ELFC are N-S striking normal faults which most obviously affect the central part of the study area, across the southern Akapnou Forest to the Vasilikos River. The AFD north of Vasa is in particular broken up by numerous structures with this orientation. The faults dip steeply and throw down both

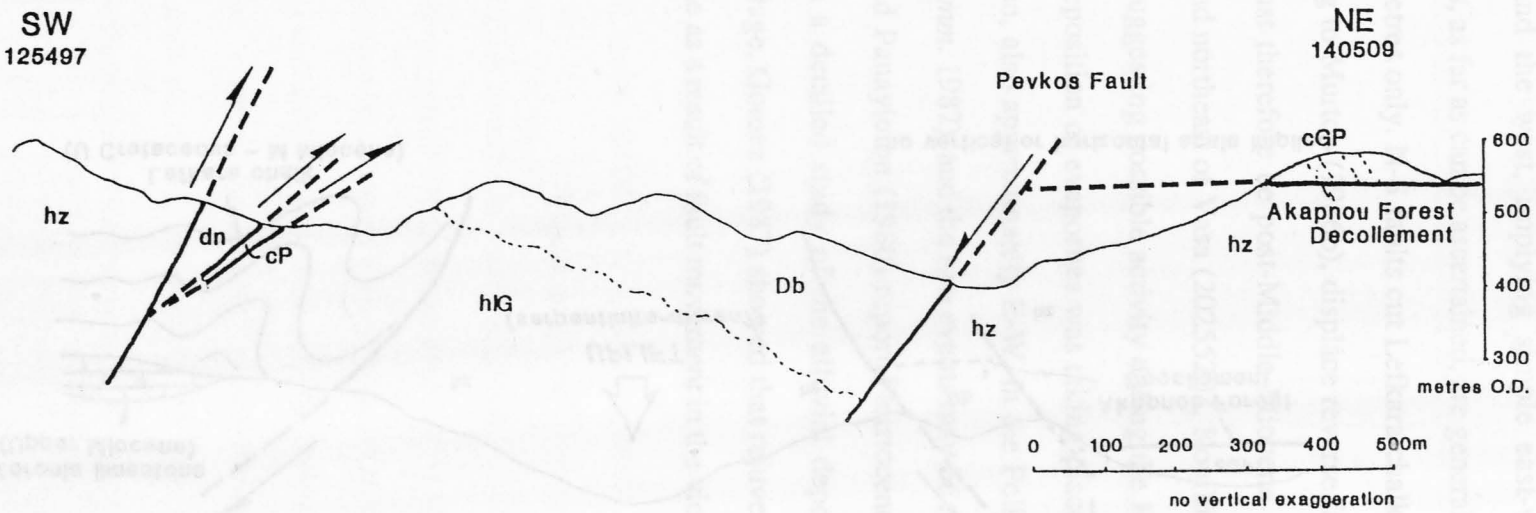

Figure 5.30: Section across the sheeted dyke outcrops in the Pevkos area, showing truncation of the Akapnou Forest Décollement by the Pevkos Fault, and the possibly reactivated reverse structures parallel to the Pevkos Fault

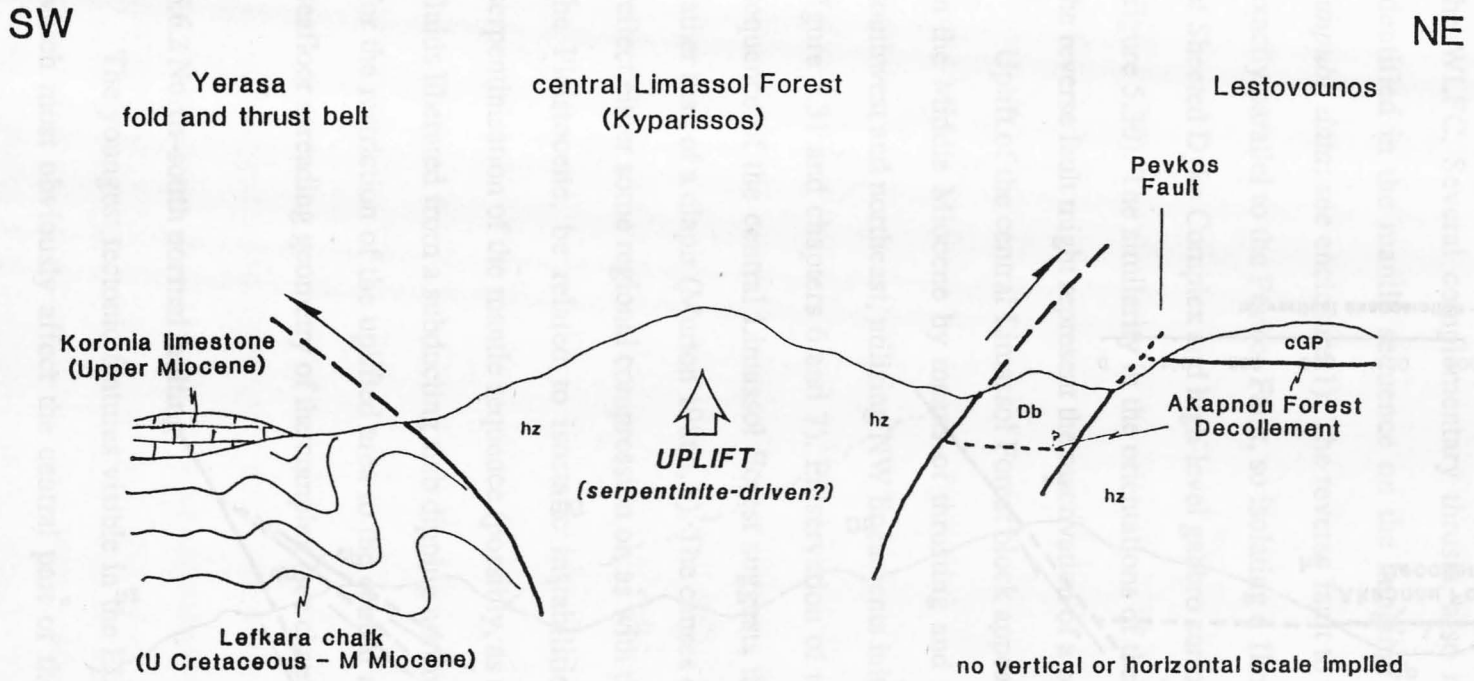

Figure 5.31: Cartoon cross section across the central Limassol Forest, to illustrate the Middle Miocene uplift and overthrusting of the serpentinised harzburgite massif along pre-existing WNW-trending lineaments.

to the east and the west, implying simple east-west extension across the area. Displacements, as far as can be ascertained, are generally in the order of a few metres to a few tens of metres only. N-S faults cut Lefkara chalks in the Asgata–Monagroulli area and, according to Murton (1986b), displace reverse faults of the Yerasa fold and thrust belt. They must therefore be post-Middle Miocene in age. Near Monagroulli village (18694554) and northeast of Vasa (20255203, Koufkia) gypsum is found along the N-S fault planes, suggesting possible activity during the Messinian (Upper Miocene), when widespread deposition of evaporites was taking place. This coincides with a period of rapid extension, also approximately E-W, in the Polis graben in western Cyprus (L.C. Ward *pers. comm.* 1987), and the two events may be related.

Searle and Panayiotou (1980) report Pleistocene valley gravels cut by these N-S faults and, in a detailed study of the alluvial deposits of the Vasilikos River near Kalavasos village, Gomez (1987) showed that rejuvenation of the river occurred in the late Pleistocene as a result of fault movement in the vicinity of the Kalavasos Mines.

CHAPTER 6:
Lava–Sediment Relationships

6.1 Introduction

Field and palaeomagnetic evidence suggests that the block rotation, and hence fault activity, described in the previous chapter (sections 5.4 and 5.5) post-dated the cessation of volcanism in the ELFC. However, a strong angular unconformity exists everywhere between the steeply-tilted lavas and the almost horizontally-disposed Lefkara Formation chalks lying on top of the ophiolite, so the block rotation must have preceded chalk deposition. Uranium–lead ages of 91.6 ± 1.4 Ma obtained from zircons in plagiogranites (Mukasa and Ludden 1987) imply a Cenomanian (95.5–91 Ma: Hallam *et al.* 1985) to Turonian (91–89.5 Ma) formation age for the Troodos crust, and the lower part of the Lefkara Formation is Maastrichtian (71.5– 66Ma); hence the deformation must have occurred entirely within the Upper Cretaceous.

Developed discontinuously between the lavas and the chalks, often in fault-controlled depressions in the lava surface, are brown umbers and well-bedded pink radiolarites which together comprise the Perapedhi Formation (figure 6.1). These range in age from Turonian to Maastrichtian (see below), and thus straddle the period in which the tectonism is inferred to have taken place. Angular unconformities at differing stratigraphic levels within the Perapedhi Formation document the movements of individual fault blocks and give information as to the overall mechanism of deformation. This chapter examines the relationships between the lavas and these sediments with a view to constraining the timing and sequence of deformation.

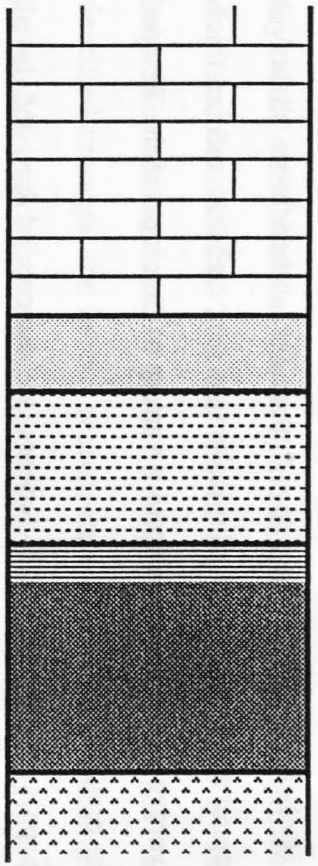

thickness:	lithology:	formation:	age:
			66Ma
0-40m	Lower Lefkara: white chalk and marl, chert-free	Lefkara	MAASTRICHTIAN
0-200m+ (in south)	bentonite clay (+ exotics in south = Moni mélange)	Kannaviou	71.5Ma
			CAMPANIAN
0-30m	pink radiolarites and radiolarian shales		
			84Ma
0-5m	umberiferous shales		CONIACIAN/SANTONIAN?
			89.5Ma
		Perapedhi	
0-35m	manganiferous brown umber		TURONIAN
	IGNEOUS BASEMENT		

Figure 6.1: Composite stratigraphic column of Upper Cretaceous sediments, Cyprus. Age range from Hallam *et al.* (1985).

6.2 Sedimentary Stratigraphy

6.2.1 The Perapedhi Formation

The name 'Perapedhi Formation' was proposed by Wilson (1959) for the umbers and radiolarian shales which in places immediately overlie pillow lavas. The first sediments are rich dark brown umbers, which form 'pods' usually a few metres in thickness and extending laterally for a few tens of metres, apparently infilling hollows in the lava surface. The largest deposit in the ELFC, at Kremmos tis Kamilas (near Dhrapia: see section 6.4.1), is more than 35m thick. The umbers are very fine-grained sediments, amorphous except for occasional microcrystalline goethite and rare quartz (Robertson and Hudson 1973). They may either be massive or well-bedded, in places have silicified layers, and sometimes contain volcaniclastic detritus (see below) and pale, probably radiolarian-rich, bands. Chemical analysis (Robertson and Hudson *op. cit.*; Guillemot and Nesteroff 1980) shows that umbers are rich in iron and manganese oxides, and are also enriched in the base metals with respect to the overlying pelagic sediments. They are very similar to iron-rich sediments found on modern ridge flanks (*e.g.* Boström and Peterson 1966, 1969; Guillemot and Nesteroff *op. cit.*) and are thought to be chemical precipitates deposited rapidly upon the oxidation of hot Fe, Mn-rich fluids discharged from submarine vents at the waning stages of convective hydrothermal circulation (Robertson and Hudson 1973, 1974).

Robertson and Hudson (1973) showed that the metal content of the umbers decreased progressively with stratigraphic height, correlating with an increase in clay content (Robertson 1975). The upper umbers, or 'umberiferous shales', are much paler in colour and are frequently fissile; Robertson (*op. cit.*) documented thicknesses of 0.5-4.5m (average 2.7m) for them from a variety of outcrops of the Perapedhi Formation across the ophiolite as a whole.

The pale brown clay-rich umbers are succeeded by, and in places initially

interbedded with, pink radiolarites and radiolarian mudstones. Their distribution is also restricted and they usually, but not always, overlie umbers. The thickest deposit of radiolarite is at the Vathyrkakas lava basin, Vavla (see sections 3.4.3 and 6.4.3), where 30-35m of pink siliceous radiolarite finely interbedded with friable grey radiolarian shales directly overlie lavas and brecciated sheeted dykes. The pink material is tough, has a porcellaneous texture and conchoidal fracture, and contains abundant radiolaria.

6.2.2 The Moni mélange

Succeeding the radiolarites in the northern ELFC, and again spatially restricted, are grey to pink thixotropic clays up to *c.*10m thick. The clays, which contain bentonite, appear to be finely bedded but are internally homogeneous, and outcrops are degraded very rapidly by weathering. They are considered to be lateral equivalents of the much thicker Kannaviou Formation of southwestern Cyprus (Robertson and Hudson 1974; see section 7.4.1) and are succeeded by white, laminated, chert-free chalks of the Lower Lefkara Formation.

Two kilometres to the northeast of Monagroulli bentonite clays similar to those described above, with a general grey-green to reddish colour, appear on top of the lavas and, where present, the umbers. Significantly, however, at this locality (20594678 Kladhefteries) a sheet of indurated brecciated serpentinite is contained within the clay immediately above the contact with the lavas. In the surrounding area, and elsewhere to the south, a variety of lithologies, predominantly sedimentary, and unknown in any of the supra-ophiolite successions to the north, form blocks lying haphazardly within the clay, which itself thickens markedly to attain a thickness of approximately 200m south of Moni and Parekklisha. This was named the 'Moni mélange' by Henson *et al.* (1949), and was studied in detail by Pantazis (1967) and Robertson (1977a). The latter authors identified amongst the blocks representatives of all the lithologies occurring in the disrupted Triassic–Cretaceous volcanosedimentary successions of the Mamonia Complex

of southwestern Cyprus (see section 7.4.2). In addition they found lithologies, such as the pale yellow, poorly cemented 'Parekklisha Sandstone', which are found nowhere else in Cyprus. Some blocks of the latter are immense–up to 1.5km in length (Robertson *op. cit.*)–leading Pantazis to think them autochthonous. Also included within the mélange are huge sheets of serpentinite, up to 5km long and 40m thick (similar to the fragment described above from Monagroulli), which are elongate in a northwesterly direction.

The increasing thickness of the clays towards the south implies that a southward-dipping palaeoslope existed at the time of Moni clay deposition. The absence of exotic blocks in the small outcrops of bentonite clay overlying radiolarites in the northern ELFC, together with the Mamonia-like affinity of the majority of the olistoliths in the Monagroulli to Parekklisha area, suggests that they were introduced from the present-day southwest, probably by either a submarine gravity-sliding mechanism (Pantazis 1967, Robertson 1977a), or by shedding from active strike-slip fault scarps (Swarbrick 1980), into the unconsolidated sediments. This event must have been relatively short-lived, as the mélange is overlain, as elsewhere along the southern Troodos margin, by undeformed Lefkara chalks. The regional setting and significance of the Moni mélange is discussed in chaper 7.

6.2.3 Age of the Perapedhi and Kannaviou Formations

The supra-ophiolite sediments were initially thought to be of Jurassic age, following earlier suggestions that the Troodos Massif might be Triassic (*e.g.* Henson *et al.* 1949, Wilson 1959), but C.G. Allen (in Pantazis 1967) and subsequently Mantis (1970) recognised an Upper Cretaceous (early Campanian) fauna in the radiolarian sediments of the Perapedhi Formation. More recently Blome and Irwin (1985) recovered radiolaria from bands within the large umber deposit at the Mangaleni open-cast mine near Parekklisha, which they suggested were of Turonian age, similar to that deduced for the ophiolite itself. This is in accord with observations of modern axial ridge systems, which suggest that umber formation is unlikely to persist for more than *c.*1 Ma after the

cessation of volcanism in a particular area (Rona *et al.* 1976, Lonsdale 1977, Boyle and Robertson 1984). A significant gap, of some 5.5 Ma (following the time scale of Hallam *et al.* 1985), is therefore implied between the deposition of the umber and radiolarite successions. A.H.F. Robertson (*pers. comm.* 1987) has suggested that this time period might be spanned by the umberiferous shales; clearly, more micropalaeontological investigations are necessary.

The Kannaviou Formation, including the Moni mélange, has been shown on micropalaeontological grounds to be Campanian to Maastrichtian (Robertson 1977a, b), and the immediately overlying Lower Lefkara chalks contain coccoliths and foraminifera also of Maastrichtian age (Robertson and Hudson 1974).

6.3 Angular Relationships, Asgata

Robertson (1975), Adamides (1980) and Searle and Panayiotou (1980) noticed the strong angular unconformity that exists between the steeply tilted lavas in the Kalavasos Mines and the almost horizontally disposed overlying umbers. This relationship is also observed in the Asgata area: pillow lavas dip at 75° or more towards the northeast, and may be overlain directly by umberiferous shales which are horizontal, or dip at no more than 20° southeastwards. Frequently, however, the sediments are separated from pillowed flows by a breccia formed of broken pillow fragments set in a fine-grained orange haematitic matrix. These breccias are effectively conformable with the overlying Perapedhi Formation, and are developed intermittently along the southern margin of the ELFC.

6.3.1 Pillow collapse breccias

The breccias, henceforth referred to as 'pillow collapse breccias' range in thickness from 0-30m. They are best developed in the Asgata area, at Mavridhia (in the Kalavasos Mines) and near Parekklisha, although some disaggregation of pillows at the lava–sediment interface is common across the whole margin of the ELFC (see below). The breccias are effectively conformable with the overlying sub-horizontal sediments, and have a gradational lower boundary cutting obliquely across the tilted lava flows beneath.

A typical collapse breccia is composed of a chaotic jumble of blocks of pillow averaging *c*.20cm in size, with chilled margins preserved, and smaller shards of green devitrified glass. The packing arrangement of the clasts is often very open, and the thicker breccia deposits are in places matrix-supported. The breccias are often intimately associated with dark manganiferous umbers, which may form pods enclosed entirely within the breccias (plate 6.1). Contacts between the umber and matrix-rich breccia are frequently gradational at both top and bottom: the first few centimetres of clast-free sediment are orange, the same as the breccia matrix, and then there is a rapid change in colour over a few millimetres to the typical dark brown of the umber proper. There is no difference in the texture of the sediment across this contact and in places, as noticed by Robertson (1975), the colour change appears to transgress obliquely across fine-scale sedimentary laminations. Rarely, as at 23134829 (Konnin, Asgata), the collapse breccias themselves have partly umberiferous matrices (plate 6.2). These observations suggest that no primary sedimentary distinctions exist between the brown umber and orange ferruginous material, but that the colour difference is instead related to some diagenetic effect. Chemical analyses reported by Robertson (*op. cit.*) show that the orange material differs from umber only in its deficiency in manganese.

The occurrence of pillow collapse breccias in the ELFC is restricted, and a clear fault control can be demonstrated. At Asprolaona, 2km west of Asgata, breccias are observed on the downthrown hanging wall of the shallowly southward-dipping fault described in

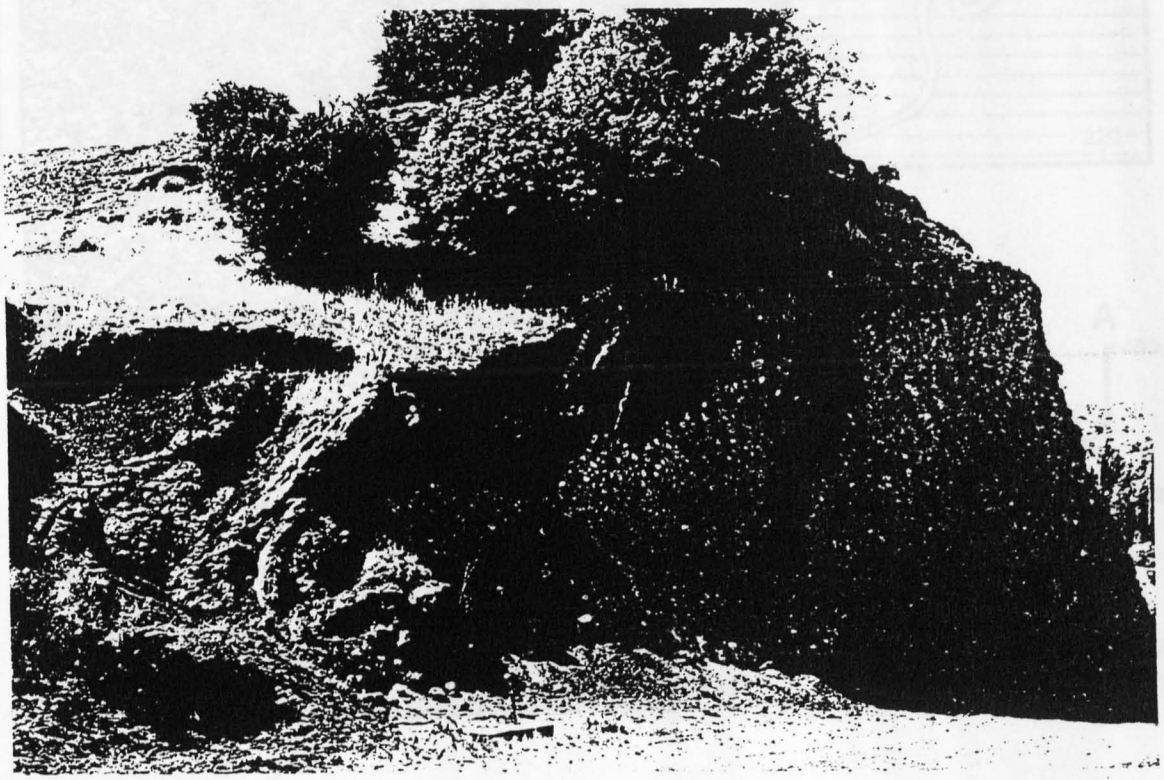

Plate 6.1: Pillow collapse breccias and deformed, partly silicified, manganiferous umbers. Note umber pod to right of picture totally enclosed by lava breccia. Roadside exposure, 0.5km SE of Asgata.

Plate 6.2: Pillow collapse breccia. Note dominantly matrix-supported fabric, occasional curved margins to clasts which are remnants of pillow margins, and partly ferruginous (orange), partly umberiferous (brown) matrix. 23134829 Konnin, Asgata.

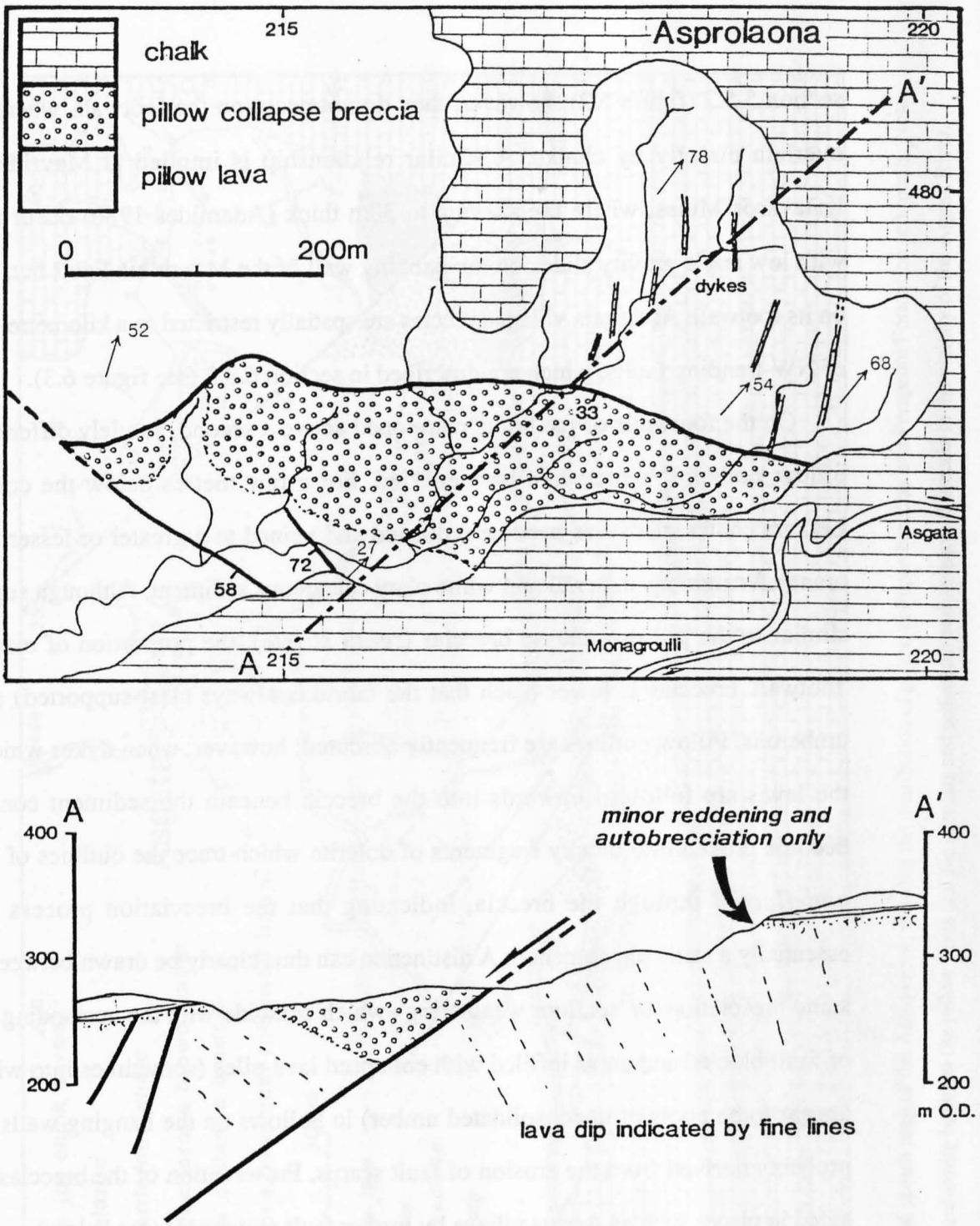

Figure 6.2: Geological map and cross section of the Asprolaona area, 2km west of Asgata. Haematitic matrix-supported pillow collapse breccias occur on the hanging wall of a low-angle southward-dipping normal fault, and may be derived by degradation of the fault scarp. No such breccias are preserved on the footwall of the structure to the north; instead only slight reddening and static brecciation of the pillow lavas and dykes is visible in the uppermost few metres below the contact with the chalk.

section 5.5.2 (figure 6.2); however, they do not occur on the footwall, where lavas are overlain directly by chalks. A similar relationship is implied at Mavridhia, in the Kalavasos Mines, where breccias up to 30m thick (Adamides 1980) occur associated with low angle gravity slides on the hanging wall of the Mavridhia Fault but, again, not on its footwall. At Asgata village breccias are spatially restricted to a kilometre-wide zone of NW-trending faults, which are described in section 6.3.2 (see figure 6.3).

On the footwalls of the faults mentioned above a second, subtlely different type of pillow 'collapse' breccia can be identified. For a few metres below the contact with Lefkara chalks, the lavas become reddened and veined to a greater or lesser degree by orange ferruginous material and white platy calcareous sediment. Although superficially similar to the pillow collapse breccias (*sensu stricto*), the proportion of matrix in the 'footwall' breccias is lower (such that the fabric is always clast-supported) and is not umberous. Pillow outlines are frequently obscured; however, when dykes which intrude the lavas are followed upwards into the breccia beneath the sediment contact, they become broken into blocky fragments of dolerite which trace the outlines of the dykes *undeflected* through the breccia, indicating that the brecciation process here was essentially a static phenomenon. A distinction can thus clearly be drawn between areas of static brecciation–or 'seafloor weathering'–which coincide with the upstanding footwalls of fault blocks, and areas infilled with collapsed lava piles (sometimes into what would appear to be pools of unconsolidated umber) in hollows on the hanging walls of faults, probably derived from the erosion of fault scarps. Preservation of the breccias has been aided in places such as Asgata village by further fault movement (see below).

6.3.2 Relationship of the Perapedhi sediments to faulting

Chaotically infolded manganiferous umbers and pillow collapse breccias at the prominent outcrop on the Kalavasos road, 0.5km southeast of Asgata (239485; plate 6.1) are succeeded by a further 15-20m of regularly bedded brown umber dipping at about 24°

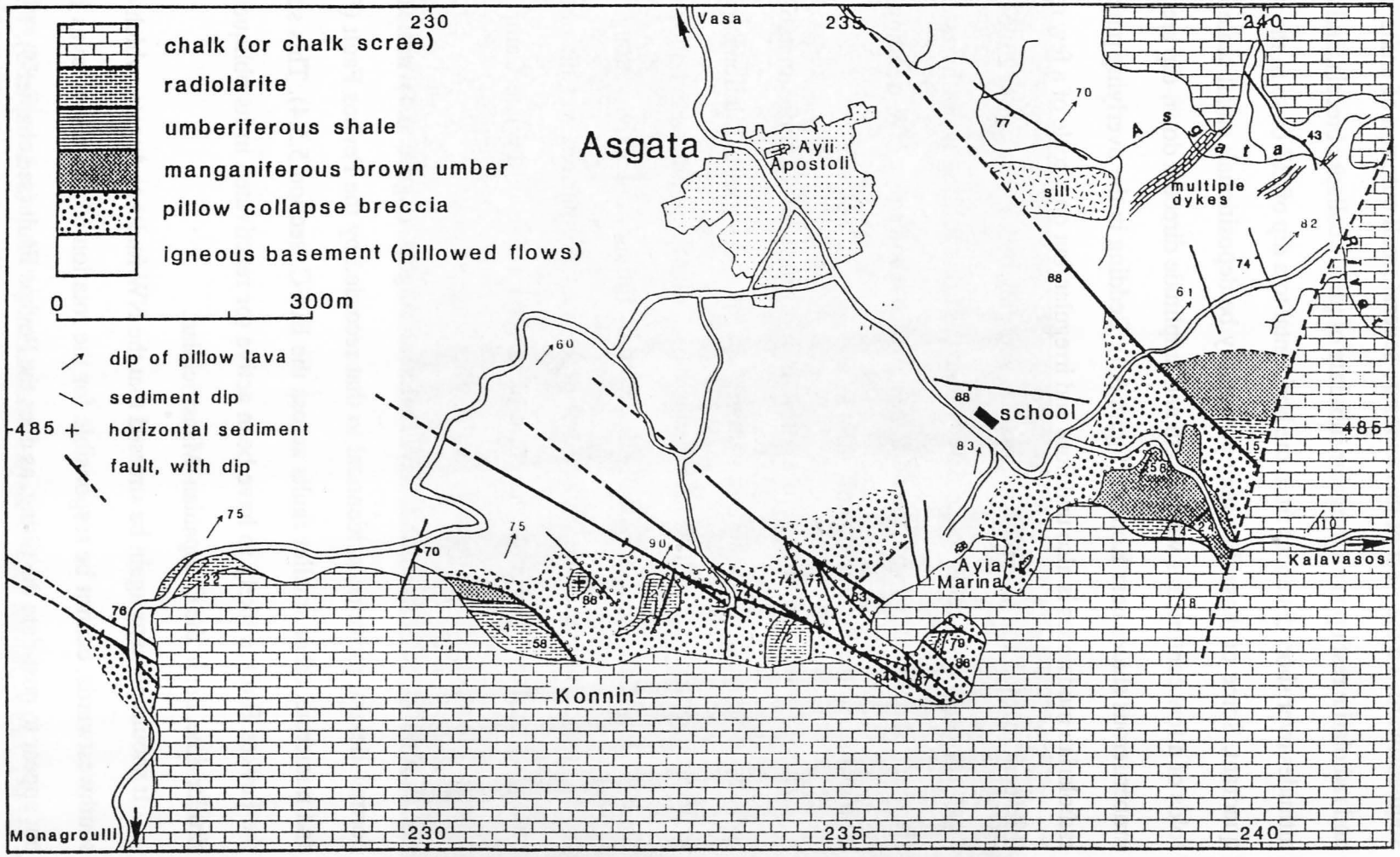

Figure 6.3: Geological sketch map of the Asgata area, showing the distribution of pillow collapse breccias and Perapedhi Formation sediments. Note the strong angular unconformity between the pillow lavas and the breccias and sediments and absence of breccia in the vicinity of the Asgata River.

southeastward. To the west of this exposure several small outcrops of umberiferous shale and radiolarite rest upon an irregular substrate of pillow collapse breccia, and vary in their attitudes over short distances from the horizontal to a dip of 20° or so in the southeastern quadrant. Some of these dips may potentially be depositional: small scale open slump folds of a few centimetres wavelength and amplitude directed down-dip are observed in umberiferous shales near Konnin (figure 6.3). Bedding in the overlying pink and brown radiolarian mudstones is also undulose and irregular, but on a scale of a few metres rather than centimetres, and pale pink radiolarites and grey bentonite clays at 23064827 display large zig-zag slump folds (plate 6.3). The axis of this folding is northwesterly, and the slumping is directed towards the northwest, which is towards a NW-trending fault which bounds the radiolarite outcrop only 40m away.

This syn-sedimentary deformation is indicative of tectonic instability during radiolarite deposition (in the Campanian), and its close spatial relationship to the NW faulting suggests a causal link: perhaps the radiolarites accumulated in hollows created by the NW faults and were periodically disturbed by further fault activity along them. These faults bound, and in some places definitely cut, radiolarites, yet do not affect the overlying chalks. They must therefore have been active in the late Campanian–early Maastrichtian period, and possibly at an earlier stage as well.

Fault-slip data from the NW faults at Asgata (figure 6.4) indicate oblique normal–dextral movement, identical to that recorded by the Pevkos Fault (figure 5.28) and numerous other smaller faults across the ELFC (section 5.5.4). This suggests that the Pevkos Fault is likely to have been active (or reactivated in its oblique sense) at a similar time, *i.e.* in the Campanian–Maastrichtian.

It should perhaps again be stressed that the NW faults at Asgata, which dip at *c.*60° southwestwards, cannot be responsible for the rotation of the pillow lavas in this area, but appear to post-date the tilting, as does the Pevkos Fault (see chapter 5). The timing of the bodily rotation of the lavas (and the rest of the crustal sequence) in the Asgata area cannot be constrained as precisely as can the activity of the NW faults, but appears to

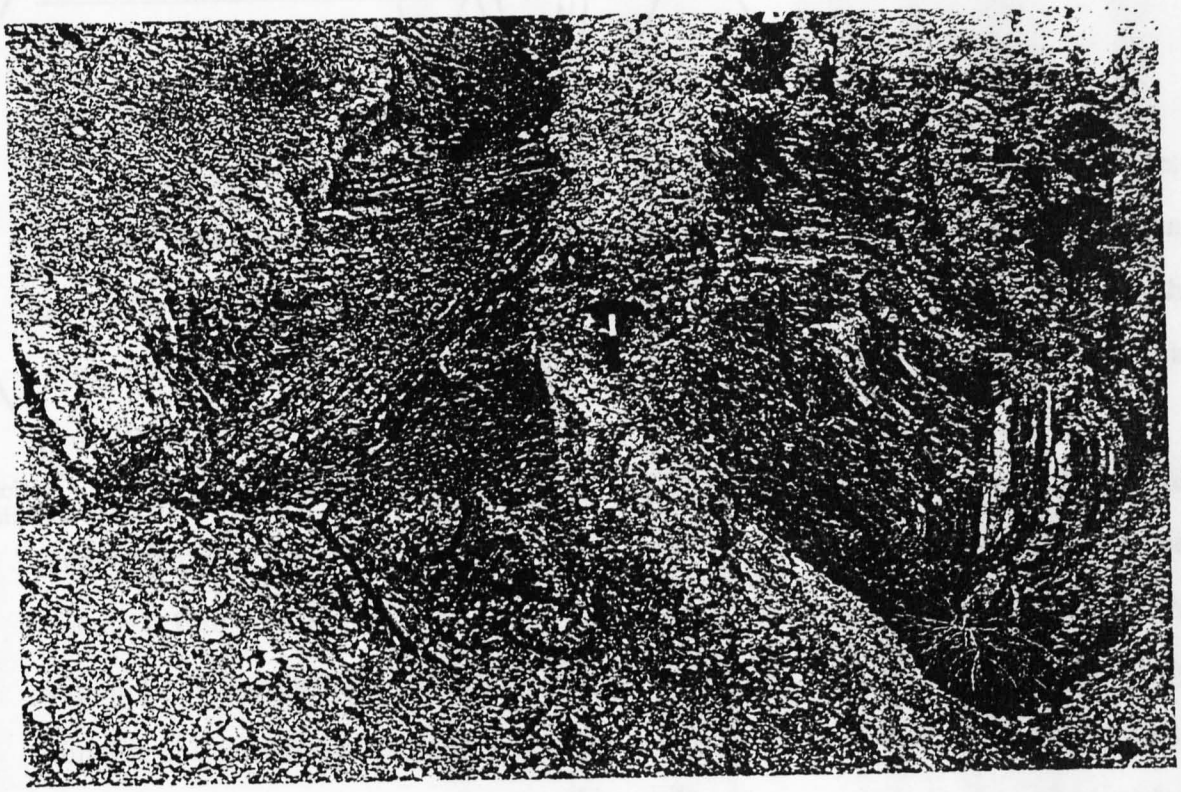

Plate 6.3: Zig-zag slump folding in radiolarian clays, 23134829 Konnin, Asgata. The axis of the slump folding is northwesterly, and 'downslope' is towards the northeast, which is towards a NW-trending oblique-slip fault a few tens of metres away. The soft-sediment deformation is thought to result from activity of this structure in the late Campanian–early Maastrichtian.

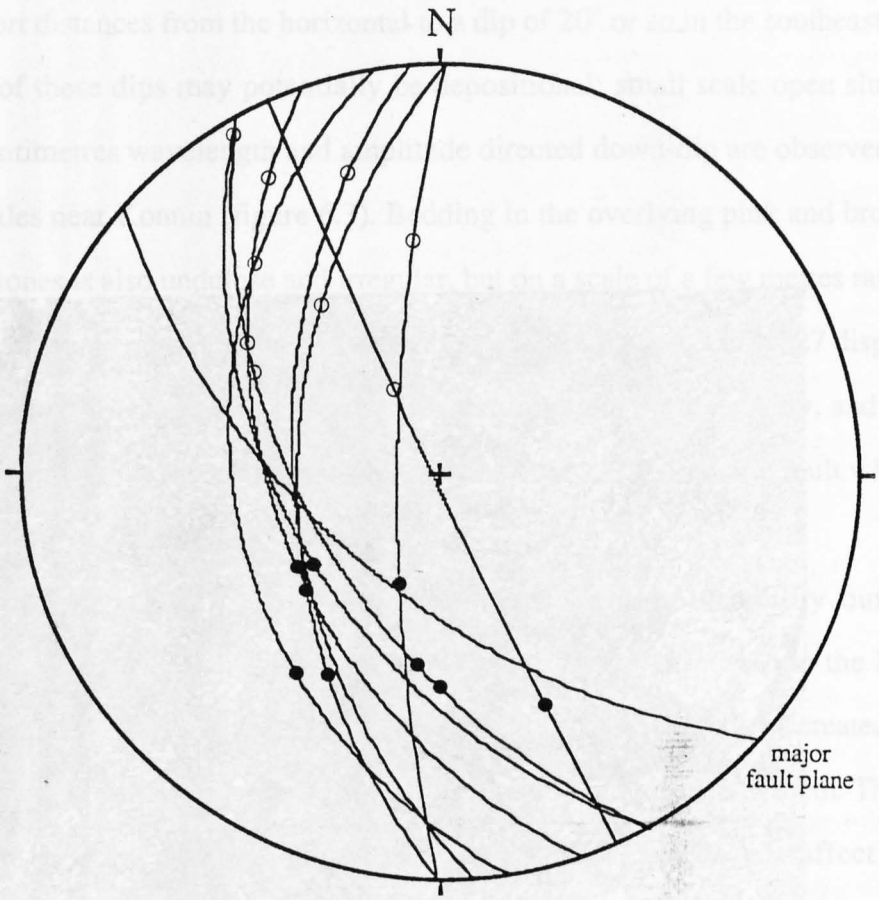

Figure 6.4: Fault planes and slickenside lineations from Konnin, Asgata. Lithological relationships indicate oblique dextral–normal sense of slip. This slip vector is almost identical to that of the Pevkos Fault (*cf.* figure 5.28).

have occurred prior to, or during, the deposition of the manganiferous umbers and creation of the pillow collapse breccias, and certainly before the accumulation of the umberiferous shales.

6.4 Angular Relationships, Dhrapia–Vavla

6.4.1 The Kalavasos Mines and Dhrapia

The Mavridhia area of the Kalavasos Mines is unfortunately now inaccessible; however, Robertson (1975) describes from there similar relationships to those given above for Asgata. Thick pillow collapse breccias are apparently partially intercalated with manganiferous umbers, and together these are overlain unconformably by pink radiolarites.

In the neighbourhood of Dhrapia the Perapedhi sediments are much more accessible and the angular relationships are very well revealed. On the road immediately south of the village a 10m thick manganiferous umber deposit, lying on breccias and pillowed flows dipping *c.*70° northeastward, itself dips at 36° towards the northeast. Small northeasterly dipping oblique slip faults (normal–dextral) reduce the dip to 23° on the northern side of the outcrop. A hundred metres to the east of the village a small pod of umber contains abundant 'dropstones' of lava fragments up to 10cm in diameter, and layers of graded volcaniclastic sediment composed of lava debris several centimetres thick, cross-laminated and fining upwards from grit to silt grade are common.

The most significant outcrop, however, and by far the most spectacular, lies at Kremmos tis Kamilas, 0.75km northeast of Dhrapia village. The umber here is 35m thick, making it one of the largest deposits in Cyprus (plate 6.4). It lies upon 200-300m of lava and diabase scree breccia (which should not be confused with the pillow collapse breccias: compare plate 6.2 with plate 3.10) infilling a large fault-controlled trough that

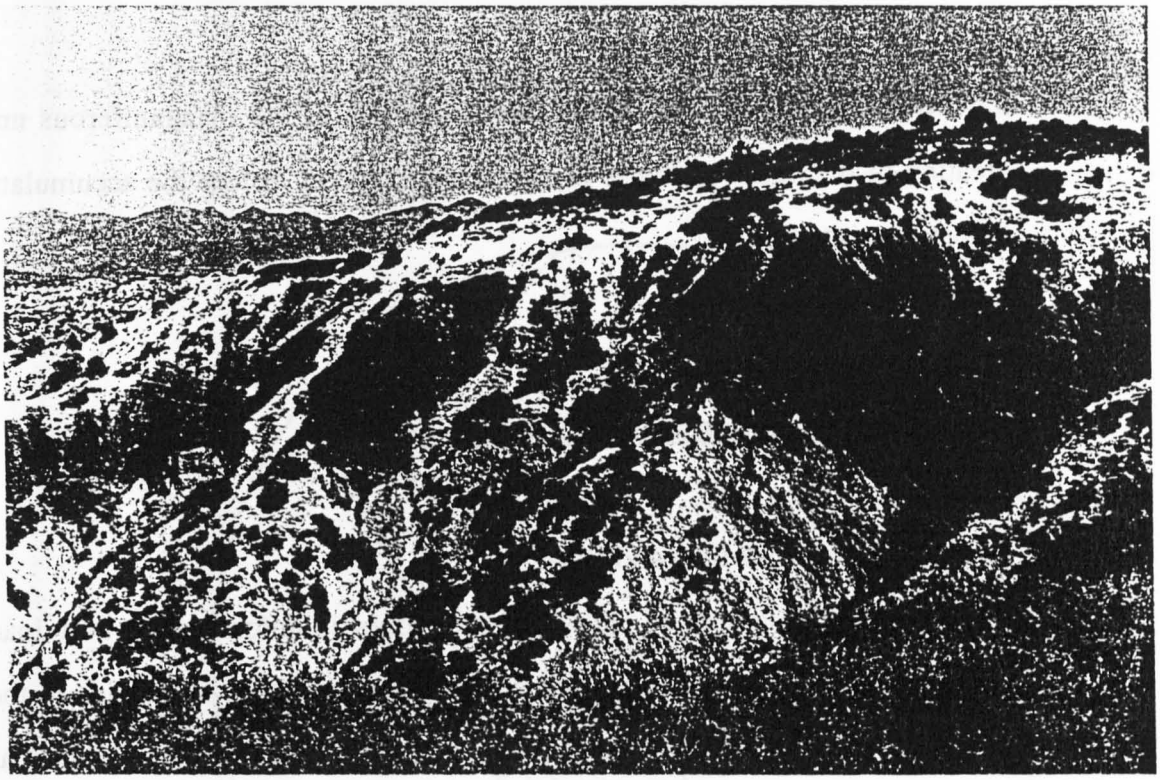

Plate 6.4: Angular unconformity in 35m thick umber deposit, Dhrapia. Dips decrease from ~35° at the base to <10° NE at the top of the deposit; note also a 4m block of diabase breccia lying within the umber to the left of the picture. The umbers lie on 200m+ of transform-related trough infill breccias, here showing vague stratification indicating a moderate NE dip. 261520 Kremmos tis Kamilas, Dhrapia.

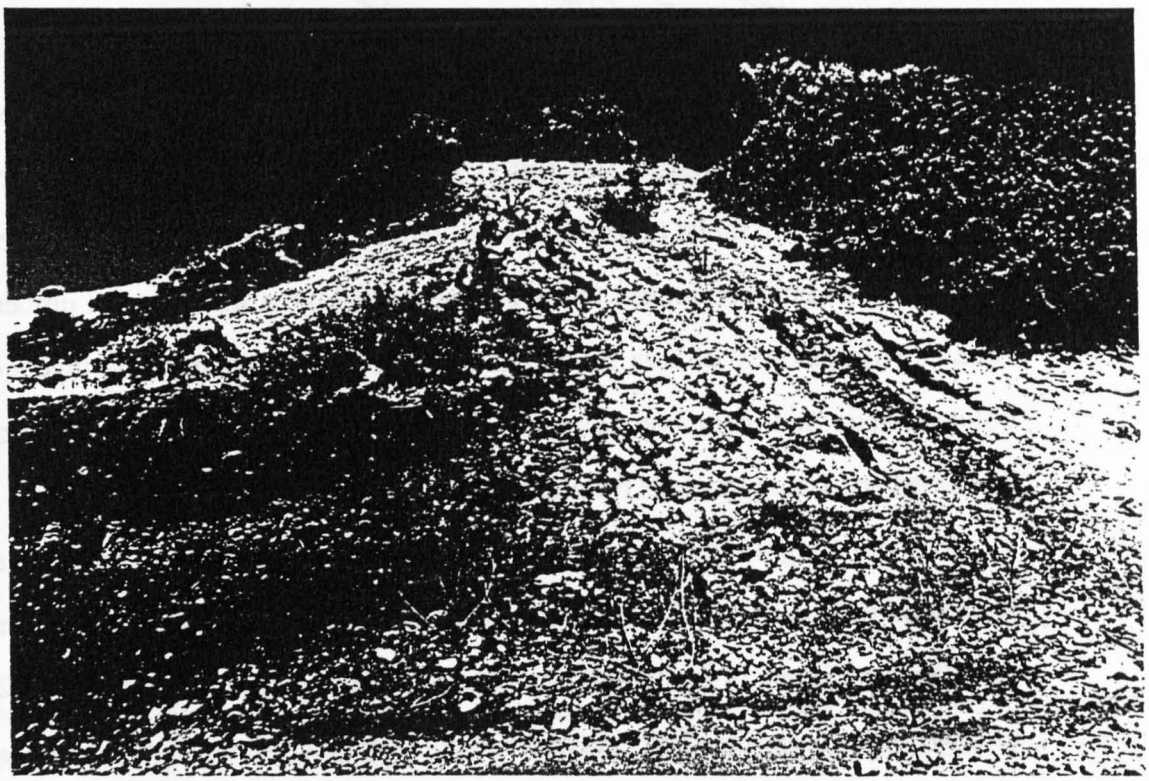

Plate 6.5: Umbers and intercalated lava breccias, Parsata. The umbers conformably overlie pillow lavas dipping at ~45-65° NE, and are overlain unconformably by poorly-exposed slump-folded radiolarites (not shown). 24245370 Parsata village.

was active during the transform phase of the seafloor spreading history of the complex (see section 3.4.1). Vague indications of stratification within the trough infill breccias suggest a moderate northeasterly dip, similar to that of the pillowed flows near Dhrapia village and in the Kalavasos Mines. At the base of the umber deposit, which displays considerable relief, partly silicified umbers dip at up to 36° northeastward; however, a progressive angular unconformity *within* the umber sequence (plate 6.4) reduces this to *c.*10° in the same sense at the contact with the overlying pink bentonite clays (no radiolarite is present here). This indicates that the Dhrapia area was being tilted northeastwards *during* umber accumulation. A 5m diameter 'dropstone' of lithified diabase scree breccia lying near the base of the umber deposit (plate 6.4) and frequent graded volcaniclastic layers attest to considerable tectonic instability at this time, and Robertson (1975) describes wedge-shaped bodies of umber within the sequence, resulting from syn-depositional slumping in response to progressive tilting.

6.4.2 Parsata

Immediately southwest of Parsata village umbers again crop out, lying atop aphyric UPL. Here, both lavas and umbers are tilted at approximately 50-60° northeastward and, unlike the outcrops at Asgata and Dhrapia, there is *no* detectable angular unconformity between them. This relationship is also observed 1km to the southeast of Parsata at 251535 Palaeodhrapia, where a small, steeply-dipping 1.5m thick pod lies conformably upon NE-tilted pillows and lava breccias. At Parsata village itself manganiferous brown umbers form a 10m thick succession becoming paler (more clay-rich?) in its upper part, and containing a few thin, slightly contorted, silicified layers. These are overlain by a 2m lava breccia horizon with an umber matrix and subsequent rapid alternations of breccia and umber (plate 6.5). In the 2m breccia layer lava blocks at the base are up to 30cm in diameter, but fine upwards such that the upper clasts average 1-5cm only. Cross-laminated gritty–silty layers also occur in the umbers above this horizon.

The umbers and breccias are overlain unconformably by several metres of poorly exposed porcellaneous pink radiolarites and friable radiolarian shales. At the contact the radiolarites dip at 30° northeastward, implying that 20-30° of tilting of the umbers northeastward took place prior to their deposition. Above this contact, however, dips of 60-70°, even 90°, are observed, suggesting angular distortion of the bedding, probably demarking cylindrical syn-sedimentary slump folds. No bedding is preserved in the succeeding 10m or so of bentonite clay, but the Lefkara chalks dip at 10-15° towards the northeast only, so rotation may have continued throughout the period of radiolarite accumulation and into that of the clay deposition.

6.4.3 Vathyrkakas, Vavla

In the lava basin at Vathyrkakas (see section 3.4.3) umbers are absent, but instead 30-35m of radiolarite has accumulated. In the lower part of the hollow the radiolarites conformably overlie pillowed and brecciated lavas dipping gently northwards (20-30°), but sweep up to bank at a steep angle against the present hillside and palaeo-topographic high of dolerite scree breccia, which forms the flank of the basin towards the northwest (plate 6.6). The radiolarites closest to this contact have a (presumably depositional) dip of as much as 60°, and display spectacular slump folds directed down-dip, away from the hillside (plate 6.7).

6.5 Synthesis: Sequence and Timing of Faulting

From the previous two sections it is clear that there is a systematic change in the angular relationships between lavas and umbers, and within the Perapedhi Formation itself, across the ELFC (figure 6.5). At Asgata only the lowermost umbers intercalated with pillow collapse breccias appear to have been involved with the tilting; otherwise manganiferous umber, and certainly umberiferous shale, deposition post-dated the

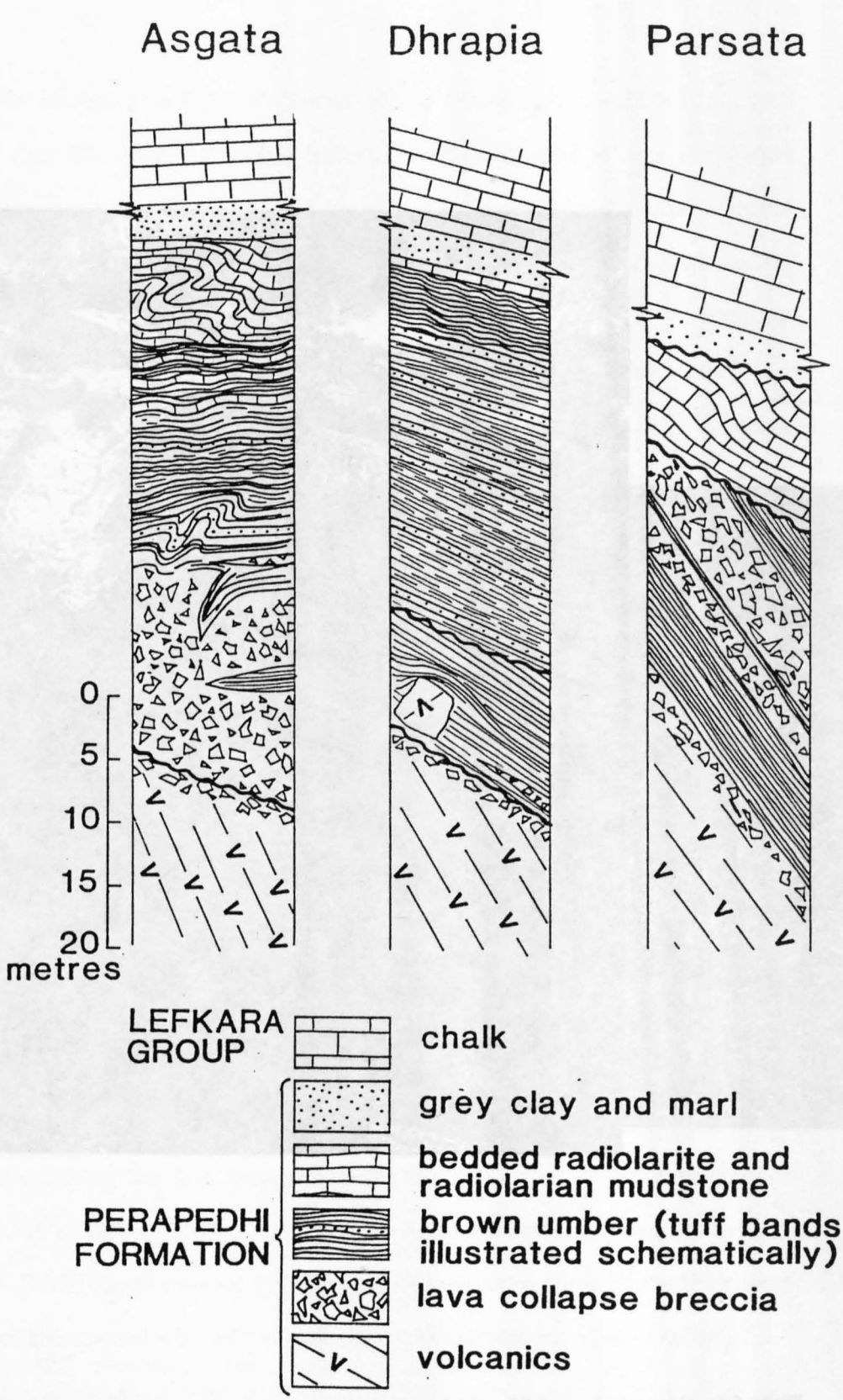

Figure 6.5: Summary of lava–sediment relationships, showing the progressively later timing for block tilting from south (Asgata) to north (Parsata).

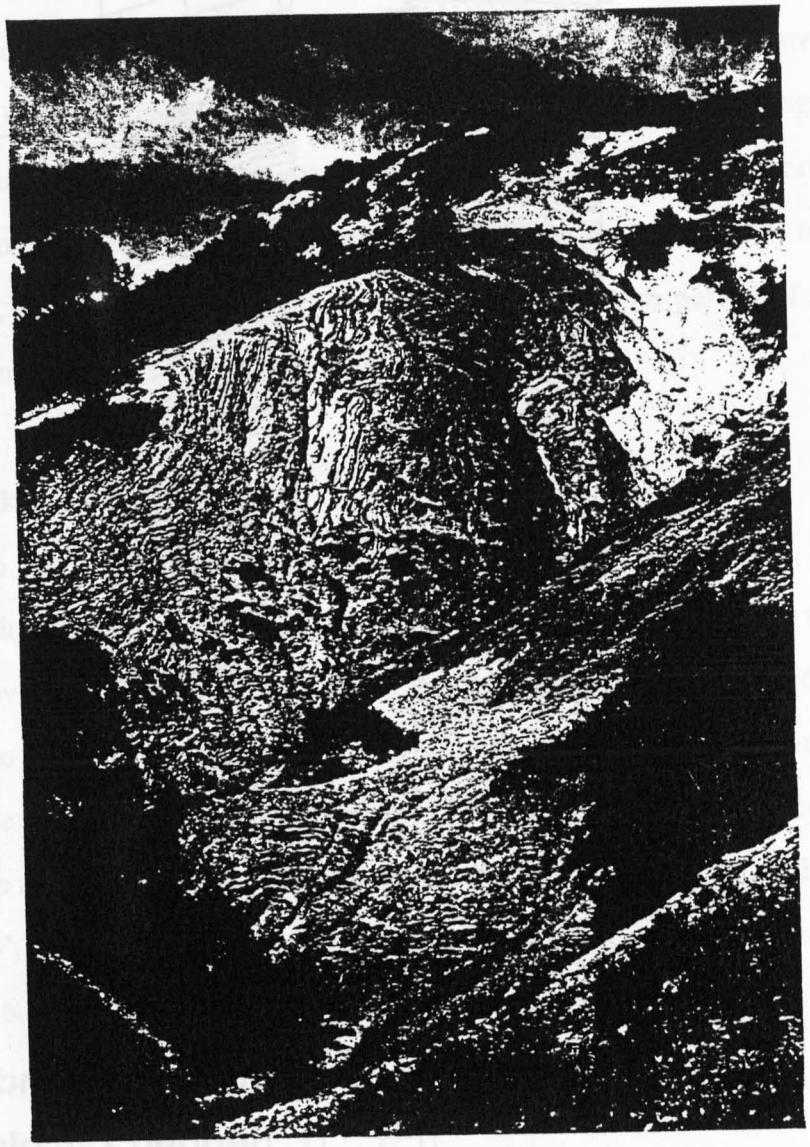

Plate 6.6: General view of 35m thick radiolarite outcrop, Vavla. Pink porcellaneous radiolarites and radiolarian shales bank up to the right of the picture against a hill of fault brecciated sheeted dykes aproned by fossil scree. Note the irregularity of bedding in the sediments. 239554 Vathyrkakas, Vavla.

Plate 6.7: Detail of large-scale slump folding in the more steeply dipping parts of the radiolarite outcrop (plate 6.6). 23965539 Vathyrkakas, Vavla.

rotation of the lavas. At Dhrapia tilting started prior to, but continued throughout, umber deposition, and at Parsata it entirely post-dated the umbers, although the presence of breccias at the top of the sequence suggests that the area became tectonically unstable as umber deposition ceased; tilting then took place prior to and during radiolarite accumulation.

These observations suggest that the extensional deformation spanned a period of some 5-10 Ma, from umber deposition in the Turonian to radiolarite accumulation in the Campanian (section 6.2.3); furthermore, assuming that the lithostratigraphic units are approximately chronostratigraphically equivalent (*i.e.* that the umbers, for example at Asgata and Parsata, are of similar age), the relationships imply that fault activity was diachronous, and that the locus of local block tilting propagated northwards across the ELFC with time. Although the assumption of time equivalence in the supra-ophiolite sediments is implicitly incorrect on a regional scale, where the ages of hydrothermal sediments must necessarily increase with distance from the ridge axis, over the short distances involved in the context of the ELFC (<5km from Asgata to Parsata), significant diachroneity in umber deposition is considered unlikely.

A mechanism for the extensional deformation can thus be suggested in which normal faulting propagates into the unextended footwall (here, northwards into the Arakapas Fault Belt; figure 6.6). Such 'footwall propagation' in successive generations of normal faults is well documented from extensional basin margins (Gibbs 1984), and implies that the collapse of the fault blocks is largely passive and gravity-driven, in response to regional tensional stresses acting on the hanging wall. This is in accord with the observations of numerous small-scale gravity-slip features in the ELFC.

The lava–sediment relationships also shed light on the temporal relationship between the earlier extension dominated tectonism so prominent in the northern part of the ELFC (section 5.4) and later strike-slip dominated tectonism most obvious in the south (section 5.5). In Asgata, the later NW-trending oblique strike-slip faults were definitely active in

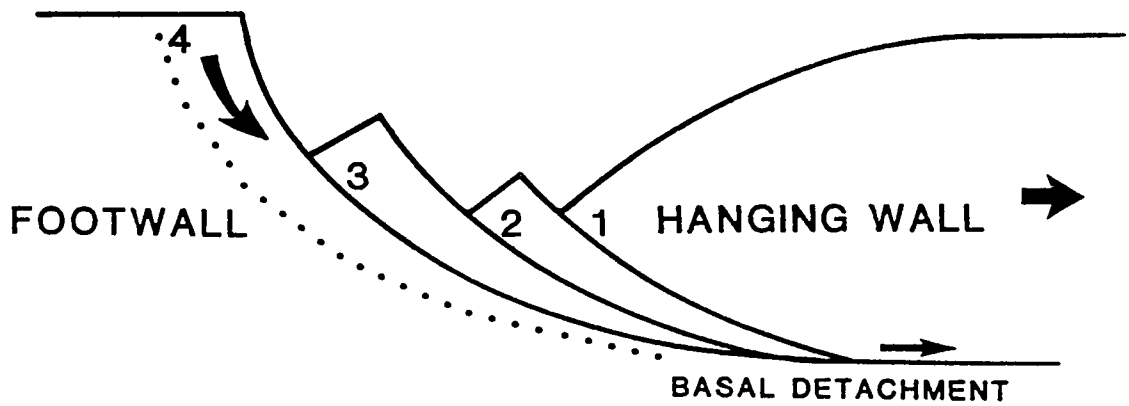

Figure 6.6: Schematic diagram illustrating the order of fault block activity in an extensional system, as deduced from relationships in the ELFC. Individual fault blocks are cut sequentially from the non-extended footwall by gravity collapse (1 = earliest; 4 = latest). In this analogy the Arakapas Fault Belt (*i.e.* the present-day north) is to the left and the southern ELFC, or Anti-Troodos fragment, is represented by the relatively less extended hanging wall. Modified after Gibbs (1984).

the late Campanian–early Maastrichtian (section 6.3.2), but the syn-sedimentary deformation suggests that they may also have been active during radiolarite deposition earlier in the Campanian. Given that tilting of the Parsata block continued throughout the period of radiolarite accumulation there, and probably through bentonite clay deposition as well–*i.e.* certainly in the Campanian, and possibly into the Maastrichtian–no significant time gap can be envisaged between the extension dominated and strike-slip dominated phases of deformation, and they may indeed overlap. The implications of the timing of the two 'episodes' or 'phases' of deformation in a regional plate tectonic context are discussed in the following chapter.

CHAPTER 7:
The Tectonic Evolution of the ELFC

7.1 Introduction

In preceding chapters it has been demonstrated that the ELFC has had a complex, multi-phase tectonic history. Earlier syn-volcanic deformation, which in the northern part of the area involved modification at a transform fault of oceanic crust generated at a spreading ridge axis, has been largely obliterated by later post-volcanic deformation, involving the oblique extensional reactivation of the transform fault over the period from the cessation of seafloor spreading related processes in the Turonian through to the end of the Cretaceous.

In this chapter details of these tectonic episodes are summarised. Observations from the ELFC of the syn-volcanic processes are discussed in section 7.2 in terms of the geometry of the Southern Troodos Transform Fault (STTF) and the spreading structure of the Troodos ophiolite as a whole. A brief analogy is drawn with modern oceanic ridge and transform systems.

The regional significance of the ELFC post-volcanic deformation in the wider context of the Upper Cretaceous plate tectonic framework of the Eastern Mediterranean is briefly reviewed in sections 7.3 and 7.4. In particular, possible links between the ELFC tectonism and the 90° anticlockwise rotation of the Cyprus microplate, which commenced in the Campanian to Maastrichtian interval, are explored (section 7.5), and implications for microplate rotation mechanisms discussed.

7.2 Reconstruction of the Oceanic Geometry of Southern Troodos

7.2.1 Summary of the accretionary geometry of the ELFC

In the Akapnou Forest, in the northern ELFC, tectonised harzburgites, massive dunites and cumulate ultramafics are traversed by, and locally juxtaposed along, vertical E-W serpentinite shear zones (section 5.3). These shear zones may be up to 100m wide and can be traced laterally for more than 1km. They have scaley schistose serpentinite fabrics and contain phacoids up to 20m in length of the above lithologies. Slickensides associated with the shear zones indicate transcurrent slip. The structures are identical to the serpentinite mélanges described by Murton (1986b) from the WLFC, and are thought to have been planes along which the major part of the transform motion occurred.

It is less easy to demonstrate evidence for equivalent structures at higher stratigraphic levels, with the reactivation of many pre-existing structures during the post-volcanic tectonism. However, activity on several major structures from a very early stage can be demonstrated. The Vasilikos Reservoir and Mavridhia Faults in the Kalavasos Mines area, in particular, are shown to have been originally vertical and almost certainly transform-parallel and perpendicular to the strike of the Sheeted Dyke Complex and mineralised faults in the LPL.

The spatial extent to which the ELFC was affected by transform deformation can be deduced from the lava stratigraphy. Simonian and Gass (1978) showed that the zone of transcurrent faulting in the AFB was coincident with an irregular bathymetric depression, infilled by lava flows and volcaniclastic sediments derived by the submarine erosion of fault scarps. The resulting complex lava stratigraphy can be identified in the northern ELFC also, with fault-controlled troughs at Layia and Dhrapia infilled by dyke-rock and lava scree breccias, separated by a relatively upstanding block (in the Parsata area) upon which a thin, irregular UPL sequence was extruded onto a fault-brecciated Sheeted Dyke Complex and tilted LPL basement.

To the south of Dhrapia the volcaniclastic sediments thin dramatically across the Vasilikos Reservoir Fault, and disappear entirely adjacent to the Mavridhia Fault in the Kalavasos Mines area. Interlava sediments are nowhere observed in the lava sequences further to the south; instead the lava stratigraphy of the southern ELFC is more similar to that of northern Troodos, implying a return to a more subdued bathymetry. Since no major transform-parallel features have been identified south of the Mavridhia Fault, it is concluded that a southern margin to the STTF can be drawn in this region. On a map of the present-day geology of the ELFC this boundary, coincidentally, lies close to the line of the prominent late E-W fault (which post-dates block rotation and therefore has no direct relationship to the transform) extending from Gyrisman tou Kanniou on the Asgata–Vasa road westwards to Pevkos (enclosure 1). Removing the effects of the post-volcanic extension, a north-south width of approximately 5km is estimated for the transform across the eastern part of the LFC.

To the south of the boundary lies crust which must have been generated at an 'Anti-Troodos' ridge axis, on the opposite side of the STTF to the remainder of the Troodos Massif. Approximately 50km^2 of Anti-Troodos crust is preserved in the southern ELFC, from Asgata to Parekklisha. A pronounced northeasterly structural grain, reflected both in the orientation of major mineralised faults and in the consistent trend of dykes of the sheeted complex, initially suggests a similar orientation for the Anti-Troodos ridge axis; however, the effect of the later post-volcanic deformation has been to impart clockwise rotations upon fault blocks in the southern ELFC and, in accommodating this, at least some of the NE faults have been rotated in the same sense. The original orientation of the ridge axis may therefore have been closer to N-S or NNE-SSW. The available palaeomagnetic data are too sparse to be unequivocal, but do not support a progressive swing in original dyke intrusion direction from N-S through NE-SW to ENE-WSW as the transform is approached, as has been suggested by some authors for sheeted dykes generated at the Troodos ridge axis north of the AFB (see section 7.2.3).

7.2.2 Implications for the geometry of the Southern Troodos Transform Fault

The 5km estimate for the width of the STTF across the eastern half of the LFC and AFB, which is typical of many oceanic transform fault zones, is significantly less than Murton's (1986a) estimate of not less than 10km for the western half. This is based upon the presence of E-W serpentinite mélange zones across the entire width of the WLFC, and occurrence of volcaniclastic breccias along its southern margin near Akrounda. The paucity of 'transform sequence' intrusives in the ELFC, coupled with the lack of significant angular unconformities in the lava sequences there, contrasting with the major progressive unconformity in the Trimiklini area in the WLFC (Murton 1986b), suggest that the synmagmatic extension, documented by Murton in the WLFC, was considerably less significant in the east. Such along-strike variations are known from modern oceanic transform faults, particularly from medium- and fast-slipping systems, where strain rates are relatively high and the thermal, and hence mechanical, contrast between the two opposed slabs of lithosphere is small (Fox and Gallo 1984). In such a dynamic environment a single strike-slip fault zone appears geometrically unstable and a complex geometry, involving the distribution of strain across extensional or compressional relay zones, is likely. A possible reconstruction of the geometry of the STTF might, therefore, look something like figure 7.1, in which the syn-magmatic transtension, progressive uplift of lithospheric mantle and concomitant magmatism reported by Murton (1986a, b; — and Gass 1986) is restricted to an extensional relay zone centred on the present-day WLFC. In this reconstruction the STTF is shown as a sinistrally-slipping structure, with the clockwise deviation of sheeted dykes north of the AFB taken as a primary feature of the spreading fabric, *i.e.* intrusion of the dykes into a sigmoidal stress field, as demonstrated for the fast-slipping Quebrada and Gofar fracture zones on the East Pacific Rise (Searle 1983). Such extensional relay zones have been described from modern oceanic systems, for example the Tamayo (Macdonald *et al.* 1979) and Orozco transforms (Project Rose Scientists 1981); thus the model for the STTF appears to have

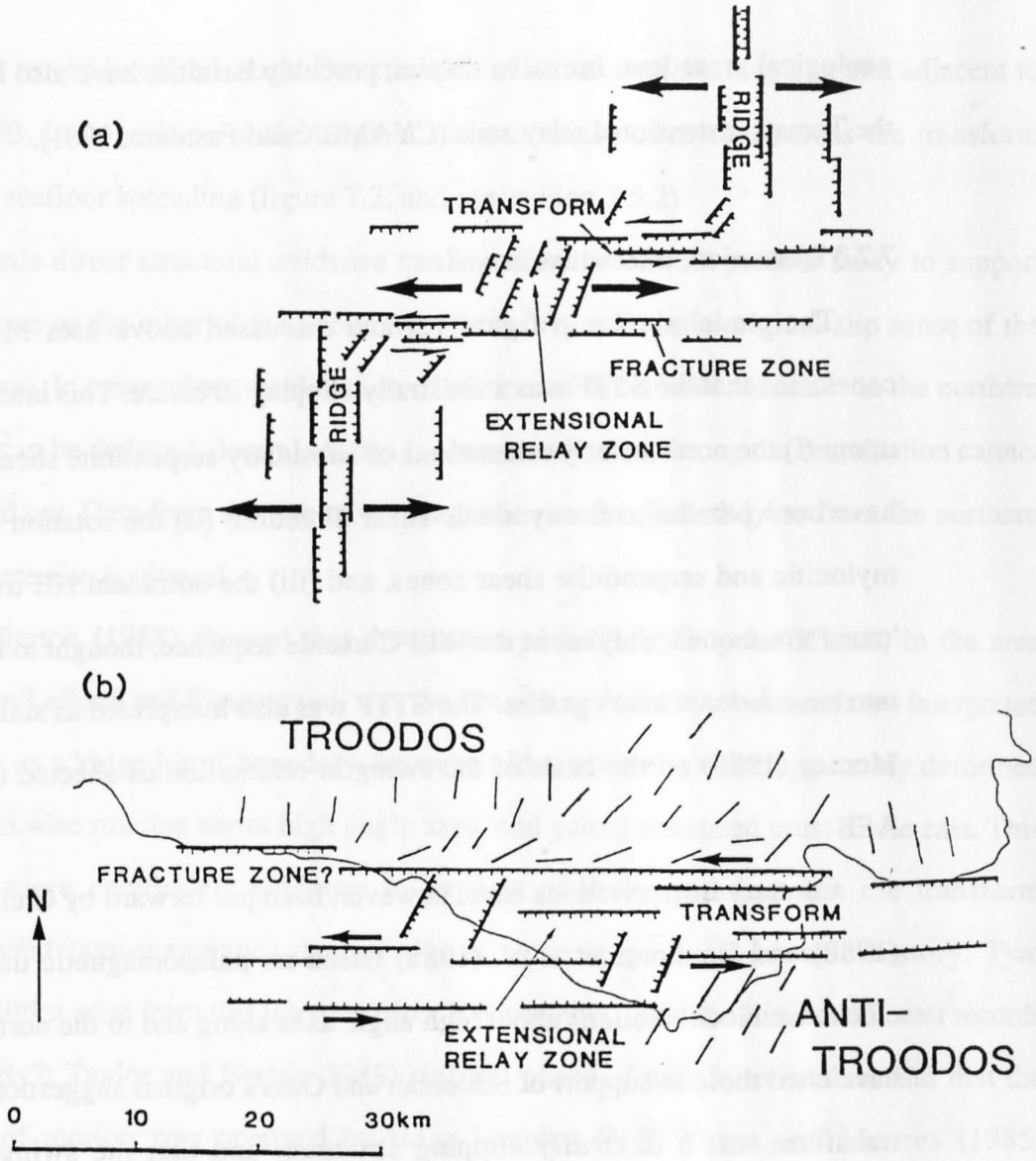

Figure 7.1 (a): Morphotectonic features associated with a medium slip-rate (*c.*6cm/yr) oceanic transform fault. Ridge axis swings into transform over several kilometres, and two principal strike-slip displacement zones are linked by an extensional relay zone (modified after Fox and Gallo 1984). Fracture zone' = inactive (non-strike slip) portion of transform.

(b): Interpretative reconstruction of the geometry of the Southern Troodos Transform Fault. The broad area of transtensional deformation in the western part of the Limassol Forest Complex contrasts with the relatively narrow well-defined transform-tectonised zone in the east. Spreading fabric denoted by thin dashed lines; north = present-day orientation.

geological precedent. Intrusive diapirs, probably basaltic, have also been reported from the Tamayo extensional relay zone (CYAMEX and Pastouret 1981).

7.2.3 Discussion: alternative models

The model shown in figure 7.1 and discussed above uses Murton's (1986a, b) conclusion that the STTF was a sinistrally-slipping structure. This interpretation he based upon: (i) the northeasterly orientations of subsidiary serpentinite shear zones, thought to have been parallel to the synthetic shear direction; (ii) the rotation of microfabrics in mylonitic and serpentinite shear zones, and (iii) the dominant NE trend of syntectonic 'transform sequence' dykes in the WLFC mantle sequence, thought to have been intruded into *en-echelon* tension gashes. The STTF was also interpreted as sinistral by Varga and Moores (1985) on the basis of the swing in orientation of sheeted dykes north of the AFB.

Contrary interpretations have, however, been put forward by Clube (1985), Allerton (1988) and Bonhommet *et al.* (1988) based on palaeomagnetic data. They measure clockwise block rotations about high angle axes along and to the north of the AFB, and have cited these in support of Simonian and Gass's original suggestions in 1978 that the transform was a *dextrally* slipping structure, and that the swing of sheeted dyke orientations was imposed by fault drag (Clube and Robertson 1986; Allerton *op. cit.*; Bonhommet *et al. op. cit.*). These authors have not, however, demonstrated that the rotations they document to the north of the AFB are syn-volcanic, *i.e.* that they relate to spreading processes, rather than to subsequent deformation. Clube (*op. cit.*) reports taking his palaeomagnetic samples from largely undeformed lava flows unconformably overlying a pervasively brecciated sheeted dyke basement; hence the rotations must necessarily have post-dated the main tectonic processes that caused the brecciation. This study has shown the importance of the widespread reactivation of transform-parallel structures after the cessation of volcanism in the ELFC, so the clockwise rotations could

instead record localised *dextral re*activation of transform lineaments in and adjacent to the AFB, in opposition to the original *sinistral* sense of motion across the transform during seafloor spreading (figure 7.2, and see section 7.5.2).

Little direct structural evidence can be offered from the present study to support either one or the other of the above hypotheses regarding the original slip sense of the transform. In cases where the direction of motion on small E-W structures in the northern ELFC can be deduced, dextral motion is always indicated but, again, reactivation cannot be ruled out. Data from the two palaeomagnetic sites in sheeted dykes from the northern ELFC are also equivocal.

Allerton (1988) showed that the eastern part of the Troodos Massif, in the area between Lefkara and Stavrovouni, was the site of a major intrusive boundary– interpreted by him as a 'ridge jump' boundary–between old crust to the west, apparently deformed by clockwise rotation about high angle axes, and young unrotated crust to the east. This offers more convincing evidence in support of the suggestion that the transform underwent (syn-magmatic) dextral slip at some stage in its oceanic history. Two possibilities arise from this interpretation, if accepted: (i) that the Limassol Forest records an (early?: Taylor and Nesbitt 1988) sinistral phase of transform motion, and that the sense of motion was reversed by ridge jumping (*N.B.* Varga and Moores (1985) suggest that the Troodos Massif records evidence for several ridge jumps); and (ii) that the transform that was *always* dextral, and that fabrics and dyke orientations in the WLFC have been modified by clockwise rotation.

The second possibility has potentially fundamental implications for the significance of the tectonism recorded in the eastern and western parts of the LFC. In this scenario both the WLFC and ELFC record oblique dextral strike slip plus extension, the former syn-magmatic and the latter post-magmatic. These may therefore be manifestations of the same process, but with the WLFC hot, and therefore accommodating transtensional magmatism (adiabatic remelting of lithospheric mantle) and the ELFC cold, already

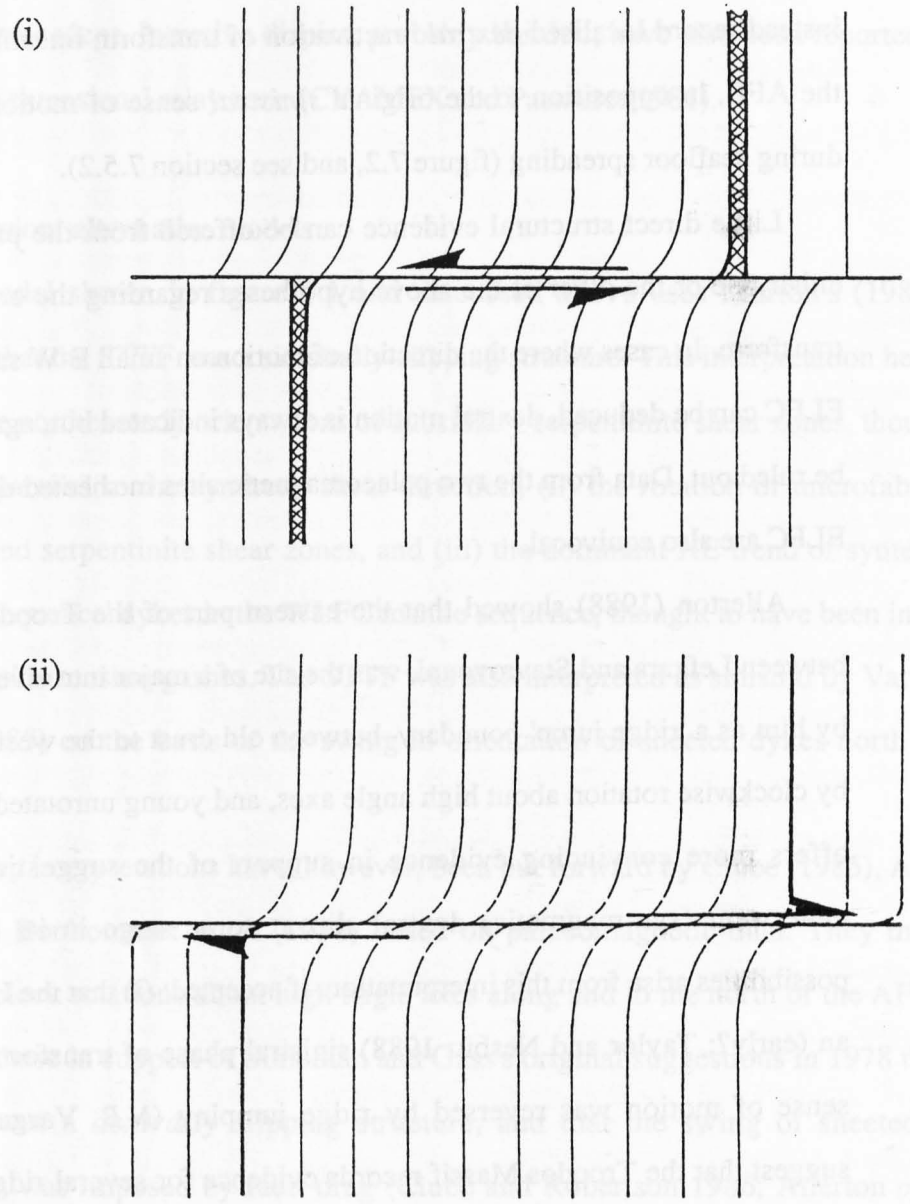

Figure 7.2: Reinforcement of dyke swing by dextral reactivation of an originally sinistrally-slipping transform fault, as postulated for the Southern Troodos Transform Fault. In medium–fast slipping systems the spreading axis adjacent to the transform swings towards the opposite ridge axis by up to 45° (diagram i); this has been explained (Searle 1983) as due to dyke intrusion into a sigmoidal stress field. The primary swing of dyke fabric is in the opposite sense to that which would be induced by fault drag during transform motion. However, reactivation of the transform as a dextral transcurrent fault would reinforce the swing beyond its theoretical 45° maximum (diagram ii).

Active ridge axes in (i) denoted by thick ornamented lines; fine lines represent theoretical spreading fabric (*i.e.* fault scarps in oceans, sheeted dykes in ophiolites).

serpentinised, and instead undergoing brittle fracture. However, this model has several inherent problems, most notably that the episode of transtension and 'transform sequence' magmatism in the WLFC appears to be short-lived (estimated at *c.*0.25Ma by Murton 1986b), whereas the oblique extension and dextral strike-slip affecting the ELFC is thought to persist for some 20Ma (see chapter 6 and section 7.5).

In the absence of further palaeomagnetic studies, therefore, possibility (i) above, that the Troodos spreading geometry was non steady-state, and led to reversals in the sense of slip along the transform, may be most applicable.

7.3 Rotation of the Cyprus Microplate

7.3.1 Timing of the rotation: palaeomagnetic evidence

The discovery that lavas and gabbros across the entire width of the Troodos ophiolite possessed stable westerly-directed primary remanent magnetisation vectors was made by Moores and Vine (1971), and led them to conclude that the ophiolite had been rotated as a coherent body by 90° in an anticlockwise sense. An attempt to constrain the timing of the rotation, by means of a systematic examination of the magnetic properties of the overlying *in situ* sedimentary cover, was first made by Shelton and Gass (1980), who suggested an Upper Miocene age for the rotation; however, more detailed studies by Clube (1985; — *et al.* 1985) indicated that it occurred at a much earlier stage, and was complete by the end of the Lower Eocene. Furthermore, declinations of 320-330° for normally-polarised sites in Maastrichtian Lower Lefkara chalks showed that *c.*60° of the rotation took place *within* the Upper Cretaceous.

At Margi, on the northern flank of Troodos, both lavas and umbers (and also the lowermost radiolarites) have comparable westerly-directed magnetisation vectors (Clube 1985). Although only a limited number of sites have been drilled in the Perapedhi Formation, magnetic declinations directed slightly more towards the north in the upper

part of the radiolarite succession have been tentatively correlated with the first signs of rotation by Clube (*op. cit.*, p.56); however, the major part of the rotation must have occurred very rapidly between the late Campanian and early Maastrichtian, *i.e.* an interval of only 5-10Ma only. This implies a rotation rate in the order of 6-12°/Ma which, although exceptionally rapid, has modern geological precedent in the island of Viti Levu, Fiji, which has rotated by at least 90° in the last 7Ma, at an angular rate of some 14°/Ma (Malahoff *et al.* 1982).

7.3.2 Size of the rotated microplate

No rotations of comparable magnitude have been detected in the surrounding regions of the Eastern Mediterranean, whether southern Turkey (Lauer 1985, Clube 1985), the Levant (Ron and Eyal 1985) or northern Africa (Van der Voo and French 1974). The size of the rotated crustal unit is therefore likely to be small, possibly little bigger than the Troodos Massif itself, and its boundaries may potentially be preserved in the successions surrounding the ophiolite.

To the north of the Troodos mountains gravity (Gass and Masson-Smith 1963), magnetic (Aubert and Baroz 1974) and borehole (Cleintaur *et al.* 1977) data suggest that ophiolitic basement underlies the entire Mesaoria plain. However, this basement appears to be truncated abruptly by a steep fault or faults close to, but not exactly coincident with, the present topographic expression of the Plio-Pleistocene thrust belt of the Kyrenia Range (Robertson and Woodcock 1986). Within the Kyrenia mountains are preserved Permian–Lower Cretaceous platform carbonates, which were pervasively brecciated prior to the deposition of Campanian turbidites (containing a variety of clasts including ophiolite-derived detritus). They were then overlain by Maastrichtian limestones and limestone breccias interbedded with mafic–acid (within-plate??) volcanics (Baroz 1980, Robertson and Woodcock 1986). No palaeomagnetic data exist from northern Cyprus, but Robertson and Woodcock (*op. cit.*) speculate that the succession from the Kyrenia

Range is unrotated, and documents the fragmentation of a carbonate platform, possibly by underthrusting in the first instance, and then by strike-slip faulting against Troodos-type crust upon the rotation of the latter.

The tectonic evolution of the area to the southwest of the Troodos Massif is highly complex, and its origin and significance is, in many respects, still contentious. Beneath a largely undeformed Maastrichtian–Recent sedimentary cover, similar to that deposited elsewhere in Cyprus, a highly disrupted basement is composed of chaotically deformed, largely allochthonous, Triassic to Middle Cretaceous rocks. According to Swarbrick (1980) these are cut by high-angle arcuate shear zones intruded by serpentinite, along which blocks of Troodos-type ophiolitic crust became entrained in Maastrichtian times. This heterogeneous basement is referred to as the Mamonia Complex. Preliminary palaeomagnetic results (Clube 1985) show that the Triassic–Cretaceous portions of the Mamonia Complex do *not* share the westerly-directed magnetic remanence vector of Troodos, and so must have suffered a different, probably more complex, rotation history. However, westerly-directed magnetisation vectors obtained from the Akamas peninsula, which is the largest of the ophiolitic fragments associated with the Mamonia Complex, imply that it has suffered a rotation history similar to that of the main Troodos Massif.

It is clear, therefore, that the relationship between the Mamonia Complex and the Troodos ophiolite is likely to be of critical importance in an understanding of the timing and mechanism of microplate rotation. In order to investigate this more fully a synopsis of current opinion as to the tectonic evolution of southwestern Cyprus is given below.

7.4 Regional Setting: A Synopsis of the Geology of Southwestern Cyprus

7.4.1 The Kannaviou Formation

Along the western margin of the Troodos Massif the lateral equivalent of the Moni mélange and the thin, discontinuous bentonite clays that overlie the Perapedhi Formation in the ELFC is a sequence of bentonite clays and volcaniclastic sands up to 750m in thickness (Robertson 1977b). This is the Kannaviou Formation (Lapierre 1968), dated on micropalaeontological evidence as early Campanian to middle Maastrichtian in age (Mantis 1970, Ealey and Knox 1975). At the base of the deposit, which is locally unconformable upon Troodos pillow lavas (Robertson and Hudson 1974), radiolarites and clays predominate. Volcaniclastic sandstones and siltstones become more important higher in the succession, and contain fragments derived from three distinct sources, *viz*: (i) Troodos-type material, (ii) andesitic–dacitic pumice and ash, and (iii) terrigenous detritus derived from the allochthonous sedimentary lithologies (Robertson 1977b). The pumiceous material is highly evolved and apparently of calc-alkaline (volcanic arc) affinity, distinct from the chemistry of Troodos (Ealey and Knox 1975, Clube and Robertson 1986); a suitable source, however, does not lie within the present confines of the island. Kannaviou lithologies conformably overlie slivers of Troodos basement entrained within the Mamonia Complex, including the Akamas peninsula at the northwestern tip of the island. They do not, however, lie upon the allochthonous Triassic–Cretaceous lithologies (Swarbrick 1980).

7.4.2 The Mamonia Complex

The allochthonous non-ophiolitic part of the Mamonia Complex is sub-divided into two groups: the predominantly igneous Dhiarizos Group, of Triassic age, and the wholly sedimentary Upper Triassic to Mid-Cretaceous Ayios Photios Group (Swarbrick and Robertson 1980). The Dhiarizos Group is composed mostly of alkaline trachytic pillow

lavas of 'within-plate' affinity (Lapierre 1975; Pearce 1975), intercalated with and overlain by fine pelagic limestones and radiolarites, and occasional pyroclastic tuffs and agglomerates. The Ayios Photios Group is wholly sedimentary, consisting basically of Upper Triassic siliciclastic turbidites (derived from a metamorphic, and hence continental, source: Henson *et al.* 1949) succeeded by pelagic and hemi-pelagic sequences, including calciturbidites.

Also associated with the Mamonia Complex are slivers of highly deformed greenschist to amphibolite grade metamorphic rocks, usually adjacent to blocks of the Dhiarizos Group, which are spatially associated with the serpentinite fault lineaments (Lapierre 1975, Ealey and Knox 1975, Spray and Roddick 1981). Spray and Roddick (*op. cit.*) showed that the protoliths to these rocks were alkali basalts (potentially belonging to the Dhiarizos Group), mid-ocean ridge type basalts, and associated siliceous and calcareous sediments, which were modified by dynamothermal metamorphism at temperatures of up to 600°C. Structural fabrics indicative of deformation at this temperature are parallel to the serpentinite fault lineaments bounding the outcrops, and are modified by local folding indicative of dextral strike slip (assuming no post-metamorphic rotation). $^{40}Ar/^{39}Ar$ geochronology of the rocks (Spray and Roddick *op. cit.*) indicates metamorphism between 90 and 83Ma (*i.e.* Coniacian–Santonian).

Most authors agree that the Ayios Photios Group represents part of a Mesozoic passive continental margin succession (Robertson and Woodcock 1979, Swarbrick *op. cit.*, Malpas and Xenophontos 1987). The Dhiarizos Group volcanics are thought to represent seamounts and volcanic islands created during rifting at the margins of an ocean basin in the Triassic, upon which were built fringing coral reefs (Clube and Robertson 1986, Malpas and Xenophontos *op. cit.*).

Deformation of the Ayios Photios Group is extreme. Stratigraphic sequences reported by Robertson and Woodcock (1979), Swarbrick and Robertson (1980) *etc.* are reconstructed from a chaotic aggegate of blocks tens of metres to several kilometres wide

and up to 200m thick. Intense (primarily soft-sediment) folding of the sediments is common, and many sequences are inverted. Structural studies indicate predominant fold vergence and facing directions towards the present-day northeast, suggesting emplacement from the southwest (Robertson and Woodcock 1979, Swarbrick 1980). The Ayios Photios sedimentary sheets consistently lie with low angle tectonic contact upon the Dhiarizos Group, which is less deformed.

The deformation has been interpreted as a result of the collapse of the Ayios Photios Group continental margin oceanwards over the Dhiarizos Group by gravity sliding, in response to limited underthrusting of the margin (Gass 1959, Robertson and Woodcock 1979, Swarbrick 1980, Clube and Robertson 1986); alternatively other authors (Pearce 1975, Moores *et al.* 1984 and I.G. Gass *pers. comm.* 1988) regard the entire Mamonia Complex as a subduction accretionary prism.

The origin and significance of the metamorphic rocks within the Mamonia Complex is not fully understood, and no convincing explanation has yet been proposed. They have been variously interpreted in terms of: exotic fragments from an externally metamorphosed terrain (Ealey and Knox 1975); slivers of a sub-ophiolitic metamorphic sole (Woodcock and Robertson 1977); shear heating along the arcuate fault lineaments (Swarbrick 1979); metamorphism at a ridge–transform intersection (Spray and Roddick 1981), or formation by the juxtaposition of hot (near-ridge) Troodos-type crust against older marginal mid-ocean ridge crust along a westerly, probably transpressional, continuation of the STTF (Clube and Robertson 1986).

7.4.3 Juxtaposition of Troodos against the Mamonia Complex

Emplacement of the Ayios Photios Group over the Dhiarizos Group occurred sometime after the deposition of the youngest Ayios Photios sediments (probably Hauterivian (122-118Ma): Ealey and Knox 1975), but prior to the deposition of the unconformably overlying Maastrichtian Lefkara chalks. According to Swarbrick (1980), the gravity sliding/thrusting event *pre-dated*, and was entirely unrelated to, activity along

the high-angle serpentinous shear zones, which juxtapose the deformed older 'Mamonia basement' (*i.e.* combined Ayios Photios and Dhiarizos Group blocks) against slivers of ophiolitic basement and the Troodos Massif itself. The shear zones are arranged in two regionally extensive lineaments with arcuate outline, parallel both to the southwest coast of Cyprus and the southwestern margin of the Troodos Massif (figure 7.3), and isolate a sliver of Mamonia basement up to 15km wide between them. The inferred continuation of the lineaments beneath areas of younger sediment, based on borehole and gravity information (R.E. Swarbrick *in* Clube and Robertson 1986), is shown by dashed lines in figure 7.3.

The more southwesterly of the lineaments, at Phasoula (Swarbrick *op. cit.*), is a zone totalling up to 3km in width of thin, vertical, anastomosing strands of schistose serpentinite with a WNW trend (figure 7.4). The westerly continuation of the zone swings round to a N-S attitiude at the Baths of Aphrodite. At several places, *e.g.* the Mavrokolymbos dam and at the margin of the Akamas peninsula, massive serpentinite has (according to Swarbrick *op. cit.*) protruded up the fault zone and flowed as sub-horizontal sheets onto the ophiolitic basement.

Fragments of Troodos-type basement entrained within these arcuate fault zones are overlain by continuous sequences of Kannaviou Formation sediments, even passing conformably in places up into Lefkara chalks; hence it is difficult to envisage the Mamonia basement being emplaced *over* the ophiolite fragments, as suggested by Lapierre (1975). Instead, it is more likely that the two basement types were juxtaposed by transcurrent movements along the arcuate fault lineaments (Swarbrick *op. cit.*). This is supported by observations of local deformation fabrics in blocks adjacent to the fault zones (Clube and Robertson 1986).

The ophiolitic fragments entrained in the shear zones are lithologically and geochemically most similar to the transform-tectonised areas of crust from the STTF: most pillow lavas have primitive 'group III' boninitic chemistry (Cameron 1985) and are

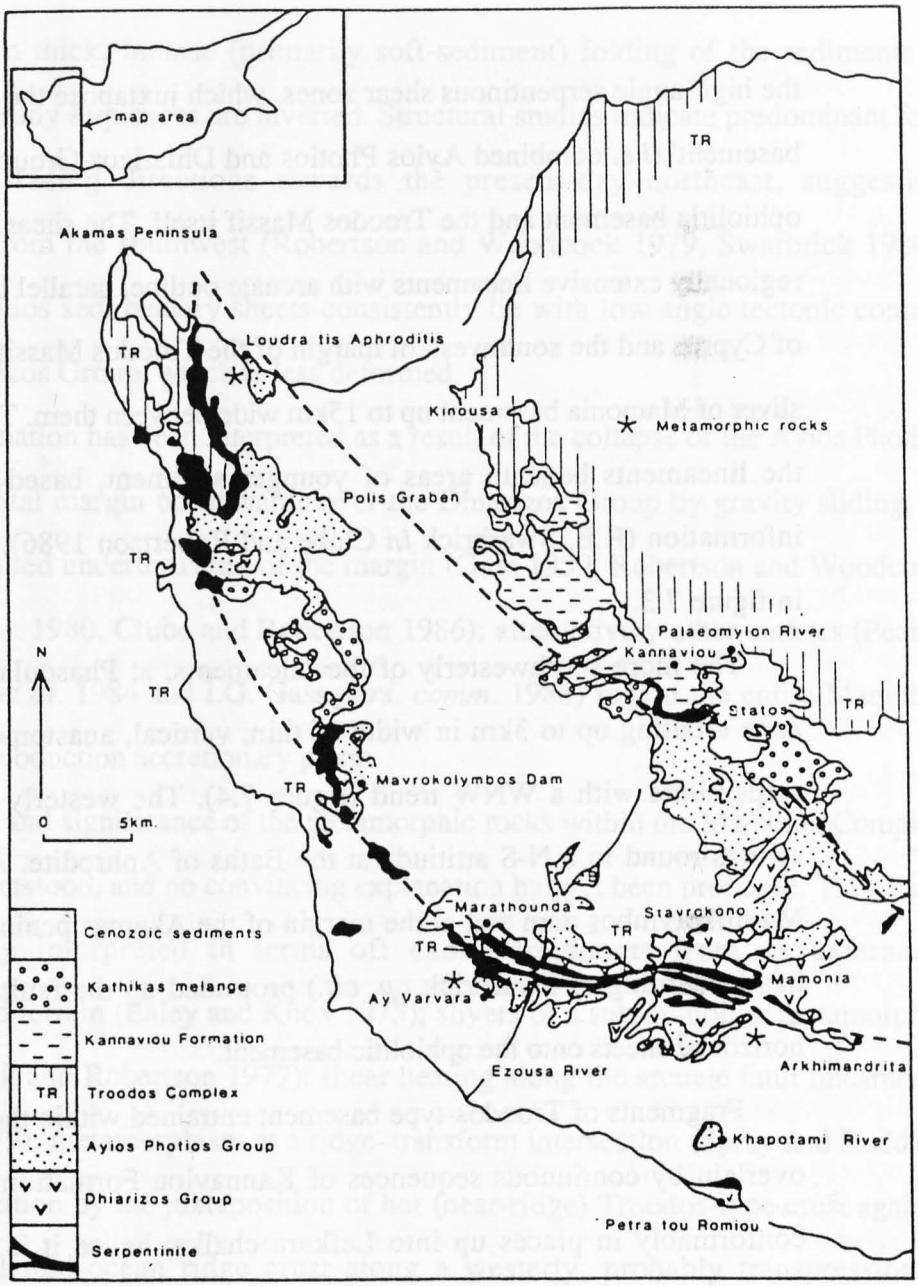

Figure 7.3: Simplified geological map of southwestern Cyprus showing the inferred distributions of Mamonia basement (Ayios Photios and Dhiarizos Groups) and Troodos basement blocks, separated by arcuate serpentinite shear zones. Dashed lines indicate inferred limits of the Mamonia basement block. Simplified after Clube and Robertson (1986).

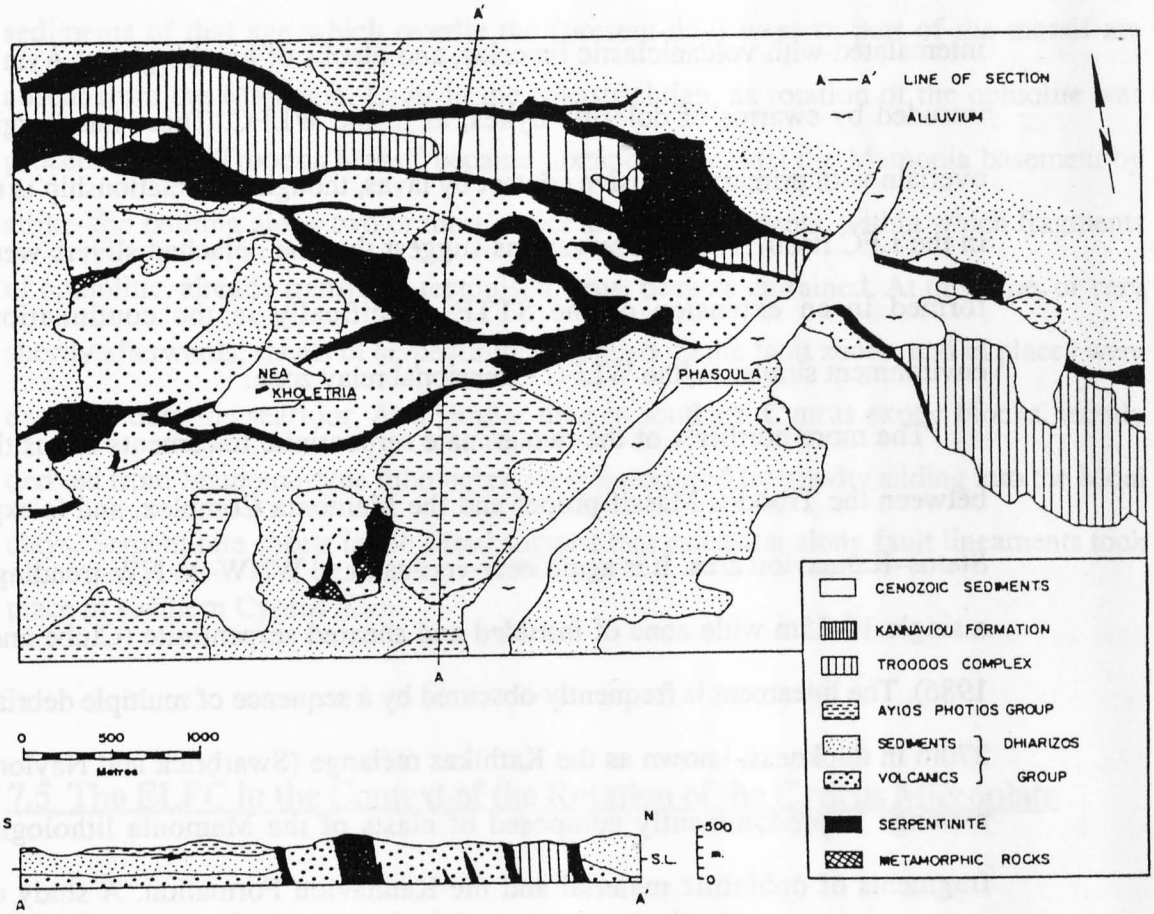

Figure 7.4: Sketch map and cross section of anastomosing serpentinite fault lineaments at Phasoula, showing slivers of Troodos-type basement interleaved amongst blocks of Mamonia basement. From Swarbrick (1980).

intercalated with volcaniclastic breccias, and blocks of harzburgite at Ayia Varvara are intruded by swarms of doleritic dykes, as in the WLFC. These harzburgites are also overlain with primary extrusive contact by lavas, though this relationship is not observed in the LFC itself. These observations suggest that the detached slivers were originally formed in an extension of the STTF, specifically in the continuation of, or an environment similar to, the WLFC extensional relay zone.

The more northerly of the two arcuate serpentinite lineaments forms the boundary between the Troodos Massif proper and the Mamonia Complex, and is exposed in the Statos–Kannaviou area. It is again near-vertical, and WNW- to NW-trending, but is here a single 10-25m wide zone of intruded and sheared serpentinite (Clube and Robertson 1986). The lineament is frequently obscured by a sequence of multiple debris flows up to 270m in thickness, known as the Kathikas mélange (Swarbrick and Naylor 1980). The mélange is predominantly composed of clasts of the Mamonia lithologies, but also fragments of ophiolitic material and the Kannaviou Formation. A study of thickness variations and direction of mass flow in the Kathikas mélange (Swarbrick and Naylor *op. cit.*) has shown that the source of the mélange is coincident with the fault lineaments themselves, leading to an interpretation of the deposit as being shed from fault scarps during activity along the fault lineaments (Swarbrick 1980). Serpentinite clasts are rare in the mélange, suggesting that serpentinite protrusion largely post-dated this activity. Intercalated between, and thus dating, individual debris flows in the Kathikas mélange are bands of pelagic chalk of Maastrichtian age. These pass conformably up into the Lefkara Formation.

In summary, the Mamonia Complex can be regarded as the product of two distinct tectonic events. Deformation of the Ayios Photios passive continental margin and its emplacement onto the Dhiarizos Group ocean margin sequence took place sometime in the Middle–Upper Cretaceous. In Campanian and early Maastrichtian times the Mamonia basement was still separated from Troodos, as the Kannaviou Formation volcaniclastic

sediments of that age which overlie the (present-day) western part of the massif are absent from the Mamonia. Later in the Maastrichtian, as rotation of the ophiolite was proceeding, the Troodos Massif became juxtaposed against the Mamonia basement by strike-slip faulting along two or more major arcuate lineaments, within which fragments of ophiolitic, already transform-tectonised, crust became entrained. At this time, or very shortly afterwards, sheets of serpentinite protruded up the fault zones, and in places were extruded onto the seafloor. At a similar time in southern Cyprus exotic blocks, mostly derived from Mamonia-type lithologies, were introduced by gravity sliding into the Moni clays. Serpentinite sheets in the Moni suggest that extrusion along fault lineaments took place in southern Cyprus also.

7.5 The ELFC in the Context of the Rotation of the Cyprus Microplate

7.5.1 Summary of post-volcanic deformation in the ELFC

The present-day Southern Troodos margin was subjected to a protracted period of extension immediately following the cessation of volcanism there, continuing from the Turonian (91-89.5Ma: Hallam *et al.* 1985) through into the Campanian (84-71.5Ma), and possibly the Maastrichtian (71.5-66Ma). It is evident that the Southern Troodos Transform Fault acted as a weak lineament, and extensional strain was preferentially accommodated in the already transform-tectonised northern half of the ELFC. Transform-parallel structures were reactivated as normal faults, and rotated 'falling domino' style, together with the greater part of the 4km-thick axis-generated crustal sequence, above a basal detachment surface, the Akapnou Forest Décollement. This décollement horizon was located in serpentinised cumulate ultramafics, a few hundred metres above the petrological Moho. Palaeohorizontals (*e.g.* pillow lavas and intercalated volcaniclastic sediments) were tilted steeply northeastward, and the originally vertical faults rotated to a low angle with a shallow south or southwesterly dip. Tilting of

the fault blocks was frequently accompanied by internal deformation and southward-directed gravity sliding.

The orientation of the minimum principal compressive stress (*i.e.* the extension direction, σ_3) at this time is thought to have been approximately NE-SW, as deduced from lava dips, the orientations of palaeomagnetic rotation axes, fault-slip lineations, and the NE strike of high angle 'transfer faults' (which form lateral boundaries to the rotating fault blocks and are thought to contain the local extension direction: see Lister *et al.* 1986a, b).

Crust created at the Anti-Troodos ridge in the southern half of the ELFC, and unaffected by transform tectonism, behaved more coherently during this extensional phase. The low angle normal faults with extreme displacements characteristic of the northern ELFC are not apparent, and block rotations are of smaller magnitude. In contrast, lavas to the north were tilted moderate degrees towards the southwest, about steeply northward-dipping antithetic normal faults.

Continued extension was manifested in the creation of a new set of normal faults which cut through the previously rotated fault blocks and the Akapnou Forest Décollement. The majority of the new faults have a WNW or NW strike and a downward displacement towards the southwest, and they do not appear to have given rise to further tilting. The most prominent of these structures is the Pevkos Fault, which can be traced for more than 8km. This later set of normal faults may have been initiated as the earlier faults rotated to a low angle, became mechanically incapable of accommodating further extension in the same stress regime and 'locked up'.

In the southern ELFC many of the NW-trending structures now possess oblique, sometimes multiple, slickenside lineations on their fault surfaces, suggesting that they, in turn, were reactivated, but with a predominantly strike-slip (dextral) sense of motion. At the same time many NE-trending fractures were initiated (or, in places, originally ridge parallel features reactivated), with oblique normal-sinistral motion. Palaeomagnetic data

from the vicinity of the Pevkos Fault suggest that the two fault sets, in concert, accommodated clockwise rotations of fault blocks about steeply inclined axes. The similarity in fault plane and fault-slip lineation orientations across much of the southern ELFC suggest that analogous clockwise rotations might be widespread. This phase of deformation can be dated with reference to the overlying sediments as (probably late) Campanian (*i.e.* syn- to post-radiolarite) to early Maastrichtian (pre-Lefkara chalk).

7.5.2 Relevance of the ELFC deformation to microplate rotation

The most southerly outcrop of the Troodos ophiolite proper is at Parekklisha, where lavas are overlain by Moni mélange. Moni mélange crops out again, and has been recovered from boreholes, on the Akrotiri peninsula (Bear and Morel 1960, Hadjistavrinou and Constantinou 1977); here, however, it lies on top of folded Mesozoic radiolarites identical to lithologies in the Ayios Photios Group further to the west (see Bear and Morel *op. cit.* plate VIII). It would appear, therefore, that the Akrotiri peninsula is underlain by Mamonia Complex basement. If the Mamonia here does not allochthonously overlie Troodos basement (for which no evidence has been propounded anywhere else in Cyprus) a major lineament similar to that exposed at Statos and Kannaviou must separate Troodos and Mamonia basement types, and should exist buried beneath the Maastrichtian to Recent sedimentary cover somewhere between Akrotiri and Parekklisha. Such a lineament could potentially be a continuation of the vertical WNW- to NW-trending Statos fault zone itself, which can be traced intermittently for 5km to the southeast of Statos village, before being buried finally beneath later sediment (Swarbrick 1980); on direct extrapolation it would pass approximately beneath Limassol (figure 7.5).

As discussed in section 7.4.3, Swarbrick (1980) and Swarbrick and Naylor (1980) have shown that the Troodos Massif and the Mamonia Complex were juxtaposed along the Statos lineament in the Maastrichtian, during which time the major part of the anticlockwise rotation of Troodos took place (Clube 1985). The continuation of this

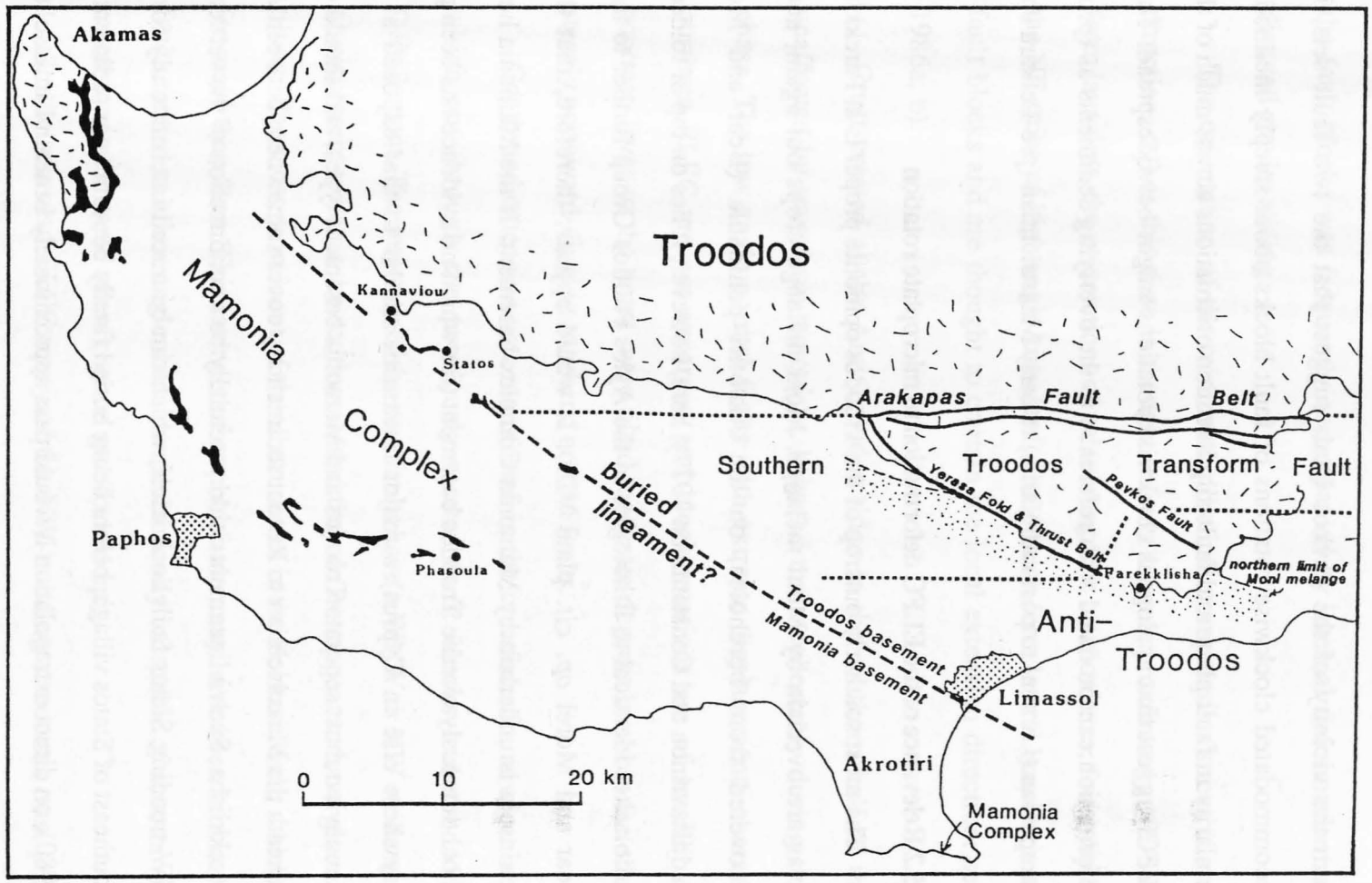

Figure 7.5: Inferred continuation of the NW-trending serpentinite shear zone separating Troodos and Mamonia basement types at Statos/Kannaviou. Mamonia lithologies exposed on the Akrotiri peninsula suggest that a continuation of this lineament passes between Akrotiri and Parekklisha. The postulated trace of the Southern Troodos Transform Fault, which is thought to be truncated by the lineament, is indicated by a fine dashed line. Note the NW trends both of major fault zones in the Limassol Forest, and the limit of Moni clay occurrence. Exposed igneous basement is shown with stippled ornament, and serpentinite black.

inferred lineament is coincident with the trough in which the Moni mélange had been deposited, and in which blocks of Mamonia-type lithologies and serpentinite sheets were introduced in Maastrichtian times. These may have been shed from active strike-slip fault scarps, as suggested by Swarbrick (1980). Pantazis (1967) identifies E-W oriented fold axes within the Moni clay matrix; if these really exist (and most of the outcrops today have been so degraded that bedding is no longer visible) they are compatible with deformation associated with dextral strike slip along a WNW-striking lineament (figure 7.6(a)). They do not necessarily imply northward-directed compression, as claimed by Clube and Robertson (1986).

At the same time in the ELFC the WNW- to NW-trending faults at Pevkos, Asgata *etc.* (and possibly the precursor to the Yerasa Fold and Thrust Belt, bordering the WLFC), which are exactly parallel to the Statos lineament, were reactivated in a dextral slip sense, and clockwise block rotations accommodated about subsidiary NE faults. The clockwise rotations are measured relative to the overall anticlockwise rotation of the Troodos Massif (*N.B.* a clockwise rotation = *less* of an *anti*clockwise rotation), hence they record less *overall* rotation and may be interpreted as a result of drag at the margin of the rotating microplate (figure 7.6(b)). Clube (1985) and Clube and Robertson (1986) document magnetisation vectors in the northwest quadrant for sites along the westerly continuation of the southern Troodos margin, and these almost certainly record analogous clockwise rotations at the edge of the microplate. It is predicted that detailed structural studies along the southwestern margin would reveal a similar faulting pattern to that described from the ELFC. Suggested geometrical relationships along the southern Troodos margin at this time, in the early Maastrichtian, are summarised in figure 7.7.

7.5.3 Significance of the extensional reactivation of the STTF

It has been demonstrated above that the dextral strike-slip and oblique faulting in the ELFC is related to the *actual* rotation of the Cyprus microplate in late Campanian to early Maastrichtian times. However, this phase of fault activity represents only the culmination

(a)

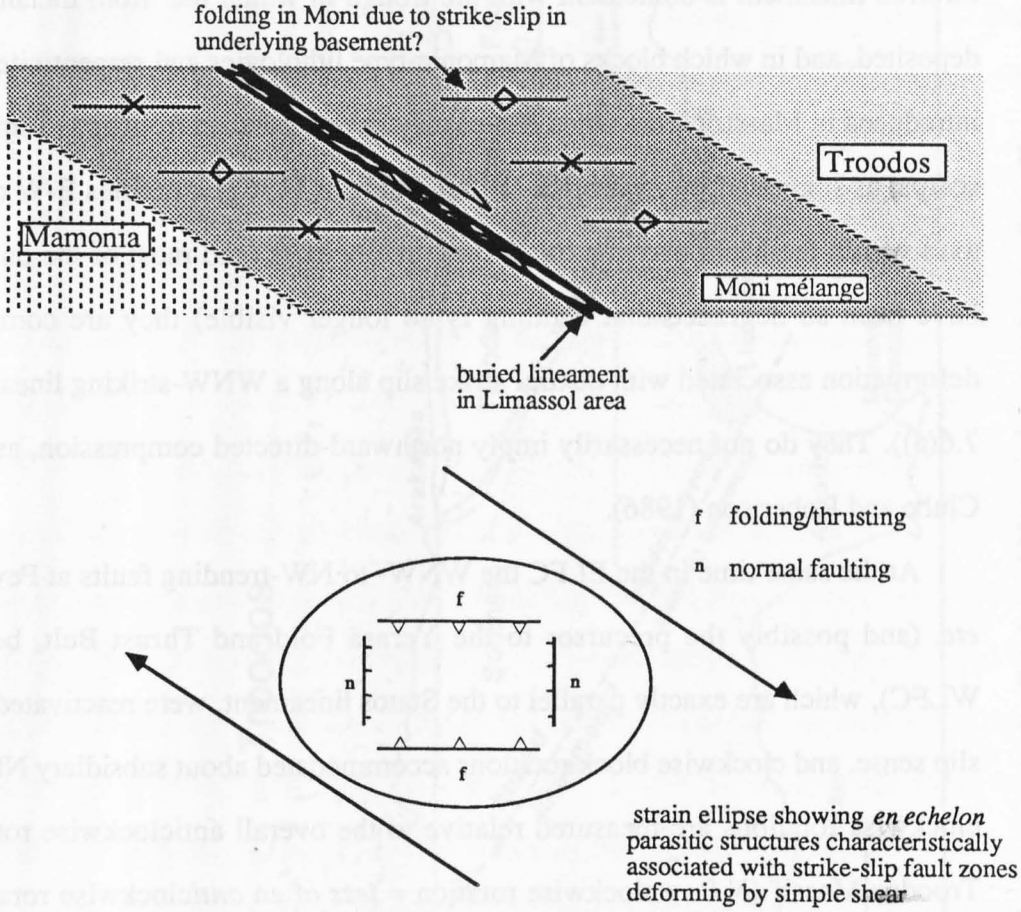

sketch section:

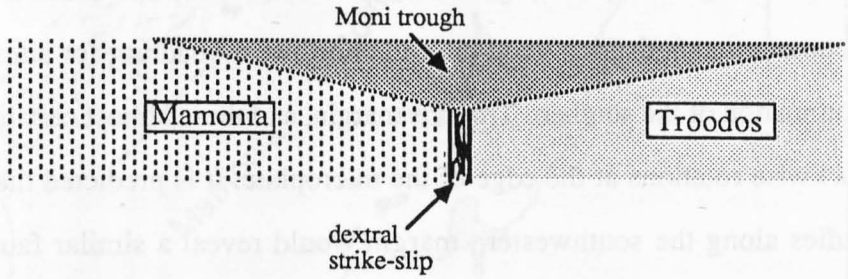

Figure 7.6 (a): Schematic illustration of fold orientations within the Moni mélange, and their interpretation as a response to strike-slip movement along the underlying Troodos–Mamonia lineament. Present-day north is up the page.

(b)

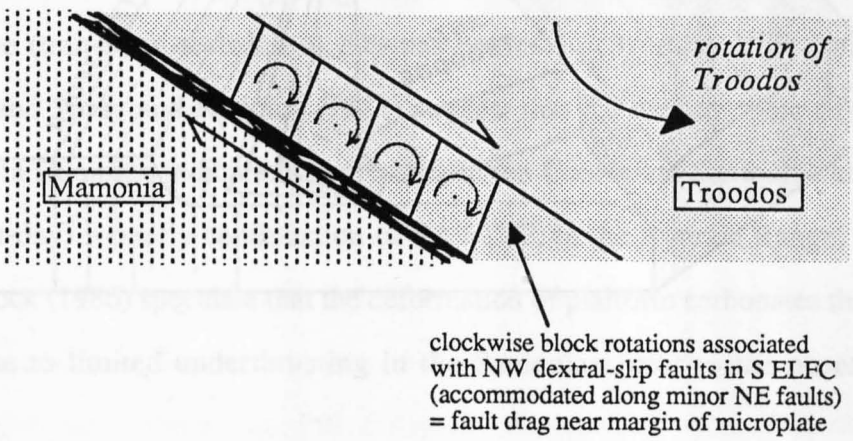

Figure 7.6 (b): Schematic illustration of clockwise block rotations close to (but not necessarily at) the margin of the Troodos ophiolite, induced during the overall anticlockwise rotation of the microplate.

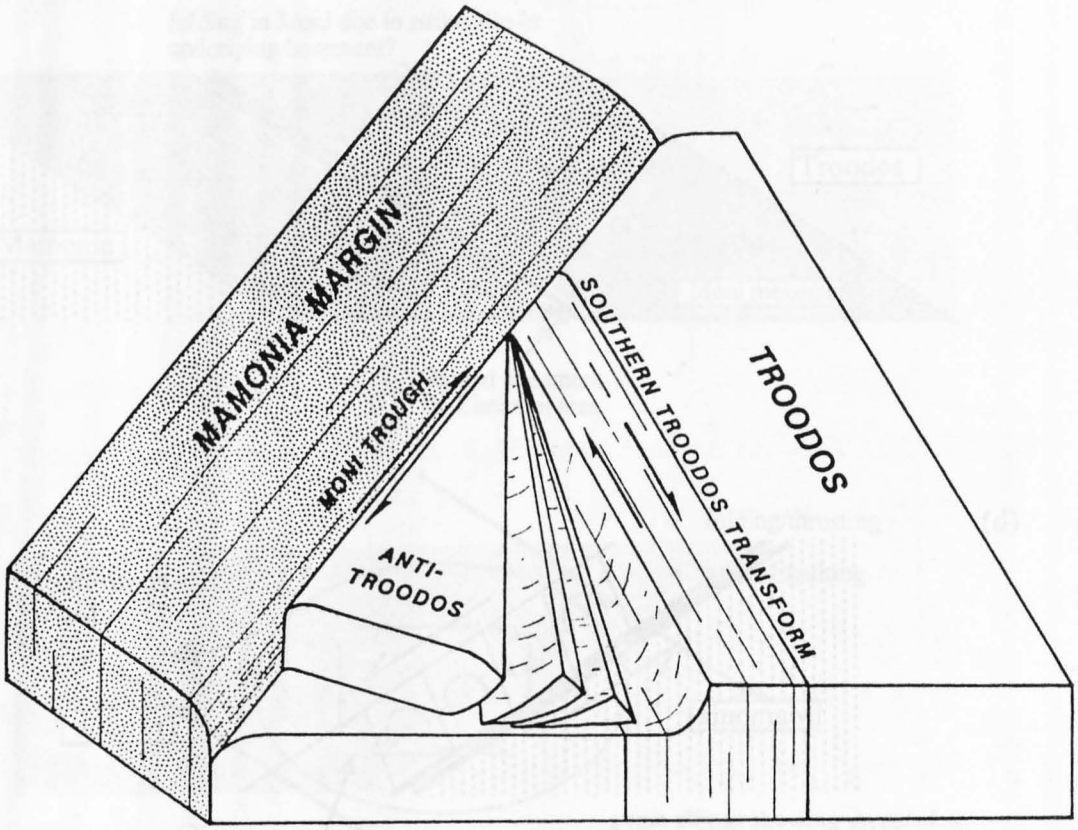

Figure 7.7: Suggested configuration of the southern Troodos margin in the early Maastrichtian. Significant anticlockwise rotation of Troodos ophiolite has commenced, and the ophiolite has been brought close to the fragmented remnants of a Mesozoic passive margin ('Mamonia margin') along a dextral strike-slip lineament blanketed by bentonite clay (the 'Moni trough'). In the vicinity of southern Troodos the lineament is slightly oblique to the trend of the Southern Troodos Transform Fault, thus incorporating transform-tectonised ophiolitic blocks into the Mamonia Complex to the present-day west (details not shown), and preserving a wedge-shaped fragment of the Anti-Troodos plate to the east. Frictional drag imparts localised clockwise block rotations close to the boundary of the rotating microplate, and also along the Southern Troodos Transform Fault itself, where originally sinistrally-slipping faults are reactivated in a dextral sense.

of a protracted period of tectonism in the ELFC. Over the preceding period, from the cessation of volcanism in the Turonian right up to the onset of microplate rotation–some 20Ma–the transform fault was subjected to sustained oblique extensional reactivation.

In order to investigate the significance of the post-magmatic extension it is necessary to examine the nature of deformation occurring in adjoining areas at the same period of time. Unfortunately only limited evidence has so far been documented. Along the western margin of Troodos northward-directed thrusting has been recognised (C. Xenophontos *pers. comm.* 1986), but this appears to involve the Kannaviou Formation and so is likely to be of Maastrichtian or later age. Early thrusting has, however, been reported from the (transform-tectonised) Akamas peninsula (Brumley J. Marton *pers. comm.* 1988), and Spray and Roddick (1981) suggest that the metamorphic slivers within the Mamonia Complex indicate transpression in the Coniacian–Santonian along a possible (present-day) westerly continuation of the STTF. In the Kyrenia Range, Robertson and Woodcock (1986) speculate that the deformation of platform carbonates there occurred in response to limited underthrusting in the Santonian prior to the onset of strike-slip faulting.

On the northern flank of the Troodos Massif the angular conformity of the Perapedhi–Lefkara sequences, spanning the Turonian to Maastrichtian interval, suggests that this area was situated in a stable, internal portion of what was to become the microplate. Deformation along the southern Troodos margin at this time, in contrast, presumably reflects the response of a weak lineament (*i.e.* the transform fault) to stress applied to an otherwise rigid platelet. The observations quoted above from southwestern Cyprus, suggesting that the original continuation of the transform to the present-day west was subjected to transpression or compression prior to microplate rotation, at the same time as the transform in the vicinity of the ELFC was undergoing extension, are compatible with the interpretation that this stress was an anticlockwise torque, applied about a local pole of rotation.

7.5.4 Implications for rotation mechanisms

The interpretation of the Turonian–Campanian extension across the STTF as a response to an anticlockwise torque has implications for possible mechanisms of microplate rotation. Various plate tectonic configurations that might account for the rotation have been proposed by previous authors, and in addition several environments where analogous rotations have taken place in the recent past have been identified. These are depicted in cartoon form in figure 7.8 and discussed briefly in the light of new constraints imposed by the present study.

Any model for the rotation must take into account the geochemical evidence that requires Troodos to have been created above a subduction zone. Most authors believe that this subduction zone dipped northwards beneath Troodos in the Upper Cretaceous, similar to the present day subduction configuration (see chapter 1), from regional considerations (Sengör and Yilmaz 1981, Robertson and Dixon 1985), and by analogy with other Neotethyan ophiolites to the east (*viz.* Baër-Bassit and Hatay), which were emplaced southwards onto the Arabian continental margin in the late Campanian to early Maastrichtian (Parrot 1977b, Tinkler *et al.* 1981).

The model preferred here notes the exact coincidence in timing between the emplacement of Baër-Bassit and Hatay and the major part of the rotation of the Cyprus microplate. It is suggested, following Clube and Robertson (1986), that rotation may have taken place with the collision of the major continental promontary of Arabia with a northward dipping intraoceanic subduction zone (model (e), figure 7.8). No collision occurs to the west, but an anticlockwise torque is induced in the over-riding plate, causing its fragmentation and potential anticlockwise rotation. Although final emplacement of the ophiolites took place in the Campanian–Maastrichtian, K-Ar radiometric age dates of 88 ± 2Ma from the metamorphic sole of Baër-Bassit (Thuizat *et al.* 1981) indicate that compressional deformation and intra-oceanic slicing was

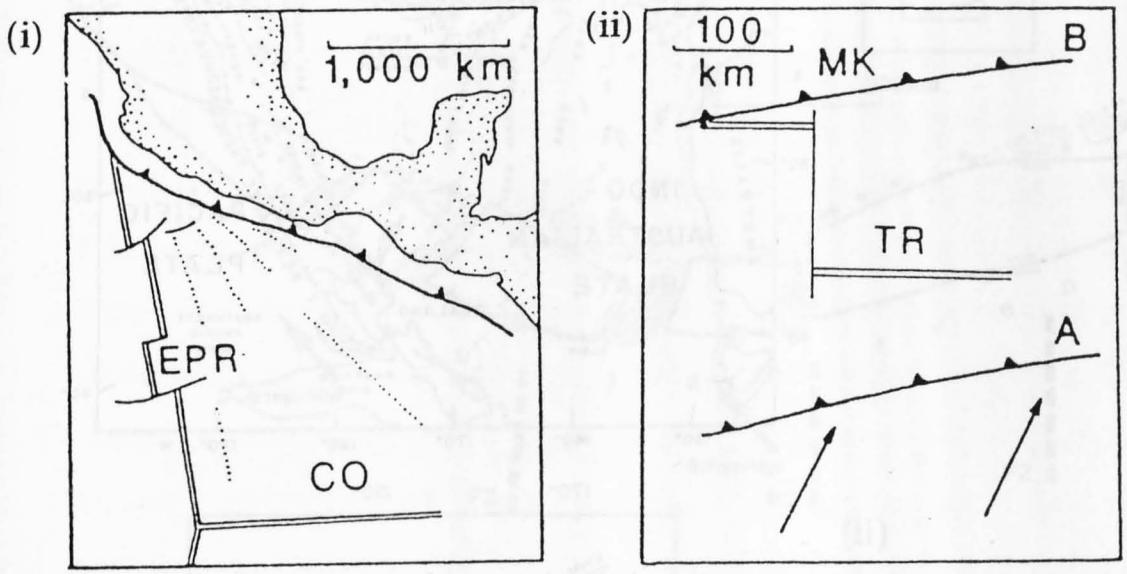

Figure 7.8 (a): is based upon present-day observations of the fragmentation and anticlockwise rotation of the Farallon plate upon its subduction beneath the west coast of North America (diagram (i)). Rotation is interpreted as a response to the difficulty of subducting young, hot, buoyant lithosphere (Atwater 1970). The position of the rotating plate on the downgoing slab requires, in the context of Cyprus, either a reversal of subduction polarity from southward- to northward-dipping subduction zone, similar to that inferred for the Woodlark Basin to the northeast of Australia (E.M. Moores *pers. comm.* 1987), or a second subduction zone of similar polarity dipping beneath the first to account for the geochemistry (diagram (ii)). There is no evidence for any subduction flip beneath the southern part of Neotethys (Sengör and Yilmaz 1981); however, Clube *et al.* (1985) and Clube and Robertson (1986) suggest that northward subduction beneath the Kyrenia Range in the Santonian in addition to (northward) subduction to the south of Cyprus may have facilitated rotation in the manner described above (diagrams from Clube *et al.* 1985). (i) EPR = East Pacific Rise; CO = Cocos Ridge. (ii) MK = Kyrenia margin; TR = Troodos.

(i)

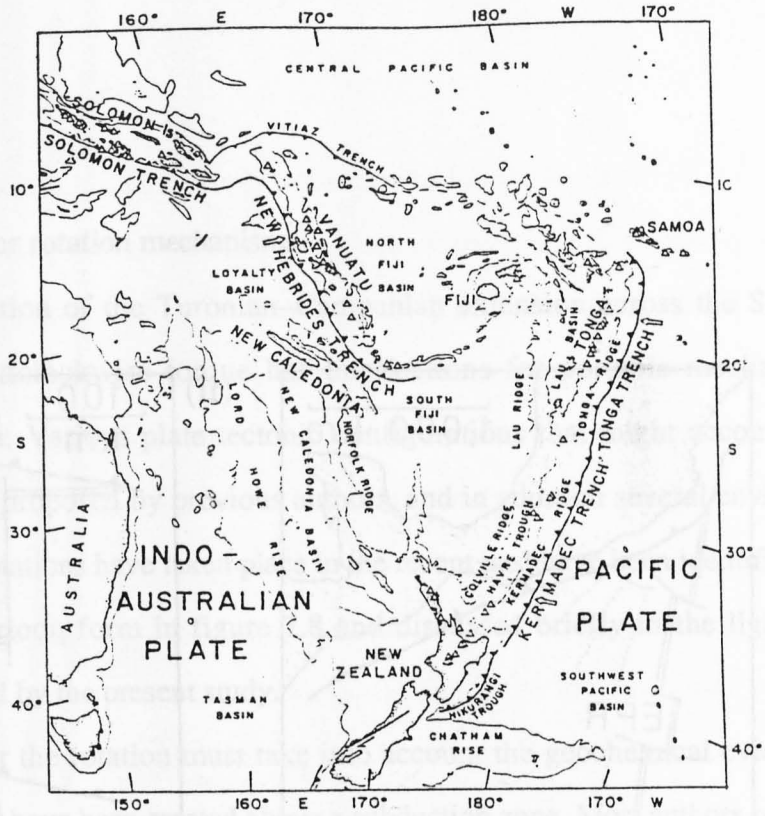

(ii)

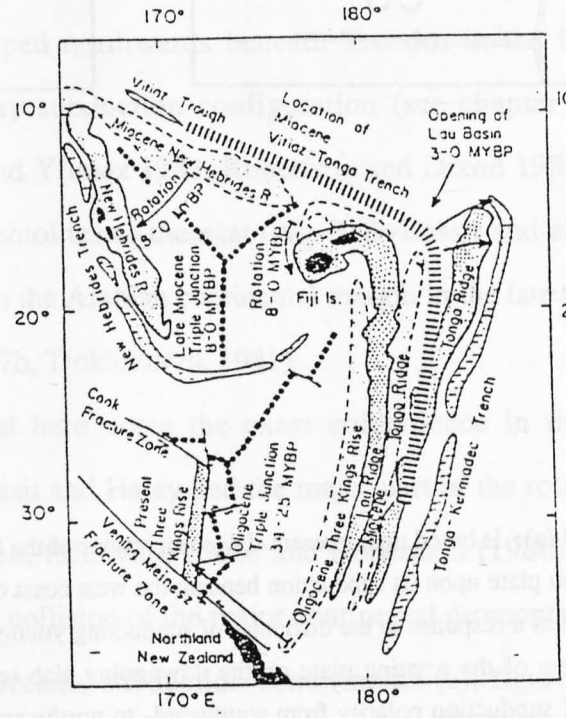

Figure 7.8 (b): follows observations from the Fiji–Lau basins from the Western Pacific, where a 90° anticlockwise rotation of the island of Viti Levu has occurred. Viti Levu is situated in a broad zone of distributed deformation close to a trench–trench transform (Malahoff *et al.* 1982, Hamburger and Isacks 1988), and rotation has been accommodated by complex reorientations of spreading centres and short-lived propagating rifts. There is no evidence from the Eastern Mediterranean of magmatism having continued whilst rotation was under way, nor for the creation of the Neotothyan ophiolites at a trench–trench transform; however, the spreading geometry in the supra-subduction zone Fiji–Lau basins offers a useful illustration of potential complexities in spreading processes during the creation of Troodos (*cf.* Varga and Moores 1985). (i) from Hamburger and Isacks (1988); (ii) from Malahoff *et al.* (1982).

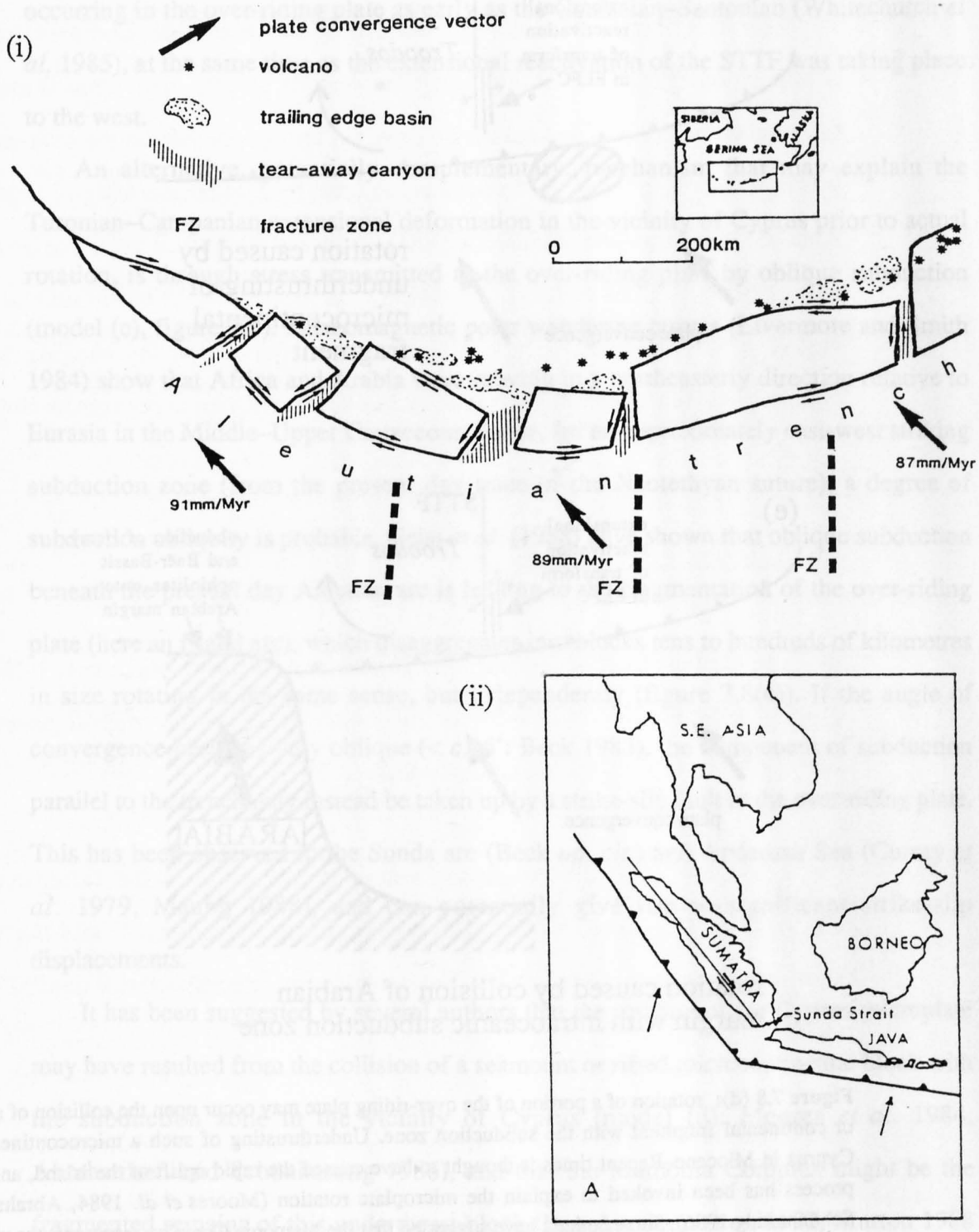

Figure 7.8 (c): illustrates a mechanism for block rotation in the over-riding plate in response to oblique subduction. Geist *et al.* (1988) have recently described the disaggregation of the Aleutian island arc and large-scale block rotation within such a setting (diagram (i)). At angles of convergence more oblique than *c.*45° the applied torque may instead be accommodated by formation of a strike-slip fault in the over-riding plate (diagram (ii): Beck 1983).

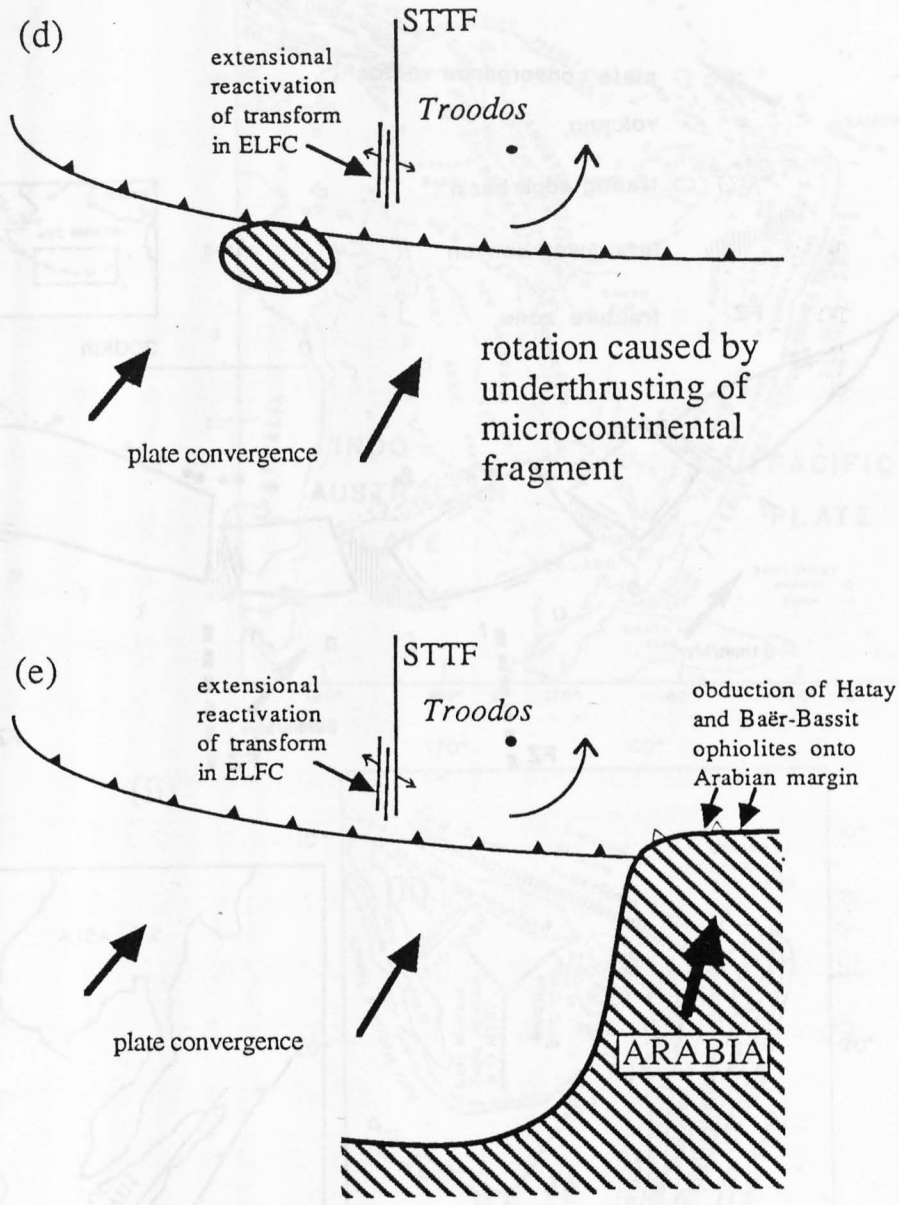

Figure 7.8 (d): rotation of a portion of the over-riding plate may occur upon the collision of a seamount or continental fragment with the subduction zone. Underthrusting of such a microcontinent beneath Cyprus in Miocene–Recent times is thought to have caused the rapid uplift of the island, and a similar process has been invoked to explain the microplate rotation (Moores *et al.* 1984, Abrahamsen and Schönharting 1986). Some authors have suggested that the Mamonia Complex represents the remnants of this underthrust block (Ben-Avraham *et al.* 1982, Murton 1988 *in prep.*); however, this is difficult to reconcile with evidence from the ELFC for extension in the oceanic upper plate at this time.

(e): The preferred model: a variation of model (d) in which fragmentation and anticlockwise rotation of the 'fore-arc' occurs with the collision of a major continental promontary (here Arabia) to the east with the subduction zone. This model can explain the southward obduction of ophiolites (*viz.* Hatay, Baër-Bassit) onto the continental margin at the same time as rotation is taking place to the west, and also reconcile evidence for extensional deformation in the 'fore-arc' prior to and during rotation.

occurring in the over-riding plate as early as the Coniacian–Santonian (Whitechurch *et al.* 1985), at the same time as the extensional reactivation of the STTF was taking place to the west.

An alternative, potentially complementary, mechanism that may explain the Turonian–Campanian extensional deformation in the vicinity of Cyprus prior to actual rotation, is through stress transmitted to the over-riding plate by oblique subduction (model (c), figure 7.8). Palaeomagnetic polar wandering curves (Livermore and Smith 1984) show that Africa and Arabia were moving in a northeasterly direction relative to Eurasia in the Middle–Upper Cretaceous; hence, for an approximately east-west striking subduction zone (from the present day trace of the Neotethyan suture), a degree of subduction obliquity is probable. Geist *et al.* (1988) have shown that oblique subduction beneath the present day Aleutian arc is leading to the fragmentation of the over-riding plate (here an island arc), which disaggregates into blocks tens to hundreds of kilometres in size rotating in the same sense, but independently (figure 7.8(c)). If the angle of convergence becomes very oblique (< *c.*45°: Beck 1983), the component of subduction parallel to the trench may instead be taken up by a strike-slip fault in the over-riding plate. This has been observed in the Sunda arc (Beck *op. cit.*) and Andaman Sea (Curray *et al.* 1979, Maung 1988), and can potentially give rise to significant strike-slip displacements.

It has been suggested by several authors that the rotation of the Cyprus microplate may have resulted from the collision of a seamount or rifted microcontinental block with the subduction zone in the vicinity of Cyprus (model (d): Moores *et al.* 1984, Abrahamsen and Schönharting 1986), and that the Mamonia Complex might be the fragmented remains of this underthrust block (Ben-Avraham *et al.* 1982, Murton 1988 *in prep.*). Although Cyprus has undoubtedly been underthrust by such material in the Miocene–Recent, such a collisional model is *not* compatible with evidence from the ELFC for sustained extension in the period leading up to rotation and *cannot* account for the actual rotation of the microplate.

The exact status and tectonic setting of the Mamonia Complex prior to its juxtaposition against the Troodos ophiolite remains unclear, with opinion divided as to the original position of the continental margin rocks, whether on the over-riding plate (perhaps separated from the Troodos ocean crust by a transform margin, as inferred for Antalya: Robertson and Woodcock 1985, Clube and Robertson 1986), or on the down-going slab (I.G. Gass *pers. comm.* 1988). The possibility of the Mamonia Complex having being transported significant distances laterally on the hanging wall of an obliquely consuming subduction zone (*à la* Beck 1983) should perhaps be emphasised.

7.6 Summary of Conclusions

(i) The northern part of the ELFC was deformed in a 5km wide, now E-W trending fossil transform fault. To the south of this transform a fragment of crust generated at an Anti-Troodos ridge axis is recognised within the ELFC.

(ii) Immediately after the cessation of volcanism in the area, in the Turonian (*c.*90Ma), the Troodos and Anti-Troodos plates were obliquely separated, and the transform reactivated as a normal fault system. Extensional activity persisted until (late?) Campanian times (*c.*72Ma).

(iii) In the late Campanian to early Maastrichtian interval the Troodos ophiolite suffered *c.*60° of anticlockwise rotation, and was juxtaposed by movement along arcuate strike-slip fault lineaments against the Mamonia Complex, which represents the fragmented remains of a Mesozoic passive margin. At the same time in the southern ELFC NW-trending faults, parallel to the inferred Troodos–Mamonia contact, became dextrally reactivated. Clockwise block rotations about high-angle axes associated with these faults,

and perhaps with E-W transform-related lineaments in the Arakapas Fault Belt also, were induced by fault 'drag' as bulk rotation of the ophiolite proceeded.

(iv) Actual rotation of the Cyprus microplate is thought to be a direct consequence of the collision in Campanian–Maastrichtian times of the Arabian continent to the east with a northward-dipping intraoceanic subduction zone (above which Troodos itself was sited). This collision would have caused the fragmentation and likely anticlockwise rotation of the over-riding plate to the west.

(v) The extensional reactivation of the transform fault in the ELFC prior to actual rotation probably corresponds to an anticlockwise torque put upon the Troodos–Anti-Troodos ocean floor, and was induced either by the initial stages of collision to the east (with the Coniacian–Santonian age of intra-oceanic slicing and metamorphic sole formation in the Baër-Bassit ophiolite), or by oblique subduction beneath Troodos, or a combination of these.

References:

Abbey, S., 1980. Studies in 'standard samples' for use in the general analysis of silicate rocks and minerals. *Geostand. Newslett.* 4, 163-190

Abrahamsen, N. and Schönharting, G., 1986. Palaeomagnetic timing of the rotation and translation of Cyprus. *Earth Planet. Sci. Lett.* 81, 409-418

Adamides, N.G., 1980. The form and environment of formation of the Kalavasos ore deposits–Cyprus. *In:* Panayiotou, A. (ed.), *Proceedings of the International Ophiolite Symposium, Cyprus, 1979.* Cyprus Geological Survey Dept., 117-127

Adamides, N.G., 1984. Cyprus volcanogenic sulphide deposits in relation to their environment of formation. *Unpubl. Ph.D. thesis,* Univ. of Leicester, 383pp.

Aktas, G. and Robertson, A.H.F., 1985. The Maden Complex, SE Turkey: evolution of a Neotethyan active margin. *In:* Dixon, J.E. and Robertson, A.H.F. (eds.), *The Geological Evolution of the Eastern Mediterranean,* Spec. Publ. Geol. Soc. No.17, 375-402

Aldiss, D.T., 1978. Granitic rocks of ophiolites. *Unpubl. Ph.D. thesis,* Open Univ., 198pp.

Allen, C.R., 1975. The petrology of a portion of the Troodos plutonic complex, Cyprus. *Unpubl. Ph.D. thesis,* Univ. of Cambridge, 161pp.

Allerton, W.S.Q., 1988. Palaeomagnetic and structural studies of the Troodos ophiolite, Cyprus. *Unpubl. Ph.D. thesis,* Univ. East Anglia, 232pp.

Allerton, W.S.Q. and Vine, F.J., 1987. Spreading structure of the Troodos ophiolite, Cyprus: some palaeomagnetic constraints. *Geology* 15, 593-597

Anderson, E.M., 1951. The dynamics of faulting and dyke formation with implications to Britain. Oliver and Boyd (Edinburgh and London) Second Edition 206pp.

Angelier, J. and Mechler, P., 1977. Sur une méthode graphique de recherche des constraintes principales également utilisable en tectonique et en séismologie: la méthode des dièdres droits. *Bull. Soc. Geol. Fr.* 19, 1309-1318

Anonymous, 1972. Penrose field conference on ophiolites. *Geotimes* 17, 24-25

Aubert, M. and Baroz, F., 1974. Structure profonde de la chaîne du Pentadaktylos et de la Mésaoria (Chypre). *Rév. Inst. Fr. Pét.* 29, 361-373

Auboin, J., 1965. Geosynclines. *Elsevier, Amsterdam* 335pp.

Bagnall, P.S., 1960. The geology and mineral resources of the Pano Lefkara–Larnaca area. *Cyprus Geol. Surv. Dept. Mem.* No.5, 116pp.

Bagnall, P.S., 1964. Wrench faulting in Cyprus. *J. Geol.* 72, 327-345

Baroz, F., 1980. Volcanism and continent–island arc collision in the Pentadaktylos range, Cyprus. *In:* Panayiotou, A. (ed.), *Proceedings of the International Ophiolite Symposium, Cyprus, 1979.* Cyprus Geological Survey Dept., 73-85

Bartholemew, I.D., 1983. The primary structures and fabrics of the upper mantle and lower crust from ophiolite complexes. *Unpubl. Ph.D. thesis*, Open University, 520pp.

Bear, L.M., 1960. The geology and mineral resources of the Akaki-Lythrodonda area. *Cyprus Geol. Surv. Dept. Mem.* No.3, 122pp.

Bear, L.M. and Morel, S.W., 1960. The geology and mineral resources of the Agros–Akrotiri area. *Cyprus Geol. Surv. Dept. Mem.* No.3

Beccaluva, L. and Serri, G., 1988. Boninitic and low-Ti subduction-related lavas from intraoceanic arc–back-arc systems and low-Ti ophiolites: a reappraisal of their petrogenesis and original tectonic setting. *In:* Wezel, F.-C. (ed.) *The origin and evolution of arcs.* Tectonophys. 146, 291-315

Bechon, F., 1982. Evolution spatio-temporelle du volcanisme de la zone d'Arakapas (Chypre). *Unpubl. Ph.D. thesis*, Univ. de Nancy, 116pp.

Beck, M.E., 1983. On the mechanism of tectonic transport in zones of oblique subduction. *Tectonophys.* 93, 1-11

Bellamy, C.V. and Jukes-Browne, A.J., 1905. The Geology of Cyprus. *London, Crown Agents*

Ben-Avraham, Z.; Nur, A. and Jones, D., 1982. The emplacement of ophiolites by collision. *J. Geophys. Res.*87, 3861-3867

Ben-Avraham, Z., Kempler, D. and Ginzburg, A., 1988. Plate convergence in the Cyprean Arc. *In:* Wezel, F.-C. (ed.), The Origin and Evolution of Arcs. *Tectonophys.* 146, 237-240

Benn, K. and Laurent, R., 1987. Intrusive suite documented in the Troodos ophiolite plutonic complex, Cyprus. *Geology* 15, 821-824

Biju-Duval, B.; Lapierre, H. and Letouzey, J., 1976. Is the Troodos Massif (Cyprus) allochthonous? *Bull. Soc. Géol. France* 7 t.XVIII, no.5

Bishopp, D.W., 1952. Some new features of the geology of Cyprus. *Compt. Rend. 19th. Int. Geol. Congr.*15, 13

Blome, C.D. and Irwin, W.P., 1985. Equivalent radiolarian ages from ophiolitic terrains of Cyprus and Oman. *Geology* 13, 401-404

Bonatti, E., 1976. Serpentinite protrusions in the oceanic crust. *Earth Planet. Sci. Lett.* 32, 107-113

Bonatti, E. and Honnorez, J., 1976. Sections of the Earth's Crust in the Equatorial Atlantic. *J. Geophys. Res.* 81, 4104-4116

Bonhommet, N.; Roperch, P. and Calza, F., 1988. Palaeomagnetic arguments for block rotations along the Arakapas fault (Cyprus). *Geology* 16, 422-425

Boström, K. and Peterson, M.N.A., 1966. Precipitates from hydrothermal exhalations of the East Pacific Rise. *Econ. Geol.* 61, 1258-1264

Boström, K. and Peterson, M.N.A., 1969. The origin of aluminium-poor ferromanganoan sediments on active volcanic ridges. *Mar. Geol.* 7, 427-447

Bowen, N.L. and Tuttle, O.F., 1949. The system MgO–SiO_2–H_2O. *Geol. Soc. Am. Bull.* 60, 439-460

Boyle, J.F. and Robertson, A.H.F., 1984. Evolving metallogenesis at the Troodos spreading axis. *In:* Gass, I.G.; Lippard, S.J. and Shelton, A.W. (eds.): *Ophiolites and Oceanic Lithosphere.* Spec. Publ. Geol. Soc. Lond. No. 14, Blackwell Scientific Publ., Oxford, 169-181

Brongniart, A., 1827. Classification et caractères mineralogiques des roches homogènes et hétérogenes. *Paris: F.G. Levrault*

Brooks, C. and Hart, S.R., 1974. On the significance of komatiite. *Geology* 2, 107-110

Brown, M.A., 1982. Chromite deposits and their ultramafic host rocks in the Oman ophiolite. *Unpubl. Ph.D. thesis*, Open University, 263pp.

Browning, P., 1982. The petrology, geochemistry, and structure of the plutonic rocks of the Oman Ophiolite. *Unpubl. Ph.D. thesis*, Open University, 404pp.

Brunn, J.H., 1961. Les sutures ophiolitiques. Contribution à l'étude des relations entre phénomènes magmatique et orogéniques. *Rev. Géogr. Phys. Géol. Dyn.* 4, 89-96, 181-202

Bullard, E.C.; Everett, J.E. and Smith, A.G., 1965. Fit of continents around the Atlantic. *In:* Blackett, P.M.S.; Bullard, E.C. and Runcorn, S.K. (eds.), A Symposium on Continental Drift. *Phil. Trans. Roy. Soc. Lond.* A258, 41-75

Butler, R.W.H., 1982. The terminology of structures in thrust belts. *J. Struct. Geol.* 4, 239-245

Cameron, W.E., 1980. Comment and reply on "Role of multistage melting in the formation of oceanic crust." *Geology* 8, 562

Cameron, W.E., 1985. Petrology and origin of primitive lavas from the Troodos ophiolite, Cyprus. *Contrib. Mineral. Petrol.* 89, 239-255

Cameron, W.E.; McCulloch, M.T. and Walker, D.A., 1983. Boninite petrogenesis: chemical and Nd-Sr isotopic constraints. *Earth Planet. Sci. Lett.* 65, 75-89

Cameron, W.E. and Nisbet, E.G., 1982. Phanerozoic analogues of komatiitic basalts. *In:* Arndt, N.T. and Nisbet, E.G. (eds.) *Komatiites* George Allen & Unwin, 29-50

Cameron, W.E.; Nisbet, E.G. and Dietrich, V.J., 1979. Boninites, komatiites and ophiolitic basalts. *Nature* 280, 550-553

Cann, J.R., 1970. Rb, Sr, Y, Zr, Nb in some ocean-floor basaltic rocks. *Earth Planet. Sci. Lett.* 10, 7-11

Cann, J.R., 1979. Metamorphism in the ocean crust. *In:* Talwani, M.; Harrison, C.G. and Hayes, D.E. (eds.): *Deep drilling results in the Atlantic Ocean Crust.* Maurice Ewing Series 2, A.G.U., Washington, Geodynamics Project, Sci. Rep. 48, 230-238

Carr, J.H. and Bear, L.M., 1960. The geology and mineral resources of the Peristerona–Lagoudhera area. *Cyprus Geol. Surv. Dept. Mem.* No.2, 79pp.

Carter, R.M., 1975. A discussion and classification of sub-aqueous mass transport with particular application to grain-flow, slurry-flow and fluxoturbidites. *Earth Sci. Rev.* 11, 145-177

Casey, J.F. & Karson, J.A., 1981. Magma chamber profiles from the Bay of Islands ophiolite Complex. *Nature* .292, 295-301

Cleintaur, M.R.; Knox, G.J. and Ealey, P.J., 1977. The geology of Cyprus and its place in the Eastern Mediterranean framework. *Geol. Mijn.* 56, 66-82

Clube, T.M.M., 1985. The palaeorotation of the Troodos microplate. *Unpubl. Ph.D. thesis* Univ. of Edinburgh, 275p.

Clube, T.M.M.; Creer, K.M. and Robertson, A.H.F., 1985. Palaeorotation of the Troodos microplate, Cyprus. *Nature* 317, 522-525

Clube, T.M.M. and Robertson, A.H.F., 1986. The palaeorotation of the Troodos microplate, Cyprus, in the Late Mesozoic–Early Cenozoic plate tectonic framework of the Eastern Mediterranean. *Surv. in Geophys.* 8, 375-437

Coish, R.A. and Church, W.R., 1979. Igneous geochemistry of mafic rocks in the Betts Cove ophiolite, Newfoundland. *Contrib. Mineral. Petrol.* 70, 29-39

Coish, R.A.; Hickey, R. and Frey, F.A., 1982. Rare earth element geochemistry of the Betts Cove ophiolite, Newfoundland: complexities in ophiolite formation. *Geochim. Cosmochim. Acta* 46, 2117-2134

Coleman, R.G., 1977. Ophiolites. Ancient Oceanic Lithosphere? *Springer-Verlag* 229pp.

Coleman, R.G. and Peterman, Z.E., 1975. Oceanic plagiogranite. *J. Geophys. Res.* 80, 1099-1108

Constantinou, G., 1972. The geology and genesis of the sulphide ores of Cyprus. *Unpubl. Ph.D. thesis*, University of London, 275pp.

Crawford, A.J.; Beccaluva, L. and Serri, G., 1981. Tectono-magmatic evolution of the West-Philippine–Mariana region and the origin of boninites. *Earth Planet. Sci. Lett.* 54, 346-356

Crawford, A.J. and Cameron, W.E., 1985. Petrology and geochemistry of Cambrian boninites and low-Ti andesites from Heathcote, Victoria. *Contrib. Mineral. Petrol.* 91, 93-104

Crawford, A.J. and Keays, R.R., 1978. Cambrian greenstone belts in Victoria: marginal sea crust slices in the Lachlan Foldbelt of southeastern Australia. *Earth Planet. Sci. Lett.* 41, 197-208

Cullis, C.G. & Edge, A.G., 1927. Report on the cupriferous deposits of Cyprus. London Crown Agents 48pp.

Curray, J.R.; Moore, D.G.; Lawver, L.A.; Emmel, F.J.; Raitt, R.W.; Henry, M. and Kieckhefer, R., 1979. Tectonics of the Andaman Sea and Burma. *In:* Geological and geophysical investigations of continental margins. AAPG Memoir No.29, 189-198

CYAMEX and Pastouret, L., 1981. Submersible structural study of Tamayo transform fault: East Pacific Rise. 23°N (Project Rita). *Marine Geophys. Res.* 4, 381-401

Dallwitz, W.B.; Green, D.H. and Thompson, J.E., 1966. Clinoenstatite in a volcanic rock from the Cape Vogel area, Papua. *J. Petrol.* 7, 375-403

Deer, W.A.; Howie, R.A. and Zussman, J., 1966. An Introduction to the Rock Forming Minerals. Longman, 528pp.

DeSitter, L.U., 1958. Boudins and parasitic folds in relation to cleavage and folding. *Geol. Mijnbouw* 20, 272-286

Dick, H.J.B., 1977. Partial melting in the Josephune peridotite I, the effect on mineral composition and its consequences for geobarometry and geothermometry. *Am. J. Sci.* 277, 801-832

Dietz, R.S., 1961. Continent and ocean basin evolution by speading of the sea floor. *Nature* 190, 854-857

Donaldson, C.H., 1976. An experimental investigation of olivine morphology. *Contrib. Mineral. Petrol.* 57, 183-213

Dubertret, L., 1955. Geologie des roches vertes du Nord-Ouest de la Syrie et du Hatay. *Notes et mem. Moyen-Orient* 6, 2-179

Duncan, R.A. and Green, D.H., 1980. Role of multistage melting in the formation of oceanic crust. *Geology* 8, 22-26

Duncan, R.A. and Green, D.H., 1987. The genesis of refractory melts in the formation of oceanic crust. *Contrib. Mineral. Petrol.* 96, 326-342

Ealey, P.J. and Knox, G.J., 1975. The pre-Tertiary rocks of SW Cyprus. *Geol. Mijn.* 54, 85-100

Eaton, S., 1986. The sedimentology of Mid-Late Miocene carbonates and evaporites in Southern Cyprus. *Unpubl. Ph.D. thesis*, University of Edinburgh.

Elthon, D. and Stern, C., 1978. Metamorphic petrology of the Sarmiento ophiolite complex, Chile. *Geology* 6, 464-468

Ewart, A. and Bryan, W.B., 1972. Petrography and geochemistry of the igneous rocks from Eua, Tongan Islands. *Geol. Soc. Am. Bull.* 83, 3281

Flower, M.F.J. and Levine, H.M., 1987. Petrogenesis of a tholeiite–boninite sequence from Ayios Mamas, Troodos ophiolite: evidence for splitting of a volcanic arc? *Contrib. Mineral. Petrol.* 97, 509-524

Fox, P.J. and Gallo, D.G., 1984. A tectonic model for ridge transform–ridge plate boundaries: implications for the structure of oceanic lithosphere. *Tectonophys.* 104, 205-242

Frey, F.A.; Suen, C.J. and Stockman, H.W., 1985. The Ronda high temperature peridotite: Geochemistry and petrogenesis. *Geochim. Cosmochim. Acta* 49, 2469-2491

Gass, I.G., 1958. Ultrabasic pillow lavas from Cyprus. *Geol. Mag.* 95, 241-251

Gass, I.G., 1959. Geology of the Akamas peninsula. *Cyprus Geol. Surv. Dept. Ann. Rept. for 1958* 18-28

Gass, I.G., 1960. The geology and mineral resources of the Dhali area. *Cyprus Geol. Surv. Dept. Mem.* No.4, 116pp.

Gass, I.G., 1968. Is the Troodos Massif of Cyprus a Fragment of Mesozoic Ocean Floor? *Nature* v.220, 39-42

Gass, I.G., 1980. The Troodos massif: Its role in the unravelling of the ophiolite problem and its significance in the understanding of constructive plate margin processes. *In:* Panayiotou, A. *(ed.), Proceedings of the International Ophiolite Symposium, Cyprus, 1979.* Cyprus Geological Survey Dept., 23-35

Gass, I.G. & Masson-Smith, D., 1963. The geology and gravity anomalies of the Troodos Massif, Cyprus. *Phil. Trans. Roy. Soc.* v. A255, 417-467

Gass, I.G.; Neary, C.R.; Plant, J.; Robertson, A.H.F.; Simonian, K.O.; Smewing, J.D.; Spooner, E.T.C. and Wilson, R.A.M., 1975. Comments on "The Troodos ophiolitic complex was probably formed in an island arc" by A. Miyashiro and subsequent correspondence by A. Hynes and A. Miyashiro. *Earth Planet. Sci. Lett.* 25, 236-238

Gass, I.G. & Smewing, J.D., 1973. Intrusion, extrusion and metamorphism at constructive plate margins: evidence from the Troodos Massif, Cyprus. *Nature* 242, 26-29

Gass, I.G. & Smewing, J.D., 1981. Ophiolites: obducted oceanic lithosphere. *In:* Emiliani, C. (ed.): *The Sea (Vol. VII): The Oceanic Lithosphere.* Wiley Interscience, 339-362

Gaudry, A., 1862. Géologie de l'île de Chypre. *Mem. Soc. Geol. France* Sér. 2, vii 149

Geist, E.L.; Childs, J.R. and Scholl, D.W., 1988. The origin of summit basins of th Aleutian ridge: implications for block rotation of an arc massif. *Tectonics* 7, 327-341

George, R.P., Jr., 1975. The internal structure of the Troodos ultramafic complex, Cyprus. *Unpubl. Ph.D. thesis,* Stony Brook, State Univ. New York, 223pp.

George, R.P., Jr., 1978. Structural petrology of the Olympus ultramafic complex in the Troodos ophiolite, Cyprus. *Geol. Soc. Am. Bull.* 89, 845-865

Georgiou, E., 1987. The Akapnou Forest plutonic complex and the associated chromite occurrences. *Abstracts of Papers, Troodos 87 Ophiolites and Oceanic Lithosphere.* Geol. Surv. Dept., Nicosia, Cyprus, 139

Gibbs, A.D., 1984. Structural Evolution of Extensional Basin Margins. *J. Geol. Soc. London.* 141, 609-620

Gillis, K.M. and Robinson, P.T., 1988. Distribution of alteration zones in the upper oceanic crust. *Geology* 16, 262-266

Gomez, B., 1987. The alluvial terraces and fills of the Lower Vasilikos Valley, in the vicinity of Kalavasos, Cyprus. *Trans. Inst. Br. Geogr.* NS12, 345-359

Gordon-Smith, J., 1963. An Interim Report on the Kalavasos Mines. *Unpubl. manuscript* Hellenic Mining Co., Cyprus.

Greenbaum, D., 1972. Magmatic processes at ocean ridges: evidence from the Troodos Massif, Cyprus. *Nature Phys. Sci.* 238, 18-21

Green, D.H., 1973. Experimental studies on a model upper mantle composition at high pressure under water-saturated and water-undersaturated conditions. *Earth Planet. Sci. Lett.* 19, 37-53

Green, D.H., 1976. Experimental testing of "equilibrium" partial melting of peridotite under water-saturated, high-pressure conditions. *Canadian Mineralogist* 14, 255-268

Gregory, R.T. and Taylor, H.P., Jr., 1981. An oxygen isotope profile in a section of Cretaceous oceanic crust, Samail ophiolite: evidence for $\delta^{18}O$ buffering of the oceans by deep (>5km) seawater–hydrothermal circulation at mid-ocean ridges. *J. Geophys. Res.* 86, 2737-2755

Guillemot, D. and Nesteroff, W.D., 1980. Les dépots métallifères crétacés de Chypre: comparaison avec leurs homologues actuals du Pacifique. *In:* Panayiotou, A. (ed.), *Proceedings of the International Ophiolite Symposium, Cyprus, 1979.* Cyprus Geological Survey Dept., 139-146

Hadjistavrinou, Y. and Constantinou, G., 1977. Hydrogeology of the Akrotiri peninsula. *Cyprus Geol. Surv. Dept. Bull.* No.7

Hall, J.M.; Fisher, B.E.; Walls, C.C.; Hall, S.L.; Johnson, P.H.; Bakor, A.R.; Agrawal, V.; Persaud, M. and Sumaiang, R.M., 1987. Vertical distribution and alteration of dykes in a profile through the Troodos Ophiolite. *Nature* 326, 780-782

Hallam, A.; Hancock, J.M.; La Brecque, J.L.; Lowrie, W. and Channell, J.E.T., 1985. Jurassic to Palaeogene: Part I. *In:* Snelling, N.J. (ed.), The Chronology of the Geological Record. *Mem. Geol. Soc. Lond.* No.10, 118-140

Hancock, P.L., 1985. Brittle microtectonics: principles and practice. *J. Struct. Geol.* 7, 437-457

Hanson, G.N., 1980. Rare earth elements in petrogenetic studies of igneous systems. *Ann. Rev. Earth Planet. Sci.* 8, 371-406

Harte, B., 1976. Rock nomenclature with particular relation to deformation and recrystallisation temperatures i nolivine-bearing xenoliths. *J. Geol.* 85, 279-288

Henson, S.R.F.; Browne, R.V. and McGinty, J., 1949. Synopsis of the stratigraphic and geological history of Cyprus. *Q. Jl. Geol. Soc. Lond.* 105, 1-41

Hess, H.H., 1962. History of Ocean Basins. *In:* Petrologic studies: a volume to honour A.F. Buddington. *Geol. Soc. America* 599-620

Hickey, R.L. and Frey, F.A., 1982. Geochemical characteristics of boninite series volcanics: implications for their source. *Geochim. Cosmochim. Acta* 46, 2099-2115

Hubbert, M.K. and Rubey, W.W., 1959. Role of fluid pressure in mechanics of overthrust faulting: I. Mechanisms of fluid-filled porous solids and its application to overthrust faulting. *Geol. Soc. Am. Bull.* 70, 115-166

Huppert, H.E. and Sparks, R.S.J., 1980a. Restrictions on the compositions of mid-ocean ridge basalts: a fluid dynamical investigation. *Nature* 286, 46-48

Huppert, H.E. and Sparks, R.S.J., 1980b. The fluid dynamics of a basaltic magma chamber replenished by influx of hot, dense ultrabasic magma. *Contrib. Mineral. Petrol.* 75, 279-289

Huppert, H.E. and Sparks, R.S.J., 1985. Cooling and contamination of mafic and ultramafic magmas during ascent through continental crust. *Earth Planet. Sci. Lett.* 74, 371-386

Hynes, A., 1975. Comment on "The Troodos ophiolitic complex was probably formed in an island arc" by A. Miyashiro. *Earth Planet. Sci. Lett.* 25, 213-216

Irving, A.J., 1978. A review of experimental studies of crystal/liquid partitioning. *Geochim. Cosmochim. Acta* 42, 743-770

Ismail, I.A.H. and Murrell, S.A.F., 1976. Dilatancy and the strength of rocks containing pore water under undrained conditions. *Geophys. J. Roy. astron. Soc. London* 44, 107-134

Jackson, E.D., 1961. Primary textures and mineral associations in the ultramafic zone of the Stillwater Complex, Montana. *USGS Prof. Paper* 358, 106pp.

Jackson, E.D., 1971. The origin of ultramafic rocks by cumulus processes. *Fortschr. Mineralogie* 48, 128-174

Jackson, J.A. and McKenzie, D.P., 1983. The geometrical evolution of normal fault systems. *J. Struct. Geol.* 5, 471-482

Jankhof, K., 1945. Changes in ground level produced by the earthquakes of April 14 to 18 1928 in southern Bulgaria. *In: Tremblements de Terre en Bulgarie* 29-31, Institut meteorologique central de Bulgarie, Sofia, 131-136 (in Bulgarian)

Jørgensen, K.A. and Brooks, C.K., 1981. The Troodos ophiolite: petrology of a fresh glassy basalt. *Bull. Geol. Soc. Denmark* 30, 43-50

Kempler, D. and Ben-Avraham, Z., 1987. The tectonic evolution of the Cyprean Arc. *Annales Tectonicae* 1, 58-71

Kidd, R.G.W., 1977. A model for the process of formation of the upper oceanic crust. *Geophys. J. Roy. astron. Soc. London* 50, 149-183

Kidd, R.G.W. and Cann, J.R., 1974. Chilling statistics indicate an ocean floor spreading origin for the Troodos complex, Cyprus. *Earth Planet. Sci. Lett.* 24, 151-155

Kikuchi, Y., 1890. On pyroxenic components in certain volcanic rocks from Bonin Islands. *J. Colloid Sci. Imp. Jpn.* 3, 67-89

Komatsu, M., 1980. Clinoenstatite in volcanic rocks from the Bonin Islands. *Contrib. Mineral. Petrol.* 74, 329-338

Kushiro, I., 1969. The system forsterite–diopside–silica with and without water at high pressures. *Am. J. Sci.* 267-A, 269

Kushiro, I., 1972. Effect of water on the composition of magmas formed at high pressures. *J. Petrol.* 13, 311-314

Lapierre, H., 1975. Les formations sédimentaires et éruptives des nappes de Mamonia et leurs relations avec le massif de Troodos (Chypre occidentale). *Mém. Soc. géol. Fr., Paris* 123, 420pp.

Lapierre, H. and Rocci, G., 1967. Le massif pluto-volcanique basique de Kellaki, (Chypre) I–Étude pétrographique et structurale. *Sciences de la Terre* 12, 145-181

Lauer, J.-P., 1985. Geodynamic evolution of Turkey and Cyprus based on palaeomagnetic data. *In:* Dixon, J.E. and Robertson, A.H.F. (eds.), *The Geological Evolution of the Eastern Mediterranean,* Spec. Publ. Geol. Soc. No.17, 483-491

Liou, J.G., 1974. Mineralogy and chemistry of glassy basalts, Coastal Range ophiolites, Taiwan. *Geol. Soc. Am. Bull.* 85, 1-10

Lippard, S.J.; Shelton, A.W. & Gass, I.G., 1986. The ophiolite of northern Oman. *Mem. Geol. Soc. Lond.* No.11, 178pp.

Lister, G.S.; Etheridge, M.A. and Symonds, P.A., 1986. Detachment faulting and the evolution of passive continental margins. *Geology* 14, 246-250

Livermore, R.A. and Smith, A.G., 1984. Some boundary conditions for the evolution of the Mediterranean region. *In:* NATO A.R.I., Erice, Sicily. Volume on Mediterranean tectonics.

Loizides, G., 1971. Geological Report on Kalavasos Proposed Damsite. *Unpubl. Rep. Cyprus Geol. Surv. Dept.* Nicosia, Cyprus, 26pp.

Lonsdale, P., 1977. Deep-tow observations at the mounds abyssal hydrothermal field, Galapagos Rift. *Earth Planet. Sci. Lett.* 36, 92-110

Luyendyk, B.P.; Kamerling, M.J. and Terres, R., 1980. Geometric model for Neogene crustal rotations in southern California. *Geol. Soc. Am. Bull.* 91, 211-217

Macdonald, A.H. and Fyfe, W.S., 1985. Rate of serpentinisation in seafloor environments. *Tectonophys.* 116, 123-135

Macdonald, K.C., 1982. Mid-ocean ridges: fine-scale tectonic, volcanic and hydrothermal processes within the plate boundary zone. *Ann. Rev. Earth Planet. Sci. Lett.* 10, 155-90

Macdonald, K.C.; Kastens, K.; Miller, S. and Spiess, F.N., 1979. Deep-tow studies of the Tamayo transform fault. *Mar. Geophys. Res.* 4, 37-70

Macdonald, W.D., 1980. Net tectonic rotation, apparent tectonic rotation, and the structural tilt correction in palaeomagnetic studies. *J. Geophys. Res.* B7, 3659-3669

Malahoff, A.; Hammond, S.R.; Naughton, J.J.; Keeling, D.L. and Richmond, R.N., 1982. Geophysical evidence for post-Miocene rotation of the island of Viti Levu, Fiji, and its relationship to the tectonic development of the North Fiji Basin. *Earth Planet. Sci. Lett.* 57, 398-414

Malpas, J.; Calon, T. and Xenophontos, C., 1987. Plutonic rocks of the Troodos ophiolite.*In:* Xenophontos, C. and Malpas, J. (eds.) *Troodos 87 Ophiolites and Oceanic Lithosphere.*Field Excursion Guidebook. Geol. Surv. Dept., Nicosia, Cyprus, 158-181

Malpas, J. and Robinson, P.T., 1987. Chromite Mineralisation in the Troodos Ophiolite, Cyprus. *In:* Stowe, C.W. (ed.): *Evolution of Chromium Ore Fields.* Van Nostrand Reinhold, 220-237

Malpas, J. and Xenophontos, C., 1987. The Mamonia Complex and its relation to the Troodos ophiolite. *In:* Xenophontos, C. and Malpas, J. (eds.) *Troodos 87 Ophiolites and Oceanic Lithosphere.*Field Excursion Guidebook. Geol. Surv. Dept., Nicosia, Cyprus, 234-259

Maltman, A.J., 1978. Serpentinite textures in Anglesey, North Wales, United Kingdom. *Geol. Soc. Am. Bull.* 89, 972-980

Mantis, M., 1970. Upper Cretaceous-Tertiary Foraminiferal Zones in Cyprus. *Sci. Res. Centre Cyprus, Epithris,* 3, 227-241

Maung, H., 1987. Transcurrent movements in the Burma–Andaman Sea region. *Geology* 15, 911-912

McBirney, A.R. and Noyes, R.M., 1979. Crystallisation and layereing of the Skaergaard intrusion. *J. Petrol.* 20, 487-554

McCulloch, M.T. and Cameron, W.E., 1983. Nd-Sr isotopic study of primitive lavas from the Troodos ophiolite, Cyprus: evidence for a subduction-related setting. *Geology* 11, 727-731

McKenzie, D.P., 1970. Plate tectonics of the Mediterranean region *Nature* 226, 239-243

McKenzie, D.P., 1972. Active tectonics of the Mediterranean region. *Geophys. J. R. Astron. Soc.* 30, 109-185

McKenzie, D.P., 1984. The generation and compaction of partially molten rock. *J. Petrol.* 25, 715-765

McKenzie, D.P., 1985. The extraction of magma from the crust and mantle. *Earth Planet. Sci. Lett.* 74, 81-91

McKenzie, D.P. and Jackson, J.A., 1983. The relationship between strain rates, crustal thickening, palaeomagnetism, finite strain and fault movements within a deforming zone. *Earth Planet. Sci. Lett.* 65, 182-202

McKenzie, D.P. and Jackson, J.A., 1986. A block model of distributed deformation by faulting. *J. Geol. Soc. London* 143, 349-353

Menard, H.W. and Atwater, T., 1969. Origin of fracture zone topography. *Nature* 222, 1037-1040

Menzies, M.A. and Allen, C.R., 1974. Plagioclase lherzolite–residual mantle relationships within two Eastern Mediterranean ophiolites. *Contrib. Mineral. Petrol.* 45, 197-213

Miyashiro, A., 1973. The Troodos ophiolitic complex was probably formed in an osland arc. *Earth Planet. Sci. Lett.* 19, 218-224

Miyashiro, A., 1975a. Origin of the Troodos and other ophiolites: A reply to Hynes. *Earth Planet. Sci. Lett.* 25, 217-222

Miyashiro, A., 1975b. Origin of the Troodos and other ophiolites: A reply to Moores. *Earth Planet. Sci. Lett.* 25, 227-235

Montigny, R.; Bougault, H.; Bottinga, Y. and Allègre, C.J., 1973. Trace element geochemistry and genesis of the Pindos ophiolite suite. *Geochim. Cosmochim. Acta* 37, 2135-2147

Moores, E.M., 1975. Discussion of '"Origin of Troodos and other ophiolites": A reply to Hynes' by Akiho Miyashiro. *Earth Planet. Sci. Lett.* 25, 223-226

Moores, E.M.; Robinson, P.T.; Malpas, J. and Xenophontas, C., 1984. Model for the origin of the Troodos massif, Cyprus, and other mideast ophiolites. *Geology* 12, 500-503

Moores, E.M. and Vine, F.J., 1971. The Troodos Massif, Cyprus and other ophiolites as oceanic crust: evaluation and implications. *Phil. Trans. Roy. Soc. Lond.* A268, 443-466

Morton, W.H. and Black, R., 1975. Crustal attenuation in Afar. *In:* Pilger, A. and Rösler, A. (eds.) *Afar Depression of Ethiopia* Inter-Union Commision on Geodynamics, Sci Rep. 14. E. Schweizerbart'sche Verlagsbuchhandlung, Stuttgart, 55-65

Mousoulos, L., 1957. Συμβολ η εις την μελετην των κοιτασματον Χαλκουχου Σιδηροπυριτου της Νησου Κυπρου. Κοιτασματολογικαι ερευναι εισ την μεταλλαφορον περιοχην Καλαβασου. *Ann. Geol. Pays Hell.* 8, 269-320

Mukasa, S.B. and Ludden, J.N., 1987. Uranium-lead ages of plagiogranites from the Troodos ophiolite, Cyprus, and their tectonic significance. *Geology* 15, 825-828

Murrell, S.A.F. and Ismail, I.A.H., 1976. The effect of decomposition of hydrous minerals on the mechanical properties of rocks at high pressures and temperatures. *Tectonophys.* 31, 207-258

Murton, B.J., 1986a. Anomalous oceanic lithosphere formed in a leaky transform fault: evidence from the Western Limassol Forest Complex, Cyprus. *J. Geol. Soc. London.* 143, 845-854

Murton, B.J., 1986b. The tectonic evolution of the Western Limassol Forest Complex, Cyprus. *Unpubl. Ph.D. thesis,* Open Univ., 332pp.

Murton, B.J. and Gass, I.G., 1986. Western Limassol Forest Complex, Cyprus: Part of an Upper Cretaceous leaky transform fault. *Geology* 14, 255-258

Murton, B.J. and MacLeod, C.J., 1987. The Limassol Forest and Arakapas Fault Belt. *In:* Xenophontos, C. and Malpas, J. (eds.) *Troodos 87 Ophiolites and Oceanic Lithosphere.*Field Excursion Guidebook. Geol. Surv. Dept., Nicosia, Cyprus, 214-233

Nakamura, N., 1974. Determination of REE, Ba, Fe, Mg, Na and K in carbonaceous and ordinary chondrites. *Geochim. Cosmochim. Acta* 38, 757-775

Natland, J.H., 1981. Crystal morphologies and pyroxene compositions in boninites and tholeiitic basalts from Deep Sea Drilling Project Holes 458 and 459B in the Mariana fore-arc region. *In:* Hussong, D.M., Uyeda, S. *et al. Init. Repts. DSDP 60* Washington (US Govt. Printing Office), 681-707

Navon, O. and Stolper, E., 1987. Geochemical consequences of melt percolation: the upper mantle as a chromatographic column. *J. Geol.* 95, 285-307

Nicholls, I.A. and Harris, K.C., 1980. Experimental rare earth element partition coefficients for garnet, clinopyroxene and amphibole coexisting with andesitic and basaltic liquids. *Geochim. Cosmochim. Acta* 44, 287-308

Nicholls, I.A. and Ringwood, A.E., 1973. Effect of water on olivine stability in tholeiites and the production of silica-saturated magmas in the island-arc environment. *J. Geol.* 81, 285-300

Nicolas, A. and Poirier, A., 1976. Crystalline plasticity and solid state flow in metamorphic rocks. Wiley, New York, 444pp.

Nur, A.; Ron, H. and Scotti, O., 1986. Fault mechanics and the kinematics of block rotations. *Geology* 14, 746-749

O'Hara, M.J., 1965. Primary magmas and the origin of basalts. *Scott. J. Geol. 1*, 19-40

O'Hara, M.J., 1985. Importance of the 'shape' of the melting regime during partial melting of the mantle. *Nature* 314, 58-62

Panayiotou, A., 1977. Geology and geochemistry of the Limassol Forest plutonic complex and the associated Cu-Ni-Co-Fe sulphide and chromite deposits, Cyprus. *unpubl. Ph.D thesis,* Univ. New Brunswick, 341pp.

Pantazis, Th. M., 1967. The Geology and Mineral Resources of the Pharmakas-Kalavasos Area. *Cyprus Geol. Surv. Dept. Mem.* No. 8, 190p.

Parrot, J.-F., 1977b. Ophiolites du Nord-Ouest Syrien et evolution de la croute oceanique Tethysienne au cours du Mesozoique. *Tectonophys.* 41, 251-268

Pearce, J.A., 1975. Basalt geochemistry used to investigate past tectonic environments on Cyprus. *Tectonophysics* 25, 41-67.

Pearce, J.A., 1980. Geochemical evidence for the genesis and eruptive setting of lavas from Tethyan ophiolites. *In:* Panayiotou, A. (ed.), *Ophiolites: Proc. Int. Oph. Symp., Cyprus, 1979.* Geol. Surv. Dept., Nicosia, Cyprus, 261-272

Pearce, J.A., 1982. Trace element characteristics of lavas from destructive plate boundaries. *In:* Thorpe, R.S. (ed.), *'Andesites'* John Wiley & Sons, 525-548

Pearce, J.A., 1983. Role of the sub-continental lithosphere in magma genesis at active continental margins. *In:* Hawkesworth, C.J. and Norry, M.J. (eds.) *'Continental Basalts and Mantle Xenoliths'* Shiva Publishing, 230-249

Pearce, J.A. and Cann, J.R., 1971. Ophiolite origin investigated by discriminant analysis using Ti, Zr and Y. *Earth Planet. Sci. Lett.* 12, 339-349

Pearce, J.A. and Cann, J.R., 1973. Tectonic setting of basic volcanic rocks determined using trace element analysis. *Earth Planet. Sci. Lett.* 19, 290-300

Pearce, J.A.; Lippard, S.J. and Roberts, S., 1984. Characteristics and tectonic significance of supra-subduction zone ophiolites. *Spec. Publ. Geol. Soc. Lond.* 16, 77-94

Pedersen R.B., 1986. The nature and significance of magma chamber margins in ophiolites: examples from the Norwegian Caledonides. *Earth Planet. Sci. Lett.* 77, 100-112

Petersen, J., 1891. Der boninit von Peel Island. *Jb. Hamburg. Wiss. Anst.* 8, 341-9

Potts, P.J.; Tindle, A.G. and Isaacs, M.C., 1983. On the precision of electron microprobe data: a new test for the homogeneity of mineral standards. *Am. Min.* 68, 1237-1242

Potts, P.J.; Webb, P.C. and Watson, J.S., 1984. Energy dispersive X-ray fluorescence analysis of silicate rocks for major and trace elements. *X-ray Spectr.* 13

Potts, P.J.; Williams Thorpe, O.; Isaacs, M.C. and Wright, D.W., 1985. High-precision instrumental neutron-activation analysis of geological samples employing simultaneous counting with both planar and coaxial detectors. *Chem. Geol.* 48, 145-155

Prichard, H.M., 1979. A petrographic study of the process of serpentinisation in ophiolites and the ocean crust. *Contrib. Mineral. Petrol.* 68, 231-241

Proffett, J.M., 1977. Cenozoic geology of the Yerington district, Nevada, and implications for the nature of Basin and Range faulting. *Geol. Soc. Am. Bull.* 88, 247-266

Project Rose Scientists, 1981. Microearthquake activity along the Orozco farcture zone: preliminary results from Project Rose. *J. Geophys. Res.* 86, 3783-3790

Raleigh, C.B. and Paterson, M.S., 1965. Experimental Deformation of Serpentinite and Its Tectonic Implications. *J. Geophys. Res.* 70, 3965-3985

Rautenschlein, M.; Jenner, G.A.; Hertogen, J.; Hofmann, A.W.; Kerrich, R.; Schmincke, H.-U. and White, W.M., 1985. Isotopic and trace element composition of volcanic glasses from the Akaki Canyon, Cyprus: implications for the origin of the Troodos ophiolite. *Earth Planet. Sci. Lett.* 75, 369-383

Remond, S., 1986. Diversité des cumulats ophiolitiques du Massif du Limassol Forest (Chypre). *Unpubl. Ph.D. thesis*, Univ. de Nancy

Ricou, L.E., 1971. Le croissant ophiolitique peri-arabe, une ceinture de nappes mises en place au Cretace Superieur. *Revue de Geographic Phys. Geol. Dyn.* 13, 327-349

Roberts, J.L., 1970. The intrusion of magma into brittle rocks. *In:* Newall, G. and Rast, N. (eds.): *Mechanics of igneous intrusion.* Geol. J. Spec. Issue No. 2, 287-339

Robertson, A.H.F., 1975. Cyprus umbers: basalt-sediment relationships on a Mesozoic ocean ridge. *J. Geol. Soc. London.* 131, 511-531

Robertson, A.H.F., 1977a. The Moni Melange, Cyprus: an olistostrome formed at a destructive plate margin. *J. Geol. Soc. London.* 133,447-466

Robertson, A.H.F., 1977b. Tertiary uplift history of the Troodos massif, Cyprus. *Geol. Soc. Am. Bull.* 88, 1763-1772

Robertson, A.H.F., 1977c. Tertiary uplift history of the Troodos massif, Cyprus. *Geol. Soc. Am. Bull.* 88, 1763-1772

Robertson, A.H.F. 1978. Metallogenesis along a fossil oceanic fracture zone: Arakapas Fault Belt, Troodos Massif, Cyprus. *Earth Planet.Sci. Lett.* 41, 317-329

Robertson, A.H.F. and Dixon, J.E., 1985. Aspects of the geological evolution of the Eastern Mediterranean. *In:* Dixon, J.E. and Robertson, A.H.F. (eds.), *The Geological Evolution of the Eastern Mediterranean,* Spec. Publ. Geol. Soc. No.17, 1-74

Robertson, A.H.F. and Hudson, J.D., 1973. Cyprus umbers: chemical precipitates on a Tethyan ocean ridge. *Earth Planet. Sci. Lett.* 18, 93-101

Robertson, A.H.F. and Hudson, J.D., 1974. Pelagic sediments in the Cretaceous and Tertiary history of the Troodos Massif, Cyprus. *Spec. Publs int. Ass. Sediment.* 1, 403-436

Robertson, A.H.F. and Woodcock, N.H., 1979. Mamonia Complex, southwest Cyprus: evolution and emplacement of a Mesozoic continental margin. *Geol. Soc. Am. Bull.* 90, 651-665

Robertson, A.H.F. and Woodcock, N.H., 1985. The SW segment of the Antalya Complex, Turkey, as a Mesozoic–Tertiary Tethyan continental margin. *In:* Dixon, J.E. and Robertson, A.H.F. (eds.), *The Geological Evolution of the Eastern Mediterranean,* Spec. Publ. Geol. Soc. No.17, 251-271

Robertson, A.H.F. and Woodcock, N.H., 1986. The role of the Kyrenia Range lineament, Cyprus, in the geological evolution of the eastern Mediterranean area. *Phil. Trans. Roy. Soc. Lond.* A317, 141-177

Robinson, P.T.; Melson, W.G.; O'Hearn, T. and Schmincke, H.-U., 1983. Volcanic glass compositions of the Troodos ophiolite, Cyprus. *Geology* 11, 400-404

Roeder, P.L. and Emslie, R.F., 1970. Olivine–liquid equilibrium. *Contrib. Mineral. Petrol.* 29, 257-289

Rogers, N.W.; MacLeod, C.J. and Murton, B.J., 1988 *in press*. Petrogenesis of boninites from the Limassol Forest Complex, Cyprus. *In:* Crawford, A.J. (ed), *Boninites and related rocks*. Geo. Allen and Unwin.

Ron, H. and Eyal, Y., 1985. Intraplate deformation by block rotation and mesostructures along the Dead Sea transform, Northern Israel. *Tectonics* 4, 85-105

Rona, R.A.; Harbison, R.H.; Bassinger, B.G.; Scott, R.B. and Nalwalk, A.J., 1976. Tectonic fabric and hydrothermal activity of Mid-Atlantic ridge, Lat. 26°N. *Geol. Soc. Am. Bull.* 87, 661-74

Rosencrantz, E., 1983. The structure of sheeted dykes and associated rocks in the North Arm massif, Bay of Islands ophiolite complex, and the intrusive process at spreading centres. *Can. J. Earth Sci.* 20, 787-801

Rothery, D.A., 1982. The evolution of the Wuqbah block and the applications of remote sensing in the Oman ophiolite. *Unpubl. Ph.D. thesis,* Open Univ. 414pp.

Rothery, D.A., 1983. The base of a sheeted dyke complex, Oman ophiolite: implications for magma chambers at oceanic spreading axes. *J. Geol. Soc. Lond.* 140, 287-296

Rubey, W.W. and Hubbert, M.K., 1959. Role of fluid pressure in mechanics of overthrust faulting, II. *Geol. Soc. Am. Bull.* 70, 167-206

Schiffman, P.; Smith, B.M.; Varga, R.J. and Moores, E.M., 1987. Geometry, conditions and timing of off-axis hydrothermal metamorphism and ore-deposition in the Solea graben. *Nature* 325, 423-425

Schilling, J.-G., 1971. Sea-floor evolution: rare-earth evidence. *Phil. Trans. Roy. Soc. London* A268, 663-706

Schmincke, H.-U.; Rautenschlein, M.; Robinson, P.T. and Mehegan, J.M., 1983. Troodos extrusive series of Cyprus: A comparison with oceanic crust. *Geology* 11, 405-409

Searle, D.L., 1967. The geology of the Kalavasos mining district. *Unpubl. Rep. Geol. Surv. Dept. Cyprus.* 66p.

Searle, D.L. and Constantinou, G., 1967a. The geology of the Asgata–Dhrapia–Vasa area. *Unpubl. Rept. Cyprus Geol. Surv. Dept.* 23pp.

Searle, D.L. and Constantinou, G., 1967b. The geology of the Kalavasos mining district. *Unpubl. Rept. Cyprus Geol. Surv. Dept.* 66pp.

Searle, D.L. and Vokes, F.M., 1969. Layered ultrabasic lavas from Cyprus. *Geol. Mag.* 106, 515-530

Searle, D.L. and Panayiotou, A., 1980. Structural implications in the evolution of the Troodos massif, Cyprus. *In:* Panayiotou, A. (ed.), *Proceedings of the International Ophiolite Symposium, Cyprus, 1979.* Cyprus Geological Survey Dept., 50-60

Searle, R.C., 1983. Multiple, closely spaced transform faults in fast-slipping fracture zones. *Geology* 11, 607-610

Sengör, A.M.C. and Yilmaz, Y., 1981. Tethyan evolution of Turkey: a plate tectonic approach. *Tectonophys.* 75, 181-241

Sengör, A.M.C.; Yilmaz, Y. and Sungurlu, 1985. Tectonics of the Mediterranean Cimmerides: nature and evolution of the western termination of Palaeo-Tethys. *In:* Dixon, J.E. and Robertson, A.H.F. (eds.), *The Geological Evolution of the Eastern Mediterranean,* Spec. Publ. Geol. Soc. No.17, 77-112

Shelton, A. W. & Gass, I.G., 1980. Rotation of the Cyprus microplate. *In:* Panayiotou, A. (ed.), *Proceedings of the International Ophiolite Symposium, Cyprus,1979.* Cyprus Geological Survey Dept., 61-65

Sibson, R.H., 1977. Fault rocks and fault rock mechanisms. *J. Geol. Soc. London.* 133, 191-213

Simonian, K.O., 1975. The geology of the Arakapas Fault Belt area, Troodos Massif, Cyprus. *Unpubl. Ph.D. thesis,* Open Univ., 151p.

Simonian, K.O. and Gass, I.G., 1978. Arakapas fault belt, Cyprus: A fossil transform fault. *Geol. Soc. Am. Bull.* 89, 1220-1230

Smewing, J.D., 1975. Metamorphism of the Troodos massif, Cyprus. *Unpubl. Ph.D. thesis,* Open Univ.

Smewing, J.D.; Simonian, K.O. & Gass, I.G., 1975. Metabasalts from the Troodos Massif, Cyprus: Genetic Implication Deduced from Petrography and Trace Element Geochemistry. *Contrib. Mineral. Petrol.* 51, 49-64.

Smith, A.G. and Briden, J.C., 1977. Mesozoic–Cenozoic Palaeocontinental Maps. *Cambridge University Press* 63pp.

Smith, A.G. and Spray, J.G., 1985. A half-ridge transform model for the Hellenic–Dinaric ophiolites.*In:* Dixon, J.E. and Robertson, A.H.F. (eds.), *The Geological Evolution of the Eastern Mediterranean,* Spec. Publ. Geol. Soc. No.17, 629-644

Spencer, J.E., 1984. Role of tectonic denudation in warping and uplift of low-angle normal faults. *Geology* 12, 95-98

Spooner, E.T.C.; Beckinsale, R.D.; Fyfe, W.S. and Smewing, J.D., 1974. ^{18}O enriched ophiolitic metabasic rocks from E. Liguria (Italy), Pindos (Greece) and Troodos (Cyprus). *Contrib. Mineral. Petrol.* 47, 41-62

Spooner, E.T.C.; Chapman, H.J. and Smewing, J.D., 1977. Strontium isotopic contamination and oxidation during ocean floor hydrothermal metamorphism of the ophiolitic rocks of the Troodos Massif, Cyprus. *Geochim. Cosmochim. Acta* 41, 873-890

Spray, J.G.; Bébien, J; Rex, D.C. and Roddick, J.C., 1985. Age constraints on the igneous and metamorphic evolution of the Hellenic–Dinaric ophiolites. *In:* Dixon, J.E. and Robertson, A.H.F. (eds.), *The Geological Evolution of the Eastern Mediterranean,* Spec. Publ. Geol. Soc. No.17, 619-628

Spray, J.G. and Roddick, J.C., 1981. Evidence for Upper Cretaceous transform fault metamorphism in West Cyprus. *Earth Planet. Sci. Lett.* 55, 273-291

Stakes, D.S.; Taylor, H.P., Jr. and Fisher, R.L., 1984. Oxygen isotope and geochemical characterisation of hydrothermal alteration in ophiolite complexes and modern oceanic crust. *In:* Gass, I.G.; Lippard, S.J. and Shelton, A.W. (eds.): *Ophiolites and Oceanic Lithosphere.* Spec. Publ. Geol. Soc. Lond. No. 14, Blackwell Scientific Publ., Oxford, 199-214

Steinmann, G., 1906. Geologische Beobachtungen in den Alpen (II). Die Schardtsche Überfaltungstheorie und die geologische Bedeutung der Tiefseeabsätze und der ophiolithischen Massengesteine. *Ber. Natf. Ges. Freiburg i. B.* 16, 1-49

Steinmann, G., 1927. Die ophiolithischen Zonen in dem mediterranean Kettenbirge. *14th. Int. Geol. Congr. Madrid* 2, 638-667

Sun, S.-S. and Nesbitt, R.W., 1978. Geochemical regularities and significance of ophiolitic basalts. *Geology* 6, 689-693

Swarbrick, R.E., 1979. The sedimentology and structure of SW Cyprus and its relationship to the Troodos Complex. *Unpubl. PhD thesis* Univ. Cambridge

Swarbrick, R.E., 1980. The Mamonia Complex of SW Cyprus: a Mesozoic continental margin and its relationship to the Troodos complex. *In:* Panayiotou, A. (ed.), *Proceedings of the International Ophiolite Symposium, Cyprus, 1979.* Cyprus Geological Survey Dept., 86-92

Swarbrick, R.E. and Naylor, M.A., 1980. The Kathikas mélange, SW Cyprus: late Cretaceous submarine debris flows. *Sedimentology* 27, 63-78

Swarbrick, R.E. and Robertson, A.H.F., 1980. Revised stratigraphy of the Mesozoic rocks of southern Cyprus. *Geol. Mag.* 117, 547-563

Taylor, R.N., 1988. The stratigraphy, geochemistry and petrogenesis of the Troodos Extrusive Sequence, Cyprus. *Unpubl. PhD thesis* Univ. Southampton 317pp.

Taylor, R.N. and Nesbitt, R.W., 1988. Light rare-earth enrichment of supra-subduction zone mantle: evidence from the Troodos ophiolite, Cyprus. *Geology* 16, 448-451

Thuizat, R.; Whitechurch, H.; Montigny, R. and Juteau, T., 1981. K-Ar dating of some infraophiolitic metamorphic soles from the eastern Mediterranean: new evidences for oceanic thrustings before obduction. *Earth Planet. Sci. Lett.* 52, 302-310

Tinkler, C.; Wagner, J.-J.; Delaloye, M. and Selçuk, H., 1981. Tectonic history of the Hatay ophiolites (South Turkey) and their relation with the Dead Sea rift. *Tectonophys.* 72, 23-41

Van der Laan, S.R.; Flower, M.F.J. and Koster van Groos, A.F., 1988, *in press.* Eutectic- and peritectic-type boninites: the role of water in olivine-orthopyroxene saturation. *In:* Crawford, A.J. (ed), *Boninites and related rocks.* Geo. Allen and Unwin.

Van der Voo, R. and French, R.B., 1974. Apparent polar wandering for the Atlantic bordering continents: late Carboniferous to Eocene. *Earth Sci. Rev.* 10, 99-119

Varga, R.J. and Moores, E.M., 1985. Spreading structure of the Troodos ophiolite, Cyprus. *Geology* 13, 846-850

de Vaumas, E., 1959. The principal geomorphological regions of Cyprus. *Cyprus Geol. Surv. Dept. Ann. Rept. for 1958*, 38-42

de Vaumas, E., 1961. Further contributions to the geomorphology of Cyprus. *Cyprus Geol. Surv. Dept. Ann. Rept. for 1960* 24-34

Vine, F.J. and Matthews, D.H., 1963. Magnetic anomalies over ocean ridges. *Nature* 199, 947-949

Vine, F.J. and Smith, G.C., 1987. Structure and physical properties of the Troodos crustal section at ICRDG drillholes CY-1, 1a and 4. *Abstracts of Papers, Troodos 87 Ophiolites and Oceanic Lithosphere.* Geol. Surv. Dept., Nicosia, Cyprus, 44

Wager, L.R. and Deer, W.A., 1939. Geological investigations in East Greenland, Part III, The petrology of the Skaergaard Intrusion, Kangerdlugssuaq, East Greenland. *Meddr. Grønland* 105, 1-352

Wager, L.R. and Brown, G.M., 1968. Layered igneous rocks. *Oliver and Boyd* Edinburgh, 588pp.

Wegener, A., 1924. The Origin of Continents and Oceans. *Methuen,* London 212pp. (English translation of 3rd. German edition of 1922).

Wernicke, B. and Burchfiel, B.C., 1982. Modes of extensional tectonics. *J. Struct. Geol.* 4, 105-115

Whitechurch, H.; Juteau, T. and Montigny, R., 1985. Role of the Eastern Mediterranean ophiolites (Turkey, Syria, Cyprus) in the history of NeoTethys. *In:* Dixon, J.E. and Robertson, A.H.F. (eds.), *The Geological Evolution of the Eastern Mediterranean,* Spec. Publ. Geol. Soc. No.17, 301-317

Wilcox, R.E.; Harding, T.P. and Seely, D.R., 1973. Basic Wrench Tectonics. *Amer. Assocn. Petrol. Geol. Bull.* 57, 74-96

Wilson, J.T., 1965. A new class of faults and their bearing on continental drift. *Nature* 207, 343-347

Wilson, R.A.M. 1959. The geology of the Xeros-Troodos area. *Cyprus Geol. Surv. Dept. Mem.* No.1, 135pp.

Woodcock, N.H., 1987. Kinematics of strike-slip faulting, Builth Inlier, Mid-Wales. *J. Struct. Geol.* 9, 353-363

Woodcock, N.H. and Fischer, M., 1986. Strike-slip duplexes. *J. Struct. Geol.* 8, 725-735

Woodcock, N.H. and Robertson, A.H.F., 1977. Origins of some ophiolite-related metamorphic rocks of the 'Tethyan belt. *Geology* 5, 373

Young, K.D.; Jancin, M.; Voight, B. and Orkan, N., 1985. Transform deformation of Tertiary rocks along the Tjörnes Fracture Zone, North Central Iceland. *J. Geophys. Res.* 90, 9986-10,010

APPENDIX 1:
Analytical Techniques

A1.1 Whole-Rock Major and Trace Element Analysis

A1.1.1 XRF sample preparation

Weathered surfaces were removed from samples using a hydraulic rock splitter, so that only fresh material was analysed. Samples were split into *c.*1 inch cubes, and then crushed in a hardened steel jaw crusher. A sub-sample of approximately 100g of the rock was separated by coning and quartering, and this material ground to 200 mesh size in an agate 'tema' swing mill or ball mill.

Trace elements were analysed on pressed powder pellets. These were prepared by mixing about 8g of rock powder with 6-12 drops of a PVP binder, and then pressing the powder into a 3cm diameter pellet using a hydraulic press.

The major elements were analysed on glass beads. The beads were made by mixing 0.4g of pre-dried rock powder with a lithium metaborate/tetraborate flux ('Spectraflux 100B') in the ratio 6:1, and fusing the mixture in a platinum crucible in a muffle furnace at 1100°C for 20 minutes. A flux loss correction was applied, and a percentage weight loss on ignition calculated for each sample by baking *c.*2.5g of rock powder in a silica crucible at 1000°C for 15 minutes, and measuring the weight loss.

A1.1.2 X-ray fluorescence analysis

The samples were analysed for both the major and trace elements on a Link Systems MECA 10-44 energy dispersive X-ray fluorescence spectrometer (ED-XRF). This incorporates a low power (49W) silver anode side window X-ray tube operated in pulsed mode with maximum settings of 49kV or 1mA, and a Si(Li) detector with a resolution of

165eV at 5.9keV. Samples were also analysed with a cobalt anode X-ray tube for the elements Cr and Ba. The ED-XRF was calibrated against international standards covering a wide range of compositions. For major elements glass beads were counted twice for 800 seconds at 45kV, 0.3mA with a 127μm silver primary beam filter. Instrumental drift was monitored by analysing USGS standard AGV-1 (major elements) (see table A1.1) and USGS GSP-1 (trace elements) four times per batch (of sixteen samples).

Detection limits for the major elements are generally quoted as 0.05wt%, except for the light elements Na, Al, Mg and Si, for which detection limits range from 0.21wt% (Si) to 0.96wt% (Na). Precision is better than 1% relative (at 2σ), except for Al (2%), Mg (3%), and Na (10%). For the trace elements detection limits are 6ppm for Rb, Sr Y, Nb, and Ni. Precision for all trace elements is about 2% at the 100ppm level, confirmed by duplicate runs of all analyses. Full details of analytical techniques are given in Potts *et al.* (1984).

Normal Zr detection limits for ED-XRF are in the order of 15ppm. The ELFC lavas, however, are notable for their exceptionally low Zr contents, down to <6ppm in some picrites (Taylor 1988). In order to improve the detection limit, therefore, a special Zr calibration ('calibration F') was devised by P.J. Potts for this study, using all available international standards with low Zr contents. These were (with preferred values): AGV-1 (230ppm); BCR-1 (191ppm); GSP-1 (500ppm); BHVO-1 (180ppm); BIR-1 (18ppm); DNC-1 (38ppm); MICA-Mg (20ppm); AN-G (15ppm); BE-N (270ppm); JG-1 (110ppm) and AL-1 (43ppm). Detection limits with this calibration are estimated to be in the range 5-10ppm Zr.

element:	Abbey (1980):	16/12/85:	11/8/86:	26/8/87:
SiO_2	59.61	59.33	59.38	59.43
TiO_2	1.06	1.08	1.08	1.07
Al_2O_3	17.19	17.01	17.2	17.25
Fe_2O_3	6.78	6.93	6.84	6.83
MnO	0.10	0.10	0.10	0.10
MgO	1.52	1.50	1.55	1.54
CaO	4.94	5.03	4.96	4.99
Na_2O	4.32	4.21	4.24	4.30
K_2O	2.92	2.91	2.91	2.91
P_2O_5	0.51	0.49	0.49	0.54

Table A1.1: Analyses of the standard AGV-1 over the period of this study, compared to the recommended values (Abbey 1980).

A1.2 Instrumental Neutron Activation Analysis

Instrumental neutron activation analysis (INAA) was carried out on 12 lavas from the ELFC by N.W. Rogers, to determine concentrations of the rare-earth elements (REE) and of Ta, Hf, Sc, and Co. The results are presented in appendix 4.

Rock powders were dried overnight in an oven at 110°C. Approximately 0.3g of each powder was weighed accurately into polythene capsules, and lids sealed to prevent leakage of radioactive powder. Irradiation capsules were then stacked in a polythene cylinder. A pre-weighed lacquered iron foil was placed between each irradiation capsule to monitor neutron flux variations along the length of the cylinder. Each irradiation cylinder contained nine samples and two standards (irradiation standard AC (OURS) and an internal standard sample of Whin Sill).

Samples were irradiated in a core tube at the Imperial College reactor centre at Ascot in a thermal flux of 5×10^{12} n $cm^{2}s^{-1}$ for 24-30 hours. Following irradiation the samples were left for a week for the short-lived radio-isotopes to decay, and then were 'counted' at the Open University using two detectors–a planar low energy photon spectrometer, and a coaxial Ge(Li) detector–on either side of the sample capsule. Data were processed using spectroscopy amplifiers and a multichannel analyser. Photopeak data were corrected for neutron flux variations using the iron foil data. A detailed description of counting conditions, peak fitting, calibration and corrections is given in Potts *et al.* (1985).

A1.3 Mineral Analysis

The mineral chemistries of a range of lavas (and a tectonised harzburgite) from the ELFC were investigated by electron microprobe. All the data were collected from polished thin sections of the samples on a fully automated, wavelength dispersive,

Cambridge Instruments Microscan 9 electron probe microanalyser at the Open University. Results of mineral analyses are presented in appendix 5. Whole-rock analysis of fresh glass was possible in some of lava specimens, and these results are incorporated into appendix 3.

Routine silicate analysis was performed at an accelerating potential of 20kV, a specimen current of 30.5nA, and a typical spot size of 10-15μm. The beam was, however, defocussed for whole-rock glass analysis. Initial calibration (for each session) was achieved with respect to natural and synthetic primary standards, and this calibration checked against a secondary basalt glass standard, ABG. If the ABG analysis for any element fell outside the expected range, then a recalibration for that element would be caried out until a satisfactory value obtained. The ABG standard was reanalysed every few hours to check for calibration drift.

A detailed review of general operating strategy and a statistical assessment of microprobe data has been made by Browning (1982), and also by Potts *et al.* (1983).

APPENDIX 2:
Sample Localities

SAMPLE:	GRID REF:	LOCALITY:	DESCRIPTION:
85/4	23584833	Asgata (school)	olØ UPL
85/21	24024882	Asgata (river)	glassy olØ UPL
85/29	23864886	Asgata (river)	glassy olØ UPL
85/34	21065018	Asgata–Vasa road	Sheeted Dyke Complex
85/35	21065018	Asgata–Vasa road	Sheeted Dyke Complex
85/37	20165035	Asgata–Vasa road	Sheeted Dyke Complex
85/38	20165035	Asgata–Vasa road	Sheeted Dyke Complex
85/63	14935130	Kellaki–Parekklisha road	dyke cutting layered sequence
85/66	15035116	Kellaki–Parekklisha road	dyke cutting layered sequence
85/68	14845115	Kellaki–Parekklisha road	dyke cutting layered sequence
85/69	14775120	Kellaki–Parekklisha road	dyke cutting layered sequence
85/83	14775120	Kellaki–Parekklisha road	dyke cutting layered sequence
85/89	14775120	Kellaki–Parekklisha road	dyke cutting layered sequence
85/90	14775120	Kellaki–Parekklisha road	dyke cutting layered sequence
85/98	14855102	Kellaki–Parekklisha road	dyke cutting layered sequence
85/99	14835097	Kellaki–Parekklisha road	dyke cutting layered sequence
85/101	14815054	Kellaki–Parekklisha road	dyke cutting layered sequence
85/108	24785101	Mandra tou Alykou, KM	olØ UPL
85/109	24785101	Mandra tou Alykou, KM	vitreous interpillow glass (UPL)
85/110	24805112	Mandra tou Alykou, KM	glassy olØ UPL
85/113	24865120	Mandra tou Alykou, KM	picrite (base of flow)
85/114	24875120	Mandra tou Alykou, KM	picrite (base of flow)
85/115	24875120	Mandra tou Alykou, KM	picrite (middle of flow)
85/116	24875120	Mandra tou Alykou, KM	picrite (top of flow)
85/117	24875120	Mandra tou Alykou, KM	glassy ol-opxØ lava in picrites
85/121	24865121	Mandra tou Alykou, KM	picrite (base of flow)
85/122	24865121	Mandra tou Alykou, KM	picrite (middle of flow)
85/123	24865121	Mandra tou Alykou, KM	picrite (top of flow)
85/124	24865120	Mandra tou Alykou, KM	picrite (base of flow)
85/127	24855114	Mandra tou Alykou, KM	vitreous interpillow glass (UPL)
85/135	19765116	Vasa village	cross-cutting dyke, isotropic gabbros
85/148	12335226	Prastion	cross-cutting dyke, isotropic gabbros
85/160	24415068	Petra, KM	aphyric LPL
85/161	24415068	Petra, KM	aphyric UPL
85/171	23334825	Asgata (Konnin)	spherulitic olØ UPL
85/172	23924864	Asgata (river)	olØ UPL
85/173	24074872	Asgata (river)	aphyric UPL
85/177	24325076	Petra, KM	olØ UPL
85/178	24325076	Petra, KM	glassy UPL
85/179	24325076	Petra, KM	glassy UPL
85/180	24325076	Petra, KM	aphyric LPL
85/181	24325076	Petra, KM	aphyric LPL
85/182	24325076	Petra, KM	aphyric LPL
85/183	24325076	Petra, KM	aphyric UPL
85/184	24325076	Petra, KM	aphyric LPL
85/185	24345070	Petra, KM	aphyric LPL
85/186	24345070	Petra, KM	aphyric LPL

SAMPLE:	GRID REF:	LOCALITY:	DESCRIPTION:
86/18	21445299	Mazoukambos, Vasil. R.	(multiple) dyke cutting harzburgite
86//20	21495303	Mazoukambos, Vasil. R.	dyke cutting harzburgite
86/28	22255291	Mazoukambos, Vasil. R.	dyke cutting harzburgite
86/37	22685445	Neron tou Mashala	foliated crush rock, AFD
86/41	23945535	Vathyrkakas, Vavla	glassy olØ lava
86/43	23905530	Vathyrkakas, Vavla	aphyric lava
86/44	23905529	Vathyrkakas, Vavla	aphyric lava
86/45	23875527	Vathyrkakas, Vavla	aphyric lava
86/46	23815510	Vathyrkakas, Vavla	aphyric lava
86/49	23835531	Vathyrkakas, Vavla	aphyric lava
86/55	22235303	Mazoukambos, Vasil. R.	dyke cutting shear zone
86/56	24765147	Mandra tou Alykou, KM	glassy olØ UPL
86/63	25015301	Palaeodhrapia	aphyric 'LPL'
86/64	25025303	Palaeodhrapia	aphyric 'LPL'
86/72	24845354	Palaeodhrapia–Parsata	aphyric 'UPL'
86/74	24845115	Mandra tou Alykou, KM	vitreous interpillow glass (UPL)
86/82	23955540	Vathyrkakas, Vavla	porcellaneous radiolarite
86/84	23045141	Vasilikos Reservoir (S bank)	aphyric LPL
86/85	23125140	Vasilikos Reservoir (S bank)	aphyric LPL
86/96	23445091	Polemikon, KM	aphyric LPL
86/106	23745102	Kalavasos Dam sluice	vitreous interpillow glass (LPL)
86/108	23745102	Kalavasos Dam sluice	aphyric LPL
86/110	23835105	Kalavasos Dam sluice	vitreous interpillow glass (LPL)
86/111	23745099	Kalavasos Dam sluice	aphyric LPL
86/141	16464771	3km NNE Parekklisha	fresh aphyric lava
86/144	19114617	Monagroulli	opxØ glassy lava
86/146	18754608	Monagroulli	glassy olØ lava
86/147	18694585	Monagroulli	glassy opx cumulate lava
86/159	19344561	Monagroulli	cross-cutting dyke in Sheeted Dyke Complex
86/160	19344561	Monagroulli	cross-cutting dyke in Sheeted Dyke Complex
86/161	18054602	1.5km NNE Pyrgos	glassy aphyric lava
86/163	17914658	Ornithouri	aphyric Basal Group lava
86/169	19455450	Akapnou Forest	tectonised harzburgite
86/170	19455450	Akapnou Forest	dyke cutting harzburgite
86/175	21805305	Mazoukambos, Vasil. R.	(multiple) dyke cutting harzburgite
86/179	24175367	Parsata village	aphyric lava
86/180	24115364	Parsata village	aphyric lava

abbreviations:

olØ = olivine-phyric
opxØ = orthopyroxene-phyric

LPL = Lower Pillow Lava
UPL = Upper Pillow Lava

KM = Kalavasos Mines
Vasil. R. = Vasilikos River

APPENDIX 3:

XRF Analyses

Sample	85/4	85/21	85/29	85/34	85/35	85/37	85/38	85/63	85/66	85/68	85/69
SiO2	55.76	52.18	53.93								
TiO2	0.34	0.28	0.4								
Al2O3	14.58	12.5	13.97								
Fe2O3	9.02	9.25	8.67								
MnO	0.09	0.16	0.17								
MgO	8.31	13.43	10.03								
CaO	6.27	11	10.99								
Na2O	0.43	0.87	1.56								
K2O	5.17	0.25	0.2								
P2O5	0.03	0.06	0.06								
S	0	0.01	0.02								
L.O.I.	5.2	5.75	4.43								
Ti				3303	2574	1922	2417	1738	1725	1668	2910
V		196	207	272			224	257			197
Cr	1018	792	712	89	72	471	562	141	98	934	473
Ni	121	335	262	46	34	149	195	66	85	154	250
Rb	43	9	6	3	10	9	6	4	5	3	2
Sr	62	300	214	102	116	63	190	206	362	224	89
Y	4	8	10	16	15	7	12	8	9	7	13
Zr	16	19	27	39	31	15	27	14	21	13	39
Nb	2.2	2.6	2.8	2.5	3.4	2.6	1.6	2.3	2.6	1.6	2.4
Ba		50	92	93			85	113			88
Mg no.	67	76.2	71.8								

Sample	85/83	85/89	85/90	85/98	85/99	85/101	85/108	85/109G	85/110	85/113	85/114	85/115	85/116
SiO2							51.96	56.23	53.8	46.51	47.55	50.2	50.93
TiO2							0.42	0.42	0.41	0.13	0.14	0.2	0.25
Al2O3							15.7	15	14.91	5.95	7.02	10.07	13.24
Fe2O3							8.62	7.69	8.65	9.91	9.7	9.24	8.98
MnO							0.09	0.14	0.16	0.15	0.16	0.16	0.18
MgO							8.37	7.71	8.97	31.94	27.77	20.05	14.53
CaO							12.12	11.38	11.12	4.87	7.03	9.17	10.98
Na2O							1.27	1.31	1.74	0.46	0.49	0.68	0.66
K2O							1.34	0.12	0.14	0.05	0.09	0.16	0.18
P2O5							0.1		0.08	0.03	0.03	0.05	0.04
S							0.01		0.02	0.01	0.01	0.02	0.02
L.O.I.							5.36	2.2	3.9	4.77	4.88	4.7	6.23
Ti	1937	1805	2102	1625	1338	794							
V		184	180	215	138	122	174		230		128		
Cr	1144	1379	1511	300	1015	922	364		559	2281	2020	1625	834
Ni	315	527	573	98	119	117	110		157	1418	1208	685	159
Rb	2	3	1	4	3	2	20		5	4	5	6	7
Sr	102	119	100	45	240	187	77		88	5	27	95	249
Y	8	9	8	10	7	2	8		10	2	3	6	7
Zr	23	16	20	19	13	9	26		26	7	8	9	14
Nb	2.7	1.6	1.7	2.1	1.4	1.4	2.3		2.2	2.1	2.3	2.4	3.1
Ba		97	101	55	46	57	116		101		36		
Mg no.							68.1	68.8	69.5	87.6	86.3	82.7	78.1

Sample	85/117	85/119	85/121	85/122	85/123	85/124	85/127G	85/135	85/148	85/160	85/161	85/171	85/172
SiO2	54.11	48.61	47.27	52.42	51.5	46.95	55.72			51.4	50.76	53.46	53.73
TiO2	0.27	0.29	0.15	0.23	0.29	0.11	0.44			0.27	0.31	0.31	0.42
Al2O3	13.49	13.17	7.27	11.99	14.3	6.45	15.77			13.27	13.24	13.82	14.89
Fe2O3	8.83	9.41	9.57	8.95	8.56	9.8	7.54			9.39	9.03	8.72	9.64
MnO	0.16	0.17	0.14	0.16	0.15	0.15	0.16			0.13	0.21	0.21	0.1
MgO	10.34	11.61	27.67	14.16	11.37	30.54	6.71			11	12.91	9.66	8.88
CaO	11.97	13.92	6.88	10.63	12.35	5.42	11.85			11.34	11.46	12.18	7.63
Na2O	0.48	0.53	0.82	1.18	0.82	0.44	1.66			0.47	0.44	1.24	0.68
K2O	0.24	2.21	0.1	0.2	0.59	0.06	0.13			2.64	1.59	0.3	3.94
P2O5	0.08	0.08	0.1	0.05	0.05	0.06				0.07	0.04	0.06	0.07
S	0.02	0.01	0.02	0.02	0.01	0.02				0.01	0.01	0.03	0.02
L.O.I.	4.37	9.27	4.63	4.84	6.73	4.25	4.15			6.48	6.95	5.19	4.98
Ti								1966	1579				
V	229		121	204	266	105							171
Cr	615	818	1961	1017	909	2041		316	119	696	977	886	592
Ni	156	206	1147	353	154	1306		81	53	149	394	172	229
Rb	7	26	5	7	14	3		4	2	25	15	9	30
Sr	101	72	23	144	122	8		71	93	66	69	305	175
Y	8	11	3	7	8	3		14	4	8	5	9	14
Zr	12	13	8	9	10	7		17	11	12	16	15	27
Nb	3	2.9	2.8	3	2.7	2		2.2	1	2.7	1.9	2.5	3.2
Ba	52		42	73	409	33							136
Mg no.	72	73.1	86.4	77.7	74.5	87.3	66.2			72	75.9	70.9	67

Sample	85/173	85/177	85/178	85/179	85/180	85/181	85/182	85/183	85/184	85/185	85/186
SiO2	50.26	49.01	53.36	53.37	54.22	54.01	52.48	51.99	54.57	50.75	51.48
TiO2	0.48	0.32	0.32	0.33	0.3	0.27	0.25	0.49	0.26	0.49	0.48
Al2O3	16.05	14.64	13.75	13.75	14.09	13.51	14.48	16.07	13.12	15.99	16.57
Fe2O3	8.84	8.8	8.92	8.93	8.4	8.57	8.69	8.39	9.04	8.58	8.6
MnO	0.21	0.11	0.16	0.16	0.14	0.11	0.15	0.15	0.11	0.16	0.15
MgO	10.63	10.78	10.76	10.78	9.87	9.92	8.66	9.57	9.63	8.99	9.24
CaO	9.92	13.12	11.82	11.76	9.65	9.07	9.52	8.01	12.33	11.51	8.85
Na2O	0.77	0.7	0.68	0.71	0.42	2.86	3.15	1.93	0.44	1.92	2.48
K2O	2.79	2.44	0.15	0.11	2.84	1.62	2.56	3.32	0.41	1.55	2.06
P2O5	0.05	0.08	0.07	0.07	0.06	0.05	0.04	0.06	0.07	0.05	0.09
S	0.01	0.01	0.02	0.03	0.01	0.01	0.01	0.01	0.01	0.01	0.01
L.O.I.	7.37	8.99	3.34	3.25	4.66	5.51	7.04	7.29	2.05	7.94	6.57
Ti											
V	201				246	234	204	193			
Cr	536	1194	877	922	582	729	592	242	748	305	267
Ni	243	256	219	255	236	165	138	105	152	101	87
Rb	20	19	6	6	25	21	29	28	15	15	17
Sr	159	54	52	50	47	321	154	103	23	108	129
Y	13	8	9	9	3	8	8	10	7	12	12
Zr	29	17	18	17	13	9	10	29	12	29	28
Nb	2.2	2	2.8	2.1	2.6	2.1	2	2.9	2.7	2.4	2.5
Ba	188				107	69	58	114			
Mg no.	72.6	72.9	72.6	72.6	72.1	71.8	68.7	71.5	70.1	69.7	70.3

Sample	86/18	86/20	86/28	86/41	86/43	86/44	86/45	86/46	86/49	86/55	86/56	86/63	86/64
SiO2				54.92	53.85	53.22	52.33	54.7	53.32		53.92	58.22	55.34
TiO2				0.37	0.59	0.64	0.57	0.59	0.5		0.41	0.79	0.7
Al2O3				13.84	17.3	17.66	15.07	16.58	14.71		14.87	15.58	16.89
Fe2O3				8.53	7.19	8.8	9.44	7.93	9.56		8.81	9.33	7.78
MnO				0.33	0.12	0.13	0.11	0.12	0.28		0.16	0.12	0.07
MgO				10.44	10.48	10.66	13.58	8.5	12.83		8.93	5.28	6.54
CaO				9.64	7.09	5.09	4.45	6.24	6.09		11.24	7.46	9.96
Na2O				1.61	2.36	1.76	1.55	2.61	0.39		1.39	2.92	2.24
K2O				0.29	0.93	1.95	2.85	2.69	2.59		0.19	0.16	0.4
P2O5				0.06	0.08	0.08	0.05	0.05	0.13		0.07	0.1	0.09
S				0.01	0.01	0.01	0	0	0.01		0.02	0.01	0.01
L.O.I.				7.29	5.69	7.92	6.51	2.98	6.39		3.79	1.94	1.96
Ti	2451	1977	1241							1646			
V													
Cr	76	163	1388	1069	223	637	234	193	749	831	291	89	255
Ni	53	55	434	184	87	188	79	57	241	164	123	16	52
Rb	1	3	2	8	7	46	17	24	17	1	5	2	15
Sr	60	81	28	286	170	165	164	114	176	3	131	154	146
Y	14	12	7	11	10	15	12	13	25	10	13	19	16
Zr	20	20	10	25	36	36	33	34	28	12	25	46	45
Nb	5.4	5.6	3.6	2.2	2.8	2.9	2.6	2.8	2.8	4.6	3	3.5	3.4
Ba													
Mg no.				72.9	76.2	72.7	76	70.2	74.7		69	55.5	64.9

Sample	86/72	86/74WR	86/74G	86/84	86/85	86/96	86/106	86/108	86/110WR	86/110G	86/111	86/141	86/144
SiO2	51.43	54	54.89	54.26	54.89	52.55	55.59	59.21	54.94	55.49	71.19	54.12	54.47
TiO2	0.78	0.41	0.43	0.75	0.75	0.58	0.48	0.61	0.45	0.5	0.66	0.42	0.29
Al2O3	18.62	14.87	15.61	15.75	16.13	17.64	15.88	16.63	16.18	16.28	12.74	15.05	14.23
Fe2O3	8.97	8.78	7.64	9.52	9.03	9.71	9.47	7.95	7.7	7.24	5.28	8.25	9.18
MnO	0.31	0.15	0.16	0.19	0.16	0.24	0.14	0.12	0.13	0.14	0.08	0.15	0.15
MgO	10.22	9.1	7.66	7.27	7.06	10.25	6.43	4.37	7	6.69	1.21	8.25	8.6
CaO	4.85	11.02	11.7	6.75	5.21	3.18	10.49	8.13	11.77	11.51	5.47	11.9	11.91
Na2O	1.2	1.42	1.72	5.09	6.57	0.41	1.3	2.65	1.56	1.99	2.66	1.57	0.86
K2O	3.4	0.13	0.13	0.34	0.09	5.15	0.14	0.26	0.19	0.14	0.53	0.14	0.2
P2O5	0.17	0.09		0.08	0.08	0.3	0.05	0.06	0.05		0.16	0.11	0.09
S	0.04	0.02		0.01	0.02	0.01	0.03	0.01	0.02		0.02	0.03	0.02
L.O.I.	7.43	2.1	3.89	2.99	4.31	7.46	3.32	3.36	2.38	4.07	0.97	3.48	3.8
Ti													
V													
Cr	346	276		61	58	73	185	85	229		111	547	419
Ni	113	126		23	20	54	35	23	51		11	125	78
Rb	32	5		3	1	39	4	6	4		14	3	5
Sr	305	85		109	91	109	74	136	99		101	93	120
Y	25	12		22	20	24	15	18	14		20	14	10
Zr	55	27		40	41	31	27	48	30		43	28	13
Nb	3.2	3		3.4	2.8	3.4	3.7	3.3	4.6		3	2.4	3.5
Ba													
Mg no.	71.5	69.5	68.8	62.7	63.2	69.9	59.9	54.7	66.7	67	33.5	68.8	67.3

All samples recast to 100% (anhydrous). Samples marked with the suffix 'G' are whole-rock microprobe analyses of fresh glass ('LOI' = difference between total and 100%).

Sample	86/144G	86/146	86/147	86/159	86/160	86/161	86/163	86/170	86/175	86/179	86/180
SiO2	55.6	53.91	54.79			54.06	56.46			52.43	51.77
TiO2	0.27	0.44	0.27			0.49	0.38			0.35	0.36
Al2O3	15.07	14.86	11.96			15.18	14.15			14.92	15.04
Fe2O3	8.21	8.5	9.47			9.16	8.54			8.61	9.48
MnO	0.17	0.15	0.15			0.16	0.18			0.15	0.27
MgO	7.65	9.71	11.76			8.85	9.3			11.5	12.01
CaO	12.28	10.55	10.53			10.25	6.41			9.97	9.96
Na2O	0.63	1.61	0.83			1.6	4.41			0.91	0.64
K2O	0.11	0.15	0.22			0.21	0.07			1.08	0.43
P2O5		0.09	0.04			0.07	0.07			0.06	0.03
S		0.02	0.02			0.03	0.06			0.01	0.01
L.O.I.	4.06	3.1	3.62			4.05	2.95			5.83	5.68
Ti				2261	1749			1629	1709		
V											
Cr		697	878	121	338	532	388	1509	996	820	854
Ni		244	173	41	73	193	97	667	189	227	196
Rb		5	5	9	4	6	1	1	6	19	7
Sr		96	74	106	62	105	63	16	229	258	548
Y		12	9	15	11	14	11	9	12	11	17
Zr		29	14	17	18	34	22	15	13	16	19
Nb		2.5	3.2	3.3	3.4	3.8	2.3	2.8	3.4	3.6	2.9
Ba											
Mg no.	67.2	71.5	73.2			68	70.6			74.6	73.6

APPENDIX 4:
INAA Analyses

sample:	85/21	85/29	85/110	85/117	85/122	85/179	85/180
La	(0.7)	1.5	0.86	(0.4)	(0.3)	(0.6)	(0.7)
Ce	—	3.5	3.2	(1.8)	(2.2)	(1.4)	(2.7)
Nd	(2.1)	2.15	2.9	—	—	(1.8)	2.9
Sm	0.46	0.85	0.83	0.35	0.28	0.54	0.25
Eu	0.22	0.34	0.35	0.16	0.13	0.24	0.13
Tb	0.23	0.25	0.29	0.21	0.15	0.23	0.11
Yb	1.15	1.19	1.25	1.27	1.07	1.22	0.69
Lu	0.20	0.20	0.20	0.22	0.18	0.21	0.11
Ta	0.10	0.07	0.07	0.13	0.10	0.07	0.12
Hf	0.34	0.68	0.61	0.34	0.22	0.44	0.25
Sc	41.0	38.3	38.8	44.2	40.2	39.6	49.0
Co	51.1	43.7	40.6	39.6	56.8	43.6	57.0

sample:	85/184	85/186	86/56	86/110	86/111	CHONDRITE:
La	(0.4)	1.0	1.3	1.0	2.5	0.328
Ce	—	3.6	3.2	2.8	5.37	0.865
Nd	(1.8)	2.9	(2.6)	—	5.2	0.630
Sm	0.34	0.92	0.77	0.88	1.48	0.203
Eu	0.17	0.44	0.35	0.40	0.61	0.077
Tb	0.21	0.36	0.26	0.24	0.51	0.052
Yb	1.03	1.24	1.25	1.30	1.91	0.22
Lu	0.17	0.20	0.20	0.20	0.31	0.0339
Ta	0.11	0.10	0.10	0.07	0.12	
Hf	0.32	0.73	0.76	0.98	1.28	
Sc	47.0	41.0	39.4	37.5	24.9	
Co	42.7	30.8	37.0	29.1	9.7	

Chondrite normalising values from Nakamura (1974).
85/29, 85/110 and 85/117 also analysed by isotope dilution by N.W. Rogers. Results given in Rogers *et al.* (1988).
Values in parentheses are below normal detection limits and are not used on plots.
— not detected

APPENDIX 5:
Microprobe Analyses

SAMPLE:	harzburgite 86/169 WAA	86/169 WAB	86/169 WAC	86/169 WAD	86/169 WAE
MINERAL:	OLIVINE	OLIVINE core	OLIVINE rim	OLIVINE	OLIVINE
SiO2	41.76	41.77	41.88	41.88	41.67
FeO	8.53	8.31	8.26	8.34	8.44
MnO	0.14	0.12	0.12	0.14	0.12
MgO	49.85	49.72	49.58	49.37	49.63
Cr2O3	0.02	0.02	0.02	0.02	0.02
NiO	0.44	0.39	0.41	0.42	0.42
TOTAL	100.74	100.33	100.27	100.17	100.3
Fo%	91.2	91.4	91.5	91.3	91.3

SAMPLE:	harzburgite 86/169 WAF	86/169 WAG	86/169 WAH
MINERAL:	OLIVINE	OLIVINE	OLIVINE
SiO2	41.87	41.97	41.63
FeO	8.51	8.41	8.34
MnO	0.11	0.14	0.14
MgO	49.80	49.66	49.59
Cr2O3	0.03	0.00	0.00
NiO	0.42	0.38	0.38
TOTAL	100.74	100.56	100.02
Fo%	91.3	91.3	91.4

SAMPLE:	harzburgite 86/169 WBD	86/169 WBE	86/169 WBF	86/169 WBG	86/169 WBH
MINERAL:	OPX	OPX	OPX	OPX	OPX
SiO2	57.33	56.45	57.48	57.50	57.21
TiO2	0.02	0.02	0.04	0.02	0.04
Al2O3	2.22	1.93	1.86	2.10	1.82
FeO	5.51	5.39	5.26	5.38	5.46
MnO	0.14	0.14	0.13	0.13	0.13
MgO	33.02	32.22	32.58	32.28	32.82
CaO	1.00	2.28	1.69	1.86	1.69
Na2O	0.01	0.03	0.01	0.01	0.01
Cr2O3	0.77	0.75	0.72	0.86	0.65
NiO	0.12	0.12	0.09	0.11	0.09
TOTAL	100.14	99.33	99.86	100.25	99.92
En%	89.70	87.40	88.70	88.10	88.50
Fs%	8.40	8.20	8.00	8.20	8.20
Wo%	1.90	4.40	3.30	3.70	3.30
Mg#	91.40	91.40	91.70	91.50	91.50

SAMPLE:	harzburgite 86/169 WBB	86/169 WBC
MINERAL:	CPX	CPX
SiO2	53.42	53.20
TiO2	0.13	0.13
Al2O3	3.08	3.02
FeO	2.80	2.87
MnO	0.09	0.09
MgO	17.77	17.93
CaO	20.21	20.01
Na2O	0.17	0.15
Cr2O3	1.14	1.14
NiO	0.05	0.06
TOTAL	98.86	98.60
En%	52.50	52.80
Fs%	4.60	4.80
Wo%	42.90	42.40
Mg#	91.90	91.80

SAMPLE:	harzburgite 86/169 WCA	86/169 WCB	86/169 WCC	86/169 WCD
MINERAL:	CHROME-SP	CHROME-SP	CHROME-SP	CHROME-SP
SiO2	0.57	0.95	0.11	0.14
TiO2	0.18	0.22	0.15	0.22
Al2O3	20.81	22.90	21.07	21.70
FeO	13.89	15.91	13.91	14.81
Fe2O3	3.22	1.83	2.95	2.42
MnO	0.12	0.14	0.15	0.12
MgO	14.48	13.62	13.93	13.59
CaO	0.01	0.05	0.01	0.03
Cr2O3	46.82	44.12	47.19	46.98
NiO	0.10	0.10	0.12	0.13
TOTAL	100.21	99.85	99.59	100.14
Mg#	65.00	60.40	64.10	62.00
Cr#	60.10	56.40	60.00	59.20
Fe'''/R'''	3.80	2.20	3.40	2.80

SAMPLE:	glassy lava	(flow unit d)			
	85/29 YYA	85/29 YYD	85/29 YYE	85/29 YYH	
MINERAL:	OLIVINE	OLIVINE	OLIVINE	OLIVINE	
	microphen	phen rim	phen rim	phen	
SiO2	40.98	40.78	40.69	41.11	
FeO	12.70	11.31	13.14	11.57	
MnO	0.20	0.20	0.20	0.20	
MgO	47.36	47.79	46.60	47.83	
CaO	0.23	0.24	0.24	0.23	
Cr2O3	0.05	0.02	0.05	0.03	
NiO	0.21	0.24	0.20	0.23	
TOTAL	101.73	100.58	101.12	101.20	
Fo%	86.9	88.3	86.3	88.0	

SAMPLE:	glassy lava	(flow unit d)			
	85/110 ZRA	85/110 ZRB	85/110 ZRC	85/110 ZRD	85/110 ZRE
MINERAL:	OLIVINE	OLIVINE	OLIVINE	OLIVINE	OLIVINE
	phen	phen	microphen	core phen	——rim phen
SiO2	40.60	40.59	40.67	40.57	40.29
FeO	11.90	13.06	12.52	11.62	12.59
MnO	0.20	0.22	0.22	0.20	0.20
MgO	46.79	45.75	46.13	46.79	46.34
CaO	0.21	0.26	0.24	0.23	0.26
Cr2O3	0.03	0.03	0.03	0.02	0.03
NiO	0.20	0.14	0.14	0.15	0.12
TOTAL	99.93	100.05	99.97	99.58	9.83
Fo%	87.5	86.2	86.8	87.8	86.8

SAMPLE:	glassy lava	(flow unit d)			
	85/110 ZRF	85/110 ZRG	85/110 ZQE	85/110 ZPB	85/110 ZPC
MINERAL:	OLIVINE	OLIVINE	OLIVINE	OLIVINE	OLIVINE
	rim phen	——core phen	microphen	core phen	——rim phen
SiO2	40.73	40.66	40.46	40.88	40.63
FeO	12.11	11.59	12.08	10.80	10.95
MnO	0.19	0.17	0.20	0.17	0.17
MgO	46.97	46.88	46.74	47.44	47.19
CaO	0.21	0.20	0.23	0.22	0.20
Cr2O3	0.02	0.02	0.02	0.03	0.05
NiO	0.18	0.20	0.18	0.27	0.24
TOTAL	100.41	99.72	99.93	99.81	99.43
Fo%	87.4	87.8	87.3	88.7	88.5

SAMPLE:	glassy lava (flow unit d)			
	86/56 WEA	86/56 WEB	86/56 WEC	86/56 WEF
MINERAL:	OLIVINE	OLIVINE	OLIVINE	OLIVINE
SiO2	41.33	41.38	41.10	41.15
FeO	11.96	12.07	12.00	12.44
MnO	0.19	0.17	0.19	0.22
MgO	46.35	46.07	45.82	45.78
CaO	0.20	0.21	0.20	0.24
Cr2O3	0.03	0.02	0.02	0.02
NiO	0.20	0.20	0.21	0.15
TOTAL	100.26	100.12	99.54	100.00
Fo%	87.4	87.2	87.2	86.8

SAMPLE:	aphyric lava	(flow unit a)		
	86/111 WFC	86/111 WFD	86/111 WFE	86/111 WFF
MINERAL:	PLAG	PLAG	PLAG	PLAG
	tabular phen	——core	——to	——rim
SiO2	48.19	49.12	49.12	48.52
TiO2	0.04	0.02	0.04	0.02
Al2O3	31.93	31.77	31.75	32.26
FeO	1.05	0.73	0.79	0.82
MnO	0.00	0.02	0.03	0.03
MgO	0.20	0.08	0.08	0.08
CaO	15.98	15.51	15.60	16.00
Na2O	1.66	2.03	2.08	1.64
K2O	0.22	0.01	0.01	0.02
TOTAL	99.27	99.29	99.50	99.39
An%	83.0	80.8	80.5	84.3
Ab%	15.6	19.1	19.4	15.6
Or%	1.4	0.1	0.1	0.1

SAMPLE:	glassy lava (flow unit e)				
	85/117 ZJG	85/117 ZJH	85/117 ZJI	85/117 ZJJ	85/117 ZFA
MINERAL:	OLIVINE	OLIVINE	OLIVINE	OLIVINE	OLIVINE
	edge phen	edge phen	phen	small phen	edge phen
SiO2	40.23	40.28	40.47	40.31	40.99
FeO	11.08	10.79	10.50	11.23	10.68
MnO	0.17	0.19	0.19	0.17	0.16
MgO	47.33	47.28	47.56	48.86	47.38
CaO	0.23	0.22	0.22	0.23	0.23
Cr2O3	0.05	0.05	0.03	0.03	0.05
NiO	0.21	0.21	0.24	0.21	0.21
TOTAL	99.32	99.02	99.21	99.04	99.71
Fo%	88.4	88.6	89.0	88.2	88.8

SAMPLE:	glassy lava	(flow unit e)		
	85/117 ZFB	85/117 ZFC	85/117 ZJU	85/117 ZJV
MINERAL:	OLIVINE	OLIVINE	OLIVINE	OLIVINE
	small phen	small phen	core large phen	——edge phen
SiO2	40.94	41.00	41.34	41.25
FeO	11.47	11.26	10.22	11.58
MnO	0.19	0.16	0.16	0.20
MgO	47.42	47.57	48.28	47.18
CaO	0.22	0.26	0.22	0.23
Cr2O3	0.03	0.03	0.05	0.05
NiO	0.17	0.20	0.27	0.17
TOTAL	100.44	100.48	100.58	100.66
Fo%	88.1	88.3	89.4	87.9

SAMPLE:	glassy lava	(flow unit e)			
	85/117 ZJK	85/117 ZJM	85/117 ZJN	85/117 ZJY	85/117 ZJZ
MINERAL:	OPX	OPX	OPX	OPX	OPX
	phen	microphen	small phen	phen	microphen
SiO2	55.90	55.31	55.82	57.32	57.72
TiO2	0.06	0.06	0.06	0.04	0.06
Al2O3	2.09	1.40	1.22	1.29	1.11
FeO	8.41	7.12	7.28	7.66	7.51
MnO	0.19	0.19	0.22	0.17	0.20
MgO	30.52	31.23	30.79	31.27	31.08
CaO	2.39	2.32	2.69	2.74	2.54
Na2O	0.03	0.02	0.00	0.00	0.02
Cr2O3	0.54	0.80	0.65	0.59	0.56
NiO	0.05	0.03	0.06	0.09	0.03
TOTAL	100.18	98.48	98.79	101.11	100.83
En%	82.6	84.7	83.6	83.3	83.8
Fs%	12.8	10.8	11.1	11.5	11.3
Wo%	4.6	4.5	5.3	5.2	4.9
Mg#	86.6	88.7	88.3	87.9	88.1

SAMPLE:	glassy lava	(flow unit e)			
	85/117 ZJW	85/117 ZJX	85/117 ZJP	85/117 ZJO	85/117 ZJL
MINERAL:	OPX	————CPX	CPX	CPX	CPX
	opx/cpx comp	opx/cpx comp	rim small phen	————core	microphen
SiO2	57.08	54.44	53.69	54.83	53.34
TiO2	0.06	0.08	0.08	0.09	0.09
Al2O3	1.13	1.71	1.69	1.84	2.20
FeO	7.38	4.39	4.47	4.29	5.70
MnO	0.23	0.17	0.17	0.14	0.19
MgO	31.03	19.86	19.65	18.36	19.43
CaO	2.48	18.26	19.33	20.93	17.42
Na2O	0.02	0.05	0.05	0.03	0.08
Cr2O3	0.56	0.78	0.82	0.50	0.43
NiO	0.03	0.00	0.03	0.02	0.03
TOTAL	100.00	99.74	99.98	101.04	98.83
En%	84.0	56.0	54.5	51.3	55.3
Fs%	11.2	7.0	7.0	6.7	9.1
Wo%	4.8	37.0	38.5	42.0	35.6
Mg#	88.2	89.0	88.7	88.4	85.9

SAMPLE:	glassy lava	(flow unit e)			
	85/117 ZJR	85/117 ZJS	85/117 ZJT	85/117 ZJF	85/117 ZFD
MINERAL:	CPX	CPX	CPX	CHROME-SP	CHROME-SP
	twinned phen	——phen	microphen	incl in olivine	incl in olivine
SiO2	53.91	53.76	54.31	0.16	0.21
TiO2	0.08	0.09	0.08	0.13	0.16
Al2O3	2.06	2.17	1.83	11.19	11.52
FeO	4.65	4.64	4.57	15.35	15.41
Fe2O3				4.04	4.67
MnO	0.17	0.16	0.14	0.14	0.14
MgO	19.23	19.36	19.41	11.86	11.81
CaO	19.43	19.21	19.53	0.05	0.08
Na2O	0.05	0.03	0.06		
Cr2O3	0.97	1.13	0.90	55.91	54.44
NiO	0.02	0.02	0.02	0.06	0.04
TOTAL	100.57	100.57	100.85	98.88	98.48
En%	53.7	54.1	53.9		
Fs%	7.3	7.3	7.1		
Wo%	39.0	38.6	39.0		
Mg#	88.1	88.2	88.3	57.9	57.7
Cr#				77.0	76.0
Fe'''/R'''				5.0	5.8

SAMPLE:	glassy lava				
	86/144 VAA	86/144 VAB	86/144 VAC	86/144 VAD	86/144 VAE
MINERAL:	OPX	OPX	CPX	CPX	OPX
	——	——glomero porphyritic——		——cluster——	
SiO2	56.48	55.54	53.03	52.82	56.16
TiO2	0.02	0.04	0.06	0.08	0.06
Al2O3	0.63	1.2	1.07	1.69	0.91
FeO	8.24	8.28	4.83	4.71	8.12
MnO	0.2	0.22	0.16	0.17	0.22
MgO	31.39	30.33	19.48	18.84	31
CaO	2.17	2.65	18.77	19.56	2.33
Na2O	0.02	0	0	0.03	0
Cr2O3	0.19	0.41	0.36	0.54	0.32
NiO	0.03	0.04	0.03	0.01	0.03
TOTAL	99.37	98.71	97.79	98.45	99.15
En%	83.5	82.2	54.6	53.0	83.3
Fs%	12.3	12.6	7.6	7.4	12.2
Wo%	4.2	5.2	37.8	39.6	4.5
Mg#	87.2	86.7	87.8	87.7	87.2

SAMPLE:	glassy lava 86/144 VCA	86/144 VCB	86/144 VCC	86/144 VCD	86/144 VCE
MINERAL:	OPX	OPX	CPX	CPX	OPX
	opx/cpx comp	opx/cpx comp	opx/cpx comp	opx/cpx comp	opx/cpx comp
SiO2	56.09	55.40	53.11	53.70	55.77
TiO2	0.04	0.04	0.17	0.08	0.04
Al2O3	1.22	0.60	1.75	1.21	1.07
FeO	8.24	8.27	6.77	4.83	8.13
MnO	0.20	0.22	0.20	0.16	0.20
MgO	30.50	31.35	17.80	19.48	30.96
CaO	2.30	2.19	18.69	19.02	2.22
Na2O	0.00	0.00	0.10	0.03	0.00
Cr2O3	0.34	0.17	0.16	0.45	0.32
NiO	0.01	0.04	0.04	0.01	0.04
TOTAL	98.94	98.28	98.79	98.97	98.75
En%	82.9	83.5	50.8	54.3	83.4
Fs%	12.6	12.3	10.8	7.6	12.3
Wo%	4.5	4.2	38.4	38.1	4.3
Mg#	86.8	87.1	82.4	87.8	87.1

SAMPLE:	glassy lava 86/144 VCG	86/144 VCH	86/144 VAF	86/144 VAH
MINERAL:	CPX	OPX	CPX	CPX
	opx/cpx comp	opx/cpx comp	small phen	microphen
SiO2	51.94	56.65	52.39	52.69
TiO2	0.41	0.04	0.09	0.08
Al2O3	1.88	0.80	2.26	1.91
FeO	8.92	8.06	4.64	4.68
MnO	0.22	0.20	0.14	0.16
MgO	15.76	30.24	18.34	18.72
CaO	19.19	3.38	19.53	19.06
Na2O	0.16	0.02	0.03	0.06
Cr2O3	0.02	0.20	0.78	0.66
NiO	0.03	0.04	0.03	0.03
TOTAL	98.53	99.64	98.23	98.05
En%	45.6	81.3	52.4	53.4
Fs%	14.5	12.2	7.4	7.5
Wo%	39.9	6.5	40.2	39.1
Mg#	75.9	87.0	87.6	87.7

SAMPLE:	glassy lava	(opx phyric)			
	86/147 VDA	86/147 VDB	86/147 VDC	86/147 VDD	86/147 VDE
MINERAL:	OPX	OPX	OPX	OPX	OPX
	rim xenocryst	–core xenocryst	xenocryst	groundmass	jacketed mphen
SiO2	55.49	55.66	56.12	55.79	56.12
TiO2	0.04	0.04	0.04	0.04	0.06
Al2O3	1.03	0.85	0.96	1.14	1.05
FeO	7.51	8.19	7.42	7.82	7.64
MnO	0.20	0.20	0.20	0.17	0.17
MgO	31.88	31.16	31.86	30.87	31.50
CaO	1.83	1.99	1.87	2.23	2.00
Cr2O3	0.59	0.41	0.56	0.68	0.59
NiO	0.05	0.04	0.06	0.04	0.06
TOTAL	98.62	98.54	99.09	98.78	99.19
En%	85.2	83.8	85.3	83.7	84.6
Fs%	11.3	12.4	11.1	11.9	11.5
Wo%	3.5	3.8	3..60	4.4	3.9
Mg#	88.3	87.2	88.4	87.6	88.0

SAMPLE:	glassy lava	(opx phyric)			
	86/147 VDF	86/147 VDH	86/147 VDI	86/147 VDJ	86/147 VDK
MINERAL:	OPX	OPX	OPX	OPX	OPX
	groundmass	core xenocryst	–rim xenocryst	core———tatty	xenocryst—rim
SiO2	55.71	55.84	55.56	56.91	56.15
TiO2	0.06	0.04	0.04	0.04	0.04
Al2O3	1.18	0.98	0.60	0.87	1.16
FeO	7.99	7.27	7.81	7.38	7.84
MnO	0.20	0.17	0.19	0.19	0.19
MgO	30.66	31.99	31.44	31.75	31.03
CaO	2.56	1.82	1.93	1.80	2.07
Cr2O3	0.64	0.54	0.25	0.44	0.61
NiO	0.04	0.05	0.05	0.05	0.06
TOTAL	99.04	98.70	97.87	99.43	99.15
En%	82.9	85.6	84.5	85.4	84.1
Fs%	12.1	10.9	11.8	11.1	11.9
Wo%	5.0	3.5	3.7	3.5	4.0
Mg#	87.2	88.7	87.8	88.5	87.8

SAMPLE:	picrite	(base of flow)			
	85/121 ZHA	85/121 ZHB	85/121 ZHC	85/121 ZHD	85/121 ZHE
MINERAL:	OLIVINE	OLIVINE	OLIVINE	OLIVINE	OLIVINE
	core———large	phenocryst–rim	large phen	core large phen	core large phen
SiO2	41.45	41.29	41.78	41.40	40.83
FeO	8.97	9.56	8.43	8.58	8.75
MnO	0.12	0.16	0.14	0.14	0.12
MgO	48.88	48.60	49.76	49.32	48.72
CaO	0.23	0.23	0.22	0.23	0.24
Cr2O3	0.05	0.05	0.08	0.05	0.05
NiO	0.30	0.30	0.36	0.33	0.29
TOTAL	100.00	100.19	100.77	100.05	99.00
Fo%	90.1	90.1	91.3	91.1	90.9

SAMPLE:	picrite	(base of flow)			
	85/121 ZHF	85/121 ZHG	85/121 ZIB	85/121 ZIC	85/121 ZID
MINERAL:	OLIVINE	OLIVINE	CPX	OPX	CPX
	rim———large	phenocryst–core	rim comp	——core comp	——rim comp
SiO2	41.55	41.58	52.42	56.86	51.1
TiO2			0.19	0.06	0.26
Al2O3			3.74	0.96	5.35
FeO	8.98	8.23	5.08	6.98	5.35
MnO	0.14	0.14	0.14	0.17	0.14
MgO	49.02	49.5	17.64	31.7	15.85
CaO	0.22	0.23	19.93	2.24	21.26
Cr2O3	0.07	0.05	0.5	0.36	0.17
NiO	0.32	0.35	0.02	0.08	0.02
TOTAL	100.3	100.06	99.66	99.41	99.55
Fo% (Mg#)	90.7	91.5	86.1	89	84.1
En%			50.7	85.2	46.4
Fs%			8.2	10.5	8.8
Wo%			41.1	4.3	44.8

SAMPLE:	picrite	(base of flow)		
	85/121 ZIE	85/121 ZIF	85/121 ZIG	85/121 ZIH
MINERAL:	CHROME-SP	CHROME-SP	CHROME-SP	CHROME-SP
	incl in olivine	core———large	phenocryst–rim	rim phen
SiO2	0.45	0.16	0.19	0.16
TiO2	0.15	0.16	0.18	0.15
Al2O3	12.65	12.83	15.39	13.38
FeO	13.38	13.34	13.38	13.18
Fe2O3	3.12	3.66	5.00	3.87
MnO	0.14	0.13	0.15	0.11
MgO	13.10	13.05	13.30	13.25
CaO	0.04	0.05	0.04	0.04
Cr2O3	53.60	53.96	49.77	53.37
NiO	0.09	0.07	0.12	0.10
TOTAL	96.72	97.41	97.52	97.60
Mg#	63.6	63.5	63.9	64.2
Cr#	74.0	73.8	68.4	72.8
Fe'''/R'''	3.9	4.5	6.1	4.8

SAMPLE:	picrite	(mid flow)		
	85/122 ZUA	85/122 ZUB	85/122 ZUD	85/122 ZUE
MINERAL:	OLIVINE	OLIVINE	OLIVINE	OLIVINE
	phen	phen	phen	microphen
SiO2	40.98	41.63	41.83	40.90
FeO	10.06	9.81	10.47	10.79
MnO	0.14	0.16	0.17	0.17
MgO	48.49	48.98	48.77	48.07
CaO	0.22	0.23	0.22	0.22
Cr2O3	0.05	0.05	0.03	0.07
NiO	0.26	0.30	0.27	0.23
TOTAL	100.20	101.16	101.76	100.45
Fo%	89.6	89.9	89.2	88.8

SAMPLE:	picrite	(top of flow)			
	85/123 ZDE	85/123 ZDG	85/123 ZDH	85/123 ZDJ	85/123 ZDK
MINERAL:	OPX	OPX	OPX	CPX	CPX
	large phen	core microphen	rim microphen	acicular quench	acicular quench
SiO2	56.62	55.86	56.30	52.34	51.56
TiO2	0.04	0.06	0.06	0.19	0.21
Al2O3	1.11	1.34	1.04	3.88	5.02
FeO	8.28	7.28	7.03	5.06	5.88
MnO	0.19	0.19	0.19	0.16	0.17
MgO	31.26	31.32	31.28	18.18	17.97
CaO	2.15	2.36	2.58	18.86	18.03
Cr2O3	0.36	0.68	0.58	0.36	0.26
NiO	0.06	0.05	0.06	0.03	0.02
TOTAL	100.07	99.14	99.12	99.06	99.12
En%	83.5	84.4	84.4	52.6	52.5
Fs%	12.4	11.0	10.6	8.2	9.6
Wo%	4.1	4.6	5.0	39.2	37.9
Mg#	87.1	88.5	88.8	86.5	84.5

SAMPLE:	picrite	(base of flow)			
	85/124 ZWA	85/124 ZWB	85/124 ZWC	85/124 ZWD	85/124 ZWG
MINERAL:	OLIVINE	OLIVINE	OLIVINE	OLIVINE	OLIVINE
	rim phen	core phen	rim phen	phen	phen
SiO2	41.16	41.31	41.23	40.68	41.28
FeO	9.38	9.59	9.59	8.90	9.66
MnO	0.17	0.14	0.16	0.14	0.14
MgO	48.97	48.67	48.77	48.53	48.75
CaO	0.23	0.22	0.22	0.20	0.22
Cr2O3	0.05	0.03	0.03	0.07	0.05
NiO	0.29	0.32	0.29	0.35	0.27
TOTAL	100.25	100.42	100.29	98.87	100.37
Fo%	90.3	89.9	90.1	90.7	90.0

SAMPLE:	picrite	(base of flow)			
	85/124 ZOA	85/124 ZOC	85/124 ZOD	85/124 ZOF	85/124 ZOG
MINERAL:	CHROME-SP	CHROME-SP	CHROME-SP	CHROME-SP	CHROME-SP
	incl in olivine	core phen	rim phen	rim microphen	core microphen
SiO2	0.13	0.13	0.50	0.47	0.16
TiO2	0.15	0.16	0.16	0.16	0.15
Al2O3	12.36	12.54	12.77	12.13	12.03
FeO	12.84	13.55	19.04	17.46	14.30
Fe2O3	3.66	3.66	4.00	4.26	3.80
MnO	0.10	0.13	0.21	0.17	0.12
MgO	13.81	13.26	9.95	11.03	12.91
CaO	0.03	0.04	0.03	0.06	0.04
Cr2O3	56.59	55.74	52.42	54.06	56.54
NiO	0.10	0.07	0.04	0.06	0.09
TOTAL	99.77	99.27	99.12	99.86	100.15
Mg#	65.7	63.6	48.2	53.0	61.7
Cr#	75.4	74.9	73.4	74.9	75.9
Fe'''/R'''	4.4	4.5	5.1	5.3	4.6

SAMPLE:	vitreous glass	(flow unit d)			
	85/109 ZTB	85/109 ZTC	85/109 ZTD	85/109ZTE	85/109 ZTF
MINERAL:	OLIVINE	OLIVINE	OLIVINE	OLIVINE	OLIVINE
	microphen	microphen	microphen	microphen	microphen
SiO2	39.19	39.65	40.05	40.36	40.12
FeO	13.77	11.93	12.34	12.50	12.08
MnO	0.20	0.19	0.17	0.20	0.20
MgO	45.28	46.86	46.33	46.59	46.74
CaO	0.21	0.21	0.23	0.23	0.23
Cr2O3	0.00	0.02	0.02	0.02	0.02
NiO	0.12	0.18	0.18	0.17	0.17
TOTAL	98.77	99.04	99.32	100.07	99.56
Fo%	85.4	87.5	87.0	86.9	87.3

SAMPLE:	vitreous glass	(flow unit d)			
	85/127 ZMC	85/127 ZMD	85/127 ZMF	85/127 ZMG	85/127 ZMI
MINERAL:	OLIVINE	OLIVINE	OLIVINE	OLIVINE	OLIVINE
	microphen	microphen	microphen	microphen	microphen
SiO2	40.29	40.16	40.14	40.08	40.03
FeO	11.44	12.03	12.10	12.46	13.55
MnO	0.17	0.20	0.20	0.20	0.23
MgO	46.81	46.40	46.57	46.13	45.30
CaO	0.23	0.24	0.23	0.24	0.26
Cr2O3	0.03	0.02	0.03	0.03	0.02
NiO	0.21	0.18	0.18	0.15	0.11
TOTAL	99.18	99.23	99.45	99.29	99.54
Fo%	87.9	87.3	87.3	86.8	85.6

SAMPLE:	vitreous glass	(flow unit d)			
	85/127 ZMK	85/127 ZML	85/127 ZMN	85/127 ZMB	85/127 ZME
MINERAL:	OLIVINE	OLIVINE	OLIVINE	CPX	CPX
	microphen	microphen	microphen	microphen	microphen
SiO2	39.95	40.23	40.08	52.04	51.75
TiO2				0.15	0.21
Al2O3				2.28	3.19
FeO	13.96	13.11	12.83	4.76	5.49
MnO	0.20	0.22	0.20	0.14	0.16
MgO	44.96	45.93	45.93	17.41	17.49
CaO	0.23	0.26	0.24	20.39	19.43
Na2O				0.11	0.11
Cr2O3	0.03	0.02	0.02	0.71	0.50
NiO	0.12	0.12	0.14	0.02	0.00
TOTAL	99.45	99.89	99.44	98.01	98.33
Fo% (Mg#)	85.2	86.2	86.5	86.7	85.0
En%				50.1	50.7
Fs%				7.7	8.9
Wo%				42.2	40.4

SAMPLE:	vitreous glass	(flow unit d)			
	86/74 XAA	86/74 XAB	86/74 XAC	86/74 XAD	86/74 XAF
MINERAL:	OLIVINE	OLIVINE	OLIVINE	OLIVINE	OLIVINE
	core microphen	rim microphen	microphen	microphen	microphen
SiO2	41.00	41.00	41.02	41.26	40.91
FeO	12.15	12.32	11.79	11.81	11.58
MnO	0.20	0.20	0.19	0.19	0.17
MgO	47.70	47.58	47.57	47.72	47.71
CaO	0.21	0.21	0.20	0.20	0.22
Cr2O3	0.05	0.03	0.03	0.03	0.03
NiO	0.20	0.20	0.26	0.18	0.18
TOTAL	101.51	101.54	101.06	101.39	100.80
Fo%	87.5	87.3	87.8	87.8	88.0

SAMPLE:	vitreous glass	(flow unit a)			
	86/110 XBB	86/110 XBC	86/110 XBD	86/110 XBE	86/110 XBH
MINERAL:	CPX	CPX	CPX	CPX	CPX
	core microphen	rim microphen	microphen	microphen	microphen
SiO2	52.73	52.60	52.40	52.48	51.98
TiO2	0.13	0.15	0.15	0.15	0.25
Al2O3	2.27	2.60	2.38	2.72	3.70
FeO	3.69	3.94	4.29	3.85	5.00
MnO	0.11	0.13	0.14	0.14	0.14
MgO	18.02	17.79	17.98	17.43	17.60
CaO	21.47	21.16	21.22	21.48	20.18
Na2O	0.14	0.17	0.11	0.14	0.09
Cr2O3	1.01	1.24	0.66	1.25	0.42
NiO	0.02	0.20	0.03	0.00	0.03
TOTAL	99.59	99.80	99.36	99.64	99.39
En%	50.7	50.5	50.5	49.7	50.4
Fs%	5.8	6.3	6.7	6.2	8.0
Wo%	43.5	43.2	42.8	44.1	41.6
Mg#	89.7	89.0	88.2	89.0	86.3

SAMPLE:	vitreous glass	(flow unit a)	
	86/110 XBA	86/110 XBF	86/110 XBG
MINERAL:	PLAG	PLAG	PLAG
	phen	phen	phen
SiO2	47.01	46.04	45.80
TiO2	0.02	0.02	0.04
Al2O3	32.19	33.40	33.67
FeO	0.56	0.56	0.48
MnO	0.02	0.02	0.02
MgO	0.18	0.26	0.18
CaO	17.61	18.23	18.47
Na2O	1.60	1.15	1.12
K2O	0.01	0.02	0.01
TOTAL	99.20	99.70	99.79
An%	85.9	89.6	90.0
Ab%	14.1	10.3	9.9
Or%	0.0	0.1	0.1

APPENDIX 6:
Palaeomagnetic Data

These palaeomagnetic data were acquired with S. Allerton, who undertook all the laboratory analysis, and are also presented in Allerton (1988). Remanent magnetisation was measured in the samples after alternating field demagnetisation at 20mT, following thorough pilot demagnetisations and optical studies to investigate the magnetic carriers. Detail of the demagnetisations, and of the statistical treatment of the results, is given in Allerton (*op. cit.*).

Site B1: Pevkos

13904983 Kythreotis Quarry Sheeted Dyke Complex

HOLE:	DYKE ORIENT: (dip/strike)	SAMPLE MAGN VECTOR: DECL; INCL:	ORIG DYKE ORIENT*: DECL; INCL:	ROTATION VECTOR: DECL; INCL ¶:	ANGLE OF ROTN†:
B01/2	48°SE/240	263.6; 60.8	306.7; 0 245.3; 0	050.4; -28.3 083.1; -44.6	48.1 136.2
B01/4	43°SE/235	013.4; 88.3	304.6; 0 247.4; 0	005.4; -2.4 052.6; -53.7	58.2 105.7
B01/5	46°SE/240	171.1; 79.4	324.8; 0 227.2; 0	011.2; 12.0 060.7; -54.2	61.3 135.5
B01/6	48°SE/250	270.5; 63.4	308.6; 0 243.4; 0	049.2; -33.8 086.2; -46.9	51.3 143.1
B01/7	43°SE/250	282.4; 53.1	294.5; 0 257.5; 0	080.4; -44.0 093.6; -43.3	79.1 141.7

* pole to dyke plane

† positive angle = anticlockwise rotation by faulting

¶ negative angle = upper hemisphere

mean sample magnetisation vector:	274°; 71°	α_{95} = 15.2°
mean dyke orientation:	44°(SE)/240°	α_{95} = 6.9°

Site B2: Asgata–Vasa road

202503 Gyrisman tou Kanniou Sheeted Dyke Complex

HOLE:	DYKE ORIENT: (dip/strike)	SAMPLE MAGN VECTOR: DECL; INCL:	ORIG DYKE ORIENT*: DECL; INCL:	ROTATION VECTOR: DECL; INCL ¶:	ANGLE OF ROTN†:
B02/1	65°SE/220	277.3; 48.8	290.7; 0	063.3; -37.0	37.3
			261.3; 0	084.9; -40.3	87.4
B02/3	65°SE/220	244.6; 56.8	324.7; 0	019.7; 31.5	33.1
			227.4; 0	075.6; -40.0	128.8
B02/5	55°SE/230	270.3; 51.9	299.4; 0	063.9; -32.8	45.7
			252.6; 0	086.0; -40.5	120.8
B02/7	77°SE/210	269.8; 75.1	335.2; 0	332.7; 38.6	61.5
			216.8; 0	067.7; -49.4	106.7
B02/8	67°SE/218	354.8; 83.1	332.9; 0	340.2; 28.6	71.4
			219.4; 0	058.8; -57.6	108.5

* pole to dyke plane

† positive angle = anticlockwise rotation by faulting

¶ negative angle = upper hemisphere

mean sample magnetisation vector:	269°; 65°	α_{95} = 18.1°
mean dyke orientation:	66°(SE)/220°	α_{95} = 9.6°

Site B3: Kalavasos Mines

248512 Mandra tou Alykou — Upper Pillow Lavas

HOLE:	DYKE ORIENT: (dip/strike)	SAMPLE MAGN VECTOR: DECL; INCL¶:	PROXIMITY TO VERT*: DECL; INCL¶:	ROTATION VECTOR: DECL; INCL¶:	ANGLE OF ROTN†:
B03/1	55°NE/315	267.5; -13.7	096.0; 84.8 276.0; -31.2	140.3; 1.5 084.0; -10.4	58.6 -146.2
B03/2	50°NE/320	262.1; -49.8	096.0; 53.9 276.0; -62.1	161.2; 10.3 081.0; 7.7	86.3 -160.0
B03/3	35°NE/310	259.3; -2.5	096.0; 82.1 276.0; -33.9	143.6; 13.6 084.0; -16.2	42.3 -162.1
B03/4	45°NE/330	343.8; -25.9	096.0; 30.5 276.0; -85.5	175.6; -36.9 297.0; -10.4	99.9 140.6

* pole to palaeohorizontal

† positive angle = anticlockwise rotation by faulting

¶ negative angle = upper hemisphere

mean sample magnetisation vector:	263°; -22°	α_{95} = 39.8°
mean dyke orientation:	46°(NE)/320°	α_{95} = 11.9°

Site B4: Asgata River

239488 Argakin tis Asgatas — Upper Pillow Lavas

HOLE:	DYKE ORIENT: (dip/strike)	SAMPLE MAGN VECTOR: DECL; INCL:	ORIG DYKE ORIENT*: DECL; INCL:	ROTATION VECTOR: DECL; INCL ¶:	ANGLE OF ROTN†:
B04/1	65°SE/235	283.7; 16.0	300.6; 0	292.3; 28.2	-74.2
			251.4; 0	282.1; 24.8	-154.4
B04/2	65°SE/235	289.6; 20.5	283.8; 0	289.2; 31.7	-97.2
			268.2; 0	286.6; 29.5	-125.9
B04/3	70°SE/230	298.1; 18.6	066.4; 0	321.4; 52.5	-39.0
			125.6; 0	277.1; 9.9	67.0
B04/4	70°SE/230	286.0; 23.7	063.9; 0	113.1; -37.5	47.9
			128.1; 0	272.6; 19.0	54.5
B04/5	75°SE/250	278.3; 22.1	328.0; 0	299.1; 29.3	-29.8
			224.0; 0	278.0; 27.2	-163.2
B04/7	80°W/210	286.2; -7.9	096.0; -18.2	123.6; -16.2	90.4
			096.0; -45.8	084.7; -7.7	-103.8
B04/8	80°W/210	300.6; -13.1	096.0; -28.8	106.4; -8.3	-167.1
			096.0; -35.2	005.7; 28.2	-52.7
B04/9	40°N/260	299.3; 53.8	339.6; 0	281.9; 45.3	-154.3
			212.4; 0	307.1; 26.9	61.8
B04/10	40°N/260	298.5; -0.8	034.9; 0	119.4; -22.2	117.8
			157.1; 0	248.6; -11.3	51.2
B04/11	85°SE/230	316.1; 43.6	299.1; 0	139.6; 34.5	-34.1
			252.9; 0	099.0; -59.4	77.0
B04/12	85°SE/230	324.0; 51.9	312.5; 0	322.0; -6.0	47.4
			239.5; 0	092.9; -60.7	90.2

* pole to dyke plane

† positive angle = anticlockwise rotation by faulting

¶ negative angle = upper hemisphere

mean sample magnetisation vector (holes 1-5): 287°; 20° α_{95} = 7.2°

mean dyke orientation (holes 1-5): 70°(SE)/230°

Site B5: Dhrapia River

25485258 *c.*1km north of Dhrapia village Sheeted Dyke Complex

HOLE:	DYKE ORIENT: (dip/strike)	SAMPLE MAGN VECTOR: DECL; INCL:	ORIG DYKE ORIENT*: DECL; INCL:	ROTATION VECTOR: DECL; INCL¶:	ANGLE OF ROTN†:
B05/1	22°SE/235	157.8; 27.8	358.6; 0	039.4; 35.3	96.5
			193.4; 0	034.9; -48.8	-178.9
B05/2	22°SE/235	189.7; 48.9	327.9; 0	042.7; 11.1	70.7
			224.1; 0	057.9; -45.8	168.4
B05/3	22°SE/235	161.0; 35.0	349.8; 0	036.8; 31.4	89.9
			202.2; 0	039.9; -48.6	175.3
B05/4	25°SE/230	155.8; 47.7	338.2; 0	027.2; 28.5	84.1
			213.8; 0	042.6; -49.0	158.2
B05/5	25°E/360	153.8; 32.3	343.4; 0	034.7; 43.7	96.0
			208.6; 0	035.0; -39.7	157.4
B05/6	17°E/195	164.6; 46.5	321.8; 0	032.4; 23.7	81.0
			230.2; 0	044.1; -41.7	148.5
B05/7	32°E/340	117.2; -5.4	346.9; 0	026.5; 24.5	147.3
			205.1; 0	353.9; -49.2	179.7

* pole to dyke plane

† positive angle = anticlockwise rotation by faulting

¶ negative angle = upper hemisphere

mean sample magnetisation vector:	155°; 35°	α_{95} = 20.1°
mean dyke orientation:	15°(SE)/233°	α_{95} = 17.7°

Site B6: Klonari

15475379 Kellaki–Klonari road Sheeted Dyke Complex

HOLE:	DYKE ORIENT: (dip/strike)	SAMPLE MAGN VECTOR: DECL; INCL:	ORIG DYKE ORIENT*: DECL; INCL:	ROTATION VECTOR: DECL; INCL¶:	ANGLE OF ROTN†:
B06/1	15°SW/305	256.4; 76.0	276.0; 59.1	159.2; -38.7	-59.0
			276.0; 4.88	079.1; -52.3	143.9
B06/2	15°SW/305	230.8; 74.9	276.0; 61.8	156.8; -48.1	-66.7
			276.0; 2.2	070.9; -50.2	136.7
B06/3	7°SE/220	262.3; 64.8	276.0; 53.1	162.5; -35.3	-41.9
			276.0; 10.9	086.1; -47.6	156.0
B06/4	7°SE/220	255.2; 55.9	276.0; 62.5	156.7; -48.1	-38.1
			276.0; 1.5	084.0; -42.7	154.7
B06/7	10°SW/300	283.8; 59.7	289.1; 0	272.6; 46.5	-146.0
			262.9; 0	101.0; -45.6	-168.2
B06/8	10°SW/300	249.5; 60.0	298.1; 0	074.0; -40.6	115.6
			253.9; 0	087.6; -47.2	-172.9

* pole to dyke plane

† positive angle = anticlockwise rotation by faulting

¶ negative angle = upper hemisphere

mean sample magnetisation vector:	259°; 66°	α_{95} = 9.0°
mean dyke orientation:	9°(S)/290°	α_{95} = 6.9°

B8: Monagroulli village

19344561 River immediately NW of village Sheeted Dyke Complex

HOLE:	DYKE ORIENT: (dip/strike)	SAMPLE MAGN VECTOR: DECL; INCL:	ORIG DYKE ORIENT*: DECL; INCL:	ROTATION VECTOR: DECL; INCL¶:	ANGLE OF ROTN†:
B08/1	46°NW/245	344.5; 22.1	033.9; 0 158.1; 0	318.7; 53.7 303.9; -16.9	-113.8 75.7
B08/2	46°NW/245	344.1; 18.1	038.9; 0 153.2; 0	322.2; 53.3 300.7; -19.8	-110.0 76.2
B08/3	48°NW/230	348.8; 21.2	031.5; 0 160.5; 0	324.3; 59.3 307.2; -9.5	-106.6 87.1
B08/4	48°NW/230	348.0; 29.4	022.7; 0 160.5; 0	314.6; 59.0 307.2; -9.5	-113.1 87.1
B08/5	66°N/270	005.3; 7.8	092.0; 0 100.1; 0	234.0; -72.9 264.0; -68.9	91.4 87.4
B08/6	66°N/270	005.4; 8.6	087.4; 0 104.6; 0	034.8; 73.3 276.4; -65.4	-94.3 85.8
B08/7	48°SE/240	002.2; 23.1	283.3; 0 268.7; 0	317.6; 8.5 316.2; -3.9	118.4 100.4
B08/8	48°SE/240	000.6; 24.3	276.0; 62.9 276.0; 1.1	148.1; -64.5 316.4; 3.4	113.7 107.9
B08/9	90°/220	355.0; 26.9	054.0; 0 138.0; 0	092.0; 84.0 314.0; 3.3	-76.3 101.6
B08/10	90°/220	351.7; 25.8	058.4; 0 133.6; 0	094.2; 81.8 311.8; 1.6	-72.2 98.4

* pole to dyke plane

† positive angle = anticlockwise rotation by faulting

¶ negative angle = upper hemisphere

mean sample magnetisation vector: 355°; 21° α_{95} = 6.4°

mean dyke orientation set 1 (holes 1-6): 52°(N)/250° α_{95} = 31.0°

set 2 (holes 7&8): 48°(SE)/240°

rotation in fact represents 210° of anticlockwise rotation (and thus that the transform was left-lateral), this is obviously less likely, even though there is no intrinsic reason why rotations greater than 180° cannot be accommodated in such an environment. The size of block being rotated as a coherent unit is very small (several metres maximum between crush zones) compared with the width of the deforming zone, and may effectively represent little more than large clasts in a kilometre-sized mega-fault breccia, with the potential to rotate like ball-bearings. It is pertinent to note in this context that sites B5 and B6 were chosen as they were the only outcrops of sheeted dyke found in the northern ELFC where margins were preserved and the dykes sufficiently physically coherent to be drilled!

5.3.4 Mazoukambos, Vasilikos River

The Mazoukambos locality is a relatively inaccessible area approximately 3.5km south of Layia, at the southeastern corner of the Akapnou Forest, where the Vasilikos River has incised deeply through the mantle sequence and layered plutonics. It is described separately as the tectonic style of the area is different to anywhere else in the ELFC.

The dominant tectonic feature is a very large N-S striking serpentinite shear zone (figure 5.7) which is up to 100m in thickness and dips at 30-40° eastwards. It separates highly disrupted and rotated, mostly ultramafic, plutonic rocks on its hanging wall from harzburgite tectonites, that form the main part of the Akapnou Forest, on its footwall. To the north it thins, passes beneath a tectonic outlier or 'klippe' of Sheeted Dyke Complex at Dhikephalas (enclosure 1), and becomes markedly less obvious; to the south it disappears abruptly against undisturbed serpentinised massive dunites, and is probably removed or accommodated by an E-W serpentinite mélange zone. This suggests that it might be an early structure, and this is confirmed by its relationship to adjacent 'transform sequence' intrusives. For 0.5km to the west E-W trending multiple dykes and